Departamento de Engenharia Civil
Faculdade de Ciências e Tecnologia da Universidade de Coimbra

Post-buckling bifurcational analysis of thin-walled prismatic members in the context of the Generalized Beam Theory

Fernando Pedro Simões da Silva Dias Simão

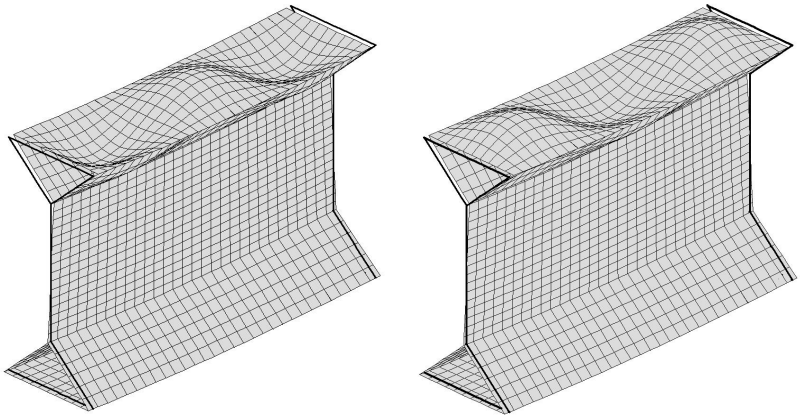

Tese apresentada para obtenção do grau de Doutor em Engenharia Civil
na Especialidade de Mecânica das Estruturas e dos Materiais

Maio de 2007

Esta dissertação foi co-financiada pelo Fundo Social Europeu, através do programa PRODEP III, Medida 5, Acção 5.3.

União Europeia

Fundo Social Europeu

ABSTRACT

This thesis presents a series of analytical models, based on the Generalized Beam Theory (GBT), to describe the buckling and post-buckling behaviour of thin-walled prismatic cold-formed steel structural members under compression and/or bending. GBT has a unique feature of enabling an theoretical significance to the structural analysis of these members, which can not be achieved by any other known method.

Initially, a review of the current state of the art in GBT is carried out, together with a review on the most recent bibliography of alternative methods for post-buckling analysis of thin-walled structures, allowing to define the specific goal of the present work – the setting up of a consistent GBT-based methodology for post-buckling analysis. Next, a consistent formulation based on the concept of Total Potential Energy in the framework of the classical GBT theory, for post-buckling analysis, was created, enabling the rigorous study of open non-branched and closed mono-cellular sections. Subsequently, a series of refinements in the GBT theory and in the adopted numerical strategies, namely in the Rayleigh-Ritz method and in the bifurcational calculus techniques, were made in order to analyze the perfect structural member, without making resource to imperfections, made by plane plates rigidly connected along the folding lines with a general cross section. Finally, the developments were illustrated and validated by the resolution of several examples, which were compared to other methods of analysis for the critical behaviour and for the post-buckling equilibrium paths, like the Finite Strip and the Finite Elements Method.

RESUMO

Esta tese descreve um conjunto de modelos analíticos, baseados na GBT ("Generalized Beam Theory"), para a descrição do comportamento crítico e pós-crítico de elementos estruturais prismáticos, formados pela união de placas planas finas, à compressão e/ou à flexão, com secção transversal de geometria qualquer. A GBT tem uma capacidade única de dar um significado teórico à analise, signioficado este que não é possível obter por nenhum outro método alternativo, tal como o Método das Faixas Finitas ou o Método dos Elementos Finitos.

Inicialmente, uma minuciosa revisão bibliográfica do estado-da-arte sobre GBT foi realizado, conjuntamente com uma revisão da bibliografia mais recente sobre os métodos alternativos para a análise pós-encurvadura de estruturas de paredes finas, com as respectivas técnicas numéricas para modelação e resolução do problema, permitindo assim estabelecer o principal objectivo deste trabalho: a criação de uma metodologia consistente, baseada na GBT, para análise pós.encurvadura de secções formadas por paredes finas planas. De seguida, uma formulação baseada no conceito de Energia Potencial Total no contexto da GBT, para análise pós-encurvadura, foi criada, permitindo o estudo rigoroso de secções abertas não ramificadas e de secções fechacas mono-celulares. Posteriormente, um conjunto de refinamentos na teoria da GBT e nas técnicas numéricas adoptadas, nomeadamente no método de Rayleigh-Ritz e nas técnicas de cálculo bifurcacional, foram realizados por forma a analisar o elemento estrutural perfeito, sem o recurso a imperfeições, realizado pelajunção rígida de placas planas, unidas ao longo das linhas longitudinais de dobragem, com secção transversal qualquer. Finalmente, os desenvolvimentos foram ilustrados e validados pela resolução de vários exemplos, que foram comparados com outros métodos de análise para o comportamento crítico e para as trajectórias de equilíbrio pós-encurvadura, como o Método das Faixas Finitas e dos Elementos Finitos.

AGRADECIMENTOS

Ao Prof.-Doutor Luís Simões da Silva, meu orientador, pela total confiança depositada no meu trabalho, pelas condições criadas e pelo apoio prestado.

À Eng. Helena Gervásio, que realizou as análises por elementos finitos do capítulo 6 para a validação da implementação da GBT, por toda a colaboração prestada.

Ao Prof. Richard Schardt, pela ajuda que me deu, na fase inicial do meu trabalho, para a compreensão da GBT.

Ao Prof.-Eng. José Luís Câncio Martins, pelo apoio que me deu na obtenção de algumas referências bibiográficas raras que, de outra forma, não teria conseguido obter.

Ao Prof.-Doutor Carlos Rebelo, por várias sugestões que se revelaram decisivas no êxito deste trabalho.

À Dra. Elisabete Machado, pelas traduções que realizou de bibliografia alemã, imprescindíveis ao realização deste trabalho.

À Dra. Isabel França e restantes Funcionárias da Biblioteca do Departamento de Engenharia Civil da Universidade de Coimbra, pela colaboração na obtenção de referências bibliográficas.

A todos os Colegas do Laboratório de Mecânica Estrutural, muito especialmente à Sandra Jordão, ao Rui Simões e ao Fernando Filipe de Oliveira.

Aos meus Pais, à minha Família e aos meus Amigos.

À Mafalda e à Matilde.

CONTENTS

Notation

1 – Latin letters

^{i}a - generalized coordinate (degree of freedom) i

A - amplitude modal function

$\boldsymbol{A}$ - vector containing the amplitude modal functions for all modes of deformation

b - plate width

$\boldsymbol{B}$ - transverse bending stiffness matrix

$\boldsymbol{C}$ - warping stiffness matrix

$\boldsymbol{D}$ - torsion stiffness matrix

E - Young modulus

f_s - displacement along the cross section perimeter

f - displacement normal to the cross section perimeter

F - force in the cross section plane

F_i - derivation of the total potential matrix with respect to generalized coordinate i

G - shear modulus

$\boldsymbol{H_{FP}}$ - Hessian matrix for the total potential energy evaluated along the fundamental path

^{ij}H - (i, j) term of the Hessian matrix for the total potential energy

L - length of a member

M - bending moment

n_A - number of active coordinates

$n_{BC,k}$ - number of adopted boundary conditions for mode of deformation k

n_C - number of generalized coordinates

n_k - number of adopted coordinate functions for mode of deformation k

n_{MD} - number of modes of deformation

P - axial force or load parameter

q - distributed load

${}^{i}q$ - sliding coordinate i

t - plate thickness

$\boldsymbol{T}$ - transformation matrix

$u(s)$ - longitudinal (warping) displacement

U_i - internal strain energy

v - displacement in Oy direction

V - total potential energy

w - displacement in Oz direction

$\mathcal{W}$ - virtual work

W - total potential energy in the W-formulation

${}^{i}W$ - generalized bimoment for mode of deformation i

2 – Greek letters

α - angle of a main plate to the horizontal axis

$\boldsymbol{\kappa}$ - tensor containing the non-linear stiffness coefficients

ε - normal extension

γ - shear distortion

φ - coordinate function

$\boldsymbol{\Phi}$ - matrix containing the amplitude modal functions

ϑ - rotation in the cross section plane of the plate's chord

κ - non-linear stiffness coefficient

μ - Poisson coefficient

Π - potential of the external loading

σ - normal stress

ξ_x - maximum exponent of variable x in a polynomial

τ - shear stress

3 – Symbols, subscripts and superscripts

$\dot{(\,)}$ - denotes differentiation along the perimeter coordinate s

$(\,)'$ - denotes differentiation along the longitudinal coordinate x

$^{ij}(\,)$ - (i,j) term of a matrix

$^{ijk}(\,)$ - (i,j,k) term of a tensor

$^{i}(\,)$ - denotes mode of deformation i

$(\,)_L$ - indicates non-linear term related to the normal longitudinal membrane stresses

$(\,)_{SH}$ - indicates non-linear term related to shear membrane stresses

$( )_T$ - indicates non-linear term related to the normal longitudinal membrane stresses

$( )_{CR}$ - inditates at Critical State

$( )_{FP}$ - inditates evaluation along the Fundamental Path

1 – INTRODUCTION

1.1 – Generalities

In recent years, the use of very slender thin-walled cross section members has become increasingly common due to their high stiffness/weight ratio. Extensive application of these members is found, in practice, in cold-formed steel members for lightweight structures (Yu 2000) or in box girder bridges (Cheung, Li and Chidiac 1996).

The analysis of thin-walled cross section members has experienced great advances over the past decades, mostly because of the vastly increased capabilities of numerical methods such as the classical finite element (FEM) or finite strip methods (FSM) (Cheung 1976). It currently constitutes an established and widespread field of research because of the inherent complexities that must be taken into account. Thin-walled cross section members are characterized by great susceptibility to instability phenomena (flexural, torsional or flexural-torsional buckling or lateral torsional buckling), related to the deformation of the member axis, combined exclusively with rigid-body displacement of the cross-sections, as well as distortional and local plate buckling, because of the high slenderness that characterizes these members. All these approaches lack a clear rationale and treat all relevant phenomena independently. It is thus difficult to identify the limits of validity and the user is easily lost in a long calculation procedure without much physical meaning. On the other hand, although the FEM is able to deal with all the complexities listed above, it is still time consuming, requires extensive calibration and does not easily allow a clear identification of the various relevant theoretical phenomena that build-up the structural response of the member. It thus requires extensive parametric studies to be able to lead to useful design guidance. Also, the usual FEM or FSM software packages require the introduction of imperfections in order to overcome the occurrence of bifurcation points

for a post-buckling analysis, thus destroying the bifurcational behaviour. This often further masks reality and extends the required work one or two orders of magnitude because of the need to obtain a reasonable envelope of all possible imperfections.

In practical design terms, the codified approach to design thin-walled cross section members consists of: i) the application of the concept of effective width (EN 1993-1-3, 2006); ii) design formulae that account on the distortional effects (Lau and Hancock 1987), and iii) more recently the Direct Strength approach (Shafer, 2003), already adopted by the American and by the Australian design codes.

Generalized Beam Theory (GBT), translated from the German "Verallgemeinerte Technische Biegetheorie" (VTB), is a complete theory devoted to the analysis of thin walled prismatic members, developed since the sixties by Schardt and his co-workers at the Technical University of Darmstadt, in Germany, and has been widely applied to study the behaviour of cold formed members. It can be regarded as a fusion between the classical Vlasov's theory for thin walled members (Vlasov 1961) and the folded plate theory (Born 1954, Girkman 1959), and is an alternative tool to the classical finite element and finite strip methods for prismatic members. It enables the analysis of thin walled prismatic members with the allowance of cross section distortion and local plate behaviour, in a one-dimensional formulation through the linear combination of pre-established orthogonal deformation patterns – the modes of deformation.

It is the aim of the present thesis to develop consistent formulations and tools to analyse the buckling and post-buckling behaviour of thin-walled prismatic members in the elastic range having a generic cross section – open or with closed cells, branched or non-branched – based on the GBT concepts, and to apply them to the characterization of the behaviour of some thin-walled prismatic members submitted to uniform compression and/or major axis bending. This chapter presents a review of the relevant aspects of GBT, FEM and FSM applied to the study of the stability of thin walled members. Given the objectives stated above, it also reviews the various methodologies for the analysis of a

general thin-walled cross section. It is supposed that the reader has a basic knowledge on the classical stability theory (Thompson and Hunt 1973 and 1984) and on the geometrically non-linear behaviour of thin-walled plated structures, so that these concepts will not be reviewed here. Finally, the chapter closes with an outline of this thesis.

1.2 – A review of the development of GBT – Generalized Beam Theory

It was not accidentally that GBT was invented in Germany during the first half of the sixties. Since the thirties, a wide range of works were developed in Germany on folded-plate structural members – members made from flat plates rigidly connected at their edges –, which are widely used in concrete or steel structures. Born (1954) summarizes several earlier theories, among which it is possible to find Gruber's and Hartenbach's flexural theories, dating back to the thirties and the forties, respectively. These theories computed the transverse flexural bending moments by modelling the folded plate member as a continuous beam and using the force method of analysis to determine the statically indeterminate bending moments at the junction of the plates. A subsequent advance in the theory of folded plate structures, also described in his book, is Güning's method, which relates the longitudinal stress resultants and the shear stresses along the cross section and then establishes an equilibrium relation between the transverse shear forces and the transversal loading; subsequently, from the transverse shear forces, the transverse bending moments are computed. From this theory, taking into account the boundary conditions of the edge plates, Girkman developed his theory (Born 1954, Girkman 1959), which already enables good quality results for the analysis of open folded plate structures – an illustration of the accuracy of Girkman's method can be found in section 2.11 of Schardt (1989), where a folded plate concrete structure subjected to transversal loading was analysed using GBT and then compared to the Girkman's method, showing a quite good agreement. In the early sixties, the crucial work on thin walled members due to Vlasov (1961), released in

the late forties in the Soviet Union, was disseminated in the west, and translated in English, French and German. From these historical facts it becomes obvious that only in the early sixties all elements were grouped together, in Germany, to create GBT.

The first known GBT publication dates from 1966 (Schardt 1966), derives from a work of Schardt to become Professor at the Technical University of Darmstadt and presents already all basic aspects of GBT, a theory devoted to the analysis of longitudinally prismatic folded-plate structures. Starting i) from the classical Vlasov assumption of negligible shear distortions along the thin walled member (Vlasov 1961), ii) using the Vlasov strategy of defining the longitudinal and transversal displacements in the plane of the plate as a sum of the product of pre-established functions defined over the member's transversal perimeter s to amplitude functions depending on the longitudinal coordinate x – Vlasov had already used a similar scheme to derive a model for thin walled closed sections, accounting for the shear deformation effects, in Chapter 4 of Vlasov (1961) – and iii) assuming linear warping displacement patterns between the edges of the plates, Schardt derived a relation between the warping displacements and the displacements along the perimeter, relating both the pre-established functions, for both displacements, along the perimeter and along the longitudinal axis. Now the displacements along the cross section plane and normal to the plates are derived from the displacements along the perimeter through a simple geometric compatible rendering process, determining also the rotations of the plates. Since these rotations differ from plate to plate, transversal bending appears so that, making resource to the folded plate theory concepts referred above, a force method problem is established in order to compute the transversal bending moments. Schardt proceeds to the establishment of the general equilibrium equation of GBT and the orthogonalization of the basic modes of deformation through a matrix eigenvalue problem – this mathematical scheme corresponds to the adoption of the principal axes and the cross section's shear centre for the computation of the cross section's geometrical properties in the Vlasov's thin walled member theory (Vlasov 1961). In this paper it is proposed to

compute the transverse membrane stresses by equilibrium – in later works of Schardt and his co-workers different proposals were made for the determination of these stresses. This work introduces already the non-linear stability analysis based on the concept of deviating forces, establishes the analogy to the beam on an elastic foundation for the differential equations system of equilibrium (Hetenyi 1952) and presents two examples of open non-branched sections.

The following works of Schardt explored the stability behaviour of a wider range of cross sections. The analysis of closed (polygonal) cross section and cylindrical members appears in Schardt (1970): due to the absence of membrane shear deformations, the torsional mode did not appear in these types of members (the first known work to consider closed sections with membrane shear distortion is the fundamental book Schardt (1989) and thus the system of equilibrium equations contains less information than necessary to enable a good analysis for general load and support conditions. At this point it is worth referring the work of Sedlacek (1971) who, based on the works of Schardt (1966) and Vlasov (1961), derived a consistent theory for the analysis of box grider bridge spans allowing cross section distortion, accounting consistently for the shear deformations. The resulting set of the modes of deformation contained already the torsional mode and gave sufficient information to the equilibrium system in order to realize an accurate analysis of closed sections. Based on Sedlacek's work, Mandić and Hajdin (1988) improve this theory by adding the effect of the secondary warping shear stress

During the seventies and eighties Schardt and his co-workers continued to apply the GBT procedures to the analysis of a wider range of problems. Among the articles found in German scientific journals it is worth mentioning Schardt and Steingaß (1970) with an application of GBT to the analysis of thin walled closed cylindrical sections, Uhlmann (1970) with an extension to open thin walled members with curved longitudinal axis, and Schardt and Zhang (1989), with a geometrically non-linear analysis of plates in the post-buckling range. Throughout this time, several thesis and monographs were supervised by

Schardt at the Technische Universität Darmstadt. Among these, Saal (1974) presents an incursion into dynamical analysis of thin walled members, Schardt and Schrade (1982) made an extensive study on purlins, including experimental work, Schrade (1984) studied channel and hat section members with small plates connecting discontinuously the member's lips, Schardt, Issmer and Mörschardt (1986) analysed the stability behaviour of plates and open sections, with some comparisons with codes, Zhang (1989) studied U-sections under eccentrically compression loading and Hanf (1989) made an incursion into the analysis of open section in the elastic-plastic range.

Among the research works made at the Technische Universität Darmstadt during the seventies and the eighties, two works deserve special attention here, due to their contribution to the advancement of GBT: the thesis of Miosga (1976) and the thesis of Möller (1982). Apart from the work of Sedlacek referred above, Miosga (1976) is the first publication that considers other basic modes of deformation than the warping modes: a second type of modes of deformation is established by imposing a unit displacement of an intermediate node (henceforth called inner node and simply consisting of a node between two consecutive folding lines or between a folding line and the section's edge) along the cross section's plane and normal to the plate that contains the inner node. These modes of deformation are crucial to characterize properly the plate buckling behaviour that occurs in thin walled prismatic members under compression or bending with shorter lengths. Later, when applied to free edge nodes, they enable the modelling of lips buckling. Miosga also presents a definition of the membrane distortion, later adopted in several works (see for example Heinz and Mark 1990), that is based on the interpretation of a deformed configuration of a plate to which a null distortion was imposed (see Miosga 1976, page 27, fig. 1.6). It is noted at this stage that this definition will not be adopted in the present thesis since it renders an incomplete formula for the membrane shear deformation. Instead, all strains will be directly derived from the classical procedures of the theory of elasticity. Secondly, Miosga (1976) also presents the non-linear terms of the virtual work referring to

the membrane shear deformation. They are computed from membrane shear forces derived by establishing the equilibrium of an elementary plate $dx \times ds$, where x and s are the longitudinal and the cross section perimeter coordinates. It is also noted at this stage that in the present work, in order to avoid inconsistencies concerning the conjugacy between stresses and strains for the derivation of the internal strain energy of the structural member, only the internal stresses derived from elasticity relations of the relevant deformations are considered, thus opting for a Lagrangian description of the system (Arantes e Oliveira 1999). Despite these two aspects, that are rebated here, the work of Miosga must be considered as one of the most crucial steps forward in the GBT research for the analysis of thin walled members, since it enabled the incorporation of the plate bending modes in the analysis, thus allowing a more precise study on the stability of thin-walled members and contains *inclusive* some relevant applications to the buckling analysis of plates, with some incursions in the post-buckling domain for compressed plates.

The other thesis from Darmstadt to be highlighted here is Möller (1982). His work purposes to analyse thin walled prismatic sections with a general cross section. In chapter 2 a consistent definition of the membrane strains is adopted but null transverse membrane deformations are imposed, and the internal strain energy is established through a consistent energy method, considering the Vlasov's formulas for the fundamental displacements of the plates (Vlasov 1961), i.e., not considering, for a mode of deformation, the relation between the amplitude modal function for the cross section displacements and the amplitude function for the longitudinal displacements, which is the first derivative of the later, as hinted above. It is noted that this relation, between the amplitude functions of the displacements along the cross section and the amplitude functions for the warping displacements, is completely general, as it will be observed in chapters 2 and 5 of the thesiss, and constitutes one of the most relevant aspects of GBT. The third chapter of Möller's thesis presents an attempt to analyse of branched sections in the context of GBT, neglecting the membrane shear deformations. Subsequently, some examples of thin-walled

sections are presented, for a bi-cellular closed section and for a simply supported plate with a reinforcement at the half-width point – this later example presents already membrane shear deformations associated with the warping of the intermediate nodes. It ends with a brief study on the vibrations of a multi-cellular beam and on the stability analysis of a squared closed section neglecting the membrane shear deformations for the GBT modelling.

During the eighties and nineties several more works on the stability analysis using GBT came to light. It is highlighted the first GBT article written in English (Schardt 1983), containing a brief presentation of GBT for stability analysis and mentioning already the need to consider a constant shear flow mode for closed sections. During the conference where this paper was presented, GBT was introduced to Davies, from the University of Salford – Prof. J. M. Davies later moved to the University of Manchester – who, by that time, had already realized a vast and very important research work on lightweight steel construction, namely on stressed skin design (Davies and Brian 1982), and later would develop several important researches on GBT, exploring the large potential of this theory to enable a better understanding of the stability behaviour of thin-walled members.

So, since the late eighties and under the supervision of Davies, several research works were made at Salford and Manchester. The first contributions of Davies are associated with Leach, whose PhD thesis (Leach 1989) contents a detailed description of the GBT procedure for open non-branched sections and an application of GBT to the linear analysis and stability analysis of these sections, making resource to the finite difference method to solve the differential equilibrium equations system, exploring to some extent the interaction between the modes of deformation, which correspond to the buckling modes, and benchmarking GBT with other methodologies. Due to Davies and Leach, several works were made, namely on the first order analysis and stability analysis of open sections submitted to compression and/or bending, exploring the modal interaction between the modes of deformation, containing also some benchmark examples comparing the GBT

results with experimental analysis (Davies and Leach 1992, 1994, Davies, Leach and Heinz 1994, Davies 1998). Due to these works, GBT was spread worldwide.

Later, with the collaboration of Jiang, Davies continued applying GBT to study the behaviour of thin-walled members. In Jiang's thesis (Jiang 1994), GBT was applied to the stability analysis of purlins. Subsequently, Davies and Jiang continued to apply GBT to explore the distortional behaviour of open sections (Davies and Jiang 1996a, 1996b and 1998) and the modal interaction of cold-formed members under compression and/or bending (Davies, Jiang and Ungureanu 1998). More recently, Davies and Kesti (2000) applied GBT to the study of flange- and web-stiffened compression members and, in particular, web-perforated sections. Finally, a recent article of Davies, Jiang and Voutay (2000) is referred here for the analysis of thin-walled members with stiffened compression flanges.

Returning to Darmstadt, in 1989 the major reference of GBT came to light: the crucial book of Schardt (1989), in German only, which contains the basic GBT statements for the establishment of the modes of deformation and for linear analysis, and collects also some developments contained in the previous thesis of the TU Darmstadt. This book is, for sure, the most cited reference in this thesis.

More recently, Schardt (1994a) presented a full and consistent linear stability analysis of open sections under uniform compression and/or uniform bending: this paper constitutes one of the most consistent GBT applications of the stability analysis of thin walled members, fully exploring the modal interaction of the modes of deformation, and constitutes the basis of several further works. The derivation of the non-linear terms for stability analysis presented in this paper is made through a similar procedure to the one presented by Vlasov (1961) – in chapter 2.3.6 of the present thesis this aspect will be explored in detail. In the same year, Schardt presented an article where the lateral torsional and distortional behaviour of channel and hat-sections is deeply analysed and where some approximate GBT-based formulae for design are developed. Recently, Schardt supervised

the thesis of Heinz (1994), concerning a study on the stability and dynamic behaviour of plates, of Conchon (2001), on the behaviour of plates in the framework of GBT, and of Haahk (2004), which contains an application of GBT to branched sections, accounting also for plate distortion.

A recent and very active pole of development of GBT is nowadays the group of Prof. Dinar Camotim, at the Instituto Superior Técnico in Lisbon. As far as is known, the vast work of this group can be structured in five research areas: the extension of GBT to thin-walled members made of orthotropic and fibre reinforced materials (Silvestre and Camotim 2002a, 2002b and 2003), the development of GBT based formulae for distortional design (Silvestre and Camotim 2004a and 2004b), the post-buckling analysis of thin-walled members (Camotim and Silvestre 2003), the analysis of aluminium structures (Gonçalves and Camotim 2003) and the plastic analysis of thin walled members (Gonçalves and Camotim 2004).

Outside Darmstadt, Manchester and Lisbon, few other groups have until now discovered the advantages of GBT, maybe because the main references are written in German. Takanashi, Ishihara and Nakamura (2000) presented a study on the stability analysis of thin-walled beams in bending and Baláž (1999) authored a paper on the linear GBT analysis of open and closed sections.

1.3 – Brief overview of the alternative methods for the stability analysis of thin-walled members

1.3.1. Introduction

In the last decade, great advances have been achieved in the knowledge on the behaviour of cold-formed structures and are summarized in three review articles that appeared in recent years. Rondal (2000) deals with the stability problems of cold-formed

members and the behaviour of the structural joints in cold-formed steel construction, and Davies (2000) includes developments in cold-formed steel construction and applications, high lighting the relevant role that GBT has gained for a deeper understanding on the stability behaviour of cold-formed structural members. More recently, Hancock (2003) updates the advances in cold-formed steel research, describes the advances in the North-American specifications and introduces briefly the Direct Strength Method and its developments, for the use in engineering practice.

The contemporary alternatives to GBT, to perform the stability analysis of thin-walled members, are the well known finite element method (FEM) and the finite strip method (FSM), which derives from the FEM. Rasmussen and Hancock (2000) contains a thorough review on the application of these techniques to the stability analysis of thin-walled cold-formed members, so only a brief review on some significant contributions will be mentioned. Finally, some aspects on experimental research, on the development of direct design methods for engineering practice, not based in GBT, and on the behaviour of thin-walled I-section members are also presented.

1.3.2. The FEM

Using the FEM method, there is an immense range of applications of this numerical tool to the stability analysis of thin-walled structures and members, so here only some recent works that explore the generality of the method are cited. The group of the Cornell University, headed by Prof. T. Peköz, make a wide use of the FEM to the analysis of thin-walled members and frames (Sarawit, Kim, Bakker and Peköz 2003). The report made by Sarawit and Peköz (2003) presents an exhaustive description of the advances recently made, covering all major aspects of the industrial steel storage racks, from the behaviour of column bases, beam-to-column connections, structural members, to the FEM analysis of entire pallet rack systems, and comparing with design methods that are or will be adopted

by current design codes. The group of the University of Timisoara, headed by Prof. D. Dubina, produces also a wide FEM based research work on cold-formed structures: two examples of this are the development of an alternative interactive buckling model, the Erosion of the Critical Bifurcation Load (ECBL) approach (Dubina, Davies, Jiang, and Ungureanu 1996) and the research on plastic buckling analysis in cold-formed construction (Dubina, Goina, Georgescu, Ungureanu, Zaharia 1998).

1.3.3. The FSM

The FSM is derived from the FEM and consists on a specialization of the FEM to the analysis of thin walled members (Schafer 1998), the only difference consisting on the longitudinal discretization of the member, as seen in Fig. 1.1: the FEM uses a mesh that discretizes the member transversally and longitudinally, while the FSM needs only transversal discretization, using currently either harmonic or spline functions in the longitudinal direction of the member. It was originally developed by Cheung (Cheung 1976, Cheung and Tham 2000) and was widely used by other authors for understanding and predicting the behaviour of cold-formed steel members and for bridge decks (Cheung, Li and Chidiac 1996) – a concise overview of the FSM can be found in Graves-Smith (1987). The work of Hancock (1978), a study on the elastic buckling of I-section beams, can be considered as a starting point on the use of the FSM as an analysis tool for the stability behaviour of thin-walled members, and several other works using a similar strategy for other types of cross sections and load conditions followed, many of them from the research group of the University of Sydney. Hancock (1981) applied the FSM to the stability analysis of I-section columns, comparing the FSM to the alternative analysis and/or design models of that time, and Kwon and Hancock (1991 and 1993) extended to the elastic post-buckling analysis of thin-walled members under bending and/or compression. Outside Sydney several other research groups also widely explored the FSM

potential for the analysis of thin-walled structures. It is highlighted here the pioneering work of Graves-Smith and Sridharan (Graves-Smith and Sridharan 1980, Sridharan and Graves Smith 1981), where a consistent formulation for the post-buckling analysis of thin-walled columns using the FSM is presented, and where an experimental observation on secondary localized buckling in a thin-walled square section tube made of silicone rubber is also addressed, as illustrated in chapter 3 of the present thesis. Among the vast range of works on FSM analysis, van Erp and Menken (1991) studied the initial post-buckling analysis of T-beams. More recently, Prola (2001) presents a large number of applications of the spline FSM to the post-buckling analysis of cold-formed members, mainly channel and rack section members, and Ovesy, Loughlan and Assaee (2004) address the analysis of the post-buckling behaviour of thin-plates using a special FSM scheme that makes resource directly to the principle of minimum potential energy. Finally, it is referred that a reliable harmonic FSM program – CUFSM – for the determination of the critical load parameter of thin-walled prismatic members under a general longitudinal normal stress loading at the extreme cross sections, developed by Schafer (1998), is available freely in internet, at www.ce.jhu.edu/bschafer.

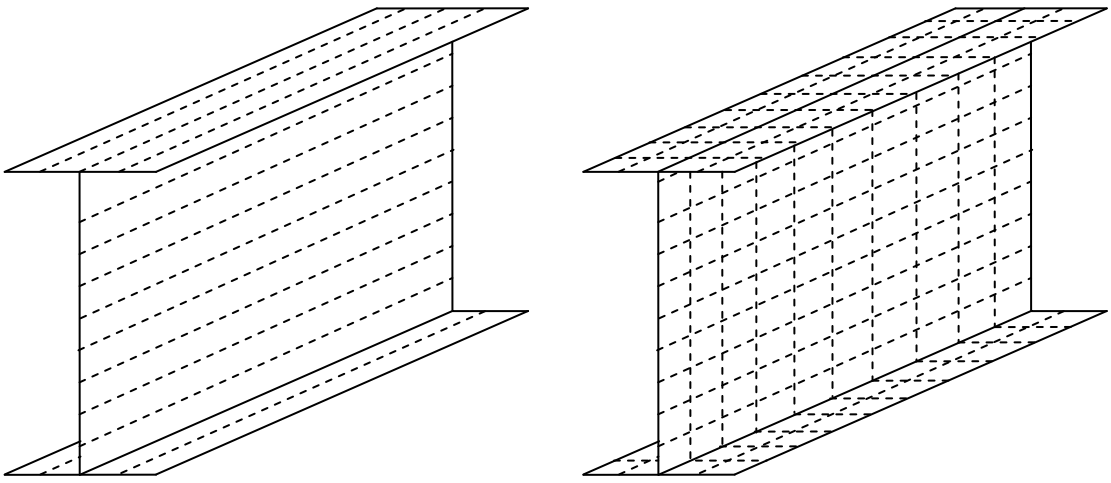

FSM discretization FEM discretization

Fig. 1.1 – FSM discretization versus FEM discretization

1.3.4. Direct design methods and experimental analysis

Several research groups are devoted today to the development of direct design methods accounting for local and distortional buckling, for application in codes and engineering practice, in order to search for alternative methods to the classical effective width approach (Winter 1962), which forms the basis of the design provisions of the Eurocode 3 – Part 1.3 (CEN 2004). Thin-walled cross sections usually adopted in cold-formed construction, like channel or rack sections, may exhibit different buckling behaviour depending on the member's length. For small lengths, local plate buckling, characterized by the fact that the folding lines of the cross section do not move when the section buckles, rules the stability behaviour of the member, while for larger lengths the member acts like an Euler column, cross section distortion being negligible and minor axis bending ruling the global behaviour. These buckling phenomena are well known and simple formulas can be derived to compute a lower bound buckling stress (Bleich 1952). However, mainly for mono-symmetric sections like channels and racks, which are widely employed in cold-formed construction, there is an intermediate length zone where buckling is neither local nor global, and occurs with the movement of at least some folding lines of the member, the cross section exhibiting distortion at buckling. So, for the engineering practice, simple design methods are needed in order to avoid the use of the more complex FEM or FSM. Starting from the formulation of the torsional and flexural buckling of an undistorted section with continuous elastic supports, firstly developed by Vlasov (1961), Lau and Hancock (1987) derived a simple procedure to determine the buckling compressive stress for the distortional mode. Later, Hancock, Kwon and Bernard (1994) derived strength design curves for some common cold-formed cross sections, dealing with distortional buckling together with the remaining critical buckling modes, in a work that became the basis of the Direct Strength Method (DSM) derived by Schafer and Peköz (Schafer 1998, Schafer and Peköz 1998b), which uses strength formulas for the gross cross section and integrates consistently local, distortional and global buckling in a practical and

simple design procedure. This method is already included in the American cold-formed steel design code and constitutes one great step forward for the engineering practice and cold-formed industry – a concise explanation of the DSM is presented in Schafer (2002).

On the other hand, the EuroCode (European Committee for Standardization 2006) allows the design of thin-walled members assisted by testing, which previously had already appeared in some ECCS recommendations (ECCS 1987). Therefore, experimental analysis gains a special relevance in cold-formed steel structures and a recent description on experimental techniques in the testing of thin-walled members can be found in Rasmussen (2000). During the last decade, a wide range of experimental works on cold-formed construction came to light, studying several relevant aspects that need special attention, like for example web crippling (Young and Hancock 2000). Here only a few and recent papers associated with the member's stability analysis will be referred. Young and Rasmussen (1998) performed an experimental research on the behaviour of cold-formed fixed-ended channel sections, which exhibit distinctive buckling behaviour compared to the pin-ended ones, thus providing an example of how the support conditions influence the buckling behaviour of thin-walled members. Comparisons to the Australian/New Zealand, American and European design codes and proposals for their design are also addressed. Schafer and Peköz (1998) carried out an experimental study regarding the characterization of the geometric imperfections and residual stresses of cold-formed members, in order to acquire important data information for numerical post-buckling analysis. Included in a research on cold formed flexural members (Schafer and Peköz 1999), Yu and Schafer (2002) carried out a series of tests on C- and Z-section beams, in order to get reliable information about stiffened elements under stress gradient and to improve the American code provisions for the design of beams. Previously, Hancock, Rogers and Schuster (1996) had performed a benchmark comparison between the distortional buckling design method for flexural members and tests. Exploring the ability of cold-formed steel construction to create any cross section shape, Narayanan and Mahendran (2003) performed a series of

experimental tests on innovative cold formed open section columns, which all failed by distortional buckling and showed very little post-buckling strength – in fact, this aspect will also be observed in the post-buckling analyses of open section columns in the later part of the present thesis. Exploring also the cold formed construction's capacity of generating different cross sections, Yan and Young (2001) developed a series of tests of thin-walled channel columns with returning lips, showing that the American design provisions are conservative for this type of cross section. At last, it is worth referring the experimental work on cold-formed sections realized at the Federal University of Rio de Janeiro by Batista (Batista, Camotim, Prola and Vasquez 1998).

1.4 – A review of the methodologies for the analysis of general thin-walled cross sections

Cold-formed, coupled with the versatility of manufacturing possibilities, allows the "invention" of arbitrary cross-sectional shapes. These sections attempt to maximize performance under certain loading conditions. Given this practical need, it is a stated objective of this thesis to develop a general procedure to deal with arbitrary cross section shapes, open or closed, branched or unbranched, mono-cell or multi-cell, or a combination of all these possibilities. A review of the current methodologies for the analysis of general cross sections are thus presented in this section

The I-section constitutes an excellent example to deal with branching. Because of its widespread use in the steel construction industry, the stability analysis of thin-walled I-sections has been the object of research for a long time. Bulson (1967), based on the traditional plate theory, presented a study on the column buckling of I-sections which, despite its simplicity, shows already the major characteristics of I-section column buckling that will be seen in the GBT analysis, namely the existence of two buckling regions: for smaller lengths local instability of the plates occurs while for larger lengths interaction

occurs between local and overall buckling modes. These aspects will be observed in the GBT analysis of I-sections performed in chapter 6. Later, several applications of the FSM to I-sections appeared. It is highlighted here the pioneering work of Hancock for the stability analysis of beams (Hancock 1978) and of columns (Hancock 1981), and the works of Sridharan (Benito and Sridharan 1985 and 1984-85, Ali and Sridharan 1989), based on FSM analysis, which showed that thin-walled I-section columns have a nearly flat post-buckling behaviour in the distortional range – in fact, in chapter 6, this behaviour will be detected by the GBT analysis. In the context of GBT, the analysis of branched sections is found very briefly in few works, such as the already referred Möller (1982). Mörschardt (1990) adopts a strategy of treating the cross section with branches, in the context of GBT, as a superposition of several non-branched sections. Based on this strategy, Dinis, Camotim and Silvestre (2006) performed several linear buckling analyses of branched cross sections. Recently, Haakh (2004) presents several applications of GBT to I-sections, where some deformation patterns involving plate's distortion are present – it is fair to say that Haakh was very close to the wholly general GBT formulation presented in this thesis.

No GBT applications were found on the analysis of multi-cellular, hollow flange beams or other cross sections having geometrical complexity other than non-branching, open branched or closed mono-cellular sections. Among the obtained literature about cold-formed and thin walled members in general having cross sections with more complex geometry, few authors focused on multi-cellular sections, although it was considered as a desired GBT enhancement (Camotim, Silvestre, Gonçalves and Borges Dinis 2004). In the context of structural engineering applications, these sections were analysed by Vlassov (1961) and Murray (1986), and also in the paper of Waldron (1986) on the derivation of the cross section properties, but all these works neglect cross section distortion[1]. Kollbrunner and Hajdin (1975) extends the classical folded plate theory to the analysis of

multi-cell sections, and uses some strategies for cross section analysis that are similar to those presented in Chapter 5 below, namely the adoption of the displacements method to derive the transverse bending moments along the cross section. More recently, Shanmungam and Balendra (1991) present an experimental study of thin-walled multi-cellular structures curved in plan, analysing perspex models and comparing the results with FEM analyses. Razaqpur and Li (1991) derived a finite element from the Vlasov's theory that accounts on the shear lag effects, appropriate to the analysis of mono-cell and multi-cell box girders, and validated the corresponding results by comparing this analysis against FEM solutions using shell elements. Jönsson (1999) presents an extension of the traditional thin-walled beam theory (Vlasov 1961, Kolbrunner and Hajdin1975, Murray 1986), to include cross section's distortion for open, mono-cell and multi-cell prismatic members, deriving the differential equilibrium conditions by establishing the equilibrium in an elementary cut-out of the member, and applying the formulation to the analysis of a triple cell bridge cross section. During the same year the book of Ignatiev and Sokolov (1999) was released, presenting an innovative method – the substructuring method – for the analysis of thin-walled plate and box-type members, based on the concept of spline interpolation of the displacement fields, together with a condensation method to compute the first n eigenvalues and eigenvectors for a stability or dynamics structural problem – those that have interest in engineering practice. At last, Pavazza and Blagojević (2005) present a study on the distortion of rectangular multi-cell cross sections under bending, assuming that beam walls are hinged along their longitudinal edges, for the accounting of the cross section distortion.

During the early nineties, a new type of cross section was developed in Australia by Palmer Tube Mills Pty Ltd, nowadays known as Smorgon Steel Tube Mills (SSTM): the hollow flange beam section (HFB), also called "Dogbone" (Avery, Mahendran and Nasir

[1] – From now on, the reader must be aware of the two different meanings of the word "distortional": it can either refer to a shear deformation at a point of the structure, or to the deformation of the cross section in its

2000). This cross section is used mainly in beam members due to its double symmetry, high major axis bending stiffness, and also to the high torsional rigidity provided by the two closed cells on the upper and lower parts of the cross section. This innovative cold formed steel section is made from a single metal strip on an electric resistance welding tube (ERW), identical to those used in the manufacturing process of square and rectangular hollow sections (Zhao and Mahendran 1998). Heldt and Mahendran (1992) present one of the first works on the analysis of HFB section members and perform buckling analyses for HFB section beams under several support conditions – it is worth highlighting the research effort on these structural members realized at the Queensland University of Technology, in Brisbane, Australia, by Mahendran and his co-workers, and below some further works of this group are referred. Despite of the high torsional stiffness of the flanges, HFB members webs are comparatively very flexible, so Pi and Trahair (1997) analysed the decrease of the resistance to lateral buckling of the HFB members due to this aspect. In order to solve the problem of low bending stiffness of the webs, Avery and Mahendran introduced web stiffeners and applied the FEM (Avery and Mahendran 1997) to the analysis of HFB members, together with some experimental work (Mahendran and Avery 1997). They showed that the reduction in the lateral buckling resistance could be effectively and economically eliminated by the adoption of a web stiffener at third points of the span. Mahendran and Doan (1999) performed FEM analyses for simply supported HFB members under uniform bending moment, which were validated against experimental tests. The most recent work on HFB section members found in the available literature is Avery, Mahendran and Nasir (2000), where some FEM analyses are performed in several HFB sections, modelling all relevant effects such as material inelasticity, residual stresses, local buckling, member instability, web distortion and geometric imperfections, covering all possible buckling modes for a wide range of cross sections – three buckling modes were detected: the local plate buckling in the compressed flange, plate buckling of the web –

---

own plane by transverse bending or transverse extension.

only for HFB members having slender web – and global distortional buckling.

1.5 – Numerical strategies for the post-buckling analysis of elastic thin-walled structures

In his doctoral dissertation "*On the stability of elastic equilibrium*", Koiter (1945) laid the basis for the analysis of the elastic post-buckling of structures. He developed an asymptotic approach in a continuous framework. Twenty years later, working independently and unaware of the fundamental Koiter's contribution (written in Dutch), the Stability research Group, in the UK, developed a similar theory but based on a discrete formulation. The two classical monographs by Thompson and Hunt (1973 and 1984) encapsulate those developments. In the present thesis it is the later discrete formulation that is followed. It is assumed that the reader is familiar with the theory, so that no review will be presented here (Hunt 1981, Thompson and Hunt 1973 and 1984).

Within the theoretical context described in the previous paragraph, the post-buckling analysis of perfect thin-walled elastic structures requires the implementation of numerical strategies that are able to deal with two aspects: i) the discretization of the problem, addressed in this thesis in the context of the Rayleigh-Ritz Method, and ii) the numerical techniques used to solve the non-linear equilibrium equations that describe the behaviour of the system. This behaviour exhibits, in most cases, a bifurcational nature in a multi-dimensional framework, thus requiring great core to ensure that the right equilibrium solutions are obtained and the equilibrium paths of the system are identified consistently.

Focusing firstly on the discretization techniques of the problem, in the present work, like in many other on the non-linear stability of elastic structural members – see, for example, Wadee, Hunt and Withing (1997) – the member's system of equilibrium differential equations are derived from an energy formulation and are rendered discrete by adopting the traditional Rayleigh-Ritz method, i.e., by approximating each of the unknown

functions by a linear combination of pre-established functions – the coordinate functions. It is known that the efficiency of the method is highly dependent on the correct choice of these coordinate functions – for a deeper review of the method it is recommended the reading of Richards (1977) – and it is required that these functions satisfy, at least, the cinematic/forced boundary conditions of the system, compliance to the static/natural boundary conditions is optional. Often, trigonometric functions are adopted but a few strategies for the definition of appropriate coordinate functions other than trigonometric ones can be found in the literature. Since Chapter 3 presents an alternative and consistent scheme to determine the coordinate functions from the relevant boundary conditions, a brief explanation on alternative procedures is presented here. In a chronological order, Storch and Strang (1988) perform a Rayleigh-Ritz analysis of a simple cantilever beam and adopt coordinate functions that either agree or do not agree with the natural boundary conditions, highlighting the effects of neglecting the natural conditions. They also discuss briefly the role of the norm of the coordinate functions and address the fact that, in this case, the adoption of trigonometric functions does not generate a complete vector space basis for the unknown functions, because a function with constant second order derivatives along the member's length was required. Orthogonal polynomials derived from the Gram-Schmidt process are used by Singh and Chakraverty (1992) for the vibration analysis of elliptic plates, and Singhvi and Kapania (1994) analyse the vibration and buckling behaviour of doubly symmetric thin-walled beams of open section for two sets of boundary conditions: fixed-fixed and pined-pined. These authors adopt several types of coordinate functions, namely orthogonal functions consisting of a combination of algebraic and trigonometric terms, simple polynomials that do not satisfy all essential boundary conditions, and Chebichev polynomials. Geannakakes (1995) uses serendipity functions to compute the natural frequencies of arbitrarily shaped plates, and Brown and Stone (1997) apply polynomial functions for the analysis of plates and conclude that polynomials series do not negatively affect convergence, for a given maximum polynomial degree, but

influence the numerical stability of the problem. Smith, Bradford and Oehlers (1999a) use orthogonal Chebichev polynomials of types 1 and 2, and also Legendre, Hermite and Laguerre polynomials to study the unilateral buckling of plates. In Smith, Bradford and Oelhers (1999b) the same authors use as displacements functions polynomials consisting of a boundary polynomial, specifying the geometric and cinematic boundary conditions, multiplied by a complete two-dimensional simple polynomial. Amabili and Graziera (1999) analyzed the vibration of simple structural models, like beam models and circular plates and shells, and rendered the system discrete by adopting the eigenfunctions of the equation of motion of the model, which are linear combinations of admissible pre-established functions that are, usually, trigonometric, hyperbolic or exponential functions. At last, Chen and Baker (2003), apply Hermite polynomials in the localized buckling analysis of a strut on a softening foundation. All in all, it can be concluded that a wide range of strategies are employed in the discrete rendering of an equilibrium system for stability or dynamical problems, and it is noted the need of a simple, systematic and general scheme for the generation of a complete set of efficient coordinate functions for the application of the Rayleigh-Ritz method to structural engineering problems – the word "efficient" refers to the fact that a desired convergence shall be reached with a minimum number of coordinate functions.

Focusing now on the step that follows the discrete rendering of the equilibrium system – the numerical strategies applied to the detection of equilibrium paths for the stability analysis of compressed structures – it is known from the classical references on the matter that straight perfect elastic structural members under compression or major axis bending exhibit most often bifurcational behaviour, so numerical techniques that follow arbitrary non-linear equilibrium paths, detect the so called stability points – turning or bifurcation points –, and allow the path switching at a bifurcation point are of major relevance in structural analysis. For this purpose, in non-linear stability analysis two numerical scheme types may be applied: the perturbation approach, based on power series

expansion techniques, and continuation methods, that bring the equilibrium curves as a set of equilibrium points – a complete summary on these techniques can be found in Riks (1984). Therefore, it is worth referring here a brief review on some relevant works on this theme but, due to large number of papers on this subject, only few works, published during the last two decades and considered more relevant in the context of the present thesis, will be referred, and the crucial works on this subject owed to Hunt and Thompson, namely Hunt (1981) and Thompson and Hunt (1973 and 1984), that are the basis of the numerical strategies employed in the forthcoming chapters for the search of non-trivial equilibrium paths, being deeply described in Chapter 3, are not reviewed here.

Following once again a chronologic order, one finds the paper of Fujikake (1988), where the positive definiteness of the tangent stiffness matrix is directly inspected at each load increment, in the sense that if it passes from positive definite to non-positive definite in the following step, it is concluded that the structure's equilibrium state became unstable. This procedure was implemented in the FEM package Adina, and was employed to the buckling analysis of a cylindrical shell. Eriksson (1988) sees the solution of a non-linear structural problem as a curve in the displacement space, resulting from a continuous variation of a load parameter and each state along the equilibrium path is described by a tangent vector describing the response to a small increment. The author then applies the procedure to snapping and buckling problems. One year after, the same author (Eriksson 1989) discusses the introduction of constraint conditions in the equilibrium equation systems for structural models showing limit points or bifurcation states, and applied to the analysis of snapping shells, buckling plates and buckling cylindrical shells. Allman (1988) computes stable equilibrium paths of discrete conservative systems by a modified Newton's method that converges only to minima, without adding any constraining condition, thus fully exploring the symmetry or bandedness of the Hessian matrix of the potential energy function. Kouhia and Mikkola (1989) present a procedure for handling simple critical points, by adding an extended Crisfield elliptical constraint equation to the

equilibrium system of the structural model. Ten years after, the same authors (Kouhia and Mikkola 1999) present a set of procedures to handle critical points showing coincident or nearly coincident buckling loads, improving some modifications to previous algorithms in order to increase their numerical robustness. In 1990 the crucial work of Allgower and Georg (1990) on numerical continuation methods comes to light, presenting a complete description of the numerical techniques developed until that date for the solution of non-linear systems, comprising the problem of bifurcations and path switching. During the same year Wriggers and Simo (1990) present a numerical formulation to compute directly the turning or bifurcation points in the context of the Finite Element Method, appending a constraint equation to characterize the presence of either a turning or a bifurcation point, and introducing a penalty regularization of the extended system in order to improve the efficiency of Newton method used to solve the equilibrium system in the neighbourhood of bifurcation points – in Wriggers (1995) further details on this subject can be found, together with a more complete explanation of the numerical strategies involved in non-linear stability analysis of structures. Huang and Atluri (1995) present a simple but very efficient approach to the stability analysis of elastic structures, monitoring the sign changes of the diagonal elements of the triangularized tangent stiffness matrix, verifying the equilibrium path's slope at critical points to distinguish between limit and bifurcational points, and applying an approximate asymptotic solution to switch to the post-buckling path. Eriksson and Pacoste (1999) explore the use of symbolic software in the large-displacement analysis of structures, using co-rotational and strain energy based formulations, discussing how the precision of the derivation of the finite elements and the efficiency of the code formulations are satisfied in the context of the symbolic programming. At last, it is worth referring two recent works of Potier-Ferry and his co-workers (Vannucci, Cochelin, Damil and Potier-Ferry 1998, Boutyour, Zahrouni, Potier-Ferry and Boudi 2004): the first work presents a strategy to compute bifurcation branches in elastic systems by adopting a perturbation technique called asymptotic-numerical

method (ANM) that associates perturbation techniques and the FEM, while the second paper combines the ANM with Padé approximants, used to detect the bifurcation points, and illustrates the adopted numerical strategies by presenting several examples on the post-buckling behaviour of different structures modelled using thin elastic shell elements.

1.6 – Outline of the thesis

Having reviewed the developments of the underlying theory, a brief summary of the content of this thesis is described in the following.

Chapter 2 starts with the detailed description of the classical Schardt's GBT formulation, fully explaining the establishment of the basic modes of deformation (the warping, the plate bending and the closed cell distortional modes), the orthogonalization procedure and the derivation of the GBT member's equilibrium condition. An explanation of the Schardt scheme for stability analysis (1994), which follows the strategy derived by Vlasov (1961) for thin-walled members with no cross section distortion, is presented. In order to apply the traditional stability procedures (Thompson and Hunt 1973) to the buckling and post-buckling analysis of thin-walled cross sections under compression and bending, a consistent formulation based on the concept of total potential energy and on the Lagrange description for geometrically non-linear analysis, accounting only on the membrane longitudinal and shear deformations since it is based on the Schardt's assumptions for the establishment of the modes of deformation, is developed. The limitations of the Schardt's formulation for stability analysis (Schardt 1994) are revealed, since it generates much fewer non-linear terms than the energy formulation. Then, an introductory application to the stability analysis of open or closed cross section columns is performed, exploring into some extent the interaction of the orthogonal modes of deformation and drawing some conclusions from the observation of the Hessian matrix, namely the fact that the stability analysis shall be made by withdrawing the line and

column related to the axial extension mode. This study considers the commonly used one half-wave sinusoidal trial functions for the modal amplitudes, in the context of the Rayleigh-Ritz method.

Chapter 3 presents the numerical strategies to derive the buckling and post-buckling behaviour of thin-walled members, in the context of the Rayleigh-Ritz method. The first part, related to the discretization of the TPE of the member, presents a natural and sequential procedure to derive the coordinate functions for each modal amplitude function, by emanating them from the relevant modal boundary conditions. Adopting, for each mode of deformation, polynomials as coordinate functions, the first coordinate function is derived from an algebraic system composed by the boundary conditions, which alone would render a homogeneous system with little numerical interest, and by a normalization rule. This later condition provides the non-homogeneous condition that enables a non-trivial solution. The following coordinate function for the same mode of deformation is then generated from the same equations system used to calculate the first coordinate function, to which an ortogonalization condition, between the coordinate function being calculated and the previous polynomial, already defined, is added. For the third coordinate function the system that generates it is composed, naturally, by the same system and by two additional rules, each one imposing the orthogonality between the third coordinate function and each of the two previously calculated polynomials. The scheme now proceeds calculating as many coordinate functions as whished, and a reference is made about the advantages of adopting the polynomial coordinate functions when compared to the usual adoption of sinusoidal functions. In order to accelerate the calculus involved and to save computer resources, a matrix scheme to compute directly the discrete TPE function, adopting the polynomials previously derived as trial functions, is developed.

The second part of chapter 3 consists on an explanation of the numerical techniques to perform buckling and post-buckling analysis of perfect members, thus enabling a full characterization of the member's behaviour without the need of making resource to

member's imperfections that would destroy the bifurcational behaviour of the structural member's equilibrium system. The proposed set of numerical techniques uses fewer assumptions and can be viewed as a simplification, as a numerical interpretation or as an updating of the traditional stability techniques (Thompson and Hunt 1973 and 1984, Hunt 1981) to the use of the today's computer capacities and to the advanced symbolic programming software MATHEMATICA (Wolfram 2003), dispensing the elimination of the passive coordinates, the use of perturbation methods and the introduction of imperfections to the structural member. From this point forward, these techniques will be used for the discrete rendering and stability analysis of the thin-walled prismatic members.

Chapter 4 applies the numerical techniques described in Chapter 3 to some preliminary examples, using the energy formulation for the traditional GBT theory, previously presented in Chapter 2.

Chapter 5 extends the energy formulation to its general form and derives additional modes of deformation in order to compute all terms of the internal strain energy. Three additional types of modes of deformation are established, each one associated with the withdrawal of three fundamental Schardt's assumptions: the linear warping between main nodes, the null membrane shear deformations for open sections or, for closed sections, the constant membrane shear flow around the closed cell, and the transversal inextensibility of the plates. By doing this, it is intended to enlarge the range of application of GBT, enabling this theory to model a wider range of phenomena, and also to unify the analysis of open and closed cross sections. Instead of the force method to compute the transversal modal bending moments, the present scheme adopts the displacements method, which is strictly needed for the establishment of the transversal extension modes of deformation. The orthogonalization procedure needs little adaptation to embrace the additional modes of deformation and highlights the fact that the enlarged GBT scheme contains the traditional GBT formulation. It is important to point out that the present methodology unifies the analysis of open and closed sections, thus formulation a wholly general GBT theory, and

allows the full description of the stress state at any point of the member, which was not possible in the classical formulation – for example, some attempts to determine the transversal membrane stresses and the shear stresses in open sections for the classical GBT theory can be found in Miosga (1976) and Schardt (1983). The concepts just presented are then validated by solving two illustrative examples – the post-buckling analyses of a rectangular hollow section column and a channel column – and by comparing the correspondent results against alternative independent solutions obtained from FEM analyses.

Chapter 6 contains the generalization of the extended GBT formulation, previously presented in Chapter 5, to the analysis of a general cross section and is illustrated here, without loss of generality, by the GBT analysis of the I-section, the rectangular two cells section and of the reinforced flange beam cross section – the presentation of these examples, by this order, pretends to illustrate the way the procedure was derived. The main difference between the formulation presented here and the previous attempts for the GBT analysis of general cross sections (Möller 1982, Mörschardt 1990 and Haakh 2004) is that in the present thesis the extended GBT scheme presented in Chapter 5 is used with little adaptation for the analysis of wholly general cross sections made by flat folded plates, thus keeping the generality of the extended GBT theory: it is required only the combining of the membrane shear deformations patterns associated with the main plates with the traditional warping modes to implement the basic warping and plate shear modes of deformation at once, generating more modes of deformation than the other GBT formulations that were applicable to open branched sections only. The present procedure is applicable to any cross section, not only to open branched ones, and explores completely the ability of the displacements method to render compatible the relative displacements at the folding lines of the cross section, needed to restore the cross section's continuity, in the sense that, for all mode types except the one related to the transverse extension of the plates, the scheme requires only the computing of the translations of the main nodes of the cross section

(nodes related to edge or folding lines), which are the input data to the displacements method problem, which, by itself and from these translations, computes the rotations at the folding lines, needing no further adaptation in order to accommodate branching nodes. Moreover, the formulation of the modes related to plate bending, inner nodes warping and transverse extension of the plates needs no adaptation for the analysis of general cross sections. Once again, several illustrative examples are presented, namely an I-section member under compression or constant major axis bending moment, a two-cells rectangular cross section column and two hollow-flange beam section members under uniform major axis bending moment, being the critical behaviour of each example validated against Finite Strip Method analyses (Schafer 2004). All in all, this formulation derives directly from the extended GBT theory presented in Chapter 5, so it makes no distinction between open or closed sections and is appropriate to analyse general cross sections, showing branching and (but not necessarily) closed cells.

Chapter 7 draws the thesis to a conclusion by summarizing the implications of the findings and remarking on possible extensions to the research presented.

2 – POST-BUCKLING FORMULATION FOR THE CLASSICAL GBT THEORY

2.1 – Introduction

In this chapter the basic statements of GBT are addressed. The first part consists of a detailed description of the GBT scheme, based on Schardt's procedures for the cross section analysis (Schardt 1989), comprehending the general assumptions of the method, the establishment of the basic modes of deformation, namely the warping, the plate bending and the closed cell distortional modes of deformation. Then, the analysis proceeds to the establishment of the linear homogeneous equilibrium conditions for the structural member and, based on this equilibrium system, to the orthogonalization procedure. This orthogonalization procedure linearly combines the basic modes of deformation and forms a new set of modes of deformation, equivalent to the basic modes in terms of enabling the same results – stresses and displacements – for the analysis of the structural member submitted to any general loading. The new set of modes of deformation, which will be used in the global analysis of the member since it introduces several simplifications into the member's equilibrium system, contains two main groups of modes of deformation: the distortional modes and the rigid-body modes. The distortional modes imply that the cross section distorts when the member is loaded, thus the classical Vlasov's theory (Vlasov 1961) is no longer applicable, while the rigid-body modes imply no cross section distortion and are equivalent to the Vlasov's axial elongation, major and minor axis bendings and shear centre torsion – hence, GBT includes the classical theory for thin-walled prismatic members, enlarging it to the analysis of cross section distortion.

Subsequently, in order to apply GBT to the stability analysis of thin-walled steel members, the procedure developed by Schardt (1994), based on Vlasov's geometrically

non-linear theory, is presented. This theory provides precise results for the stability analysis of thin-walled open section members and was widely used by several authors for the stability analysis of open sections only, under axial compression or uniform major axis bending (Schardt 1994, Davies 1998), but does not generate sufficient information for post-buckling analysis, namely because it does not contain third order terms in the equilibrium system. Therefore, a new methodology for post-buckling analysis is needed.

In order to apply the traditional stability procedures (Thompson and Hunt 1973) to the post-buckling analysis of prismatic thin-walled open or closed cross section members under a general loading, a consistent energy formulation, based on the Lagrange formulation for geometrically non-linear analysis and accounting only for the membrane longitudinal and shear deformations, since it is based on the Schardt's GBT formulation, is then developed. In contrast to Miosga's formulation for buckling and post-buckling analysis (Miosga 1976), the present energy formulation does not consider the effects of any stress calculated by partial equilibrium, so that the conjugacy between stresses and strains is kept, and is based on the Total Potential Energy concept. Finally, an introductory application to the stability analysis of an open and a closed cross section columns is presented, showing the relevant mathematical aspects for stability analysis of open and closed cross section members like, for example, the establishment of the generalized non-linear eigenvalue problem. This application considers the commonly used one half-wave sinusoidal trial functions for the modal amplitudes with the exception of the first mode of deformation, the axial elongation, which needs a special treatment in the GBT scheme, as stated in Schardt (1989).

2.2 - Basic concepts of GBT: a brief overview

2.2.1 The GBT scheme

As already stated in the introductory chapter, the whole GBT concept is based on

the characterization of the response of a prismatic thin-walled member as a linear combination of pre-established cross sectional deformation patterns, called modes of deformation. A typical thin walled cross section is represented in Fig. 2.1-a). To clarify the establishment of a warping mode of deformation, with reference to the generic cross-section of Fig. 2.1-a) and an infinitesimal slice of length *dx*, an overview of the general procedure for the warping modes – the first type of mode to be derived (Schardt, 1965) – is briefly presented as follows:

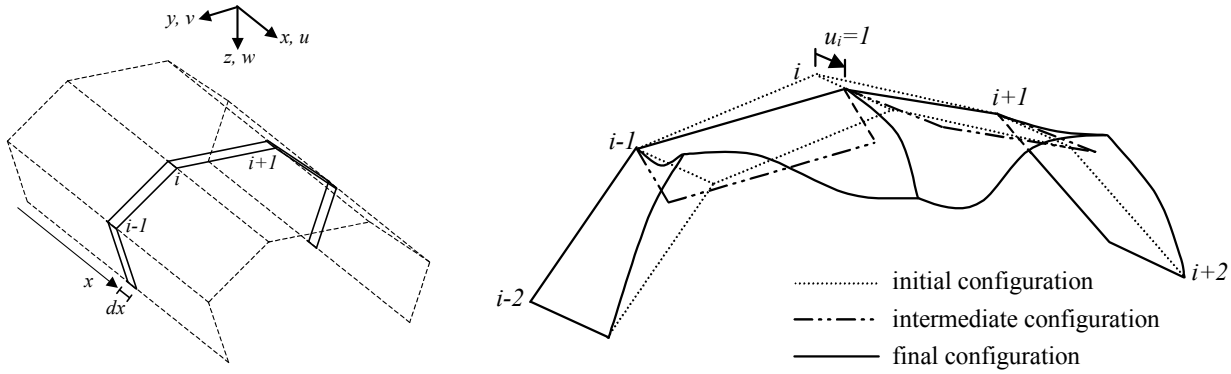

a) infinitesimal slice of a typical thin walled section

b) typical configuration for a warping mode of deformation

Fig. 2.1 – Generic thin-walled cross-section member

i) impose, to each main node in succession, a comprehensive set of linearly independent unitary warping displacement patterns along the cross-section nodal lines, see Fig. 2.1-b), assuming that the distortion of each plate is zero.

This displacement will generate some discontinuities at section *x*+*dx*, along the folding lines, as it can be seen for the intermediate configuration of Fig. 2.1-b). These

discontinuity displacements must become compatible, so:

ii) using only transversal bending displacements, render compatible the discontinuity displacements at the folding lines between any two consecutive plates, assuming that the connections between the folding plates are hinged – in this step only the nodal translations are computed;

iii) assuming the transversal displacements of the nodes computed in (ii) as prescribed displacements along the cross section, determine the rotations of the nodes that render compatible the rotation discontinuities between the plates, making resource to a force method formulation.

Only in step iii) a constitutive relation is used and only at this step all relevant modal displacements and transverse bending moments become fully determined. Next, the analysis proceeds as follows:

iv) determine the generalized geometrical cross section properties needed for the orthogonalization procedure of the modes of deformation;

v) compute the resulting cross-sectional stresses and deformations for each orthogonalized mode of deformation, and calculate all generalized geometrical properties;

vi) superimpose the relevant results for all modes of deformation, each mode k multiplied by an unknown amplitude function ${}^{k}A$ that only depends on the longitudinal coordinate x;

vii) use the global equilibrium conditions and the appropriate numerical techniques to calculate the unknown amplitude functions.

This procedure constitutes the basis of any GBT analysis and is applied also for the

establishment of other types of modes of deformation – for full details see Schardt (1989). Naturally, the establishment of the unit longitudinal displacement pattern is performed by introducing longitudinal cuts between the plates, along each folding line, in order to allow the longitudinal deformations. This leads to some non-admissible displacements that destroy the member's continuity along the cross-section perimeter at $x + dx$, thus requiring the application of a set of forces and moments along the cross section to reinstate compatibility. In the classic formulation, GBT calculates these forces and moments from the discontinuity displacements and appropriate constitutive relations by using the force method (Schardt, 1989). The scheme presented above was derived for the warping modes of deformation, but the establishment of the remaining types of modes follows a similar procedure.

It is worth noting that steps iv) to vi) are meant to simplify the problem, ease the quest for solutions and relate back to the classical rigid body modes of beam theory (axial elongation, bending and torsion): the chosen modes of deformation are transformed into a new and equivalent set of modes of deformation using a reversible linear transformation (Noble and Daniel, 1998) that render orthogonal some matrices of the linear system of equilibrium equations.

2.2.2. General assumptions

A typical thin walled cross section is represented in Fig. 2.2 and is composed of n_{PP} main walls of longitudinally constant thickness $t_{p,r}$ and width $b_{p,r}$., rigidly connected at their end nodes. At the present stage it will be considered that branching along the cross section does not occur – branched sections will be analysed in Chapter 6. A main node (from the German "Hauptknot") is defined as any point of the cross section that: i) connects two plates with different inclination angle, or ii) connects three or more plates (for branched sections only – see Chapter 6), or iii) corresponds to a point at a free edge of a plate. A main plate is thus any plate between two consecutive main nodes. In addition to

the main nodes there is another type of nodes, the inner nodes (in German called "Nebenknoten"), which are points freely defined by the user inside the plate's width and that will be associated with specific modes of deformation. It is further assumed that two consecutive main walls in non-branched sections make a nonzero continuity angle $\Delta\alpha_i$, so that the number of principal nodes is $n_{NP} = n_{PP} + 1$ for an open section, and $n_{NP} = n_{PP}$ for a closed cell. Following Schardt (1989), and with reference to Fig. 2.2, two coordinate systems are defined: (i) a local coordinate system $r_i\ s_i\ x$ for each wall *i* and (ii) a global coordinate system, *x y z* with its origin on node 1. The displacements associated with the global and the local axes are defined in Table 2.1 and Fig. 2.3.

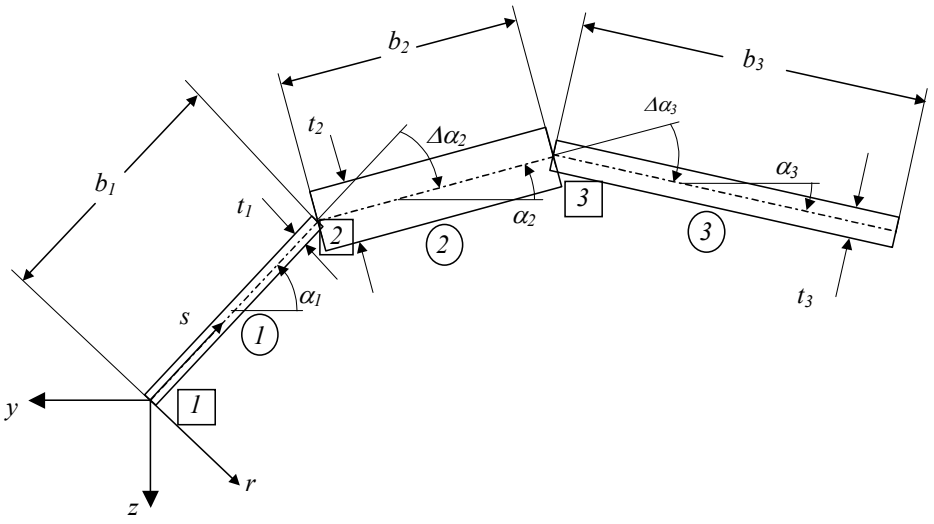

Fig. 2.2 – The cross section dimensions and the coordinate systems

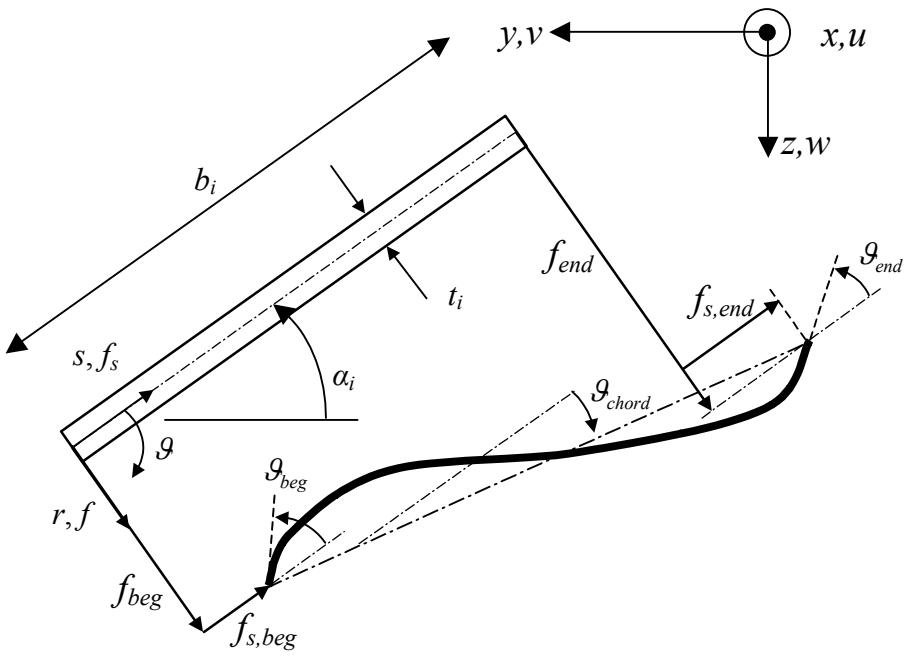

Fig. 2.3 – The relevant displacements for a generic plate

Table 2.1 – Definition of the relevant unitary displacements and transversal bending moments for mode of deformation k

	Axes	General notation	for node *i*	for wall *i* initial node	for wall *i* end node	chord
Displacements in global axes	*x*	*u*	u_i	$u_{i,beg}$	$u_{i,end}$	
	y	*v*	v_i			
	z	*w*	w_i			
Displacements in local axes	*s*	f_s		$f_{s,i,beg}$	$f_{s,i,end}$	
	r	*f*		$f_{i,beg}$	$f_{i,end}$	
	transversal rotation	ϑ		$\vartheta_{i,beg}$	$\vartheta_{i,end}$	$\vartheta_{i,chord}$
Transverse bending moment		m_s		$m_{s,i,beg}$	$m_{s,i,end}$	

In the GBT analysis, based on the concept of modes of deformation, it is supposed that the relevant displacements are given by (see Fig. 2.3):

$$u(x,s)=\sum_{k=1}^{n_{MD}} {}^{k}u(s)\times {}^{k}A'(x)$$

$$f_s(x,s)=\sum_{k=1}^{n_{MD}} {}^{k}f_s(s)\times {}^{k}A(x)$$

$$f(x,s)=\sum_{k=1}^{n_{MD}} {}^{k}f(s)\times {}^{k}A(x) \qquad (2.1, \text{a-e})$$

$$\vartheta(x,s)=\sum_{k=1}^{n_{MD}} {}^{k}\vartheta(s)\times {}^{k}A(x)$$

$$m_s(x,s)=\sum_{k=1}^{n_{MD}} {}^{k}m_s(s)\times {}^{k}A(x)$$

where ${}^{k}u(s)$, ${}^{k}f_s(s)$, ${}^{k}f(s)$, ${}^{k}\vartheta(s)$ and ${}^{k}m_s(s)$ denote, respectively, the warping displacement, the displacement along the perimeter of the plate, the displacement normal to the plate, the rotation and the transverse bending moment functions – defined along the whole cross section perimeter – for the mode of deformation k, and ${}^{k}A(x)={}^{k}A$ is the corresponding modal amplitude function, n_{MD} being the total number of modes of deformation. This definition of the displacements constitutes one of the crucial characteristics of GBT and implies no loss of generality for the definition of the displacements and stresses as long as a proper set of functions for the unitary displacements along the cross section and for the amplitudes of the modes are provided. In paragraph 2.2.3.1 it will be demonstrated that the amplitude function for the warping displacements is the first derivative of the modal amplitude function for any type of mode.

The following general assumptions are considered:

i) the cross section is considered constant along the member's longitudinal axis Ox;

ii) the material follows Hooke's law for isotropic materials;

iii) since the plates are thin, i.e., their thickness is small when compared to the

other dimensions of the plate, the Kirchoff's thin plates assumption is considered, and thus the strains in the xOs plane may be split into bending and membrane parts (Fung, 1965):

$$\varepsilon_x = \varepsilon_x^M + \varepsilon_x^B$$

$$\varepsilon_s = \varepsilon_s^M + \varepsilon_s^B \qquad \text{(2.2, a-c)}$$

$$\gamma = \gamma^M + \gamma^B .$$

iv) the von Kármán hypotheses for thin plates are adopted, with a small adjustment: the assumption of negligible shear displacements shall not be considered, due to the fact that, in cold formed prismatic elements, the plate's transversal width b may be much smaller than the longitudinal length L and so the non-linear terms related to the displacements along the plate's plane may not be negligible. It will be considered instead that, in any strain-displacement relation, the higher powers of the derivatives of u and f_s are neglected only if lower powers of the same terms are already present in that expression; so, in comparison to the usual von Kármán strain tensor for thin plates, some more terms of the complete Green's strain tensor must be added – this strategy was already used by Benito and Sridharan (1984-85) and will be relevant for the non-linear energy formulation.

The present GBT formulation assumes also the following assumptions (Schardt 1989) (later relaxed in Chapter 5), namely:

v) negligible membrane transverse strain:

$$\frac{\partial f_s}{\partial s} \approx 0 ; \qquad \text{(2.3)}$$

vi-a) negligible membrane shear distortion for open cross sections:

$$\gamma_{xs} = \frac{\partial u}{\partial s} + \frac{\partial f_s}{\partial x} \approx 0\,; \tag{2.4}$$

vi-b) constant shear flow around a closed cell, for closed sections:

$$\tau_{xs} \times t = G t \left(\frac{\partial u}{\partial s} + \frac{\partial f_s}{\partial x} \right) = cons\,tan\,t \tag{2.5}$$

vii) linear warping displacements between main nodes, i.e., the function ${}^{k}u(s)$ is linear between any two main nodes, for any mode k.

From the above hypothesis the strain-displacement relations are obtained, which are shown here for linear analysis: the parts related to bending effects are:

$$\varepsilon_x^B = -\bar{s}\frac{\partial^2 f}{\partial x^2} = \sum_{k=1}^{n_{MD}} -r\ {}^{k}f\ {}^{k}A''$$

$$\varepsilon_s^B = -\bar{s}\frac{\partial^2 f}{\partial s^2} = \sum_{k=1}^{n_{MD}} -r\ {}^{k}\ddot{f}\ {}^{k}A \tag{2.6, a-c}$$

$$\gamma_{sx}^B = -2\bar{s}\frac{\partial^2 f}{\partial s\,\partial x} = \sum_{k=1}^{n_{MD}} -2r\ {}^{k}\dot{f}\ {}^{k}A'\,,$$

while for the membrane effects, for open or closed sections:

$$\varepsilon_x^M = \frac{\partial u}{\partial x} = \sum_{k=1}^{n_{MD}} {}^{k}u\ {}^{k}A''\,, \tag{2.7}$$

and for closed sections only also:

$$\gamma_{sx}^M = \frac{\partial u}{\partial s} + \frac{\partial f_s}{\partial x} = \sum_{k=1}^{n_{MD}} \left({}^{k}\dot{u} + {}^{k}f_s \right) {}^{k}A'\,. \tag{2.8}$$

From the above expressions the elasticity relations can be derived. For the bending effects:

$$\sigma_x^B = \frac{E}{1-\mu^2}\left(\varepsilon_x^B + \mu\,\varepsilon_x^B\right) = \frac{E}{1-\mu^2}\sum_{i=1}^{n_{MD}} -\bar{s}\left({}^{i}f\ {}^{i}A'' + \mu\ {}^{i}\ddot{f}\ {}^{i}A\right)$$

$$\sigma_s^B = \frac{E}{1-\mu^2}\left(\varepsilon_s^B + \mu\,\varepsilon_x^B\right) = \frac{E}{1-\mu^2}\sum_{i=1}^{n_{MD}} -\bar{s}\left({}^{i}\ddot{f}\ {}^{i}A + \mu\ {}^{i}f\ {}^{i}A''\right) \tag{2.9, a-c}$$

$$\tau_{sx}^{B} = G\gamma_{sx}^{B} = -2G\sum_{i=1}^{n_{MD}} \bar{s}\ {}^{i}\dot{f}\ {}^{i}A' ,$$

and for membrane effects (equation (2.10 b) holds only for closed cross section members):

$$\sigma_{x}^{M} = E\varepsilon_{x}^{M} = E\sum_{i=1}^{n_{MD}} {}^{i}u\ {}^{i}A'' \qquad (2.10, \text{a-b})$$

$$\tau_{1}^{M} = G\gamma_{sx}^{M} = G\sum_{i=1}^{n_{MD}} \left({}^{i}\dot{u} + {}^{i}f_{s}\right) {}^{i}A' \ .$$

2.2.3. The establishment of the basic modes of deformation

2.2.3.1. The warping mode

In this section, the implementation of the basic modes of deformation associated with the longitudinal warping displacements is presented, following closely the statements of Schardt (1989). The warping modes were the first modes to be established (Schardt 1966) and constitute the basis of all GBT theory. Fig. 2.4 presents a transversal slice of length *dx*, at an arbitrary position *x*, that belongs to a typical thin-walled prismatic member. There, it is represented the imposition of a unitary longitudinal displacement at node *i*, placed at the folding line that connects plates *p* and *p+1*, for the establishment of mode of deformation *k*, and it becomes evident that some discontinuities occurs along the cross section at *x+dx*. Since it is supposed that along any plate the linear membrane distortion is null for any basic warping mode, the displacements of the plates *p* and *p+1* in their own plane can be completely defined. Denoting the relevant displacements for mode *k* by:

$${}^{k}f_{s}(x,s) = {}^{k}f_{s}(s) \times {}^{k}A(x) \qquad (2.11, \text{a-b})$$

$${}^{k}u(x,s) = {}^{k}u(s) \times {}^{k}U(x),$$

and noting that ${}^{k}A(x)$ and ${}^{k}U(x)$ – the amplitude functions for mode *k* associated with cross section displacements and longitudinal displacements, respectively – remain until now unrelated, the above definition of the displacements is similar to the one used by

Vlasov for the theory of closed cells (Vlasov 1961). The condition of zero membrane distortion, derived also from the assumption of Vlasov for open sections (Vlasov 1961), leads to:

$$\gamma_{xs} = \frac{\partial f_s}{\partial x} + \frac{\partial u}{\partial s} = 0 \Rightarrow \frac{\partial f_s}{\partial x} = -\frac{\partial u}{\partial s}, \tag{2.12}$$

this relation being illustrated in Fig. 2.5. Applying this relation to the plates p and $p+1$ yields:

i) for plate p: $${}^k\dot{u}\Big|_p = \frac{\partial\, {}^k u}{\partial s}\Big|_p = \frac{{}^k u_{end,p} - {}^k u_{beg,p}}{b_p} \times {}^k U(x) = \frac{1}{b_p} \times {}^k U(x) \tag{2.13}$$

ii) for plate $p+1$: $${}^k\dot{u}\Big|_{p+1} = \frac{\partial\, {}^k u}{\partial s}\Big|_{p+1} = \frac{{}^k u_{end,p+1} - {}^k u_{beg,p+1}}{b_{p+1}} \times {}^k U(x) = -\frac{1}{b_{p+1}} \times {}^k U(x). \tag{2.14}$$

Substituting these expressions in (2.12) and comparing the resulting expression with (2.11, a-b), and considering the assumption of null transversal extensibility – for any plate and for any warping mode k it implies that ${}^k f_s(s,x)$ is constant along the perimeter direction – the perimeter displacements ${}^k f_s$ can be computed as follows:

i) for plate p: $${}^k f_{s,\,p}(s,x) = {}^k f_{s,beg,\,p}\ {}^k A(x) = {}^k f_{s,end,\,p}\ {}^k A(x) = -\frac{1}{b_p}\ {}^k A(x); \tag{2.15}$$

ii) for plate $p+1$: $${}^k f_{s,\,p+1}(s,x) = {}^k f_{s,beg,\,p+1}\ {}^k A(x) = {}^k f_{s,end,\,p+1}\ {}^k A(x) = \frac{1}{b_{p+1}}\ {}^k A(x); \tag{2.16}$$

and rendering equal the coefficients of x in both members of expression (2.12) yields:

$${}^k A'(x) = {}^k U(x), \tag{2.17}$$

hence justifying expression (2-a). Note that i) this simple relation holds for any type of mode of deformation for open or closed cross sections as it will be seen below, ii) is one of the most relevant contributions of Schardt (1966) and iii) constitutes a great advance in

relation to the classical thin-walled beam theory of Vlasov (1961).

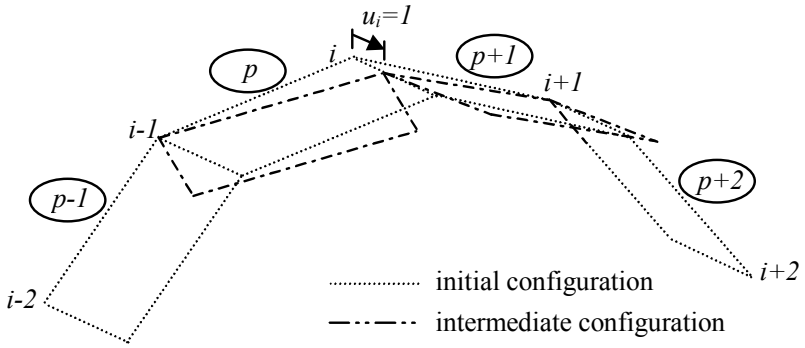

Fig. 2.4 – Imposing a unitary warping displacement at node *i*

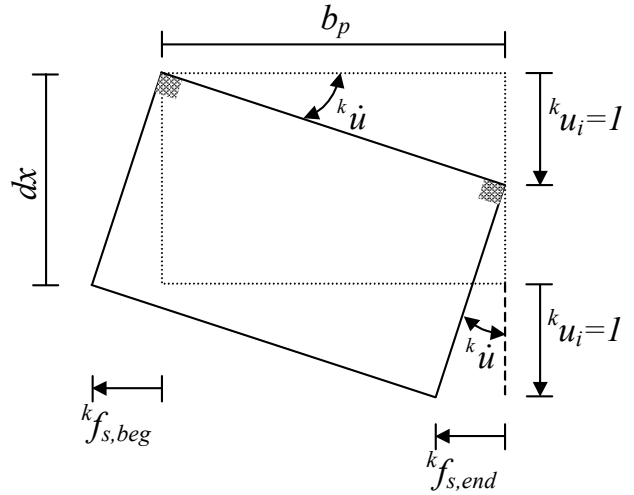

Fig. 2.5 – The in-plane displacements for plate *p*, considering a null membrane distortion

At the present stage only the displacements at $x+dx$ along the cross section plane need to be rendered compatible, given the configuration of the plates shown in Fig. 2.6 – in this figure the deformed shapes of plates *p* and *p+1* are represented by bold lines. The translation displacements at the edge nodes of the plates are rendered compatible through the process illustrated in Fig. 2.7, allowing relative rotations between consecutive plates to occur. The resulting displacements at the edges of the main plates, for plates near node *i*, in

the present case for plates *p-1* to *p+2*, are given by the general following formulas for any plate *q* that result from the geometrical compatible rendering procedure (Schardt 1989), assuming that the plates numbering is as show in Fig. 2.4:

$$ {}^{k}f_{beg,q} = \frac{{}^{k}f_{s,q}}{\tan \Delta\alpha_q} - \frac{{}^{k}f_{s,q-1}}{\sin \Delta\alpha_q} \qquad (2.18, \text{a-b}) $$

$$ {}^{k}f_{end,q} = \frac{{}^{k}f_{s,q+1}}{\sin \Delta\alpha_{q+1}} - \frac{{}^{k}f_{s,q}}{\tan \Delta\alpha_{q+1}}, $$

where

$$ \Delta\alpha_q = \alpha_q - \alpha_{q-1}, \qquad (2.19) $$

for

$$ {}^{k}f_{s,p} = -\frac{1}{b_p} \qquad (2.20, \text{a-b}) $$

$$ {}^{k}f_{s,p+1} = \frac{1}{b_{p+1}}, $$

thus obtaining:

$$ {}^{k}f_{end,p-1} = -\frac{1}{b_p \sin \Delta\alpha_p} $$

$$ {}^{k}f_{beg,p} = -\frac{1}{b_p \tan \Delta\alpha_p} $$

$$ {}^{k}f_{end,p} = \frac{1}{b_{p+1} \sin \Delta\alpha_{p+1}} + \frac{1}{b_p \tan \Delta\alpha_{p+1}} \qquad (2.21, \text{a-f}) $$

$$ {}^{k}f_{beg,p+1} = \frac{1}{b_{p+1} \tan \Delta\alpha_{p+1}} + \frac{1}{b_p \sin \Delta\alpha_{p+1}} $$

$$ {}^{k}f_{end,p+1} = -\frac{1}{b_{p+1} \tan \Delta\alpha_{p+2}} $$

$$ {}^{k}f_{beg,p+2} = -\frac{1}{b_{p+1} \sin \Delta\alpha_{p+2}}, $$

where

$$\Delta\alpha_p = \alpha_p - \alpha_{p-1}$$

$$\Delta\alpha_{p+1} = \alpha_{p+1} - \alpha_p \qquad (2.22, \text{a-c})$$

$$\Delta\alpha_{p+2} = \alpha_{p+2} - \alpha_{p+1}$$

Note that, until now, the compatible rendering procedure referred only to the main plates, allowing rotation inconsistencies between them to occur, and, from now on, no more longitudinal displacements will occur along the transversal slice. In order to eliminate the relative rotations between consecutive plates the structural model shown in Fig. 2.8, a continuous beam model related to the secondary plates connecting any two consecutive secondary plates by a hinge, which makes resource to the traditional folded plate theory (Born 1954), is adopted in order to apply the traditional force method (Ghali and Neville 1997) to the transversal slice which has the form presented in Fig. 2.7 – note that the inner nodes, and the free edge nodes as well, have null translation displacements normal to the plates. Associated with each added hinge, which was introduced in all nodes of the cross section with the exception of free edge nodes, two equal and opposite transverse bending moments – the connecting moments – acting on either side of the hinge become now the static redundant forces of the problem.

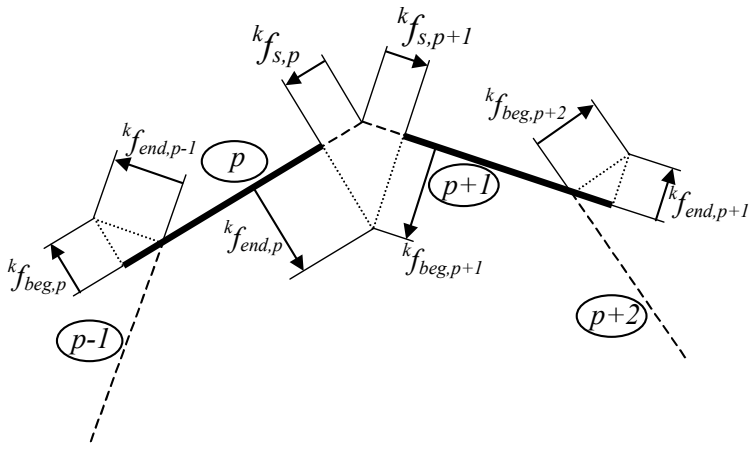

Fig. 2.6 – Rendering compatible the translation inconsistent displacements along the cross section plane

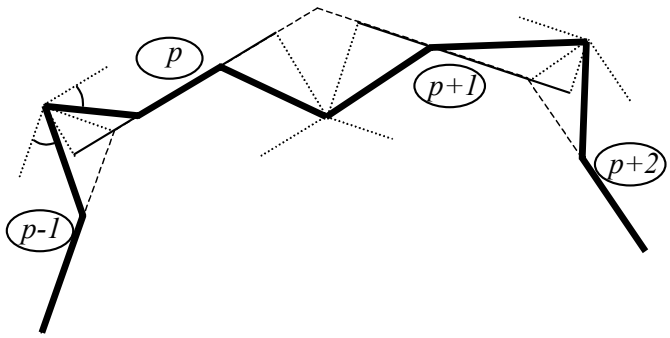

Fig. 2.7 – The transversal slice shape after rendering compatible the translations

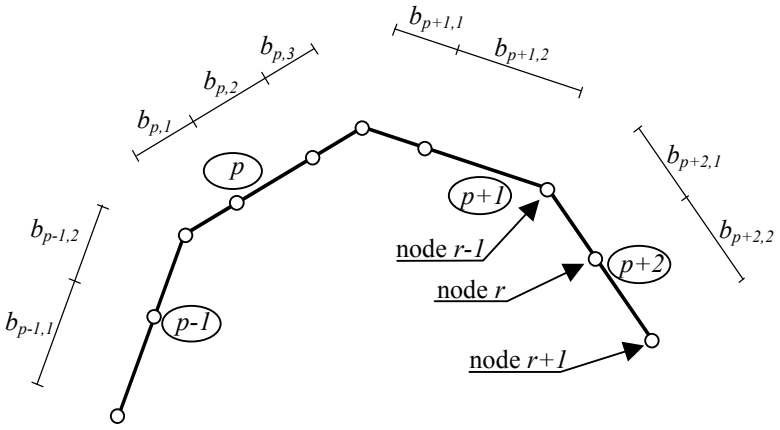

Fig. 2.8 – The structural model to render compatible the relative rotations at the plates edges, related to the secondary plates

Thus, from this point forward, a global numbering to all nodes and plates can be adopted and the flexibility matrix Δ will have the following shape:

	column $i-1$	column i	column $i+1$	column $i+2$
line $i-1$	$\frac{b_{j-2}}{6K_{j-2}}+\frac{b_{j-1}}{6K_{j-1}}$	$\frac{b_{j-1}}{6K_{j-1}}$		
line i	$\frac{b_{j-1}}{6K_{j-1}}$	$\frac{b_{j-1}}{6K_{j-1}}+\frac{b_j}{6K_j}$	$\frac{b_j}{6K_j}$	
line $i+1$		$\frac{b_j}{6K_j}$	$\frac{b_j}{6K_j}+\frac{b_{j+1}}{6K_{j+1}}$	$\frac{b_{j+1}}{6K_{j+1}}$
line $i+2$			$\frac{b_{j+1}}{6K_{j+1}}$	$\frac{b_{j+1}}{6K_{j+1}}+\frac{b_{j+2}}{6K_{j+2}}$

(2.23)

where each line or column corresponds to a specific introduced hinge: hinge i is placed between secondary plates j-1 and j. For any secondary plate j, K_j corresponds to the transversal bending stiffness coefficient and is given by the usual formula:

$$K_j = \frac{E\,t_j}{12\left(1-\mu^2\right)}. \tag{2.24}$$

The i-line of the matrix of the displacement inconsistencies $\boldsymbol{\Delta\vartheta}$ related to mode of deformation k is given by:

$${}^{k}\Delta\vartheta_i = {}^{k}\vartheta_{chord,j} - {}^{k}\vartheta_{chord,j-1} \tag{2.25}$$

where

$${}^{k}\vartheta_{chord,j} = \frac{{}^{k}f_{end,j} - {}^{k}f_{beg,j}}{b_j} \tag{2.26, a-b}$$

$${}^{k}\vartheta_{chord,j-1} = \frac{{}^{k}f_{end,j-1} - {}^{k}f_{beg,j-1}}{b_{j-1}},$$

and the connecting moments for each introduced hinge are computed by solving the force method equation:

$$\boldsymbol{\Delta}\cdot\boldsymbol{m_s} = \boldsymbol{\Delta\vartheta}. \tag{2.27}$$

In practice, the transverse bending moments can be determined all at once by matching, in matrix $\boldsymbol{\Delta\vartheta}$, the i-line to a specific hinge and the k-column to a mode of deformation. Finally, the unitary modal displacements become fully determined through the following expressions, for a general secondary plate i (Schardt 1989):

i) warping displacement (along Ox) : $${}^{k}u(s) = {}^{k}u_{i,beg} + \frac{{}^{k}u_{i,end} - {}^{k}u_{i,beg}}{b_i}\,s\,; \tag{2.28}$$

ii) normal displacement (along Or) : $${}^{k}f(s) = {}^{k}f_{i,beg}\left(1-\frac{s}{b_i}\right) + {}^{k}f_{i,end}\,\frac{s}{b_i} +$$

$$+{}^{k}m_{s,i,beg}\left(\frac{b_i}{3\,K_i}s - \frac{s^2}{2\,K_i} + \frac{s^3}{6\,b_i\,K_i}\right) + {}^{k}m_{s,i,end}\left(\frac{b_i}{6\,K_i}s - \frac{s^3}{6\,b_i\,K_i}\right); \tag{2.29}$$

iii) perimeter displacement (along Os) : ${}^{k}f_{s}(s) = {}^{k}f_{s,i,beg} = {}^{k}f_{s,i,end}$. (2.30)

It is worth referring that expression (2.28) is computed from the assumption of linear longitudinal displacements along a plate, expression (2.29) is derived from the classical equation of the elastica (Dias da Silva 2004) and the perimeter displacements of expression (2.30), due to assumption v) of chapter 2.2.2, remain constant along the plate.

2.2.3.2. The plate bending mode

The plate bending modes of deformation were first introduced by Miosga (1976) and consist in imposing a unitary displacement to each secondary or free edge node of the cross section, perpendicularly to the plate where it is placed, and no displacements along the longitudinal direction or along the perimeter. These modes are intended to model local plate buckling patterns which occur frequently in short thin-walled members under compression and/or bending. Their implementation is achieved through a similar procedure of the one used to render compatible the relative rotations of the previous paragraph – note that, for the plate bending modes, only the relative rotations that are formed at the edges of the plates need to become zero. With reference to the cross section model of Fig. 2.8 shown above, let's suppose, without loss of generality, that plate $p+2$ is an edge plate. Related to this plate, with the nodal discretization presented in Fig. 2.8, the plate bending modes of deformation k – associated with the inner node r – and $k+1$ – associated with the free edge node $r+1$ – have the form presented in Fig. 2.9.

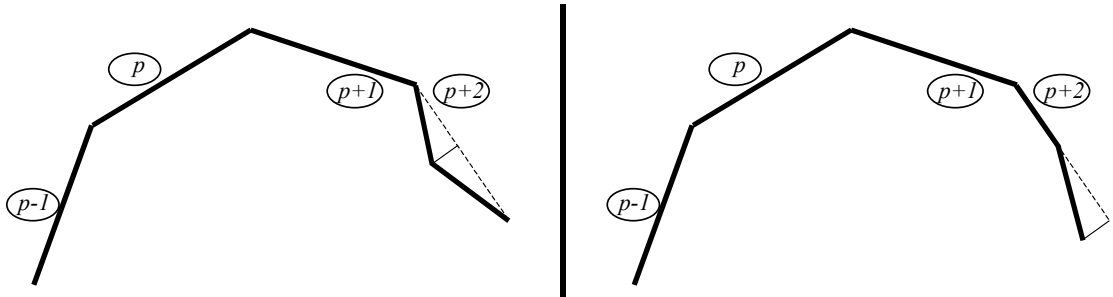

mode k – for an inner node | mode $k+1$ – for a free edge node

Fig. 2.9 – The establishment of the plate bending modes for wall $p+2$

Now the establishment of the force method problem, similar to expression (2.27), requires only the computation of vector $\Delta\vartheta$ for each mode of deformation. For mode k, the only non-zero terms in vector $\Delta\vartheta$ are:

$$ {}^{k}\Delta\vartheta_{r-1} = \frac{1}{b_{p+2,1}} \qquad (2.31, \text{a-b}) $$

$$ {}^{k}\Delta\vartheta_{r} = -\frac{1}{b_{p+2,2}} - \frac{1}{b_{p+2,1}} $$

while for mode $k+1$ the only non-zero term is:

$$ {}^{k+1}\Delta\vartheta_{r} = \frac{1}{b_{p+2,2}} . \qquad (2.32) $$

Then, the unitary cross section displacements can be entirely computed using expression (2.29), the remaining displacements being identically equal to zero.

2.2.3.3. The distortional mode for closed cells

For the modes of deformation presented above, the traditional Vlasov's assumption of null membrane shear distortions around the cross section (Vlasov 1961), applied to open section members, was considered. However, for closed cells, in addition to the warping and plate bending modes, following the classical theory of torsion of closed sections developed by von Kármán & Christensen (1944), it is currently assumed (Kollbrünner & Basler 1966) that the membrane shear flow, given by

$$F_{SH} = \tau_r \times t_r \tag{2.33}$$

for a generic point *r* of the cross section, is constant along the cross section perimeter, i.e., for any two distinct points of a closed cell r_1 and r_2, it is considered that

$$F_{SH,r_1} = F_{SH,r_2} \Leftrightarrow \tau_{r_1} \times t_{r_1} = \tau_{r_2} \times t_{r_2}, \tag{2.34}$$

and the shear deformations and stresses, instead of being negligible, will follow an elasticity law. In fact, looking at one of the first works of Schardt (1970), the analysis of a closed cell without the consideration of membrane shear deformations leads to a set of modes of deformation where torsion is not present, and in some support conditions and/or load cases the analysis of the closed cell member may not be accurate. So, an additional mode of deformation shall be added in order to give the dimension of membrane distortion to the equilibrium system, and the generic cinematic relation for the membrane distortion is considered:

$$\gamma^M = \frac{\partial u}{\partial s} + \frac{\partial f_s}{\partial x}. \tag{2.35}$$

Schardt (1989) refers three ways of considering the shear flow effect in closed cells:

i) the shear flow is constant and no warping displacements occur along the closed cell, the displacements f_s in each wall being inversely proportional to the wall's thickness, and the distortion of the cross section by transversal bending is allowed;

ii) the cross section rotates as a rigid body, the displacement of a generic point being inversely proportional to the distance of that point to the shear centre; the shear centre, which may be not constant, is determined by imposing that the shear forces cause only a torsional moment;

iii) a constant shear flow occurs along the cross section but a warping displacements pattern along the cross section is imposed in order to avoid cross

section deformation caused transversal bending.

All the methods model the shear distortion dimension of the problem in an equivalent way (Schardt), but only the first one will be used in the present work, regarding the GBT scheme's elegance and ease – it is the only procedure that does not require the direct computation of the shear centre. So, and additional mode of deformation is created, here denoted by *l*, to which corresponds the amplitude function ${}^{l}V$. During the establishment of this mode, no longitudinal displacements occur along the cross section and the shear distortions are due only to the displacements ${}^{l}f_{s}$. Hence a relation between the shear flow $\tau \cdot t$ and these displacements can be found, and considering a reference thickness t^{*}, which can be the thickness of any wall of the closed cell for which is supposed that the shear distortion is unitary, the perimeter displacement for any wall *i* comes equal to:

$$ {}^{l}f_{s,i} = \frac{t^{*}}{t_{i}}, \tag{2.36} $$

this displacement being constant along the entire width of the main wall. For a main plate *i* having a variation of thickness along the perimeter direction, as shown in Fig. 2.10, the displacement ${}^{l}f_{s,i}$ is computed considering an equivalent thickness given by

$$ t_{eq,i} = \frac{t_{i,1} \cdot b_{i,1} + t_{i,2} \cdot b_{i,2} + t_{i,3} \cdot b_{i,3}}{b_{i,1} + b_{i,2} + b_{i,3}}. \tag{2.37} $$

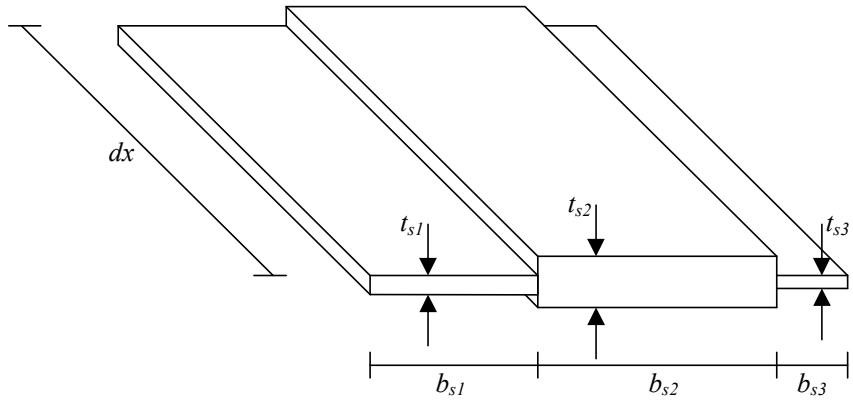

Fig. 2.10 – A wall with a transversal variation of the thickness

After finding the perimeter displacements for all the main walls, the displacements ${}^{l}f_{beg}$ and ${}^{l}f_{end}$ for any main plate are determined using the general formulas (2.18, a-b) shown in paragraph 2.2.3.1, and the force method problem can now be established, to determine the unitary transversal bending moments for mode *l*, in a similar way to the one used in the modes types presented above – see expression (2.27).

2.2.4. The GBT homogeneous equilibrium equations system

The system of equilibrium equations for a prismatic thin-walled member with length L is determined by equalizing the virtual work of the internal forces W_i and the virtual work of the exterior loading W_a, when the member is submitted to a set of cinematically compatible virtual displacements:

$$\delta W_i = \delta W_a \,. \tag{2.38}$$

Firstly, attention will be drawn to the work of the internal forces, in order to derive the homogeneous equilibrium system – this is the strategy followed by Schardt (1989), which is summarized in the following. Subsequently, the contribution of the external loading will be analysed.

The work done by the internal forces is:

$$\delta W_i = \int_0^l \int_A \left(\sigma_x \, \delta \varepsilon_x + \sigma_s \, \delta \varepsilon_s + \tau_{sx} \, \delta \gamma_{sx} \right) dA \, dx \, . \tag{2.39}$$

Noting that each part of the above expression can be split in two, one associated with the membrane effects and the other with the bending effects, the general expression will contain six parts. However, due to the assumptions exposed in paragraph 2.2.2, for open section members only four parts are not zero, while for closed sections the number of non-zero parts increases to five, yielding:

i) for open sections: $\delta W_i = \int_0^l \int_A \left(\underbrace{\sigma_x^M \, \delta \varepsilon_x^M}_{1^{st} \text{ part}} + \underbrace{\sigma_x^B \, \delta \varepsilon_x^B}_{2^{nd} \text{ part}} + \underbrace{\sigma_s^M \, \delta \varepsilon_s^M}_{=0} + \right.$

$$\left. + \underbrace{\sigma_s^B \, \delta \varepsilon_s^B}_{3^{rd} \text{ part}} + \underbrace{\tau_{sx}^M \, \delta \gamma_{sx}^M}_{=0} + \underbrace{\tau_{sx}^B \, \delta \gamma_{sx}^B}_{4^{th} \text{ part}} \right) dA \, dx \; ; \tag{2.40}$$

ii) for closed cells: $\delta W_i = \int_0^l \int_A \left(\underbrace{\sigma_x^M \, \delta \varepsilon_x^M}_{1^{st} \text{ part}} + \underbrace{\sigma_x^B \, \delta \varepsilon_x^B}_{2^{nd} \text{ part}} + \underbrace{\sigma_s^M \, \delta \varepsilon_s^M}_{=0} + \right.$

$$\left. + \underbrace{\sigma_s^B \, \delta \varepsilon_s^B}_{3^{rd} \text{ part}} + \underbrace{\tau_{sx}^M \, \delta \gamma_{sx}^M}_{4^{th} \text{ part}} + \underbrace{\tau_{sx}^B \, \delta \gamma_{sx}^B}_{5^{th} \text{ part}} \right) dA \, dx \; ; \tag{2.41}$$

Applying the elasticity and strain-displacement relations presented in paragraph 2.2.2, the following equilibrium expression is obtained:

$$\delta W_i = \sum_{i=1}^{n+1} \sum_{k=1}^{n+1} \int_0^L \left({}^{ik}C \, {}^{i}A'''' - {}^{ik}D \, {}^{i}A'' + {}^{ik}B \, {}^{i}A \right) \delta^{k} A \, dx = 0 \, . \tag{2.42}$$

Because the above expression must be valid whatever the value of $\delta^k V$, the following equilibrium system is obtained, presented in a matrix form:

$$\boldsymbol{C} \, \boldsymbol{A}'''' - \boldsymbol{D} \, \boldsymbol{A}'' + \boldsymbol{B} \, \boldsymbol{A} = \boldsymbol{0} \, . \tag{2.43}$$

It is a homogeneous system of fourth order differential equations, and the terms of the matrices are computed using the following formulas:

i) for matrix ***C***:

$$ {}^{ik}C = {}^{ik}C^{M} + {}^{ik}C^{B} \tag{2.44} $$

$$ {}^{ik}C^{M} = \int_{s} E\,t\,{}^{i}u\,{}^{k}u\,ds \tag{2.45} $$

$$ {}^{ik}C^{B} = \int_{s} \frac{E\,t^{3}}{12\left(1-\mu^{2}\right)}\,{}^{i}f\,{}^{k}f\,ds \tag{2.46} $$

ii) for matrix ***D***:

ii-1) for open section members: $ {}^{ik}D = {}^{ik}D_{1} - \left({}^{ik}D_{2} + {}^{ki}D_{2}\right) $ (2.47)

ii-2) for closed cells: $ {}^{ik}D = {}^{ik}D_{1} + {}^{ik}D_{3} - \left({}^{ik}D_{2} + {}^{ki}D_{2}\right) $ (2.48)

where:

$$ {}^{ik}D_{1} = \int_{s} \frac{G\,t^{3}}{3}\,{}^{i}\dot{f}\,{}^{k}\dot{f}\,ds \tag{2.49} $$

$$ {}^{ik}D_{2} = \int_{s} \frac{E\,t^{3}\,\mu}{12\left(1-\mu^{2}\right)}\,{}^{i}\ddot{f}\,{}^{k}f\,ds \tag{2.50} $$

$$ {}^{ik}D_{2T} = \int_{s} \frac{E\,t^{3}\,\mu}{12\left(1-\mu^{2}\right)}\,{}^{i}f\,{}^{k}\ddot{f}\,ds \tag{2.51} $$

$$ {}^{ik}D_{3} = \int_{s} G\cdot t\cdot\left({}^{i}\dot{u}+{}^{i}f_{s}\right)\cdot\left({}^{k}\dot{u}+{}^{k}f_{s}\right)ds \tag{2.52} $$

i) for matrix ***B***:

$$ {}^{ik}B = \int_{s} \frac{E\,t^{3}}{12\left(1-\mu^{2}\right)}\,{}^{i}\ddot{f}\,{}^{k}\ddot{f}\,ds \tag{2.53} $$

Note that all terms may be computed as long as the unitary displacement functions are known and the above formulas are entirely general. If these terms are calculated using the unitary modal displacements presented above – denoted by basic modes of deformation

– in general these matrices will be full. It is worth referring that the equilibrium condition system is very similar to the one obtained through the Vlasov's theory (Vlasov 1961), differing only in the additional part associated with the (zero derivative) amplitude modal functions ${}^{k}V$ – this is due to the assumption of the Vlasov's theory related to the non-distortion of the cross section.

2.2.5. The orthogonalization procedure

In the classical Vlasov's theory (Vlasov 1961), the global equilibrium matrices were in general full, preventing the uncoupling of the system of equations. In order to uncouple the equations, the determination of the geometrical cross section properties should refer to the principal axes and to the shear centre of the cross section. This corresponds to the diagonalization of the equilibrium system, is enabled by an appropriate eigenproblem and corresponds to the orthogonalization procedure in GBT.

So, having defined the equilibrium system, the second crucial concept in a GBT analysis of a thin walled member is the orthogonalization of the modes of deformation. Through this process it is intended, as much as possible, to render diagonal the linear equilibrium system matrices by means of a reversible linear transformation applied to the displacements and stress resultants of the basic modes of deformation. In other words, a non-singular n_{MD}-dimensional square matrix $\boldsymbol{T}$ is required which combines linearly the displacements and stress resultants associated with the modes of deformation in such a way that the matrices $\boldsymbol{C}$, $\boldsymbol{D}$ and $\boldsymbol{B}$ (see expressions 2.44 to 2.53 above) become diagonal or, at least, with some diagonal blocks. From the mathematical point of view it consists merely in a change of the coordinate system for the n_{MD}-dimensional vector space generated by the basic modes of deformation, and any equilibrium analysis for the prismatic member shall not be affected by this transformation. Furthermore, it is obvious that the analysis becomes simpler, enables a better physical explanation of the phenomena and allows a better definition of the boundary conditions if it makes resource to the orthogonal modes of

deformation.

In general, by the orthogonalization procedure, it is not possible to render diagonal all three matrices of the linear equilibrium system, but it is possible to render diagonal two of them and also to diagonalize a block in the remaining one. It must be stressed that the present goal is just to define a matrix $\boldsymbol{T}$ that enables the required modal transformation, independently of the procedure used to obtain it. Also, regarding the properties of linear transformations, it is important to point out that if one column of matrix $\boldsymbol{T}$ is multiplied by a non-zero scalar, the resulting matrix still enables a feasible linear transformation. This property will allow a specific normalization for each resulting mode of deformation. It is obvious that the matrices of the linear equilibrium system $\boldsymbol{C}$, $\boldsymbol{D}$ and $\boldsymbol{B}$ are the most appropriate for the determination of matrix $\boldsymbol{T}$, and the procedure proposed by Schardt (1965 and 1989) uses these matrices, giving the most relevant role to matrix $\boldsymbol{C}$ and enabling the full diagonalization of matrices $\boldsymbol{C}$ and $\boldsymbol{B}$. A remark is made in Schardt (1989) that other options may exist, namely he refers that it can be convenient to start the orthogonalization scheme by matrices $\boldsymbol{D}$ and $\boldsymbol{B}$ for closed sections, since in closed sections warping may not be very relevant – this suggestion will not be followed in the present work.

Thus, in the GBT framework, in order to render diagonal the equilibrium system's matrices, the following algebra concept will be used, which states that the orthogonalization procedure corresponds to the diagonalization of matrices through the resolution of a generalized eigenproblem (Wilkinson 1965) of the following type:

$$\boldsymbol{A}\,\boldsymbol{x} - \lambda \boldsymbol{B}\,\boldsymbol{x} = \boldsymbol{0}\,, \tag{2.54}$$

the general matrices $\boldsymbol{A}$ and $\boldsymbol{B}$ being symmetric and $\boldsymbol{B}$ also positive definite, thus invertible. For the resolution of the eigenproblem the Jacobi method (Wilkinson1965, Jiang 1996) can be adopted, and the procedure occurs in three steps:

i) first step – the following n_{MD}-dimensional eigenproblem is solved:

$$(\boldsymbol{B} - \lambda \boldsymbol{C})\boldsymbol{T} = \boldsymbol{0} \tag{2.55}$$

where the transformation matrix $\boldsymbol{T}$ stores the eigenvectors by columns and can be initially given by the identity matrix, obtaining n_{MD} eigenvalues ${}^{k}\lambda$ and n_{MD} eigenvectors ${}^{k}T$.

Ordering the eigenvectors by the increasing values of the corresponding eigenvalue, a new matrix $\boldsymbol{T}$ is formed, through which the new modes of deformation can be derived, and the equilibrium matrices are then updated as follows:

$$\boldsymbol{C} \rightarrow \boldsymbol{T}^{T}\,\boldsymbol{C}\,\boldsymbol{T} \tag{2.56}$$

$$\boldsymbol{D} \rightarrow \boldsymbol{T}^{T}\,\boldsymbol{D}\,\boldsymbol{T} \tag{2.57}$$

$$\boldsymbol{B} \rightarrow \boldsymbol{T}^{T}\,\boldsymbol{B}\,\boldsymbol{T} \tag{2.58}$$

and the actual shape of matrices $\boldsymbol{C}$ and $\boldsymbol{B}$ is, evidentely, diagonal. After this step, it is noticed that the first eigenvalues ${}^{k}\lambda$ are zero, the corresponding modes of deformation being related to the classical Vlasov's theory, but are not yet explicited as axial elongation, major and minor axis bending and shear centre's torsion. The corresponding terms in the main diagonal of the diagonalized matrix $\boldsymbol{B}$ are zero, so a second orthogonalization can take place, in the following form, for these modes of deformation:

ii) second step – the following eigenproblem, with dimension 4, is solved:

$$(\boldsymbol{D} - \lambda\ \boldsymbol{C})\boldsymbol{T} = \boldsymbol{0} \tag{2.59}$$

where matrices $\boldsymbol{D}$ and $\boldsymbol{C}$ are given by

$$\boldsymbol{C} = \begin{bmatrix} {}^{11}C & 0 & \cdots & & & & & 0 \\ 0 & {}^{22}C & 0 & \cdots & & & & 0 \\ \vdots & 0 & {}^{33}C & 0 & \cdots & & & 0 \\ & \vdots & 0 & {}^{44}C & 0 & \cdots & & 0 \\ & & \vdots & 0 & 1 & 0 & \cdots & 0 \\ & & & \vdots & 0 & 1 & & \vdots \\ & & & & \vdots & & \ddots & 0 \\ 0 & 0 & 0 & 0 & 0 & \cdots & 0 & 1 \end{bmatrix} \tag{2.60}$$

$$\boldsymbol{D} = \begin{bmatrix} {}^{11}D & {}^{12}D & {}^{13}D & {}^{14}D & 0 & \cdots & & 0 \\ {}^{21}D & {}^{22}D & {}^{23}D & {}^{24}D & 0 & \cdots & & 0 \\ {}^{31}D & {}^{32}D & {}^{33}D & {}^{34}D & 0 & \cdots & & 0 \\ {}^{41}D & {}^{42}D & {}^{43}D & {}^{44}D & 0 & \cdots & & 0 \\ 0 & 0 & 0 & 0 & 1 & 0 & \cdots & 0 \\ \vdots & \vdots & \vdots & \vdots & 0 & 1 & & \vdots \\ & & & & \vdots & & \ddots & 0 \\ 0 & 0 & 0 & 0 & 0 & \cdots & 0 & 1 \end{bmatrix}. \tag{2.61}$$

The first four columns of $\boldsymbol{T}$ are ordered according to the increasing value of the corresponding eigenvalue and replace the corresponding first columns of matrix $\boldsymbol{T}$ obtained in the first orthogonalization step. The matrices $\boldsymbol{C}$, $\boldsymbol{B}$ and $\boldsymbol{D}$ are updated using expressions (2.56) to (2.58), matrix $\boldsymbol{B}$ remains unchanged and now the first 4-dimensional main block in matrix $\boldsymbol{D}$ has only one non-zero term, ${}^{4,4}D$, which corresponds to the polar moment of inertia related to the cross section's shear centre. In matrix $\boldsymbol{C}$ the term ${}^{4,4}C$ corresponds now to the torsional warping of the cross section. Therefore, mode 4 corresponds to the classical torsion of thin-walled beams and shall be normalized in such a form that for any point of the cross section one gets:

$${}^{4}\vartheta = 1. \tag{2.62}$$

The first three terms of the main diagonal of matrix $\boldsymbol{D}$ are zero, consequently the first three modes of deformation are not influenced by torsion and correspond to the traditional phenomena of axial elongation and major and minor axis bendings – however these modes

are still mixed and to split them one makes resource to the third orthogonalization step, as follows:

iii) third step – the following eigenproblem, with dimension 3, is solved:

$$\left(\boldsymbol{\kappa}\text{-}\lambda\ \boldsymbol{C}\right)\boldsymbol{T}=\boldsymbol{0} \tag{2.63}$$

where matrix $\boldsymbol{\kappa}$ is a matrix given in the form:

$$\boldsymbol{\kappa}=\begin{bmatrix} {}^{11}\kappa & {}^{12}\kappa & {}^{13}\kappa & 0 & \cdots & 0 \\ {}^{21}\kappa & {}^{22}\kappa & {}^{23}\kappa & 0 & & \\ {}^{31}\kappa & {}^{32}\kappa & {}^{33}\kappa & 0 & & \vdots \\ 0 & 0 & 0 & 1 & & \\ \vdots & & & & \ddots & 0 \\ 0 & & \cdots & & 0 & 1 \end{bmatrix} \tag{2.64}$$

its (i,k) term being given by:

$${}^{ik}\kappa=-\frac{1}{A}\sum_{r=1}^{n_{SP}}\left({}^{i}f_{s,beg,r}\ {}^{k}f_{s,beg,r}+{}^{i}f_{beg,r}\ {}^{k}f_{beg,r}\right)b_r\,t_r\ , \tag{2.65}$$

where A is the cross section area.

Matrix $\boldsymbol{\kappa}$ has physical meaning only in the 2nd order theory of GBT, corresponding to the tensor $\boldsymbol{\kappa_{LO2}}$ in the energy formulation presented later, so it will be explained later, and the displacements f and f_s refer to the first three modes of deformation. After normalization, these three modes of deformation represent the axial elongation and major and minor axis bendings, and the first three terms of the main diagonal of matrix $\boldsymbol{C}$ correspond, respectively, to the cross sectional area and major and minor axis moment of inertia.

After the three-step procedure the sought reversible transformation matrix $\boldsymbol{T}$, which contains the resulting eigenvectors stored in columns, is already obtained and the modal displacements for the secondary plates (see table 2.1), which can be stored, for each mode of deformation, as columns of the respective displacement's matrix, are updated in the

following way (they shall be updated after each orthogonalization step):

$$\boldsymbol{u}_{beg} \rightarrow \boldsymbol{u}_{beg}\,\boldsymbol{T} \text{ and } \boldsymbol{u}_{end} \rightarrow \boldsymbol{u}_{end}\,\boldsymbol{T}$$

$$\boldsymbol{f}_{beg} \rightarrow \boldsymbol{f}_{beg}\,\boldsymbol{T} \text{ and } \boldsymbol{f}_{end} \rightarrow \boldsymbol{f}_{end}\,\boldsymbol{T}$$

$$\boldsymbol{f}_{s,beg} \rightarrow \boldsymbol{f}_{s,beg}\,\boldsymbol{T} \text{ and } \boldsymbol{f}_{s,end} \rightarrow \boldsymbol{f}_{s,end}\,\boldsymbol{T} \qquad (2.66, \text{a-e})$$

$$\vartheta_{beg} \rightarrow \vartheta_{beg}\,\boldsymbol{T} \text{ and } \vartheta_{end} \rightarrow \vartheta_{end}\,\boldsymbol{T}$$

$$\boldsymbol{m}_{s,beg} \rightarrow \boldsymbol{m}_{s,beg}\,\boldsymbol{T} \text{ and } \boldsymbol{m}_{s,end} \rightarrow \boldsymbol{m}_{s,end}\,\boldsymbol{T}\,.$$

All in all, through the orthogonalization procedure it is possible to highlight that GBT includes the classical Vlasov theory, since the first four modes derived from the orthogonalization process correspond to the Vlasov's equilibrium system equations of the member, giving a traditional significance to the resulting generalized geometrical properties for these first four modes.

After the orthogonalization procedure the homogeneous equilibrium equations system shows the following form

$$\boldsymbol{C}\,\boldsymbol{A}'''' - \boldsymbol{D}\,\boldsymbol{A}'' + \boldsymbol{B}\,\boldsymbol{A} = \boldsymbol{0} \qquad (2.67)$$

where matrices $\boldsymbol{C}$ and $\boldsymbol{B}$ and the main 4-dimensional block in matrix $\boldsymbol{D}$ are diagonal. If Schardt's simplification is adopted (Schardt 1989), neglecting the out-of-diagonal terms in matrix $\boldsymbol{D}$ for open sections, since they are negligible, then the system (2.67) becomes a set of uncoupled fourth order differential equations, which can be solved separately.

2.2.6. The generalized loading

Loading is only handled now since logically it refers to the orthogonal modes of deformation, resulting from the orthogonalization procedure presented just above. Its study is made in two parts, one related to the loading acting along the cross section plane and the other related to the loads acting along the longitudinal axis. The existence of loading implies that the equilibrium system (2.67) will no longer be homogeneous, and this

corresponds to rendering equal the virtual work of the internal forces and of the external loading (Schardt 1989), as referred above:

$$\delta W_i = \delta W_a . \tag{2.68}$$

The virtual work of the external loading δW_a is given by (Schardt 1989):

$$\delta W_a = \int_0^l \left(\sum_{r=2}^{n} q_{tr,r}(x)\delta f_{tr,r}(x) + \sum_{r=1}^{n+1} q_{x,r}(x)\delta u_r(x) \right) dx \tag{2.69}$$

which is equivalent to

$$\delta W_a = \sum_{k=1}^{n+1} \int_0^l \left(\sum_{r=2}^{n} q_{tr,r}(x)\delta^k A(x)^k f_{tr,r} + \sum_{r=1}^{n+1} q_{x,r}(x)\delta^k A'(x)^k u_r \right) dx \tag{2.70}$$

where $q_{tr,r}$ is the magnitude of the transversal load at node *r* and ${}^k f_{tr,r}$ is the displacement of node *r* in the cross section's plane along the direction of $q_{tr,r}$ for mode of deformation *k*. The second part of expression (2.70) refers to the longitudinal loading, which is a function of $\delta^k A'$, whereas the first part is a function of $\delta^k A$. This implies that two distinct approaches must be implemented, the respective terms for the global equilibrium condition being derived separately.

For the transversal loading, the modal transversal loading is given by:

$${}^k q_{TR}(x) = \sum_{r=1}^{n_{NT}} q_{tr,r} \times {}^k f_{tr,r} = \sum_{r=1}^{n_{NT}} \left[q_{y,r} \times {}^k v_r + q_{z,r} \times {}^k w_r \right] \tag{2.71}$$

where ${}^k f_{tr,r}$ denotes the displacement in the direction of $q_{tr,r}$ for mode *k* at node *r*. The last part of (2.71) is equivalent to the former part and is applicable if the load is referred to the general axes of the cross section, as shown in Fig. 2.11.

For the longitudinal loading the virtual work is given by (Schardt 1989):

$$\delta W_a^x = \int_0^l \sum_{k=1}^{n+1} \left({}^k q_x' \, \delta^k A \right) dx - \sum_{k=1}^{n+1} {}^k \tilde{q}_x \, \delta^k A \Big|_0^l \tag{2.72}$$

where

$${}^k q_x(x) = -\sum_{r=1}^{n+1} q_{x,r}'(x) \cdot {}^k u_r . \tag{2.73}$$

The second part of expression (2.72) influences only the boundary conditions and thus has no direct influence in the equilibrium equation, while the first part belongs to the equilibrium equation for mode *k*.

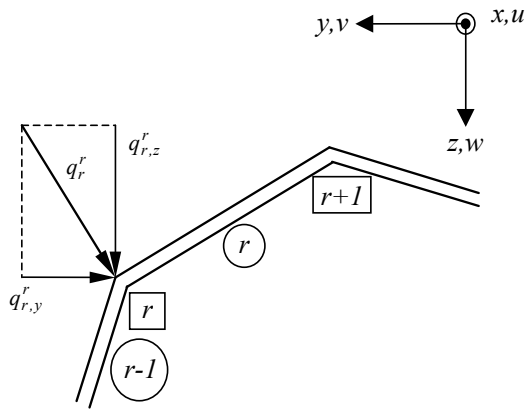

Fig. 2.11 – Transversal loading acting along the cross section's general axes

2.2.7. The GBT general equilibrium equations system

Finally, the general equilibrium equations system is given by the following expression, neglecting the out-of-diagonal terms in matrix ***D***:

$$ {}^{k}C\ {}^{k}A''''-{}^{k}D\ {}^{k}A''+{}^{k}B\ {}^{k}A={}^{k}q(x)+{}^{k}q'_x(x). \tag{2.74}$$

and it is worth defining the following quantities in order to determine the stresses and internal forces along the member (Schardt 1989):

i) the generalized bimoment is given by, for mode *k*:

$$ {}^{k}W=-{}^{k}C\ {}^{k}A''; \tag{2.75}$$

ii) the normal stresses are given by, for linear analysis:

$$ {}^{k}\sigma(s,x)=-E\frac{{}^{k}W(x)\,{}^{k}u(s)}{{}^{k}C}; \tag{2.76}$$

iii) the shear stresses are determined by, for each mode of deformation *k*:

$$ {}^{k}\tau(s)=E\frac{{}^{k}W'\int_0^s {}^{k}u(\zeta)\mathrm{d}\zeta}{{}^{k}C\times t(s)}. \tag{2.77}$$

Expression (2.77) refers to open sections only, since for closed cells the constant shear flow follows an elasticity law, and is derived by partial equilibrium for an elementary plate, so shall not be included in the global equilibrium system.

2.2.8. The Schardt's GBT formulation for stability analysis

The above formulation was derived for linear analysis and thus needs further improvements in order to perform the stability analysis of thin-walled members, which will be presented here, following the Vlasov (1961) strategy, based on the concept of deviating forces. It consists on computing the virtual work of the deviating forces generated by the longitudinal membrane stresses associated with a displacements shape l to a shape of virtual displacements k, and the corresponding classical equilibrium expression is given by:

$$\partial \mathcal{W}_i = \partial \mathcal{W}_e \tag{2.78}$$

where $\mathcal{W}_i$ and $\mathcal{W}_e$ refer to the work of the internal forces and to the work of the external loading, respectively (the above expression requires that, for any equilibrium configuration of a structural member, the external and the internal virtual works are determined for any cinematically admissible shape of the virtual displacements). By analyzing Figures 2.12 and 2.13, reproduced from Vlasov (1961) (split in two for clearer understanding), recalling expression (2.76) for the membrane longitudinal stresses in the linear analysis (Schardt 1989), here expressed in terms of the modes of deformation:

$$\sigma = \sum_{i=1}^{n_{MD}} - E \frac{{}^{i}W \, {}^{i}u}{{}^{i}C}, \tag{2.79}$$

and because matrix $\boldsymbol{C}$ becomes diagonal after the orthogonalization scheme presented above, the following deviating forces are obtained:

i) the first term of the deviating force is due to the variation of the longitudinal normal membrane stress in the plane *Osx*, for the mode of deformation *l*

$$ {}^{l}q_s^{\mathrm{I}} = \sigma\, t\, ds \frac{dx}{\rho_s} \approx \sigma\, t\, {}^{l}f_s'' ds\, dx ; \tag{2.80} $$

ii) the second term of the deviating force is due to the variation of the longitudinal normal membrane stress in the plane *Osx*, for the mode of deformation *l*

$$ {}^{l}q_s^{\mathrm{II}} = \frac{\partial \sigma}{\partial x} t \sin(\alpha_s) ds\, dx \approx \frac{\partial \sigma}{\partial x} t\, {}^{l}f_s' ds\, dx . \tag{2.81} $$

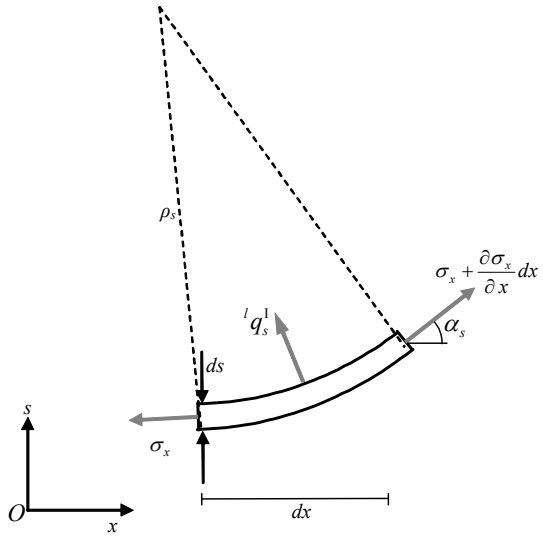

Fig. 2.12 - Computing the 2nd order terms for the equilibrium condition using the non-linear Vlasov theory: analysis along the plate's plane *Osx*

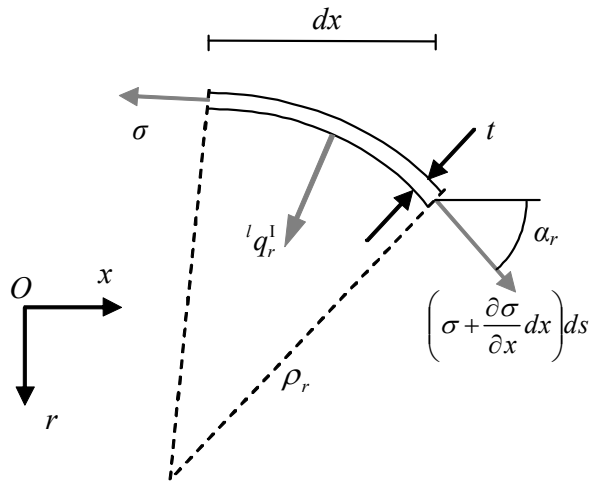

Fig. 2.13 - Computing the 2nd order terms for the equilibrium condition using the non-linear Vlasov theory: analysis normal to the plate, along plane *Orx*

Adding these two forces and using expression (2.79) the deviating force along plane *Osx* becomes

$$ {}^{l}q_s = {}^{l}q_s^{\mathrm{I}} + {}^{l}q_s^{\mathrm{II}} = \sum_{i=1}^{m} -E\frac{{}^{i}u}{{}^{i}C}t\,{}^{l}f_s\left({}^{i}W\,{}^{l}A'\right)'ds\,dx\ . \tag{2.82} $$

Applying the same procedures for the plane *Orx* the following deviating force for mode of deformation *l* is obtained

$$ {}^{l}q_{\bar{s}} = \sum_{i=1}^{m} -E\frac{{}^{i}u}{{}^{i}C}t\,{}^{l}f\left({}^{i}W\,{}^{l}A'\right)'ds\,dx\ . \tag{2.83} $$

The work of these deviating forces is determined for a virtual displacements pattern *k* – these forces will be multiplied by the displacements that occur in their plane for mode *k*, i.e., they are multiplied by:

$$ {}^{k}f_s\,\delta^{k}A \text{ - forces along the } Osx \text{ plane;} \tag{2.84} $$

$$ {}^{k}f\,\delta^{k}A \text{ - forces along the } Orx \text{ plane.} \tag{2.85} $$

By doing this, the following expression is obtained for the virtual work of the deviating forces:

$$ \delta W = \int_{L}\int_{s}\sum_{i=1}^{m}\sum_{l=1}^{m}\left[-E\frac{{}^{i}u}{{}^{i}C}t\left({}^{l}f_s\,{}^{k}f_s + {}^{l}f\,{}^{k}f\right)\left({}^{i}W\,{}^{l}A'\right)'\right]\delta^{k}A\,ds\,dx\,. \tag{2.86} $$

Defining the coefficients κ as

$$ {}^{ilk}\kappa = \int_{s} E\frac{{}^{i}u}{{}^{i}C}t\left({}^{l}f_s\,{}^{k}f_s + {}^{l}f\,{}^{k}f\right)ds\,, \tag{2.87} $$

the following expression is obtained for the virtual work of the deviating forces:

$$ \delta W = \int_{L}\sum_{i=1}^{m}\sum_{l=1}^{m} -{}^{ilk}\kappa\left({}^{i}W\,{}^{l}V'\right)'\delta^{k}A\,dx\,. \tag{2.88} $$

Noting that the virtual work of the above expression refers to fictitious forces, hence shall be added to the virtual work of the external loading (Przemieniecki 1968), when it is transferred to the first member of expression (2.67) its signal is changed; accounting also

on the definition of generalized bimoment for the mode of deformation i – see expression (2.75) – the following non-linear equilibrium equation derived by Schardt (1994) is obtained, for mode of deformation k:

$$ {}^{k}C\ {}^{k}A''''-{}^{k}D\ {}^{k}A''+{}^{k}B\ {}^{k}A+\sum_{i=1}^{n_{MD}}\sum_{j=1}^{n_{MD}}{}^{ijk}\kappa\left({}^{i}W\ {}^{j}A'\right)'=0 \qquad (2.89) $$

Note that the non-linear equilibrium conditions are derived after the orthogonalization scheme and Schardt neglects the out of diagonal terms in the linear equilibrium matrices, since he analysed only open sections. Noting that for the usual bifurcational problems it is supposed that the generalized bimoment ${}^{i}W$ is constant along the member's length, so:

$$ {}^{i}W'=0\,, \qquad (2.90) $$

and then expression (2.89) reduces to (Schardt 1994):

$$ {}^{k}C\ {}^{k}A''''-{}^{k}D\ {}^{k}A''+{}^{k}B\ {}^{k}A+{}^{i}W\sum_{j=1}^{n_{MD}}{}^{ijk}\kappa\ {}^{j}A''=0\,. \qquad (2.91) $$

Finally, this formulation was adapted to the GBT by Schardt to perform buckling analysis of columns under uniform compression and beams under uniform major axis bending moment (Schardt 1965, 1970 and 1994). Although this formulation is in most cases sufficiently accurate for the buckling analysis of open sections under uniform compression or under uniform bending moment, it becomes incomplete for post-buckling analysis, even if the usual strategy of accounting only on the geometrical nonlinear effects provoked by the longitudinal stresses is considered (Schardt 1994, Chajes 1974), due, at least, to the absence of third order terms. In the following a consistent formulation for buckling and post-buckling analysis is therefore developed, based on the concept of total potential energy. It is noted that the stability analysis using expression (2.91) corresponds to the use of the TPE formulation accounting only for the nonlinear term related to the tensor $\boldsymbol{\kappa}_{L2}$ for the definition of the internal strain energy, defined in chapter 2.3, thus taking into account only the nonlinear effects of the longitudinal membrane stresses.

2.3 – The energy formulation

2.3.1 The strain-displacements relation

Based on the assumptions presented in paragraph 2.1.2 and using $\dot{(\,)}$ and $(\,)'$ to denote differentiation with respect to *s* and *x*, respectively, the bending strain-displacement relations follow the usual linear formulation and are given by

$$\varepsilon_x^B = -r\frac{\partial^2 f}{\partial x^2} = \sum_{k=1}^{n_{MD}} -r\ {}^k f\ {}^k A''$$

$$\varepsilon_s^B = -r\frac{\partial^2 f}{\partial s^2} = \sum_{k=1}^{n_{MD}} -r\ {}^k \ddot{f}\ {}^k A \qquad \text{(2.92, a-c)}$$

$$\gamma_{sx}^B = -2r\frac{\partial^2 f}{\partial s\,\partial x} = \sum_{k=1}^{n_{MD}} -2r\ {}^k \dot{f}\ {}^k A' .$$

For a stability analysis, it is necessary to include the relevant non-linear terms in the membrane strain-displacement relations. From Fig. 2.14, the longitudinal membrane strain is given, in general, by:

$$\varepsilon_x^M = \frac{\overline{A_2B_2} - \overline{A_1B_1}}{\overline{A_1B_1}} = \sqrt{\left(1+\frac{\partial u}{\partial x}\right)^2 + \left(\frac{\partial f}{\partial x}\right)^2 + \left(\frac{\partial f_s}{\partial x}\right)^2} - 1 . \qquad (2.93)$$

Expanding equation (2.93) in Taylor series and neglecting higher-order terms yields:

$$\varepsilon_x^M = \frac{\partial u}{\partial x} + \frac{1}{2}\left(\frac{\partial f}{\partial x}\right)^2 + \frac{1}{2}\left(\frac{\partial f_s}{\partial x}\right)^2 = \sum_{k=1}^{n_{MD}}\left\{ {}^k u\ {}^k A' + \frac{1}{2}\sum_{l=1}^{n_{MD}}\left[\left({}^k f_s\ {}^l f_s + {}^k f\ {}^l f\right){}^k A'\ {}^l A'\right]\right\}. \qquad (2.94)$$

Analogously, for closed cross-section members only, from the definition of membrane shear distortion,

$$\gamma_{sx}^M = \sphericalangle\left(B_1A_1C_1\right) - \sphericalangle\left(B_2A_2C_2\right), \qquad (2.95)$$

given that

$$\sphericalangle\left(B_1A_1C_1\right)=\frac{\pi}{2}\text{ rad}, \tag{2.96}$$

and noting that by definition of scalar product of two vectors, $\overrightarrow{A_2B_2}$ and $\overrightarrow{A_2C_2}$, the angle $\sphericalangle\left(B_2A_2C_2\right)$ may be determined as a function of the displacements of A, B and C, the membrane shear distortion is given by:

$$\gamma_{sx}^{M}=\frac{\pi}{2}-arc\cos\left[\frac{\left(1+\frac{\partial u}{\partial x}\right)\frac{\partial u}{\partial s}+\left(1+\frac{\partial f_s}{\partial s}\right)\frac{\partial f_s}{\partial x}+\frac{\partial f}{\partial x}\frac{\partial f}{\partial s}}{\sqrt{\left(1+\frac{\partial u}{\partial x}\right)^2+\left(\frac{\partial f_s}{\partial x}\right)^2+\left(\frac{\partial f}{\partial x}\right)^2}\sqrt{\left(\frac{\partial u}{\partial s}\right)^2+\left(1+\frac{\partial f_s}{\partial s}\right)^2+\left(\frac{\partial f}{\partial s}\right)^2}}\right] \tag{2.97}$$

Expanding in Taylor series and neglecting higher-order terms leads to:

$$\gamma_{sx}^{M}=\frac{\partial u}{\partial s}+\frac{\partial f_s}{\partial x}+\frac{\partial f}{\partial x}\frac{\partial f}{\partial s}+\frac{\partial u}{\partial x}\frac{\partial u}{\partial s}+\frac{\partial f_s}{\partial x}\frac{\partial f_s}{\partial s}. \tag{2.98}$$

Finally, introducing the assumption of a negligible 1st order transverse membrane strain,

$$\frac{\partial f_s}{\partial s}\approx 0 \tag{2.99}$$

the membrane shear distortion of equation (11) is obtained:

$$\gamma_{sx}^{M}=\frac{\partial u}{\partial s}+\frac{\partial f_s}{\partial x}+\frac{\partial f}{\partial x}\frac{\partial f}{\partial s}+\frac{\partial u}{\partial x}\frac{\partial u}{\partial s}=$$

$$=\sum_{k=1}^{n_{MD}}\left({}^{k}\dot{u}+{}^{k}f_s\right){}^{k}A'+\sum_{k=1}^{n_{MD}}\sum_{l=1}^{n_{MD}}{}^{k}f\,{}^{l}\dot{f}\;{}^{k}A'\,{}^{l}A+\sum_{k=1}^{n_{MD}}\sum_{l=1}^{n_{MD}}{}^{k}u\,{}^{l}\dot{u}\;{}^{k}A''\,{}^{l}A'. \tag{2.100}$$

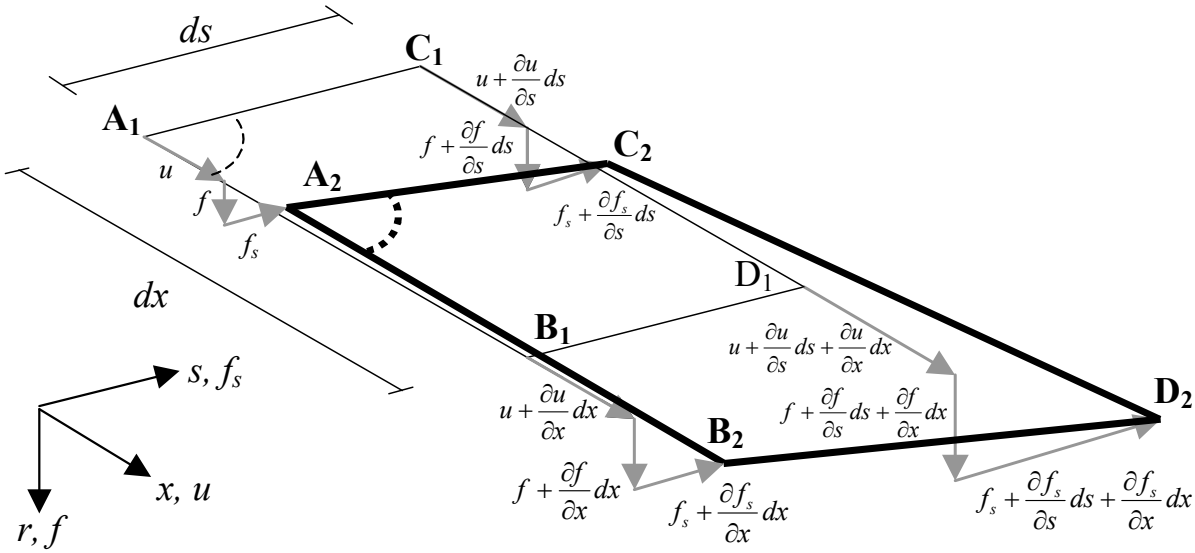

Fig. 2.14– Membrane displacements of the thin plate $ds \times dx$

2.3.2. The constitutive relations

The stress-strain relations are split into bending effects,

$$\sigma_x^B = \frac{E}{1-\mu^2}\left(\varepsilon_x^B + \mu\,\varepsilon_x^B\right) = \frac{E}{1-\mu^2}\sum_{i=1}^{n_{MD}} -r\left({}^i f\,{}^i A'' + \mu\,{}^i\ddot{f}\,{}^i A\right)$$

$$\sigma_s^B = \frac{E}{1-\mu^2}\left(\varepsilon_s^B + \mu\,\varepsilon_x^B\right) = \frac{E}{1-\mu^2}\sum_{i=1}^{n_{MD}} -r\left({}^i\ddot{f}\,{}^i A + \mu\,{}^i f\,{}^i A''\right) \qquad (2.101,\ \text{a-c})$$

$$\tau_{sx}^B = G\gamma_{sx}^B = -2G\sum_{i=1}^{n_{MD}} r\,{}^i\dot{f}\,{}^i A'.$$

and membrane effects – equation (2.102 b) holds only for closed cross section members:

$$\sigma_x^M = E\varepsilon_x^M = E\sum_{i=1}^{n_{MD}}\left\{{}^i u\,{}^i A'' + \frac{1}{2}\sum_{j=1}^{n_{MD}}\left[\left({}^i f_s\,{}^j f_s + {}^i f\,{}^j f\right){}^i A'\,{}^j A'\right]\right\} \qquad (2.102\ \text{a})$$

$$\tau_I^M = G\gamma_{sx}^M = G\left[\sum_{i=1}^{n_{MD}}\left({}^i\dot{u} + {}^i f_s\right){}^i A' + \sum_{i=1}^{n_{MD}}\sum_{j=1}^{n_{MD}} {}^i f\,{}^j\dot{f}\,{}^i A'\,{}^j A + \sum_{i=1}^{n_{MD}}\sum_{j=1}^{n_{MD}} {}^i u\,{}^j\dot{u}\,{}^i A''\,{}^j A'\right]. \qquad (2.102\ \text{b})$$

2.3.3 The internal strain energy

From the classical definition of internal strain energy (ISE),

$$U_i = \int_0^L \iint_A \left(\frac{1}{2}\sigma_x^M \varepsilon_x^M + \frac{1}{2}\tau_{sx}^M \gamma_{sx}^M + \frac{1}{2}\sigma_x^B \varepsilon_x^B + \frac{1}{2}\sigma_s^B \varepsilon_s^B + \frac{1}{2}\tau_{sx}^B \gamma_{sx}^B \right) dA\, dx, \qquad (2.103)$$

the bending terms are obtained by introducing equations (2.92, a-c) and (2.101, a-c) into equation (2.103), yielding:

$$U_i^B = \sum_{i=1}^{n_{MD}} \sum_{k=1}^{n_{MD}} \frac{1}{2} \int_0^L {}^{ik}C^B \, {}^{i}A'' \, {}^{k}A'' dx + \sum_{i=1}^{n_{MD}} \sum_{k=1}^{n_{MD}} \frac{1}{2} \int_0^L {}^{ik}D_1 \, {}^{i}A' \, {}^{k}A' dx +$$

$$+ \frac{1}{2} \sum_{i=1}^{n_{MD}} \sum_{k=1}^{n_{MD}} \int_0^L {}^{ik}D_2 \, {}^{i}A \, {}^{k}A'' dx + \frac{1}{2} \sum_{i=1}^{n_{MD}} \sum_{k=1}^{n_{MD}} \int_0^L {}^{ik}D_{2T} \, {}^{i}A'' \, {}^{k}A dx + \frac{1}{2} \sum_{i=1}^{n_{MD}} \sum_{k=1}^{n_{MD}} \int_0^L {}^{ik}B \, {}^{i}A \, {}^{k}A dx, \qquad (2.104)$$

where:

$${}^{ik}C^B = \int_s \frac{E t^3}{12\left(1-\mu^2\right)} \, {}^{i}f \, {}^{k}f \, ds$$

$${}^{ik}D_1 = \int_s \frac{G t^3}{3} \, {}^{i}\dot{f} \, {}^{k}\dot{f} \, ds$$

$${}^{ik}D_2 = \int_s \frac{E t^3 \mu}{12\left(1-\mu^2\right)} \, {}^{i}\ddot{f} \, {}^{k}f \, ds \qquad (2.105, \text{a-e})$$

$${}^{ik}D_{2T} = \int_s \frac{E t^3 \mu}{12\left(1-\mu^2\right)} \, {}^{i}f \, {}^{k}\ddot{f} \, ds$$

$${}^{ik}B = \int_s \frac{E t^3}{12\left(1-\mu^2\right)} \, {}^{i}\ddot{f} \, {}^{k}\ddot{f} \, ds$$

Analogously, the membrane contribution, which includes all non-linear terms, is obtained by introducing equations (2.94), (2.97) and (2.102, a-b) into equation (2.103), giving:

$$U_i^M = \sum_{i=1}^{n_{MD}} \sum_{k=1}^{n_{MD}} \frac{1}{2} \int_0^L {}^{ik}C^M \, {}^{i}A'' \, {}^{k}A'' \, dx + \sum_{i=1}^{n_{MD}} \sum_{k=1}^{n_{MD}} \frac{1}{2} \int_0^L {}^{ik}D_3 \, {}^{i}A' \, {}^{k}A' dx +$$

$$+\frac{1}{4}\sum_{i=1}^{n_{MD}}\sum_{k=1}^{n_{MD}}\sum_{l=1}^{n_{MD}}\int_L {}^{ikl}\kappa_{LO2}\ {}^iA''\ {}^kA'\ {}^lA'\,dx+\frac{1}{4}\sum_{i=1}^{n_{MD}}\sum_{j=1}^{n_{MD}}\sum_{k=1}^{n_{MD}}\int_L {}^{ijk}\kappa_{LO3}\ {}^iA'\ {}^jA'\ {}^kA''\,dx+$$

$$+\frac{1}{8}\sum_{i=1}^{n_{MD}}\sum_{j=1}^{n_{MD}}\sum_{k=1}^{n_{MD}}\sum_{l=1}^{n_{MD}}\int_L {}^{ijkl}\kappa_{LO4}\ {}^iA'\ {}^jA'\ {}^kA'\ {}^lA'\,dx+\frac{1}{2}\sum_{i=1}^{n_{MD}}\sum_{k=1}^{n_{MD}}\sum_{l=1}^{n_{MD}}\int_L {}^{ikl}\kappa_{SH2}\ {}^iA'\ {}^kA'\ {}^lA\,dx+$$

$$+\frac{1}{2}\sum_{i=1}^{n_{MD}}\sum_{k=1}^{n_{MD}}\sum_{l=1}^{n_{MD}}\int_L {}^{ikl}\kappa_{SH3}\ {}^iA'\ {}^kA''\ {}^lA'\,dx+\frac{1}{2}\sum_{i=1}^{n_{MD}}\sum_{j=1}^{n_{MD}}\sum_{k=1}^{n_{MD}}\int_L {}^{ijk}\kappa_{SH4}\ {}^iA'\ {}^jA\ {}^kA'\,dx+$$

$$+\frac{1}{2}\sum_{i=1}^{n_{MD}}\sum_{j=1}^{n_{MD}}\sum_{k=1}^{n_{MD}}\sum_{l=1}^{n_{MD}}\int_L {}^{ijkl}\kappa_{SH5}\ {}^iA'\ {}^jA\ {}^kA'\ {}^lA\,dx+\frac{1}{2}\sum_{i=1}^{n_{MD}}\sum_{j=1}^{n_{MD}}\sum_{k=1}^{n_{MD}}\sum_{l=1}^{n_{MD}}\int_L {}^{ijkl}\kappa_{SH6}\ {}^iA'\ {}^jA\ {}^kA''\ {}^lA'\,dx+$$

$$+\frac{1}{2}\sum_{i=1}^{n_{MD}}\sum_{j=1}^{n_{MD}}\sum_{k=1}^{n_{MD}}\int_L {}^{ijk}\kappa_{SH7}\ {}^iA''\ {}^jA'\ {}^kA'\,dx+\frac{1}{2}\sum_{i=1}^{n_{MD}}\sum_{j=1}^{n_{MD}}\sum_{k=1}^{n_{MD}}\sum_{l=1}^{n_{MD}}\int_L {}^{ijkl}\kappa_{SH8}\ {}^iA''\ {}^jA'\ {}^kA'\ {}^lA'\,dx+$$

$$+\frac{1}{2}\sum_{i=1}^{n_{MD}}\sum_{j=1}^{n_{MD}}\sum_{k=1}^{n_{MD}}\sum_{l=1}^{n_{MD}}\int_L {}^{ijkl}\kappa_{SH9}\ {}^iA''\ {}^jA'\ {}^kA''\ {}^lA'\,dx\,, \qquad (2.106)$$

where the following coefficients relate to the longitudinal membrane stress

$${}^{ik}C^M=\int_s E\,t\ {}^iu\ {}^ku\,ds \quad (1^{\text{st}}\text{ order term})$$

$${}^{ikl}\kappa_{LO2}=\int_s E\,t\ {}^iu\left({}^kf_s\ {}^lf_s+{}^kf\ {}^lf\right)ds \qquad (2.107,\text{ a-d})$$

$${}^{ijk}\kappa_{LO3}=\int_s E\,t\ {}^ku\left({}^if_s\ {}^jf_s+{}^if\ {}^jf\right)ds$$

$${}^{ijkl}\kappa_{LO4}=\int_s E\,t\left({}^if_s\ {}^jf_s+{}^if\ {}^jf\right)\cdot\left({}^kf_s\ {}^lf_s+{}^kf\ {}^lf\right)ds\,,$$

while the following arise uniquely for closed sections from the membrane shear flow contribution:

$${}^{ik}D_3=\int_s G\cdot t\cdot\left({}^i\dot{u}+{}^if_s\right)\cdot\left({}^k\dot{u}+{}^kf_s\right)ds \ (1^{\text{st}}\text{ order term})$$

$${}^{ikl}\kappa_{SH2}=\int_s G\cdot t\cdot\left({}^i\dot{u}+{}^if_s\right)\cdot{}^l\dot{f}\cdot{}^kf\,ds$$

$${}^{ikl}\kappa_{SH3}=\int_s G\cdot t\cdot\left({}^i\dot{u}+{}^if_s\right)\cdot{}^l\dot{u}\cdot{}^ku\,ds$$

$$
\begin{aligned}
{}^{ijk}\kappa_{SH\,4} &= \int_s G\cdot t\cdot {}^{i}f\cdot {}^{j}\dot{f}\cdot\left({}^{k}\dot{u}+{}^{k}f_s\right)ds \\
{}^{ijkl}\kappa_{SH\,5} &= \int_s G\cdot t\cdot {}^{i}f\cdot {}^{j}\dot{f}\cdot {}^{l}\dot{f}\cdot {}^{k}f\,ds \\
{}^{ijkl}\kappa_{SH\,6} &= \int_s G\cdot t\cdot {}^{i}f\cdot {}^{j}\dot{f}\cdot {}^{l}\dot{u}\cdot {}^{k}u\,ds \\
{}^{ijk}\kappa_{SH\,7} &= \int_s G\cdot t\cdot {}^{i}u\cdot {}^{j}\dot{u}\cdot\left({}^{k}\dot{u}+{}^{k}f_s\right)ds \\
{}^{ijkl}\kappa_{SH\,8} &= \int_s G\cdot t\cdot {}^{i}u\cdot {}^{j}\dot{u}\cdot {}^{l}\dot{f}\cdot {}^{k}f\,ds \\
{}^{ijkl}\kappa_{SH\,9} &= \int_s G\cdot t\cdot {}^{i}u\cdot {}^{j}\dot{u}\cdot {}^{l}\dot{u}\cdot {}^{k}u\,ds\,.
\end{aligned}
\qquad (2.108,\ \text{a-i})
$$

It is worth recalling that all of the above expressions are computed taking into consideration the expressions of the displacements for mode *k* at plate *i* (Schardt 1989) presented above – see expressions (2.28), (2.29) and (2.30).

2.3.4. The potential energy of the external loading

The potential of the external loading is given, in general, by

$$
\begin{aligned}
\Pi = &\int_L \sum_{k=1}^{n_{MD}}\sum_{r=1}^{n_{NT}}\left\{q_{y,r}(x)\,{}^{k}v_r + q_{z,r}(x)\,{}^{k}w_r\right\}{}^{k}A\,dx + \int_L \sum_{k=1}^{n_{MD}}\sum_{r=1}^{n_{NT}}\left\{-q_{x,r}(x)\,{}^{k}u_r\right\}{}^{k}A'\,dx + \\
&+ P\times {}^{1}A'\Big|_{x=x_1} + \sum_{k=2}^{n_{MD}}\left({}^{k}v_{\bar{r}}\,F_y + {}^{k}w_{\bar{r}}\,F_z\right){}^{k}A\Big|_{x=x_2} + {}^{2}M\,{}^{2}A'\Big|_{x=x_3} + {}^{3}M\,{}^{3}A'\Big|_{x=x_3}\,,
\end{aligned}
\qquad (2.109)
$$

where $q_{y,r}(x)$, $q_{z,r}(x)$ and $q_{x,r}(x)$ denote general longitudinally distributed loads applied at node *r* in the *y*, *z* and *x* directions, respectively, *P* denotes an axial force applied at $x = x_1$, *F* is a concentrated force in the cross section plane applied at $x = x_2$ and with vertical and horizontal components F_y and F_z. ${}^{2}M$ and ${}^{3}M$ denote the components of an applied bending moment at $x = x_3$ with respect to the principal cross section axes.

2.3.5 The total potential energy

Combining equations (2.104), (2.106) and (2.109) yields the total potential energy function:

$$
\begin{aligned}
V = &\sum_{i=1}^{n_{MD}}\sum_{k=1}^{n_{MD}}\frac{1}{2}\int_0^L \left({}^{ik}C^M + {}^{ik}C^B\right){}^{i}A''\,{}^{k}A''\,dx + \sum_{i=1}^{n_{MD}}\sum_{k=1}^{n_{MD}}\frac{1}{2}\int_0^L \left({}^{ik}D_1 + {}^{ik}D_3\right){}^{i}A'\,{}^{k}A'\,dx + \\
&+\frac{1}{2}\sum_{i=1}^{n_{MD}}\sum_{k=1}^{n_{MD}}\int_0^L {}^{ik}D_2\,{}^{i}A\,{}^{k}A''\,dx + \frac{1}{2}\sum_{i=1}^{n_{MD}}\sum_{k=1}^{n_{MD}}\int_0^L {}^{ik}D_{2T}\,{}^{i}A''\,{}^{k}A\,dx + \frac{1}{2}\sum_{i=1}^{n_{MD}}\sum_{k=1}^{n_{MD}}\int_0^L {}^{ik}B\,{}^{i}A\,{}^{k}A\,dx + \\
&+\frac{1}{4}\sum_{i=1}^{n_{MD}}\sum_{k=1}^{n_{MD}}\sum_{l=1}^{n_{MD}}\int_L {}^{ikl}\kappa_{\sigma 2}\,{}^{i}A''\,{}^{k}A'\,{}^{l}A'\,dx + \frac{1}{4}\sum_{i=1}^{n_{MD}}\sum_{j=1}^{n_{MD}}\sum_{k=1}^{n_{MD}}\int_L {}^{ijk}\kappa_{\sigma 3}\,{}^{i}A'\,{}^{j}A'\,{}^{k}A''\,dx + \\
&+\frac{1}{8}\sum_{i=1}^{n_{MD}}\sum_{j=1}^{n_{MD}}\sum_{k=1}^{n_{MD}}\sum_{l=1}^{n_{MD}}\int_L {}^{ijkl}\kappa_{\sigma 4}\,{}^{i}A'\,{}^{j}A'\,{}^{k}A'\,{}^{l}A'\,dx + \frac{1}{2}\sum_{i=1}^{n_{MD}}\sum_{k=1}^{n_{MD}}\sum_{l=1}^{n_{MD}}\int_L {}^{ikl}\kappa_{SH2}\,{}^{i}A'\,{}^{k}A'\,{}^{l}A\,dx + \\
&+\frac{1}{2}\sum_{i=1}^{n_{MD}}\sum_{k=1}^{n_{MD}}\sum_{l=1}^{n_{MD}}\int_L {}^{ikl}\kappa_{SH3}\,{}^{i}A'\,{}^{k}A''\,{}^{l}A'\,dx + \frac{1}{2}\sum_{i=1}^{n_{MD}}\sum_{j=1}^{n_{MD}}\sum_{k=1}^{n_{MD}}\int_L {}^{ijk}\kappa_{SH4}\,{}^{i}A'\,{}^{j}A\,{}^{k}A'\,dx + \\
&+\frac{1}{2}\sum_{i=1}^{n_{MD}}\sum_{j=1}^{n_{MD}}\sum_{k=1}^{n_{MD}}\sum_{l=1}^{n_{MD}}\int_L {}^{ijkl}\kappa_{SH5}\,{}^{i}A'\,{}^{j}A\,{}^{k}A'\,{}^{l}A\,dx + \\
&+\frac{1}{2}\sum_{i=1}^{n_{MD}}\sum_{j=1}^{n_{MD}}\sum_{k=1}^{n_{MD}}\sum_{l=1}^{n_{MD}}\int_L {}^{ijkl}\kappa_{SH6}\,{}^{i}A'\,{}^{j}A\,{}^{k}A''\,{}^{l}A'\,dx + \\
&+\frac{1}{2}\sum_{i=1}^{n_{MD}}\sum_{j=1}^{n_{MD}}\sum_{k=1}^{n_{MD}}\int_L {}^{ijk}\kappa_{SH7}\,{}^{i}A''\,{}^{j}A'\,{}^{k}A'\,dx + \frac{1}{2}\sum_{i=1}^{n_{MD}}\sum_{j=1}^{n_{MD}}\sum_{k=1}^{n_{MD}}\sum_{l=1}^{n_{MD}}\int_L {}^{ijkl}\kappa_{SH8}\,{}^{i}A''\,{}^{j}A'\,{}^{k}A'\,{}^{l}A'\,dx + \\
&+\frac{1}{2}\sum_{i=1}^{n_{MD}}\sum_{j=1}^{n_{MD}}\sum_{k=1}^{n_{MD}}\sum_{l=1}^{n_{MD}}\int_L {}^{ijkl}\kappa_{SH9}\,{}^{i}A''\,{}^{j}A'\,{}^{k}A''\,{}^{l}A'\,dx - \\
&-\int_L \sum_{k=1}^{n_{MD}}\sum_{r=1}^{n_{NT}}\left\{q_{y,r}(x)\,{}^{k}v_r + q_{z,r}(x)\,{}^{k}w_r\right\}{}^{k}A\,dx - \int_L \sum_{k=1}^{n_{MD}}\sum_{r=1}^{n_{NT}}\left\{-q_{x,r}(x)\,{}^{k}u_r\right\}{}^{k}A'\,dx - \\
&-P\times {}^{1}A'\Big|_{x=x_1} - \sum_{k=2}^{n_{MD}}\left({}^{k}v_{\bar{r}}\,F_y + {}^{k}w_{\bar{r}}\,F_z\right){}^{k}A\Big|_{x=x_2} - {}^{2}M\,{}^{2}A'\Big|_{x=x_3} - {}^{3}M\,{}^{3}A'\Big|_{x=x_3}. \qquad (2.110)
\end{aligned}
$$

2.4 – The particular case of a simply supported compressed column

2.4.1. Introduction

In order to illustrate the application of the general formulation derived above the Rayleigh-Ritz method will be used, approximating the modal amplitude functions ${}^{k}A(x)$ by a set of coordinate functions ${}^{k}A_i(x)$, as shown in equation (2.111):

$$ {}^{k}A(x) \approx {}^{k}a_1 {}^{k}\varphi_1(x) + {}^{k}a_2 {}^{k}\varphi_2(x) + {}^{k}a_3 {}^{k}\varphi_3(x) + \ldots, \qquad (2.111) $$

where the coordinate functions ${}^{k}\varphi_i(x)$ must respect the cinematic boundary conditions and the coordinates ${}^{k}a_i$ become the unknowns of the problem (in Chapter 5 a deeper analysis on the Rayleigh-Ritz method will be presented). Concentrating, at the present stage, on the application to an open or closed simply supported compressed column with flexible end plates, a suitable and usual approximation consists of sinusoidal amplitude functions given by:

$$ \text{mode1: } {}^{1}A(x) \approx {}^{1}a \frac{x^2 \sqrt{5}}{L^{5/2}} \qquad (2.112, \text{a-b}) $$

$$ \text{remaining modes: } {}^{k}A(x) \approx {}^{k}a \sin \frac{\pi x}{L} \quad \text{for } k=2,\ldots, n_{MD}, $$

${}^{1}a$ and ${}^{k}a$ being the unknown degrees-of-freedom. It is noted that the approximation function for the first mode of deformation is not sinusoidal in order to allow for constant axial force along the length of the member – below, in Chapter 3, the choice of the adequate coordinate functions will be object of deeper analysis and it is noticed here that other boundary conditions or different loading cases follow identical procedures, given an adequate choice of amplitude functions. For this particular case of a compressed column, the potential of the external loads is simply given by

$$ \Pi = P \times {}^{1}A' \big|_{x=L}, \qquad (2.113) $$

so that substitution of equations (2.112 a-b) into the total potential energy function (2.110)

and integration along the length yields:

$$V = V_1\ {}^1a + V_{11}\ {}^1a^2 + \sum_{i=2}^{n_{MD}} V_{ii}\ {}^ia^2 + \sum_{i=2}^{n_{MD}}\sum_{j=2}^{n_{MD}} V_{ij}\ {}^ia\ {}^ja +$$

$$+ \sum_{i=2}^{n_{MD}}\sum_{j=2}^{n_{MD}} \left(V_{1ij}\ {}^1a\ {}^ia\ {}^ja + V_{11ij}\ {}^1a^2\ {}^ia\ {}^ja \right) + \sum_{i=2}^{n_{MD}}\sum_{j=2}^{n_{MD}}\sum_{k=2}^{n_{MD}} \left(V_{ijk}\ {}^ia\ {}^ja\ {}^ka + V_{1ijk}\ {}^1a\ {}^ia\ {}^ja\ {}^ka \right) +$$

$$+ \sum_{i=2}^{n_{MD}}\sum_{j=2}^{n_{MD}}\sum_{k=2}^{n_{MD}}\sum_{l=2}^{n_{MD}} V_{ijkl}\ {}^ia\ {}^ja\ {}^ka\ {}^la\,. \qquad (2.114)$$

where

$$V_1 = -P\frac{2\sqrt{5}}{L^{3/2}}$$

$$V_{11} = \frac{10}{L^4}{}^1C$$

$$V_{ii} = \frac{\pi^4}{4L^3}\left({}^iC^M + {}^iC^B\right) + \frac{L}{4}\,{}^iB + \frac{\pi^2}{4L}\left({}^{ii}D_1 + {}^{ii}D_3\right) - \frac{\pi^2}{4L}\left({}^{ii}D_2 + {}^{ii}D_{2T}\right)$$

$$V_{\substack{ij \\ i\neq j}} = \frac{\pi^2}{4L}\left({}^{ij}D_1 + {}^{ij}D_3\right) - \frac{\pi^2}{4L}\left({}^{ij}D_2 + {}^{ij}D_{2T}\right)$$

$$V_{1ij} = \frac{\pi^2\sqrt{5}}{4L^{7/2}}\left({}^{1ij}\kappa_{\sigma 2} + {}^{ij1}\kappa_{\sigma 3}\right) - \frac{\pi^2\sqrt{5}}{2L^{7/2}}\left({}^{ij1}\kappa_{SH3} + {}^{i1j}\kappa_{SH7}\right) \qquad (2.115,\ \text{a-i})$$

$$V_{ijk} = -\frac{\pi^3}{6L^3}\left({}^{ijk}\kappa_{\sigma 2} + {}^{ijk}\kappa_{\sigma 3}\right) + \frac{\pi}{3L}\left({}^{ijk}\kappa_{SH2} + {}^{ijk}\kappa_{SH4}\right) - \frac{\pi^3}{3L^3}\left({}^{ijk}\kappa_{SH3} + {}^{ijk}\kappa_{SH7}\right)$$

$$V_{11ij} = \frac{5\pi^2}{L^6}\ {}^{1i1j}\kappa_{SH9}$$

$$V_{1ijk} = \frac{2\pi\sqrt{5}}{3L^{7/2}}\left({}^{ij1k}\kappa_{SH6}\right) - \frac{2\pi^3\sqrt{5}}{3L^{11/2}}\left({}^{1ijk}\kappa_{SH9} + {}^{ij1k}\kappa_{SH9}\right)$$

$$V_{ijkl} = \frac{3\pi^4}{64L^3}\ {}^{ijkl}\kappa_{\sigma 4} + \frac{\pi^2}{16L}\ {}^{ijkl}\kappa_{SH5} - \frac{\pi^4}{16L^3}\ {}^{ijkl}\kappa_{SH6} - \frac{\pi^6}{16L^5}\ {}^{ijkl}\kappa_{SH9}\,,$$

with $i, j, k, l \geq 2$. It is noted that, in the case of a compressed column, all terms in ${}^{ijkl}\kappa_{SH8}$ vanish upon integration.

2.4.2. Equilibrium equations

Differentiating the total potential energy function (2.114) with respect to the several degrees of freedom yields the equilibrium equations of the system (Thompson & Hunt 1973). Specifically, for $i=1$, yields

$$\frac{\partial V}{\partial {}^{1}a} = V_1 + 2V_{11}\ {}^{1}a + \sum_{i=2}^{n_{MD}}\sum_{j=2}^{n_{MD}}\left(V_{1ij}\ {}^{i}a\ {}^{j}a + 2V_{11ij}\ {}^{1}a\ {}^{i}a\ {}^{j}a\right) +$$

$$+\sum_{i=2}^{n_{MD}}\sum_{j=2}^{n_{MD}}\sum_{k=2}^{n_{MD}} V_{1ijk}\ {}^{i}a\ {}^{j}a\ {}^{k}a = 0\,, \tag{2.116}$$

while for the remaining degrees of freedom $(i \geq 2)$,

$$\frac{\partial V}{\partial {}^{i}a} = 2V_{ii}\ {}^{i}a + \sum_{\substack{j=2\\ i\neq j}}^{n_{MD}}\left(V_{ij}+V_{ji}\right){}^{j}a + \sum_{j=2}^{n_{MD}}\left[\left(V_{1ij}+V_{1ji}\right)\ {}^{1}a\ {}^{j}a + \left(V_{11ij}+V_{11ji}\right)\ {}^{1}a^{2}\ {}^{j}a\right] +$$

$$+\sum_{j=2}^{n_{MD}}\sum_{k=2}^{n_{MD}}\left[\left(V_{ijk}+V_{jik}+V_{kji}\right)\ {}^{j}a\ {}^{k}a + \left(V_{1ijk}+V_{1jik}+V_{1kji}\right)\ {}^{1}a\ {}^{j}a\ {}^{k}a\right] +$$

$$+\sum_{j=2}^{n_{MD}}\sum_{k=2}^{n_{MD}}\sum_{l=2}^{n_{MD}}\left[\left(V_{ijkl}+V_{jikl}+V_{kjil}+V_{ljki}\right)\ {}^{j}a\ {}^{k}a\ {}^{l}a\right] = 0\,. \tag{2.117}$$

Equation (2.116) can be solved with respect to ${}^{1}a$, giving

$${}^{1}a = \frac{-V_1 - \sum_{i=2}^{n_{MD}}\sum_{j=2}^{n_{MD}} V_{1ij}\ {}^{i}a\ {}^{j}a - \sum_{i=2}^{n_{MD}}\sum_{j=2}^{n_{MD}}\sum_{k=2}^{n_{MD}} V_{1ijk}\ {}^{i}a\ {}^{j}a\ {}^{k}a}{2V_{11} + 2\sum_{i=2}^{n_{MD}}\sum_{j=2}^{n_{MD}} V_{11ij}\ {}^{i}a\ {}^{j}a} \tag{2.118}$$

or, in the case of an open cross section,

$${}^{1}a = \frac{-V_1 - \sum_{i=2}^{n_{MD}}\sum_{j=2}^{n_{MD}} V_{1ij}\ {}^{i}a\ {}^{j}a}{2V_{11}}\,, \tag{2.119}$$

because of the inexistence of a shear flow.

2.4.3. Pre-buckling solution and sliding coordinate transformation

Equations (2.116) and (2.117) yield a pre-buckling (fundamental) solution defined by

$$ {}^{1}a_F = -\frac{V_1}{2V_{11}}, \quad {}^{i}a_F = 0 \text{ for } i = 2,\ldots,n_{MD}. \tag{2.120} $$

In order to simplify further calculations, it is worth applying a sliding coordinate transformation (Thompson & Hunt 1973):

$$ {}^{i}a = {}^{i}a_F + {}^{i}q,\ i = 1,\ldots,n_{MD} \tag{2.121} $$

to yield a trivial fundamental solution:

$$ {}^{i}q = 0,\ i = 1,\ldots,n_{MD}. \tag{2.122} $$

The resulting total potential energy function, now denoted by W, is given by

$$ W = W_0 + W_{11}\,{}^{1}q^2 + \sum_{i=2}^{n_{MD}}\sum_{j=2}^{n_{MD}}\left(W_{ij}\,{}^{i}q\,{}^{j}q + W_{1ij}\,{}^{1}q\,{}^{i}q\,{}^{j}q + W_{11ij}\,{}^{1}q^2\,{}^{i}q\,{}^{j}q\right) + $$

$$ + \sum_{i=2}^{n_{MD}}\sum_{j=2}^{n_{MD}}\sum_{k=2}^{n_{MD}}\left(W_{ijk}\,{}^{i}q\,{}^{j}q\,{}^{k}q + W_{1ijk}\,{}^{1}q\,{}^{i}q\,{}^{j}q\,{}^{k}q\right) + \sum_{i=2}^{n_{MD}}\sum_{j=2}^{n_{MD}}\sum_{k=2}^{n_{MD}}\sum_{l=2}^{n_{MD}}\left(W_{ijkl}\,{}^{i}q\,{}^{j}q\,{}^{k}q\,{}^{l}q\right) \tag{2.123} $$

where

$$ W_0 = -\frac{V_1^2}{4V_{11}} $$

$$ W_{11} = V_{11} $$

$$ W_{ij} = \begin{cases} \text{if } i = j,\ W_{ii} = V_{ii} + V_{11ii}\dfrac{V_1^2}{4V_{11}^2} - V_{1ii}\dfrac{V_i}{2V_{11}} \\ \text{if } i \neq j,\ W_{ij} = V_{ij} + V_{11ij}\dfrac{V_1^2}{4V_{11}^2} - V_{1ij}\dfrac{V_i}{2V_{11}} \end{cases} $$

$$ W_{1ij} = V_{1ij} - \frac{V_{11ij}V_1}{V_{11}} \tag{2.124, a-h} $$

$$ W_{ijk} = V_{ijk} - \frac{V_{1ijk}V_1}{2V_{11}} $$

$$W_{1ijk} = V_{1ijk}$$

$$W_{11ij} = V_{11ij}$$

$$W_{ijkl} = V_{ijkl} .$$

2.4.4. Eigenvalue analysis

The critical loads of the compressed column are now easily evaluated by setting to zero the determinant of the Hessian matrix of the total potential energy function, evaluated along the fundamental path of the system (Thompson & Hunt 1973):

$$\det\left(\boldsymbol{H}_{\boldsymbol{F}}\right) = \left| \left. \frac{\partial^2 W}{\partial^{\,i} q \, \partial^{\,j} q} \right|_F \right| = \begin{vmatrix} 2W_{11} & 0 & 0 & \cdots & 0 \\ & 2W_{22} & W_{23}+W_{32} & \cdots & W_{2n_{MD}}+W_{n_{MD}2} \\ & & 2W_{33} & \cdots & W_{3n_{MD}}+W_{n_{MD}3} \\ & \text{Symmetric} & & \ddots & \vdots \\ & & & & 2W_{n_{MD}n_{MD}} \end{vmatrix} = 0 \tag{2.125}$$

Analysing equation (2.125) the following conclusions can be drawn:

i) the first row and the first column have all terms equal to zero with the exception of the term ${}^{11}H_F$, which is not dependant of *P*; so, when finding the roots of the determinant $\boldsymbol{H}_{\boldsymbol{F}}$, only the submatrix formed by the last $(n_{MD} - 1)$ rows and columns shall be considered;

ii) for closed cross sections, the terms W_{ij}, for $i=j$ and $i \neq j$, in the $V_{11ij}\frac{V_1^2}{4V_{11}^2}$ part, contain a quadratic factor in P, which is dependent of coefficient ${}^{11ij}\kappa_{SH9}$; so, for closed section members only, if third order coefficients are taken into account for the determination of the critical loads, a non-linear eigenvalue problem will occur (Mirasso & Godoy 1992) – this fact will have a small influence for the value of the critical loads, so in the example presented below, only second order terms will be considered for the closed cross section;

iii) for open or closed cross sections, the terms W_{ij}, for $i = j$ and $i \neq j$, contain, in general, a linear term in P in the part $V_{1ij}\frac{V_i}{2V_{11}}$, so all coefficients for $i, j \geq 2$ will have a constant part and a linear part in P – thus the eigenvalue problem is established.

Regarding the first conclusion above, the eigenvalue-eigenvector problem will have dimension $(n_{MD}-1)$, since coordinate ${}^1q$ will always be passive. From the third conclusion, the shape of any term (i, j) of $\boldsymbol{H}_F$, for any $i, j \geq 2$, is ${}^{ij}H_0 + {}^{ij}H_1 P$, and the generalized eigenproblem can be established in the form (Hangai & Kawamata 1972):

$$\left(\boldsymbol{H}_o + P \cdot \boldsymbol{H}_1\right)\boldsymbol{q} = 0, \tag{2.126}$$

being the non-zero terms in the eigenvectors $\boldsymbol{q}$, if properly normalized, regarded as the "participation" of their relative mode of deformation in the overall buckling – note that in this particular case each coordinate ${}^iq$ is related to a specific mode of deformation.

2.5 – Chapter synopsis

This chapter starts by presenting a brief overview of the Schardt's GBT scheme for the analysis of thin-walled open or closed cross section members, in terms of the establishment of the modes of deformation, their orthogonalization and the Schardt's approach to stability analysis. Afterwards, the Schardt's GBT scheme was developed through the frame of a consistent energy formulation, eliminating inconsistencies in the former theories and enabling the Schardt's GBT theory to analyse open or closed sections submitted to a general loading in the buckling and in the post-buckling ranges. Finally, a theoretical application to the stability analysis was realized. The developments of this chapter are based on several contributions of the author to scientific journals (Simões da Silva and Simão 2002 and Simão and Simões da Silva 2004a) and to international scientific conferences (Simão and Simões da Silva 2002, 2003a and 2003b).

3 – NUMERICAL SOLUTION STRATEGIES FOR BUCKLING AND POST-BUCKLING ANALYSIS

3.1 – Introduction

The previous chapter introduced an energy formulation for the GBT non-linear analysis of thin-walled prismatic members, deriving a functional in the yet unknown modal amplitude functions ${}^{k}A(x)$ and in the load parameter P, for the modelling of the geometrically non-linear behaviour of the structural member. In this chapter, the numerical strategies used to perform the GBT energy analysis of a prismatic thin-walled member subjected to any conservative loading and to a wide range of supporting conditions, are presented in the context of the derived energy formulation and the classical stability theory for discrete systems (Hunt 1981, Thompson and Hunt 1973 and 1984). These numerical strategies comprehend two distinct parts: i) the discretization of the energy functional and the corresponding integration along the member's length, in order to turn the energy functional into a gradient potential function in a set of discrete coordinates ${}^{k}a$ and the load parameter P, and ii) the establishment and solution of the member's equilibrium system, now expressed in terms of a finite set of discrete generalized coordinates and a control parameter.

The first part develops a discretization procedure for the member's TPE in the context of the Rayleigh-Ritz method (RRM) for which, instead of the commonly used trigonometric functions, each amplitude modal function ${}^{k}A(x)$ is approximated by a set of normalized orthogonal polynomials derived directly from the relevant modal boundary conditions. This procedure presents several advantages when compared to the traditional use of trigonometric functions, as follows:

i) Since the coordinate functions are computed from the boundary conditions, the computed functions can model a wider range of boundary conditions and the user can choose, among all boundary conditions that apply to the problem, those that shall be taken into account – note that the RRM requires only to account for all cinematic (forced) boundary conditions, and, in some occasions, it ca be advantageous to neglect some static (natural) conditions in terms of the completeness of the set of trial functions, as it will be seen below.

ii) The use of orthonormal polynomials as coordinate functions leads to smoother approximations for the stresses and displacements, due to the continuity of any order derivative of the polynomials and also to the fact that no additional orthogonality conditions are added to the problem than those required by the method, whereas the use of trigonometric functions always carries the introduction of orthogonality conditions between the coordinate functions themselves and also between their derivatives.

iii) The polynomials can form a complete set of trial functions – it is seen below that it suffices to withdraw the natural boundary conditions.

iv) The scheme enables fast convergence, owing to the orthogonality between the polynomials, and favours easy integrations that can be made through a matrix procedure.

The scheme proposed here uses one-dimensional polynomials only, since it is devoted to the GBT analysis; nevertheless, it may be generalized to *n*-dimensional problems with little adaptations, thus generating polynomials in *n* variables. All in all, by defining the coordinate functions this way, a sequential scheme to build an infinite-dimensional orthogonal complete base for the vector space of the coordinate functions that respect the considered boundary conditions is created for the problem under observation, keeping the problem as general as possible and improving the convergence speed of the

solution procedure. At the end of the first part, an integration procedure is proposed that benefits from the use of polynomials as coordinate functions, performing the integration in a matricial form, deriving directly the gradient potential function.

The second part of the chapter concerns the stability analysis of the thin-walled structural straight members. It is known, from the classical references on this subject (see, for example, Croll and Walker 1972), that most of these mechanical systems, submitted to axial or bending forces, exhibit bifurcational behaviour. Hence a numerical tool is needed that: i) computes equilibrium paths derived from an already known equilibrium state, ii) enables the search and analysis of critical points along the already known equilibrium path, determining whether they are bifurcational points or not, and if the corresponding equilibrium state is stable or not, and iii) searches alternative equilibrium points in the neighbourhood of the computed critical point and outside the initial (primary) equilibrium path, respecting the bifurcational formalism and analysing the stability of the found non-trivial equilibrium state. The scheme presented below is adapted from the traditional nonlinear stability theory for discrete systems developed by Hunt and Thompson (Hunt 1981, Thompson and Hunt 1973 and 1984). The stability procedures due to these authors use perturbation techniques (Murdock 1999) to deal with the bifurcation phenomena, which become very heavy if a large number of coordinates is required by the analysis. The procedure presented below, devoted to perfect structures – hence not requiring the use of imperfections to overcome bifurcation points and thus enabling a full comprehension on the involved bifurcation phenomena – can be viewed as a numerical approach to the classical stability procedures, adapted for the use of the advanced symbolic programming software MATHEMATICA (Wolfram 2003), and is based in as few concepts as possible: the definition of an equilibrium point and the analysis of the stability of an equilibrium state.

Finally, a description of the software developed to perform the post-buckling analysis is presented, aimed at organizing the concepts previously explained and showing how they connect in order to perform a buckling and post-bucking analysis.

3.2 – The application of the Rayleigh-Ritz method – the use of polynomial coordinate functions

3.2.1 The derivation of the coordinate functions and the natural discretization

In the previous chapter, in the context of GBT, the thin-walled structural member's behaviour is described by its total potential energy V, which is a functional in the n_{MD} amplitude modal functions ${}^{k}A(x)$ and their first two derivatives, all yet unknown, together with a unique control parameter P that measures the magnitude of the applied loading system that appears in a linear form – hence the designation of specialized system – in the following form:

$$V = \int_0^L F\left[{}^{k}A(x), {}^{k}A'(x), {}^{k}A''(x), P\right] dx\,,\ k = 1,\ldots,n_{MD}\,. \tag{3.1}$$

Expression (3.1) shall be transformed into a gradient potential function that depends on a finite set of discrete generalized coordinates ${}^{i}a$ and the scaling factor P,

$$V = V\left({}^{i}a, P\right),\ i = 1,\ldots,n_C\,, \tag{3.2}$$

so that the stability procedures may be applied (Hunt 1981, Thompson and Hunt 1973 and 1984). This process comprehends two distinctive parts: the discretization, presented below, and the integration, described subsequently.

The discretization is performed in the context of the Rayleigh-Ritz Method (Richards 1977), by approximating each amplitude modal function ${}^{k}A(x)$ by a finite set of pre-established coordinate functions ${}^{k}\varphi_i(x)$, previously defined along the member's length – in mathematical notation along the closed interval $[0, L]$ – as follows:

$${}^{k}A(x) = {}^{k}a_1\,{}^{k}\varphi_1(x) + {}^{k}a_2\,{}^{k}\varphi_2(x) + \ldots + {}^{k}a_{n_k}\,{}^{k}\varphi_{n_k}(x), \tag{3.3}$$

where n_k is the number of adopted coordinate functions for the amplitude function of mode k. The coefficients ${}^{k}a_i$ become the unknowns of the problem and are henceforth denoted

generalized coordinates.

Trigonometric functions, usually sinusoidal ones, are commonly adopted as coordinate functions, but they exhibit several disadvantages, as already mentioned: they carry several difficulties in the computational treatment, for example their integration can be very heavy if several half-waves are used, need a complex treatment to model more peculiar boundary conditions, and the use of polynomials provides smoother approximations for the longitudinal variation of the displacements (Prola 2001). Also, it has been observed experimentally (Young and Rasmussen 1998) that the boundary conditions can influence the buckling behaviour of thin-walled compressed channel columns more that the mere change of the effective member's length.

For practical GBT applications the boundary conditions can be considered mode by mode and, without loss of generality, can be considered as homogeneous (Richards 1977), in the following form:

$$ {}^{k}A^{(i)}\Big|_{x=\bar{x}} = 0 , \tag{3.4}$$

where $\bar{x}$ refers to a specific value of x inside $[0,L]$, usually 0 or L, and superscript (i) refers to the i^{th} derivative of ${}^{k}A$. These boundary conditions can be either cinematic (forced) or static (natural) but, in the context of the RRM, the adopted coordinate functions ${}^{k}\varphi_i$ must respect only the cinematic boundary conditions. If, in addition, the coordinate functions respect also the static boundary conditions, usually but not always convergence is improved, in the sense that less coordinate functions are needed to achieve the intended precision. So, the efficiency of this method depends strongly on the correct choice of the coordinate functions, as emphasized by Richards (1977), and the choice of orthonormal functions ${}^{k}\varphi_i$ over the member's length, defined by (Courant and Hilbert 1953):

$$ \int_L {}^{k}\varphi_i \; {}^{k}\varphi_j \, dx = \begin{cases} c \text{ if } i = j \\ 0 \text{ if } i \neq j \end{cases} , \tag{3.5}$$

accelerates the convergence of the method. In expression (3.5), the first condition is a

normalization rule, where c is a real positive constant usually taken equal to *1* or to the member's length L. Alternatively, the normalizing condition of expression (3.5) can also be written as (Singh and Chakraverty 1992):

$$\sqrt{\int_L {}^k\varphi_i \, {}^k\varphi_i \, dx} = c, \tag{3.6}$$

whereas the second condition constitutes an orthogonality condition. Grouping together the boundary conditions for each mode of deformation, a homogeneous system is obtained, and it has a trivial solution of no numerical interest. However, if the normalizing condition of expression (3.5) is added, the resulting system is no longer homogeneous and becomes the basis of a sequential procedure that generates a set of appropriate coordinate functions for the mode of deformation k in the following way.

To initiate the procedure, assume that the first coordinate function for a general mode k is given by the following polynomial

$${}^k\varphi_1 = a_{1,0} + a_{1,1}\, x + \ldots + a_{1,n_k}\, x^{n_{BC,k}} \tag{3.7}$$

where the $a_{1,0},\ldots,a_{1,n_{BC,k}}$ are yet unknown coefficients and $n_{BC,k}$ is the number of boundary conditions that apply to mode of deformation k. Obviously, the set of the considered boundary conditions must contain all the cinematic ones, but there is freedom to choose, among the static conditions, those, if any, that shall be considered in the procedure. The $n_{BC,k}$ chosen boundary conditions are then used sequentially to define the first $n_{BC,k}$ coefficients of the polynomial, $a_{1,0},\ldots,a_{1,n_{BC,k}-1}$, as a linear function of the highest order coefficient of the polynomial $a_{1,n_{BC,k}}$:

$$a_{1,0} = a_{1,0}\left(a_{1,n_{BC,k}}\right),\ldots,\, a_{1,n_{BC,k}-1} = a_{1,n_{BC,k}-1}\left(a_{1,n_{BC,k}}\right) \tag{3.8}$$

Subsequently, the normalization condition of expression (3.5) gives a simple quadratic equation in $a_{1,n_{BC,k}}$:

$$\int_0^L \left[{}^k\varphi_1\left(a_{1,n_{BC,k}}, x\right)\right]^2 dx = c, \tag{3.9}$$

that can be easily solved, thus obtaining two symmetrical roots, the positive one being retained. Polynomial (3.7) is now completely defined and the determination of the second polynomial can start right away. It is important to point out at this stage that choosing the arbitrary positive constant c of the orthogonality condition in (3.5) equal to one will usually lead to polynomials that take very small values for long members. This can be avoided by normalizing the coordinate function with respect to the member's length L or to L^2, instead of unity. By doing this, the resulting polynomial shows more reasonable values along the member's length, independently of its value – below the influence of the normalization factor on the integrals and functional values along the member's length will be illustrated for a specific function.

The second coordinate polynomial is now set up in the form:

$$ {}^{k}\varphi_2 = a_{2,0} + a_{2,1}\,x + \ldots + a_{2,n_k}\,x^{n_k} + a_{2,n_{BC,k}+1}\,x^{n_{BC,k}+1}, \tag{3.10} $$

i.e., it is established in the same way as the first polynomial but is one order higher. Like the previous polynomial, the n_k boundary conditions are used sequentially to determine all the $a_{2,0},\ldots,a_{2,n_{BC,k}-1}$ as linear functions of $a_{2,n_{BC,k}}$ and $a_{2,n_{BC,k}+1}$, the (unknown) coefficients of the higher order parts:

$$ a_{2,0} = a_{2,0}\left(a_{2,n_{BC,k}}, a_{2,n_{BC,k}+1}\right), \ldots, a_{2,n_{BC,k}-1} = a_{2,n_{BC,k}-1}\left(a_{2,n_{BC,k}}, a_{2,n_{BC,k}+1}\right). \tag{3.11} $$

Next, imposing the orthogonality condition between ${}^{k}\varphi_1$ (already known) and ${}^{k}\varphi_2$ in the form:

$$ \int_0^L \left[{}^{k}\varphi_1(x) \times {}^{k}\varphi_2\left(a_{2,n_{BC,k}}, a_{2,n_{BC,k}+1}, x\right)\right] d\,x = 0\,, \tag{3.12} $$

yields coefficient $a_{2,n_{BC,k}}$ as a function of coefficient $a_{2,n_{BC,k}+1}$:

$$ a_{2,n_{BC,k}} = a_{2,n_{BC,k}}\left(a_{2,n_{BC,k}+1}\right). \tag{3.13} $$

Finally, coefficient $a_{2,n_{BC,k}+1}$ is determined by choosing the positive root of the normalization condition for ${}^{k}\varphi_2$ along the member's length:

$$\int_0^L \left[{}^k\varphi_2\left(a_{2,n_{BC,k}+1}, x\right)\right]^2 d\,x = c\,, \tag{3.14}$$

The process may be repeated as many times as needed, providing an infinite set of functions suitable to approximate the unknown amplitude modal function ${}^k A(x)$.

This calculation is sequential and can be used indefinitely, bringing a set of orthonormal polynomials over the member's length that respect the adopted boundary conditions since they are derived from them, hence the designation "natural discretization". Therefore, these polynomials are appropriate to be used as coordinate functions in the context of the Rayleigh-Ritz method, since they full fill all the applicable requirements for the set of appropriate coordinate functions (Storch and Strang 1988):

i) they satisfy the cinematic/forced boundary conditions of the mode, being optional their obedience to the static/natural boundary conditions;

ii) they are linearly independent along the problem's domain, i.e., for any set of *n* coordinate functions ${}^k\varphi_i(x)$ the relation

$$\sum_{i=1}^{n} {}^i a\ {}^k\varphi_i(x) = 0 \tag{3.15}$$

holds if and only if

$${}^i a = 0\,,\ \forall\, x \in \left]\, 0, L\, \right[, \tag{3.16}$$

which is equivalent to say that none of the functions ${}^k\varphi_i(x)$ can be obtained as a linear combination of the remaining ones, along the problem's domain – in the present case they are not only linearly independent but they are orthogonal;

iii) the functions ${}^k\varphi_i(x)$ form a complete set of functions; in other words, the function

$${}^k A_n(x) = \sum_{i=1}^{n} {}^i a\ {}^k\varphi_i(x) \tag{3.17}$$

converges to any admissible function ${}^{k}A(x)$ in $[0, L]$ as the number of trial functions increases, or, in other words, the following expression holds:

$$\lim_{n\to\infty} \int_0^L \left[{}^{k}A(x) - {}^{k}A_n(x)\right]^2 dx = 0 . \tag{3.18}$$

By adopting the polynomial coordinate functions derived through the scheme presented above, it is intended that the Rayleigh-Ritz method converges to the correct solution of the system of differential equations as fast as possible, i.e., using as few coordinate functions as possible. This is achieved without loss of generality since the computed set of allowable polynomial coordinate functions is infinite and complete along the member's length, paying attention to the first Weierstrass' approximation theorem, which states that any function defined along an interval in $\mathbb{R}$ can be approximated as closely as desired by a polynomial (Nathanson 1964) – this theorem proves that expression (3.18) applies to the set of orthonormal polynomials derived through the scheme presented just above.

Finally it is worth referring that the static boundary conditions are considered here in a linear form, thus resulting in simple expressions for each mode in the form of (3.4). A more refined theory would bring more complex static boundary conditions that could involve more than one mode at a time if they were derived from the non-linear equilibrium system, and so the scheme would become very complex, perhaps not possible. However, the formulation presented here and illustrated below is still appropriate and general for the Rayleigh-Ritz method, due to the fact that the method only requires the obedience to the cinematic/forced boundary conditions, which, being related only to the displacements, are linear in engineering problems, even for a non-linear geometrical analysis – it consists merely to impose a null value to a displacement, which is computed from the amplitude modal functions in a linear form. Note that similar approaches, where the static boundary conditions involve only first order equations, are currently adopted in the context of the

non-linear stability of structural members – see, for example, Yamada and Croll (1999) for the stability analysis of axially compressed thin-walled cylinders, or Sridharan and Graves Smith (1981) for the FSM analysis of thin-walled prismatic structures.

3.2.2 Illustrative examples of appropriate coordinate functions for GBT stability analysis

3.2.2.1 The coordinate function for the axial elongation mode – mode 1

Having presented the background procedure, some polynomial coordinate functions, appropriate for buckling and post-buckling analysis of a thin-walled compressed columns or beams in the context of the energy formulation of GBT, are derived below for several boundary conditions – note that not all will be used in the forthcoming examples but are presented here to illustrate the possibilities of the scheme.

Applying the procedure to the first mode of deformation – axial elongation –, requires a special implementation (Schardt 1989) in order to be integrated in the general theory of GBT. For a column considering axial displacement restricted at $x = 0$ and free at $x = L$, the corresponding boundary conditions are:

i) cinematic conditions: ${}^{1}A\big|_{x=0} = 0$ and ${}^{1}A'\big|_{x=0} = 0$; (3.19 a-b)

ii) static conditions: ${}^{1}A''\big|_{x=L} = 0$ and ${}^{1}A'''\big|_{x=L} = 0$. (3.19 c-d)

Expression (3.19 a) is used for consistency only, since ${}^{1}A$ appears in the member's total potential energy only in its first and second derivatives. This case illustrates a typical situation where it is advantageous to neglect the static conditions: if the static conditions are taken into account, it is not possible to simulate a load case with constant axial force along the length of the member, so only the cinematic conditions of expression (3.19 a-b) are retained. Therefore, accounting only on the boundary conditions given by (3.14 a-b), the coordinate polynomial is simply given by

$${}^{1}\varphi_{1} = {}^{1}a_{1,0} + {}^{1}a_{1,1}\,x + {}^{1}a_{1,2}\,x^{2}. \qquad (3.20)$$

Using sequentially condition (3.19 a) and condition (3.19 b), by this order, yields:

$$ {}^{1}a_{1,0} = 0 \tag{3.21} $$

and

$$ {}^{1}a_{1,1} = 0 . \tag{3.22} $$

Finally, applying the normality rule of (3.5), considering $c = 1$, leads to

$$ {}^{1}a_{1,2} = \frac{\sqrt{5}}{L^2} . \tag{3.23} $$

and the first coordinate function becomes fully defined in the form:

$$ {}^{1}\varphi_1 = \frac{x^2 \sqrt{5}}{L^2} . \tag{3.24} $$

When a column is axially loaded at one end, a linear equilibrium analysis leads to a constant longitudinal stress resultant – axial effort – and to a linear longitudinal displacements configuration along the member's length. Figure 3.1 presents a plot of function ${}^{1}\varphi_1$ and its first two derivatives for a member's length of $L = 300\,\text{mm}$. Recalling that the generalized bimoment for mode of deformation *k* is given by (Schardt 1989):

$$ {}^{k}W = -{}^{k}C \; {}^{k}A'' , \tag{3.25} $$

which, for mode of deformation 1 (axial elongation), corresponds to the traditional normal force. The sufficiency of this function to achieve an optimal approximation for ${}^{1}A$ for the stability analysis of compressed columns becomes evident by looking at the graphics shown in Fig. 3.1, where it can be seen that the second derivative of ${}^{1}\varphi_1$ is constant along the member's length, thus allowing a constant axial force along the member. Hence, it is appropriate to model the axial elongation mode for a compressed column and this property illustrates the advantage of neglecting the static boundary conditions for a practical case.

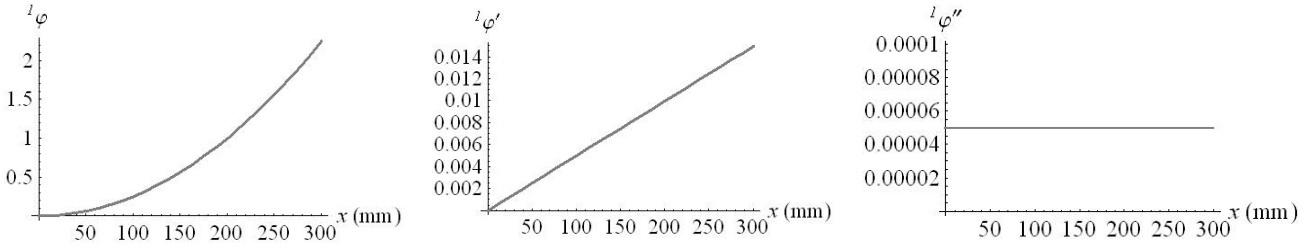

a) Function $^{1}\varphi$ b)1st derivative c) 2nd derivative

Fig. 3.1 – Function $^{1}\varphi$ and its first two derivatives for *L=300* mm

3.2.2.2 The coordinate functions for the higher modes: the pined-pined boundary conditions

For modes 2 and higher and allowing warping at the end sections – end plate with negligible bending inertia at both ends – the modal boundary conditions are:

i) cinematic conditions: $^{k}A\big|_{x=o} = 0$ and $^{k}A\big|_{x=L} = 0$; (3.26 a-b)

ii) static conditions: $^{k}A''\big|_{x=o} = 0$ and $^{k}A''\big|_{x=L} = 0$. (3.26 c-d)

If the static boundary conditions of (3.26 c-d) are used, the first polynomial is of 4th order and has five unknown coefficients, given by

$$^{k}\varphi_{1} = {}^{k}a_{1,0} + {}^{k}a_{1,1}\,x + {}^{k}a_{1,2}\,x^{2} + {}^{k}a_{1,3}\,x^{3} + {}^{k}a_{1,4}\,x^{4}, \quad (3.27)$$

where $^{k}a_{1,0}$, $^{k}a_{1,1}$, $^{k}a_{1,2}$, $^{k}a_{1,3}$ and $^{k}a_{1,4}$ are yet unknown. Using sequentially expressions (3.26 a), (3. 26 b), (3. 26 c) and (3. 26 c), by this order, leads to:

$$^{k}a_{1,0} = 0, \quad (3.28 \text{ a-d})$$

$$^{k}a_{1,1} = -{}^{k}a_{1,2}L - {}^{k}a_{1,3}\,L^{2} - {}^{k}a_{1,4}\,L^{3},$$

$$^{k}a_{1,2} = 0,$$

$$^{k}a_{1,3} = -2\,{}^{k}a_{1,4}\,L.$$

Finally, imposing the normality rule of expression (3.5) with respect to the member's length yields:

$$\int_L {}^k\varphi_1^2\, dx = L \Rightarrow \quad {}^k a_{1,4} = -\frac{3\sqrt{\frac{70}{31}}}{L^4} \quad \vee \quad {}^k a_{1,4} = \frac{3\sqrt{\frac{70}{31}}}{L^4}. \tag{3.29}$$

The positive root is retained and the first coordinate polynomial for mode k becomes fully defined in the form:

$${}^k\varphi_1 = \sqrt{\frac{70}{31}}\left(\frac{3}{L}x - \frac{6}{L^3}x^3 + \frac{3}{L^4}x^4\right). \tag{3.30}$$

If a different value was chosen to normalize the polynomial, different values for ${}^k a_{1,4}$ would be obtained, and the polynomial would be equal to:

$$\int_L {}^k\varphi_1^2\, dx = 1 \Rightarrow \quad {}^k a_{1,4} = \frac{3\sqrt{\frac{70}{31}}}{L^{\frac{9}{2}}} \text{ and } {}^k\varphi_1 = \sqrt{\frac{70}{31}}\left(\frac{3}{L^{\frac{3}{2}}}x - \frac{6}{L^{\frac{7}{2}}}x^3 + \frac{3}{L^{\frac{9}{2}}}x^4\right); \tag{3.31}$$

$$\int_L {}^k\varphi_1^2\, dx = L^2 \Rightarrow \quad {}^k a_{1,4} = \frac{3\sqrt{\frac{70}{31}}}{L^{\frac{7}{2}}} \text{ and } {}^k\varphi_1 = \sqrt{\frac{70}{31}}\left(\frac{3}{\sqrt{L}}x - \frac{6}{L^{\frac{5}{2}}}x^3 + \frac{3}{L^{\frac{7}{2}}}x^4\right). \tag{3.32}$$

The second polynomial has now the following form

$${}^k\varphi_2 = {}^k a_{2,0} + {}^k a_{2,1}\, x + {}^k a_{2,2}\, x^2 + {}^k a_{2,3}\, x^3 + {}^k a_{2,4}\, x^4 + {}^k a_{2,5}\, x^5 \tag{3.33}$$

where coefficients ${}^k a_{2,0}$ to ${}^k a_{2,5}$ are yet unknown, and the use of the boundary conditions is performed in the same way as for the first polynomial, yielding the same results for the first four coefficients. Imposing the orthogonality rule between ${}^k\varphi_2$ and ${}^k\varphi_1$ of expression (3.30), the following relation between ${}^k a_{2,4}$ and ${}^k a_{2,5}$ is obtained:

$$\int_L \left({}^k\varphi_1\ {}^k\varphi_2\right) dx = 0 \Rightarrow \quad {}^k a_{2,4} = -\frac{5\ {}^k a_{2,5}\, L}{2}. \tag{3.34}$$

Finally, the normality rule (3.5) yields for ${}^k a_{2,5}$:

$$\int_L {}^k\varphi_2^2\, dx = L \Rightarrow \quad {}^k a_{2,5} = -\frac{6\sqrt{\frac{462}{5}}}{L^5} \quad \vee \quad {}^k a_{2,5} = \frac{6\sqrt{\frac{462}{5}}}{L^5}. \tag{3.35}$$

Again, accounting only for the positive root of (3.35) yields the following expression for the second coordinate polynomial:

$${}^k\varphi_2 = \sqrt{\frac{462}{5}} \times \left(-\frac{1}{L}x + \frac{6}{L^5}x^5\right) + \sqrt{2310} \times \left(\frac{2}{L^3}x^3 - \frac{3}{L^4}x^4\right). \tag{3.36}$$

The scheme may proceed indefinitely, building a set of orthonormal polynomials that are adequate to approximate the unknown amplitude modal function ${}^{k}A$. The first five polynomials are listed below, and Fig. 3.2 presents a plot of these functions and their first two derivatives for a member's length of $L=400$:

$$ {}^{k}\varphi_1 = \sqrt{\frac{70}{31}}\left(\frac{3}{L}x - \frac{6}{L^3}x^3 + \frac{3}{L^4}x^4\right) \qquad (3.37, \text{a-e}) $$

$$ {}^{k}\varphi_2 = \sqrt{\frac{462}{5}} \times \left(-\frac{1}{L}x + \frac{6}{L^5}x^5\right) + \sqrt{2310} \times \left(\frac{2}{L^3}x^3 - \frac{3}{L^4}x^4\right) $$

$$ {}^{k}\varphi_3 = \sqrt{\frac{2730}{7781}} \times \left(\frac{27}{L}x - \frac{736}{L^3}x^3 + \frac{2073}{L^4}x^4\right) + \sqrt{\frac{84630}{251}} \times \left(-\frac{66}{L^5}x^5 + \frac{22}{L^6}x^6\right) $$

$$ {}^{k}\varphi_4 = \sqrt{\frac{462}{1345}} \times \left(-\frac{41}{L}x + \frac{17796}{L^5}x^5\right) + $$

$$ + \sqrt{\frac{2310}{269}} \times \left(\frac{472}{L^3}x^3 - \frac{2073}{L^4}x^4 - \frac{2730}{L^6}x^6 + \frac{780}{L^7}x^7\right) $$

$$ {}^{k}\varphi_5 = \sqrt{\frac{39270}{111193}} \times \left(\frac{57}{L}x - \frac{6016}{L^3}x^3 + \frac{37341}{L^4}x^4 - \frac{96018}{L^5}x^5 + \frac{123370}{L^6}x^6\right) + $$

$$ + \sqrt{\frac{9856770}{443}} \times \left(-\frac{312}{L^7}x^7 + \frac{78}{L^8}x^8\right). $$

Another option for the derivation of the coordinate functions that approximate the amplitude modal function ${}^{k}A$ is the use of the cinematic boundary conditions only, i.e., only those that are required by the Rayleigh-Ritz method, which are given by expressions (3.26 a) and (3.26 b). If this option is considered, the scheme generates the following first five coordinate polynomials, all normalized to L:

$$ {}^{k}\varphi_1 = -\frac{\sqrt{30}\,x}{L} + \frac{\sqrt{30}\,x^2}{L^2} \qquad (3.38, \text{a-e}) $$

$$ {}^{k}\varphi_2 = \sqrt{210}\left(\frac{x}{L} - 3\frac{x^2}{L^2} + 2\frac{x^3}{L^3}\right) $$

$$ {}^{k}\varphi_3 = \sqrt{10}\left(-9\frac{x}{L} + 51\frac{x^2}{L^2} - 84\frac{x^3}{L^3} + 42\frac{x^4}{L^4} \right) $$

$$ {}^{k}\varphi_4 = \sqrt{2310}\left(\frac{x}{L} - 9\frac{x^2}{L^2} + 26\frac{x^3}{L^3} - 30\frac{x^4}{L^4} + 12\frac{x^5}{L^5} \right) $$

$$ {}^{k}\varphi_5 = \sqrt{1365}\left(-2\frac{x}{L} + 26\frac{x^2}{L^2} - 114\frac{x^3}{L^3} + 222\frac{x^4}{L^4} - 198\frac{x^5}{L^5} + 66\frac{x^6}{L^6} \right). $$

These polynomials, illustrated in Figure 3.3, are of lower order than those given by expression (3.27). Therefore the later require less integrations and less computer resources for the calculation of the total potential energy. Moreover, as for the axial elongation mode, if a constant major axis bending moment is required for the stability analysis of simply supported beams, the bending moment is given by (Schardt 1989):

$$ {}^{2}W = -{}^{2}C \; {}^{2}A'' , \tag{3.39} $$

and therefore the coordinate functions set that approximate ${}^{2}A$ must result in a constant 2nd order derivative. This is only achievable if function (3.38 a) is taken, since its 2nd order derivative is constant – see Figure 3.3 – or, in other words, if the static boundary conditions are withdrawn.

3.2.2.3 The coordinate functions for the higher modes: the fixed-fixed boundary conditions

The coordinate functions for modes of deformation 2 and higher for the case of fixed-fixed boundary conditions, without the allowance of warping at the edge sections, are computed. The relevant boundary conditions are now all cinematic and are given by:

$$ {}^{k}A\big|_{x=o} = 0 , \; {}^{k}A\big|_{x=L} = 0 , \; {}^{k}A'\big|_{x=o} = 0 \text{ and } {}^{k}A'\big|_{x=L} = 0 \tag{3.40 a-d} $$

and the sequential procedure leads to the following first five orthonormal polynomials:

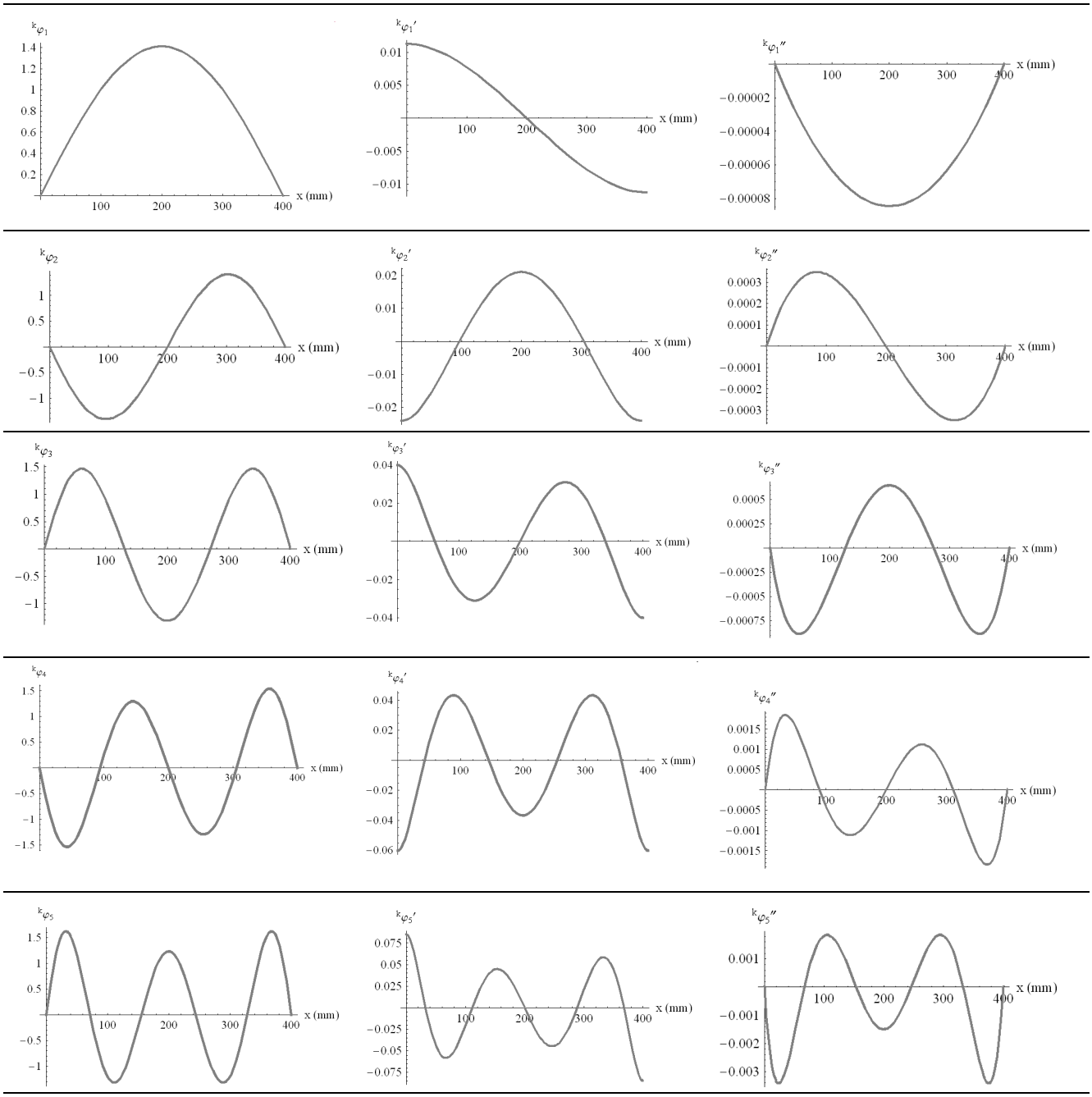

a) Functions ${}^{k}\varphi_i$ b)1st derivative c) 2nd derivative

Fig. 3.2 – Functions ${}^{k}\varphi_1$, ${}^{k}\varphi_2$, ${}^{k}\varphi_3$, ${}^{k}\varphi_4$ and ${}^{k}\varphi_5$, and their first two derivatives, for *L=400*, for pined-pined – free-to-warp edge cross sections, using the cinematic and the static boundary conditions, normalized to *L*

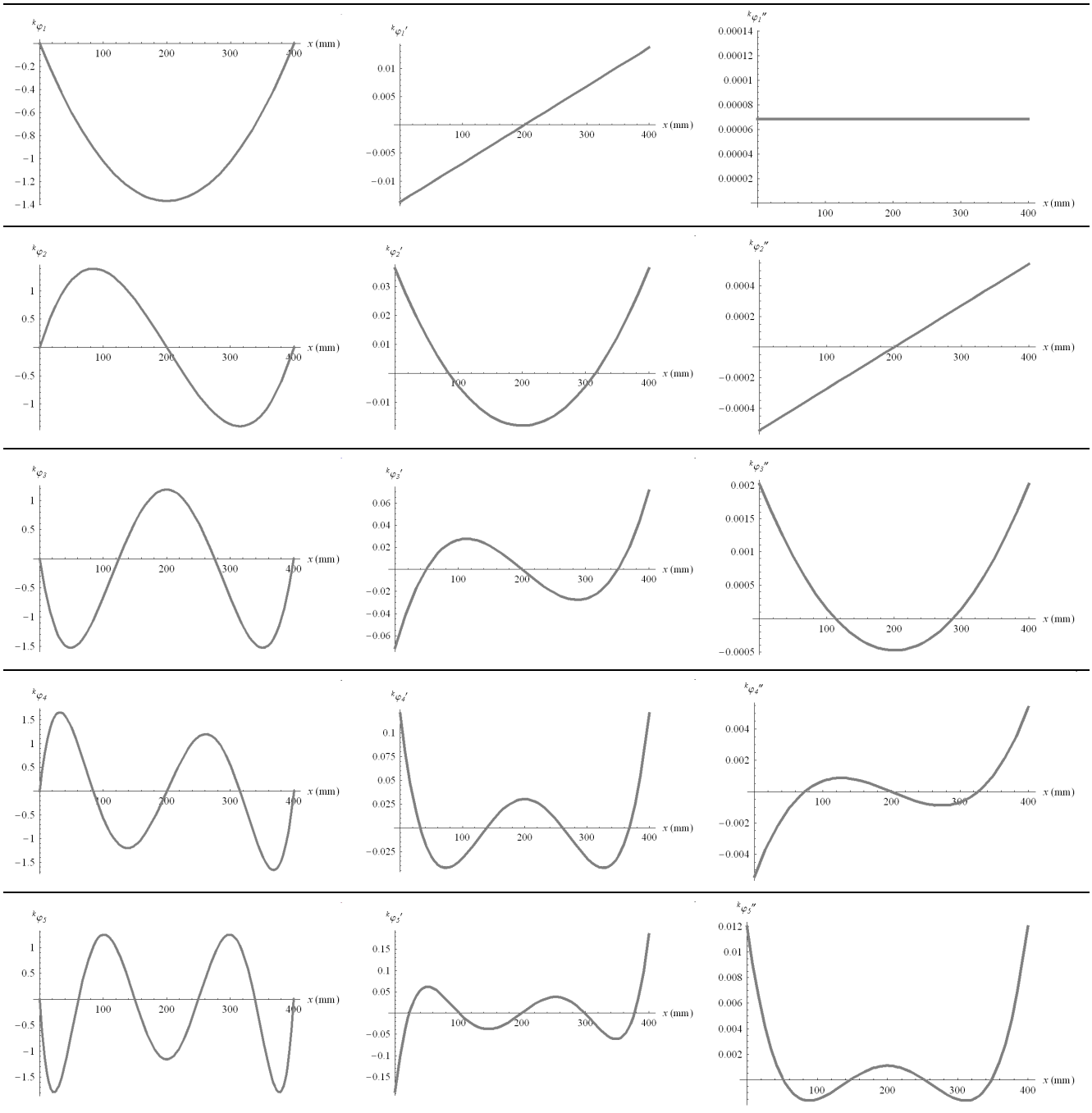

Fig. 3.3 – Functions $^{k}\varphi_1$, $^{k}\varphi_2$, $^{k}\varphi_3$, $^{k}\varphi_4$ and $^{k}\varphi_5$, and their first two derivatives, for *L=400*, for pined-pined – free-to-warp edge cross sections, using the cinematic boundary conditions only, normalized to *L*

$$ {}^{k}\varphi_1 = \sqrt{70}\left(\frac{3}{L^2}x^2 - \frac{6}{L^3}x^3 + \frac{3}{L^4}x^4\right) \qquad (3.41,\ a\text{-}e) $$

$$ {}^{k}\varphi_2 = \sqrt{770}\times\left(-\frac{3}{L^2}x^2 + \frac{12}{L^3}x^3 - \frac{15}{L^4}x^4 + \frac{6}{L^5}x^5\right) $$

$$ {}^{k}\varphi_3 = \sqrt{182}\times\left(\frac{15}{L^2}x^2 - \frac{96}{L^3}x^3 + \frac{213}{L^4}x^4 - \frac{198}{L^5}x^5 + \frac{66}{L^6}x^6\right) $$

$$ {}^{k}\varphi_4 = \sqrt{770}\times\left(-\frac{15}{L^2}x^2 + \frac{138}{L^3}x^3 - \frac{465}{L^4}x^4 + \frac{732}{L^5}x^5 - \frac{546}{L^6}x^6 + \frac{156}{L^7}x^7\right) $$

$$ {}^{k}\varphi_5 = \sqrt{2618}\times\left(\frac{15}{L^2}x^2 - \frac{186}{L^3}x^3 + \frac{873}{L^4}x^4 - \frac{2018}{L^5}x^5 + \frac{2496}{L^6}x^6 + \frac{1560}{L^6}x^6 + \frac{390}{L^6}x^6\right), $$

plotted in Fig. 3.4 for $L=400$ mm.

3.2.2.4 The coordinate functions for the higher modes: the fixed-pinned boundary conditions

In order to show the ability of the present procedure to simulate several and distinct boundary conditions, the coordinate functions for fixed-pinned boundary conditions are presented. The considered boundary conditions are:

$$ {}^{k}A\big|_{x=o} = 0,\ {}^{k}A\big|_{x=L} = 0,\ {}^{k}A'\big|_{x=o} = 0 \text{ and } {}^{k}A''\big|_{x=L} = 0, \qquad (3.42\ a\text{-}d) $$

so the static condition at $x=L$ is also considered, and the first five polynomials, shown in Fig. 3.5 for a member's length $L=300$ mm, take the following form:

$$ {}^{k}\varphi_1 = \frac{9\sqrt{\frac{70}{19}}}{L^{3/2}}x^2 - \frac{15\sqrt{\frac{70}{19}}}{L^{5/2}}x^3 + \frac{6\sqrt{\frac{70}{19}}}{L^{7/2}}x^4 \qquad (3.43,\ a\text{-}e) $$

$$ {}^{k}\varphi_2 = -\frac{3\sqrt{\frac{10010}{19}}}{L^{3/2}}x^2 + \frac{141\sqrt{\frac{770}{247}}}{L^{5/2}}x^3 - \frac{159\sqrt{\frac{770}{247}}}{L^{7/2}}x^4 + \frac{3\sqrt{\frac{14630}{13}}}{L^{9/2}}x^5 $$

$$ {}^{k}\varphi_3 = \frac{39\sqrt{\frac{910}{43}}}{L^{3/2}}x^2 - \frac{3045\sqrt{\frac{70}{559}}}{L^{5/2}}x^3 + \frac{6333\sqrt{\frac{70}{559}}}{L^{7/2}}x^4 - \frac{5511\sqrt{\frac{70}{559}}}{L^{9/2}}x^5 + \frac{132\sqrt{\frac{910}{43}}}{L^{11/2}}x^6 $$

$$ {}^{k}\varphi_4 = -\frac{15\sqrt{\frac{10010}{1247}}}{L^{3/2}}x^2 + \frac{15449\sqrt{\frac{770}{16211}}}{L^{5/2}}x^3 - \frac{49776\sqrt{\frac{770}{16211}}}{L^{7/2}}x^4 + \frac{74874\sqrt{\frac{770}{16211}}}{L^{9/2}}x^5 - $$

$$-\frac{4102\sqrt{\frac{10010}{1247}}}{L^{11/2}}x^6+\frac{26\sqrt{\frac{430430}{29}}}{L^{13/2}}x^7$$

$${}^k\varphi_5=\frac{9\sqrt{\frac{185878}{29}}}{L^{3/2}}x^2-\frac{7669\sqrt{\frac{2618}{2059}}}{L^{5/2}}x^3+\frac{34824\sqrt{\frac{2618}{2059}}}{L^{7/2}}x^4-\frac{78234\sqrt{\frac{2618}{2059}}}{L^{9/2}}x^5+$$

$$+\frac{2496\sqrt{\frac{2618}{2059}}}{L^{11/2}}x^6-\frac{1560\sqrt{\frac{2618}{2059}}}{L^{13/2}}x^7+\frac{390\sqrt{\frac{75922}{71}}}{L^{15/2}}x^8.$$

3.2.3 – Matrix scheme for the integration of the internal strain energy

Once chosen the relevant coordinate functions, the modal amplitude functions have the following form:

$${}^kA\approx{}^ka_1\ {}^k\varphi_1(x)+\ldots+{}^ka_{n_k}\ {}^k\varphi_{n_k}(x),\ k=1,\ldots,n_{MD} \tag{3.44}$$

(remember that n_k represents the number of orthonormal polynomials adopted for the modal amplitude function k), all functions ${}^kA$ becoming a function of x and of the generalized coordinates ${}^ia$, and their n^{th} order derivative is now given by:

$${}^kA^{(n)}={}^ka_1\ {}^k\varphi_1^{(n)}(x)+\ldots+{}^ka_{n_k}\ {}^k\varphi_{n_k}^{(n)}(x),\ k=1,\ldots,n_{MD}. \tag{3.45}$$

A global numbering can now be adopted for the generalized coordinates, and n_C denotes the total number of generalized coordinates and trial functions of the problem, and the total potential energy presents the following form:

$$V=\int_0^L F\left[{}^ka,\ {}^k\varphi(x),\ {}^k\varphi'(x),\ {}^k\varphi''(x),P\right]dx,\ k=1,\ldots,n_C, \tag{3.46}$$

where

$$F\left[{}^ka,\ {}^k\varphi(x),\ {}^k\varphi'(x),\ {}^k\varphi''(x),P\right],\ k=1,\ldots,n_C, \tag{3.47}$$

is a polynomial in the control parameter P, in the generalized ${}^ka$ coordinates and in x, or in other words, whose any of its parts belonging to the internal strain energy is given by the product of a term of a tensor related to a generalized mechanical property times the coordinate functions (or their 1st or 2nd order derivatives, being dependent of x) times the generalized coordinates ${}^ka$. The part related to the potential of the external loading is given

by the product of a coordinate function times a stress pattern linearly dependent of the control parameter *P*.

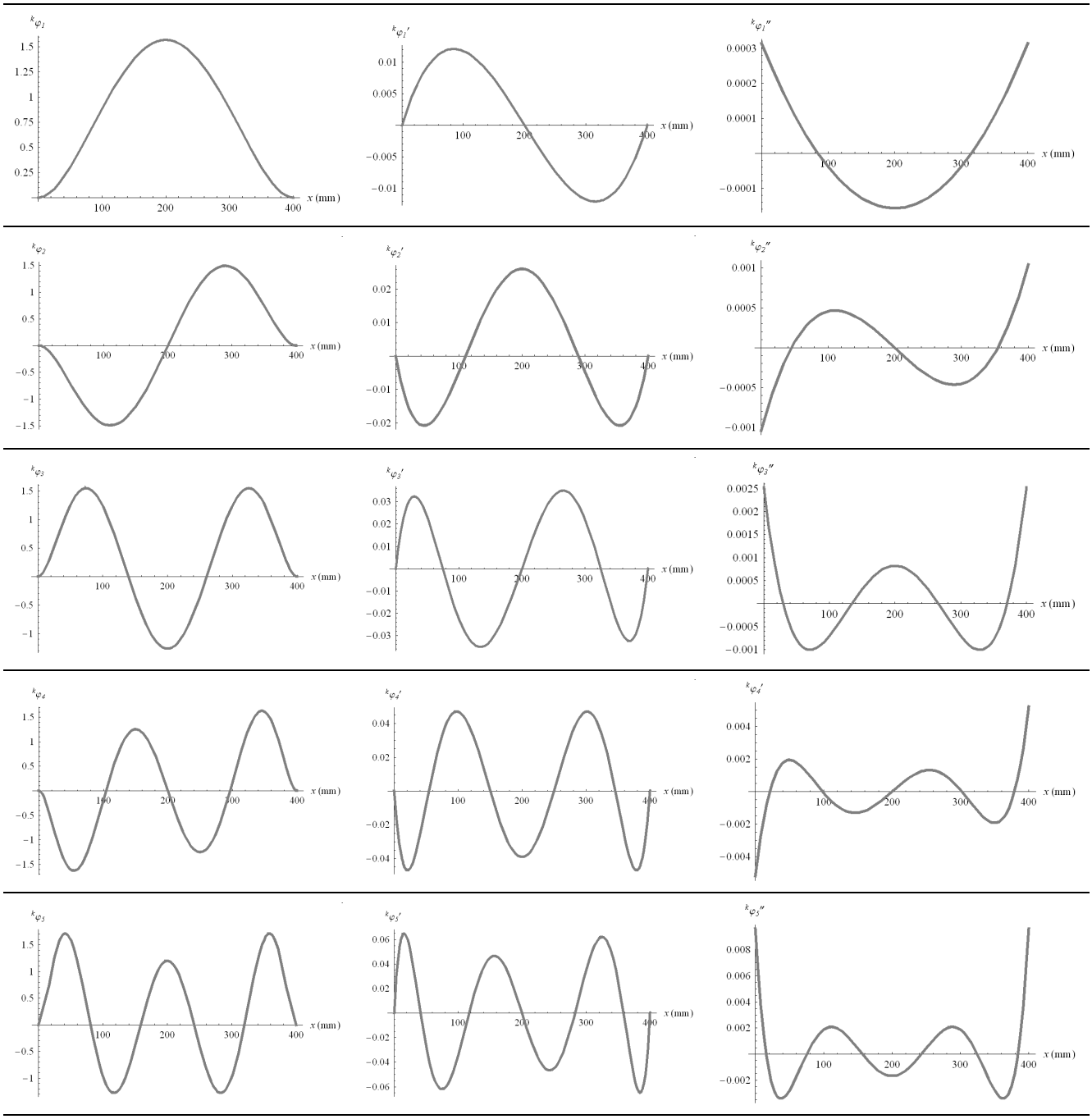

a) Functions ${}^{k}\varphi_i$ b)1st derivative c) 2nd derivative

Fig. 3.4 – Functions ${}^{k}\varphi_1$, ${}^{k}\varphi_2$, ${}^{k}\varphi_3$, ${}^{k}\varphi_4$ and ${}^{k}\varphi_5$, and their first two derivatives, for *L=400*, for fixed-fixed and warping restrained edge cross sections

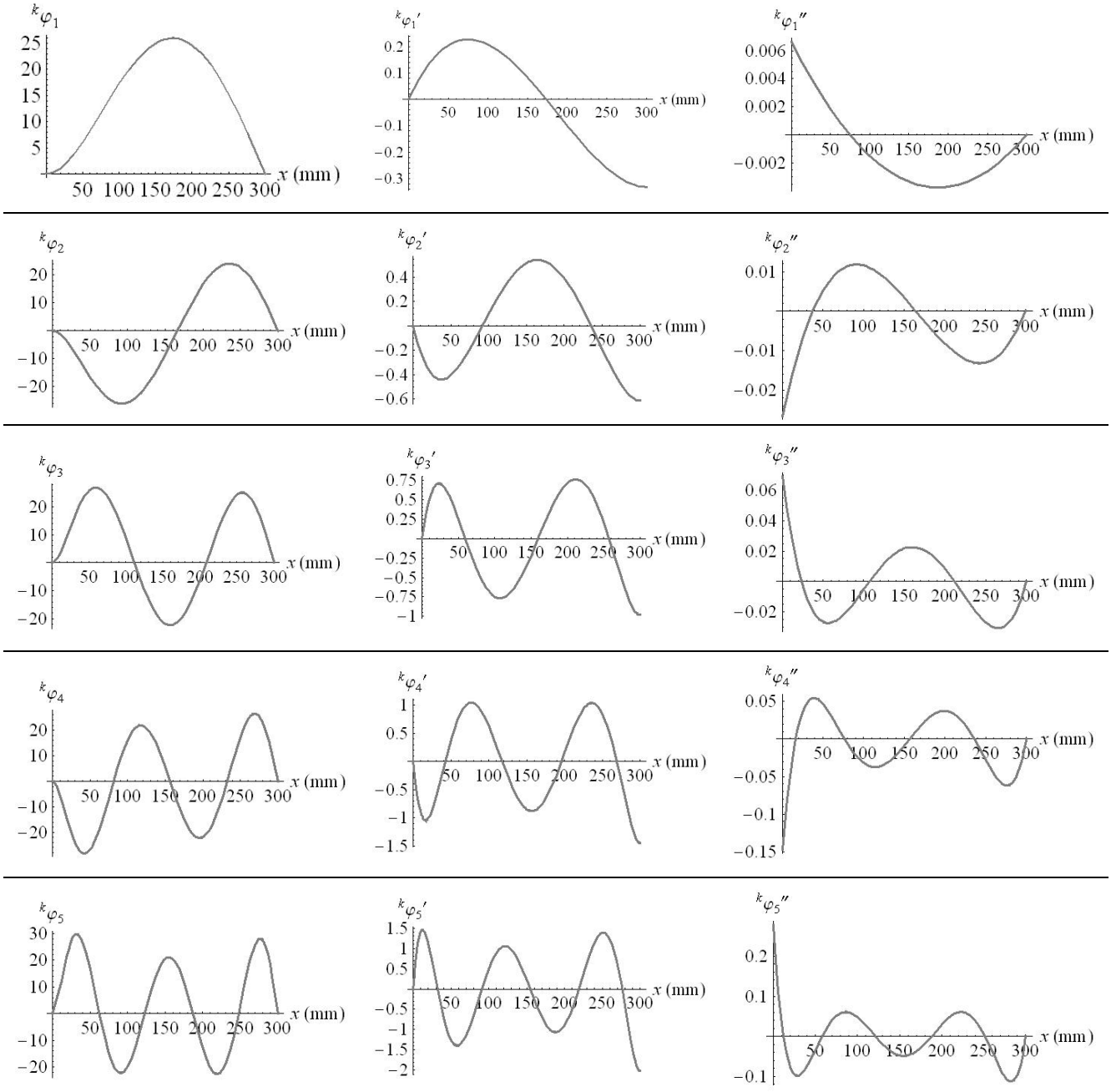

a) Functions $^k\varphi$ b)1st derivative c) 2nd derivative

Fig. 3.5 – Functions $^k\varphi_1$, $^k\varphi_2$, $^k\varphi_3$, $^k\varphi_4$ and $^k\varphi_5$, and their first two derivatives, for *L=300* mm, for fixed-pinned boundary conditions and accounting also for the static boundary condition

The aim of the integration procedure is to group the terms corresponding to the same power of *x*, thus generating a vector dependent only of the generalized coordinates, and to integrate along the member's length by summing all these coefficients, each one

multiplied by the integration of the correspondent power of x along the member's length; in other words, for the generic coefficient of x^j in (3.47), this coefficient is multiplied by $\frac{L^{j+1}}{j+1}$ and subsequently added to the internal strain energy polynomial – the following presentation concerns only the computation of the internal strain energy parts, because the ones related to the potential of the external loading are usually very easy to calculate, since they are simple and linear terms.

To perform the integration of the ISE parts, first the set of all amplitude modal functions ${}^kA$ from expression (3.3) are stored in the following matrix:

$$\boldsymbol{\Phi}_0 = \boldsymbol{\Phi}_{0,\, n_{MD}\times(\xi_x+1)} \tag{3.48}$$

where ξ_x is the maximum power of x for all modal amplitude functions, and the term ${}^{ir}\boldsymbol{\Phi}_0$ represents the coefficient of x^{r-1} for the amplitude function associated with mode of deformation i, all these coefficients being linear polynomials in the generalized coordinates ${}^ka$. Similar storage form can be derived for the set of derivatives of ${}^kA$, the first two – those that have relevance for the problem – being denoted by $\boldsymbol{\Phi}_{d1}$ and $\boldsymbol{\Phi}_{d2}$ and having dimensions $\left(n_{MD}\times\xi_x\right)$ and $\left(n_{MD}\times\xi_x-1\right)$, respectively.

The calculus of the integral in the TPE is made through a matrix scheme based on the fact that the coefficient of x^n of the product of the m polynomials ${}^1\varphi(x),\ldots,{}^m\varphi(x)$ is given in general by:

$$\sum_{i_1=1}^{(n+1)}\left\{{}^1\varphi_{i_1}\times\sum_{i_2=1}^{(n+1)-i_1+1}{}^2\varphi_{i_2}\times\left[\sum_{i_3=1}^{(n+1)-(i_1+i_2)+2}{}^3\varphi_{i_3}\times\ldots\times\left(\sum_{i_{m-1}=1}^{(n+1)-(i_1+i_2+\ldots+i_{m-2})+(m-2)}{}^{m-1}\varphi_{i_3}\times{}^m\varphi_{[(n+1)-(i_1+i_2+\ldots+i_{m-2})+(m-2)-i_{m-1}+1]}\right)\right]\right\} \tag{3.49}$$

where ${}^i\varphi_j$ denotes the coefficient of x^{j-1} for polynomial ${}^i\varphi$. The above expression can be easily proven by natural induction and, noting that in the definition of the TPE expression the integration is made between 0 and L for all terms, it can be applied to the calculus of the TPE as follows – it is illustrated in the following for some representative cases:

i) calculus of the part related to matrix $\boldsymbol{D_2}$: the maximum power of the product is given by the sum of the maximum powers of the polynomials stored in $\boldsymbol{\Phi}_0$ and $\boldsymbol{\Phi}_{d2}$, being equal to $\xi_{TOT} = 2\xi_x - 2$, and the part of ISE associated with $\boldsymbol{D_2}$ is:

$$V_i^{\boldsymbol{D_2}} = \frac{1}{2}\sum_{r=0}^{\xi_{TOT}} \left\{ \frac{L^{r+1}}{r+1} \times \sum_{i=1}^{n_{MD}} \sum_{k=1}^{n_{MD}} {}^{ik}D_2 \times \sum_{s=1}^{r+1} {}^{i,s}\boldsymbol{\Phi}_0 \times {}^{k,[(r+1)-s+1]}\boldsymbol{\Phi}_{d2} \right\}; \tag{3.50}$$

ii) calculus of the part related to the second-order tensor $\boldsymbol{\kappa_{L2}}$: the maximum power is equal to $\xi_{TOT} = 3\xi_x - 4$ and the part of the ISE related to $\boldsymbol{\kappa_{L2}}$ is:

$$V_i^{\boldsymbol{\kappa_{L2}}} = \frac{1}{4}\sum_{r=0}^{\xi_{TOT}} \left\{ \frac{L^{r+1}}{r+1} \times \sum_{i=1}^{n_{MD}} \sum_{k=1}^{n_{MD}} \sum_{l=1}^{n_{MD}} {}^{ikl}\boldsymbol{\kappa}_{L2} \times \left[\sum_{s_1=1}^{r+1} {}^{i,s_1}\boldsymbol{\Phi}_{d2} \times \sum_{s_2=1}^{(r+1)-s_1+1} {}^{k,s_2}\boldsymbol{\Phi}_{d1} \times {}^{l,[(r+1)-s_1+1]-s_2+1}\boldsymbol{\Phi}_{d1} \right] \right\}; \tag{3.51}$$

iii) calculus of the part related to the third-order tensor $\boldsymbol{\kappa_{L4}}$: the maximum power is equal to $\xi_{TOT} = 4\xi_x - 4$ and the part of the ISE related to $\boldsymbol{\kappa_{L4}}$ is given by:

$$V_i^{\boldsymbol{\kappa_{L4}}} = \frac{1}{8}\sum_{r=0}^{\xi_{TOT}} \left\{ \frac{L^{r+1}}{r+1} \times \sum_{i=1}^{n_{MD}} \sum_{j=1}^{n_{MD}} \sum_{k=1}^{n_{MD}} \sum_{l=1}^{n_{MD}} {}^{ijkl}\boldsymbol{\kappa}_{L4} \times \right.$$

$$\left. \times \left[\sum_{s_1=1}^{r+1} {}^{i,s_1}\boldsymbol{\Phi}_{d1} \times \sum_{s_2=1}^{(r+1)-s_1+1} {}^{j,s_2}\boldsymbol{\Phi}_{d1} \times \sum_{s_3=1}^{(r+1)-(s_1+s_2)+1} {}^{k,s_3}\boldsymbol{\Phi}_{d1} \times {}^{l,[(r+1)-(s_1+s_2)+2]-s_3+1}\boldsymbol{\Phi}_{d1} \right] \right\}. \tag{3.52}$$

The calculation of the remaining parts of the TPE becomes now trivial and it is important to point out that the above scheme is devoted to the use the symbolic computing software, like MATHEMATICA (Wolfram 2003), exploring the vast resources that this type of software enables, although it can be adapted for numerical computer languages like FORTRAN.

3.2.4 Choice of the normalization factor for the polynomial coordinate functions – a way for minimising numerical instability problems

The choice of the normalization factor c in the normalization rule of expression (3.5) provokes great changes in the magnitude of the coordinate polynomial functions along the interval $[0, L]$ and therefore in the corresponding integrals for the calculus of the TPE. This fact, rarely object of research in applied mechanics, is illustrated in Figure 3.6, where the graphics of functions (3.30), (3.31) and (3.32) for $L=300$ mm, together with their first and second derivatives, are presented, while Tables 3.1 to 3.3 show the most relevant integration values of coordinate function (3.22) as its derivatives as they appear in the TPE of the member, for several member's lengths.

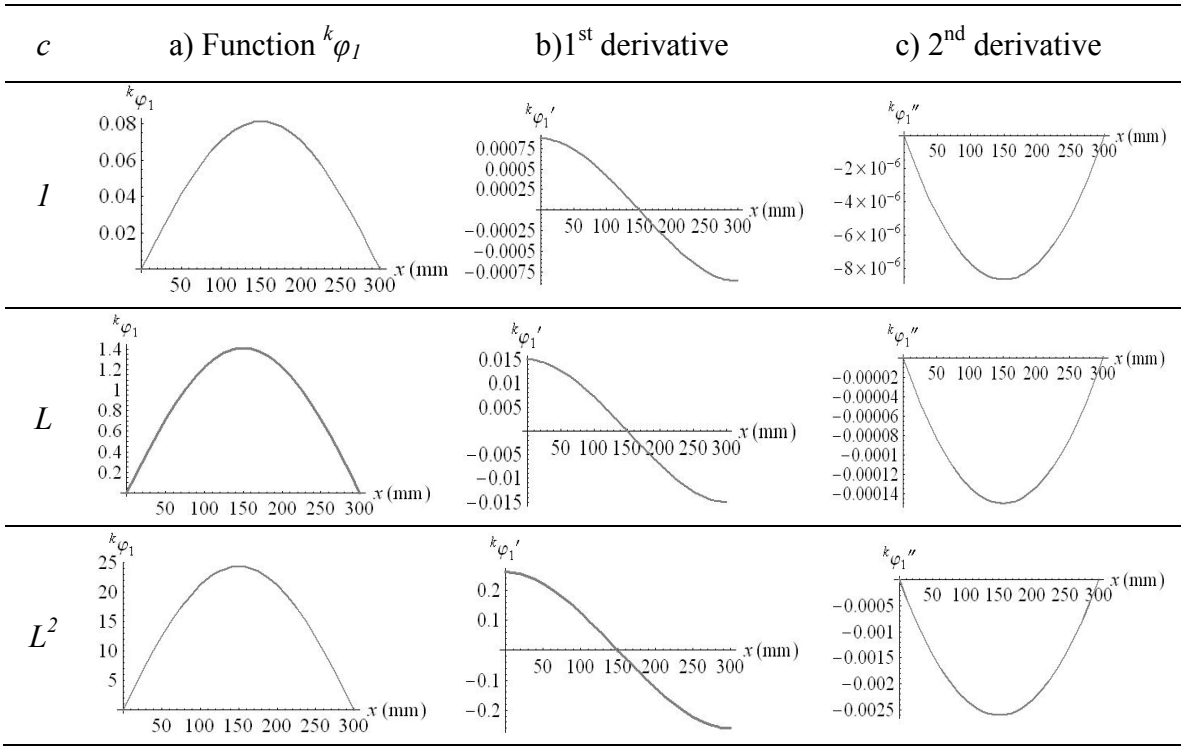

Fig. 3.6 – Function ${}^k\varphi_1$ and its first two derivatives, for L=300, for pined-pined boundary conditions, accounting also on the static conditions: influence of the normalization factor c

A deeper look at Fig. 3.6 highlights the variation of the maximum value of ${}^k\varphi_1$ as normalization factor c changes from 1 to L and to L^2, for which the maximum value the

function reaches along the interval $[0,300]$ passes from about *0.08* to *1.4* or *25*, respectively, but more dramatic changes occur in the function's derivatives, specially for the function's second derivative, where a ratio of about *100* is observed between the maximum values of the 2nd derivative of ${}^{k}\varphi_1$ for $c=1$ and $c=L^2$. Since the function ${}^{k}\varphi_1$ itself and its first and second derivatives are present in the calculation of the TPE of the member, it becomes evident that this variation in the values the function and its derivatives along the member's length, due only to the normalization factor, influences the numerical stability of the solution procedure. Tables 3.1 to 3.3 illustrate this fact by computing the most relevant integrals that appear in the TPE expression for several lengths. It is clear that the choice of the normalization factor results in great changes in the values of the integrals: for example, it is seen that the integrals related to the geometrical property κ_{LO2} are about *10* times greater that the integrals associated with κ_{LO4} for $c=1$, but for $c=L^2$ the terms related to κ_{LO2} can be *100* times less than the others. Knowing that the maximum magnitude in tensor κ_{LO2} is about 10 times smaller than the maximum term of κ_{LO4}, it becomes evident that the normalization factor must be carefully chosen if balanced expressions are pretended in the equilibrium system, so that the numerical efficiency of the structural stability procedures used to analyse the member's behaviour is optimized. Knowing that the TPE is a polynomial in the generalized coordinates, as it will be seen below, the strategy adopted in the examples presented below is to consider a normalization factor for the coordinate polynomials and for a specific member's length that generates parts in the TPE of the same magnitude order, as far as possible and especially for the 2nd and 3rd order parts, so that balanced equations appear in equilibrium system and the numerical problems due to the presence, in the same expression, of numbers with different magnitudes are minimized. In other words, knowing that the greatest term in tensor κ_{LO2} or κ_{LO3} is of magnitude x, usually the magnitude of the greatest term in tensor κ_{LO4} is of magnitude $O\left(x\times 10^3\right)$, so it is convenient to chose a normalization factor for the coordinate polynomials that, in some part, compensates this difference in order to derive a

more balanced TPE polynomial. It was observed that the most reliable numerical behaviour occurred, usually, for the normalization factor equal to L or L^2 but a deeper analysis of this phenomenon requires an extensive analysis of the equilibrium system from the point of view of computational efficiency (Golub and Van Loan 1996), which may contain very large expressions and become hard to handle. Thisis considered to be beyond the scope of the present work and beyond the available computer resources. Moreover, with today's evolution of small personal computers to 64-bit processors, that compute numbers with 31 decimal places instead of 15 for the traditional 32-bit processors (like the computer available to the author), these numerical problems tend to be less relevant in the near future.

L (mm)	$\int \varphi \times \varphi \, dx$	$\int \varphi \times \varphi'' \, dx$	$\int \varphi' \times \varphi' \, dx$	$\int \varphi'' \times \varphi'' \, dx$	$\int \varphi'' \times \varphi' \times \varphi' \, dx$	$\int \varphi' \times \varphi' \times \varphi' \times \varphi' \, dx$
50	1	-3.948387E-03	3.948387E-03	1.560774E-05	-1.382013E-06	4.755731E-07
100	1	-9.870968E-04	9.870968E-04	9.754839E-07	-6.107691E-08	1.486166E-08
300	1	-1.096774E-04	1.096774E-04	1.204301E-08	-4.353428E-10	6.115910E-11
500	1	-3.948387E-05	3.948387E-05	1.560774E-09	-4.370308E-11	4.755731E-12
1000	1	-9.870968E-06	9.870968E-06	9.754839E-11	-1.931421E-12	1.486166E-13
1500	1	-4.387097E-06	4.387097E-06	1.926882E-11	-3.115060E-13	1.957091E-14
2000	1	-2.467742E-06	2.467742E-06	6.096774E-12	-8.535757E-14	4.644269E-15
2500	1	-1.579355E-06	1.579355E-06	2.497239E-12	-3.127138E-14	1.521834E-15
3000	1	-1.096774E-06	1.096774E-06	1.204301E-12	-1.376675E-14	6.115910E-16
3500	1	-8.057933E-07	8.057933E-07	6.500517E-13	-6.879721E-15	2.829614E-16
4000	1	-6.169355E-07	6.169355E-07	3.810484E-13	-3.772307E-15	1.451334E-16
4500	1	-4.874552E-07	4.874552E-07	2.378866E-13	-2.220346E-15	8.053873E-17
5000	1	-3.948387E-07	3.948387E-07	1.560774E-13	-1.382013E-15	4.755731E-17

Table 3.1 – Variation of the TPE integrals of the coordinate function (3.22) against the member's length (polynomial normalized to *1*)

L (mm)	$\int \varphi \times \varphi \, dx$	$\int \varphi \times \varphi'' \, dx$	$\int \varphi' \times \varphi' \, dx$	$\int \varphi'' \times \varphi'' \, dx$	$\int \varphi'' \times \varphi' \times \varphi' \, dx$	$\int \varphi' \times \varphi' \times \varphi' \times \varphi' \, dx$
50	50	-1.974194E-01	1.974194E-01	7.803871E-04	-4.886152E-04	1.188933E-03
100	100	-9.870968E-02	9.870968E-02	9.754839E-05	-6.107691E-05	1.486166E-04
300	300	-3.290323E-02	3.290323E-02	3.612903E-06	-2.262108E-06	5.504319E-06
500	500	-1.974194E-02	1.974194E-02	7.803871E-07	-4.886152E-07	1.188933E-06
1000	1000	-9.870968E-03	9.870968E-03	9.754839E-08	-6.107691E-08	1.486166E-07
1500	1500	-6.580645E-03	6.580645E-03	2.890323E-08	-1.809686E-08	4.403455E-08
2000	2000	-4.935484E-03	4.935484E-03	1.219355E-08	-7.634613E-09	1.857708E-08
2500	2500	-3.948387E-03	3.948387E-03	6.243097E-09	-3.908922E-09	9.511463E-09
3000	3000	-3.290323E-03	3.290323E-03	3.612903E-09	-2.262108E-09	5.504319E-09
3500	3500	-2.820276E-03	2.820276E-03	2.275181E-09	-1.424534E-09	3.466277E-09
4000	4000	-2.467742E-03	2.467742E-03	1.524194E-09	-9.543266E-10	2.322134E-09
4500	4500	-2.193548E-03	2.193548E-03	1.070490E-09	-6.702541E-10	1.630909E-09
5000	5000	-1.974194E-03	1.974194E-03	7.803871E-10	-4.886152E-10	1.188933E-09

Table 3.2 – Variation of the TPE integrals of coordinate function (3.21) against the member's length (polynomial normalized to L)

L (mm)	$\int \varphi \times \varphi \, dx$	$\int \varphi \times \varphi'' \, dx$	$\int \varphi' \times \varphi' \, dx$	$\int \varphi'' \times \varphi'' \, dx$	$\int \varphi'' \times \varphi' \times \varphi' \, dx$	$\int \varphi' \times \varphi' \times \varphi' \times \varphi' \, dx$
50	2.500E+03	-9.870968E+00	9.870968E+00	3.901935E-02	-1.727516E-01	2.972332E+00
100	1.000E+04	-9.870968E+00	9.870968E+00	9.754839E-03	-6.107691E-02	1.486166E+00
300	9.000E+04	-9.870968E+00	9.870968E+00	1.083871E-03	-1.175426E-02	4.953887E-01
500	2.500E+05	-9.870968E+00	9.870968E+00	3.901935E-04	-5.462884E-03	2.972332E-01
1000	1.000E+06	-9.870968E+00	9.870968E+00	9.754839E-05	-1.931421E-03	1.486166E-01
1500	2.250E+06	-9.870968E+00	9.870968E+00	4.335484E-05	-1.051333E-03	9.907774E-02
2000	4.000E+06	-9.870968E+00	9.870968E+00	2.438710E-05	-6.828606E-04	7.430830E-02
2500	6.250E+06	-9.870968E+00	9.870968E+00	1.560774E-05	-4.886152E-04	5.944664E-02
3000	9.000E+06	-9.870968E+00	9.870968E+00	1.083871E-05	-3.717022E-04	4.953887E-02
3500	1.225E+07	-9.870968E+00	9.870968E+00	7.963134E-06	-2.949680E-04	4.246189E-02
4000	1.600E+07	-9.870968E+00	9.870968E+00	6.096774E-06	-2.414277E-04	3.715415E-02
4500	2.025E+07	-9.870968E+00	9.870968E+00	4.817204E-06	-2.023291E-04	3.302591E-02
5000	2.500E+07	-9.870968E+00	9.870968E+00	3.901935E-06	-1.727516E-04	2.972332E-02

Table 3.3 – Variation of the TPE integrals of the coordinate function (3.23) against the member's length (polynomial normalized to L^2)

3.3 – The stability procedures and bifurcational analysis

3.3.1 Introduction

After the natural discretization and the integration procedures presented above, the

TPE becomes a polynomial gradient potential function on the generalized coordinates and on a single external control parameter, here referring to the applied load P, in the form:

$$V = V\left({}^{1}a,\ldots,\ {}^{n_C}a,\ P\right), \tag{3.53}$$

where n_C denotes the total number of generalized coordinates. P appears in expression (3.24) in a linear form, hence its designation of specialized system (Thompson and Hunt 1984). At the present stage, function (3.53) is ready to be analysed using the traditional stability procedures, and it is taken as axiomatic that (Thompson and Hunt 1973, Hunt 1981):

Axiom 1: a stationary value of the TPE with respect to the generalized coordinates is necessary and sufficient for the equilibrium of the system;

Axiom 2: a complete relative minimum of the TPE with respect to the generalized coordinates is necessary and sufficient for the stability of an equilibrium state of the system.

From Axiom 1 the member's equilibrium system is defined as:

$$V_i\left({}^{1}a,\ldots,\ {}^{n_C}a,\ P\right) = \frac{\partial V}{\partial\ {}^{i}a} = 0\,,\ i=1,\ldots,\ n_C \tag{3.54}$$

where, in the present case, V_i are polynomials in ${}^{i}a$ and P, hence can be treated as smooth functions. From Axiom 2 the sign of the determinant of the Hessian matrix of the TPE at any equilibrium state, whose general term is given by:

$${}^{ij}H = \frac{\partial^2 V}{\partial\ {}^{i}a\ \partial\ {}^{j}a},\ i = 1,\ldots,n_c \text{ and } j = 1,\ldots,n_c\,, \tag{3.55}$$

rules the stability of the equilibrium state, in the sense that a positive sign implies a stable equilibrium state while a negative sign implies that the equilibrium state is unstable. In the transition between stable and unstable equilibrium states, along an equilibrium path, $\boldsymbol{H}$ becomes singular and, obviously, its determinant becomes zero. For initially stable equilibrium paths rising with increasing values of the load parameter, a bifurcation point or a limit point state may occur when $\boldsymbol{H}$ becomes singular. The limit point state may be

identified by a direct inspection of the fundamental path, plotting the curve $P - {}^{i}a$, where ${}^{i}a$ is any appropriate coordinate, or by computing the slope of the equilibrium path at the singular point, being zero at limit point (Huang and Atluri 1995). This case has little interest for the problem under observation, since from the practice it is known that thin walled straight prismatic members under compression or bending show bifurcational behaviour. So, the basic problem consists of i) determining the sets of values of ${}^{i}a$ and P that satisfy system (3.54) – the so called equilibrium paths – from the known equilibrium point related to the unloaded state of the member by any appropriate numerical method, then ii) at each point in the ${}^{i}a$–P space that satisfies (3.54), of analysing the stability of the corresponding equilibrium state by calculating the value of the determinant of the TPE Hessian matrix $\boldsymbol{H}$ through expression (3.55), detecting the eventual existence of critical points and detecting if they are related to limit point or to bifurcational states, and finally iii) if a critical point along an equilibrium path has been reached corresponding to a bifurcational state, to switch from the already known equilibrium path to another distinct one, adopting the appropriate numerical techniques for this path switching.

3.3.2 From the unloaded state to the critical state

Due to the physical properties of the equilibrium system of structural members, the unloaded state defined by:

$$P = 0 \text{ and } {}^{i}a = 0\,,\ i=1,\ldots,\ n_C, \tag{3.56}$$

is a particular and stable solution of (3.54), and, since it is known that there is a unique equilibrium path emerging from a non-critical equilibrium state on varying a single control (Thompson and Hunt 1973), the unique equilibrium path emerging from the unloaded state – the fundamental path (FP) – can be easily computed from this equilibrium state by the power series method (Kreiszig 1999) in the following way: first, it is assumed that the FP can be expressed as a Taylor expansion in the neighbourhood of the unloaded state in the

following form:

$$ {}^{i}a_{FP}(P) = {}^{i}a_{(1)}P + {}^{i}a_{(2)}P^2 + {}^{i}a_{(3)}P^3 + \dots \ , \ i=1,\dots, n_C, \tag{3.57} $$

where coefficients ${}^{i}a_{(j)}$ are yet unknown. For most situations in practice this assumption is not restrictive, since the FP is almost linear in the range of interest – between the unloaded state and the lowest critical point. Here P was chosen to be the control parameter, but other variables of the system – any appropriate generalized coordinate – could have been chosen as the controller, which would correspond to the displacements control technique, the adoption of an appropriate generalized coordinate as a controller being needed in the cases where limit points may occur in the region of interest, which is not the present case. Then, expression (3.57) is introduced into the equilibrium system (3.54), giving:

$$ V_i\left({}^{j}a_{(k)},\ P\right) = 0 \ , \ i=1,\dots, n_C, j=1,\dots, n_C, \tag{3.58} $$

and all coefficients ${}^{j}a_{(k)}$ are determined by equalling to zero all coefficients of the powers in P, since along an equilibrium path all equilibrium equations V_i of system (3.54) must vanish for any value of P. In practice, although the FP is quasi-linear between the unloaded state and the lowest critical point, it was observed that expansions at least of third order are required for the column in compression, and at least of fifth order for the simply supported beam under constant major axis bending moment, in order to define with sufficient precision not only the bifurcational load parameter P_{CR} but also the first critical state, i.e., the values of the generalized coordinates ${}^{i}a$ at the critical state.

The resulting FP intersects other equilibrium paths – post-buckling paths, yet unknown – at points of bifurcation, which are to be found. So, associated with the FP, a sliding coordinate transformation – the W-transformation – is introduced in the form (Thompson and Hunt 1973, Hunt 1981):

$$ {}^{i}a = {}^{i}a_{FP}(P) + {}^{i}q \ , \ i=1,\dots, n_C, \tag{3.59} $$

this transformation being valid only outside the neighbourhood of limit points of the FP (Hunt 1981). For thin-walled prismatic members under compression or bending, this

assumption is not restrictive because, as said above, the FP is usually almost linear in the range of interest, i.e., between the unloaded state and the first critical point. Note that the FP is given, in the ${}^{i}q$–P space, as a trivial solution in terms of the sliding coordinates ${}^{i}q$. Hence a new TPE function W is defined in terms of the sliding coordinates as (Thompson and Hunt 1973):

$$W\left({}^{i}q,P\right)=V\left({}^{i}a_{FP}\left(P\right)+{}^{i}q,P\right). \tag{3.60}$$

In general, the linearity in P disappears in expression (3.60) but the equilibrium and the stability conditions pass over unchanged to the W function with respect to the generalized coordinates ${}^{i}q$ (Thompson and Hunt 1973, Hunt 1981). Therefore, the equilibrium system can be computed either from (3.54) by applying directly substitution (3.59):

$$W_i\left({}^{i}q,P\right)=V_i\left({}^{i}a_{FP}\left(P\right)+{}^{i}q,P\right)=0\,,\ i=1,\ldots,n_C\,, \tag{3.61}$$

or by deriving directly (3.60) with respect to the sliding coordinates ${}^{i}q$:

$$W_i\left({}^{i}q,P\right)=\frac{\partial W}{\partial\,{}^{i}q}=0,\ i=1,\ldots,n_C\,. \tag{3.62}$$

The fundamental path remains stable until it reaches a critical point, which is associated with the vanishing of the second variation of W with respect to the generalized coordinates, thus the critical points along the FP are computed by equalling to zero the determinant of the Hessian matrix of W along the FP, denoted by $\boldsymbol{H}_{FP}$:

$$\det\left(\boldsymbol{H}_{FP}\right)=\left|\frac{\partial^2 W}{\partial\,{}^{i}q\ \partial\,{}^{j}q}\right|_{FP}=0\,, \tag{3.63}$$

determined, for ${}^{i}q=0$, $i=1,...,n_c$, directly from (3.630) or by applying (3.59) to expression (3.55). Instead of equalling to zero the determinant of the Hessian matrix, the critical loads can be determined by solving the following generalized eigenproblem, equivalent to equation (3.63), that computes the critical loads and the buckling modes:

$$\left[\boldsymbol{H}_{FP}\right]\left\{{}^{i}\overline{q}\right\}=0\,. \tag{3.64}$$

Due to the shape of $\boldsymbol{H}_{FP}$ – see paragraph 2.4.4 for a simple and illustrative example – equation (3.64) can be presented in the following form:

$$\left[\boldsymbol{H}_{FP}\right]\left\{{}^{i}\overline{q}\right\}=0 \Leftrightarrow \left[\boldsymbol{H}_{FP}^{(0)}+\boldsymbol{H}_{FP}^{(1)}P+\boldsymbol{H}_{FP}^{(2)}P^{2}+\boldsymbol{H}_{FP}^{(3)}P^{3}+\ldots\right]\left\{{}^{i}\overline{q}\right\}=0\,, \tag{3.65}$$

corresponding to a non-linear eigenproblem, which can be solved using an appropriate numerical technique (Mirasso and Godoy 1992) that enables the calculation of the eigenvalues – the critical loads, the lowest one having the most relevant physical interest –, and their corresponding eigenvectors – the critical modes. This technique requires, at first, that the following eigenvalue problem is solved

$$\frac{1}{P}\left[\boldsymbol{H}_{FP}^{(0)}\right]\left\{\overline{\boldsymbol{q}}\right\}=-\left[\boldsymbol{M}_{(0)}\right]\left\{\overline{\boldsymbol{q}}\right\}, \tag{3.66}$$

where matrix $\boldsymbol{M}$ is given by

$$\boldsymbol{M}_{(0)}=\boldsymbol{H}_{FP}^{(1)}, \tag{3.67}$$

and the corresponding lowest value of P, the relevant critical load denoted by $P_{CR,(1)}$, is retained. The inverse of P is adopted in the eigenproblem formulation to avoid infinite solutions for the eigenvalues or the need to reduce the dimension of the eigenproblem, as seen in the example at paragraph 2.4. Then, the second-member matrix $\boldsymbol{M}$ is updated in the form:

$$\boldsymbol{M}_{(1)}=\boldsymbol{H}_{FP}^{(1)}+P_{CR,(1)}\boldsymbol{H}_{FP}^{(2)}+P_{CR,(1)}^{2}\boldsymbol{H}_{FP}^{(3)}+P_{CR,(1)}^{3}\boldsymbol{H}_{FP}^{(4)}+\ldots \tag{3.68}$$

and once again the eigenproblem

$$\frac{1}{P}\left[\boldsymbol{H}_{0}\right]\left\{\overline{\boldsymbol{q}}\right\}=-\left[\boldsymbol{M}_{(1)}\right]\left\{\overline{\boldsymbol{q}}\right\}, \tag{3.69}$$

is solved. The procedure continues until convergence of P_{CR} is achieved, which usually requires few iterations, when, for two consecutive iterations i and $i+1$, it is obtained:

$$P_{CR(i+1)}-P_{CR(i)}\leq \text{tolerance}\,. \tag{3.70}$$

After having achieved convergence of the lowest eigenvalue of P at iteration n, the buckling modes are then determined by computing the eigenvectors for the problem:

$$\frac{1}{P}\left[\boldsymbol{H}_{0}\right]\left\{\overline{\boldsymbol{q}}\right\}=-\left[\boldsymbol{M}_{(n)}\right]\left\{\overline{\boldsymbol{q}}\right\}, \tag{3.71}$$

and the one corresponding to P_{CR}, denoted by $\left\{{}^{i}\overline{q}\right\}_{CR}$, defines the relevant buckling mode

for which the correspondent post-buckling equilibrium path will be searched. Furthermore, through expression (3.57) P_{CR} defines the values of all coordinates ${}^{i}a$ at the critical state, henceforth deonted by ${}^{i}a_{CR}$, and thus defining completely the critical state, and $\left\{{}^{i}\overline{q}\right\}_{CR}$, being the relevant buckling mode, defines the direction of the tangent line of the post-buckling path at the critical state (Wriggers 1995, Krätzig 1995) for the space of the sliding coordinates.

3.3.3 Searching post-buckling equilibrium paths near the critical state: Thompson and Hunt's approach using the elimination of the passive coordinates

The study of efficient numerical procedures for searching post-critical equilibrium paths in the neighbourhood of critical points, for the analysis of the equilibrium system of loaded perfect members given in the form of expression (3.54), has been a relevant research subject in structural engineering over the years, due to the many mathematical difficulties that arise in the treatment of these problems, and several strategies were presented in Chapter 1. Special relevance is made now to the techniques developed by Hunt and Thompson (Thompson and Hunt 1973 and 1984, Hunt 1981), which are briefly reviewed here and are based on perturbation methods (Murdock 1999) that compute the post-buckling equilibrium path as Taylor expansions from the relevant critical state.

So, in relation to the problem stated in chapter 3.3.1 – the search of equilibrium curves in the ${}^{i}a$-P space for the equilibrium system given by (3.54), and at each solution in analysing the stability of the equilibrium state – after having defined the fundamental equilibrium path as a function of an appropriate control parameter Λ, which can be the load parameter P or any appropriate coordinate ${}^{i}a$, whichever is appropriate in the range of interest – in the following it is assumed, with no loss of generality, that the control parameter is actually the acting load P, because it is the most usual case in practice – in the

form:

$$ {}^{k}a = {}^{k}a(P), \quad k = 1,\ldots,n_c , \tag{3.72} $$

having always a non-null component in the P-direction in the region of interest in the ${}^{i}a$–P space, which excludes limit points and defines the fundamental path as a single valued path with respect to P. The localized set of incremental coordinates is then introduced in the form

$$ {}^{i}a = {}^{i}a_{FP}(P) + {}^{i}q \ , \ i=1,\ldots, n_C, \tag{3.73} $$

implying a one-to-one correspondence between ${}^{i}a$ and ${}^{i}q$, and the origin of the new coordinate system slides along the fundamental path – these two aspects are only true in the absence of limit points. A new function is derived for the TPE in terms of ${}^{i}q$, as above:

$$ W({}^{i}q,P) = V({}^{i}a_{FP}(P) + {}^{i}q,P), \tag{3.74} $$

and the equilibrium and stability axioms pass over unchanged to the new TPE function. Furthermore, $W({}^{i}q,P)$ has the following property:

$$ \left.\frac{\partial W^{n+1}}{\partial^{i}q \, \partial P^{n}}\right|_{FP} = 0, \quad \forall i = 1,\ldots,n_c \text{ and } \forall n = 0,1,2,\ldots \tag{3.75} $$

since function $\dfrac{\partial W}{\partial^{i}q}$ it is identically null along the FP, for any i from *1* to n_c.

The Hessian matrix of W along the FP,

$$ \boldsymbol{W}_{ij}\big|_{FP} = \left.\frac{\partial^2 W}{\partial^{i}q \, \partial^{j}q}\right|_{FP}, \ i = 1,\ldots,n_c \text{ and } j = 1,\ldots,n_c \tag{3.76} $$

rules the stability of equilibrium and, since it is supposed that the FP is initially stable, for low values of P matrix $\boldsymbol{W}_{ij}\big|_{FP}$ is positive definite. With increasing P, a m-fold point of bifurcation C is found in the FP, for $P = P^{C}$, and $\boldsymbol{W}_{ij}^{C}$ is singular with rank n_c-m (co-rank m). The procedure shown in section 3.3.2 follows closely the present scheme until this stage, only adding the eigenproblem formulation of expression (3.64), but from this point forward it will be seen that some changes will be introduced.

Returning to the Thompson and Hunt's scheme, it proceeds by splitting the coordinates in two subsets, one of *m* active coordinates (in the present chapter, henceforth denoted by Latin suffices) and another of n_c-*m* passive coordinates (in the present chapter, henceforth denoted by Greek suffices), in such a way that the Hessian's submatrix corresponding to the passive coordinates only is non-singular at the critical state:

$$\det\left(\boldsymbol{W}_{\alpha\beta}^{C}\right)=\left|\frac{\partial^2 W}{\partial^{\alpha}q\partial^{\beta}q}\right|^{C}\neq 0\,. \tag{3.77}$$

The two sets are not necessarily unique, which means that more than one admissible set of active coordinates can be established. For the most relevant case in engineering practice, i.e. for *m=1*, it means that more than one coordinate can be chosen to be the active one and thus to control the search of the post-buckling equilibrium path in the neighbourhood of the relevant critical state.

Subsequently, all n_c-*m* passive coordinates are expressed as a function of the active coordinates and the control parameter in the form:

$${}^{\alpha}q={}^{\alpha}q\left({}^{i}q, P\right) \tag{3.78}$$

and are introduced in the equilibrium equations related to the passive coordinates only, yielding the n_c-*m* equilibrium equations:

$$W_{\alpha}\left[{}^{i}q,\ {}^{\alpha}q\left({}^{i}q, P\right), P\right]\equiv 0\,. \tag{3.79}$$

In fact, it can be seen in subsequent works by Hunt, like for example Hunt and Lucena Neto (1991) and Lucena Neto (1992), that the passive coordinates can be made dependent of the active ones only, without being dependent of the control parameter, in the neighbourhood of the relevant critical state in the form:

$${}^{\alpha}q={}^{\alpha}q\left({}^{i}q\right). \tag{3.80}$$

This is allowed by the application of the implicit function's theorem (Poston and Stewart 1978, Troger and Steindl 1991). Returning to expression (3.78), assuming that the elimination of the passive coordinates is made by assuming they are given by a series expansion in ${}^{i}q$ and *P* from the critical state, the coefficients can be computed through the

power series method and a new potential function is thus obtained, defined by:

$$\mathscr{W}\left({}^{i}q, P\right) = W\left[{}^{i}q,\ {}^{\alpha}q\left({}^{i}q, P\right), P\right]. \tag{3.81}$$

It is highlighted that the passive coordinates are not simply neglected, and any contamination effect they provoke in the buckling modes is considered (Hunt 1981). The set of *m* equilibrium equations is given in general by:

$$\mathscr{W}_{,} = \frac{\partial \mathscr{W}}{\partial {}^{\cdot}q}, \tag{3.82}$$

which enable the computing of the post-buckling equilibrium paths. In most of the cases in practice, there is only one active coordinate and one control parameter, corresponding to the case where matrix $\boldsymbol{W}_{ij}^{C}$ of (3.77) has co-rank *1*, so (3.82) becomes a simple equation whose solution yields the pretended post-buckling equilibrium path.

The scheme presented here is one among several procedures of reducing the system's dimension in the analysis of dynamical systems – see for example Steindl and Troger (2001) – and Hunt, Thompson and their co-workers applied it to perform post-buckling analysis of structural engineering systems having a relatively small number of coordinates. In this thesis it was observed that this procedure becomes inefficient in practice if a high number of coordinates is required, sometimes not applicable even with the nowadays computer resources, due to the need of manipulation of very large expressions that requires large computer resources, so an alternative procedure is derived below to compute the post-buckling equilibrium paths in the context of the use of advanced symbolic programming (Wolfram 2003) and based on continuation methods.

3.3.4 Searching post-buckling equilibrium paths near the critical state: the direct search approach using coordinate control

Going back to the problem under observation – the search of post-buckling

equilibrium paths in the neighbourhood of an already known critical equilibrium state –, as an alternative to the scheme of Thompson and Hunt presented above, which is based on perturbation procedures, the post-buckling equilibrium paths are determined numerically in this thesis by solving directly the non-linear transformed equilibrium system (3.61) or (3.62), which was previously manipulated in order to ensure that the resulting equilibrium state stays outside the equilibrium path. The procedure presented in the following is devoted to simple bifurcation problems, for which $m=1$, the most common situation in practice, is greatly inspired in the Thompson and Hunt's scheme and shall be viewed as an adaptation of the traditional stability procedures to the use of continuation methods in the context of symbolic programming software MATHEMATICA (Wolfram 2003). It relies only on the definition of an equilibrium path – any line in the R^{n_C+1} space that solves the equilibrium system (3.25) – and also on the following theorems (Thompson and Hunt 1973):

Theorem 1: an initially stable (primary) equilibrium path rising monotonically with the loading parameter cannot become unstable without intersecting a further distinct (secondary) equilibrium path;

Theorem 2: an initially stable equilibrium path rising with the loading parameter cannot approach an unstable equilibrium state, from which the system would exhibit a finite dynamic snap, without the approach of an equilibrium path (which may or may not be an extension of the original path) at values of the loading parameter less than that of the unstable state.

These theorems apply to the present problem and, due to the shape of the FP, which is almost linear in the range of interest, i.e., between the unloaded and the relevant critical state, a secondary equilibrium path must emerge from the critical state since here the determinant of the Hessian matrix becomes zero, passing from positive to negative, and thus the FP ceases to be stable, although the values of the control parameter P rise. Therefore, among all equilibrium paths in the R^{n_C+1} vector space related to the sliding

coordinates and the load parameter P that solve the equilibrium system (3.54), it is sought the one that intersects the FP at the relevant critical state determined above. So, from the above paragraph some information about this post-buckling equilibrium path (PBP) can be obtained: it contains the critical state defined by the n_{C+1} dimensional vectors $\left({}^{i}a_{CR}, P_{CR}\right)$, $i = 1,\ldots,n_C$, or by $\left(0,\ldots,0,P_{CR}\right)$ in terms of the sliding coordinates, and from this point, follows approximately the direction of the critical eigenvector in the ${}^{i}a$-P or ${}^{i}q$-P vector space.

The search of this equilibrium path is performed using simple continuation methods, determining a number of points in the R^{n_C+1} space of the sliding coordinates and the load parameter belonging to the solution curve of interest. The post-buckling equilibrium path is thus defined by the set of n_K points in the form:

$$\left\{\left\{{}^{i}q_k\right\}, P_k\right\}, i = 1,\ldots,n_C, k = 1,\ldots,n_K, \tag{3.83}$$

being $\left(0,\ldots,0,P_{CR}\right)$ part of this set, and the first step to define (3.83) is to chose one active coordinate as the controller, denoted by ${}^{control}q$. Following Thompson and Hunt (1973 and 1984), it is required for this coordinate that the matrix obtained by removing the *control* line and *control* column of the Hessian matrix at the critical state is non-singular:

$$\det\left(\boldsymbol{W}_{ij}^{C}\right) = \left|\frac{\partial^2 W}{\partial^i q \partial^j q}\right|^{C} \neq 0, \quad \begin{cases} i = 1,\ldots,n_C \wedge i \neq control \\ j = 1,\ldots,n_C \wedge j \neq control \end{cases}. \tag{3.84}$$

Since ${}^{control}q$ is active in the post-buckling range, its corresponding term in the buckling mode must be non-zero and in most cases it is convenient to chose as the controller the coordinate that has a high coefficient in the buckling mode $\left\{{}^{i}\overline{q}\right\}_{CR}$, obtained through (3.64), but not necessarily the highest. Subsequently, a set of n_K positive and negative prescribed values are attributed to ${}^{control}q$ and the equilibrium system becomes dependent of the remaining coordinates and of the load parameter:

$$W_i\left({}^{j}q, P\right) = 0, i = 1,\ldots,n_c, \quad j = 1,\ldots,n_c \wedge j \neq control, \tag{3.85}$$

thus having n_C unknowns and n_C equations. By placing the equilibrium equation related to

${}^{control}q$ at the end of the system, the corresponding Jacobian matrix has a symmetric $(n_C - 1)\times(n_C - 1)$ dimensional block along the main diagonal, which is very useful for numerical purposes, and is written in the form:

$$\boldsymbol{J} = \left[\begin{array}{c|c} \dfrac{\partial W_i}{\partial^j q} & \dfrac{\partial W_i}{\partial P} \\ (\text{symmetric block}) & \\ \hline \dfrac{\partial W_{control}}{\partial^j q} & \dfrac{\partial W_{control}}{\partial P} \end{array}\right], \quad \begin{cases} i = 1,\ldots,n_c \wedge i \neq control \\ j = 1,\ldots,n_c \wedge j \neq control \end{cases}. \tag{3.86}$$

Therefore, the set (3.83) is defined by giving a sequence of pre-established non-zero, positive and negative, values with increasing modulus to ${}^{control}q$ and, for each value, by determining the corresponding solution of (3.85). Care shall be taken upon the choice of the lowest attributed value for ${}^{control}q$, for the sequences associated with positive and negative values of ${}^{control}q$, denoted by ${}^{control}q_{(1)}$: in the thesis it was chosen by analysing directly ill conditioning phenomena of the Jacobian matrix, in order to reduce the numerical instability of the procedure, and the first value was adopted when the respective Jacobian matrix was well conditioned and whose inverse was correctly determined. Note that, at the critical state, the Jacobian matrix is singular, hence not invertible, and in a neighbourhood around the critical state this matrix is ill-conditioned (Fellipa 2001), being very difficult, even not possible, to determine its inverse, and any adopted method for solving the non-linear algebraic system (3.85) may lead to incorrect solutions (Golub and Van Loan 1996). Following Wriggers (1995) and Krätzig (1995), as a first approximation of the solution of equilibrium system (3.85), in order to move away from the critical state, the terms related to the passive coordinates are computed by making resource to the relevant buckling mode vector $\{{}^i\overline{q}_{CR}\}$, $i = 1,...,n_C$, in the form:

$${}^i q_{(0)} = {}^i\overline{q}_{CR} \times \frac{{}^{control}q_{(1)}}{{}^{control}\overline{q}_{CR}}, \quad i = 1,\ldots,n_C, \tag{3.87}$$

which means that the first approximation for the solution of the equilibrium system follows

the critical buckling mode, and the term related to the load parameter is considered equal to P_{CR}. Then, the traditional Newton-Raphson method (Jennings and McKeown 1992) is applied to solve the resulting algebraic non-linear system (3.85), and the obtained solution is then used as a first approximation for the next step, related to the second prescribed value for ${}^{control}q$. Finally, the PBP is defined by the set of resulting points, each being a solution of the equilibrium system (3.85). Fig. 3.7 gives a geometrical representation of the presented scheme in the R^{n_C+1} space.

Having found the first equilibrium point outside the equilibrium path, it is possible to opt between proceeding with this scheme by giving increasing values to ${}^{control}q$ (positive and negative), hence forcing the resulting equilibrium points to move outwards the FP, which is valid as long as the equilibrium points move away from the FP in the ${}^{j}a$-P hyper-plane, or by any other appropriate method (Allgower and Georg 1990). Moreover, it is also possible to compute the PBP either through the transformed equilibrium system of (3.85) or by the initial one, from (3.54), as long as it is known the way coordinate ${}^{control}a$, related to ${}^{control}q$ through transformation (3.59), evolves along the PBP, which is not difficult to obtain. The stability of the obtained equilibrium states can be evaluated through the usual process, by evaluating at each equilibrium point the sign of the determinant of the corresponding Hessian matrix. By doing this, the search of secondary critical states becomes possible for the adopted discretization, following the same scheme as above, shooting a polynomial in an appropriate parameter when a critical point becomes near and searching alternative equilibrium points outside the secondary path – if a more refined discretization was possible, regarding the available computational capacities, since the energy system (3.54) is conservative, thus keeping its volume and dimensions in the R^{n_C+1} space (Thompson and Stewart 2002), this scheme would proceed to the search of secondary bifurcations which would implicate, almost certainly, the appearance of localized phenomena (Coman 2004). These localized buckling phenomena were already observed, either experimentally (Graves-Smith and Sridharan 1980) or analytically (Lord,

Champneys and Hunt 1997, Hunt, Peletier, Champneys, Woods, Ahmer Wadee, Budd and Lord 2000), in some types of thin-walled prismatic members under compression or bending and in the near future it is wished to analyse them in the context of the extended GBT formulation, as sufficient computer resources become available to the author. Finally, it is important to highlight that the use of symbolic programming software, like MATHEMATICA in the present case, allows the analyst to choose the appropriate coordinate for the definition of the equilibrium path that solves system (3.85), and one coordinate might be appropriate for one section of the equilibrium path, while for another section another coordinate can make easier the involved computations – by choosing the appropriate coordinate to control the solving procedure for each section of the equilibrium path, the analyst can turn the sometimes complex problem of searching solution paths in highly non-linear systems into a sequence of much easier problems.

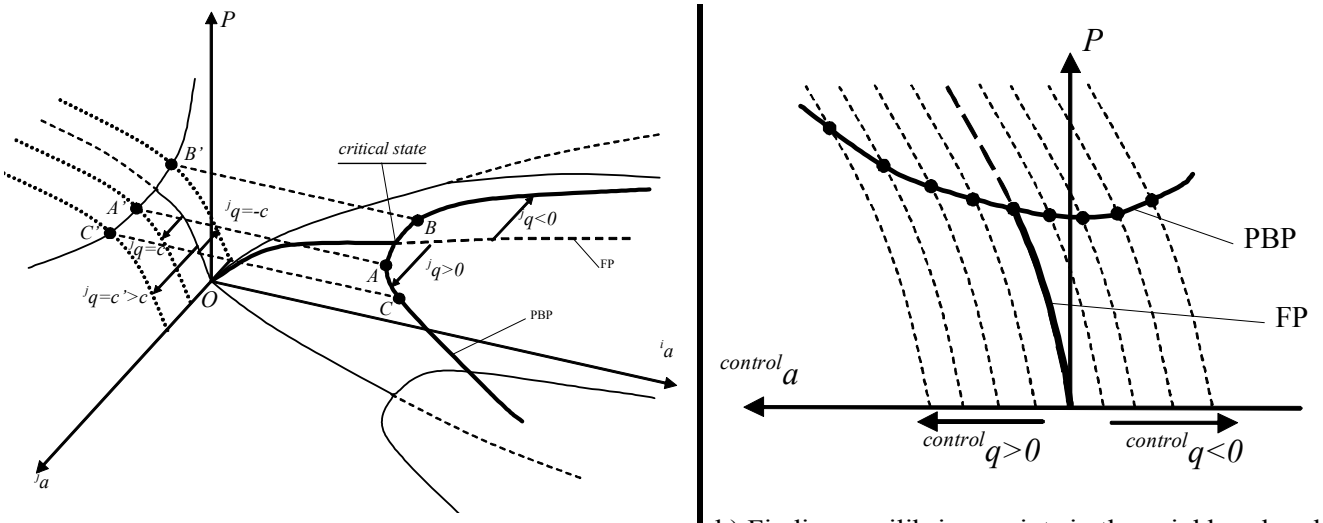

a) General overview

b) Finding equilibrium points in the neighbourhood of the FP (hyper-plane ^{j}a-P)

Fig. 3.7 – Direct search of post-buckling paths in the neighbourhood of the critical point through continuation methods

3.4 – Computer implementation of the stability procedures

Regarding the optimization of the computational resources, several worksheets running on the software MATHEMATICA were implemented to solve the examples shown in the following chapter. They comprise: i) the calculus of the TPE, ii) the linear stability analysis, in the sense of the characterization of the critical behaviour of the member in relation to the member's length, and iii) the post-buckling analysis for a specific length of the member. In the following, a general presentation of these programs is made, to clarify the application of the concepts just presented to practical member stability analysis.

The calculus of the ISE is the hardest task in the overall analysis, and usually the one that limits the number of adopted polynomial coordinate functions per mode of deformation (it may take several… weeks, continuously, to compute the ISE for one single example), due to the heavy calculations involved, and is realized according to Fig. 3.8.

The input data consists in the adopted number of modes of deformation and generalized coordinates, respectively n_{MD} and n_C, a vector containing the definition of all amplitude modal functions, each one expressed in the form of expression (3.44), and the set of generalized properties, which were previously computed using the formulas shown in chapter 2.3.3. The ISE is then calculated making resource to the matrix scheme of chapter 3.2.3, which already considers the adopted coordinate functions to approximate each modal amplitude function ${}^{k}A$. The potential of the external loading is computed by expression (2.109) of chapter 2.3.4 and then the TPE becomes fully defined, being a function of the generalized coordinates ${}^{1}a,\ldots,{}^{n_C}a$ and of the load parameter P. It is noted here that for post-buckling analysis the member's length L is defined as the worksheet starts while for linear stability analysis the TPE may stay also dependent of L, due to the available computer resources, both being related to a specific cross section and load case.

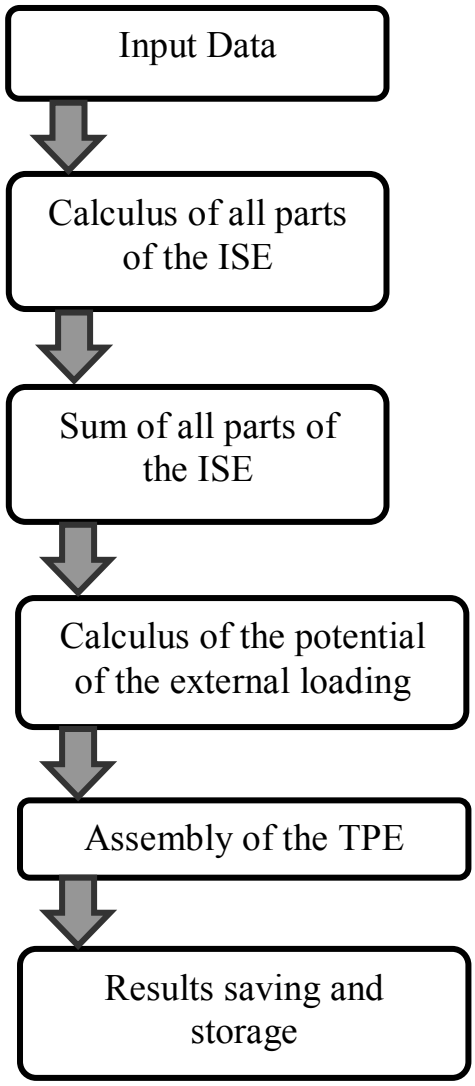

Fig. 3.8 – Flowchart of the program for calculation of the TPE

It is highlighted here that GBT constitutes, in a certain way, a way of discretization, which introduces unavoidable errors in the solution. Also, the thin-walled prismatic structural members under analysis show very small ratios thickness/length, due to their very small thickness, and so their analysis may be very susceptible to numerical locking phenomena that often occurs in FSM or FEM analyses of thin-walled members, which can destroy completely the accuracy of the solution (Cook, Malkus and Plesha 1989, Lanzo, Garcea and Casciaro 1995, Garcea 2001). These phenomena can also affect any GBT non-linear analysis and usually decrease as the discretization becomes smaller, but refined GBT

discretizations, which imply a large number of inner nodes, may not be possible since they demand large computer resources. Although in certain cases locking can appear in linear analyses, it is often due to errors in the calculus of the non-linear terms of the TPE – one possible cause is the unavoidable errors that occur in the calculus of the difference of very large numbers, the error usually being greater than the correct value (Lanzo, Garcea and Casciaro 1995). A common way to assure the accuracy of the analysis, overcoming this problem, is to consider the fewest number of non-linear terms, obviously as long as the accuracy of the analysis is not affected. Apart certain types of problems that deal with local non-linear effects, like patch loading or non-correct support conditions, in thin-walled prismatic cold-formed members the main cause of geometric non-linearity are the membrane longitudinal stresses and strains, so very often it is adopted the assumption of accounting only for the non-linear effects related to the longitudinal membrane stresses. This strategy is used by Thompson and Hunt (1984) for the analysis of compressed plates, by Schafer (1997) in the context of the FSM, and also by Schardt (1994) in the GBT stability analysis for open cross sections. In the context of the GBT formulation presented in chapter 3, it implies the consideration of only the higher order parts associated with the tensors $\boldsymbol{\kappa}_{LO2}$, $\boldsymbol{\kappa}_{LO3}$ and $\boldsymbol{\kappa}_{LO4}$ in expression 2.110 in the member's global analysis. This strategy was adopted in several examples and has generated very good results when it was compared to other methods of analysis, like the FSM (Schafer 2003).

The linear stability analysis is performed through the scheme presented in Fig. 3.6. The input data is the TPE, which depends on the generalized coordinates ${}^{1}a,\ldots,{}^{n_C}a$, the load parameter P and the member's length L. The equilibrium equations system is obtained by expression (3.54), deriving the TPE in order to each generalized coordinate and the FP is determined through the power series method, assuming each coordinate given by expression (3.57) and rendering to zero each coefficient of every power of P in each equation of the equilibrium system. It is possible to prove that, in this step and for a specific member's length L, only one matrix inversion is required, independently of the

approximation adopted for the generalized coordinates, in a similar way as done by Hunt (1981) for the post-buckling analysis through a perturbation scheme. The matrix inversion is made making resource to the MATHEMATICA appropriate instruction. The *W*-transformation is then applied, the Hessian matrix is deduced through expression (3.63) and the eigenproblem that will determine the critical state is established in the form given by expression (3.65). The procedure explained in Mirasso and Godoy (1992) is then applied, noting that in expression (3.65) matrix $\boldsymbol{H}_{FP}^{(1)}$ is not invertible – see chapter 2.4, where this is proved for column analysis in the context of the classical GBT theory. This difficulty is easily overcome by making resource to the relevant properties of the eigenvalue problems (Wilkinson 1965) so that the first step of the eigenproblem must be expressed in the following form:

$$\left(\boldsymbol{H}_{FP}^{(1)} + \frac{1}{P} \boldsymbol{H}_{FP}^{(0)} \right) \{q\} = \boldsymbol{0} \,, \tag{3.88}$$

and is solved using the MATHEMATICA own appropriate instructions. The lowest eigenvalue, denoted by $P_{CR,1}$ is then retained and used to update the eigenproblem, through the scheme proposed in Mirasso and Godoy (1992), in the following form

$$\left(\boldsymbol{H}_{FP}^{(1)} + \left(\boldsymbol{H}_{FP}^{(2)} \; P_{CR,1}^{2} + \boldsymbol{H}_{FP}^{(3)} \; P_{CR,1}^{3} + \ldots \right) + \frac{1}{P} \boldsymbol{H}_{FP}^{(0)} \right) \{q\} = \boldsymbol{0} \,. \tag{3.89}$$

Usually one or two iterations are sufficient to achieve convergence, then the eigenvector is determined, using the MATHEMATICA instruction for determining eigenvectors, and the one that corresponds to the lowest eigenvalue P_{CR} represents the relevant buckling mode. Finally, the critical loads and the buckling modes are saved and stored in a file, in order to draw the graphics of the critical behaviour – loads and modes – in relation to the member's length. For the examples presented throughout this thesis, due to computer limitations, the maximum number of adopted polynomials for modes of deformation 2 and higher, for post-buckling column analysis, was five, which implies more than 90 generalized coordinates if about 20 modes of deformation are adopted.

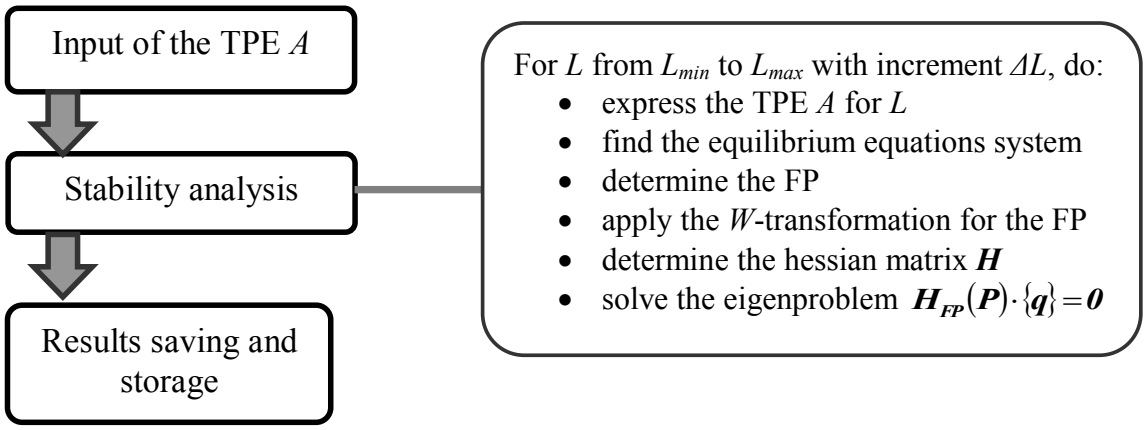

Fig. 3.9 – Flowchart of the program for stability analysis

The post-buckling analysis is performed for a specific member's length using the scheme presented in Fig. 3.10 below, and follows the procedure used for linear stability analysis described above until the determination of the critical state along the FP. Then, based on the concepts presented in chapter 3.3, the post-buckling equilibrium path is determined and, at each equilibrium point, the determinant of the Hessian matrix is calculated to enable the full characterization of the equilibrium state. The algebraic equilibrium system (3.85) may be solved by any appropriate numerical method (Stoer and Bulirsch 1993, Jennings and McKeown 1992). A Newton-Raphson scheme was adopted here, benefiting from the internal procedures of Mathematica (Wolfram 2003). The initial values of the unknowns influence the convergence of the method, so, in order to improve the efficiency of the numerical method, the initial value of the sliding coordinates for the first iteration is taken proportional to the eigenvector of the problem (3.89) that corresponds to the critical load.

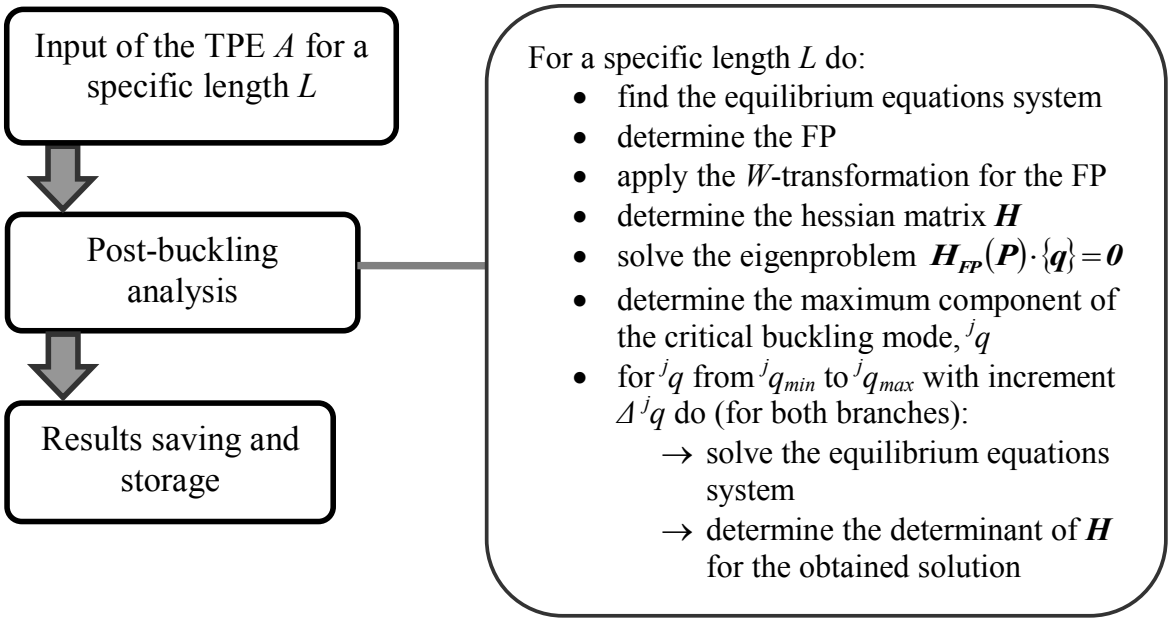

Fig. 3.10 - Flowchart of the program for post-buckling analysis

3.5 – Chapter synopsis

This chapter contains the numerical developments that were needed to implement the post-buckling analysis of thin-walled perfect members through the unified energy formulation of GBT. At first, a structured and sequential scheme that derives the appropriate coordinate functions from the relevant modal boundary conditions, in the context of the Rayleigh-Ritz method, was presented. The graphics of the resulting functions prove their adequacy for the buckling and post-buckling analysis and the advantages of adopting these functions instead of trigonometric ones. As referred in Chapter 1, Storch and Strang (1988) performed a Rayleigh-Ritz analysis for a simple cantilever beam and addressed the fact that the adoption of trigonometric functions can not render a complete vector space basis for the unknown functions, since they can not simulate a function with constant second order derivative along the member's length. In fact, in the scheme presented just above, this aspect is also perceived and explained: for

functions respecting all cinematic boundary conditions, this limitation is related to the obedience to the natural boundary conditions of the system for the functions derived above, so if a complete set of coordinate functions is needed to analyse a general case, natural boundary conditions must be removed from the problem. So, one has to opt between a faster convergence, that usually – but not always – is obtained from the obedience to the natural boundary conditions, or the completeness of the functions set, which renders completely general the RRM analysis. In most cases the second option is more advisable, since, usually, it carries only one or two more coordinate functions per unknown to achieve a similar convergence to the first option.

Subsequently, the stability procedures that permit the calculus of the sought equilibrium paths were described. They are based on the traditional bifurcational calculus adapted to the stability analysis by Thompson and Hunt, but were improved here in the context of an advanced programming software, in order to avoid the more complicated computations based on the perturbations scheme – with the modern symbolic software programming like MATHEMATICA, needed to manipulate the member's equilibrium system, it was observed that, as the number of discrete coordinates increases, it is easier to invert a matrix than to make a series development of the passive coordinates in terms of the active one. The numerical techniques just presented will be applied to several illustrative examples in the following chapters, in the context of the energy formulation for the classical or extended GBT theories. This chapter is based on two articles from the author that were presented in two international scientific conferences (Simão and Simões da Silva 2003b and 2004b).

4 – ILLUSTRATIVE EXAMPLES FOR THE CLASSICAL GBT FORMULATION

4.1 – Introduction

This chapter presents some applications of the energy formulation derived above, in the context of the classical GBT theory, to the linear and non-linear stability analysis of open non-branched and closed mono-cellular section thin-walled sections under uniform compression or major axis bending moment. The objective of these examples is to validate the implementation of the unified post-buckling energy formulation developed in Chapter 2 and the implementation of the numerical techniques presented in Chapter 3. The validation examples comprise i) the comparative stability analysis of a mono-cellular ad a channel cross section columns, ii) the linear stability analysis of a closed mono-cellular simply supported beam, and iii) the post-buckling analysis of a simply supported channel column. These validation examples are not intended to reproduce real situations but only to highlight the features of the formulation that was developed. In particular, an ideal elastic material was considered, without any concern about actual levels of plasticity.

4.2 – Comparative analysis of an open and of a closed cross section columns

The present example compares the linear stability behaviour of a closed mono-cellular and of a channel section member under uniform compression. The closed cross section – case 1 – consists of a RHS $80\times40\times2$ member while the open section – case 2 – was chosen to have the same height, width and cross sectional area as and also to fulfil

EC3 – part 1.3 recommendations for lip slenderness (EC3 2006). Fig. 4.1 illustrates the cross section geometry and the nodal discretization for the chosen sections. Young's modulus is $E = 210$ GPa and the Poisson ratio is $\mu = 0.3$. The warping functions, the cross section displacements and the transverse bending moments are shown in Figures 4.2, 4.3 and 4.4. These figures illustrate some important aspects: for the closed section, only one distortional mode, here referred in the most restrictive sense of the word distortional – the mode that is associated with distortional buckling, is generated (mode 5), while for the channel section two distortional modes – symmetric distortional mode 5 and anti-symmetric distortional mode 6 – are generated. The remaining distortional modes, here in wider sense, i.e., modes associated with non-zero terms of the diagonal matrix $\boldsymbol{B}$, deal just with plate and/or lip bending and are associated with null displacements of the main nodes along the cross section plane, except for the free nodes of the lips.

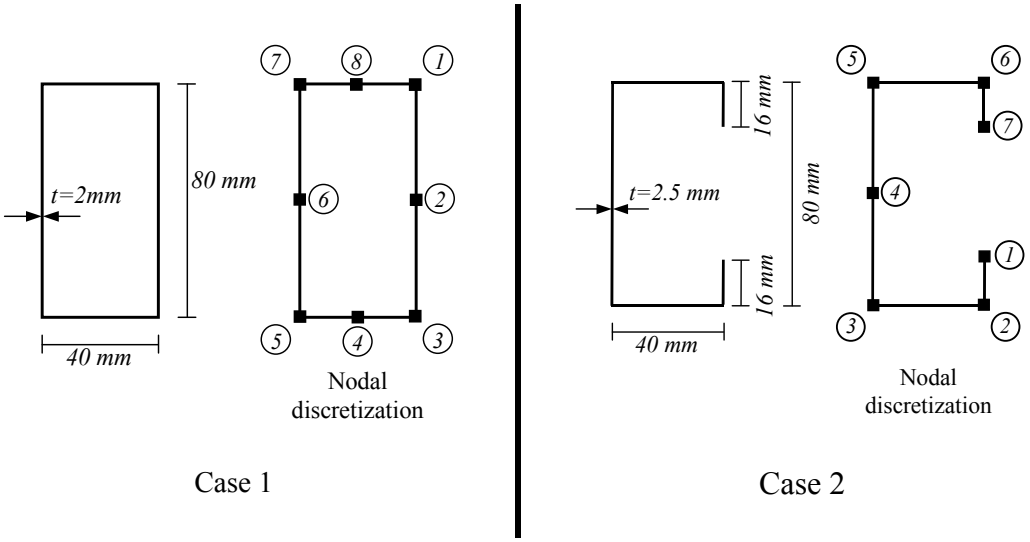

Fig. 4.1 – Definition of cross sections dimensions and nodal discretization

The boundary conditions are assumed to model a simply supported column, as shown in Fig. 4.5, so that the trigonometric functions:

$$ {}^{k}\varphi = sin\frac{\pi x}{L} \tag{4.1} $$

are chosen as trial functions for modes 2 to 9, while for mode 1 polynomial (3.24) is chosen to model a column with an end free to move along the longitudinal direction. For a compressive axial force P applied at one end – see Fig. 4.5 – the potential of the external load is simply given by:

$$ \Pi_{P,1} = P \times {}^{1}V' \Big|_{x=L} = {}^{1}a \frac{2\sqrt{5}}{L^{3/2}} P \,. \tag{4.2} $$

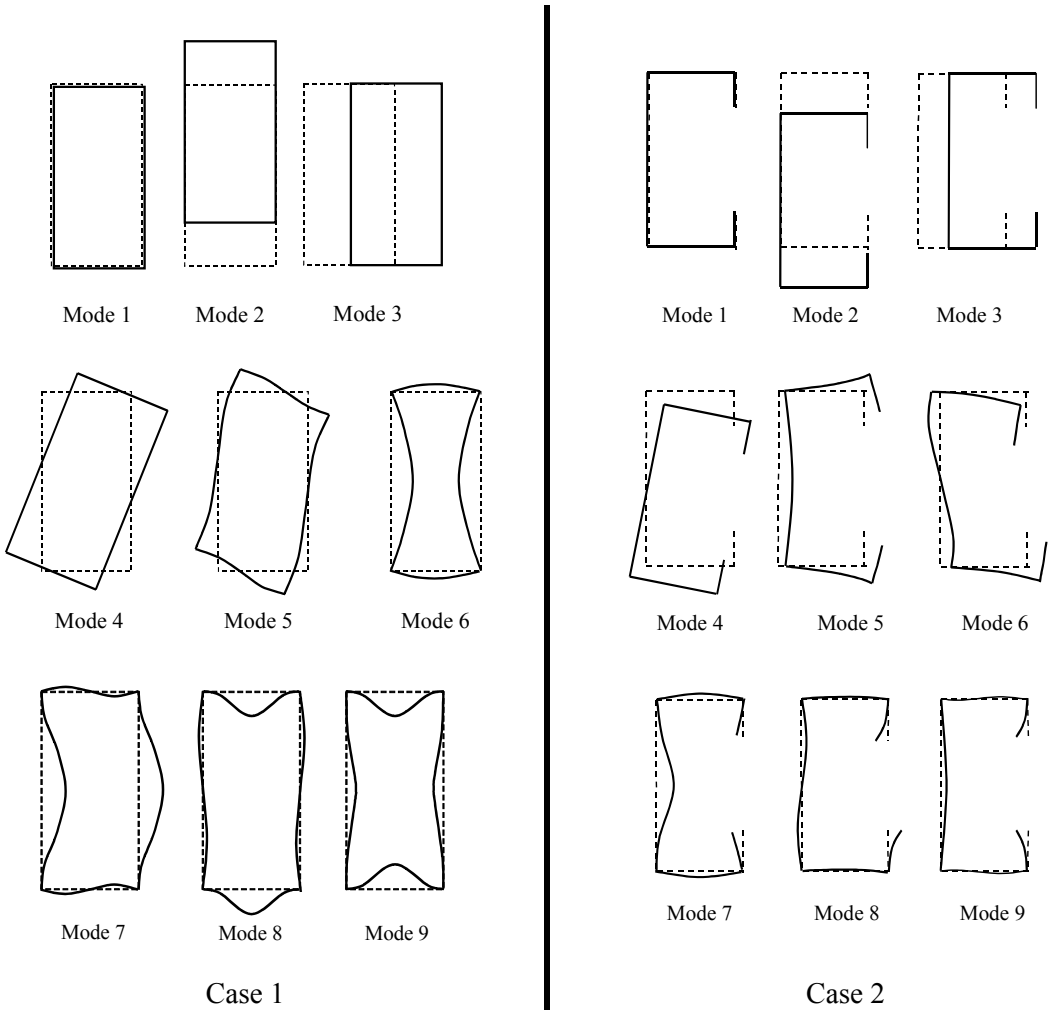

Fig. 4.16 – Shape of the unitary modal cross section displacements

Since both cases are related to equal cross section areas – that is equivalent to say,

in GBT notation, to equal values of ${}^{1}C$ (Schardt 1989) – their fundamental paths are equal and given by:

$${}^{1}a_{1} = 2.21832 \times 10^{-6} \times L^{5/2}, \tag{4.3}$$

all other coordinates being equal to zero. Applying the standard stability procedures presented in Chapter 3, the critical loads of Fig. 4.6 are obtained, together with the modal participation coefficients.

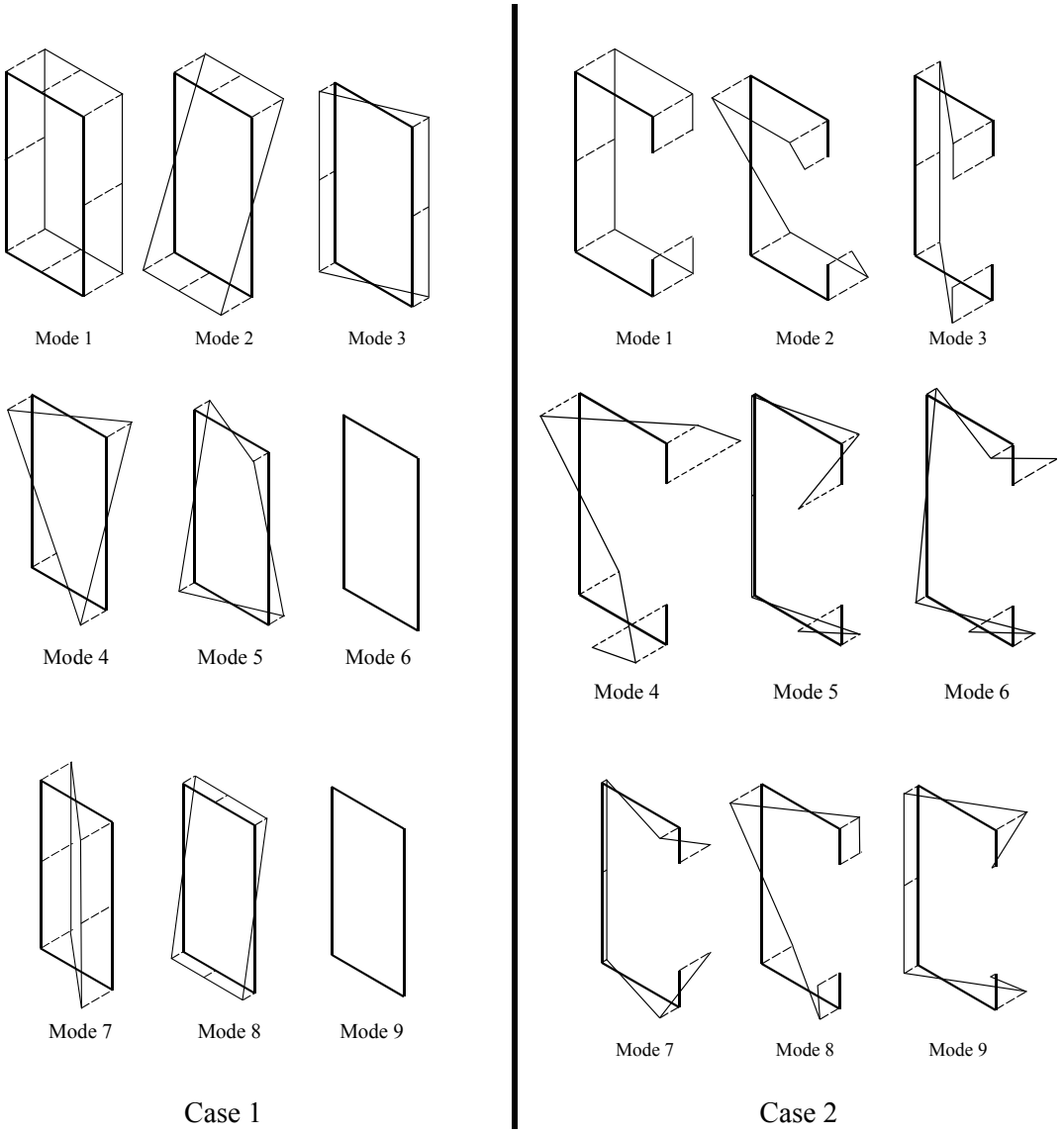

Fig. 4.3 – Shape of the unitary modal warping displacements

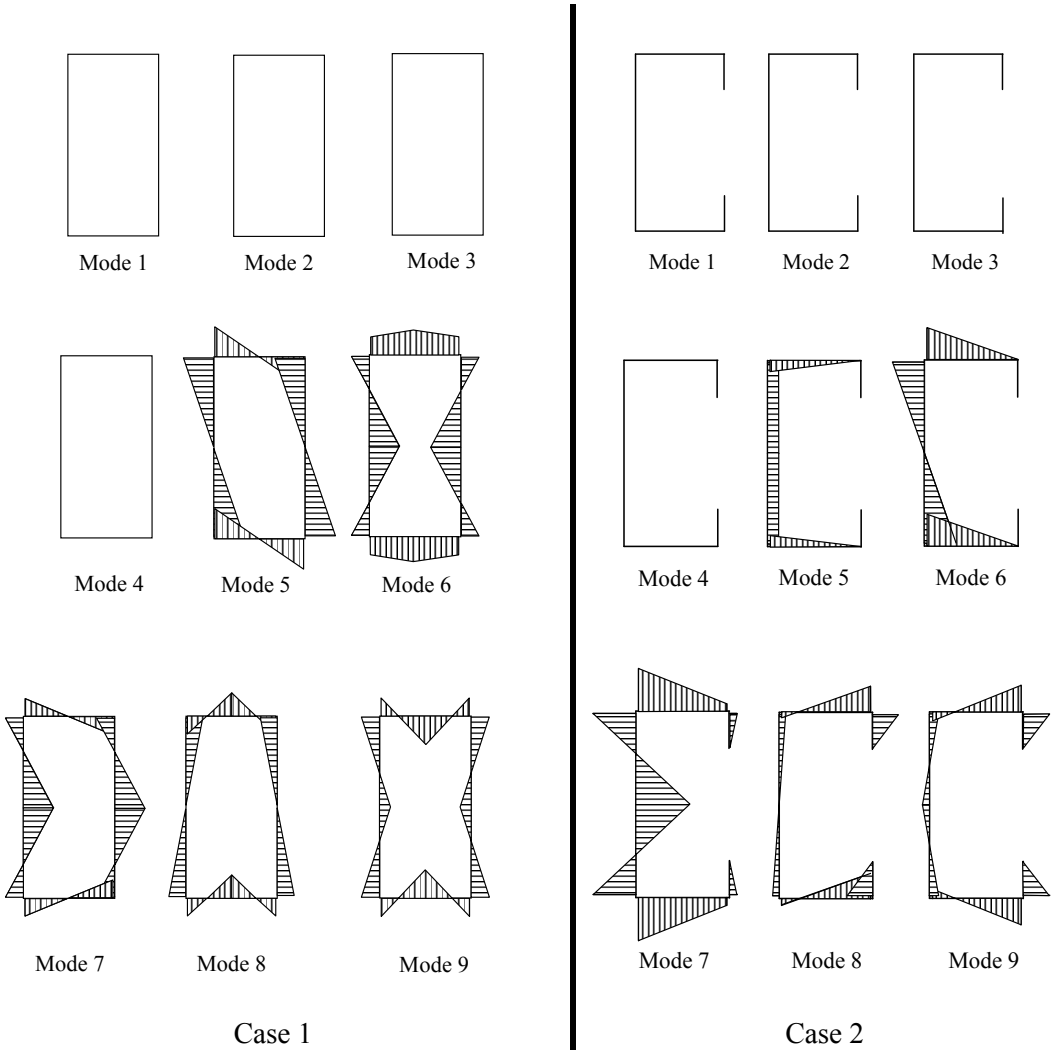

Fig 4.4– Shape of the modal transverse bending diagrams

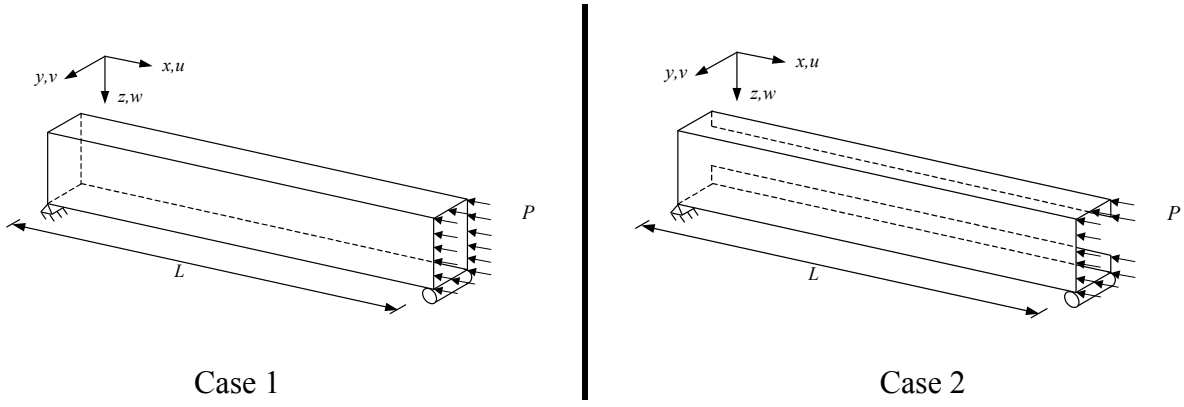

Figure 4.5 – The simply supported compressed column

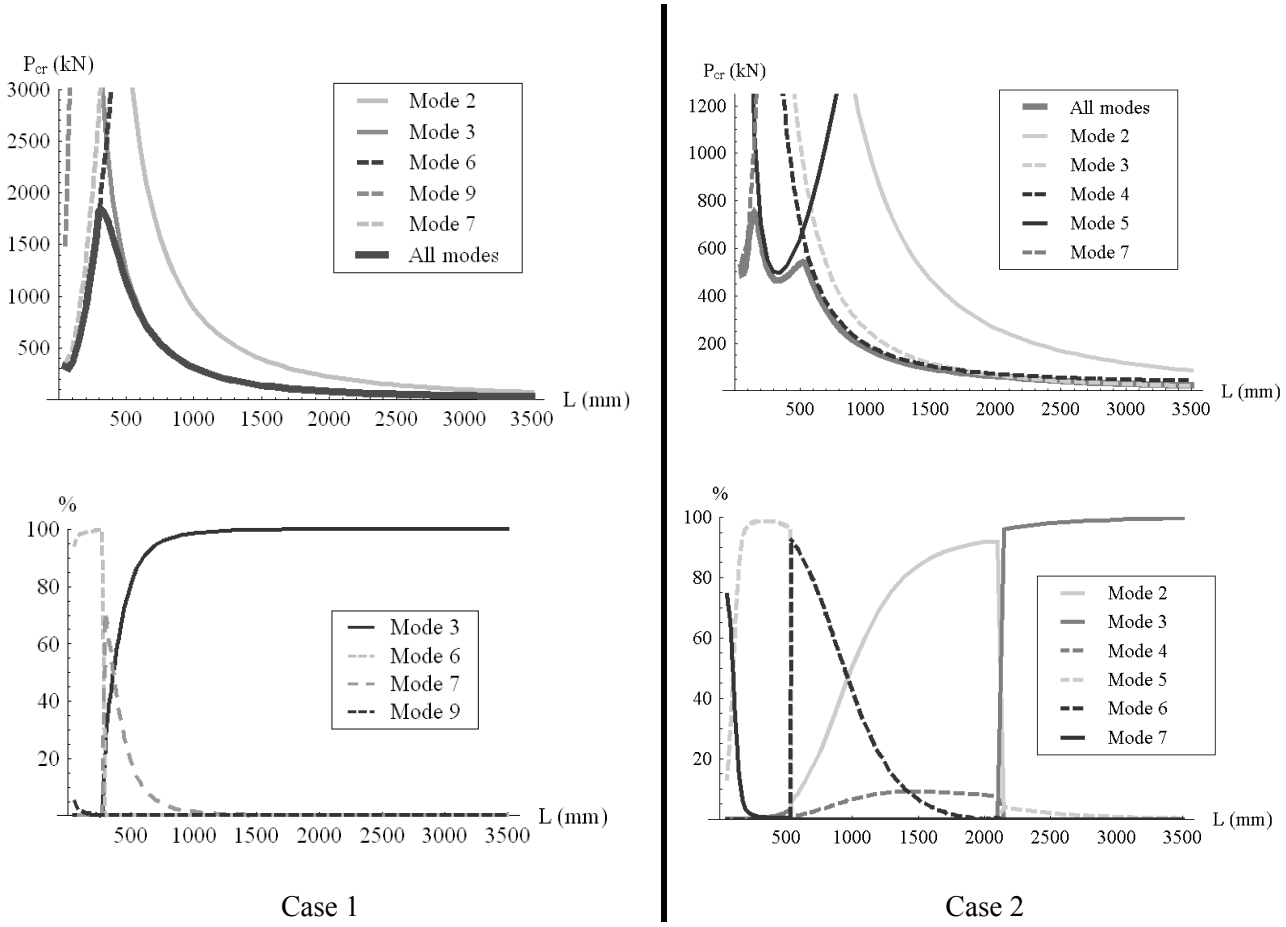

Fig. 4.6 – Buckling loads and modal participations for cases 1 and 2

For case 1, the existence of three buckling regions is clearly perceptible. The first region, where modes 6 and 9 are predominant, corresponds to the local plate buckling zone, for lengths smaller than 400 mm. Then, as the member length increases, the second region occurs, where modes 3 and 7 interact, this phenomenon being related to global buckling – minor axis bending – influenced by buckling of the compressed web, linked to the asymmetric distortional mode. Finally, for lengths longer than 1500 mm, the third region occurs, where mode 3 (minor axis bending) alone governs the behaviour of the member. It is important to notice that individual mode buckling loads for modes 4 and 5 are much greater than the buckling loads for all modes, as can be observed in Figure 4.7.

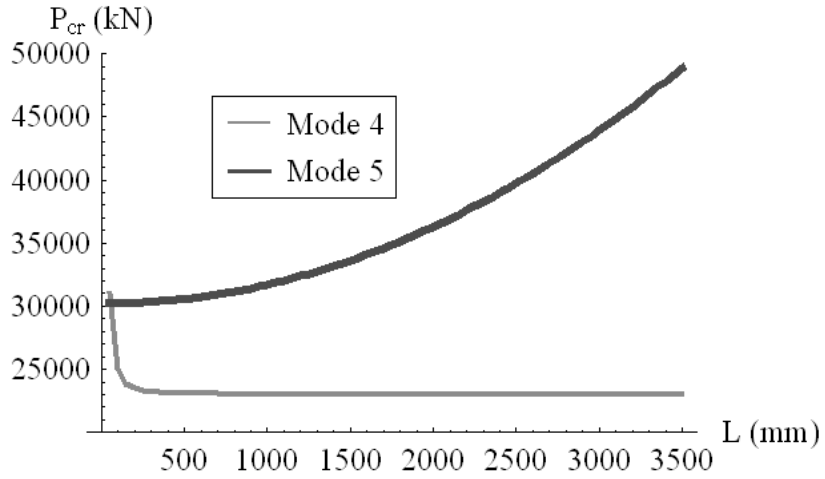

Fig. 4.7 - Single mode buckling loads for modes 4 and 5 for case 1

The buckling behaviour for case 2 is far more complex, being a mono-symmetric open cross section. Four buckling regions can be identified. The first region corresponds to lengths smaller than 100 mm and local plate buckling rules the column behaviour, which, in GBT notation, is expressed by the strong influence of mode 7. Then, a second region occurs for lengths up to 530 mm and mode 5 controls the buckling loads, corresponding to the symmetric distortional buckling zone. In the third region, that can be denoted as the anti-symmetrical flexural-distortional buckling range, for column lengths between 530 mm and 2100 mm, modes 2, 4 and 6 control the behaviour – in this zone at first, mode 6 (asymmetric distortional mode) governs the behaviour but smoothly major axis bending (mode 2) takes the most relevant role. Finally, for lengths higher than 2100 mm, minor axis bending controls alone the behaviour of the column.

Observing Fig. 4.8 it is seen that the buckling load for smaller lengths is lower for the closed section than for the channel, due to its smaller thickness. For higher lengths the buckling loads become higher for the closed section due to the higher minor axis bending stiffness.

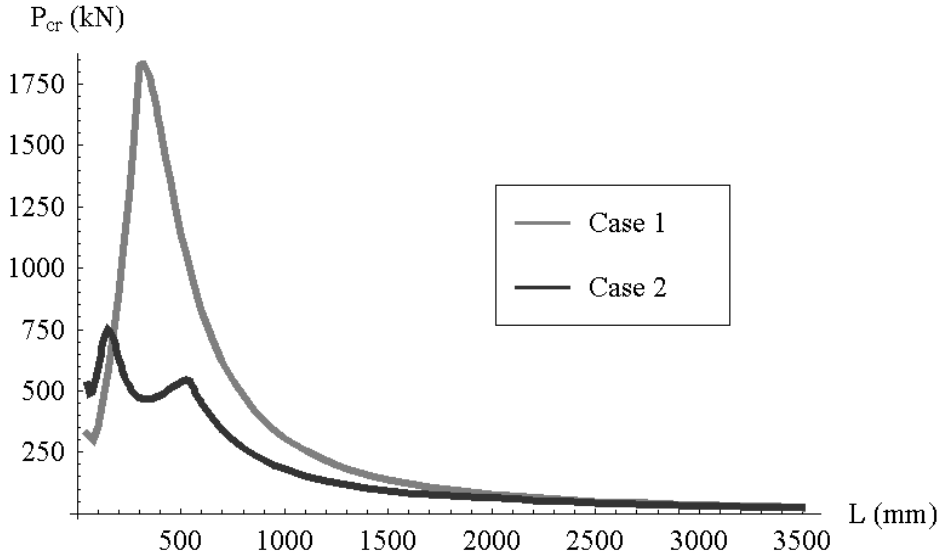

Fig. 4.8 – All modes bifurcation loads for cases 1 and 2

A last note to refer that the analysis just performed used only one half-wave per mode of deformation, like in several stability works (see, for example, Davies), so in this introductory example the multi-wave effect that often occurs in plated structures (Bleich 1952) was not modelled, hence was not observed. In forthcoming examples this phenomenon will be analysed.

4.3 – Stability analysis of a closed cross section member under uniform major axis bending moment

In the literature a wide range of works on the stability of open section members under major axis bending moment may be found, which use FSM (Prola 2001), or GBT (Davies, Jiang & Ungureanu 1998), or even FEM. It is thought that closed cross section beams have high resistance to buckling, due to the high stiffness of these sections to torsional effects, so that flexural-torsional buckling is not relevant. However, the following

example shows that the cross section's distortion induces a relevant decrease of the critical moment when compared to the traditional rigid cross section analysis.

Here the closed cross section member of the previous example is submitted to two equal and opposite major axis bending moments M, at both ends of the member. The potential of the external loads is now given by:

$$\Pi_M = M \times \left(-{}^2V' \big|_{x=0} + {}^2V' \big|_{x=L} \right). \tag{4.4}$$

and a small adjustment was made to the coordinate functions. The coordinate function related to mode of deformation 2 is no longer sinusoidal, instead polynomial (3.38 a) is chosen to allow a uniform and constant linear major axis bending moment. Assuming that both ends are longitudinally fixed and thin plates are used at the edge cross sections, the critical moments are determined for a range of lengths, leading to the results of Fig. 4.9. Fig. 4.9 highlights that there are two sets of lengths: the smaller lengths – smaller than about 350 mm – for which local plate modes rule the buckling load, related to the buckling of the compressed flange, and the higher lengths range – over about 350 mm – for which the rigid body mode 3 and the distortional mode 5 control the buckling behaviour of the beam. In contrast to the compressed column, the distortional mode is very important for all the higher lengths range, the critical moments resulting from the combination of all modes being much smaller than the critical bending moments arising from the analysis with the rigid body modes 3 and 4 only. Therefore, the neglect of the cross section distortion mode results in a gross overestimation of the critical moments.

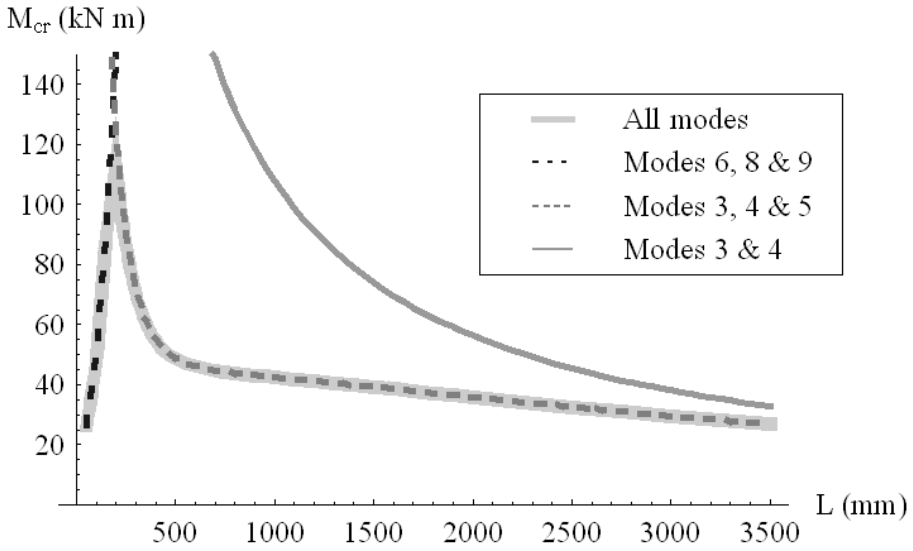

Fig. 4.9 – Critical major axis bending moments

The modal buckling loads were determined by equalling to zero the determinant of the TPE Hessian matrix (Thompson & Hunt 1973), in the context of the Rayleigh-Ritz method, as in the previous example. To show the precision of this method with only one coordinate function, the critical moments were calculated also using the FSM program CUFSM (Schafer 2003) in Fig. 4.10 and the bifurcation moments for modes 3 and 4 only, corresponding to neglecting the cross section distortion, were compared to the classical critical moment formula (Trahair 1993) in Fig. 4.11. It can be observed a very good fitting between both curves, for both cases.

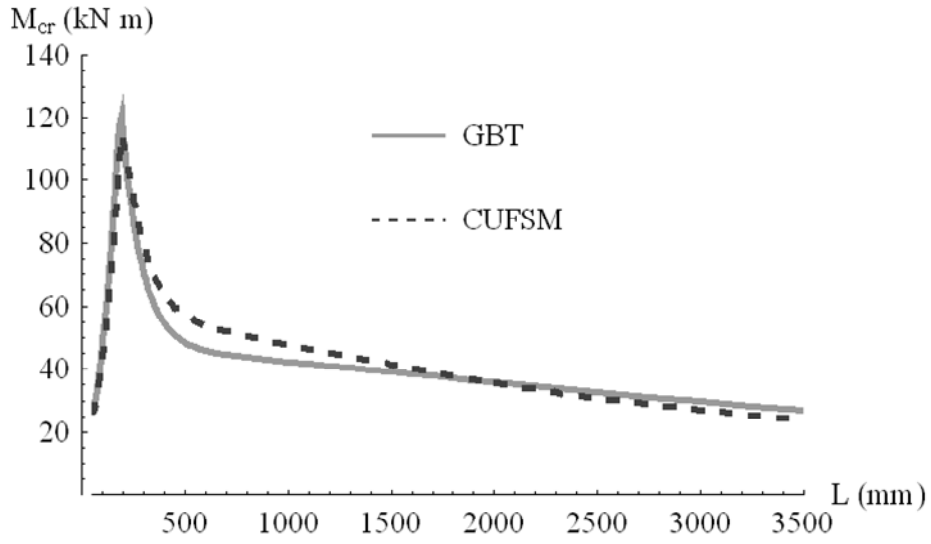

Fig.4.10 – Comparison between the stability procedures using GBT and CUFSM (Schafer 1998)

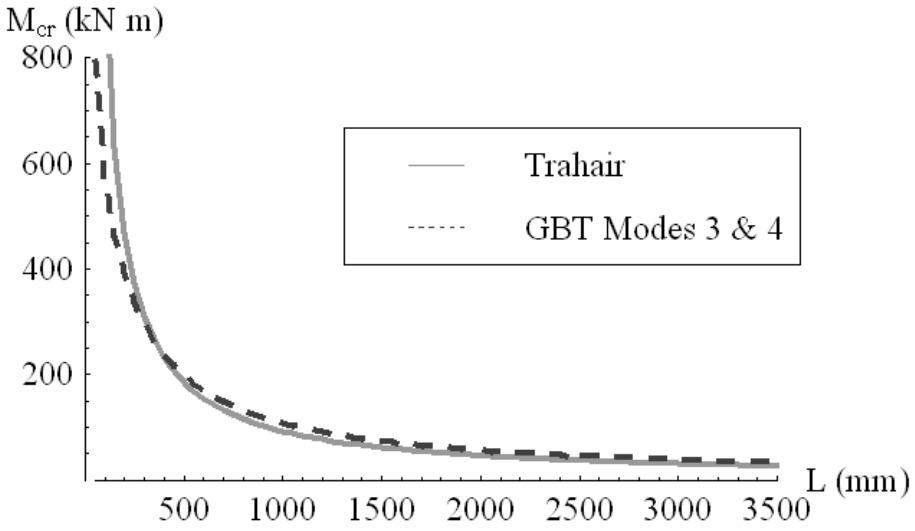

Fig.4.11 – Comparison between the stability procedures using Rayleigh-Ritz method and the classical formula (Trahair 1993)

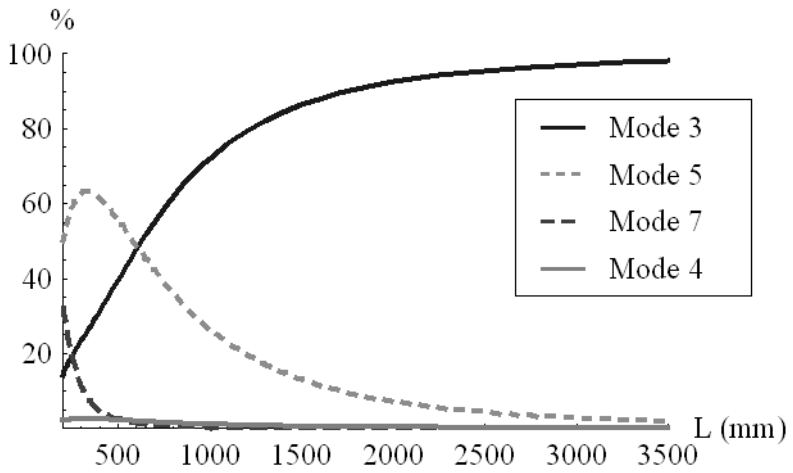

Fig. 4.12 – Modal participation factors for strong axis bending for member lengths larger than 200 mm

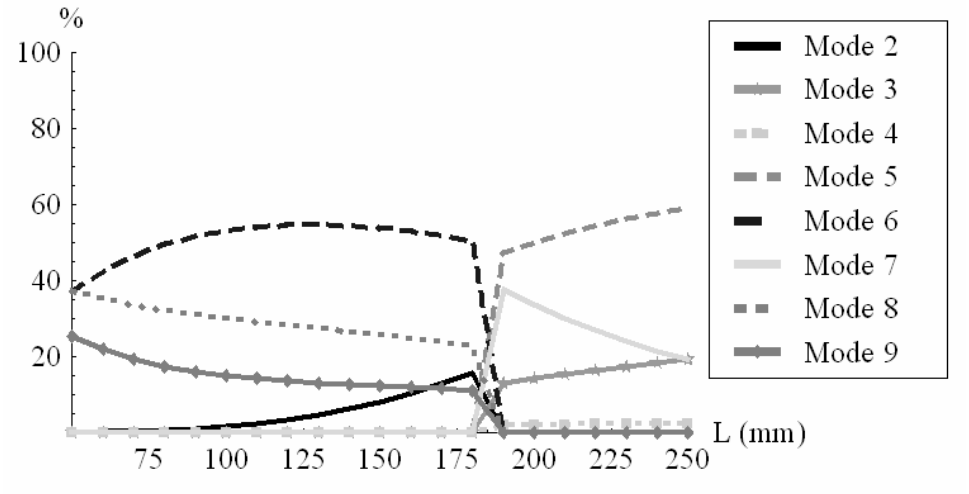

Fig. 4.13 – Modal participation factors for strong axis bending for member lengths between 50 and 200 mm

The participation factor of the modes is presented in Figures 4.12 and 4.13. Fig. 4.12 puts in evidence the dominance of modes 3 and 5 for the higher lengths range, mode 5 being more important for intermediate lengths and mode 3 more important for the higher lengths. Mode 4 plays a minor role for all lengths. For the smaller lengths, in Fig. 4.13, it can be see that first, for very small lengths, modes 6, 8 and 9 control the buckling behaviour, with mode 2 having a small but very significant role – it corresponds to the

influence of the local buckling of the compressed flange on the bending stiffness. Then, abruptly, the relevance of these modes ceases and modes 3, 5 and 7 start to rule the buckling behaviour. As the member's length increases, modes 3 and 5 progressively control the global buckling behaviour, and mode 7 for lengths higher than 600 mm has no relevance.

4.4 – Post-buckling analysis of an open cross section column

4.4.1. Introduction

Finally, to illustrate the potential of the GBT energy formulation developed above, an example on the post-buckling analysis of an open channel section is presented. The channel cross section used in paragraph 4.2 was chosen, with similar nodal discretization.

4.4.2 Buckling behaviour

The critical behaviour is presented in Fig. 4.14 for member lengths between 50 and 3500 mm, and polynomial (3.24) is chosen as trial function for mode 1, while the first three polynomials of (3.37) are considered as coordinate functions for the remaining modes. For case one, only the first polynomial was considered, and for cases 2 and 3 the first two and three polynomials of (3.37) were adopted, respectively. The lowest eigenvalue was used here to describe the member critical behaviour. In the present problem and, due to the shape of $\boldsymbol{H}_{FP}$, coordinate 1 (related to axial elongation mode) is passive for all values of the load factor P and thus can be ignored in the eigenvalue analysis. Figure 4.14 illustrates the decrease of critical load with the number of approximating polynomials, this decrease being more relevant when local or distortional buckling are dominant – significant decrease occurs for the smaller lengths (lengths up to about 250mm) when local plate buckling of the web rules the bifurcational behaviour – and almost negligible for global buckling. For example, the use of just one half-wave curve stiffens the member up

to *46%* for *L=160* mm, when compared to cases 2 or 3. When the critical behaviour is governed mainly by minor axis bending, the use of additional coordinate functions is not necessary, because a good convergence is obtained with only one polynomial per mode.

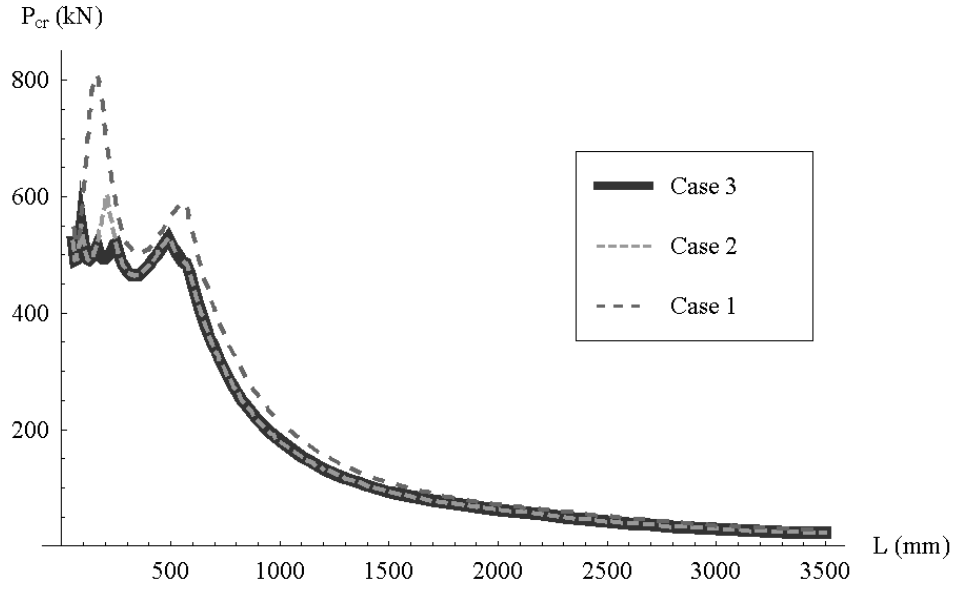

Fig. 4.14: Member's critical loads for the three analysed cases

4.4.3 Post-Buckling behaviour

In order to perform the post-buckling analysis, consider a length of *400* mm submitted to a uniform axial compression load at one end, as indicated in Fig. 4.5 – case 2. For this length, the critical behaviour is governed mainly by mode of deformation 5 (symmetric distortion), and the lowest critical load is $P_{cr}=481.05$ kN. The corresponding eigenvector is presented in Table 4.2, where it can be seen that mode 5 – symmetrical distortion – plays the most relevant role. In this table, for each mode of deformation, the first coordinate corresponds to the generalized coordinate associated with polynomial (3.37 a), and the second and the third coordinates correspond to polynomials (3.37 b) and (3.37 c), respectively.

Next, the post-buckling solutions are obtained by searching non-trivial equilibrium

paths around the critical point. Fig. 4.15 shows the post-buckling paths for coordinates ${}^{1}a$ and ${}^{11}a$, Fig. 4.16 presents the horizontal displacement of node 4 and the relative vertical displacement between nodes 1 and 7 in the post-buckling domain, Fig. 4.17 displays the post-buckling axial displacements of nodes 5 and 6, and Fig. 4.18 gives an overall post-buckling member shape. Fig. 4.15 highlights the stability of both post-buckling equilibrium paths, the one related to negative values of ${}^{11}a$ exhibiting a slightly negative slope in the neighbourhood of the critical point, while the other branch has always a positive slope, hence this bifurcation is clearly a non-symmetric one. Having negative slope, the branch related to ${}^{11}a < 0$ is unstable around the bifurcation point, corresponding to the inwards deformation. However, as the values of coordinate ${}^{11}a$ move away from the fundamental path, the post-buckling path gains a positive slope and the equilibrium becomes stable.

mode n.	3			5			7			9		
coordinate	${}^{5}a$	${}^{6}a$	${}^{7}a$	${}^{11}a$	${}^{12}a$	${}^{13}a$	${}^{17}a$	${}^{18}a$	${}^{19}a$	${}^{23}a$	${}^{24}a$	${}^{25}a$
coefficient	0.96	0	0	98.13	0	0.40	-0.49	0	0	-0.02	0	0

Table 4.1 – Coefficients of the 1st eigenvector

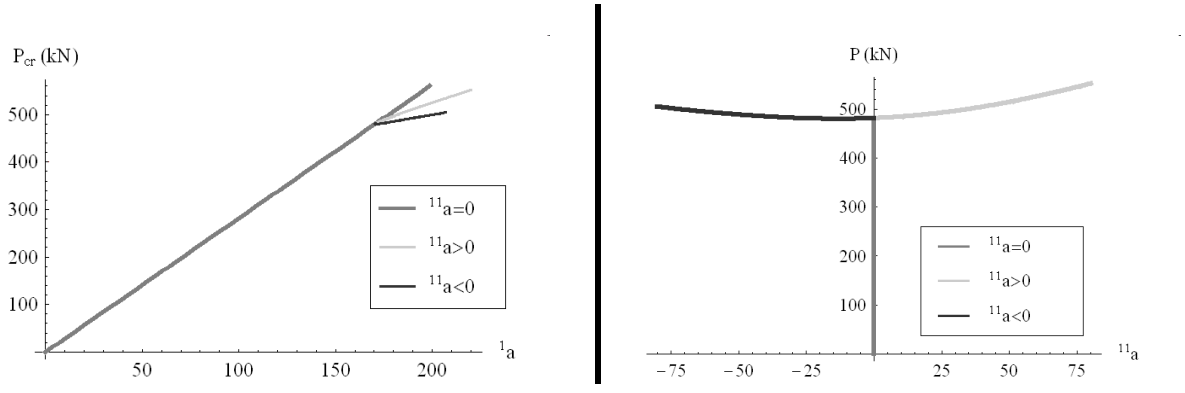

Fig. 4.15 – Post-buckling equilibrium paths for coordinates ${}^{1}a$ and ${}^{11}a$

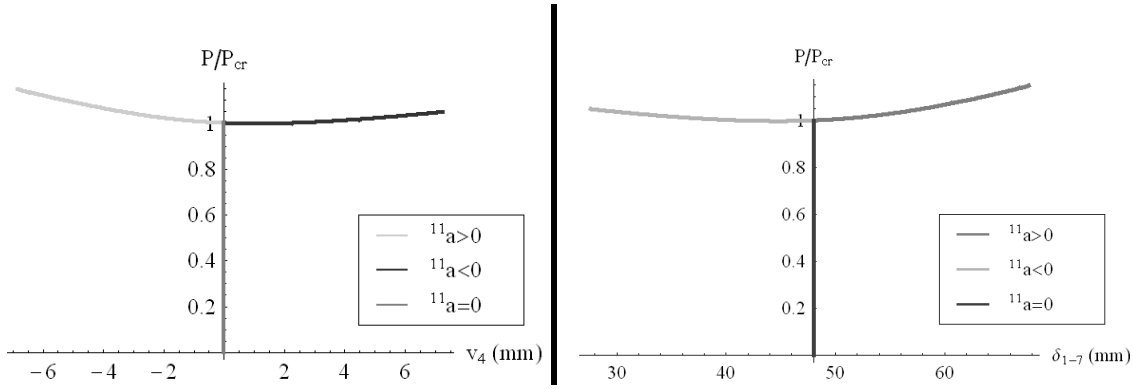

Fig. 4.16 – Post-buckling displacements (v4: horizontal displacement of node 4; δ1-7: relative vertical displacement between nodes 1 and 7)

Looking at Fig. 4.19, where the longitudinal membrane stresses along two illustrative cross sections are presented for the critical point and for two points of both post-buckling branches, it can be concluded that, mainly due to the modal interaction between modes 5 and 3, the path relative to $^{11}a < 0$ is associated with a stresses increase in the flanges near the lips, while the other branch carries a stress increase at the web, this configuration being more stable.

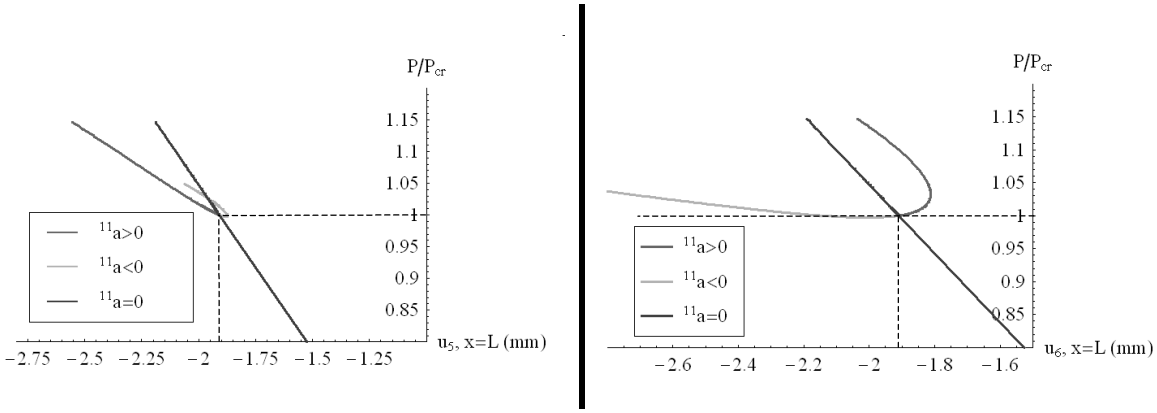

Fig. 4.31– Post-buckling axial displacements for nodes 5 and 6

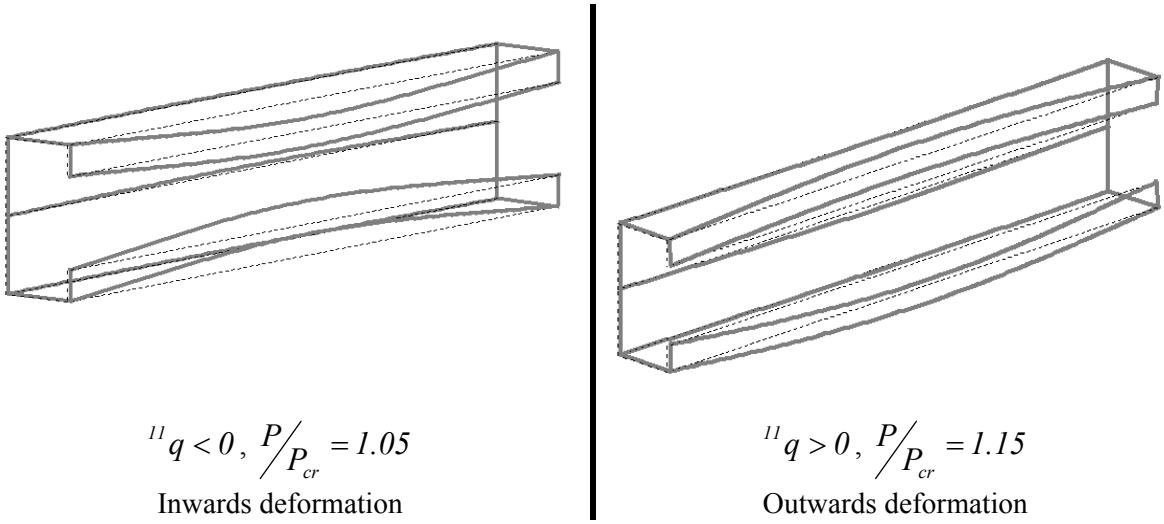

Fig. 4.18 – Post-buckling member's configuration

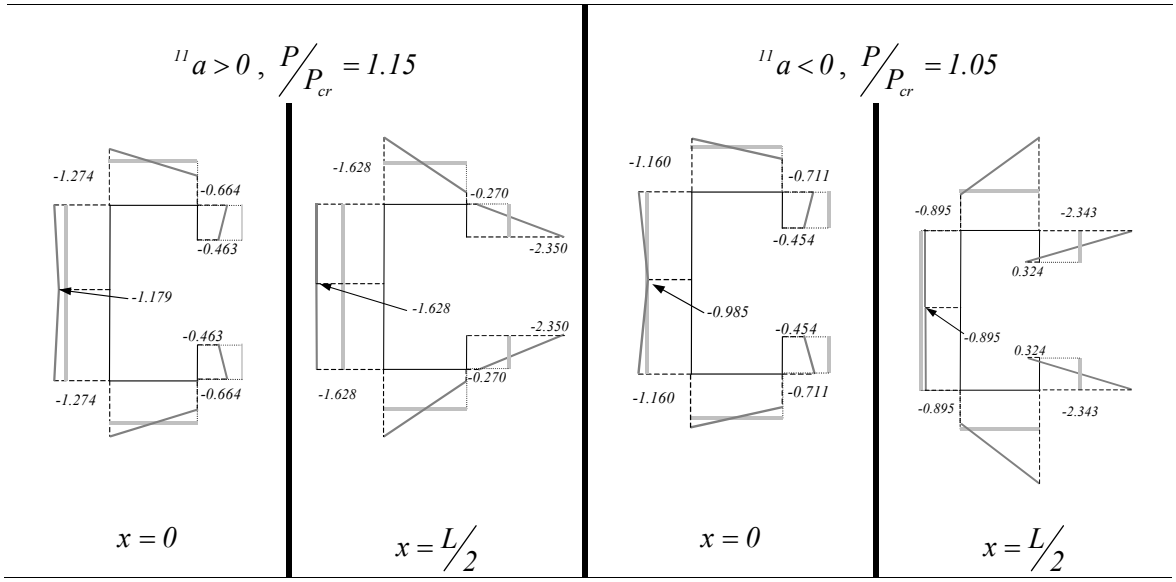

Fig. 4.19 – Longitudinal stresses for the critical state (light grey) and for post-buckling states (dark grey) ($\times 10^9$ Pa)

4.4 – Chapter synopsis

This chapter presented three simple examples to illustrate the ability of the GBT energy formulation to model the critical and post-critical behaviour of open and closed cross sections under uniform compressive load or major axis bending moment. These

examples were previously used to illustrate the theoretical developments in one scientific journal paper (Simão and Simões da Silva 2004) and in three international conference papers (Simão and Simões da Silva 2002, 2003a and 2003b). It is highlighted once again that the examples presented above, made during an initial phase of this thesis, were pretended to illustrate the features of the GBT only, and not to reproduce real situations. Therefore, they were realized with no concern upon the stress levels neither to plasticity.

5 – POST-BUCKLING FORMULATION FOR THE EXTENDED GBT THEORY

5.1 – Introduction

Since GBT combines pre-established modes of deformation, one crucial requirement is to consider modes of deformation that enable a complete characterization of all relevant phenomena involved in the member's behaviour, i.e., in the member's deformations and stresses that occur when it is subjected to an external action such as an external loading, and consequently a complete characterization of all relevant terms in the total potential energy. The most important modes for the analysis of thin-walled folded-plate members were already derived by Schardt (1989) and Miosga (1976), but some important phenomena need additional information. The plate bending modes of deformation, first introduced by Miosga (1976), intended to enable a multi-linear transverse bending moments diagrams along the cross section perimeter. Until then, GBT was limited to have a linear shape between any two consecutive main nodes. With the plate bending mode, the GBT methodology gained the ability to analyse a wider range of phenomena, like the local plate buckling behaviour in thin-walled members. An experimental work of Graves-Smith and Sridharan (1980) shows, for a thin-walled squared hollow section column with such a length that plate buckling occurs as a first critical state, that secondary critical states deal with the change of the distance between two consecutive folding lines: this is illustrated in Fig. 5.1, showing the various stages of a compression test of a thin-walled RHS column. Fig. 5.1-a) shows the state associated with the fundamental path and Figures 5.1-b) and -c) present the deformation of the member for increasing load values, in the local plate buckling range. Then, suddenly, a secondary critical state occurs and a terciary path emerges from it, associated with a localized deformation of the cross

section that involves a curved shape for the folding lines, illustrated at Fig. 5.1-d). The equilibrium path emerging from the secondary critical point is unstable and therefore the secondary critical state defines the maximum load capacity of the elastic column. Observation of Fig. 5.1 - d) shows clearly that the existing modes of deformation for closed sections presented in Chapter 2 could not model the deformations related to the terciary path, since they do not allow transverse extension of the plates.

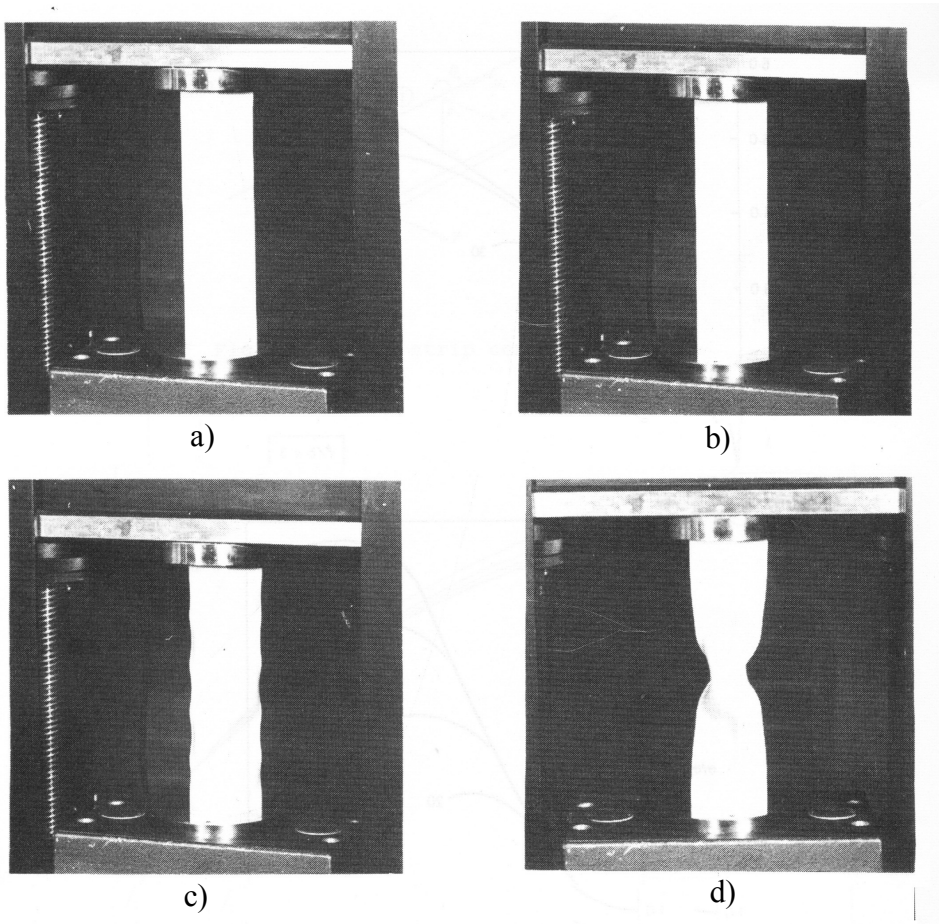

Fig. 5.1 – An experimental test of a thin-walled square hollow section under compression (Graves-Smith and Sridharan 1980)

Moreover, the traditional GBT analysis is not able to define precisely the membrane stress state at any point of the member, even for linear analysis: the inconsistency for the definition of the shear and normal transverse membrane stresses is noted by comparing the various proposals for the definition of the transverse membrane

stress (Schardt 1965, Schardt 1989 and Heinz and Mark 1990).

To overcome these limitations of the classical GBT theory, it is adopted here a strategy of taking up each simplifying hypothesis of Schardt (1989) and, for the establishment of each additional mode of deformation, of imposing displacement patterns that go against these assumptions. It is intended that the validity of the former assumptions becomes a result of the member equilibrium analysis, instead of a hypothesis at the starting point of the problem. This strategy is not new: it was already used by Schardt (1989) for the analysis of closed cells in the context of GBT, and here is extended to other situations. Also, it can be observed that using this strategy Schardt derived GBT from the classical Vlasov theory. It is obvious that adding more modes of deformation renders the analysis more cumbersome and, for several practical applications, the additional modes may not be relevant. Also, the modes of deformation presented below, in addition to the classical ones, may not form a complete set of all possible modes. In principle, the limit is one's imagination, and just one condition applies to consider additional modes: any newly added mode must be linearly independent from all previous modes. During the definition of the modes, only first order properties are needed to establish the orthogonalization problem, with the exception of axial elongation and bending around the principal axes (Schardt, 1989). After the orthogonalization procedure, for all modes of deformation, the non-linear properties will be computed and no restriction is made to which coefficients are present for a given mode of deformation. In other words, for example in the classical formulation, the non-linear terms related to shear distortion were not taken into account for the analysis of open sections (Schardt, 1994; Simão and Simões da Silva, 2002), whereas in the present chapter they will be considered. Among the simplifying statements (Schardt, 1989) that will be relaxed, one finds: (i) the assumption of negligible transverse membrane strain, (iia) the assumption of negligible distortion in open sections and (iib) the hypothesis that imposes the shear flow around a closed cell to be constant, (iii) the hypothesis of linear warping displacements between the folding lines of the cross section, and (iv) the

assumption of negligible transverse extensions.

From the mathematical point of view, the displacement, along the direction of any coordinate axis, of a point belonging to any plate of a thin-walled prismatic member can be regarded as a function, in the sense that to the generic point of the plate corresponds one and only one displacement. So, any displacement of a generic point of a plate can be regarded as a function of the plate's transverse coordinate s and longitudinal coordinate x, continuous since no fracture is admitted along the plate. This function can thus be approximated, as closely as wished, by a polynomial in s and x (Natanson 1964), so that one can speak in terms of a polynomial instead of a generic function. The definition of a polynomial of two variables, s and x, is given in general by the sum of the products of a polynomial in x by a polynomial in s (Caraça 1954), and so the formulas (2.1, a-e) presented in chapter 2..2.2 can be completely general if the polynomials in s, related to the modes of deformation, and in x, referred in this work to the polynomial coordinate functions in the context of the Rayleigh-Ritz method, provide that generality. So, it is the aim of the present chapter to enlarge the field of the referred formulas for the polynomials in s, by defining alternative polynomials in s, along the cross section perimeter, that may improve the GBT analysis skills. This is achieved by the introduction of additional modes of deformation that model more general deformation patterns of the cross section and of its plates, namely i) the plate distortional mode (defined for each plate), ii) the inner nodes warping modes and iii) the plate's transversal extension modes. As seen in Chapter 3, the generality of the polynomials in x is assured by a sequential scheme that provides a set of proper coordinate functions, in the context of the Rayleigh-Ritz method, for the analysis of the member's global equilibrium.

5.2 – The general energy formulation

5.2.1. Introduction

In order to prepare the background for the establishment of alternative modes of deformation, general elasticity relations are derived, and a more general formula for the internal strain energy is thus obtained (cf. equation 2.110). It is intended that all generalized geometric properties derived here become fully defined by all modes of deformation, as it will be seen in chapter 5.3.

5.2.2. The complete strain-stress relations and constitutive relations

The bending strain-displacement relations follow the usual linear formulation for thin plates and are given by:

$$\varepsilon_x^B = -r\frac{\partial^2 f}{\partial x^2} = \sum_{k=1}^{n_{MD}} -r\ {}^k f\ {}^k A''$$

$$\varepsilon_s^B = -r\frac{\partial^2 f}{\partial s^2} = \sum_{k=1}^{n_{MD}} -r\ {}^k \ddot{f}\ {}^k A \qquad \text{(5.1, a-c)}$$

$$\gamma_{sx}^B = -2r\frac{\partial^2 f}{\partial s\,\partial x} = \sum_{k=1}^{n_{MD}} -2r\ {}^k \dot{f}\ {}^k A' .$$

For a stability analysis the membrane strain-displacement relations must include the relevant non-linear terms, as seen in Chapter 2. Taking into account Fig. 5.2 and neglecting higher order terms, ε_x^M and γ_{sx}^M are given by:

$$\varepsilon_x^M = \frac{\overline{A_2B_2} - \overline{A_1B_1}}{\overline{A_1B_1}} \approx \frac{\partial u}{\partial x} + \frac{1}{2}\left(\frac{\partial f}{\partial x}\right)^2 + \frac{1}{2}\left(\frac{\partial f_s}{\partial x}\right)^2 =$$

$$= \sum_{k=1}^{n_{MD}} \left\{ {}^k u\ {}^k A'' + \frac{1}{2}\sum_{l=1}^{n_{MD}} \left[\left({}^k f_s\ {}^l f_s + {}^k f\ {}^l f \right) {}^k A'\ {}^l A' \right] \right\}. \qquad \text{(5.2)}$$

$$\gamma_{sx}^M = \sphericalangle\left(B_1A_1C_1\right) - \sphericalangle\left(B_2A_2C_2\right) =$$

$$= \frac{\pi}{2} - arc\cos\left[\frac{\left(1+\frac{\partial u}{\partial x}\right)\frac{\partial u}{\partial s}+\left(1+\frac{\partial f_s}{\partial s}\right)\frac{\partial f_s}{\partial x}+\frac{\partial f}{\partial x}\frac{\partial f}{\partial s}}{\sqrt{\left(1+\frac{\partial u}{\partial x}\right)^2+\left(\frac{\partial f_s}{\partial x}\right)^2+\left(\frac{\partial f}{\partial x}\right)^2}\sqrt{\left(\frac{\partial u}{\partial s}\right)^2+\left(1+\frac{\partial f_s}{\partial s}\right)^2+\left(\frac{\partial f}{\partial s}\right)^2}}\right] \approx$$

$$\approx \frac{\partial u}{\partial s}+\frac{\partial f_s}{\partial x}+\frac{\partial f}{\partial x}\frac{\partial f}{\partial s}+\frac{\partial u}{\partial x}\frac{\partial u}{\partial s}+\frac{\partial f_s}{\partial x}\frac{\partial f_s}{\partial s} =$$

$$= \sum_{k=1}^{n_{MD}}\left({}^k\ddot{u}+{}^kf_s\right){}^kA' + \sum_{k=1}^{n_{MD}}\sum_{l=1}^{n_{MD}} {}^k f\, {}^l\dot{f}\, {}^kA'\, {}^lA + \sum_{k=1}^{n_{MD}}\sum_{l=1}^{n_{MD}} {}^k u\, {}^l\ddot{u}\, {}^kA''\, {}^lA' + \sum_{k=1}^{n_{MD}}\sum_{l=1}^{n_{MD}} {}^k f_s\, {}^l\dot{f}_s\, {}^kA'\, {}^lA \tag{5.3}$$

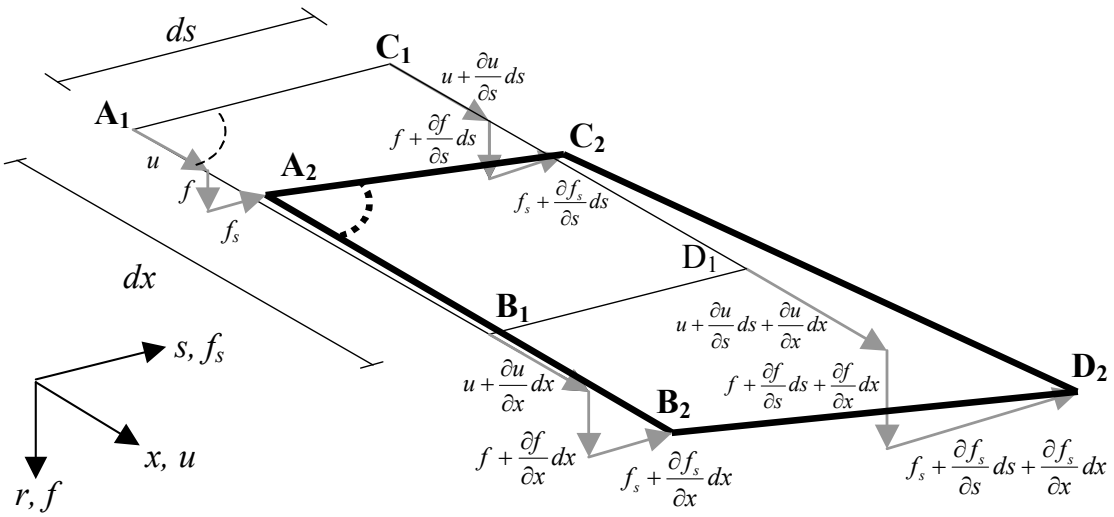

Fig. 5.2 – Membrane displacements of the thin plate $ds \times dx$

Because it is intended to relax some assumptions of the classical GBT theory, expression (5.3) will be considered in its full form, in opposition to the formulation derived in chapter 2.3. The transverse membrane extension must be considered and again from Fig. 5.2 it can be computed as:

$$\varepsilon_s^M = \frac{\overline{A_2C_2}-\overline{A_1C_1}}{\overline{A_1C_1}} \approx \frac{\partial f_s}{\partial s}+\frac{1}{2}\left(\frac{\partial u}{\partial s}\right)^2+\frac{1}{2}\left(\frac{\partial f}{\partial s}\right)^2 =$$

$$= \sum_{k=1}^{n_{MD}} {}^k\dot{f}_s\, {}^kA + \frac{1}{2}\sum_{k=1}^{n_{MD}}\sum_{l=1}^{n_{MD}} {}^k\ddot{u}\, {}^l\ddot{u}\, {}^kA'\, {}^lA' + \frac{1}{2}\sum_{k=1}^{n_{MD}}\sum_{l=1}^{n_{MD}} {}^k\dot{f}\, {}^l\dot{f}\, {}^kA\, {}^lA \tag{5.4}$$

The membrane strains were determined above by using the "engineering strain" concept (Crisfield, 1991). This option is consistent with the Lagrangian description for plates and the use of the Green strains (Fung, 1965), since in the analysis only the first terms of the series expansion are considered, any square term in ∂u and ∂f_s being neglected only if it is present in the same expression in a linear form – this is commonly referred as "Simplified Lagrangian description" (Garcea 2001), and the conjugacy between strains and stresses is therefore assured.

For isotropic materials, the stress-strain relations are, for bending effects,

$$\sigma_x^B = \frac{E}{1-\mu^2}\left(\varepsilon_x^B + \mu\,\varepsilon_x^B\right)$$

$$\sigma_s^B = \frac{E}{1-\mu^2}\left(\varepsilon_s^B + \mu\,\varepsilon_x^B\right) \qquad \text{(5.5, a-c)}$$

$$\tau_{sx}^B = G\gamma_{sx}^B .$$

while for membrane effects are

$$\begin{bmatrix}\sigma_x^M\\ \sigma_s^M\\ \tau_{sx}^M\end{bmatrix} = \begin{bmatrix}\frac{E}{1-\mu^2} & \frac{E\mu}{1-\mu^2} & 0\\ \frac{E\mu}{1-\mu^2} & \frac{E}{1-\mu^2} & 0\\ 0 & 0 & G\end{bmatrix} \times \begin{bmatrix}\varepsilon_x^M\\ \varepsilon_s^M\\ \gamma_{sx}^M\end{bmatrix}. \qquad \text{(5.6)}$$

5.2.3. The internal strain and the total potential energy

From the classical definition of internal strain energy,

$$U_i = \frac{1}{2}\int_0^L\int_A \left(\sigma_x^M\,\varepsilon_x^M + \sigma_s^M\,\varepsilon_s^M + \tau_{sx}^M\,\gamma_{sx}^M + \sigma_x^B\,\varepsilon_x^B + \sigma_s^B\,\varepsilon_s^B + \tau_{sx}^B\,\gamma_{sx}^B\right) dA\,dx\,, \qquad \text{(5.7)}$$

the bending terms are obtained by introducing equations (5.1, a-c) and (5.5, a-c) into equation (5.7),

$$U_i^B = \sum_{i=1}^{n_{MD}}\sum_{k=1}^{n_{MD}} \frac{1}{2}\int_0^L {}^{ik}C^B \; {}^{i}A'' \; {}^{k}A'' dx + \sum_{i=1}^{n_{MD}}\sum_{k=1}^{n_{MD}} \frac{1}{2}\int_0^L {}^{ik}D_1 \; {}^{i}A' \; {}^{k}A' dx +$$

$$+\frac{1}{2}\sum_{i=1}^{n_{MD}}\sum_{k=1}^{n_{MD}}\int_0^L {}^{ik}D_2 \; {}^{i}A \; {}^{k}A'' dx + \frac{1}{2}\sum_{i=1}^{n_{MD}}\sum_{k=1}^{n_{MD}}\int_0^L {}^{ik}D_{2T} \; {}^{i}A'' \; {}^{k}A dx + \frac{1}{2}\sum_{i=1}^{n_{MD}}\sum_{k=1}^{n_{MD}}\int_0^L {}^{ik}B^B \; {}^{i}A \; {}^{k}A dx \,, \tag{5.8}$$

where

$${}^{ik}C^B = \int_s \frac{E t^3}{12\left(1-\mu^2\right)} \; {}^{i}f \; {}^{k}f \, ds \tag{5.9, a-e}$$

$${}^{ik}D_1 = \int_s \frac{G t^3}{3} \; {}^{i}\dot{f} \; {}^{k}\dot{f} \, ds$$

$${}^{ik}D_2 = \int_s \frac{E t^3 \mu}{12\left(1-\mu^2\right)} \; {}^{i}\ddot{f} \; {}^{k}f \, ds$$

$${}^{ik}D_{2T} = \int_s \frac{E t^3 \mu}{12\left(1-\mu^2\right)} \; {}^{i}f \; {}^{k}\ddot{f} \, ds$$

$${}^{ik}B^B = \int_s \frac{E t^3}{12\left(1-\mu^2\right)} \; {}^{i}\ddot{f} \; {}^{k}\ddot{f} \, ds$$

The determination of the membrane contribution was derived in chapter 2 using the classical assumptions of GBT (Schardt, 1989). Here it is extended to include the influence of the transverse strains, thus enabling the consideration of the full membrane constitutive law. It is obtained by introducing equations (5.2), (5.3), (5.4) and (5.6) into equation (5.7), and is presented in the form

$$U_i^M = U_i^{M,L} + U_i^{M,T} + U_i^{M,SH} \tag{5.10}$$

where superscripts ^{L}, ^{T} and ^{SH} refer to the parts associated with longitudinal, transverse and shear membrane deformations, respectively. The terms related to the longitudinal membrane stresses are:

$$U_i^{M,L} = \sum_{i=1}^{n_{MD}}\sum_{k=1}^{n_{MD}} \frac{1}{2}\int_0^L {}^{ik}C^M \; {}^{i}A'' \; {}^{k}A'' dx + \sum_{i=1}^{n_{MD}}\sum_{k=1}^{n_{MD}} \frac{1}{2}\int_0^L {}^{ik}D_4 \; {}^{i}A \; {}^{k}A'' dx +$$

$$+\frac{1}{4}\sum_{i=1}^{n_{MD}}\sum_{k=1}^{n_{MD}}\sum_{l=1}^{n_{MD}}\int_L {}^{ikl}\kappa_{L2}\ {}^{i}A''\ {}^{k}A'\ {}^{l}A'\,dx+\frac{1}{4}\sum_{i=1}^{n_{MD}}\sum_{j=1}^{n_{MD}}\sum_{k=1}^{n_{MD}}\int_L {}^{ijk}\kappa_{L3}\ {}^{i}A'\ {}^{j}A'\ {}^{k}A''\,dx+$$

$$+\frac{1}{8}\sum_{i=1}^{n_{MD}}\sum_{j=1}^{n_{MD}}\sum_{k=1}^{n_{MD}}\sum_{l=1}^{n_{MD}}\int_L {}^{ijkl}\kappa_{L4}\ {}^{i}A'\ {}^{j}A'\ {}^{k}A'\ {}^{l}A'\,dx+\frac{1}{4}\sum_{i=1}^{n_{MD}}\sum_{j=1}^{n_{MD}}\sum_{k=1}^{n_{MD}}\int_L {}^{ijk}\kappa_{L5}\ {}^{i}A'\ {}^{j}A'\ {}^{k}A''\,dx+$$

$$+\frac{1}{4}\sum_{i=1}^{n_{MD}}\sum_{j=1}^{n_{MD}}\sum_{k=1}^{n_{MD}}\int_L {}^{ijk}\kappa_{L6}\ {}^{i}A\ {}^{j}A\ {}^{k}A''\,dx+\frac{1}{4}\sum_{i=1}^{n_{MD}}\sum_{k=1}^{n_{MD}}\sum_{l=1}^{n_{MD}}\int_L {}^{ikl}\kappa_{L7}\ {}^{i}A\ {}^{k}A'\ {}^{l}A'\,dx+$$

$$+\frac{1}{8}\sum_{i=1}^{n_{MD}}\sum_{j=1}^{n_{MD}}\sum_{k=1}^{n_{MD}}\sum_{l=1}^{n_{MD}}\int_L {}^{ijkl}\kappa_{L8}\ {}^{i}A'\ {}^{j}A'\ {}^{k}A'\ {}^{l}A'\,dx+\frac{1}{8}\sum_{i=1}^{n_{MD}}\sum_{j=1}^{n_{MD}}\sum_{k=1}^{n_{MD}}\sum_{l=1}^{n_{MD}}\int_L {}^{ijkl}\kappa_{L9}\ {}^{i}A\ {}^{j}A\ {}^{k}A'\ {}^{l}A'\,dx \tag{5.11}$$

where

$${}^{ik}C^{M}=\int_s \frac{E}{1-\mu^2}t\ {}^{i}u\ {}^{k}u\,ds \quad (1^{\text{st}}\text{ order term}) \tag{5.12, a-j}$$

$${}^{ik}D_4=\int_s \frac{E\,\mu}{1-\mu^2}t\ {}^{i}\dot{f}_s\ {}^{k}u\,ds \quad (1^{\text{st}}\text{ order term})$$

$${}^{ikl}\kappa_{L2}=\int_s \frac{E}{1-\mu^2}t\ {}^{i}u\left({}^{k}f_s\ {}^{l}f_s+{}^{k}f\ {}^{l}f\right)ds$$

$${}^{ijk}\kappa_{L3}=\int_s \frac{E}{1-\mu^2}t\ \left({}^{i}f_s\ {}^{j}f_s+{}^{i}f\ {}^{j}f\right){}^{k}u\,ds$$

$${}^{ijkl}\kappa_{L4}=\int_s \frac{E}{1-\mu^2}t\left({}^{i}f_s\ {}^{j}f_s+{}^{i}f\ {}^{j}f\right)\cdot\left({}^{k}f_s\ {}^{l}f_s+{}^{k}f\ {}^{l}f\right)ds$$

$${}^{ijk}\kappa_{L5}=\int_s \frac{E\mu}{1-\mu^2}t\ {}^{i}\dot{u}\ {}^{j}\dot{u}\ {}^{k}u\ ds$$

$${}^{ijk}\kappa_{L6}=\int_s \frac{E\mu}{1-\mu^2}t\ {}^{i}\dot{f}\ {}^{j}\dot{f}\ {}^{k}u\ ds$$

$${}^{ikl}\kappa_{L7}=\int_s \frac{E\,\mu}{1-\mu^2}t\ {}^{i}\dot{f}_s\ \left({}^{k}f_s\ {}^{l}f_s+{}^{k}f\ {}^{l}f\right)ds$$

$${}^{ijkl}\kappa_{L8}=\int_s \frac{E\,\mu}{1-\mu^2}t\ {}^{i}\dot{u}\ {}^{j}\dot{u}\ \left({}^{k}f_s\ {}^{l}f_s+{}^{k}f\ {}^{l}f\right)ds$$

$$ {}^{ijkl}\kappa_{L9} = \int_s \frac{E\,\mu}{1-\mu^2} t\ {}^i\dot{f}\ {}^j\dot{f}\ \left({}^k f_s\ {}^l f_s + {}^k f\ {}^l f\right) ds\,. $$

Similarly, the strain energy due to transverse membrane stresses is given by:

$$ U_i^{M,T} = \sum_{i=1}^{n_{MD}}\sum_{k=1}^{n_{MD}} \frac{1}{2}\int_0^L {}^{ik}B^M\ {}^i A\ {}^k A\, dx + \sum_{i=1}^{n_{MD}}\sum_{k=1}^{n_{MD}} \frac{1}{2}\int_0^L {}^{ik}D_{4T}\ {}^i A''\ {}^k A\, dx + $$

$$ + \frac{1}{4}\sum_{i=1}^{n_{MD}}\sum_{j=1}^{n_{MD}}\sum_{k=1}^{n_{MD}}\int_L {}^{ijk}\kappa_{T2}\ {}^i A'\ {}^j A'\ {}^k A\, dx + \frac{1}{4}\sum_{i=1}^{n_{MD}}\sum_{j=1}^{n_{MD}}\sum_{k=1}^{n_{MD}}\int_L {}^{ijk}\kappa_{T3}\ {}^i A\ {}^j A\ {}^k A\, dx + $$

$$ + \frac{1}{4}\sum_{i=1}^{n_{MD}}\sum_{j=1}^{n_{MD}}\sum_{k=1}^{n_{MD}}\int_L {}^{ijk}\kappa_{T4}\ {}^i A'\ {}^j A'\ {}^k A\, dx + \frac{1}{4}\sum_{i=1}^{n_{MD}}\sum_{k=1}^{n_{MD}}\sum_{l=1}^{n_{MD}}\int_L {}^{ikl}\kappa_{T5}\ {}^i A\ {}^k A'\ {}^l A'\, dx + $$

$$ + \frac{1}{8}\sum_{i=1}^{n_{MD}}\sum_{j=1}^{n_{MD}}\sum_{k=1}^{n_{MD}}\sum_{l=1}^{n_{MD}}\int_L {}^{ijkl}\kappa_{T6}\ {}^i A'\ {}^j A'\ {}^k A'\ {}^l A'\, dx + \frac{1}{8}\sum_{i=1}^{n_{MD}}\sum_{j=1}^{n_{MD}}\sum_{k=1}^{n_{MD}}\sum_{l=1}^{n_{MD}}\int_L {}^{ijkl}\kappa_{T7}\ {}^i A\ {}^j A\ {}^k A'\ {}^l A'\, dx $$

$$ + \frac{1}{4}\sum_{i=1}^{n_{MD}}\sum_{k=1}^{n_{MD}}\sum_{l=1}^{n_{MD}}\int_L {}^{ikl}\kappa_{T8}\ {}^i A''\ {}^k A'\ {}^l A'\, dx + \frac{1}{8}\sum_{i=1}^{n_{MD}}\sum_{j=1}^{n_{MD}}\sum_{k=1}^{n_{MD}}\sum_{l=1}^{n_{MD}}\int_L {}^{ijkl}\kappa_{T9}\ {}^i A'\ {}^j A'\ {}^k A'\ {}^l A'\, dx + $$

$$ + \frac{1}{4}\sum_{i=1}^{n_{MD}}\sum_{k=1}^{n_{MD}}\sum_{l=1}^{n_{MD}}\int_L {}^{ikl}\kappa_{T10}\ {}^i A\ {}^k A\ {}^l A\, dx + \frac{1}{8}\sum_{i=1}^{n_{MD}}\sum_{j=1}^{n_{MD}}\sum_{k=1}^{n_{MD}}\sum_{l=1}^{n_{MD}}\int_L {}^{ijkl}\kappa_{T11}\ {}^i A'\ {}^j A'\ {}^k A\ {}^l A\, dx + $$

$$ + \frac{1}{8}\sum_{i=1}^{n_{MD}}\sum_{j=1}^{n_{MD}}\sum_{k=1}^{n_{MD}}\sum_{l=1}^{n_{MD}}\int_L {}^{ijkl}\kappa_{T12}\ {}^i A\ {}^j A\ {}^k A\ {}^l A\, dx + \frac{1}{4}\sum_{i=1}^{n_{MD}}\sum_{k=1}^{n_{MD}}\sum_{l=1}^{n_{MD}}\int_L {}^{ikl}\kappa_{T13}\ {}^i A''\ {}^k A\ {}^l A\, dx $$

$$ + \frac{1}{8}\sum_{i=1}^{n_{MD}}\sum_{j=1}^{n_{MD}}\sum_{k=1}^{n_{MD}}\sum_{l=1}^{n_{MD}}\int_L {}^{ijkl}\kappa_{T14}\ {}^i A'\ {}^j A'\ {}^k A\ {}^l A\, dx \qquad (5.13) $$

where

$$ {}^{ik}B^M = \int_s \frac{E}{1-\mu^2} t\ {}^i\dot{f}_s\ {}^k\dot{f}_s\, ds \quad (1^{\text{st}}\text{ order term}) \qquad (5.14,\ \text{a-o}) $$

$$ {}^{ik}D_{4T} = \int_s \frac{E\,\mu}{1-\mu^2} t\ {}^i u\ {}^k\dot{f}_s\, ds \quad (1^{\text{st}}\text{ order term}) $$

$$ {}^{ijk}\kappa_{T2} = \int_s \frac{E}{1-\mu^2} t\ {}^i\dot{u}\ {}^j\dot{u}\ {}^k\dot{f}_s\, ds $$

$$ {}^{ijk}\kappa_{T3} = \int_s \frac{E}{1-\mu^2} t\ {}^i\dot{f}\ {}^j\dot{f}\ {}^k\dot{f}_s\, ds $$

$$^{ijk}\kappa_{T4} = \int_s \frac{E\,\mu}{1-\mu^2} t \left({}^{i}f_s \, {}^{j}f_s + {}^{i}f \, {}^{j}f \right) {}^{k}\dot{f}_s \, ds$$

$$^{ikl}\kappa_{T5} = \int_s \frac{E}{1-\mu^2} t \, {}^{i}\dot{f}_s \, {}^{k}\dot{u} \, {}^{l}\dot{u} \, ds$$

$$^{ijkl}\kappa_{T6} = \int_s \frac{E}{1-\mu^2} t \, {}^{i}\dot{u} \, {}^{j}\dot{u} \, {}^{k}\dot{u} \, {}^{l}\dot{u} \, ds$$

$$^{ijkl}\kappa_{T7} = \int_s \frac{E}{1-\mu^2} t \, {}^{i}\dot{f} \, {}^{j}\dot{f} \, {}^{k}\dot{u} \, {}^{l}\dot{u} \, ds$$

$$^{ikl}\kappa_{T8} = \int_s \frac{E\,\mu}{1-\mu^2} t \, {}^{i}u \, {}^{k}\dot{u} \, {}^{l}\dot{u} \, ds$$

$$^{ijkl}\kappa_{T9} = \int_s \frac{E\,\mu}{1-\mu^2} t \left({}^{i}f_s \, {}^{j}f_s + {}^{i}f \, {}^{j}f \right) {}^{k}\dot{u} \, {}^{l}\dot{u} \, ds$$

$$^{ijk}\kappa_{T10} = \int_s \frac{E}{1-\mu^2} t \, {}^{i}\dot{f}_s \, {}^{k}\dot{f} \, {}^{l}\dot{f} \, ds$$

$$^{ijkl}\kappa_{T11} = \int_s \frac{E}{1-\mu^2} t \, {}^{i}\dot{u} \, {}^{j}\dot{u} \, {}^{k}\dot{f} \, {}^{l}\dot{f} \, ds$$

$$^{ijkl}\kappa_{T12} = \int_s \frac{E}{1-\mu^2} t \, {}^{i}\dot{f} \, {}^{j}\dot{f} \, {}^{k}\dot{f} \, {}^{l}\dot{f} \, ds$$

$$^{ikl}\kappa_{T13} = \int_s \frac{E\,\mu}{1-\mu^2} t \, {}^{i}u \, {}^{k}\dot{f} \, {}^{l}\dot{f} \, ds$$

$$^{ijkl}\kappa_{T14} = \int_s \frac{E\,\mu}{1-\mu^2} t \left({}^{i}f_s \, {}^{j}f_s + {}^{i}f \, {}^{j}f \right) {}^{k}\dot{f} \, {}^{l}\dot{f} \, ds$$

Finally, the membrane shear contribution is given by:

$$U_i^{M,SH} = \sum_{i=1}^{n_{MD}} \sum_{k=1}^{n_{MD}} \frac{1}{2} \int_0^L {}^{ik}D_3 \, {}^{i}A' \, {}^{k}A' \, dx + \frac{1}{2} \sum_{i=1}^{n_{MD}} \sum_{k=1}^{n_{MD}} \sum_{l=1}^{n_{MD}} \int_L {}^{ikl}\kappa_{SH2} \, {}^{i}A' \, {}^{k}A' \, {}^{l}A \, dx +$$

$$+ \frac{1}{2} \sum_{i=1}^{n_{MD}} \sum_{k=1}^{n_{MD}} \sum_{l=1}^{n_{MD}} \int_L {}^{ikl}\kappa_{SH3} \, {}^{i}A' \, {}^{k}A'' \, {}^{l}A' \, dx + \frac{1}{2} \sum_{i=1}^{n_{MD}} \sum_{j=1}^{n_{MD}} \sum_{k=1}^{n_{MD}} \int_L {}^{ijk}\kappa_{SH4} \, {}^{i}A' \, {}^{j}A \, {}^{k}A' \, dx +$$

$$+ \frac{1}{2} \sum_{i=1}^{n_{MD}} \sum_{j=1}^{n_{MD}} \sum_{k=1}^{n_{MD}} \sum_{l=1}^{n_{MD}} \int_L {}^{ijkl}\kappa_{SH5} \, {}^{i}A' \, {}^{j}A \, {}^{k}A' \, {}^{l}A \, dx +$$

$$+\frac{1}{2}\sum_{i=1}^{n_{MD}}\sum_{j=1}^{n_{MD}}\sum_{k=1}^{n_{MD}}\sum_{l=1}^{n_{MD}}\int_L {}^{ijkl}\kappa_{SH6}\ {}^{i}A'\ {}^{j}A\ {}^{k}A''\ {}^{l}A'\,dx+\frac{1}{2}\sum_{i=1}^{n_{MD}}\sum_{j=1}^{n_{MD}}\sum_{k=1}^{n_{MD}}\int_L {}^{ijk}\kappa_{SH7}\ {}^{i}A''\ {}^{j}A'\ {}^{k}A'\,dx+$$

$$+\frac{1}{2}\sum_{i=1}^{n_{MD}}\sum_{j=1}^{n_{MD}}\sum_{k=1}^{n_{MD}}\sum_{l=1}^{n_{MD}}\int_L {}^{ijkl}\kappa_{SH8}\ {}^{i}A''\ {}^{j}A'\ {}^{k}A'\ {}^{l}A\,dx+$$

$$+\frac{1}{2}\sum_{i=1}^{n_{MD}}\sum_{j=1}^{n_{MD}}\sum_{k=1}^{n_{MD}}\sum_{l=1}^{n_{MD}}\int_L {}^{ijkl}\kappa_{SH9}\ {}^{i}A''\ {}^{j}A'\ {}^{k}A''\ {}^{l}A'\,dx+\frac{1}{2}\sum_{i=1}^{n_{MD}}\sum_{k=1}^{n_{MD}}\sum_{l=1}^{n_{MD}}\int_L {}^{ikl}\kappa_{SH10}\ {}^{i}A'\ {}^{k}A'\ {}^{l}A\,dx+$$

$$+\frac{1}{2}\sum_{i=1}^{n_{MD}}\sum_{j=1}^{n_{MD}}\sum_{k=1}^{n_{MD}}\sum_{l=1}^{n_{MD}}\int_L {}^{ijkl}\kappa_{SH11}\ {}^{i}A'\ {}^{j}A\ {}^{k}A'\ {}^{l}A\,dx+$$

$$+\frac{1}{2}\sum_{i=1}^{n_{MD}}\sum_{j=1}^{n_{MD}}\sum_{k=1}^{n_{MD}}\sum_{l=1}^{n_{MD}}\int_L {}^{ijkl}\kappa_{SH12}\ {}^{i}A''\ {}^{j}A'\ {}^{k}A'\ {}^{l}A\,dx+\frac{1}{2}\sum_{i=1}^{n_{MD}}\sum_{j=1}^{n_{MD}}\sum_{k=1}^{n_{MD}}\int_L {}^{ijk}\kappa_{SH13}\ {}^{i}A'\ {}^{j}A\ {}^{k}A'\,dx+$$

$$+\frac{1}{2}\sum_{i=1}^{n_{MD}}\sum_{j=1}^{n_{MD}}\sum_{k=1}^{n_{MD}}\sum_{l=1}^{n_{MD}}\int_L {}^{ijkl}\kappa_{SH14}\ {}^{i}A'\ {}^{j}A\ {}^{k}A'\ {}^{l}A\,dx+$$

$$+\frac{1}{2}\sum_{i=1}^{n_{MD}}\sum_{j=1}^{n_{MD}}\sum_{k=1}^{n_{MD}}\sum_{l=1}^{n_{MD}}\int_L {}^{ijkl}\kappa_{SH15}\ {}^{i}A'\ {}^{j}A\ {}^{k}A''\ {}^{l}A'\,dx+$$

$$+\frac{1}{2}\sum_{i=1}^{n_{MD}}\sum_{j=1}^{n_{MD}}\sum_{k=1}^{n_{MD}}\sum_{l=1}^{n_{MD}}\int_L {}^{ijkl}\kappa_{SH16}\ {}^{i}A'\ {}^{j}A\ {}^{k}A'\ {}^{l}A\,dx \qquad (5.15)$$

where

$${}^{ik}D_3=\int_s Gt\left({}^{i}\dot{u}+{}^{i}f_s\right)\left({}^{k}\dot{u}+{}^{k}f_s\right)ds\ \ (1^{\text{st}}\text{ order term}) \qquad (5.16,\text{ a-p})$$

$${}^{ikl}\kappa_{SH2}=\int_s Gt\left({}^{i}\dot{u}+{}^{i}f_s\right){}^{k}f\ {}^{l}\dot{f}\,ds$$

$${}^{ikl}\kappa_{SH3}=\int_s Gt\left({}^{i}\dot{u}+{}^{i}f_s\right){}^{k}u\ {}^{l}\dot{u}\,ds$$

$${}^{ijk}\kappa_{SH4}=\int_s Gt\ {}^{i}f\ {}^{j}\dot{f}\left({}^{k}\dot{u}+{}^{k}f_s\right)ds$$

$${}^{ijkl}\kappa_{SH5}=\int_s G\ t\ {}^{i}f\ {}^{j}\dot{f}\ {}^{k}f\ {}^{l}\dot{f}\,ds$$

$${}^{ijkl}\kappa_{SH6}=\int_s Gt\ {}^{i}f\ {}^{j}\dot{f}\ {}^{k}u\ {}^{l}\dot{u}\ ds$$

$$^{ijk}\kappa_{SH7} = \int_s G\,t\;{}^{i}u\;{}^{j}\dot{u}\left({}^{k}\dot{u}+{}^{k}f_s\right)ds$$

$$^{ijkl}\kappa_{SH8} = \int_s G\;t\;{}^{i}u\;{}^{j}\dot{u}\;{}^{k}f\;{}^{l}\dot{f}\;ds$$

$$^{ijkl}\kappa_{SH9} = \int_s G\,t\;{}^{i}u\;{}^{j}\dot{u}\;{}^{k}u\;{}^{l}\dot{u}\,ds$$

$$^{ikl}\kappa_{SH10} = \int_s G\,t\left({}^{i}\dot{u}+{}^{i}f_s\right){}^{k}f_s\;\;{}^{l}\dot{f}_s\;ds$$

$$^{ijkl}\kappa_{SH11} = \int_s G\,t\;{}^{i}f\;{}^{j}\dot{f}\;{}^{k}f_s\;{}^{l}\dot{f}_s\,ds$$

$$^{ijkl}\kappa_{SH12} = \int_s Gt\;{}^{i}u\;{}^{j}\dot{u}\;{}^{k}f_s\;{}^{l}\dot{f}_s\;ds$$

$$^{ijk}\kappa_{SH13} = \int_s G\,t\;{}^{i}f_s\;\;{}^{j}\dot{f}_s\;\left({}^{k}\dot{u}+{}^{k}f_s\right)ds$$

$$^{ijkl}\kappa_{SH14} = \int_s G\,t\;{}^{i}f_s\;{}^{j}\dot{f}_s\;{}^{k}f\;{}^{l}\dot{f}\;ds$$

$$^{ijkl}\kappa_{SH15} = \int_s G\,t\;{}^{i}f_s\;{}^{j}\dot{f}_s\;{}^{k}u\;{}^{l}\dot{u}\,ds$$

$$^{ijkl}\kappa_{SH16} = \int_s G\,t\;{}^{i}f_s\;\;{}^{j}\dot{f}_s\;\;{}^{k}f_s\;{}^{l}\dot{f}_s\,ds\,.$$

All of the above expressions are computed taking into consideration the following definitions of the displacements for mode *k* at plate *i* (Schardt 1989):

i) warping displacement (along *Ox*) : $^{k}u(s) = {}^{k}u_{i,beg} + \dfrac{{}^{k}u_{i,end} - {}^{k}u_{i,beg}}{b_i}s$; (5.17)

ii) normal displacement (along *Or*) : $^{k}f(s) = {}^{k}f_{i,beg}\left(1-\dfrac{s}{b_i}\right)+{}^{k}f_{i,end}\dfrac{s}{b_i}+$

$$+{}^{k}m_{s,i,beg}\left(\frac{b_i}{3K_i}s-\frac{s^2}{2K_i}+\frac{s^3}{6b_iK_i}\right)+{}^{k}m_{s,i,end}\left(\frac{b_i}{6K_i}s-\frac{s^3}{6b_iK_i}\right); \quad (5.18)$$

and the displacements along the perimeter are assumed to vary linearly between the edges of the plate:

iii) perimeter displacement (along *Os*) : $${}^{k}f_{s}(s) = {}^{k}f_{s,i,beg} + \frac{{}^{k}f_{s,i,end} - {}^{k}f_{s,i,beg}}{b_i} s \,. \qquad (5.19)$$

Combining equations (5.8), (5.11), (5.13) and (5.15) yields the total potential energy function:

$$V = U_i^B + U_i^{M,L} + U_i^{M,T} + U_i^{M,SH} - \Pi \qquad (5.20)$$

where the potential of the external loading Π is given by the general expression (2.109).

The above formulation is completely general and is based on the classical procedures of the non-linear theory of elasticity (Fung 1969). If the assumptions and the procedures of the classical GBT formulation (Schardt, 1989) are considered, most of these energy terms become null, as shown in chapter 2.3 – note that now all parts of expression (5.7) were considered. Moreover, often only the non-linear terms associated with the normal longitudinal membrane extensions are considered for buckling and post-buckling analysis of thin-walled structural members – several works where this assumption is considered are, for example, Sridharan and Graves-Smith (1981), Rhodes (1991), Schardt (1994) and Schaefer (1998). This simplification constitutes the so-called "lower bound approach" and implies, in the present case, that only the non-linear terms related to the generalized geometric properties κ_{L2}, κ_{L3} and κ_{L4} are considered. The designation "lower bound" is a common expression in the specialized literature and derives from the fact that, for systems with post-critical stable behaviour (which is the case of the structural systems analysed in this work), the above simplification usually yields conservative results, and is a particular case of the complex problem of the truncation of the structural potential function that is analysed, for example, in Hunt and Williams (1984). This simplification is reasonable and in some cases may give better results than the consideration of all parts in

the non-linear member's equilibrium system, for a similar discretization of the problem. In the analysis of thin-walled prismatic members, subjected to uniform major axis bending moments or uniform compression loads that generate mainly longitudinal normal membrane stresses, these stresses (and the corresponding deformations as well) are of much higher magnitude that the shear and normal transverse membrane stresses. Moreover, in open sections shear and transverse membrane stresses are null in the neighbourhood of the edge nodes. So, they generate much smaller non-linear coefficients than the longitudinal stresses, and the corresponding coefficients may perturb drastically the numerical accuracy of the numerical algorithm used to solve the member's equilibrium equations system. Note that it is well known that it is numerically very instable if no imperfections are introduced in the model (Troger and Steindl 1990), i.e., if the perfect member is analysed using bifurcational analysis (Keller 1987). 32-bits computers[1] consider only 15 decimal places for any number, so numerical difficulties arise when, for example, one wants to invert a matrix having high spectral ratius (Golub and Van Loan 1996). It is also worth recalling that a typical numerical instability phenomenon in the analysis of thin-walled structures is the well known "membrane locking" phenomenon, associated with the fact that, in the member's equilibrium system, large coefficients coexist with much smaller coefficients in the same equation, thus generating Jacobean matrices for the non-linear system with very high spectral ratio, so very hard to invert. If bifurcational analysis is used to determine the equilibrium paths, this problem is augmented since in the neighbourhood of the critical point the Jacobean matrix of the non-linear equilibrium system has naturally a very high spectral ratio, since its lowest eigenvalue is very small and trends to zero as the equilibrium state approaches to the critical state and is hardly invertible – in the critical point it is exactly zero and the Jacobian matrix of the equilibrium system has an infinite spectral ratio and is not invertible. Moreover, it is well known that the equilibrium systems for the stability analysis of perfect structures have poor numerical stability (Troger &

[1] Such as the computer used to solve the forthcoming examples, in this thesis.

Steindl 1991). So, these causes of numerical instability may be present in the stability analysis of a real case and may collaborate with each other in the destruction of the precision of the numerical procedure used to solve the problem, so that equilibrium systems with simpler equations may compute more reliable results, even if it is known *a priori* that these results are approximate[2].

Therefore, in the following examples this simplifying assumption is often adopted, and the correspondent TPE is given simply by:

$$V = \sum_{i=1}^{n_{MD}}\sum_{k=1}^{n_{MD}} \frac{1}{2}\int_0^L {}^{ik}C^B \, {}^{i}A'' \, {}^{k}A'' dx + \sum_{i=1}^{n_{MD}}\sum_{k=1}^{n_{MD}} \frac{1}{2}\int_0^L {}^{ik}C^M \, {}^{i}A'' \, {}^{k}A'' dx +$$

$$+ \sum_{i=1}^{n_{MD}}\sum_{k=1}^{n_{MD}} \frac{1}{2}\int_0^L {}^{ik}D_1 \, {}^{i}A' \, {}^{k}A' dx + \frac{1}{2}\sum_{i=1}^{n_{MD}}\sum_{k=1}^{n_{MD}}\int_0^L {}^{ik}D_2 \, {}^{i}A \, {}^{k}A'' dx +$$

$$+ \frac{1}{2}\sum_{i=1}^{n_{MD}}\sum_{k=1}^{n_{MD}}\int_0^L {}^{ik}D_{2T} \, {}^{i}A'' \, {}^{k}A dx + \sum_{i=1}^{n_{MD}}\sum_{k=1}^{n_{MD}} \frac{1}{2}\int_0^L {}^{ik}D_3 \, {}^{i}A' \, {}^{k}A' dx +$$

$$+ \sum_{i=1}^{n_{MD}}\sum_{k=1}^{n_{MD}} \frac{1}{2}\int_0^L {}^{ik}D_4 \, {}^{i}A \, {}^{k}A'' dx + \sum_{i=1}^{n_{MD}}\sum_{k=1}^{n_{MD}} \frac{1}{2}\int_0^L {}^{ik}D_{4T} \, {}^{i}A'' \, {}^{k}A dx +$$

$$+ \frac{1}{4}\sum_{i=1}^{n_{MD}}\sum_{k=1}^{n_{MD}}\sum_{l=1}^{n_{MD}}\int_L {}^{ikl}\kappa_{L2} \, {}^{i}A'' \, {}^{k}A' \, {}^{l}A' dx + \frac{1}{4}\sum_{i=1}^{n_{MD}}\sum_{j=1}^{n_{MD}}\sum_{k=1}^{n_{MD}}\int_L {}^{ijk}\kappa_{L3} \, {}^{i}A' \, {}^{j}A' \, {}^{k}A'' dx +$$

$$+ \frac{1}{8}\sum_{i=1}^{n_{MD}}\sum_{j=1}^{n_{MD}}\sum_{k=1}^{n_{MD}}\sum_{l=1}^{n_{MD}}\int_L {}^{ijkl}\kappa_{L4} \, {}^{i}A' \, {}^{j}A' \, {}^{k}A' \, {}^{l}A' dx - \Pi \, . \qquad (5.21)$$

5.3 – The additional modes of deformation

5.3.1 Introduction

It is worth recalling here the procedure to establish the displacement patterns for a

[2] It is hoped that the recent innovations in personal computers, such as the 64-bit processors that compute numbers with 31 decimal places, together with large computing capacities, contribute to the resolution of many numerical problems that commonly arise in structural stability.

mode. Considering a transversal member slice with longitudinal length *dx*, at first a displacement is imposed to a node and/or a plate and all the necessary movements for the plates are free to happen. Then, considering the relevant constitutive relations, the discontinuities around the cross section are rendered compatible making resource to an adequate method to solve statically indeterminate structures. The traditional theory of Schardt uses the classical force method, modelling the cross section as a continuous beam, introducing a hinge in each node and setting to zero the rotational discontinuities that occur in each hinge when the displacements modal pattern is applied. Henceforth the displacement method adapted to folded plate structures will be used for the new modes of deformation. The use of this method implies that it will be necessary to solve one system of equations per mode, while in the traditional GBT procedure just one system of equations was required for all modes. Nevertheless, it is important to point out that this procedure embraces the traditional process, leading to necessarily equal resulting modal displacements. The procedure to establish the displacement patterns for a mode can be summarized as follows:

i) for each major plate (plate between folding lines or extreme lines), a consistent stiffness matrix considering the inner nodes and the corresponding transformation matrix is formulated; then the global stiffness matrix for the whole cross section is computed;

ii) the classical warping modes, the plate bending modes (Miosga, 1976), the main plate distortional modes and the inner nodes warping modes are defined – these modes can be defined using the classical procedure or the displacement method, being the later adopted here;

iii) the transverse extension modes are defined – these modes require the use of the displacement method;

iv) the modal unitary displacements and transverse bending modes are computed for all

modes and the terms related to the linear analysis can be computed, thus enabling the start of the orthogonalization procedure.

v) the orthogonalization procedure is performed, in order to simplify the global equilibrium system;

vi) the unitary modal displacements and transverse bending moments are computed for the orthogonal modes of deformation, which will be used in the global analysis of the equilibrium of the structural member.

In the following, the basic concepts to perform the steps shown above to establish the basic modes of deformation are presented. First, in order to determine the rotations and the transversal bending moments at the ends of the plates in the context of the traditional displacements method (Ghali and Neville 1997), a consistent major plate stiffness matrix is derived for all possible cases of plates: the plate between two consecutive main nodes placed inside the cross section and the initial of final edge plate. Subsequently, reference is made to the insertion of the traditional modes of deformation, presented in chapter 2, in the extended GBT formulation. Then, the set of additional modes of deformation is presented: the inner nodes warping, the main plates' transversal extension and the main plates' distortional modes of deformation.

5.3.2. Derivation of a consistent major plate stiffness matrix

The starting point of this procedure is the formulation of the plate element and its stiffness matrix. Each plate is modelled as depicted in Fig. 5.3, where a main plate with two inner nodes is illustrated (the adaptation for plates with a different number of inner nodes is trivial).

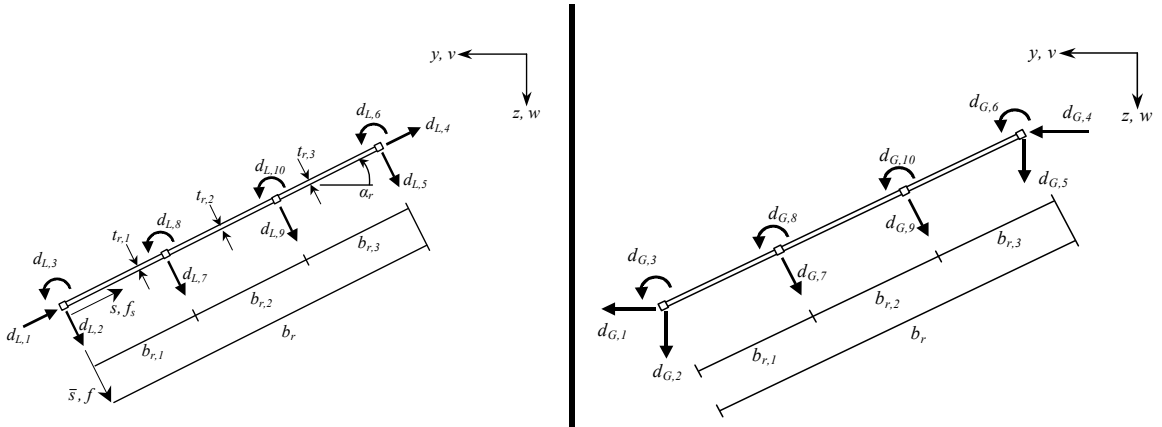

a) Local coordinates for all plates b) Global coordinates for internal plates

Fig. 5.3 – Plate displacements for a main plate *r*

The corresponding stiffness matrix in local coordinates is given by:

$$S=\begin{bmatrix}
\frac{1}{\sum_r \frac{b_r\left(1-\mu_r^2\right)}{Et_r}} & 0 & 0 & -\frac{1}{\sum_r \frac{b_r\left(1-\mu_r^2\right)}{Et_r}} & 0 & 0 & 0 & 0 & 0 & 0 \\
0 & \frac{12K_1}{b_1^3} & -\frac{6K_1}{b_1^2} & 0 & 0 & 0 & -\frac{12K_1}{b_1^3} & -\frac{6K_1}{b_1^2} & 0 & 0 \\
0 & -\frac{6K_1}{b_1^2} & \frac{4K_1}{b_1} & 0 & 0 & 0 & \frac{6K_1}{b_1^2} & \frac{2K_1}{b_1} & 0 & 0 \\
-\frac{1}{\sum_r \frac{b_r\left(1-\mu_r^2\right)}{Et_r}} & 0 & 0 & \frac{1}{\sum_r \frac{b_r\left(1-\mu_r^2\right)}{Et_r}} & 0 & 0 & 0 & 0 & 0 & 0 \\
0 & 0 & 0 & 0 & \frac{12K_3}{b_3^3} & \frac{6K_3}{b_3^2} & 0 & 0 & -\frac{12K_3}{b_3^3} & \frac{6K_3}{b_3^2} \\
0 & 0 & 0 & 0 & \frac{6K_3}{b_3^2} & \frac{4K_3}{b_3} & 0 & 0 & -\frac{6K_3}{b_3^2} & \frac{2K_3}{b_3} \\
0 & -\frac{12K_1}{b_1^3} & \frac{6K_1}{b_1^2} & 0 & 0 & 0 & \frac{12K_1}{b_1^3}+\frac{12K_2}{b_2^3} & \frac{6K_1}{b_1^2}-\frac{6K_2}{b_2^2} & -\frac{12K_2}{b_2^3} & -\frac{6K_2}{b_2^2} \\
0 & -\frac{6K_1}{b_1^2} & \frac{2K_1}{b_1} & 0 & 0 & 0 & \frac{6K_1}{b_1^2}-\frac{6K_2}{b_2^2} & \frac{4K_1}{b_1}+\frac{4K_2}{b_2} & \frac{6K_2}{b_2^2} & \frac{2K_2}{b_2} \\
0 & 0 & 0 & 0 & -\frac{12K_3}{b_3^3} & -\frac{6K_3}{b_3^2} & -\frac{12K_2}{b_2^3} & \frac{6K_2}{b_2^2} & \frac{12K_2}{b_2^3}+\frac{12K_3}{b_3^3} & \frac{6K_2}{b_2^2}-\frac{6K_3}{b_3^2} \\
0 & 0 & 0 & 0 & \frac{6K_3}{b_3^2} & \frac{2K_3}{b_3} & -\frac{6K_3}{b_3^2} & \frac{2K_2}{b_2} & \frac{6K_2}{b_2^2}-\frac{6K_3}{b_3^2} & \frac{4K_2}{b_2}+\frac{4K_3}{b_3}
\end{bmatrix} \tag{5.22}$$

where K_r is the plate stiffness given by:

$$K_r=\frac{E\,t_r^3}{12\left(1-\mu_r^2\right)} \tag{5.23}$$

The plate global displacements are given in Fig. 5.3-b) and the corresponding transformation matrix $\boldsymbol{T}$, relating local and global coordinates displacements in the form

$$\left\{d_L\right\}=\boldsymbol{T}\cdot\left\{d_G\right\}, \tag{5.24}$$

where subscripts $_L$ and $_G$ refer to local and global coordinates, respectively, is given by:

$$\boldsymbol{T} = \begin{bmatrix} -\cos\alpha_r & -\sin\alpha_r & 0 & & 0 & 0 & 0 & 0 & 0 & 0 \\ -\sin\alpha_r & \cos\alpha_r & 0 & 0 & 0 & 0 & 0 & 0 & 0 & 0 \\ 0 & 0 & 1 & 0 & 0 & 0 & 0 & 0 & 0 & 0 \\ 0 & 0 & 0 & -\cos\alpha_r & -\sin\alpha_r & 0 & 0 & 0 & 0 & 0 \\ 0 & 0 & 0 & -\sin\alpha_r & \cos\alpha_r & 0 & 0 & 0 & 0 & 0 \\ 0 & 0 & 0 & 0 & 0 & 1 & 0 & 0 & 0 & 0 \\ 0 & 0 & 0 & 0 & 0 & 0 & 1 & 0 & 0 & 0 \\ 0 & 0 & 0 & 0 & 0 & 0 & 0 & 1 & 0 & 0 \\ 0 & 0 & 0 & 0 & 0 & 0 & 0 & 0 & 1 & 0 \\ 0 & 0 & 0 & 0 & 0 & 0 & 0 & 0 & 0 & 1 \end{bmatrix} \tag{5.25}$$

Having obtained the plate displacements in global coordinates, the global stiffness matrix can be computed using the traditional procedure by summing the contributions of all plates, making resource to an adequate incidence matrix. One important exception consists of the edge plates, for which the transversal displacement at the edge node has a special significance in the context of GBT and it is advantageous to keep it in local coordinates, as it was done before with the inner nodes of the internal plates. This is illustrated in Fig. 5.4 and the corresponding transformation matrix is now trivial.

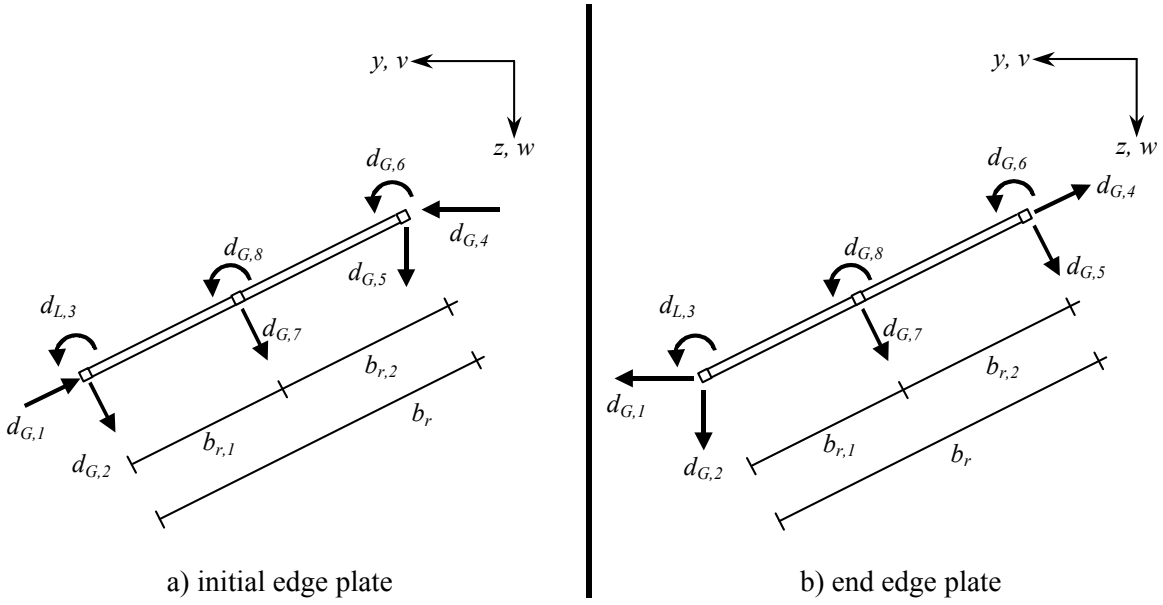

a) initial edge plate b) end edge plate

Fig. 5.4 – The particular case of the edge plates

5.3.3 The classical modes of deformation in the extended formulation

The consideration of the traditional modes of deformation, presented in chapter 2, in the extended formulation is easily achieved and will be applied to the warping and plate bending modes only, since the distortional mode for closed cells is substituted here by the plate's distortional modes, each referring to each main plate of the cross section. It requires that all translational displacements for all nodes are defined by rendering compatible the translations between the plates, considering each node as hinged (Schardt 1989). After finding the translations for the nodes of each plate, these displacements can be expressed in global coordinates by the proper transformation matrices and are considered as prescribed displacements in the global displacement method problem (Ghali and Neville, 1997), while all rotations become the unknowns of the problem. Thus, the fixation forces vector, for each mode of deformation, is defined by the prescribed translation displacements of the nodes. Below, it will be seen that this procedure can be used for all types of modes of deformation with the exception of the inner nodes warping modes, for which no compatibility rendering is required, and for the transversal extension modes, whose set of fixation forces can be trivially found. Having computed the plate displacements, this step of the cross section analysis ends with the computation of the transversal bending moments, thus enabling the full definition of the unitary modal displacements (Schardt, 1989).

5.3.4. The inner nodes warping modes

In order to neglect the assumption of linear displacements between the major nodes, related to the folding or edge lines (Schardt, 1989), it is assumed that, for a major plate, all nodes have zero warping displacements while an inner node has a unit displacement along the longitudinal axis. This displacements shape is only achievable by considering shear distortion in the plate and does not provoke any transversal

displacement, so there is no need to render compatible any displacements. It is noted that these modes of deformation are intended to model the "shear lag" phenomenon (Nakai and Yoo, 1988) and, in certain way, they were already present in the work of Möller (1982).

In the formulation of this family of modes of deformation it is possible either to assume (for simplicity) that the displacements between the nodes of the plate are linear, or to use a more rigorous formulation, ensuring continuity of the first derivative along *Os* of the warping displacements and, consequently, the continuity of the shear distortion for linear analysis, and the 1st order shear stresses distribution. Both alternatives are illustrated in Fig. 5.5 and consist of the choice between a multi-linear shape (Fig. 5.5-a) and a smooth polynomial shape (Fig. 5.5-b), for the warping displacements. In the present work, the multi-linear displacements distribution is assumed (for simplicity) and it is suggested the use of a larger number of inner nodes per plate to minimize the shear stresses discontinuities.

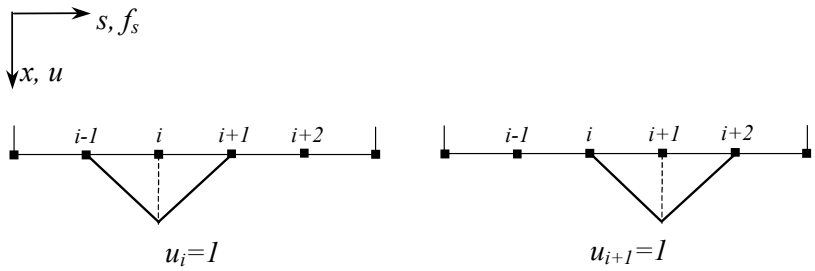

a) multi-linear function;

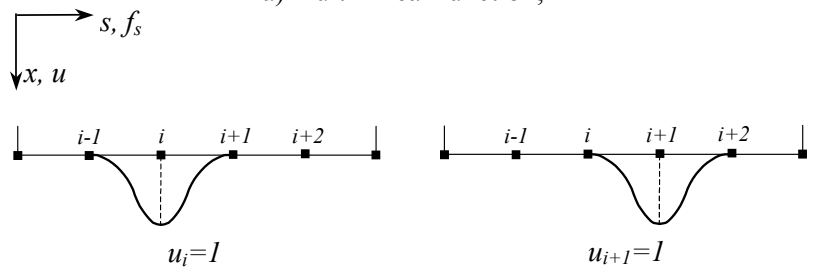

b) polynomial function

Fig. 5.5 – Alternative displacement functions

From Fig. 5.6 and the linear part of expression (5.3), and considering only the mode of deformation *k* related to $u_i = 1$, the following values for the distortion are obtained:

i) for plate *i-1*: $^{k}u_{plate\,i-1}(s,x)=\left(\frac{^{k}u_i}{b_{i-1}}s\right)\,^{k}A' \;\Rightarrow\; ^{k}\gamma_{sx,\,plate\,i-1}=\frac{^{k}u_i}{b_{i-1}}\,^{k}A'$ (5.26)

ii) for plate *i*: $^{k}u_{plate\,i}(s,x)=\left(^{k}u_i-\frac{^{k}u_i}{b_i}s\right)\,^{k}A' \;\Rightarrow\; ^{k}\gamma_{sx,\,plate\,i}=-\frac{^{k}u_i}{b_i}\,^{k}A'$ (5.27)

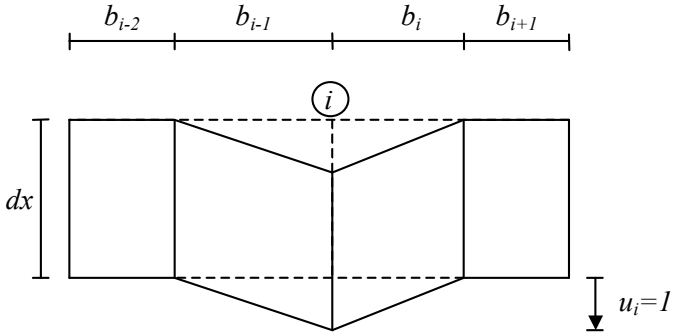

Fig. 5.6 – Membrane distortion for the inner nodes warping modes

Associated with these modes of deformation no displacements along the cross section plane occur, so for consistency, the amplitude modal function can be denoted by $^{k}A'$ and the calculus of the relevant mechanical terms can start immediately.

5.3.5. The main plates transversal extension mode

The consideration of the transversal normal stresses has been the object of several approaches in the past. Vlasov (1961) assumed that the cross section was fully rigid in the transversal direction and the corresponding strains were zero. The transversal normal stresses were thus dependant on the longitudinal stresses through the constitutive law for isotropic materials, deriving from the Poisson effect. The zero transversal membrane strain was kept in the first works of GBT, and an equilibrium model was proposed by Schardt (1989), similar to the equilibrium model for the membrane shear stresses, to compute the transverse membrane normal stresses. Assuming a rigid section's perimeter does not respect the boundary condition of a free edge of the cross section, where the transverse normal stress is null and some type of deformations must occur if longitudinal membrane

stresses are present – this phenomenon is referred in the literature as the "bulging effect". Previously, Schardt (1983) had noticed that the presence of transversal extensions would affect the member's behaviour in certain situations – one of them was the post-critical behaviour, so in this paper a non-linear term related to the transverse extension is present in the member's non-linear internal virtual work. A later work (Heinz and Mark, 1990) already considered the presence of some non-linear terms in the internal virtual work of the thin-walled member accounting for the transverse strains, but only for the classical modes, so that the first order part of the internal virtual work related to the transverse extensions was always null. The establishment of the membrane constitutive relations for the plates in their general form requires that the transverse membrane extensions are taken as unknown values, not necessarily negligible, and the corresponding first order part is given by:

$$\varepsilon_s^M = \frac{\partial f_s}{\partial s}, \tag{5.28}$$

So, in order to fully define the transverse membrane extensions, a new type of mode of deformation is established, and consists of an extension of a major plate along the cross section perimeter's direction, as shown in Fig. 5.7, generating displacements along the *Os* axis and provoking a transversal membrane extension given by:

$$\varepsilon_{s,i}^M = \frac{f_{s,i+1} - f_{s,i}}{b_i}. \tag{5.29}$$

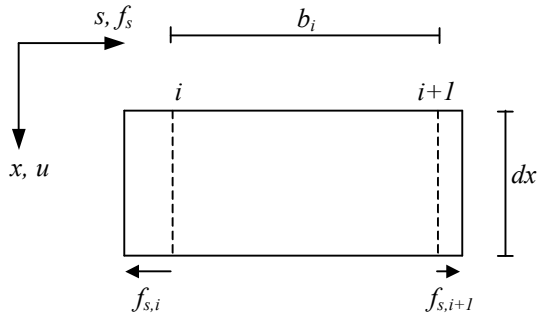

Fig. 5.7 – Transversal membrane extension for plate *I*

In the context of the matrix displacement method scheme presented above to restore cross section's continuity, the mechanical system of Fig. 5.9 is adopted and the

transverse extension of plate *i* is modelled making resource to the proper set of fixation forces. For the transverse extension of plate *i*, it can be computed as follows. Consider a simply supported portion of the plate *i* with longitudinal unitary length, and it is considered, for the sake of generality, that the thickness varies along the perimeter in the form presented in Fig. 5.8. When a load F is applied at point A, the displacement δ along *Os* is:

$$\delta = F\left(\frac{b_{r,1}\left(1-\mu_{r,1}^2\right)}{E\,t_{r,1}}+\frac{b_{r,2}\left(1-\mu_{r,2}^2\right)}{E\,t_{r,2}}+\frac{b_{r,3}\left(1-\mu_{r,3}^2\right)}{E\,t_{r,3}}\right) \tag{5.30}$$

The fixation force is thus obtained by setting the displacement δ equal to *1*:

$$F_{F,i} = \frac{1}{\left(\frac{b_{i,1}\left(1-\mu_{r,1}^2\right)}{E\,t_{i,1}}+\frac{b_{i,2}\left(1-\mu_{i,2}^2\right)}{E\,t_{i,2}}+\frac{b_{i,3}\left(1-\mu_{i,3}^2\right)}{E\,t_{i,3}}\right)} \tag{5.31}$$

and is applied on both ends of the plate, following the scheme presented in Fig. 5.9.

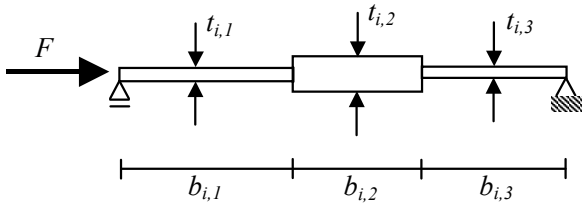

Figure 5.8 – The determination of fixation forces for plate *i*

Subsequently, the fixation forces are introduced in the mechanical system of Fig. 5.9, where all translations are prevented with the exception of those related to major plate *i*, which are set as unknowns together with all rotations at the cross section nodes. The correspondent displacement method problem is solved and the unknown displacements are determined, thus defining the unitary displacements for the mode of deformation. Fig. 5.10 illustrates the deformed shape of the mechanical model associated with the transverse

extension of plate *i*, and in most cases the plates connected to plate *i* present very small membrane deformations, showing mostly transverse bending.

The procedure presented above considers the transversal extension of an entire major plate, i.e., of a plate between two consecutive folding line nodes or edge nodes. However, this scheme can be refined to model the extension of a secondary plate, i.e., the plate delimited by two consecutive nodes, independently of their type and including the intermediate nodes, while the remaining secondary plates do not experience transversal extension directly, and hence several transversal extension modes would correspond to one major plate. The adaptation requires little change in the scheme exposed above: it would only need a more refined model for the cross section, with the introduction of additional coordinate displacements along the local axis *Os* at all inner nodes for any major plate *i*, and the fixation forces for the transverse extension of secondary plate *j*, belonging to major plate *i*, would be applied directly at the edges of the secondary plate. Then, the scheme would proceed through a similar way as the one presented just above, and some adaptations in the orthogonalization procedure are expected, since the resulting matrix $\boldsymbol{C}$ for these modes would no longer be invertible – this fact will be object of deeper discussions in the final Chapter 7. In the present thesis, this more refined procedure was not adopted since these modes showed little relevance for the examples presented below, the modes derived from the simplified scheme showing sufficient precision, and also due to the limited computer resources available. However, for more advanced non-linear stability analyses, such as localization analysis (Champneys, Hunt and Thompson 1999), it is expected that this type of modes of deformation shows greater relevance.

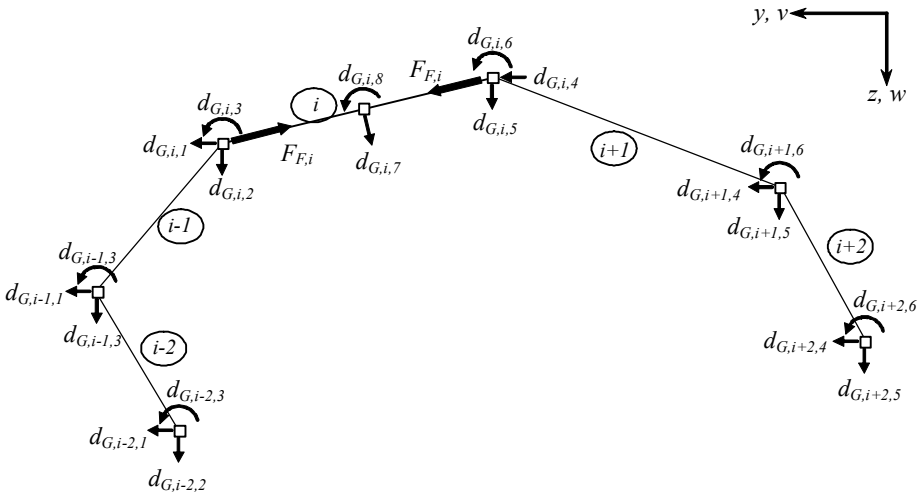

Fig. 5.9 – The mechanical system and the fixation forces $F_{F,i}$ for the extension of plate *i*

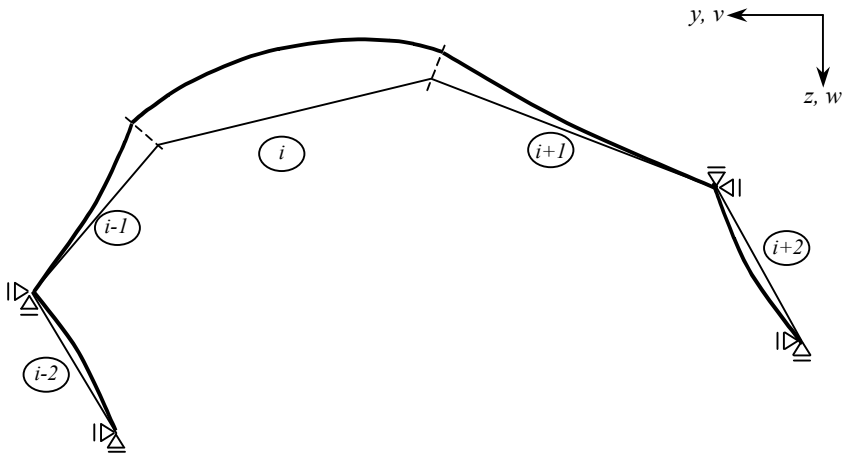

Fig. 5.10 – Deformed shape for an extension of plate *p*

5.3.6. The main plates distortional modes

Section 5.3.4 presented the inner nodes warping displacements modes, which allowed distortional deformations and shear stresses along a plate. However, these modes do not consider the distortional behaviour of a main plate as a whole and are not able to model, for example, the behaviour of a plate submitted to a shear force along the cross section perimeter's direction, because the plate's edge nodes do not move. So, following closely the methods proposed by Schardt (1989) for the analysis of mono-cellular sections and by Vlasov (1961) for the consideration of shear in multi-cellular sections, an additional

type of modes of deformation, associated with the shear deformation of the plate as a whole, for each plate of the cross section, is presented. These modes differ from Schardt's distortional mode for closed cells (Schardt 1989) because they do not require a constant shear flow around a closed cell, they just impose a distortional displacement pattern on each single plate of the section, one by one, and thus they can also be applied to open sections. Schardt's distortional mode for closed cells becomes a particular case of the present modes, i.e., it can be computed as a particular linear combination of the plate's distortion modes for a closed cell. The traditional Vlasov assumption of null membrane shear flow around an open section, which is equivalent to null membrane distortion along the member, is regarded here as possible result of the equilibrium system of the member instead of an assumption at the beginning of the analysis.

Consider a main plate *i*, belonging to a general cross section with no branching, as presented in Fig. 5.11. The displacements pattern associated with a constant shear deformation along plate *I* can be established in two different ways:

i) In Fig. 5.11-a) the constant shear deformation is applied with no warping displacements, so at $x+dx$ the plate experiences a constant (unitary) displacement $f_{s,i}$ along the perimeter's direction, and the corresponding shear deformation is given by:

$$f_{s,r} = \gamma\, dx = 1\, dx\,. \tag{5.32}$$

ii) In Fig. 5.11-b) the constant shear deformation is applied by imposing a (unitary) warping displacement $u_{end,i}$ at the final node of plate *i*, yielding the following shear deformation:

$$u_{end,i} = b_i\, \gamma = 1 \Rightarrow \gamma = \frac{1}{b_i}\,. \tag{5.33}$$

Remembering the membrane stress-strain relation for shear deformations in the

linear form:

$$\gamma_{sx}^{M} = \frac{\partial f_s}{\partial x} + \frac{\partial u}{\partial s}, \tag{5.34}$$

it is clearly recognizable that the above displacements patterns constitute the two extreme cases for the establishment of the plate *i* distortional modes, and that any linear combination of the above cases is also a feasible distortional displacement pattern.

For the second option and related to plate *i+1*, because this plate experiences no distortion a displacement occurs along the *Os* axis, equal to:

$$f_{s,r+1} = \frac{1}{b_{r+1}}. \tag{5.35}$$

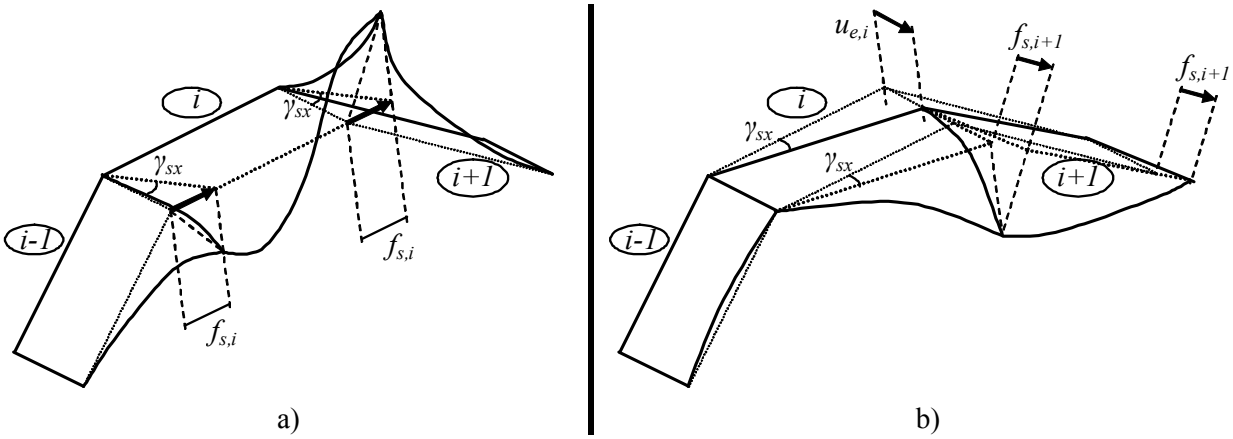

Fig. 5.11 – The *r*-plate distortional mode

As an alternative to the scheme of Fig. 5.11-b), the unitary warping displacement could be imposed to the initial node of plate *i*. All these ways are equivalent, so in the present work the pattern presented in Fig. 5.11 a) will be used. So, when a unit distortion is applied at plate *r*, at *x+dx* the section undergoes a displacement equal to *1* along *Os*, as shown in Fig. 5.12, and the displacements in the cross section plane normal to the plates are:

i) for plate *r-1*: $f_{e,r-1} = \frac{1}{\sin \Delta\alpha_r}$; (5.35)

ii) for plate r: $f_{b,r} = \dfrac{1}{tan\,\Delta\alpha_r}$ and $f_{e,r} = \dfrac{1}{tan\,\Delta\alpha_{r+1}}$, (5.36)

and the scheme proceeds by establishing the displacements method for the computing of the displacements and transverse bending moments in a similar form as the one presented in paragraphs 5.3.3 and 5.3.5. Finally, it is worth referring that it is expected these modes interact with the warping modes during the orthogonalization process, since they can be established using also warping displacements and the shear deformation may depend also from warping displacements – actually, in the forthcoming examples this fact is clearly viewed.

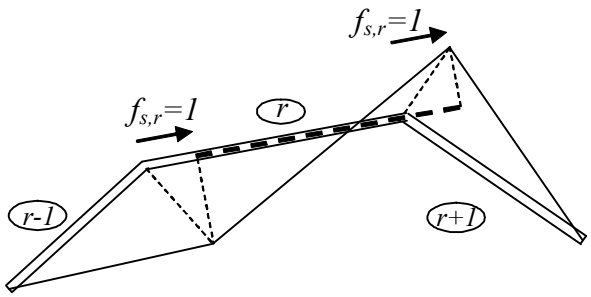

Fig. 5.12 – The r-plate distortional mode: rendering compatible the cross section displacements in the neighbourhood of plate r

5.4 – The orthogonalization procedure considering the additional modes

The next step is to include the additional modes into the traditional orthogonalization procedure, i.e., to render fully diagonal matrices ***C*** and ***B*** and to achieve a diagonal block in matrix ***D*** along the main diagonal. However, some adaptations are needed. Defining as rigid body modes those modes of deformation that have a main diagonal term of matrix ***B*** equal to zero, after the first orthogonalization step their number becomes now higher than four, which was the number of rigid body modes for the classical

GBT theory. From expressions (5.9 e) and (5.14 a) it is concluded that the rigid body modes do not exhibit transverse bending moments neither transversal extension in any point of the cross section, since the corresponding term in matrix $\boldsymbol{B}$ is zero. After the second orthogonalization step, involving only the rigid body modes, only three zero terms are obtained in the diagonal block of matrix $\boldsymbol{D}$, these terms being associated with the modes related to the Bernoulli assumption of plane sections remaining plane after deformation – the axial elongation and the major and minor axis bending (Vlasov 1961). The remaining modes that take part in the second orthogonalization step, henceforth denoted as torsional or "shear lag" modes whether they show a global cross section rotation or not[3], respectively, are associated with torsional or "shear-lag" effects, and in the forthcoming examples it is observed that:

i) for open sections, a torsional mode always occurs, independently of the number of intermediate nodes added for the cross section discretization, which confirms the Vlasov's assumption of negligible shear deformations in open sections submitted to torsion;
ii) for closed sections, there is not any mode showing constant shear flow around the closed cell, so that the Bredt's scheme for torsion analysis is a particular case and may be restrictive in some cases.
iii) For one cross section, more than one torsional mode occurs, but for open sections only one is related to null shear deformations.

Finally, concerning the transversal extension modes for edge plates, these modes generate non-zero terms only in the main diagonal of matrix $\boldsymbol{B}$, all corresponding terms in matrix $\boldsymbol{C}$ being equal to zero. Hence, these modes need not be considered in the

[3] Some modes can show "shear-lag" combined with a global cross section rotation, and are denoted as torsional modes.

orthogonalization procedure, since they are already orthogonal to the others with respect to matrices $\boldsymbol{C}$ and $\boldsymbol{B}$.

If the more general formulation was adopted by referring the transversal extension modes to the secondary plates, then it would be expected that matrix $\boldsymbol{C}$ corresponding to the transversal extension modes was not invertible, and the orthogonalization procedure could not start. Accounting on the fact that the problem here is collocated in the perpendicular direction of the warping modes, it is expected that the insertion of an additional orthogonalization step at the beginning of the problem, between matrices $\boldsymbol{B}$ and $\boldsymbol{C}$ and for the transverse extension modes only, brings two sets of transverse extension modes, corresponding to null and non-null values of main diagonal terms in matrix $\boldsymbol{C}$. These two sets of modes of deformation shall correspond to modes that do not exhibit and exhibit displacements along the cross section's plane normal to the plates, respectively. The modes belonging to the first set are considered as they are in the analysis but are removed from the subsequent orthogonalization steps, while the modes belonging to the second set are considered in the forthcoming orthogonalization procedure, and obviously accounted in the global analysis of the structural member. This idea is not more than a conjecture and was not implemented since the limited computer resources presently available to the author require that the cross section's model is as simple as possible, but in the near future will be tested – this aspect will be object of further discussion in the final chapter.

5.5 – Computer implementation for cross section analysis

In the following, a general description of the developed software is presented, in order to enable a better grasp on how the concepts presented above can form a structured scheme for the calculus of the relevant geometrical properties of an open non-branched or closed mono-cellular cross section, which will be used after to perform the stability

analysis of thin walled elements. All GBT cross section analysis embrace two major steps: i) the calculus of the unitary modal displacements and transverse bending moments, that will be used later to determine the stresses and the displacements at any point of the member, and ii) the calculus of the linear and non-linear cross section generalized geometric properties, calculated from the unitary modal displacements and transverse bending moments derived in the previous step, and that will build the global equilibrium system of the member.

In order to perform the first step a computer program was made, on a FORTRAN POWERSTATION 4.0 code, to calculate the unitary modal displacements and transverse bending moments, storing all relevant results in a text file that will be read by the following MATHEMATICA worksheets. Fig. 5.13 presents a flowchart describing the major steps involved here. The first step consists in reading a data file that includes all relevant information about the cross section, namely: i) the type of cross section, n_{CST}, the number of main nodes, n_{MN}, and the number of inner nodes, n_{IN}. Since the program, at this stage, applies only to unicellular or open non-branched sections, from this information it is possible to derive the number of main plates, n_{MP}, the number of secondary plates, n_{SP}, and the number of modes of deformation, n_{MD}. Afterwards, the relevant mechanical and geometrical properties, for each main plate i, are read from the data file, namely the number of inner nodes included in the plate, the inclination angle of the plate, α_i, the number of the corresponding initial and ending main nodes and the incidence matrix, needed to compute the global stiffness matrix of the cross section, relating the local displacements of the main plate to the global displacements adopted for the whole cross section. Next, the information about each secondary plate p is given to the program, which contains the major plate where the secondary plate p in question is included, its thickness t_p, its width b_p, its Young modulus E_p, and its Poisson coefficient μ_p. From this data it is possible to derive the shear modulus and the plate bending stiffness for each secondary plate i, given respectively by:

$$G_i = \frac{E_i}{2\left(1+\mu_i\right)} \tag{5.38}$$

$$K_i = \frac{E_i\ t_i^3}{12\left(1-\mu_i^2\right)}. \tag{5.39}$$

The next step involves the calculus of the stiffness matrices for all main plates and their assemblage to form the global stiffness matrix, making resource to the concepts presented in chapter 5.3.2. Now all relevant information is available to establish the basic modes of deformation in five steps, described by the unitary modal displacements and transverse bending moments, as follows:

i) the n_{MN} warping modes of deformation, one per main node, are derived based on the concepts exposed in the paragraph 2.2.3.1;

ii) the n_{MP} plate distortional modes, one per main plate, are derived, based on the postulated in chapter 5.3.6;

iii) the plate bending modes are established through the scheme presented in chapter 2.2.3.2, being their number equal to n_{IN} for closed sections or $n_{IN}+2$ for open non-branched sections; each mode corresponds to one inner node and, for open sections, the edge nodes generate also a plate bending mode, being treated in a similar form of the remaining inner nodes (Schardt 1989);

iv) the inner nodes are formulated directly, regarding chapter 5.3.4 and do not need to make resource to the stiffness method since no displacements along the cross section plane occur.

v) The plate's transversal extension modes are established taking into account paragraph 5.3.5.

The program proceeds to the orthogonalization scheme, based in chapters 2.2.5 and 5.4, by deriving a linear reversible transformation scheme, given by a n_{MD} dimensional

square matrix $\boldsymbol{T}$, that recombines the modes of deformation in order to simplify some linear equilibrium matrices, rendering diagonal matrices $\boldsymbol{C}$ and $\boldsymbol{B}$, and also a matrix block through the main diagonal of matrix $\boldsymbol{D}$. This transformation matrix $\boldsymbol{T}$ is derived from the three steps scheme described in the referred chapters and now the number of rigid body modes n_{RBM} – those that do not involve cross section distortion – is given by the number of zeros in the main diagonal of matrix $\boldsymbol{B}$.

Finally, the program computes and stores the unitary modal displacements and transverse bending moments for the orthogonal modes of deformation, which are obtaining by multiplying their respective values for the basic modes of deformation by the linear transformation matrix $\boldsymbol{T}$, in the following matrix form:

$$\boldsymbol{u}_{ORT} = \boldsymbol{u}_{BAS} \cdot \boldsymbol{T} \qquad \text{(5.40, a-e)}$$

$$\boldsymbol{f}_{s,ORT} = \boldsymbol{f}_{s,BAS} \cdot \boldsymbol{T}$$

$$\boldsymbol{f}_{ORT} = \boldsymbol{f}_{BAS} \cdot \boldsymbol{T}$$

$$\vartheta_{ORT} = \vartheta_{BAS} \cdot \boldsymbol{T}$$

$$\boldsymbol{m}_{s,ORT} = \boldsymbol{m}_{s,BAS} \cdot \boldsymbol{T} \,,$$

where subscripts *BAS* and *ORT* refer to the initial (basic) and the final (orthogonal) modes of deformation, respectively.

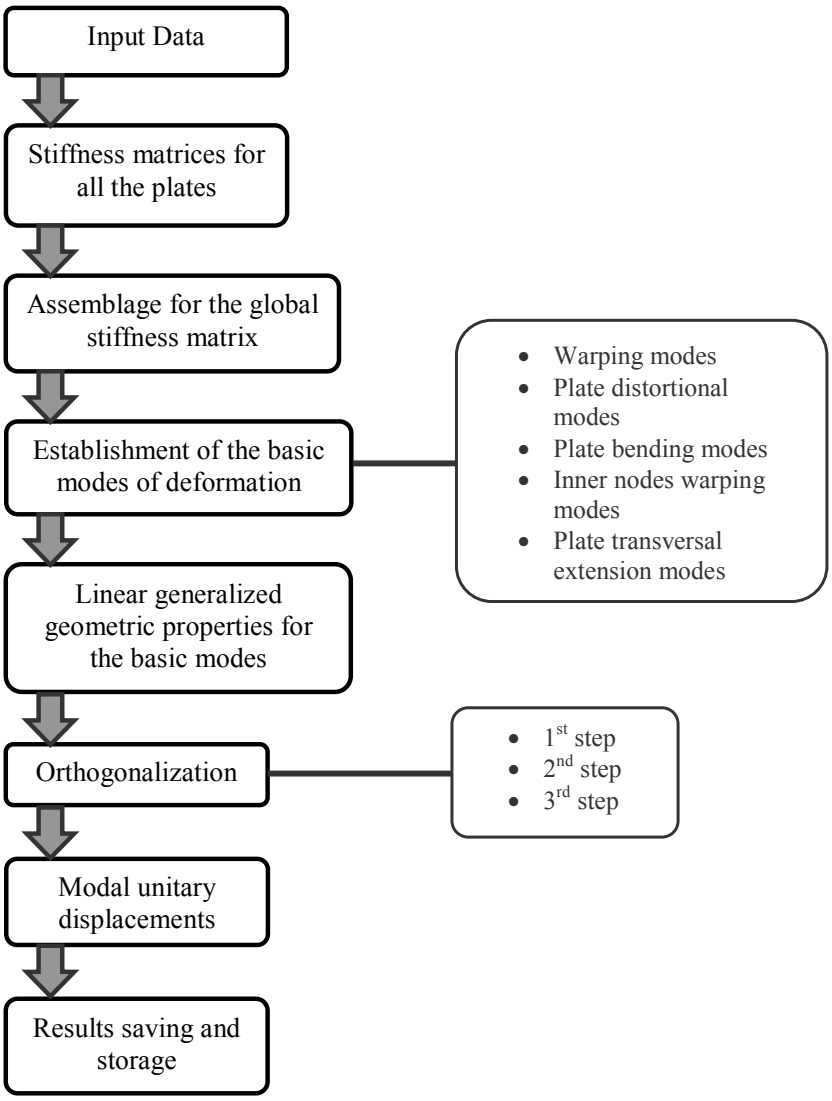

Fig. 5.13 - Flowchart of the program for calculation of the unitary modal displacements and transverse bending moments

As an alternative, after having generated the basic modes of deformation, a Mathematica worksheet was also implemented to perform the orthogonalization procedure and to derive the final modes of deformation and the corresponding generalized geometric properties

After having computed the unitary modal displacements and transverse bending moments, the calculus of the generalized geometric properties – which are given by the integration of products of functions that represent the relevant displacements along the cross section – is made through a MATHEMATICA worksheet that calculates and stores these

tensors, to build afterwards the equilibrium system. Fig. 5.14 presents a flowchart containing the relevant steps that form the program, which just requires the cross section geometrical and mechanical properties, related to the secondary plates and which were already given to the FORTRAN program, and the modal displacements given by expressions (5.40, a-e). The geometrical constants are calculated by summing, for all secondary plates, the integral, defined along each secondary plate of the cross section, of the products of the appropriate displacement functions given by the appropriate formula of expressions (5.9, a-e), (5.12, a-j), (5.14, a-o) and (5.16, a-p), where each displacement is given by the suitable formula of (5.17), (5.18) or (5.19).

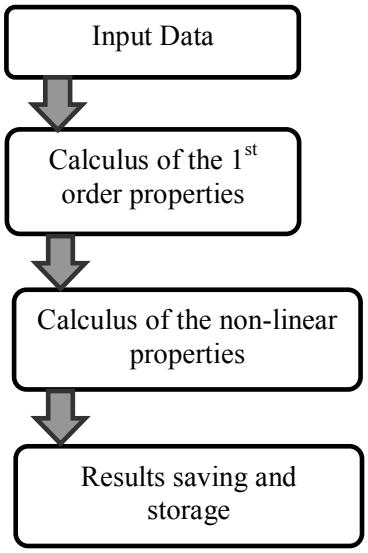

Fig. 5.14 - Flowchart of the program for calculation of the unitary modal displacements and transverse bending moments

5.6 – Benchmark example: the channel column

5.6.1 General presentation of the problem

In order to illustrate and validate the concepts just presented, the buckling and post-buckling analysis of a prismatic thin-walled channel section presented in Yap and Hancock (2006) is performed, for the common load case of uniform compression. After the

introductory presentation of the problem, a linear stability analysis is made in terms of the variation of the critical behaviour with the member's length, thus defining the general critical behaviour of the member for various boundary conditions. This diagram of the critical load versus the member's length is validated by comparing the GBT results with those arising from the FSM program CUFSM (Schafer 2003), and since this analysis considers pined-pined boundary conditions for the edge cross sections of the member, the coordinate functions (3.24) and (3.37 a-e) are adopted. Subsequently, for the length *300* mm, whose stability behaviour lies in the symmetrical distortional buckling range, and using fixed-fixed boundary conditions for the member's edge sections, hence adopting coordinate functions (3.24) for mode 1 and (3.37 a, c and e) for the remaining modes, the initial post-buckling behaviour is investigated using the lower bound approximation for the member's internal strain energy, in other words using expression (5.21) for the TPE of the member. The corresponding results are drawn and compared to those arising from the FEM analysis performed by Yap and Hancock (2006). Diagrams of the primary and secondary equilibrium paths are shown as plots of the load parameter against the vertical displacement the edge node of the lip for both cases, and a good agreement was observed. Finally, the deformed configuration of the member is presented, for a load level higher that the critical one.

The cross section is presented in Fig. 5.15-a) and consists of a 80×60 channel section with *5* mm lips and thickness equal to *1* mm. It is assumed that the member is made of steel, having $E=210$ Gpa and $\mu=0.3$. From the discretization presented in Fig. 5.15-a), which considers 3 inner nodes in the web and 1 inner node in each flange, 28 basic modes of deformation are derived, being illustrated in Fig. 5.16 for the unitary warping displacements and in 5.17 for the unitary cross sectional displacements. After the orthogonalization procedure, these modes are recombined and transformed in the new set of modes shown in Figures 5.18 and 5.19. Comparing the initial and the final modes shows how the orthogonalization procedure performs: the five types of modes of deformation,

warping (modes 1 to 6), plate distorsional (modes 7 to 11), plate bending (modes 12 to 18), inner nodes warping (modes 19 to 23) and plate transversal extension (modes 24 to 28) modes are recombined in the following way:

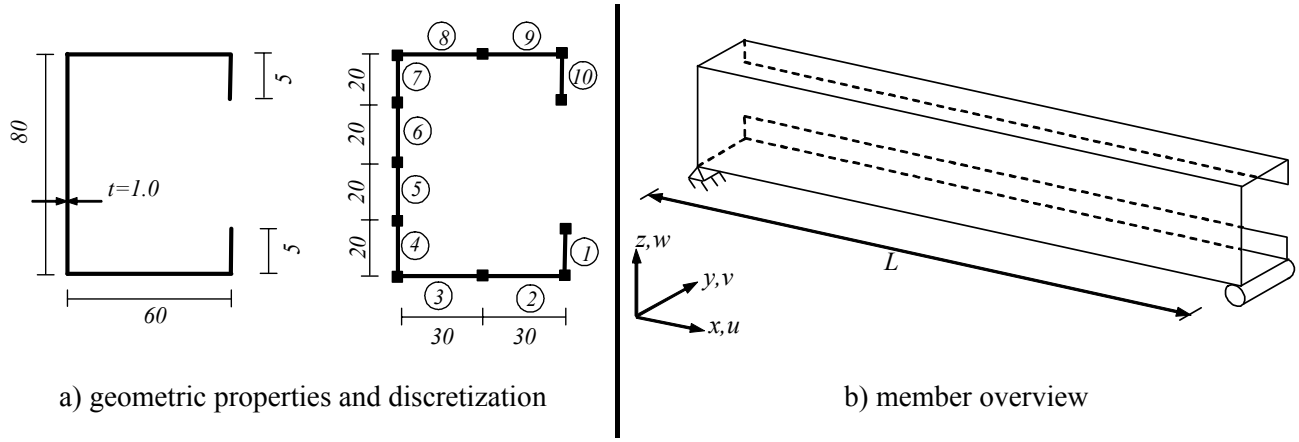

a) geometric properties and discretization b) member overview

Fig. 5.15 – The analysed cross-section and the adopted nodes (all dimensions in mm)

i) Modes 24 to 28 are still plate transversal extension modes (modes 27 and 28 remain unchanged since they are associated with edge plates of the cross section), but modes 24 to 26 are recombined in order to present symmetrical or anti-symmetrical shapes.

ii) Modes 15 to 23 derive from the warping, plate bending and plate distortional modes and present no warping displacements, as opposite to the corresponding modes in the classical GBT formulation – this fact can be interpreted as a direct influence of the plate distortional modes.

iii) Modes 5 to 14 are the torsional and "shear-lag" modes, depending whether or not they show cross section rotation, and derive from the inner nodes warping, warping and plate distortional modes. These modes are related to null terms in the main diagonal of matrix $\boldsymbol{B}$, hence are already rigid-body modes, and were determined in the second step of the orthogonalization procedure. Some of them, showing no cross section rotation, are very close to the traditional major

or minor axis bendings and represent the influence of shear-lag in the bending of structural members, a very important phenomenon that has been object of research all over the years. On the other hand, the remaining modes illustrate the influence of shear lag in torsion. All in all, these modes can be regarded as a new look at the shear lag phenomenon.

iv) Like in the traditional GBT theory, mode 1 corresponds to the axial elongation, modes 2 and 3 are the major and minor axis bendings, respectively, and mode 4 is the traditional Vlasov's warping torsion, and for the present case – an open cross section – does not carry any shear deformation, since the corresponding term in matrix $\boldsymbol{D_3}$ is null.

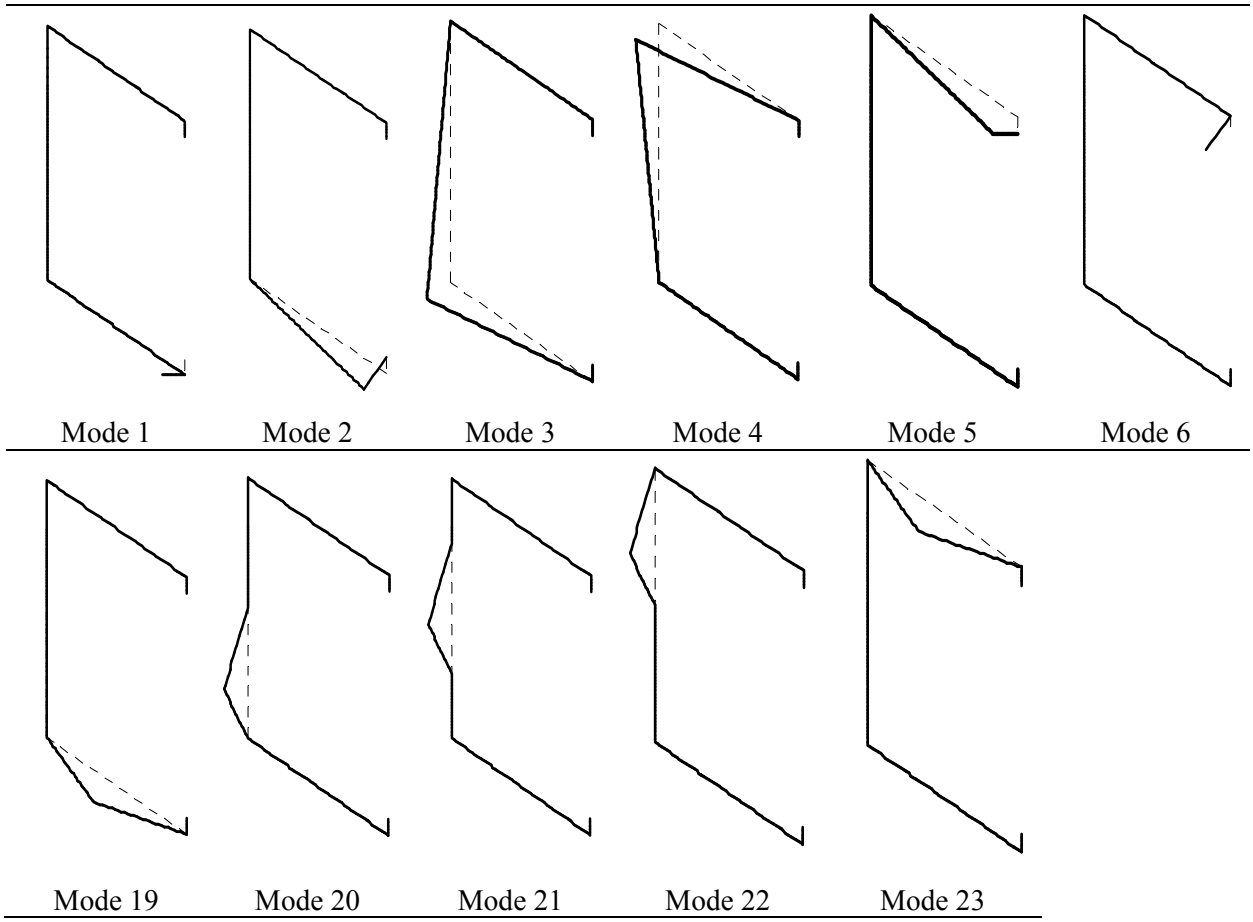

Fig. 5.16 – The unitary warping displacements for the initial modes of deformation (the remaining basic modes have null warping displacements)

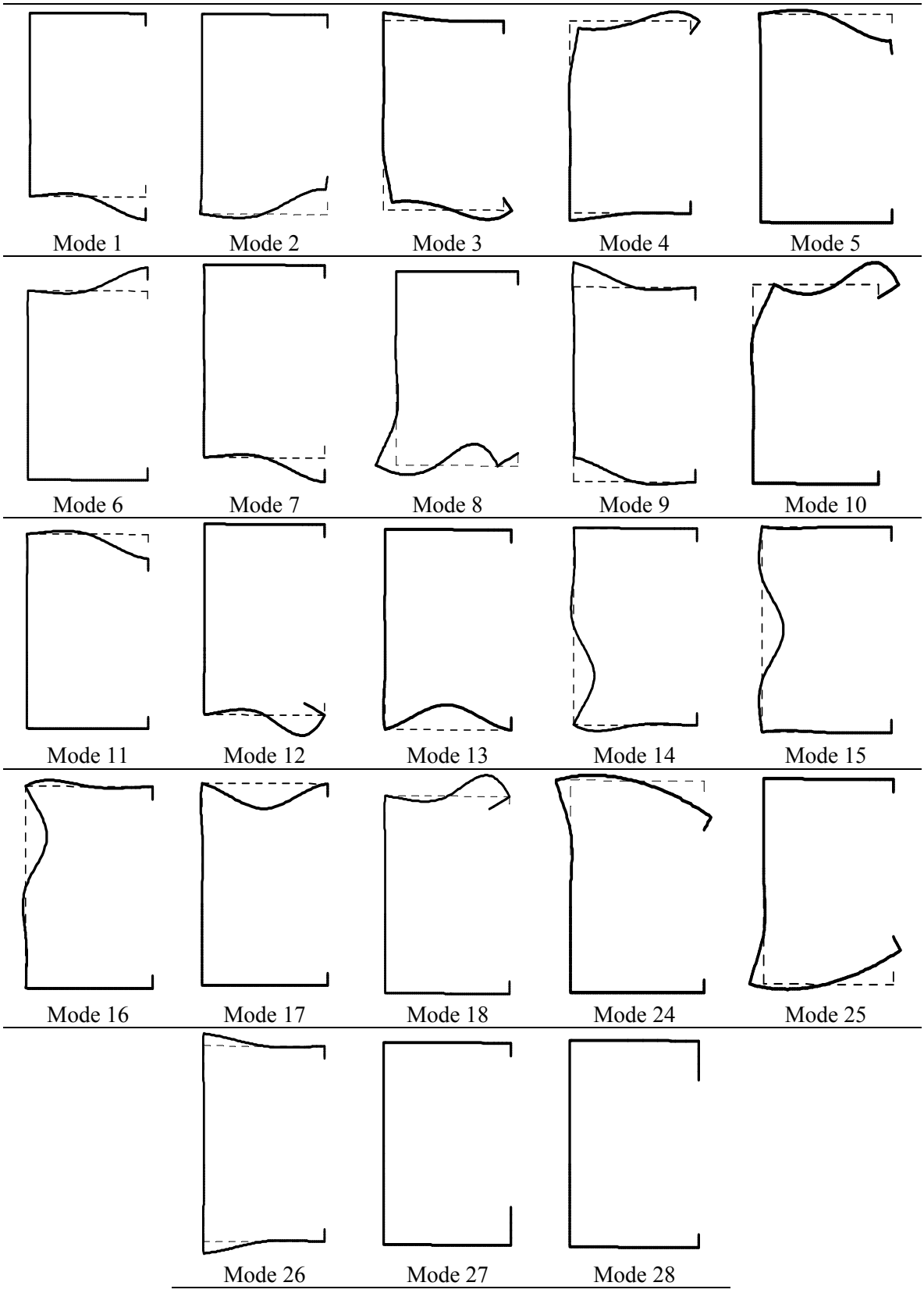

Fig. 5.17 – The unitary cross section plane displacements for the initial modes of deformation (the remaining basic modes have null displacements)

As said above, the extended GBT formulation embraces the traditional scheme, and this can be illustrated by considering in the analysis only the initial modes 1, 2, 3, 4, 5, 6, 12, 13, 14, 15, 16, 17 and 18. Their orthogonalization generates the modes represented in Figures 5.20 and 5.21, which are precisely the same generated by the traditional GBT procedure explained in Chapter 2 and applied in Chapter 4. So, the extended formulation only adds more feasible deformation patterns to the analysis, which provokes that any warping displacement is removed from the plate bending modes.

5.6.2 – The critical behaviour

At first, the critical behaviour was investigated for the uniform compressed column assuming pined-pined boundary conditions, by accounting on the coordinate functions (3.37) for modes 2 and higher – all modes were considered. Figure 5.22 presents the variation of the critical load for member's lengths between *50* and *5000* mm, adopting only the first polynomial of (3.37) as coordinate function for all modes, with the exception of mode 1 that uses function (3.24), together with the corresponding results obtained from the linear stability analysis realized by the FSM software CUFSM (Schafer 2003). This FSM program assumes a single half sine wave over the member's length for the membrane and flexural displacements, thus it models the pined-pined boundary conditions, and a perfect agreement between both analyses is observed.

Fig. 5.23 illustrates the decrease of the critical loads for the increasing number of polynomial coordinate e functions per mode of deformation, for fixed-fixed boundary conditions, i.e., for coordinate functions (3.41), since in the following paragraph the post-bucking analysis will be performed for fixed-fixed boundary conditions. The ability of the procedure shown in Chapter 3 to generate polynomial coordinate functions that model a wide range of boundary conditions is used to study the member's critical behaviour for pined-pined, fixed-fixed and pined-fixed boundary conditions, in other words considering polynomials (3.37 a), (3.43 a) and (3.41 a) as coordinate functions for modes 2 and higher, and Fig. 5.24 presents the corresponding critical behaviour of the column, highlighting the

decrease of the critical loads when the support conditions pass from fixed to pinned.

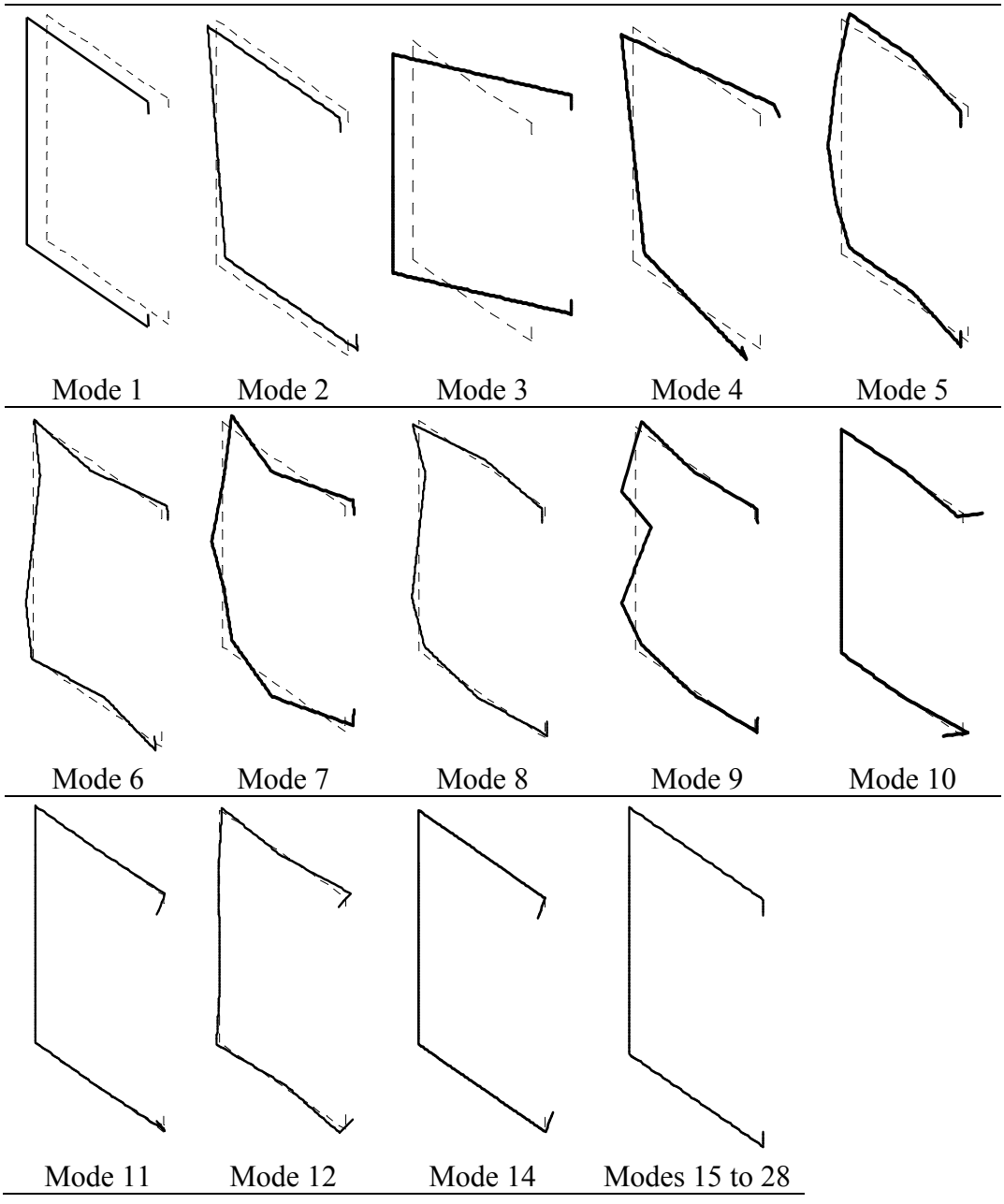

Fig. 5.18 – The unitary warping displacements for the orthogonal modes of deformation

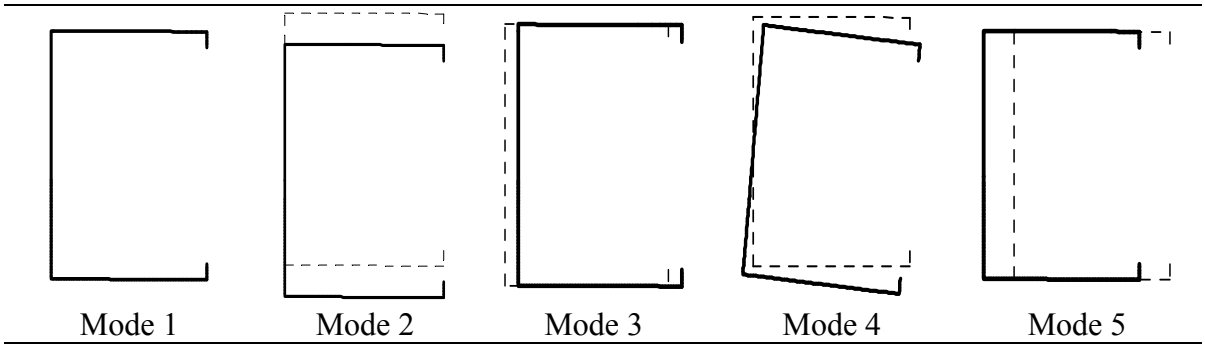

Mode 1 Mode 2 Mode 3 Mode 4 Mode 5

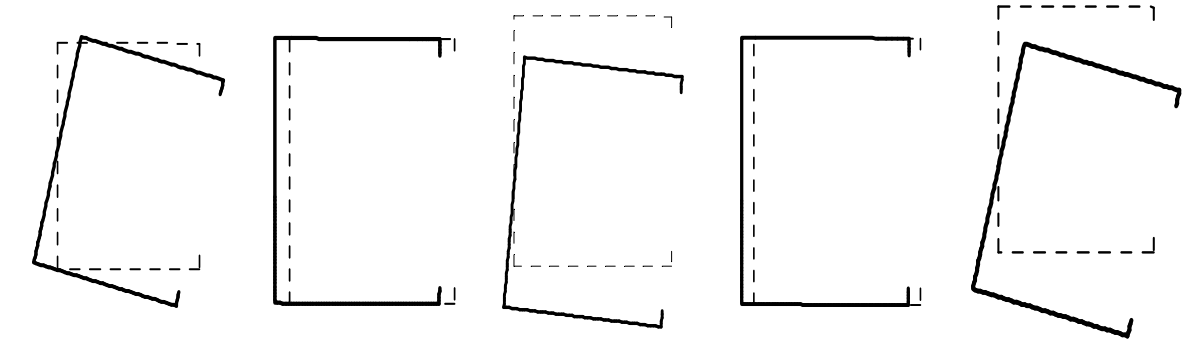

Mode 6 Mode 7 Mode 8 Mode 9 Mode 10

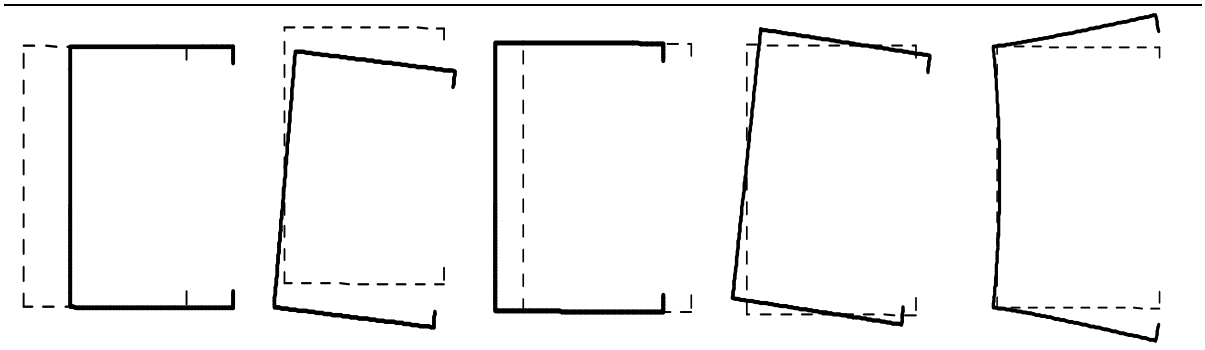

Mode 11 Mode 12 Mode 13 Mode 14 Mode 15

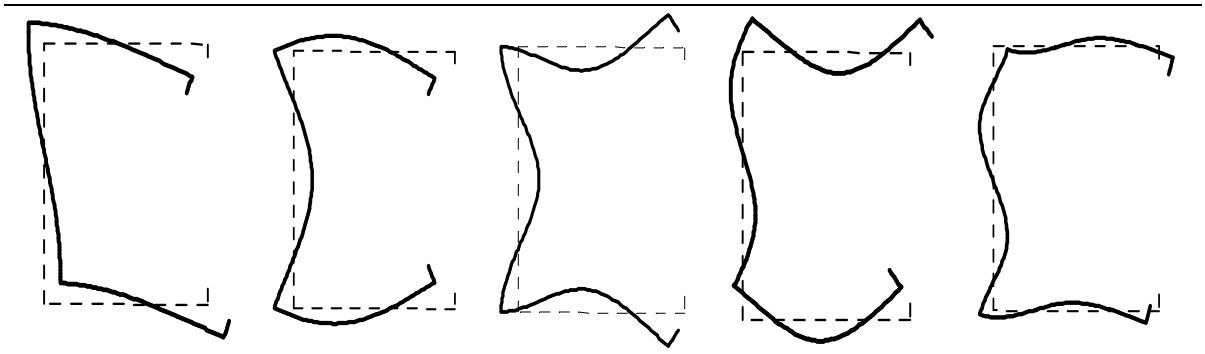

Mode 16 Mode 17 Mode 18 Mode 19 Mode 20

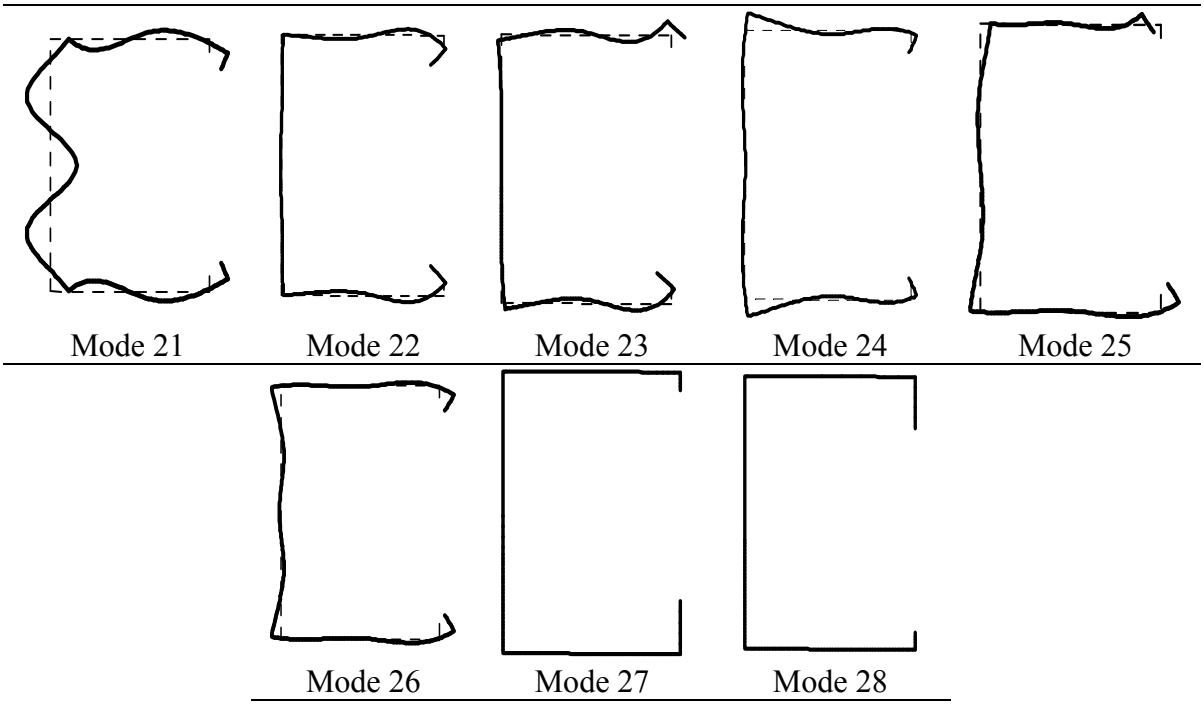

Fig. 5.19 – The unitary cross section's plane displacements for the orthogonal modes of deformation

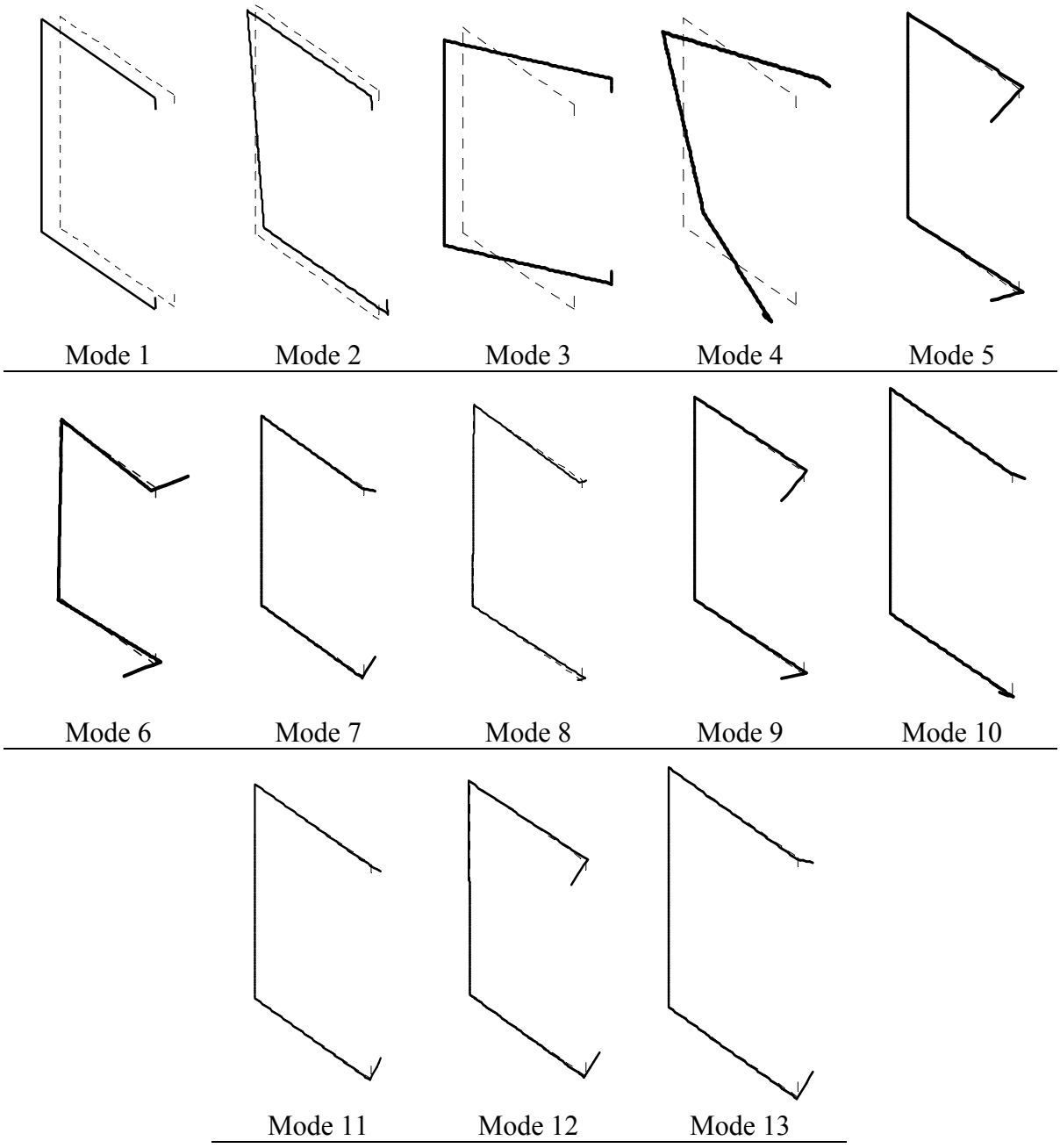

Fig. 5.20 – The unitary warping displacements for the orthogonal modes of deformation, for the classical GBT procedure

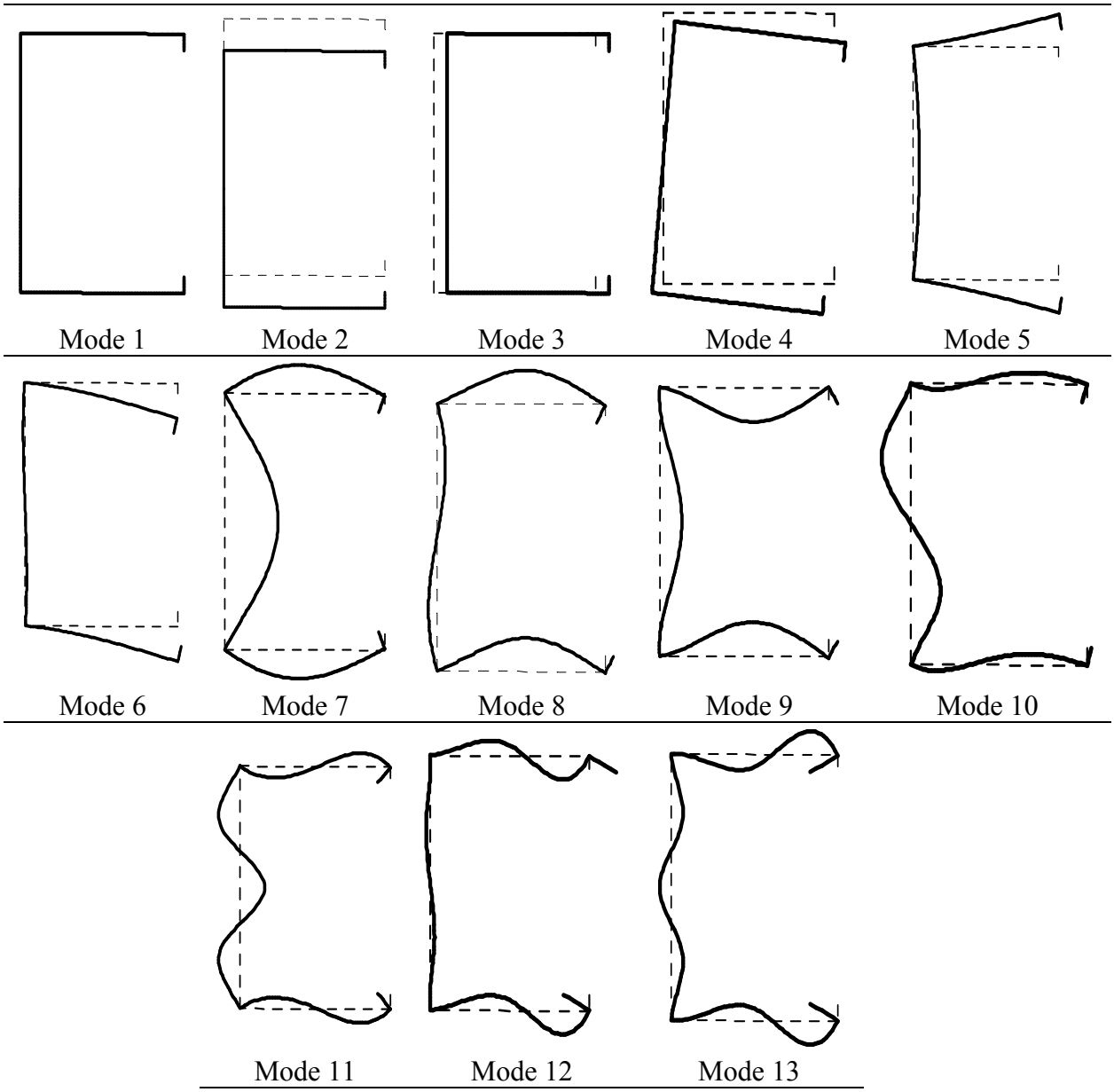

Fig. 5.21 – The unitary cross section's plane displacements for the orthogonal modes of deformation, for the classical GBT procedure

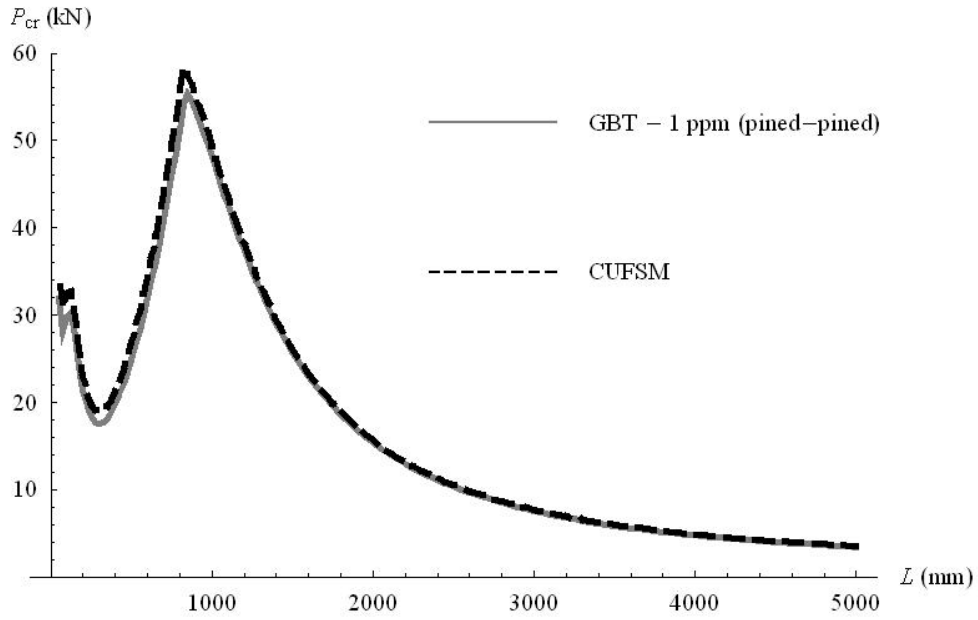

Fig. 5.22 – The critical loads for the simply supported channel column of Yap & Hancock (2006): benchmark comparison between GBT and CUFSM analysis

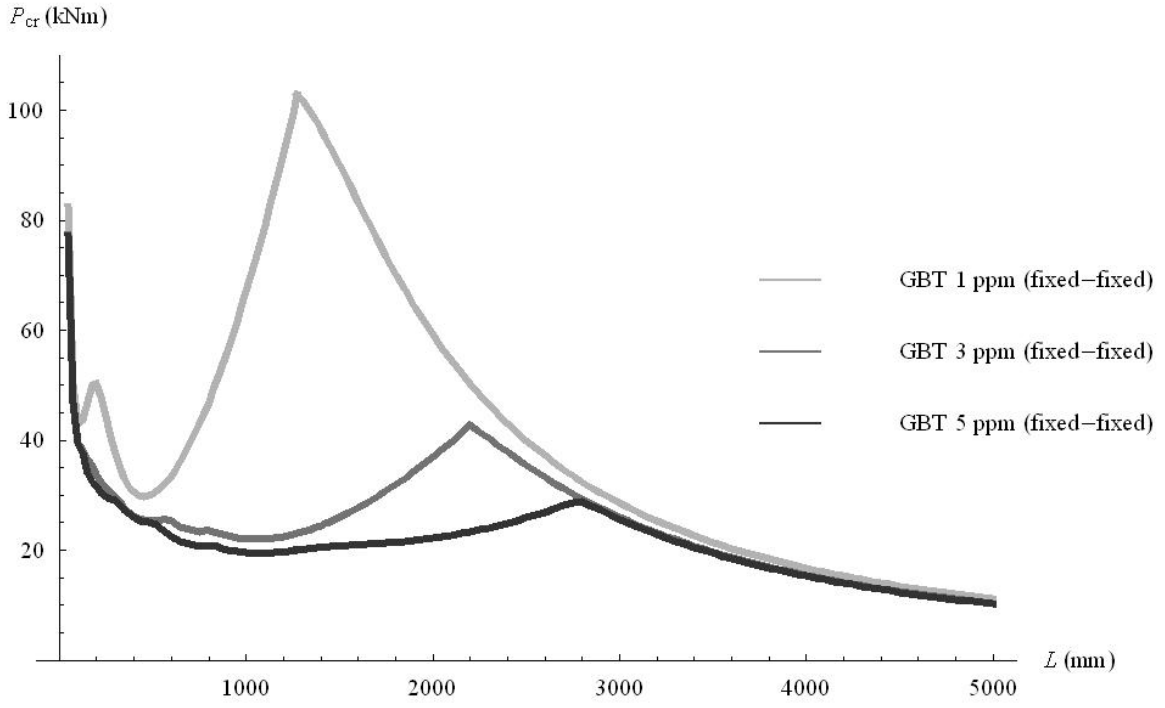

Fig. 5.23 – The critical loads for the fixed-fixed channel column of Yap & Hancock (2006): the decrease of the critical load with the increasing number of adopted polynomials

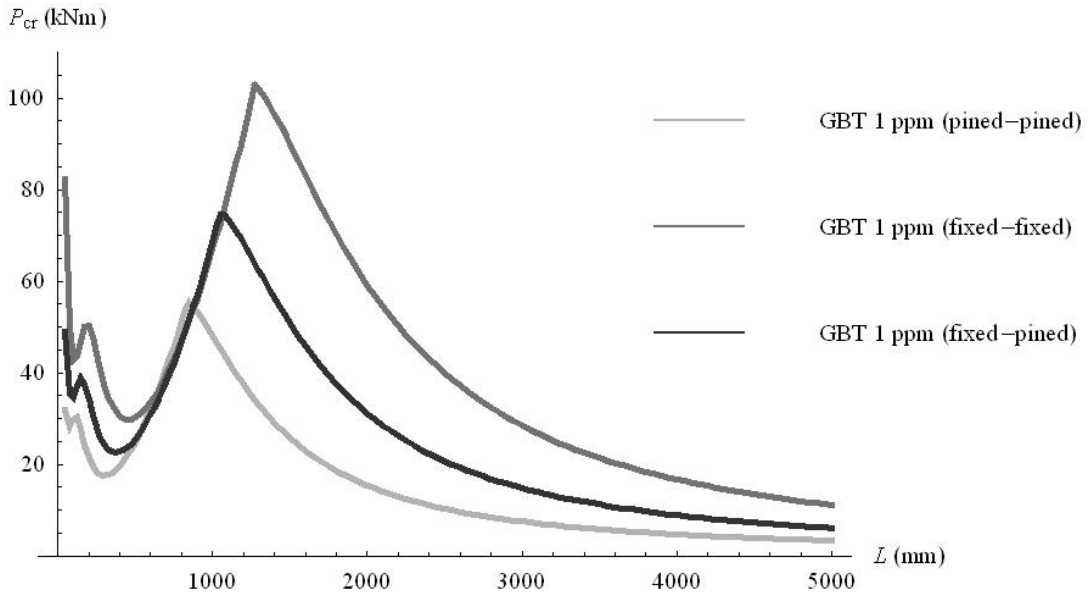

Fig. 5.24 – The critical loads for the channel column of Yap & Hancock (2006): comparison for the fixed-fixed, fixed-pined and pined-pined boundary conditions

5.6.3 – The post-buckling behaviour in the distortional range

In order to perform a benchmark comparison between GBT and FEM analyses in the post-bucking range and to validate the concepts presented above, the column's post-buckling behaviour is investigated for the length $L=300$ mm, considering fixed-fixed boundary conditions and following the example presented in Yap & Hancock (2006). Both the classical and the extended GBT formulations were used and for the latter the lower-bound approach was adopted to save computer resources, by determining the internal strain energy through the simplified energy formula (5.21). Hence, both the extended and the classical GBT formulations account on the same non-linear terms, use the same coordinate functions, given by expression (3.24) for mode 1 and (3.37 a-e) for modes 2 and higher, adopt similar discretization, given in Fig. 5.15-a, and make resource to the same no-linear stability scheme presented in chapter 3.

Fig. 5.25 presents the resulting vertical displacement of the edge node of plate *1* for the classical and the extended GBT analyses, and also for a FEM analysis taken from Yap

& Hancock (2006). A good agreement between all the analyses is noted. The classical GT formulation clearly overestimates the load parameter for a similar displacement, showing that the relation between the warping displacements and the cross section plane displacements for the distortional modes that occurs in the classical GBT scheme to render null the distortions in the member, clearly stiffens the member's behaviour, generating smaller displacements than those that really occur for a specific load level. Despite being very similar, it is observed in all analyses that the inwards deformation is slightly less stiff than the outwards one, where inwards and outwards refers to the movement of one lip in relation to the other one. In the extended GBT analysis some numerical instability was observed in the neighbourhood of the critical point, due to the larger dimension of the relative non-linear system, so the analysis of the critical state and its vicinity is not clear, but the classical GBT analysis highlights the fact that the bifurcational behaviour is non-symmetric and the inwards deformation corresponds to the non-stable branch. However, as the post-buckling displacements become bigger, the system regains stability shortly after the critical state, and the inwards equilibrium path's slope turns from negative to positive – in fact, negative path's slope occurs inside a very small neighbourhood around the critical state for the analysed example, where some post-buckling equilibrium points were determined corresponding to a load level slightly smaller that the critical load.

Fig. 5.26 represents the member's deformed configuration for $P/P_{cr} = 2$ and it can be clearly viewed that the assumption of null distortions results in smaller displacements for the classical GBT formulation – in fact, despite of giving good results for small displacements in linear analysis (Schardt 1989), this assumption shall be withdrawn in the post-buckling analysis since the resulting displacements are smaller than the ones really observed in the FEM or extended GBT analyses, and the member's post-buckling configurations in the right column of Fig. 5.26 are clearly more realistic – for example, from the classical GBT analysis, the displacements along the *Oy* axis are nearly null, and it is known that inwards and outwards deformation are associated with translational

movements of the cross sections parallel to the major axis, in the present case the *Oy* axis (Yap and Hancock 2006 present no information about this displacement, so it is not illustrated here). Finally, Fig. 5.27 presents the normal membrane longitudinal stresses along the cross section for P/P_{cr} equal to 1, 1.25 and 1.50 for the extended GBT formulation.

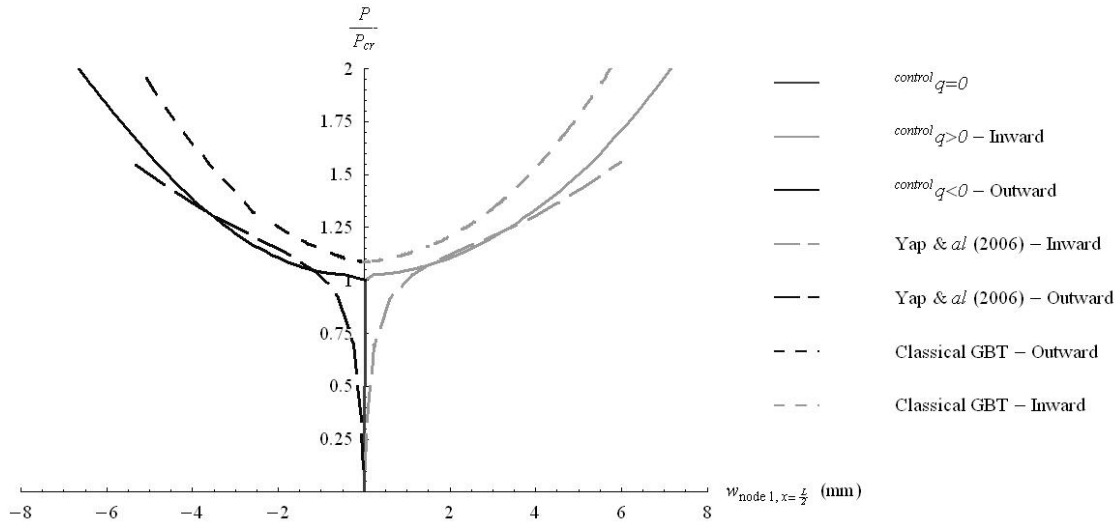

Fig. 5.25 – Vertical displacement w for node 1 at $x = L/2$: benchmark comparison between the extended and the classical GBT formulations and the FEM (Yap & Hancock 2006)

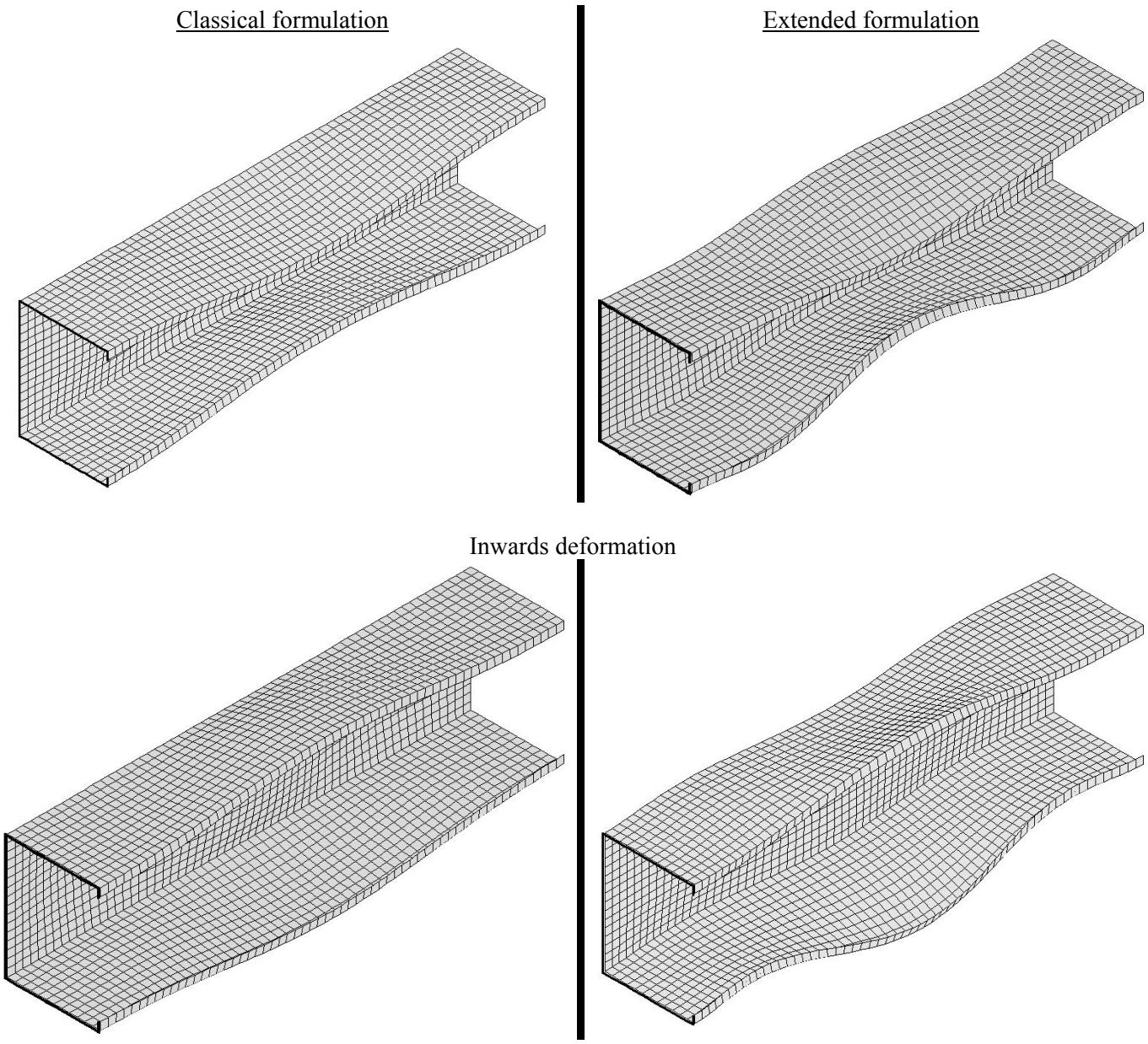

Fig. 5.26 – Column's configuration for $\frac{P}{P_{cr}} = 2$: comparison between classical and extended GBT formulations (all displacements, for both analyses, are multiplied by the same amplification factor, equal to 2)

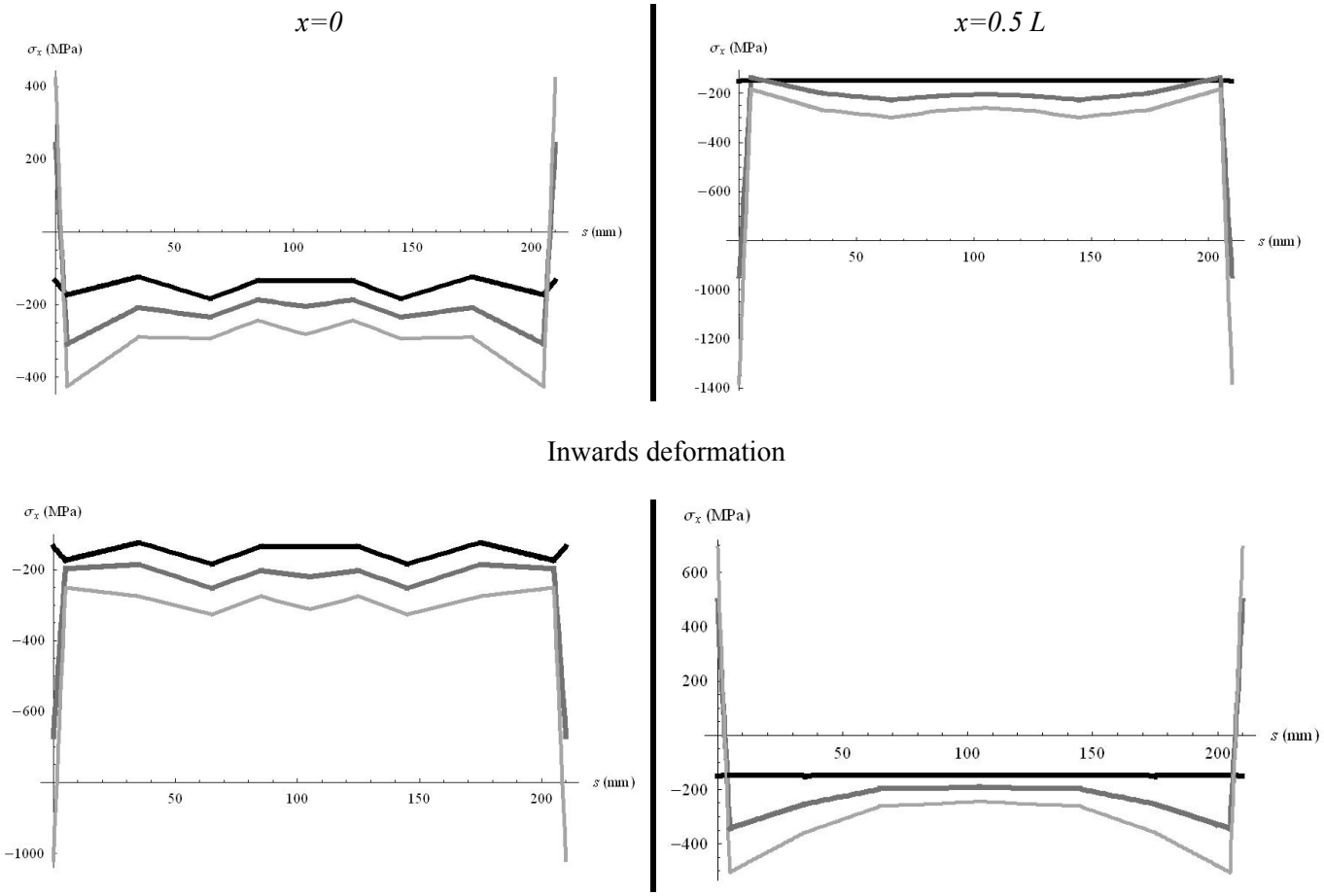

Fig. 5.27 – Longitudinal membrane stress along the (laid out) cross section, for $\frac{P}{P_{cr}}$ equal to 1, 1.25 and 1.50

5.7 – Benchmark example: the thin-walled RHS member

5.7.1 Presentation and derivation of the modes of deformation

The buckling and post-buckling behaviour of a RHS $80 \times 40 \times 1$ shown in Fig. 5.28-a) is analysed here, and validated against a FEM solution. The member is made of steel ($E = 210$ GPa , $\mu = 0.3$) and is simply supported, as shown in Fig. 5.28-b). The end plates are of negligible bending inertia, so the edge cross sections are free to warp, and one

end, at $x=L$, is free to move along the longitudinal direction.

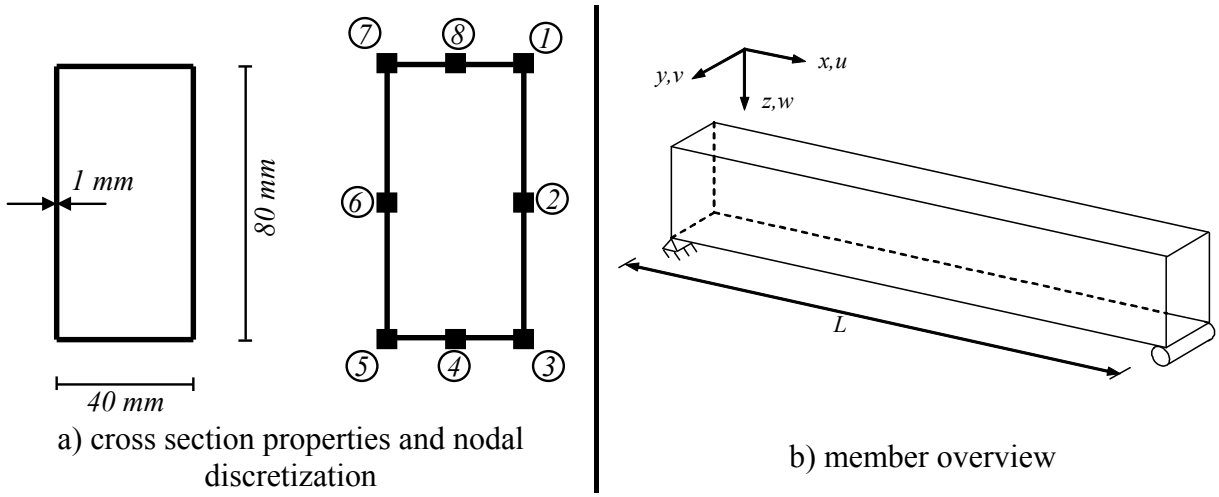

a) cross section properties and nodal discretization

b) member overview

Fig. 5.28 – The compressed column

The unitary modal displacements are presented in Fig. 5.29 for the classical GBT formulation and in Figures 5.30 and 5.31 for the extended GBT theory. In comparison to the classical GBT formulation, the number of rigid body modes – modes associated with null values for the main diagonal of equilibrium matrix $\boldsymbol{B}$ – is increased from 4 to 11. The first three modes are coincident with those resulting from the classical formulation.

Classical Bredt's torsion does not appear in the extended formulation. The Schardt formulation for closed cells (Schardt, 1989) considers the hypothesis of Bredt, by associating the shear deformation of the plates with a constant membrane shear flow around the whole closed cell, as seen chapter 2. In the extended GBT formulation different shear stress flows are allowed for each main plate, so that the classical Bredt's torsion of closed cells becomes a particular case of the extended theory: combining modes 5 and 11 in the form:

$$^{BT}\delta = 0.111031\ ^{5}\delta + 0.888969\ ^{11}\delta \tag{5.41}$$

where δ represents any unitary modal displacement or unitary modal transversal bending moment and superscript ^{BT} denotes Bredt's torsion, yields the torsional mode of the classical GBT theory. Analogously, it is possible to obtain the global distortional mode 5

of the classical formulation by a linear combination of modes 5, 11 and 13.

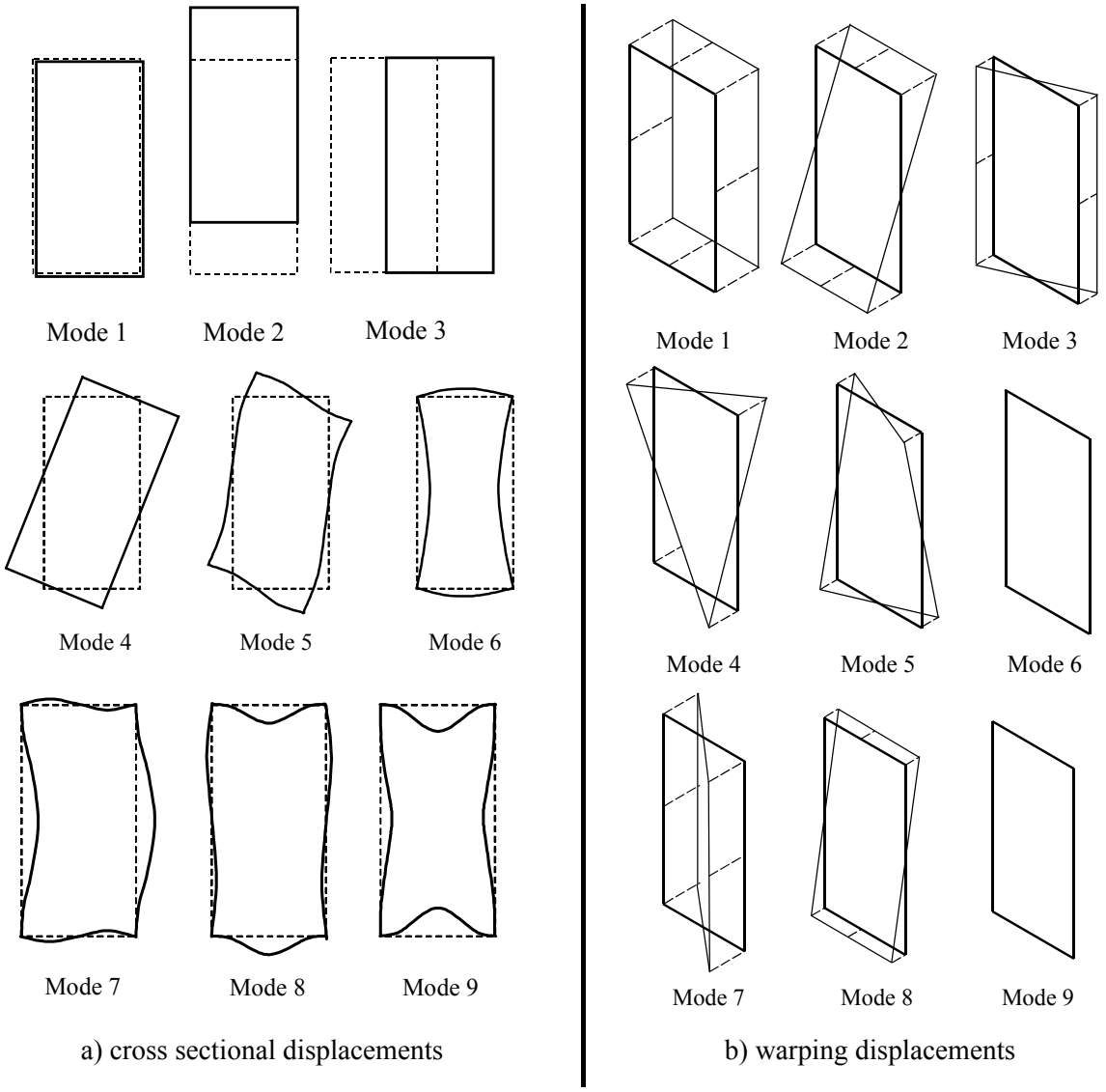

a) cross sectional displacements b) warping displacements

Fig. 5.29– Unit modal displacement shapes for the classical GBT formulation

So, establishing the initial modes using a similar scheme of the previous example, the modes generated by the extended GBT theory, after the orthogonalization, can be grouped in the following sets:

i) Modes 17 to 20 deal mainly with transverse extension of the plates.

ii) Modes 12 and 14 to 16 are associated with the transverse bending of the plates, and will take the most relevant roles in the local plate buckling range.

iii) Among the distortional modes and with the exception of those related to the plates' transverse extension, mode 13 is the only one that presents global rotations of the cross section plates, provoking displacements of the main nodes along the cross section plane.

iv) Modes 5 and 11 are the torsional modes, whose combination can produce the Bredt's torsional mode, as referred above.

v) Modes 4 and 6 to 10 are the so-called shear-lag modes, here related to bending (modes 6, 7, 9 and 10) or axial elongation (modes 4 and 9). It is expectable that a more refined cross section discretization renders shear-lag modes associated with torsion too.

vi) Mode 1 refers to the traditional axial elongation and modes 2 and 3 are the traditional major and minor axis bendings.

5.7.2. The compressed column

5.7.2.1 The buckling behaviour

Using the coordinate functions presented in the expressions (3.24) for mode 1 and (3.37 a-e) for the remaining modes, applying the stability procedures presented in Chapter 3 and adopting the complete expression for the TPE, accounting for expressions (5.8), (5.11), (5.13) and (5.15) in the calculus of the internal strain energy, the column shown in Fig. 5.32, submitted to an uniform compressive force at $x=L$, was analysed, and the respective critical loads are presented in Fig. 5.33, together with the corresponding modal participation coefficients in Fig. 5.34. These figures clearly highlight a local plate buckling zone (for smaller lengths, where modes 4, 12 and 15 control the critical state) and a flexural global buckling zone (for longer columns, where modes 3, 6 and 9 govern buckling). Additionally, for smaller lengths, the discretization (number of adopted polynomials per mode) strongly influences the results. For example, for a column length of *250* mm, the use of 1 to 4 polynomials per mode leads to critical loads of *217.3* kN, *48.7*

kN, *37.6* kN, and *35.4* kN, respectively, 4 polynomials per mode being required to ensure convergence.

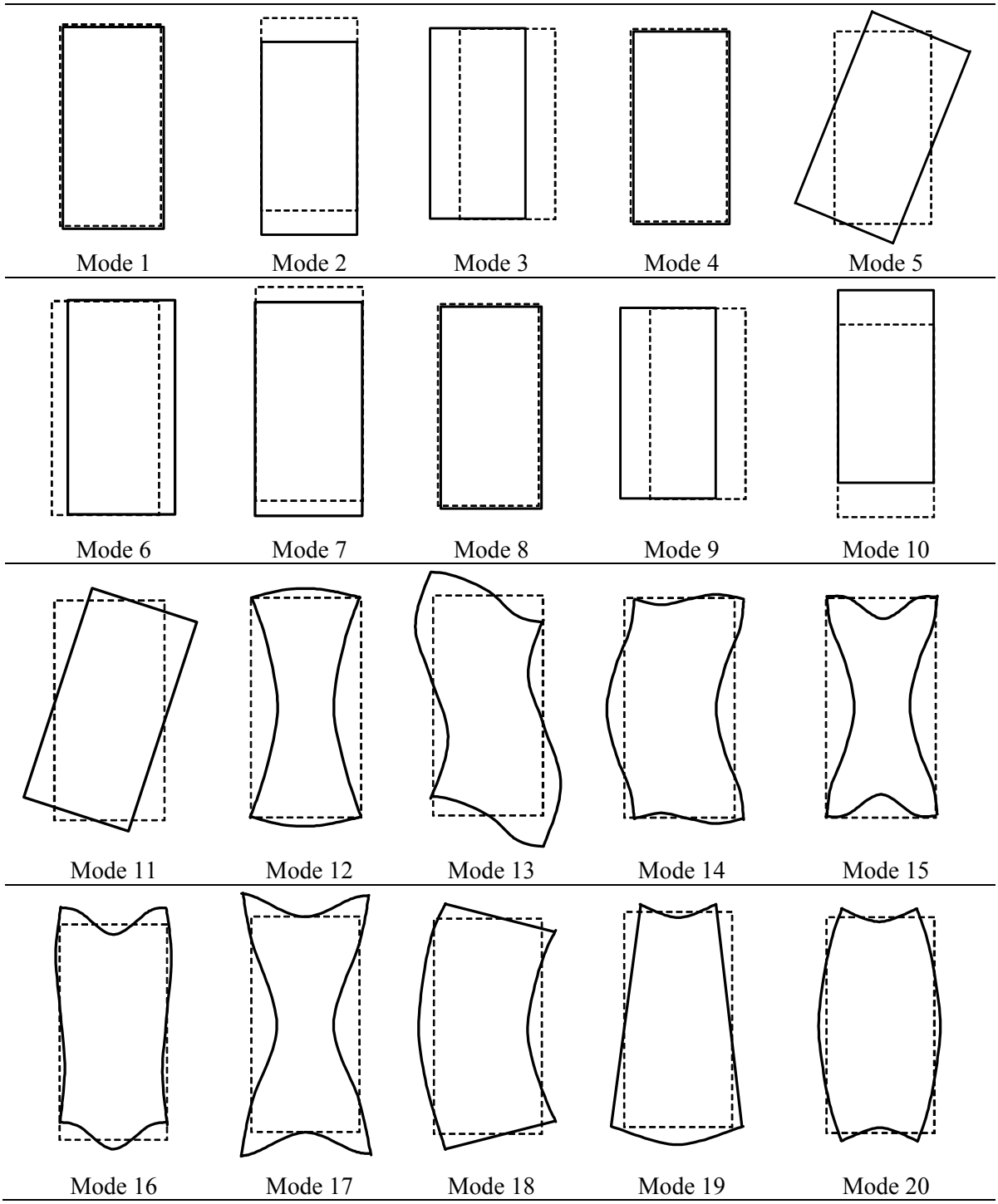

Fig. 5.30 - Unit modal displacements in the cross section plane

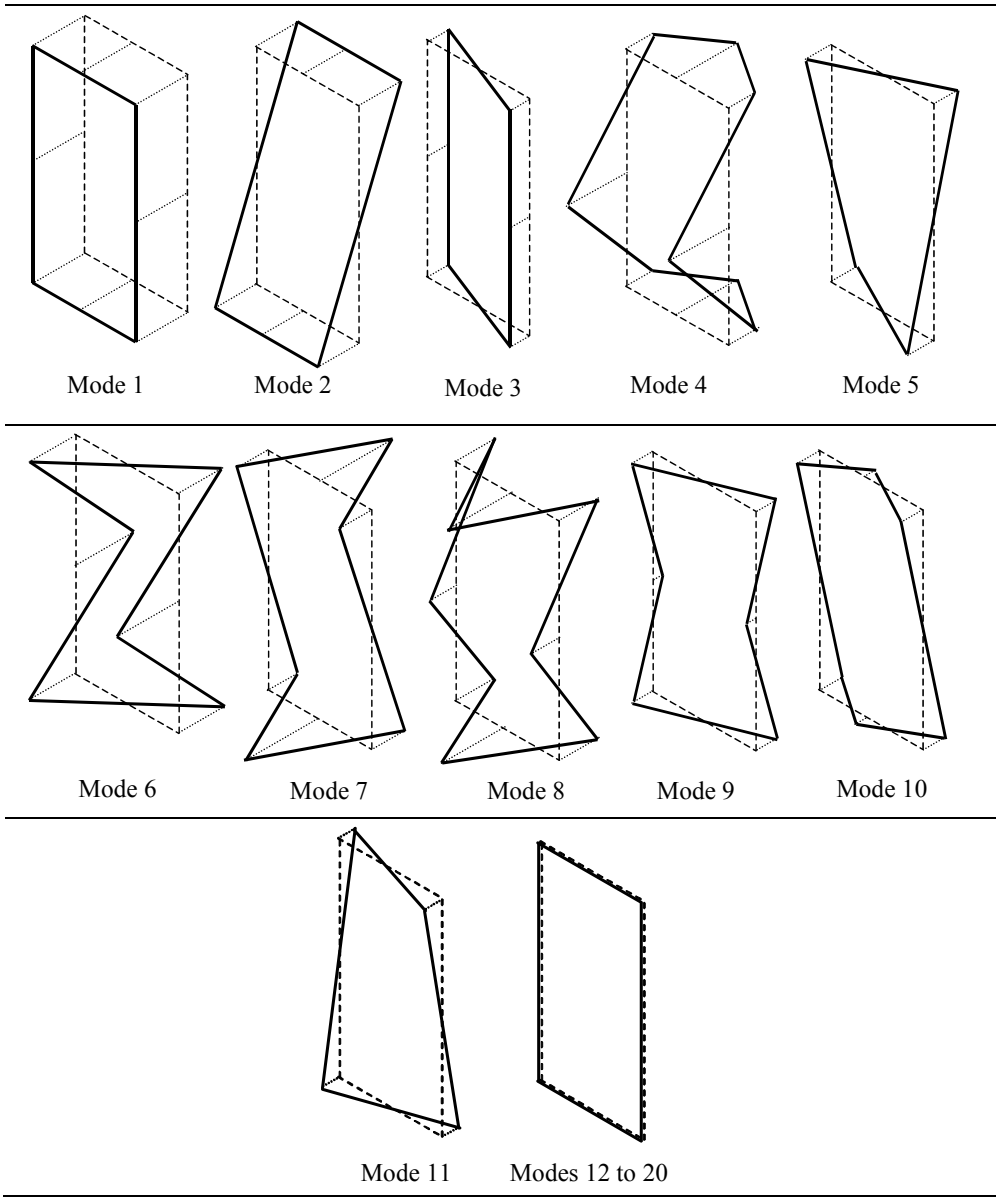

Fig. 5.31 - Unit modal warping displacements

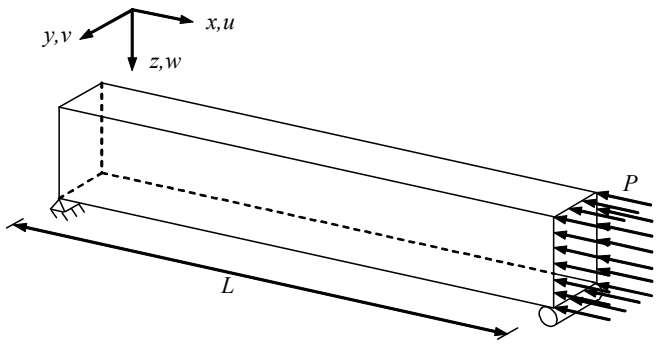

Fig. 5.32 - The compressed column

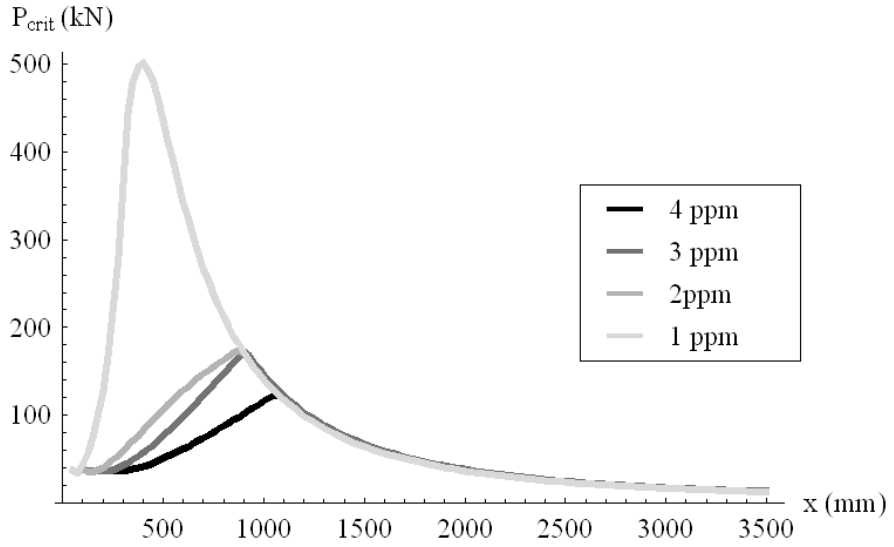

Fig. 5.33 – The critical loads for the compressed RHS column: the decrease of the critical loads with the increase of the number of the considered polynomials per mode of deformation 2 and higher

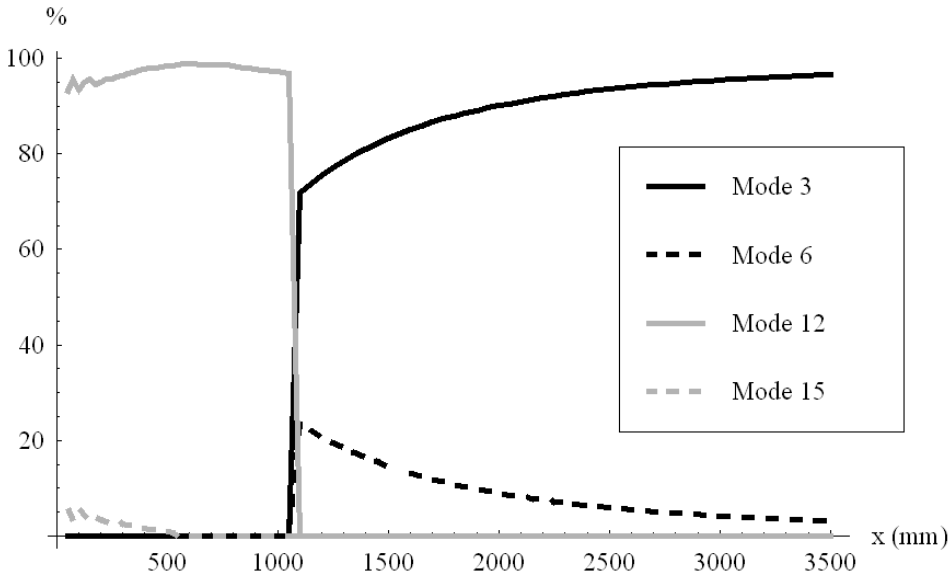

Fig. 5.34 – Modal participation coefficients (4 coordinate functions per mode)

5.7.2.2 The post-buckling behaviour in the local plate buckling range

Having identified the active coordinates and calculated the critical loads, the post-buckling behaviour is determined by searching alternative equilibrium paths in the

neighbourhood of the critical point through the scheme presented in Chapter 3. In the following the post-buckling equilibrium paths are determined for a column length of *250* mm. Fig. 5.35 presents the load-displacement curve for the longitudinal displacement of node 2, both for the classical (CF) and the extended (EF) GBT formulations. Examination of Fig. 5.35 reveals a coincidence between the CF and the EF along the fundamental and the post-critical paths. This coincidence was to be expected, because in compressed columns the additional modes of deformation do not have a great influence on the load-axial shortening relation. In contrast, for displacements in the cross-sectional plane, this exact coincidence prior to bifurcation does not occur, as can be seen in Fig. 5.36. As noted before, the presence of the additional modes in the extended formulation allows the modelling of the bulging effect (Graves Smith & Sridharan, 1980), which consists of very small but non-zero transversal displacements prior to bifurcation, a feature not possible with the classical formulation. Noting that the same coordinate functions were used for corresponding modes of deformation, the critical load for a column length of $L = 250$ mm decreases from *38.0* kN for the classical formulation to *35.4* kN for the extended formulation, a decrease of 7%.

In the post-buckling range, Fig. 5.36 shows that the analysis based on the classical formulation underestimates the member stiffness compared to the EF. Also, despite the bulging effect that occurs prior to bifurcation, the critical state of the EF can be regarded as symmetrical and stable. Fig. 5.37 presents the column's deformed configuration for $P = 2.91 \times P_{cr}$ (the displacements are exaggerated for visual clarity) showing the initial position of the end section (black line rectangle on the right). This figure was drawn through the graphic facilities of the software MATHEMATICA and it is seen that the branch associated with positive values of ${}^{31}q$ is associated with a convex bulge at $x = \frac{3}{8}L$, while a concave bulge at the same cross section occurs for negative values of the control coordinate ${}^{31}q$, ${}^{31}q$ being the sliding coordinate associated with mode 12 and coordinate

function (3.37 d). For this load level, the corners experience negligible displacements in the cross section plane.

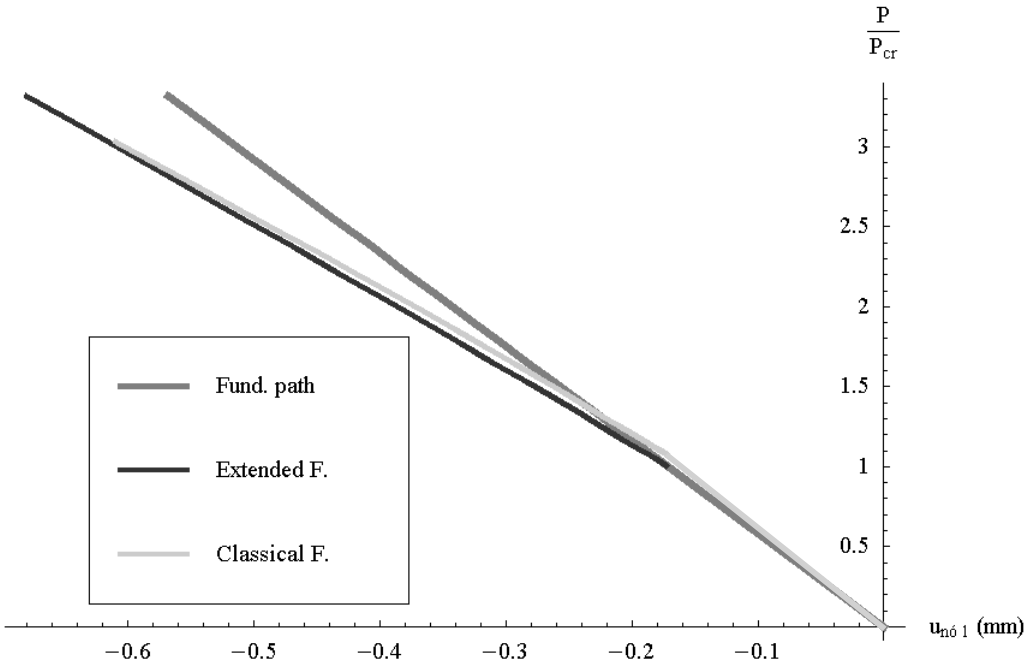

Fig. 5.35 – Compressive load – axial displacement curves for the traditional and for the extended formulations

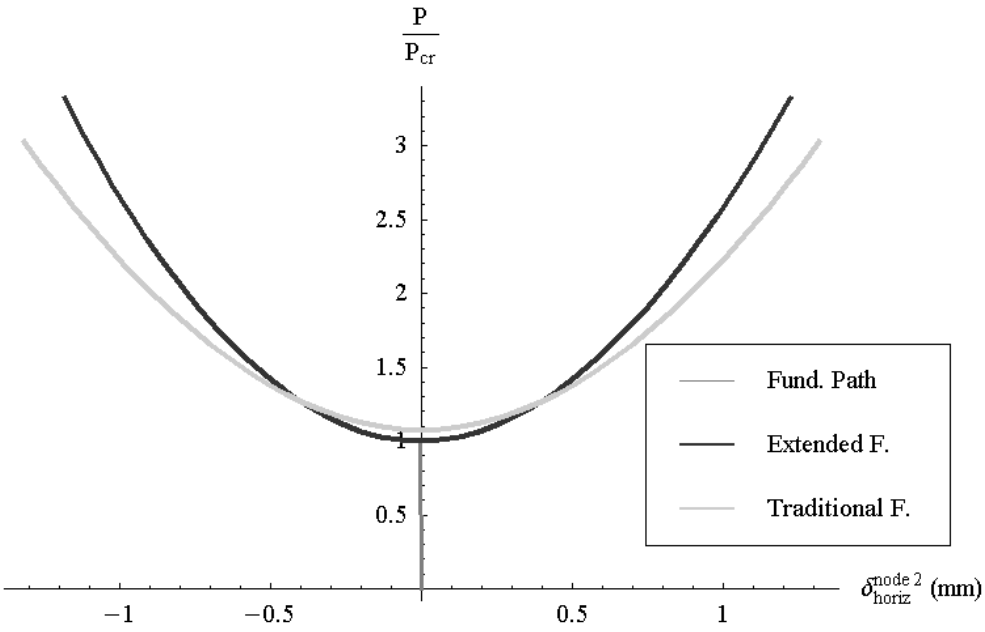

Fig. 5.36 – Compressive load – transversal displacement curves for the

traditional and for the extended formulations at node 2 and $x = \frac{3}{8}L$

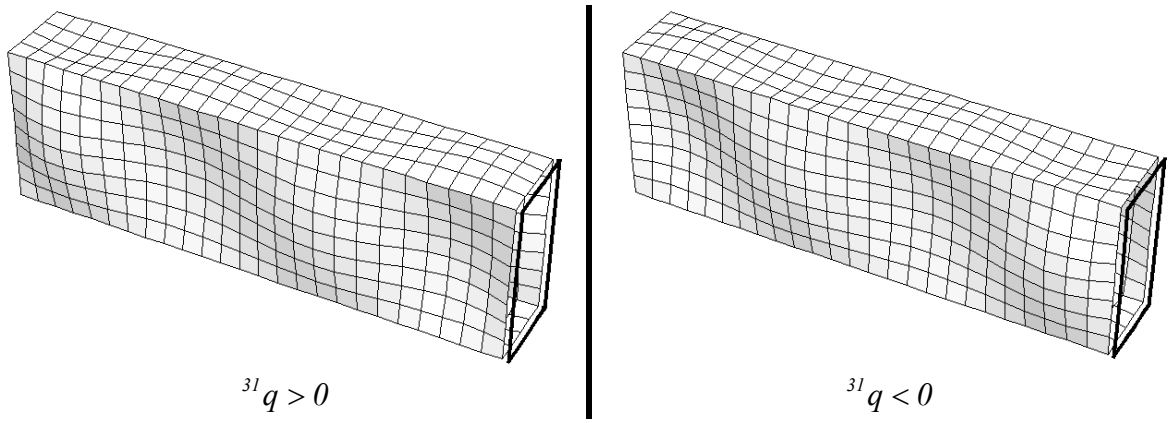

$^{31}q > 0$ $^{31}q < 0$

Fig. 5.37 - Member's deformed configuration for $P = 2.91 \times P_{CR}$ (the displacements are amplified by a factor 5)

Figures 5.38, 5.39 and 5.40 illustrate the stress diagrams along the longitudinal nodal lines 1, 2 and 4 for $^{31}\delta > 0$. The membrane shear stresses and membrane normal stresses in the transversal direction have much smaller magnitude than the longitudinal normal stresses, the shear stresses being quite small in the present case. It is noted that, despite of being small, the membrane shear and transversal stresses are determined by the present scheme. Figures 5.41 and 5.42 present normal stress diagrams along the cross section at $x = 0$ and $x = \frac{3}{8}L$. Fig. 5.41 highlights the significant relaxation of the membrane longitudinal stresses in the extreme cross section between nodes 1 and 3, due to the buckling of the corresponding plate. Figures 5.43 and 5.44 present the transverse normal membrane stresses at $x = 0$ and $x = \frac{3}{8}L$, mainly due to the Poisson effect, and Figures 5.45 and 5.46 illustrate the discontinuity that appears in the τ_{xs}^{M} -plots along a cross section due to the use of non-smooth functions in the inner nodes warping modes.

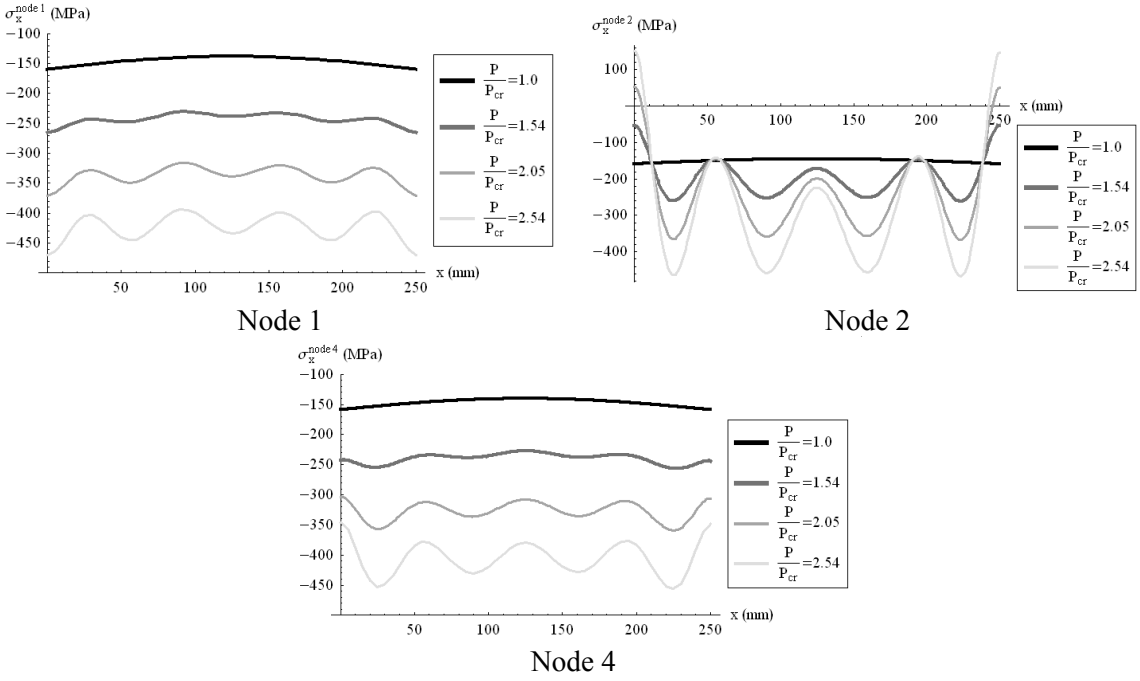

Node 1 Node 2

Node 4

Fig. 5.38 – Stresses σ_x^M along nodal lines 1, 2 and 4

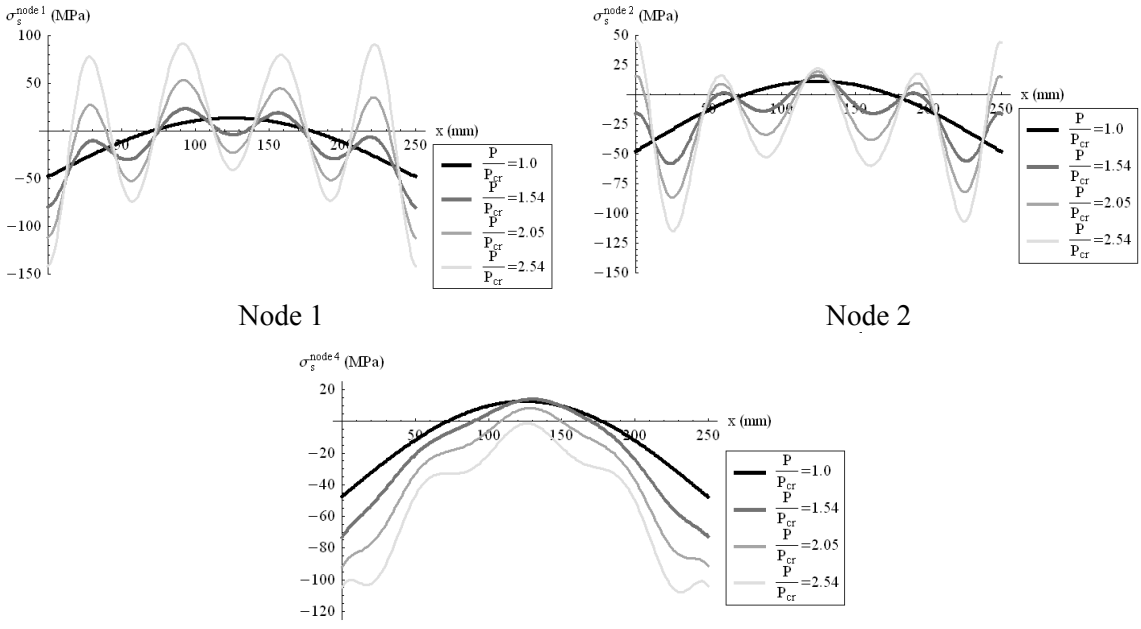

Node 1 Node 2

Node 4

Fig. 5.39 – Stresses σ_s^M along nodal lines 1, 2 and 4

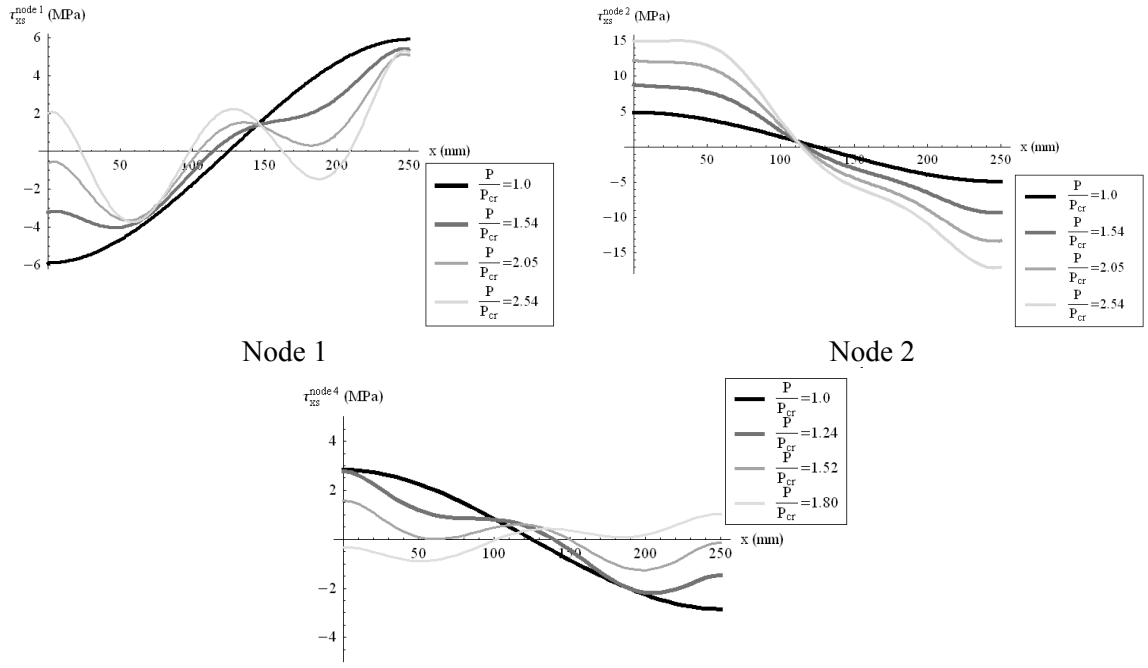

Fig. 5.40 – Stresses τ_{xs}^{M} along nodal lines 1, 2 and 4

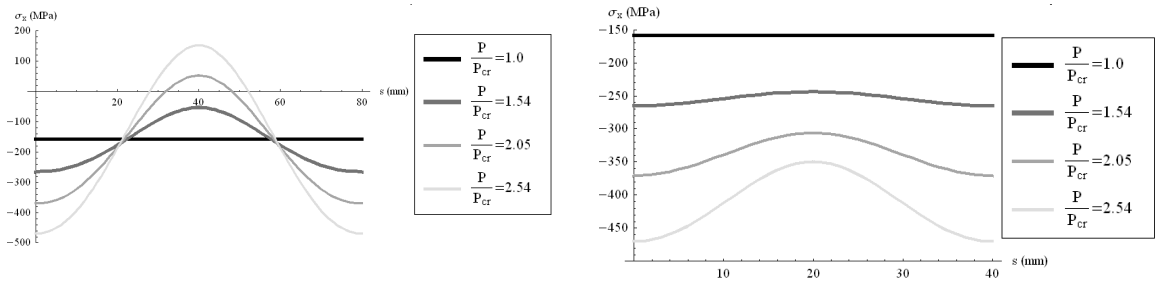

Fig. 5.41 – Stresses σ_x^M between nodes 1-2-3 and 3-4-5 for $x = 0$

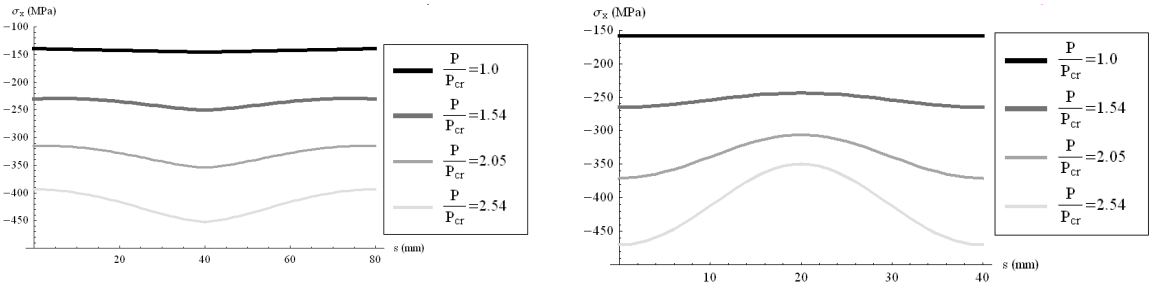

Fig. 5.42 – Stresses σ_x^M between nodes 1-2-3 and 3-4-5 for $x = \frac{3}{8}L$

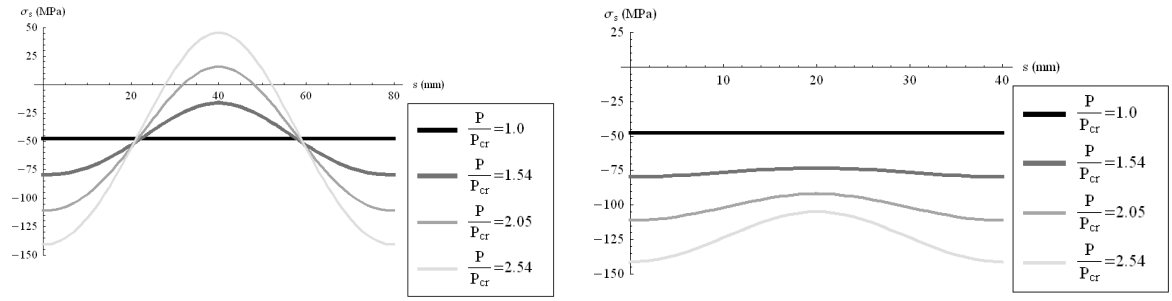

Fig. 5.43 – Stresses σ_s^M between nodes 1-2-3 and 3-4-5 for $x = 0$

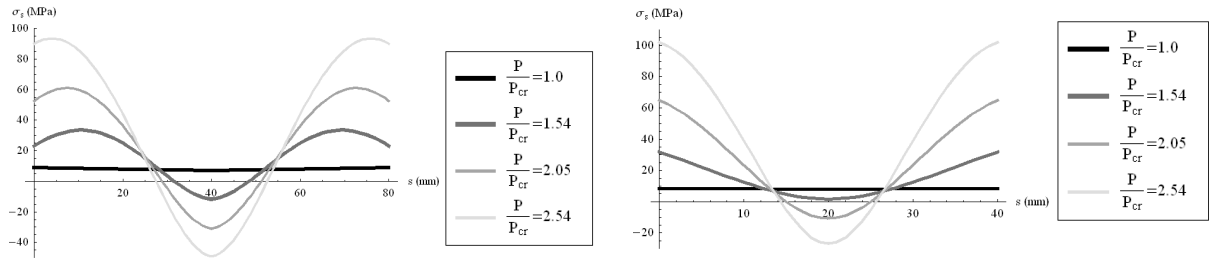

Fig. 5.44 – Stresses σ_s^M between nodes 1-2-3 and 3-4-5 for $x = \frac{3}{8}L$

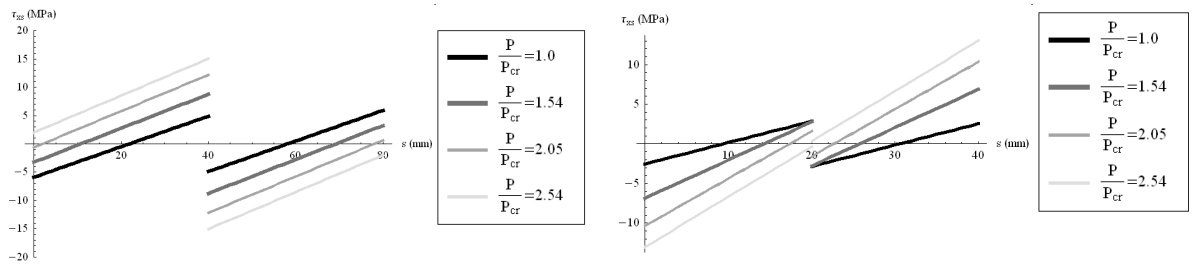

Fig. 5.45 – Stresses τ_{xs}^M between nodes 1-2-3 and 3-4-5 for $x = 0$

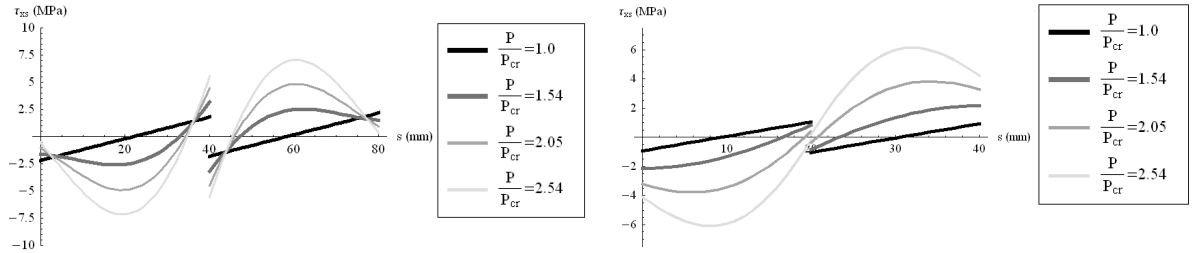

Fig. 5.46 – Stresses τ_{xs}^M between nodes 1-2-3 and 3-4-5 for $x = \frac{3}{8}L$

5.7.2.3 Comparison with a FEM analysis

The above example was analysed by the FEM (Gervásio, Simões da Silva & Simão

2004), using the commercial FEM package LUSAS (FEA 2002). The adopted finite element is an isoparametric shell element with 4 nodes (type QST4), and the adopted mesh is regular, keeping the relation between both sides of the element close to one. The adopted boundary conditions model an element which, at its extreme cross sections, the displacement of any point along the cross section plane is not allowed. To avoid numerical instability a point at the member's mid-span was fixed along the longitudinal direction. The applied loading consists of a uniform distributed load, applied along the middle line of the cross section, whose value is equal to the plate's thickness. This loading was applied at both extreme cross sections of the member and generates a unitary stress state, so the resulting load parameters correspond to the average acting stress. Several member lengths were adopted, being their values show in Table 5.1. For each case, the eigenvalues and the eigenvectors were computed, the critical loads being presented in Table 5.2 and the corresponding buckling modes, for the various analyzed lengths, being presented in Figures 5.47 to 5.50.

L	Model 1	Model 2	Model 3	Model 4	Model 5	Model 6	Model 7	Model 8
(mm)	200	250	375	500	750	1000	2000	3000

Table 5.1 – Adopted lengths for the parametric study

Mode	Critical loads (kN)							
	L=200	L=250	L=375	L=500	L=750	L=1000	L=2000	L=3000
1	36.54	36.90	37.17	37.24	37.20	37.42	37.42	17.19
2	40.29	38.72	37.50	37.25	37.27	37.45	37.45	37.23
3	42.06	40.92	39.48	38.86	38.16	38.11	38.11	37.23
4	43.29	41.74	42.04	39.52	38.38	38.38	38.38	37.73
5	44.35	43.37	42.31	41.21	39.64	38.75	38.75	37.74
6	50.16	47.88	42.54	42.14	39.70	39.47	39.47	37.79

Table 5.2 – Critical loads

The post-buckling equilibrium paths were determined by adopting an initial imperfection proportional to the first instability mode, and are represented in Figures 5.51 and 5.52, showing, for each analysed case, the longitudinal displacements of node 6 at the edge cross section, and the horizontal displacement of node 6 at the cross section where the

maximum horizontal displacement is reached, for each member's length.

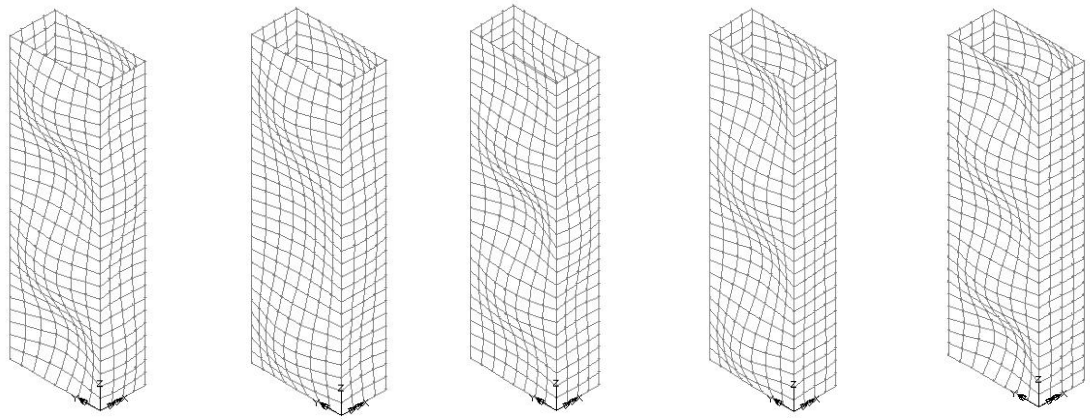

a) 1st mode b) 2nd mode c) 3rd mode d) 4th mode e) 5th mode

Fig. 5.47 – Instability modes for *L=250* mm

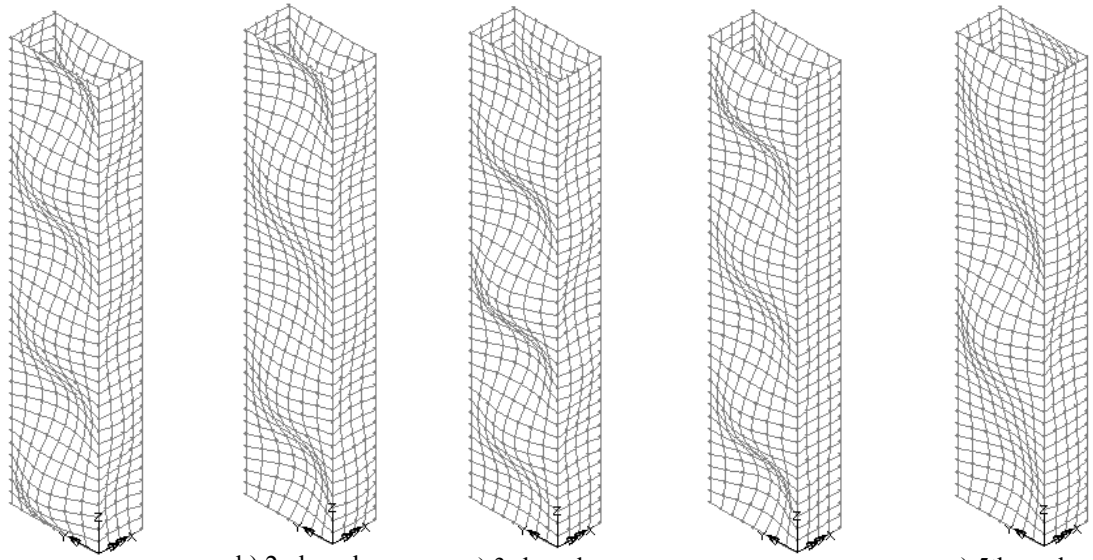

a) 1st mode b) 2nd mode c) 3rd mode d) 4th mode e) 5th mode

Fig. 5.48 – Instability modes for *L=375*mm

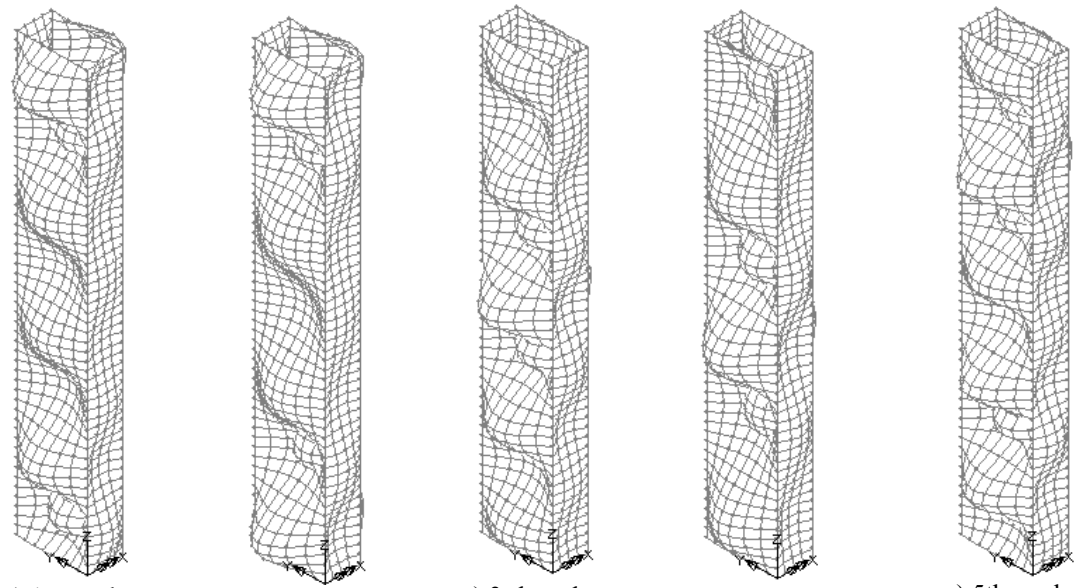

a) 1st mode b) 2nd mode c) 3rd mode d) 4th mode e) 5th mode

Fig. 5.49 – Instability modes for *L=500* mm

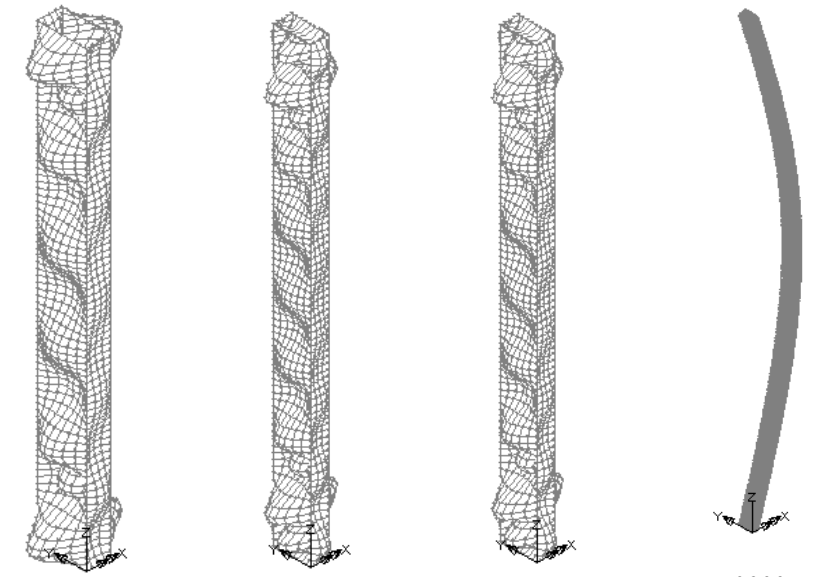

L=750 mm *L=1000* mm *L=2000* mm *L=3000* mm

Fig. 5.50 – Instability modes for the referred lengths

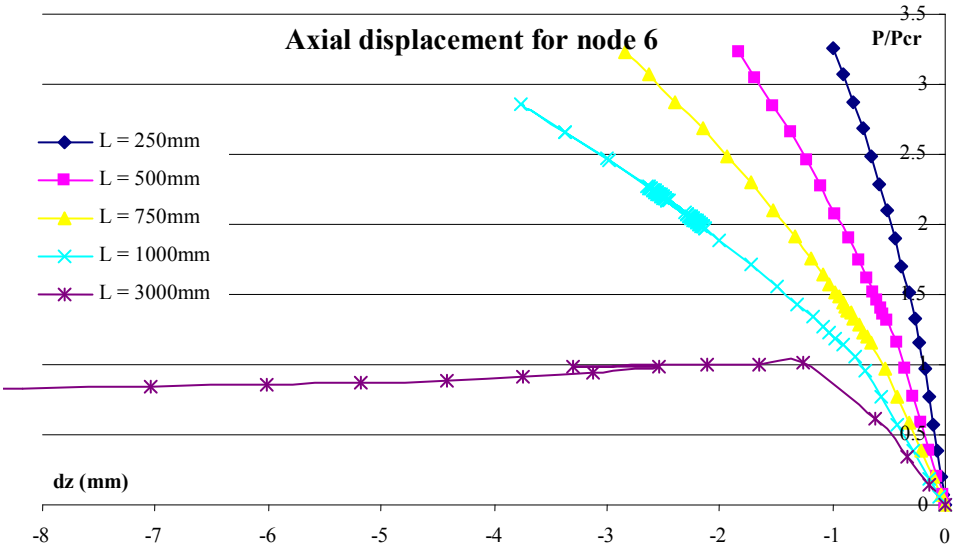

Fig. 5.51 – Post-buckling equilibrium paths for node 6 at an edge cross section

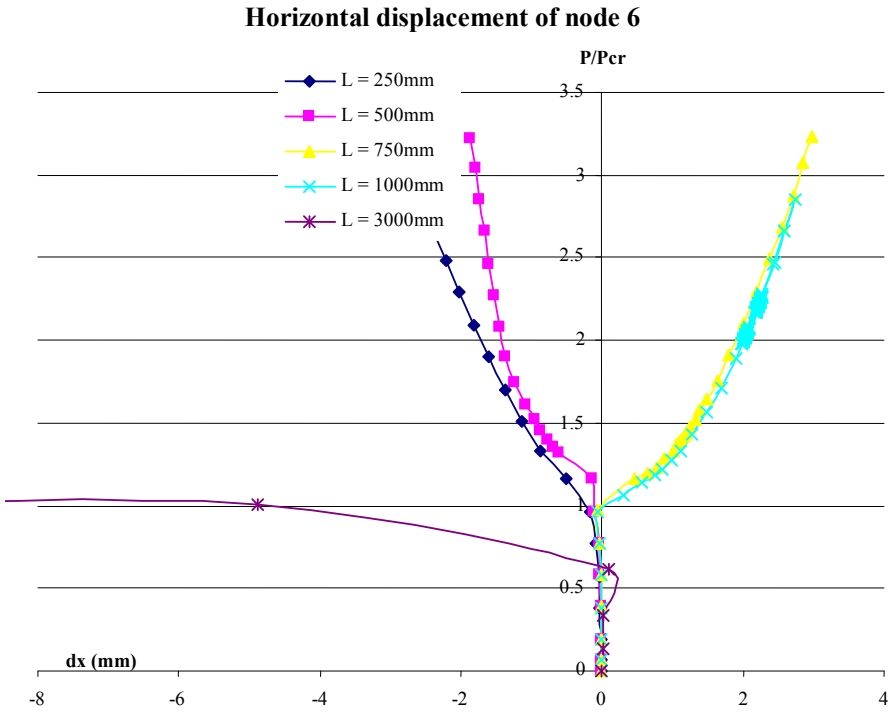

Fig. 5.52 - Post-buckling equilibrium paths for node 6 at an edge cross section

Comparing with the GBT analysis, Table 5.3 presents the critical loads for the

analysed RHS column, highlighting the better agreement between the FEM and the extended GBT analyses, while the classical GBT analysis increases the values of the critical loads about 10%. For the length's range between *375* mm and *2000* mm the GBT analysis presents higher critical loads, because the number of adopted polynomials is severely limited by the available computer resources – as the computer resources become more capable, allowing the adoption of a higher number of polynomials per mode of deformation, looking at Table 5.3 it becomes evident that the GBT method will be able to achieve as good results as the FEM analysis, enabling also additional information on the member's behaviour.

L (mm)	200	250	375	500	750	1000	2000	3000
Lusas	36.54	36.9	37.17	37.24	37.2	37.42	37.42	17.19
GBT	35.62	35.43	39.27	49.93	80.53	115.71	37.88	16.91

Table 5.3 – Critical loads for the simply supported column – comparison between the FEM and GBT (until 4 polynomials per mode)

For the length *L=250* mm – for which the critical state is associated with the local buckling of the wider cross section's plates with 4 half-waves – the post-buckling equilibrium paths were found for both analyses. Fig. 5.53 shows the agreement between both analyses – MEF e GBT – for the horizontal displacement of node 2 at $x = \frac{3}{8} L = 93.75$ mm, noting that the GBT analysis is applied to the perfect member while the FEM analysis applies to an imperfect column, GBT considers all non-linear terms of the ISE and uses in this example only the 1st to the 4th polynomials as coordinate functions due to computer limitations. Due to these factors, the GBT analysis provides more rigid results but, despite of the referred differences and limitations, has still a satisfying agreement with the FEM analysis. About the normal stresses diagram shown in Fig. 5.53b), the agreement is total in the neighbourhood of the supports, but this agreement decreases in the middle span zone, due to the existence of imperfections in he FEM model and to the limited number of adopted polynomials in the GBT analysis.

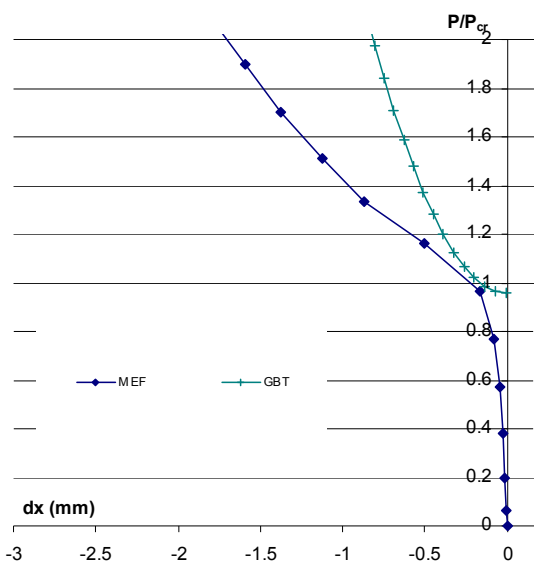

a) horizontal displacement for node 2

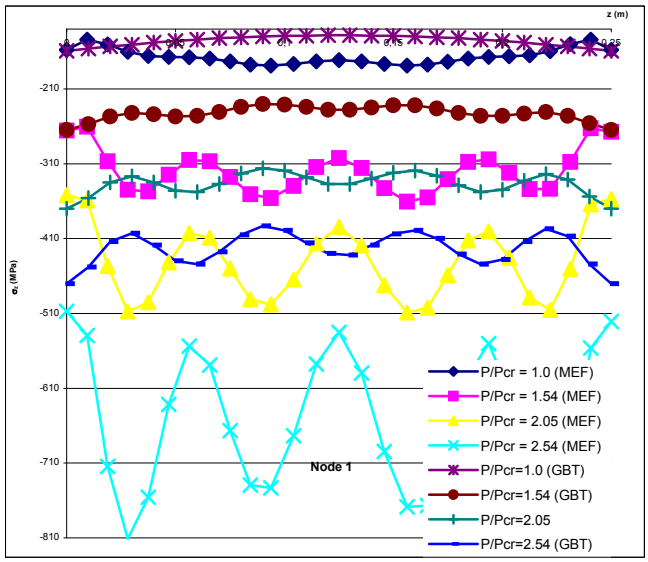

b) Longitudinal membrane stresses for node 1 along the member's length

Fig. 5.53 – Comparison between GBT and FEM analyses

5.7.3 The critical behaviour of the rectangular hollow section member under uniform major axis bending moment

The RHS prismatic member is now submitted to a uniform major axis bending moment, as shown in Fig. 5.54. Since it is assumed that the beam is simply supported and the edge sections are longitudinally restrained, the axial elongation mode was removed from the analysis and for modes 3 and higher the coordinate functions of expression (3.37) were assumed. For mode 2, in order to generate an uniform major axis bending moment, functions (3.38) were adopted. The load is introduced as a bending normal stress patterns in both edges of the member, and the respective critical loads are presented in Figures 5.55 and 5.56. Fig. 5.55 highlights the very good agreement between GBT and CUFSM analyses, the extended GBT theory provoking a small decrease of the critical load in comparison with the traditional Schardt's theory. Fig. 5.56 illustrates the influence of the number of adopted polynomials per mode of deformation in the critical load showing that a large number of polynomials is required in order to achieve a good convergence.

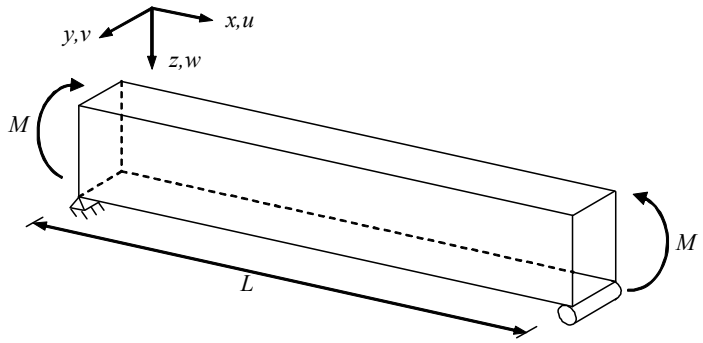

Fig. 5.54 - The beam under uniform major axis bending moment

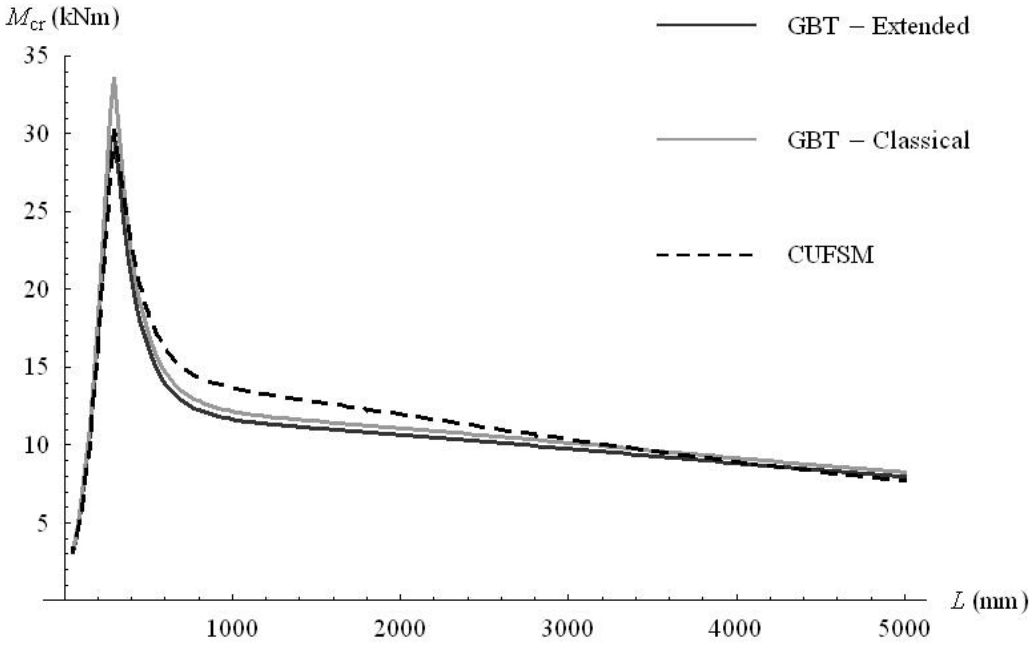

Fig. 5.55 – Critical major axis bending moments for the simply supported RHS beam: benchmark comparison between GBT – classical and extended formulations – and CUFSM analysis

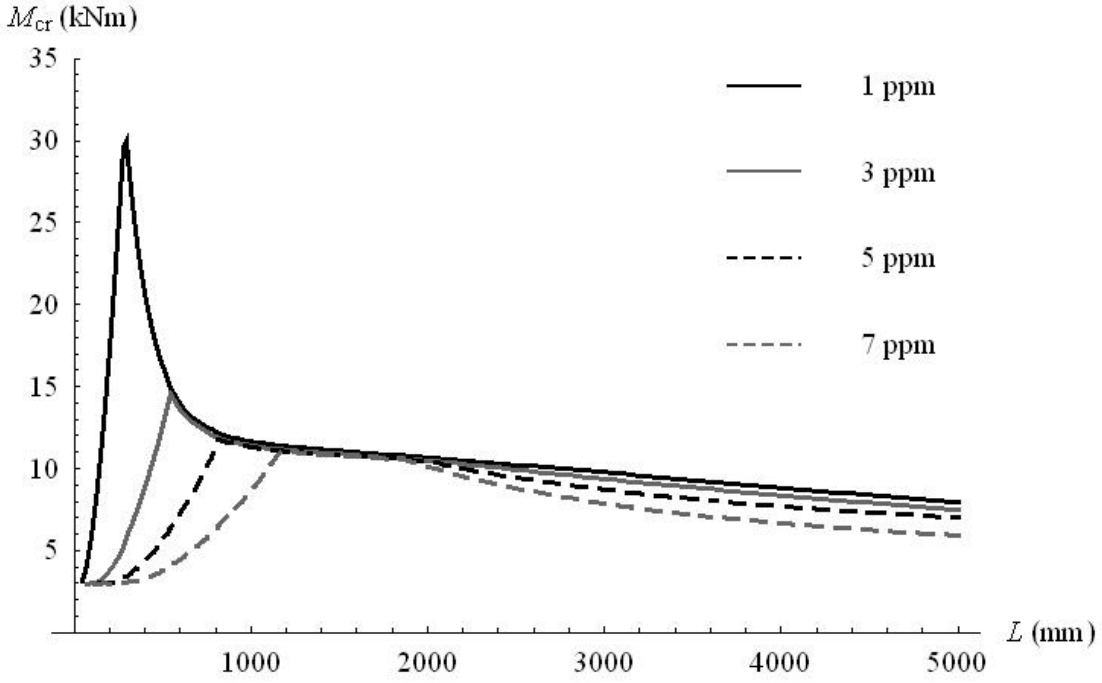

Fig. 5.56 – Critical major axis bending moments for the simply supported RHS beam: decrease of the critical major axis bending moment with the increase of the number of adopted polynomials per mode of deformation

5.8 – Benchmark example: the channel section member

5.8.1. Presentation and derivation of the modes of deformation

In the present paragraph the behaviour of a channel cross-section member, presented in Fig. 5.57, is analysed. The geometric properties were chosen in order to give the minimum critical load for the local mode range higher that the minimum critical load for the distortional lengths zone. Its dimensions are: b_w=*80*mm, b_f=*60*mm, b_{lips}=*12*mm and *t=1.35*mm, and the member is made of steel ($E = 210$ GPa and $\mu = 0.3$). A GBT analysis based on the concepts presented in chapter 3, considering one inner node at the mid-height of the web, generates 20 modes of deformation, presented in Figures 5.58 and 5.59.

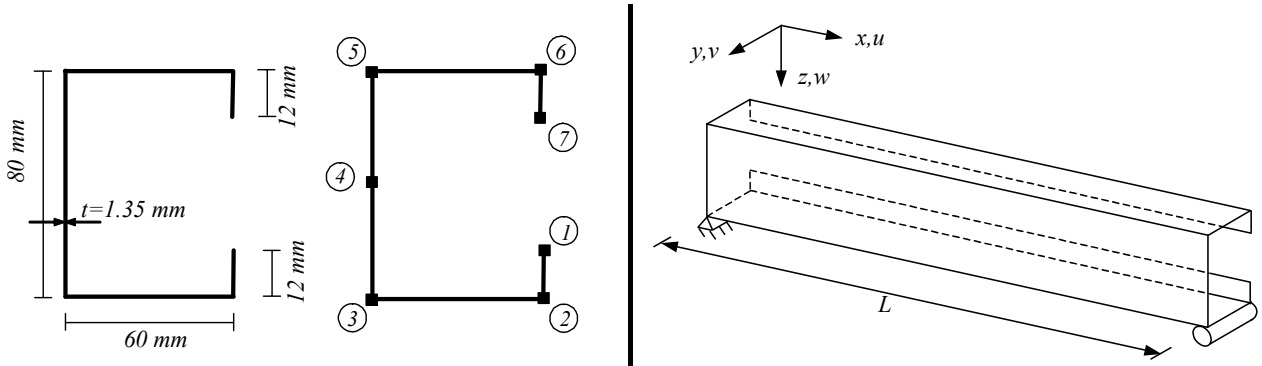

a) geometric properties and discretization b) member overview

Fig. 5.57 – The analysed cross-section and the adopted nodes

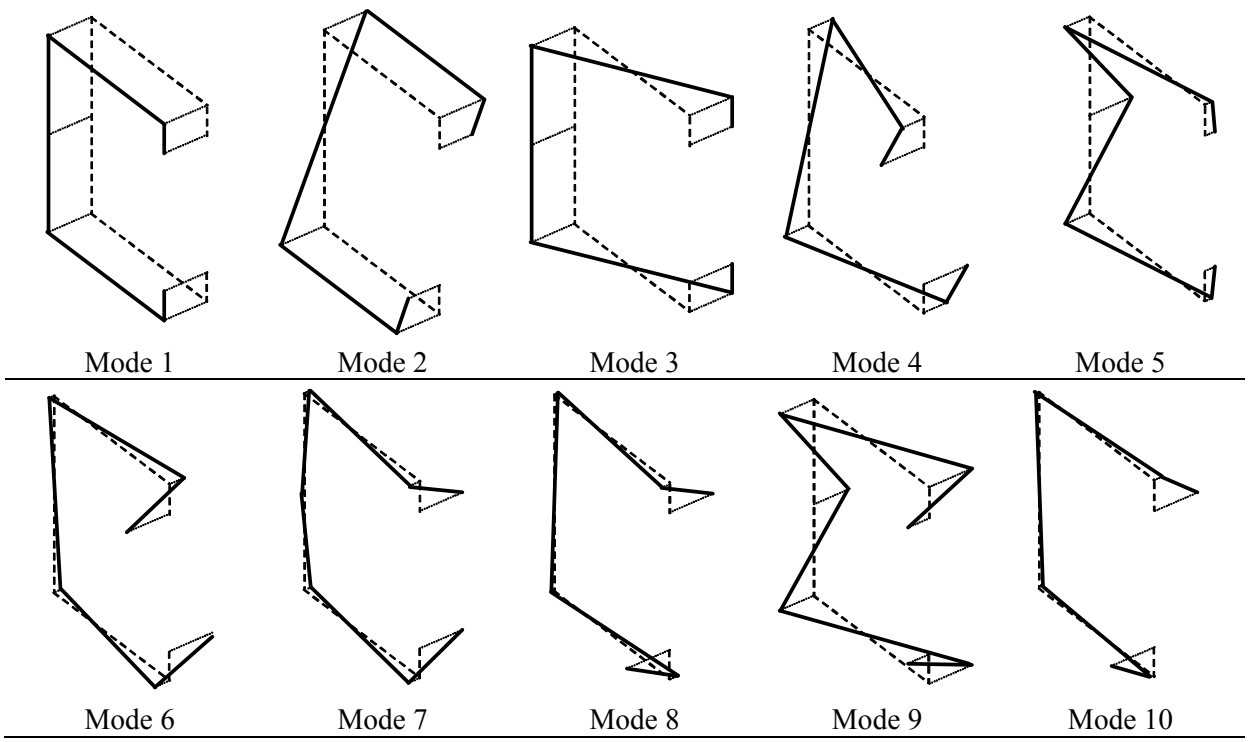

Fig. 5.58 - Unit modal warping displacements (modes 11 to 20 show no warping displacements)

5.8.2. The buckling behaviour for the compressed column

Fig. 5.60 presents the critical loads obtained from the extended GBT analysis and from the FSM program CUFSM for the channel section member under uniform compression presented in Fig. 5.57 b). For the GBT analysis the polynomial of expression

(3.37 a) was adopted for modes of deformation 2 and higher, and it is evident the very good agreement between both analyses. Improving the GBT analysis in terms of adding more polynomials per mode of deformation to the in the discretization procedure leads to the decrease of the critical loads shown in Fig. 5.61, together with the modal participation factors presented in Fig. 5.62.

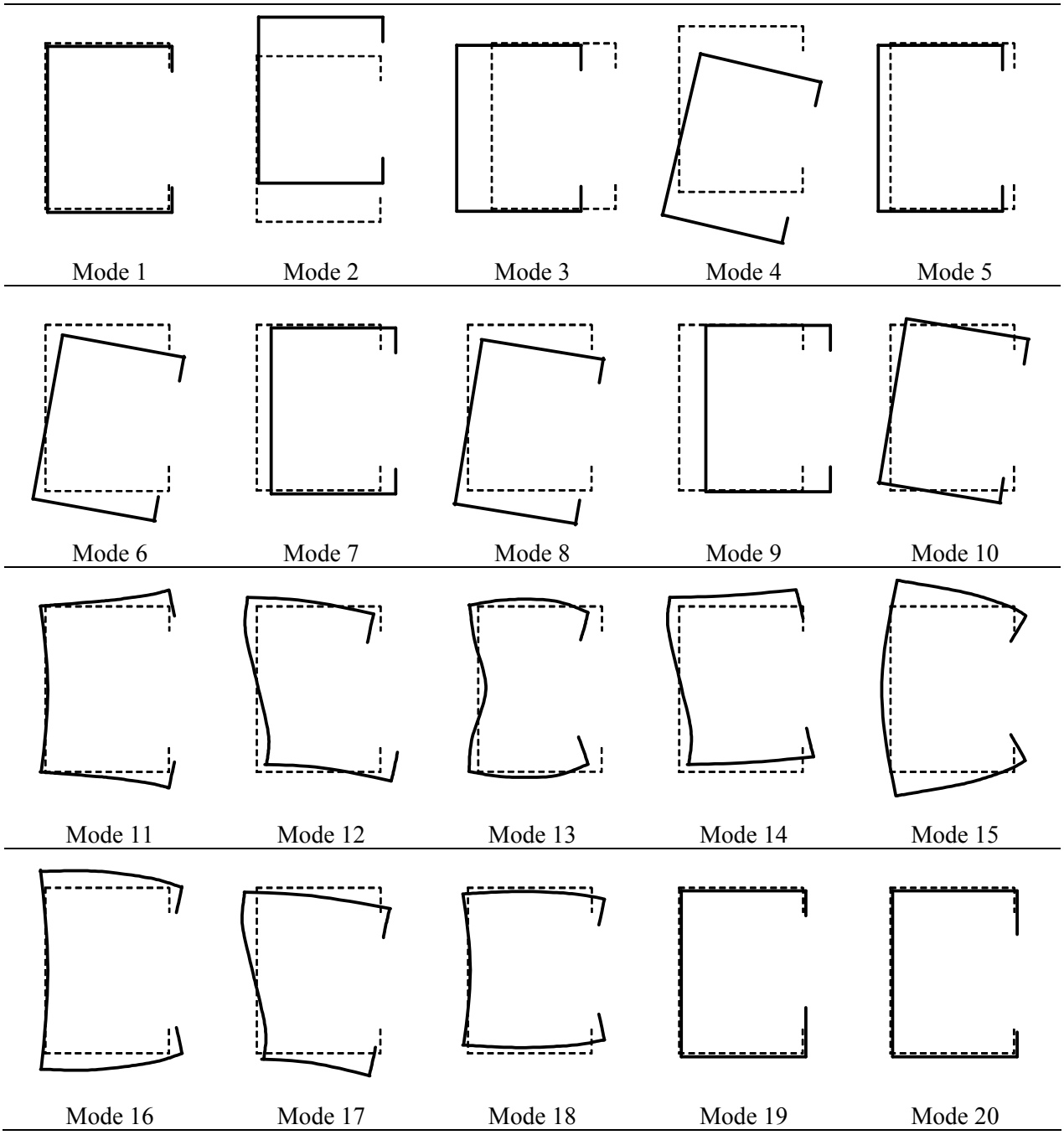

Fig. 5.59 - Unit modal displacements in the cross section plane

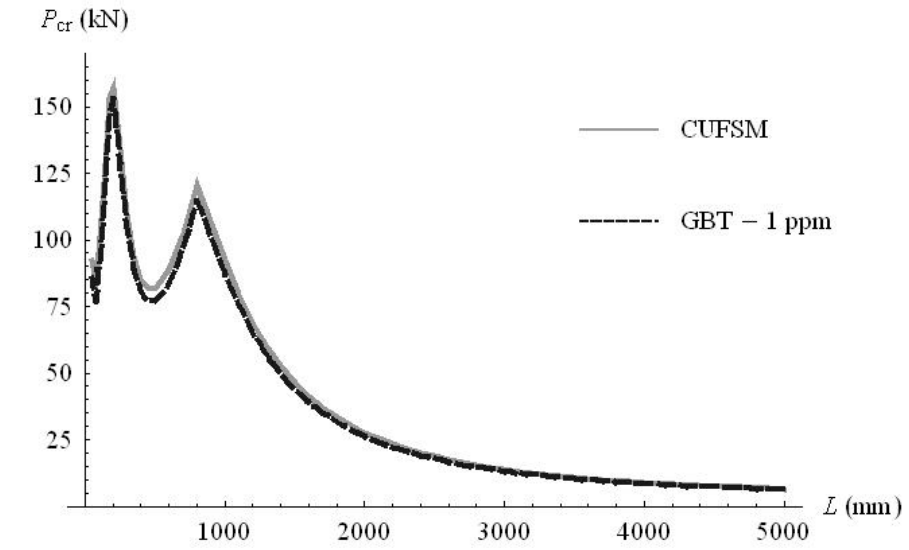

Fig. 5.60 – Buckling loads for the simply supported channel section column under a compressive force: benchmark comparison between GBT and CUFSM analysis

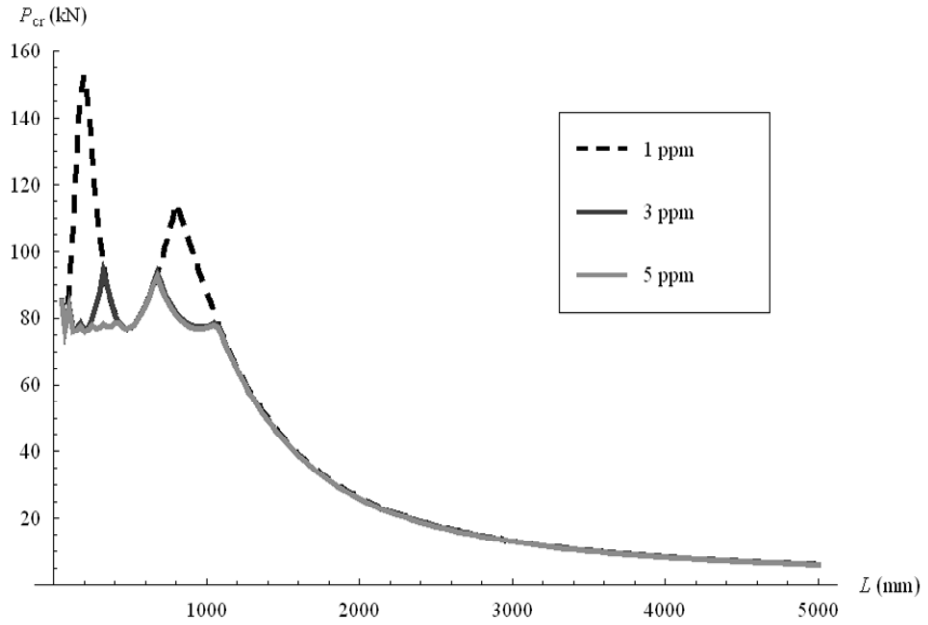

Fig. 5.61 – The critical loads for the simply supported channel column: the decrease of the critical loads with the increase of the number of adopted polynomials for modes 2 and higher

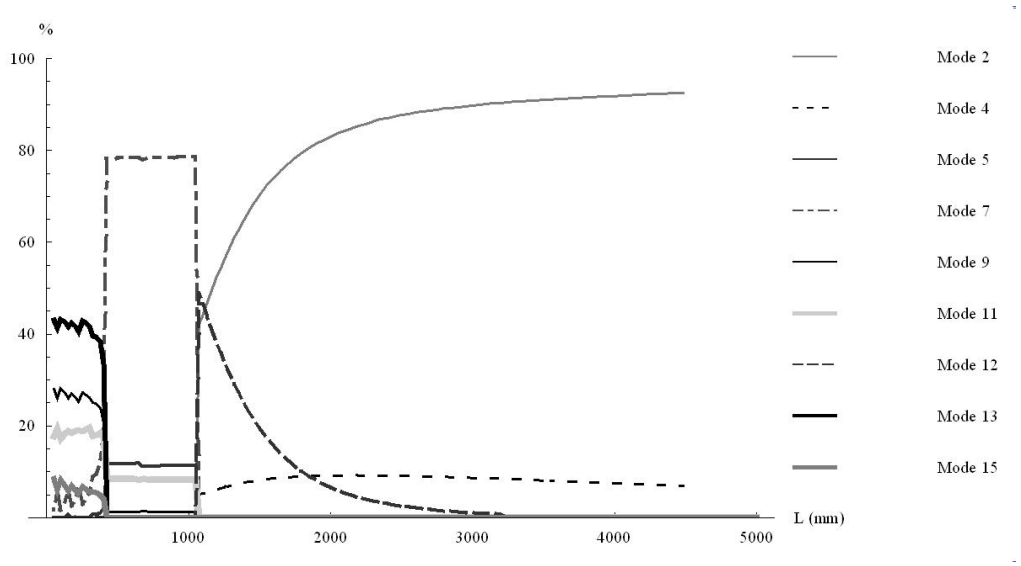

Fig. 5.62 – The participation of the modes of deformation in the critical state, for 5 polynomials per modal amplitude function

5.8.3. The post-buckling behaviour

5.8.3.1. Introduction

Having identified the critical loads and the active coordinates at bifurcation for the channel section column under analysis, the post-buckling equilibrium paths are determined here through the usual way by searching alternative equilibrium states outside the fundamental path, in the neighbourhood of the critical state associated with the lowest critical load, through the application of the appropriate numerical procedures previously described in Chapter 3. Here the post-buckling behaviour is analysed for two member lengths, 950 mm and 1100 mm. The first length fall in the symmetric distortional lengths range, the critical shape corresponding to two longitudinal half-waves, while the higher length falls in the flexural-asymmetrical range. For the two cases presented below only the first three polynomials of expression (3.37) are used for modes of deformation 2 to 20, due to computer limitations.

5.8.3.2. Post-buckling analysis for *L=950* mm

For *L=950* mm Table 5.4 resumes the main aspects of the critical state for this

length, showing the active generalized coordinates, together with their corresponding participation factors, mode of deformation and number of longitudinal half-waves. Due to the limitations of the available computer resources, only three polynomials per mode of deformation, for modes 2 to 20, were adopted in the post-buckling analysis, thus discretizing the member's total potential energy into 58 generalized coordinates – in fact, for the member's length considered, this number of generalized coordinates is sufficient for an accurate analysis. For this length and for the adopted discretization, the observed critical load is 76.862 kN and coordinate ^{26}q was chosen to control the post-buckling calculations.

Critical mode	Active coordinate	Modal participation (%)	Number of half-waves
5	^{24}a	11.67	2
7	^{26}a	78.45	2
9	^{28}a	1.29	2
11	^{23}a	8.43	2
	Sum:	99.84	

Table 5.4 – Most active modes and most active coordinates at the critical state

The post-buckling behaviour is defined by the evolution of displacements and stresses at any point of the member beyond the critical state. Fig. 5.63 shows the post-critical displacements of node 4, at the mid-height of the web, along the *y*-direction, and Fig. 5.64 illustrates the deformed shape of the channel column for $P=1.078\ P_{crit}$. Figures 5.65 and 5.66 show the longitudinal membrane normal stresses along plate 2, between nodes 2 and 3, and along the longitudinal line related to node 2. Fig. 5.67 shows the longitudinal normal membrane stresses along the column's flange, for $x=0.25\ L$. From observing these figures it is concluded that the post-buckling behaviour is symmetric and stable. For the positive branch of ^{26}q – see Figures 5.65, 5.66 and 5.67 – it is noted that in the first half of the member, for *x* between *0* and *475* mm, the membrane longitudinal normal stresses level increases in the neighbourhood of nodes 2 and 6, while for the other half of the member these stresses increase in the neighbourhood of the web. The same

phenomenon is observed in the negative branch of ^{26}q, obviously making the corresponding adjustments.

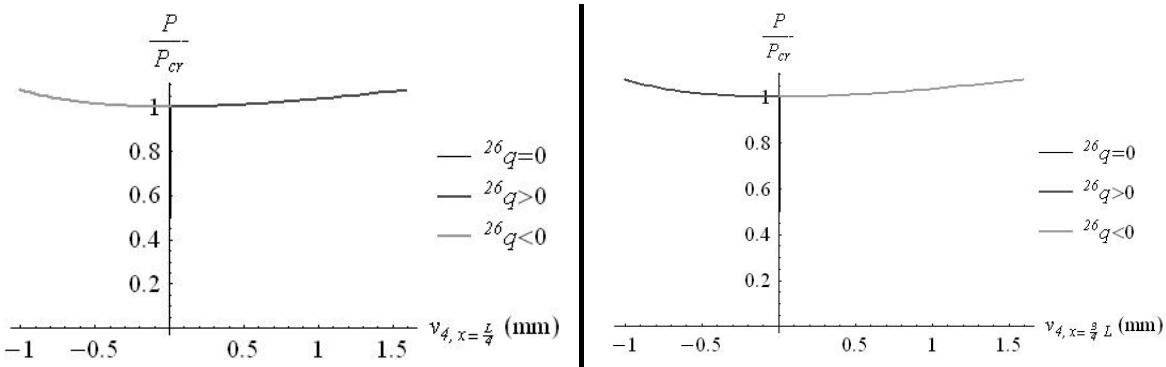

at $x=0.25\ L$ at $x=0.75\ L$

Fig. 5.63– The horizontal displacements v for node 4

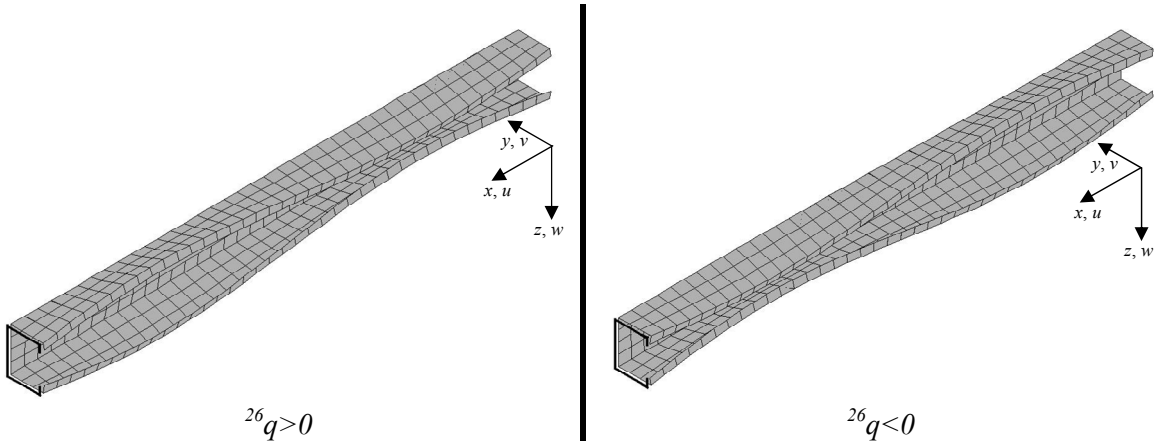

$^{26}q>0$ $^{26}q<0$

Fig. 5.64 – The column's deformed shape for $P = 1.078 \times P_{crit}$ (all displacements are amplified by factor 5)

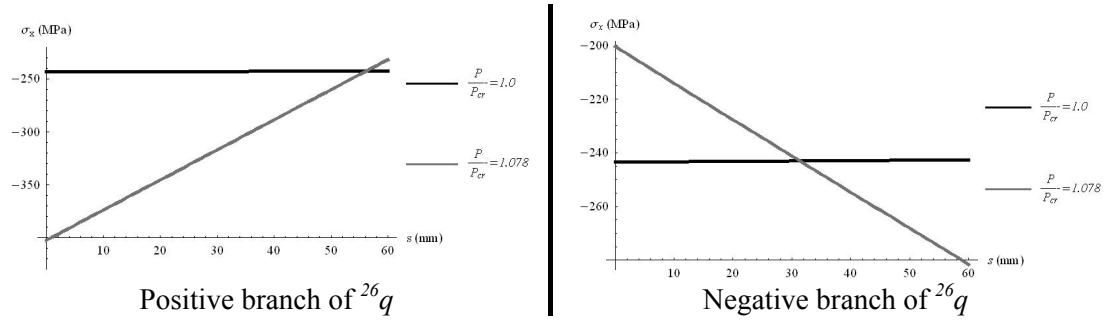

Positive branch of ^{26}q Negative branch of ^{26}q

Fig. 5.65 – The longitudinal normal membrane stresses at plate 2 (flange), between nodes 2 ($s=0$ mm) and 3 ($s=60\ mm$), for $x=0.25\ L$

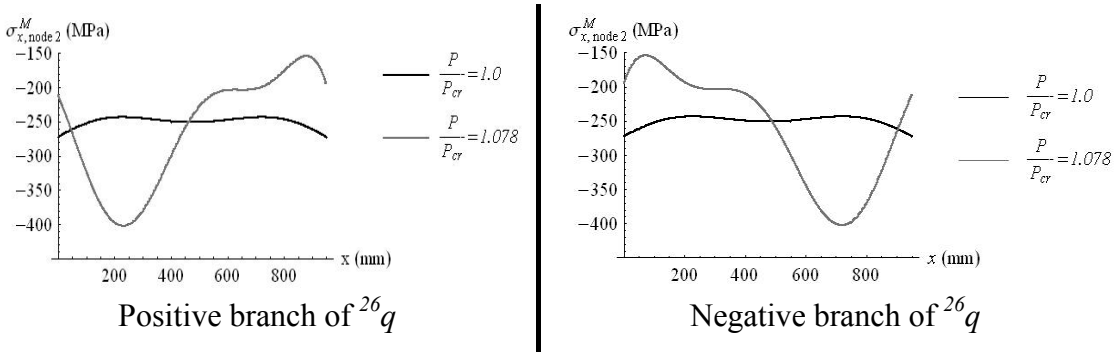

Fig. 5.66 – The longitudinal normal membrane stresses at node 2 along the member's length

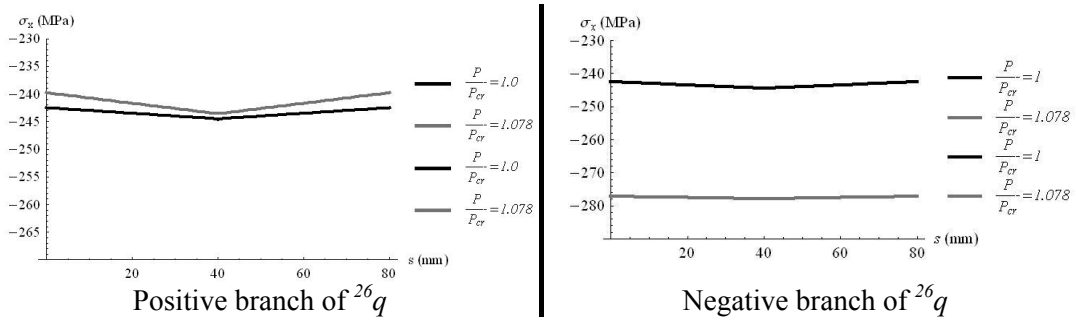

Fig. 5.67 – The longitudinal normal membrane stresses along the web, between nodes 3 ($x=0$ mm), 4 ($x=40$ mm) and 5 ($x=80$ mm), for $x=0.25\ L$

5.8.3.3. Post-buckling analysis for *L=1100* mm

The post-buckling in the flexural-distortional (asymmetric) buckling zone is investigated for a member's length of $L=1100$ mm, using the classical and the extended GBT theories, being adopted the lower bound approach given in expression (5.21) for the latter. For a discretization considering 3 polynomials per mode of deformation 2 and higher, each one given by expression (3.37), the obtained critical load is $P_{cr}=74.513$ kN for the extended GBT theory and $P_{cr}=77.771$ kN for the classical GBT formulation, the extended formulation carrying a decrease of *4.3*%. For the extended formulation, the control coordinate was chosen to be the one related to mode 12 and to the first coordinate polynomial, and the resulting post-buckling behaviour presents a curious shape, similar in both formulations: in fact, the post-buckling behaviour is unstable since, for the post-

buckling equilibrium path, concavity points downwards at the critical state for both formulations, i.e., the load level for both branches decreases as the equilibrium states move away from the critical point, where the tangent line is horizontal, this decrease being more sensible in the classical GBT formulation, as shown in Fig. 5.68, where the vertical displacement of node 1 is plotted against the load level. Subsequently, for both formulations, each branch of the post-buckling path reaches a stability point, corresponding to the minimum load capacity in the post-buckling range, and from this point forward the post-buckling equilibrium path regains a positive slope.

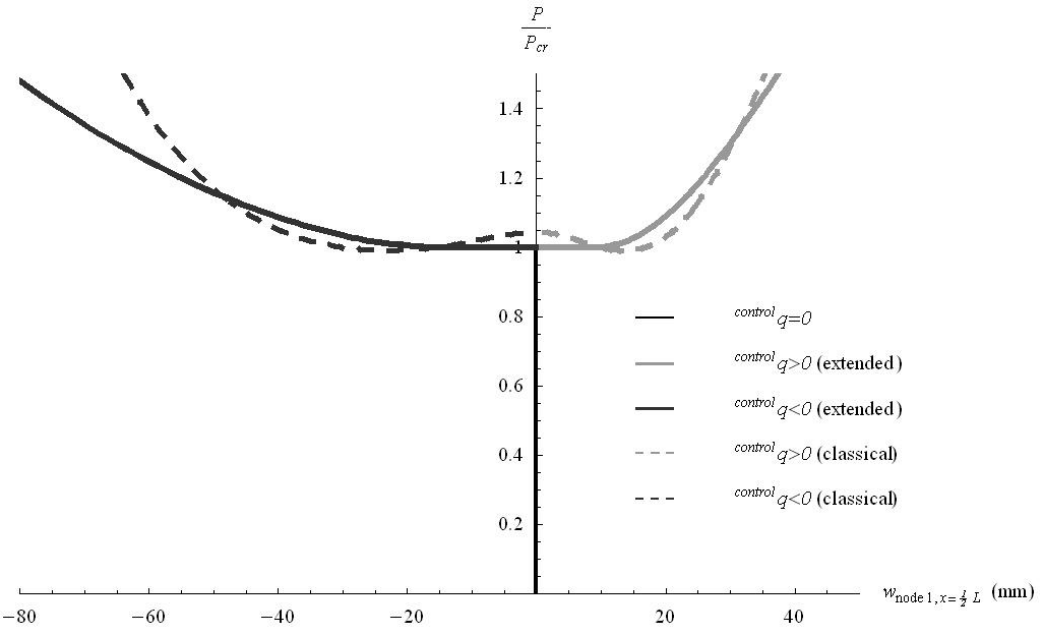

Fig. 5.68 – Vertical displacement of node 1: comparison between the extended and the classical GBT formulations

The post-buckling behaviour is symmetric and Fig. 5.69 presents the member's configuration at $P = 1.50\ P_{cr}$, while Fig. 5.70 displays the stress along the mid-span cross section at the critical state and for P equal to *93.395* kN and *112.191* kN. It is noted that very high stress levels are reached since elastic regime was assumed to the material, so that, in real cases, plasticity would occur and would limit severely the cross section's load capacity, and therefore the load capacity of the member would be much smaller than the

observed.

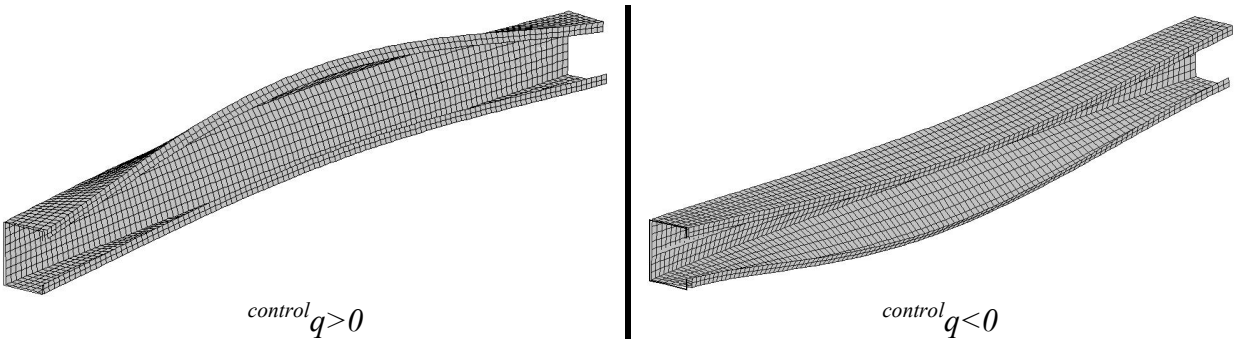

$^{control}q>0$ $^{control}q<0$

Fig. 5.69 – The column's deformed shape for $P = 1.50 \times P_{crit}$ (all displacements are amplified by factor 2)

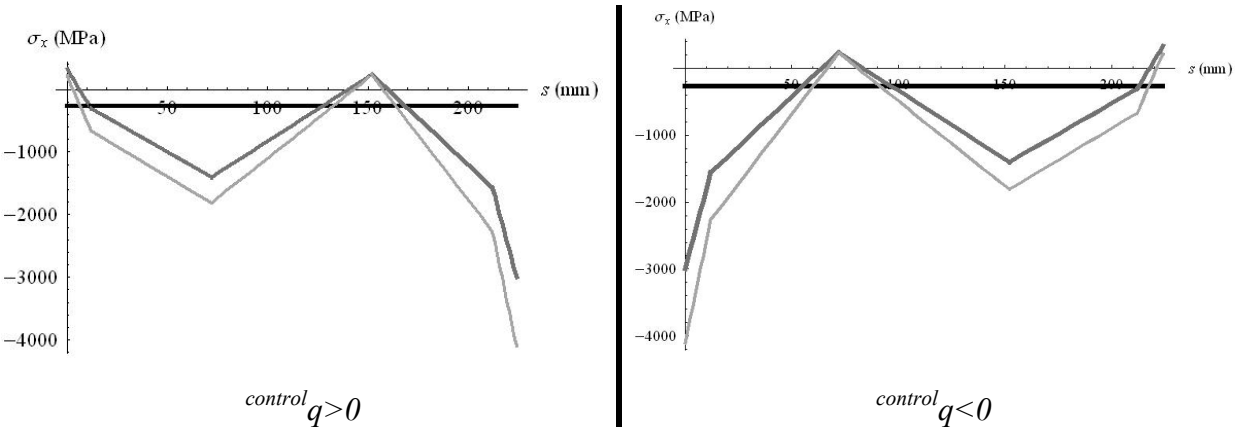

$^{control}q>0$ $^{control}q<0$

Fig. 5.70 – The longitudinal normal membrane stresses along the laid-out cross section for $P = 1.25340 \times P_{cr}$ and $P = 1.50566 \times P_{cr}$

5.9 – Chapter synopsis

In this chapter the Schardt's GBT theory, which is based on the concept of modes of deformation, was enlarged by setting up additional modes of deformation and by establishing a fully general energy formulation. It was intended to give more information about the member's behaviour to the equilibrium system, to withdraw some initial assumptions of the Schardt's theory and to unify the GBT analysis of open and closed cross sections, as in the FSM and FEM. The adopted strategy was to consider an additional

mode of deformation against each of the Schardt's restrictive assumptions, which are (Schartd 1989): i) the assumption of negligible distortion in open sections, ii) the assumption of constant shear flow around a closed cell, iii) the assumption of linear warping displacements between the folding lines of the cross section, and iv) the assumption of negligible transverse membrane extension around the cross section. The necessary modifications were presented, consisting on the modelling of additional cinematically admissible deformation patterns along the cross section's perimeter, on the consideration of additional terms in the total potential energy, derived by the classical non-linear elasticity theory for thin plates, and in slight adjustments in the orthogonalization procedure to accommodate new modes of deformation. In the setting up of the modes of deformation, the force method was replaced by the more consistent displacements method for the analysis of the cross section – in the following chapter it will be taken great profit from this change. Finally, the computer programs developed to improve the described GBT implementations were resumed and two benchmark examples were presented, to validate the presented GBT theory. The developments contained in this chapter are already presented in three articles presented in two scientific conferences (Gervásio, Simões da Silva & Simão 2004, Simão & Simões da Silva 2004b and 2005c).

6 – TOWARDS THE GBT ANALYSIS OF A GENERAL CROSS-SECTION MEMBER

6.1 – Introduction

As referred in Chapter 1, since the invention of GBT, in the middle sixties, the search of a GBT procedure devoted to the analysis of a general cross section, open or closed, branched and non-branched, has been a major research goal. Until now the GBT cross section analysis of folded-plate members was limited to open non-branched, open branched and closed mono-cellular cross section types. In the present chapter, the GBT skills will be enhanced for the analysis of a general cross section made by plane plates, which may present branching in several nodes together with several closed cells. This enhancement, based in the extended GBT formulation presented in the previous chapter, is based on the following main concepts:

i) As far as possible, it is intended that only one unified GBT formulation applies for all cross sections, in the sense that similar initial modes of deformation are generated for any cross section type, and the formulation shall be as general as possible.

ii) The procedure developed for the closed mono-cellular and open non-branched sections passes over unchanged to branched sections, open or closed, for the basic modes related to the warping of the inner nodes, since these are established directly and do not need any compatible rendering process.

iii) The procedure developed for the closed mono-cellular and open non-branched sections passes over unchanged to branched sections, open or closed, for the basic modes related to plate bending or plate transverse extension, since these

modes require only the computing of the appropriate prescribed displacements in the cross section's plane for the setting up of the appropriate displacements method problem, in order to derive the transversal rotations; in these two types of modes, no longitudinal nor plate distortion occur along the cross section.

iv) In the GBT analyses of closed mono-cellular and open non-branched sections of the Chapter 5, the warping modes were established with no distortion and the plate distortional modes were established with no warping, but it was observed that the basic modes of deformation associated with warping of the main nodes and distortion of the main plates interact between each other during the orthogonalization procedure; so, in order to perform the compatible rendering of cross section's plane displacements at branching points for these two types of modes, it is fair to combine them from the beginning, since it was observed they will combine in the final part of the orthogonalization process, in previous cases.

v) Nevertheless, the setup procedure for the warping-distortional modes shall generate all possible displacement patterns that may appear, in order to provide the most complete information to the member's equilibrium system, so that it may be necessary to neglect the traditional GBT scheme's assumption that only one mode of deformation corresponds to the warping displacement's pattern of each main node (Schardt 1989); therefore, from now on, two or more initial modes of deformation may have the same warping displacements pattern along the cross section.

vi) However, all modes of deformation that are considered in the member's analysis must be linearly independent one from the others. Therefore, in the following, some modes can be rejected if it is observed that they are linearly dependant of the remaining ones – a mathematically grounded procedure to extract them may be needed;

So, for the analysis of a general cross section, only the modes that deal with warping of the main nodes and distortion of the main plates need to be adapted for the compatible rendering of the cross section's plane displacements, to assure cross section's continuity. The remaining modes of deformation – inner nodes warping, plate bending and plate transverse extension – pass over unchanged for the analysis of general cross sections and constitute no special difficulty. It is only required to consider the proper cross section stiffness matrix and the appropriate prescribed displacements and/or fixation forces for the latter two types of modes of deformation, in the context of the displacements method procedure presented above, and the inner nodes warping modes are established directly, as before. Also, for all modes, the determination of the transverse bending moments is made trivially through the displacements method, using exactly the same procedure that was used in Chapter 5, so the existence of branching represents no special difficulty to this step, highlighting the advantage of the displacement method when compared to the force method adopted in the classical GBT theory.

The explanation presented below expresses chronologically the way the enhancement was derived. It was first derived for the I-section, after for the bi-cellular section with right angles between plates. For these cases it was seen that the traditional orthogonalization scheme performs properly, just as for open non-branched and mono-cellular sections. Subsequently, the analysis was extended to a general cross section, illustrated here without loss of generality by the hollow-flange beam section, and it was observed that the scheme generates an exaggerated number of modes of deformation, some of them being linearly dependant from the remaining ones – the excessive modes could be obtained as linear combinations of the remaining ones, those that form a vector base space. So, a zero-step was introduced in the orthogonalization procedure, associated only with matrix $\boldsymbol{C}$, to extract the linearly independent warping-plate distortional modes of deformation that constitute the base of the vector space of the modes of deformation. Like

for the open non-branched and closed mono-cellular section cases, for the new section cases the resulting orthogonal modes of deformation can be grouped in three main sets: i) the traditional modes of axial elongation and bending related to the principal axes, associated with zero-values in the ***D*** and ***B*** matrices, ii) the torsion and shear-lag modes, associated with zero values in matrix ***B*** but non-zero values in the main diagonal of matrix ***D***, and, finally, iii) the cross-sectional distortional modes that generate non-zero values in the main diagonal of matrix ***B***, present null warping displacements and some present null terms in matrix ***C***.

Finally, for each cross section case, an illustrative example was presented, showing the critical behaviour for uniform compression and/or major axis uniform bending, and post-buckling behaviour for specific lengths. Each example was benchmarked with the finite-strip program CUFSM (Schafer 2003) for the critical behaviour using one half-wave coordinate function per mode of deformation, which corresponds to the use of only the first polynomial function derived in Chapter 3, and a perfect agreement of the two analyses was observed for all examples.

6.2 – The I-section

6.2.1 Introduction

In the context of GBT, the I-section constitutes one particular and simple case of branched sections: a plate – the web – is connected at the edges to two other plates – the flanges – each one of these being formed by two plates with equal inclination angle, as shown in Fig. 6.1-a). For this cross section the GBT discretization renders six main nodes and five main plates, the corresponding numbering being presented in Fig. 6.1-b). According to the strategy used in the previous chapters, it is considered here that the nodes that connect the web to the flanges are main nodes, since each one connects two main

plates. The procedure presented below is based on the extended GBT formulation previously explained, thus keeping the unification between open and closed cross sections, and is assessed here for the warping and plate distortional modes only. Therefore, the task here is merely the computation of the warping displacements and the displacements along the cross section plane necessary to the establishment of the displacements method problem that will calculate the rotations at the nodes and transverse bending moments that will fully define each mode of deformation.

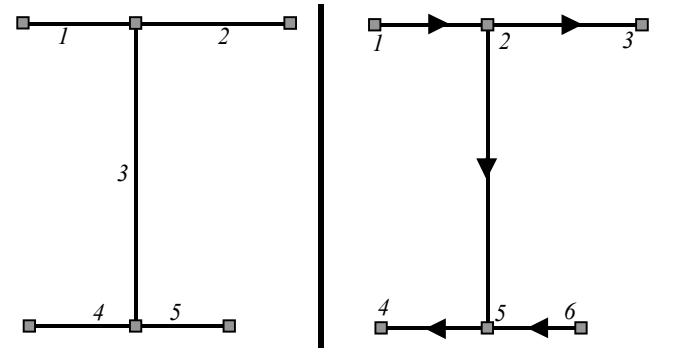

Fig. 6.1 – Typical thin-walled I-section and the main plates numbering

For the establishment of the warping and the plate distortional modes, at first one decision has to be made: is it admissible or not that a warping mode involves longitudinal displacements of more than one main node? A positive answer to this question is equivalent to assume that, for the warping modes associated with the warping of a main node, other main nodes can be forced to experience longitudinal displacements in order to render null the distortion along all plates. The alternative is to assume that any warping mode corresponds to the longitudinal displacement of only one main node, and the remaining ones stay longitudinally unmoved, keeping linear warping displacements distribution along the main plates. Then, the compatibility process required to restore the section's continuity must disregard the condition of null distortion along the plates for the

warping modes, implying that the distortional modes associated with some main plates become linear combinations of some warping modes and hence must be removed from the analysis. It is not proved that the two alternatives are equivalent, but the second option is more general and consistent with the basic assumptions of the extended GBT formulation derived in the previous chapter, so that, in the present work, it will be considered. The correspondent warping basic modes of deformation are derived below assuming that some distortions are allowed to occur in some plates, if necessary, to assure cross section's continuity. Also, for the warping of a main node, if various distinct ways are feasible for the compatible rendering process, then all must be taken into account, in order to give as many information as possible to the member's equilibrium system. As referred above, in the end of the cross section analysis, these modes are combined through the traditional orthogonalization procedure to form a new and equivalent set of orthogonal modes of deformation.

6.2.2 The basic modes involving warping of the main nodes and distortion of the main plates

A general methodology for the establishment of the warping and distortional basic modes of deformation in branched sections is presented here in the context of the extended GBT formulation. First, all feasible and linearly independent modes involving warping are set up and only after the plate distortion modes will be established – these later ones are considered only if they are not a linear combination of the warping modes previously established. In the following, concern is taken upon the determination of the nodal translation displacements only for the establishment of the basic modes of deformation, since the rotations will be determined through the displacements method by considering that the already known translational displacements act as prescribed displacements, as shown in chapter 5. Fig. 6.2 presents the global displacements numbering for the analysis of the cross section, considering only the main nodes.

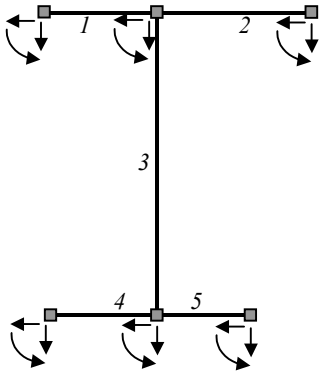

Fig. 6.2 – The global displacements at the main nodes for the I-section analysis

Beginning by the warping modes, for a main node *i* a longitudinal displacement is imposed while the remaining main nodes stay longitudinally unmoved. The configuration of the plates adjacent to the main node *i* is then drawn, assuming at first that no distortion occurs, in general destroying the cross section's continuity at various folding lines. Subsequently, the compatible rendering process starts from the main node *i* to the rest of the cross section and, when possible, the continuity of two adjacent plates is restored through the traditional GBT process (Schardt 1989). However, when two main plates have a same inclination angle or when one main node connects three or more main plates, this compatible rendering type is no longer possible. In this case, at first the compatible rendering process is made for any two plates connected to the main node in question having different inclination angle through the traditional procedure – this step defines the final position of the main node. Then, the remaining plates connected to the main node are forced to connect to its final position applying a distortional deformation pattern if necessary. In this case, several options can be admissible in this compatible rendering step for the choice of the pair of plates to be rendered compatible using the traditional GBT process, while the others are forced to distort, each option generating a distinct mode of deformation. Hence, associated with the warping of one main node, several linearly independent modes of deformation can occur and all of them shall be considered in the member's analysis.

After, the modes of deformation related to the distortion of the plates are generated. Since distortional displacements patterns have already been used for the establishment of the warping modes, it is important to find out if the present modes can or can not be generated as a linear combination of the precedent ones, in order to do not generate an indeterminate equilibrium system for the global member analysis.

In the following the above statements will be applied to the establishment of the basic modes of deformation of the typical I-section shown in Fig. 6.1. Starting at the establishment of warping mode associated with node 1, the process goes as shown in Fig. 6.3. First, a unitary longitudinal displacement is imposed to node 1, neglecting the cross section's continuity at node 2 – see Fig. 6.3-a). After, the compatible rendering between plates 1 and 3 is established by using bending displacements only, because these plates are the ones having different inclination angle that connect at node 2, where discontinuities happen – see Fig 6.3-b. The compatible rendering related to plate 2 is only achieved by imposing a distortional deformation pattern to this main plate.

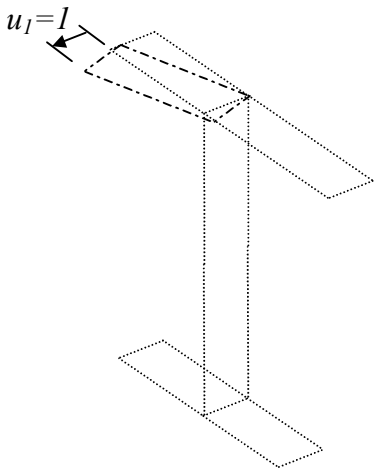

a) imposing a warping displacement to node 1, neglecting the continuity of the cross section at $x+dx$

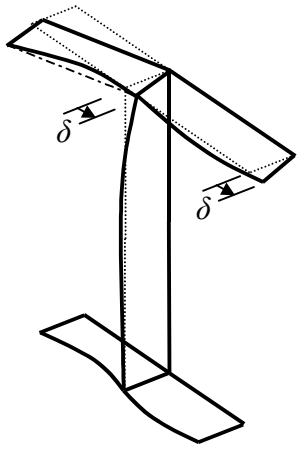

b) compatible rendering of the cross section, where $\delta = \frac{1}{b_1}$

Fig. 6.3 – Setting up the warping mode associated with node 1

For the establishment of the warping mode related to a unitary longitudinal displacement of node 2, plates 1, 2 and 3 are involved in the first step, while plates 4 and 5 remain unmoved, as shown in Fig. 6.4-a). Two ways of compatible rendering are now possible: at first one can render compatible the discontinuity displacements between plates 1 and 3 or between plates 2 and 3. After, the remaining plate will experience transversal bending and distortion to restore cross section continuity. In order to enable the maximum generality to the method, both ways shall be considered since they are distinct, hence the warping of mode 2 gives rise to two independent modes of deformation as expected above. Fig. 6.4 shows the scheme for the first option. At first, the warping displacement is imposed to node 2, neglecting cross section's continuity – see Fig. 6.4-a).Then, a compatible rendering process is established between plates 1 and 3 in the classical form, and a distortional deformation pattern, together with bending displacements, is imposed to plate 2 to assure the cross section's continuity, as illustrated in Figures 6.4-b) and 6.4-d), resulting in the final shape given in Fig. 6.4-c). Fig. 6.5 resumes the procedure for the alternative option, where the traditional GBT compatible rendering process is used between plates 2 and 3, and plate 1 distorts. All in all, for each option, the first step is to impose the warping displacement along the cross section, assuming that no distortion occurs along the cross section, which implies the existence of uniform displacements along the local *Os* axis for all main plates connecting to node 2, as shown in figures 6.4-a) and 6.5-a) for both cases. Then, the discontinuity between one horizontal plate and the web is rendered null using the traditional GBT process, which, for each option, defines the final position of main node 2. At last, the remaining horizontal plate is forced to connect to the final position of node 2 by a combination of bending and distortional displacements. These two independent modes of deformation are associated with the same warping displacements pattern and, for this cross section, only two options occur, but if plates 1 and 2 did not have the same inclination angle, more options to the compatible rendering scheme could exist and should be considered in the analysis – this fact is explored below

for the general cross section analysis. Therefore, as the cross section becomes more complex, more ways of rendering compatible the discontinuity displacements may exist and thus, in order to assure the scheme's generality, all of them should be considered in the analysis. At this stage the establishment of the remaining warping modes for the I-section is trivial.

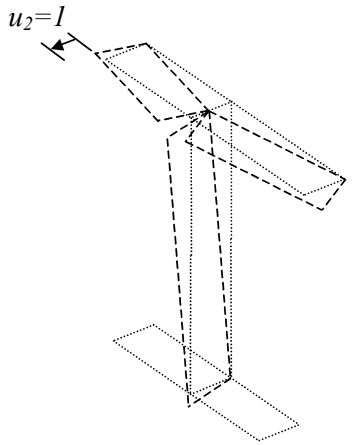

a) introduction of the warping displacement at main node 2

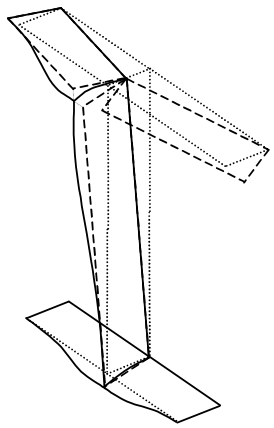

b) compatible rendering of the discontinuity between plates 1 and 3

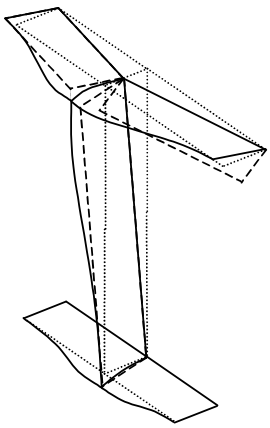

c) compatible rendering of plate 2

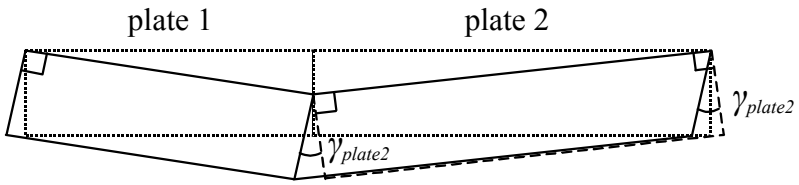

d) detail of the compatible rendering of plates 1 and 2, high lightening the distortion that occurs at plate 2, for Fig. 6.4 b)

Fig. 6.4 – Setting up the warping mode associated with node 2 – option 1

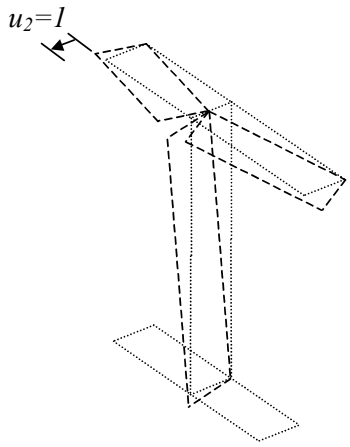

a) introduction of the warping displacement at main node 2

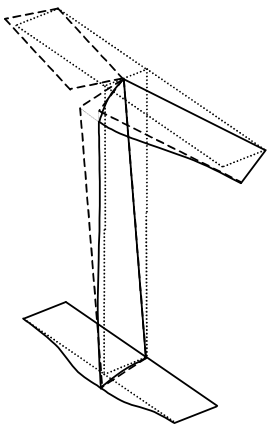

b) compatible rendering of the discontinuity between plates 2 and 3

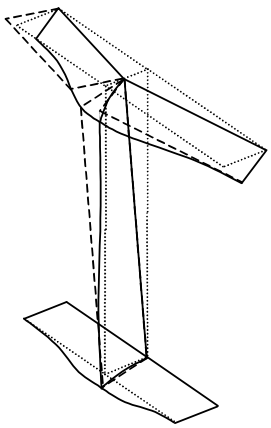

c) compatible rendering of plate 1

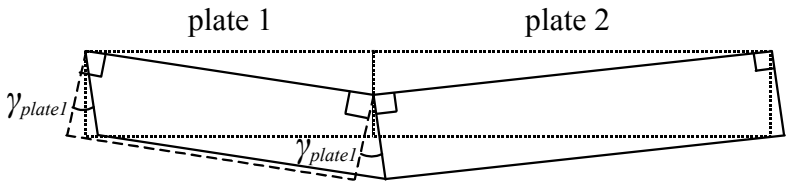

d) detail of the compatible rendering of plates 1 and 2, high lightening the distortion that occurs at plate 2

Fig. 6.5 – Setting up the warping mode associated with node 2 – option 2

Focusing now on the distortional modes of deformation, they are associated with a distortional deformation pattern of the main plates, with no longitudinal displacements along the cross section, as shown in Chapter 5. For the I-section under analysis, only three main plates are considered for these modes: the web and the two flanges, since it is physically impossible to impose a distortional deformation pattern to one half of the flange without imposing the same pattern to the other half, when no warping is allowed. However, the distortional mode associated with the top flange can be derived from the warping modes in the following way: for the warping modes related to node 2 shown

above, if one subtracts option 1 from option 2, a pure distortional pattern for the upper flange is encountered. So, owing to the use of distortional deformation patterns to establish the warping modes, some distortional modes become now redundant and must be removed from the global analysis. Therefore, only the distortional mode associated with the web is considered, since it is linearly independent of the remaining modes, and is established by imposing to the web a constant and unitary displacement along the *Os* axis, as shown in Fig. 6.6-a). The compatible rendering scheme, shown in Fig. 6.6-b) follows the normal process and considers also the strategy exposed in chapter 5.3.6. Due to the fact that both plates forming each flange have the same inclination angle, and as a consequence of the right angle between the web and the flanges, only one compatible rendering scheme is possible. However, if any of the flanges was composed by plates having different inclination angles, more than one procedure would be possible and all possibilities should be considered, as above, hence the equal inclination angle of the two plates forming the web introduces a simplification in the GBT analysis.

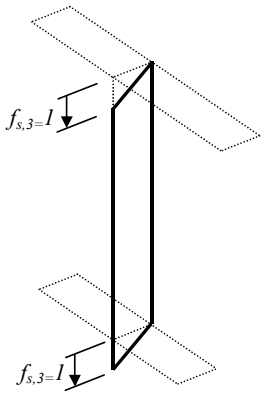

a) introduction of the distortional deformation pattern to the web

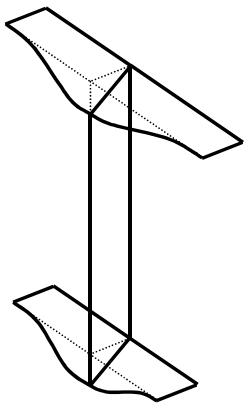

b) compatible rendering of the discontinuity displacements along the cross section

Fig. 6.6 – Setting up the mode of deformation related to the distortion of the web

6.3 – Illustrative example for the I-section

6.3.1. Presentation and derivation of the modes of deformation

The buckling and post-buckling behaviour of a thin-walled I-section member under uniform compression or bending, whose geometric properties and cross section discretization are presented in Fig. 7.27, is analysed here. The member consists of an I-section, is made of steel ($E = 210$ GPa and $\mu = 0.3$), and is regarded as two channel sections perfectly glued by their webs, in such a way that both channel webs can be modelled as one single web for the I-section. The member is simply supported with end plates of negligible bending inertia, so the coordinate functions (3.24) for mode 1 and (3.37) for the remaining modes are used.

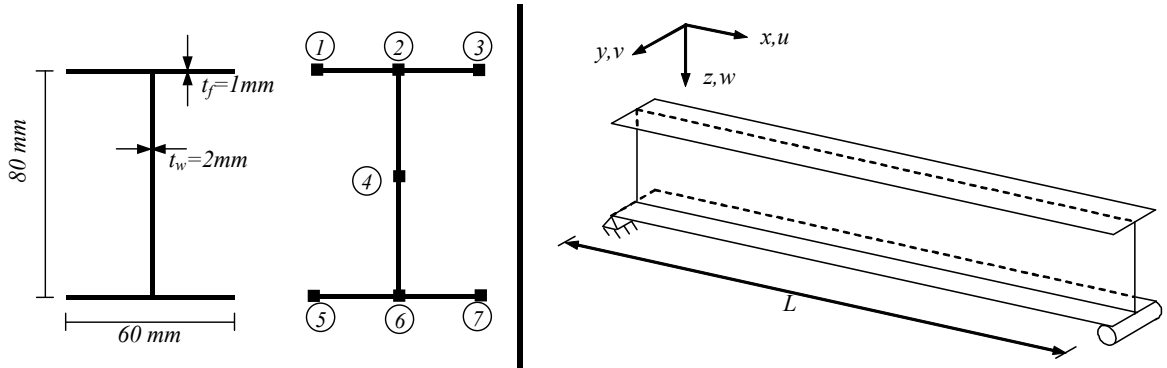

a) geometric properties and discretization b) member overview

Fig. 6.7 – The analysed cross section and the adopted nodes

For the uniformly compressed column case, an inner node at the mid-height of the web is introduced and a set of 20 orthogonal modes of deformation, whose unitary displacements patterns are shown in Figures 6.8 and 6.9, is formed. Modes 1 to 10 are associated with null values of matrix $\boldsymbol{B}$, thus can be considered as rigid body modes. Mode 1 corresponds to the axial elongation, mode 2 and mode 3 to major axis and minor axis bendings, respectively, and mode 4 corresponds to the Vlasov's torsional mode referred to the cross section shear centre. Note that, once again, in open sections the classical Vlasov's

torsional mode appears explicitly and is associated with null membrane distortion, since the corresponding term ${}^{4,4}D_3$ vanishes. Modes 5 to 10 are associated with membrane distortion, thus are not considered in the classical thin-walled theory, and it is observed that their stiffness is very high, corresponding to high values in matrix $\boldsymbol{C}$ and $\boldsymbol{D}$. The remaining modes, the distortional ones, imply cross section deformation in its own plane: modes 11 to 15 are associated mainly with transversal bending and modes 16 to 20 refer to the transversal extension of the cross section plates. For I-sections the present GBT scheme establishes more modes of deformation than the procedure of Haakh (2004), where the modes involving, for example, transversal extension of the plates and multi-linear longitudinal displacements between main nodes are not present.

6.3.2. The simply supported column under uniform compression

6.3.2.1 The buckling behaviour

Applying the standard stability procedures to the perfect column shown in Fig. 6.10 the critical loads of Figures 6.11 and 6.12 and are obtained for a length's range between 50 and 3500 mm, together with the corresponding modal participation coefficients, presented in Fig. 6.13. Fig. 6.11 highlights the perfect agreement between GBT and CUFSM analyses, while Fig. 6.12 shows the influence of the number of coordinate functions per mode of deformation 2 and higher in the member's behaviour, highlighting the wave effect along the plate buckling range. Fig. 6.13 illustrates the two buckling domains: for smaller lengths, between *50* and *900* mm, the plate bending modes rule the member's buckling, corresponding to a local plate buckling mode of the webs. For lengths higher than *900* mm, the minor axis bending governs the bifurcational behaviour.

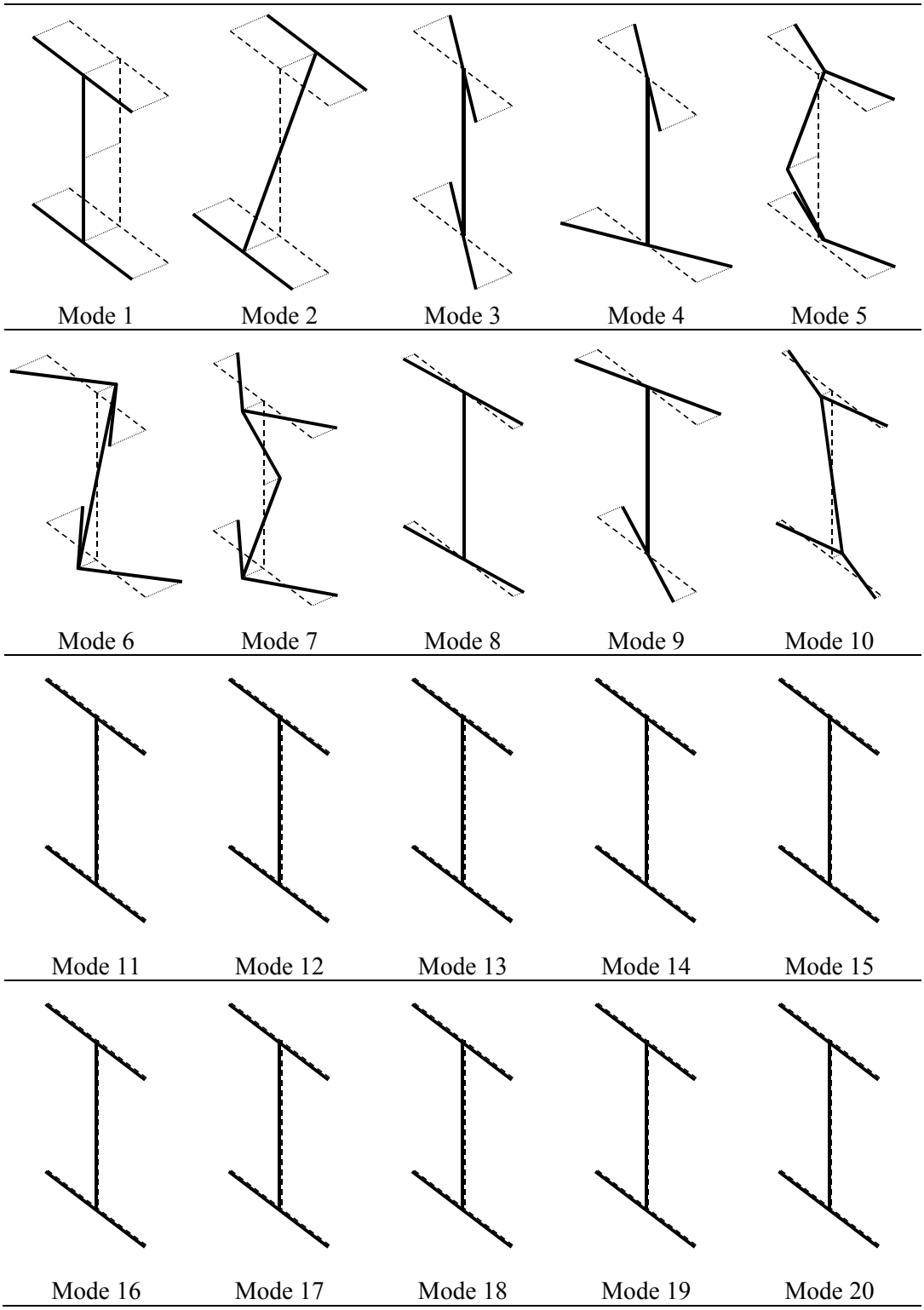

Fig. 6.8 - The unitary longitudinal warping displacements shapes for the orthogonal modes of deformation

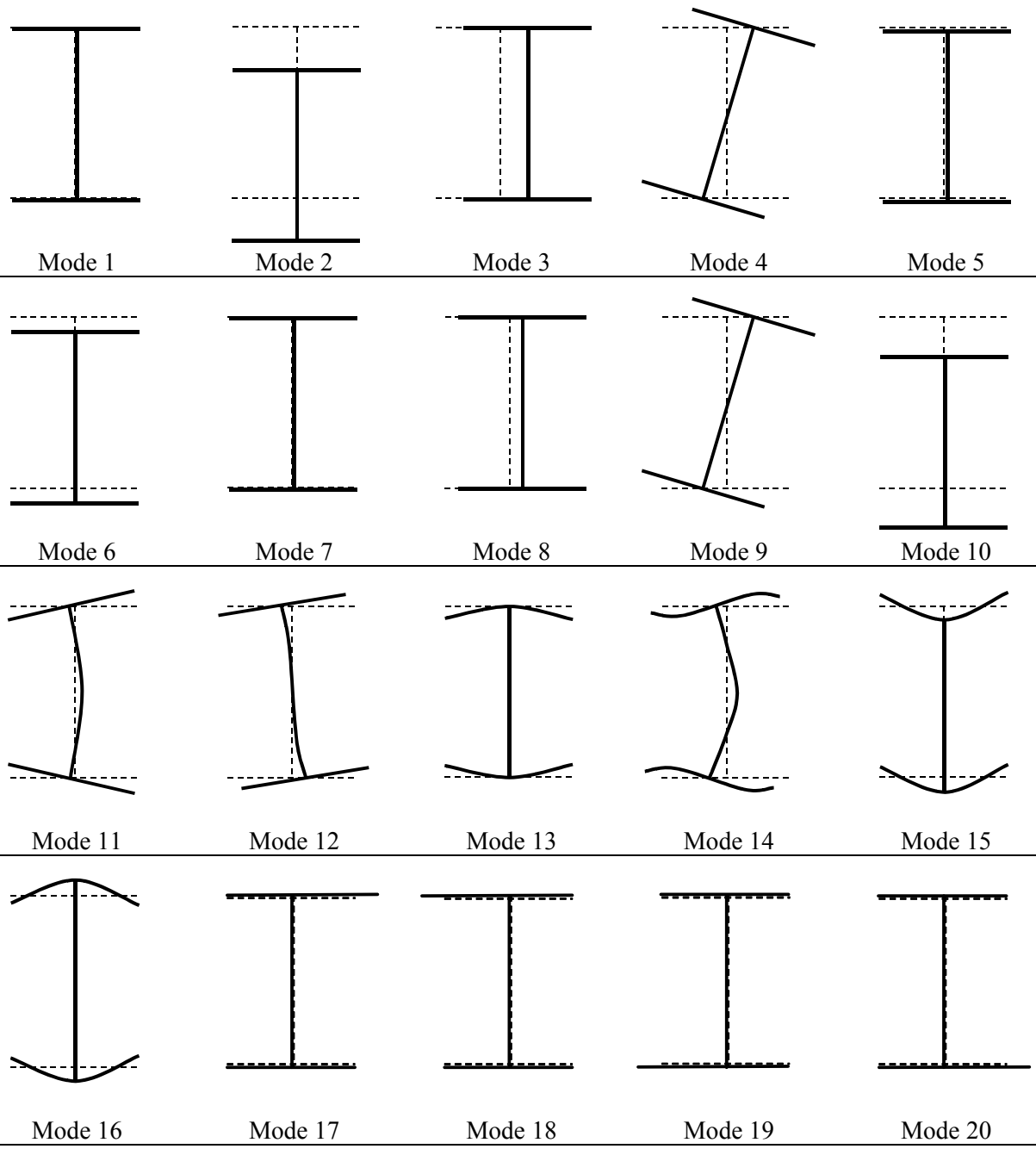

Fig. 6.9 - The unitary displacements shapes along the cross section plane for the orthogonal modes of deformation

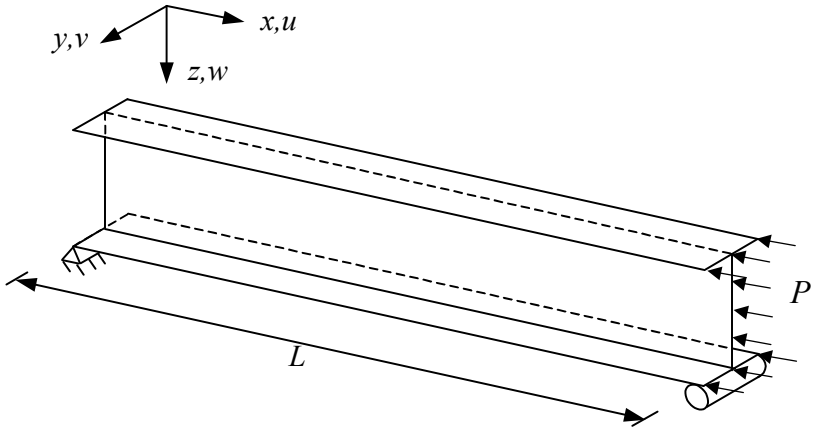

Fig. 6.10 – The compressed I-section column

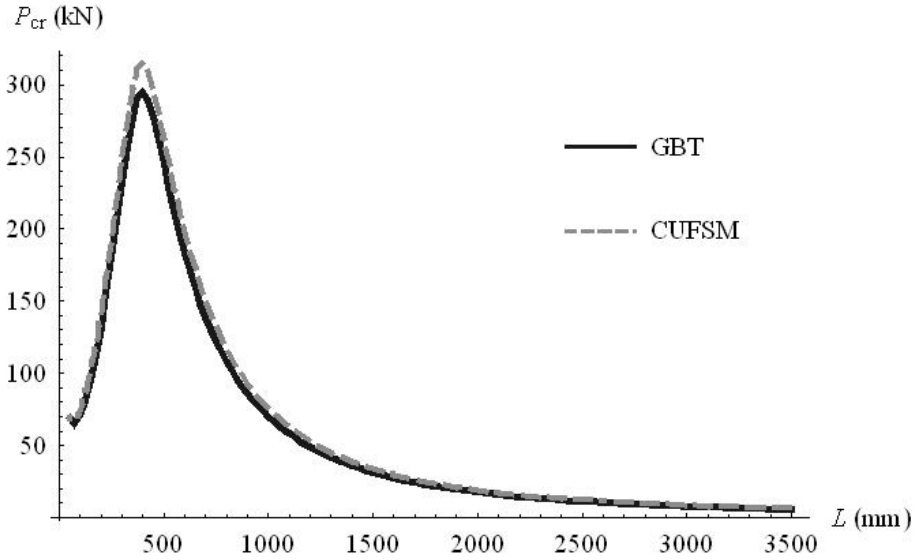

Fig. 6.11 – Buckling loads for the compressed I-section column: benchmark comparison between GBT (with only one polynomial – with one half-wave – as coordinate function for each mode of deformation) and CUFSM analysis

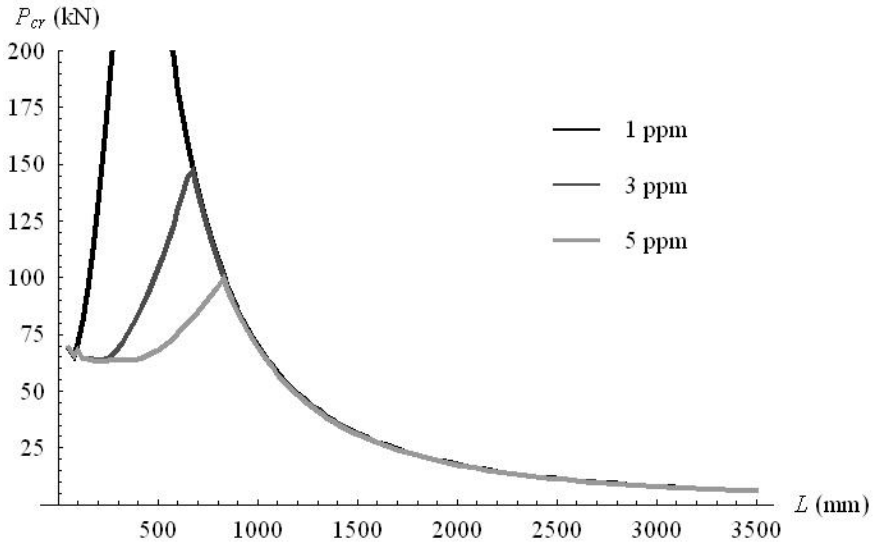

Fig. 6.12 – Buckling loads for the compressed I-section column: decrease of the critical load with the number of adopted polynomials per mode of deformation

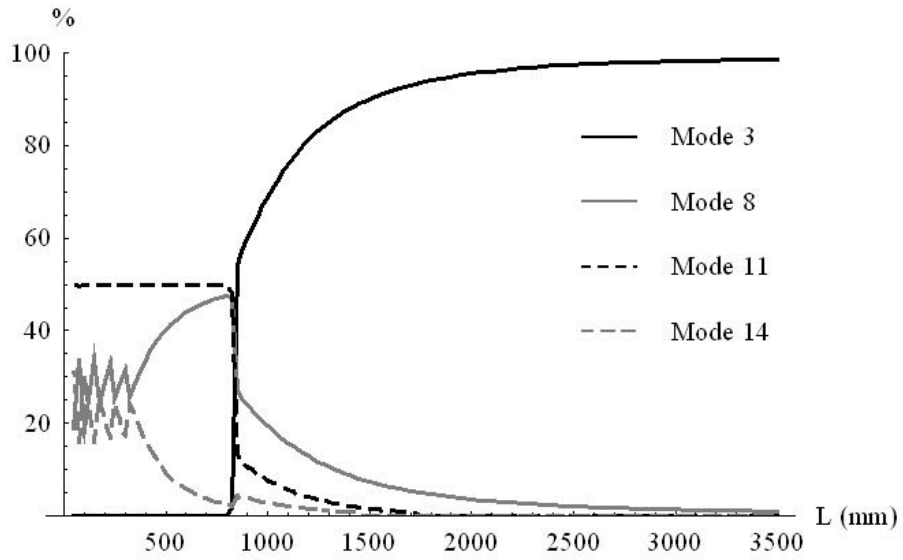

Fig. 6.13– Modal participations at the critical state for the compressed I-section column, considering 5 polynomials per mode of deformation

6.3.2.2 The post-buckling behaviour in the distortional range

Having identified the active coordinates and calculated the critical loads, the post-buckling equilibrium paths are determined for a column length of *400* mm, and, due to computer limitations, for modes 2 to 20 only the first three polynomials of expression (3.37) were adopted per mode of deformation, generating a critical load of 83.3 kN. For

this discretization, the most critical coordinate is ^{49}a, associated with mode of deformation 11 and with three half-waves, i.e., with coordinate function (3.37-c). Figures 6.14 and 6.15 present the vertical displacement *w* for node 1 and the horizontal displacement *v* for node 4 at $x = \frac{L}{2}$, respectively. These graphs show a symmetrical and stable post-buckling behaviour. Fig. 6.16 presents the member's deformed configuration for $P = 1.08 \times P_{CR}$ for each post-buckling equilibrium branch, showing also the non-deformed (initial) position of the edge cross section at *x*=*L*, highlighting the axial shortening of the member. Figures 6.17 to 6.19 show the evolution of the longitudinal membrane stress at some relevant points of the member for *x*=*L*. Fig. 6.17 puts in evidence the decrease of the applied stress at node 1 – an edge node – while for nodes 2 and 4 the stresses increase in the post-buckling range, more pronounced in node 4, as shown in Figures 6.18 and 6.19. Figures 6.20 to 6.22 show the evolution of the longitudinal membrane stress along the member's length for nodes 1, 2 and 4, respectively, and it is noted that this stress always increases for nodes 2 and 4, while in certain parts of the member's length some decrease in the post-buckling domain is observed for node 1. Figures 6.23 and 6.24 present the longitudinal stress diagrams for the upper flange and for the web, highlighting that near main nodes corresponding to folding lines the stress increases in the post-buckling range, while near the edges, for the web, or in the middle of the plate, for the flange, the stress decreases. Figures 6.25 and 6.26 show the transverse membrane stress for nodes 1 and 2 – this stress is only significant in the neighbourhood of the edge sections due to the restriction of the Poisson effect provoked by the adopted coordinate functions. Fig. 6.27 presents the membrane shear stress at node 1 along the member's length, showing always negligible values in comparison to the longitudinal stresses.

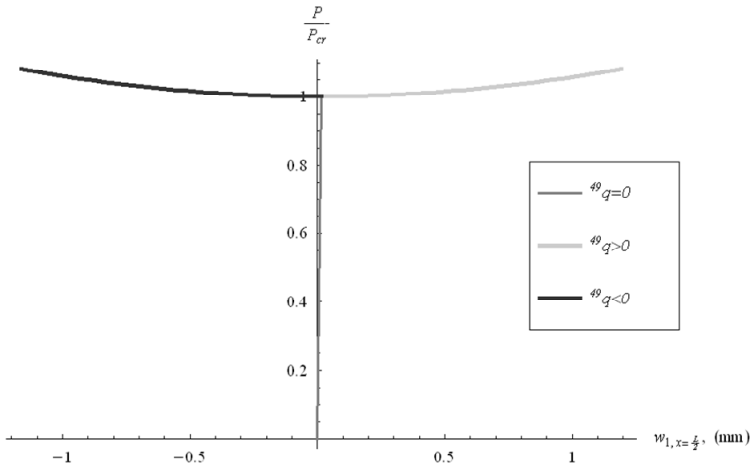

Fig. 6.14 – Vertical displacement *w* for node 1 at $x = \frac{L}{2}$

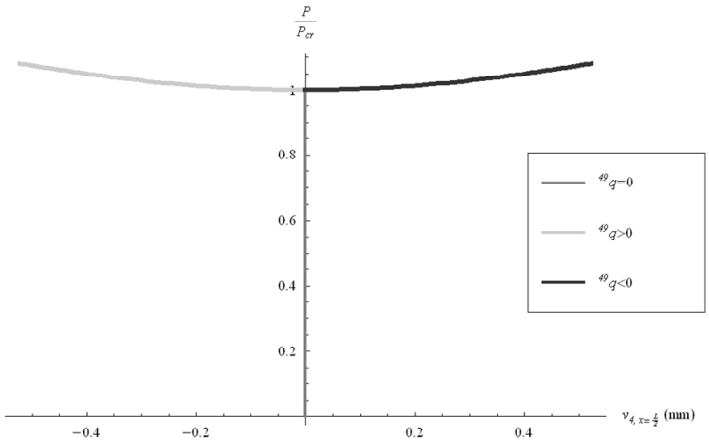

Fig. 6.15 – Horizontal displacement *v* for node 4 at $x = \frac{L}{2}$

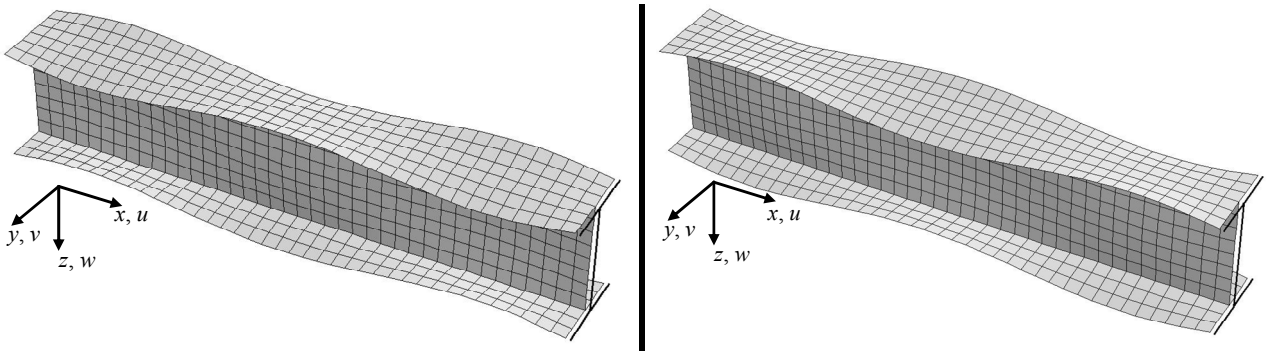

$^{49}q > 0$ $^{49}q < 0$

Fig. 6.16 – Member's deformed configuration for $\frac{P}{P_{CR}} = 1.08$, for (all displacements are amplified by a factor 5)

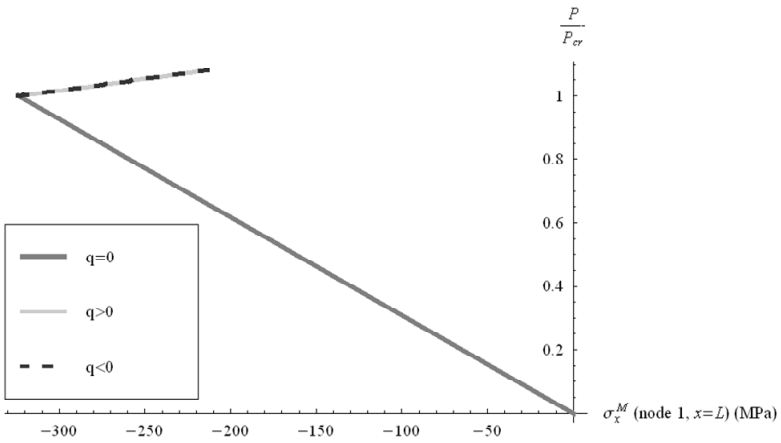

Fig. 6.17 – Longitudinal membrane stresses at node 1, for $x = L$

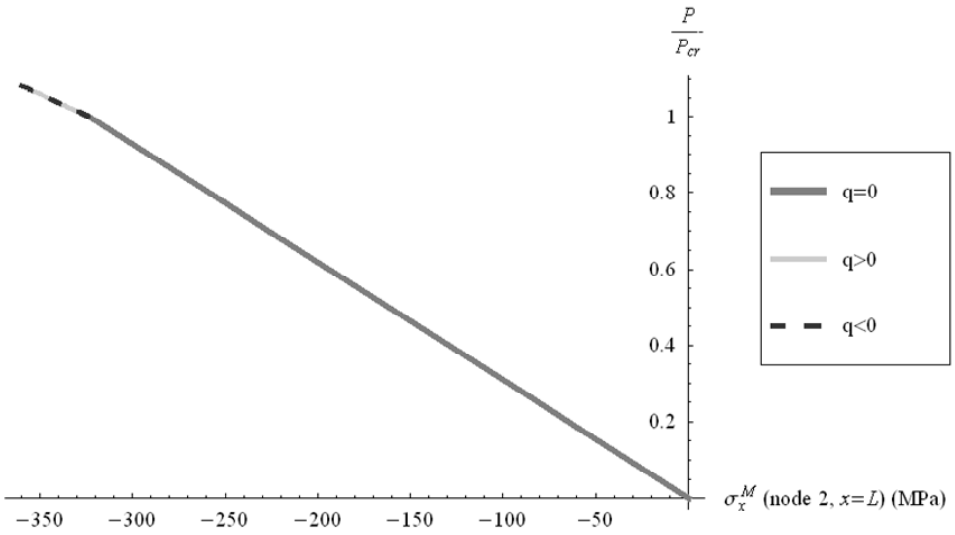

Fig. 6.18 – Longitudinal membrane stresses at node 2, for $x = L$

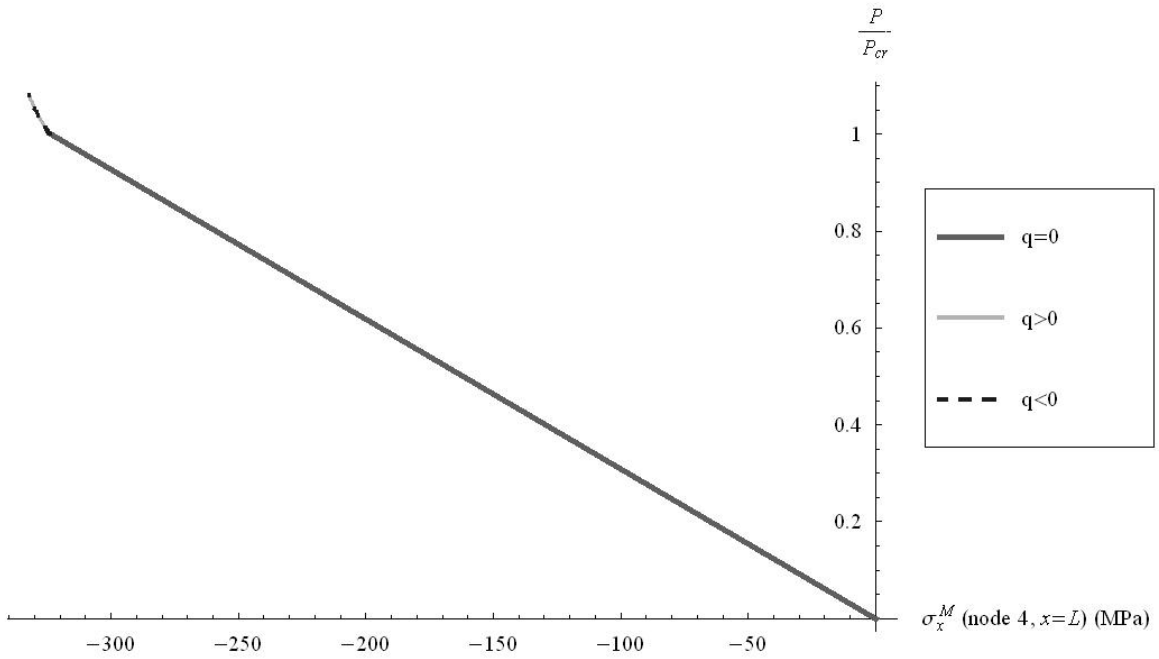

Fig. 6.19 – Longitudinal membrane stresses at node 4, for $x = L$

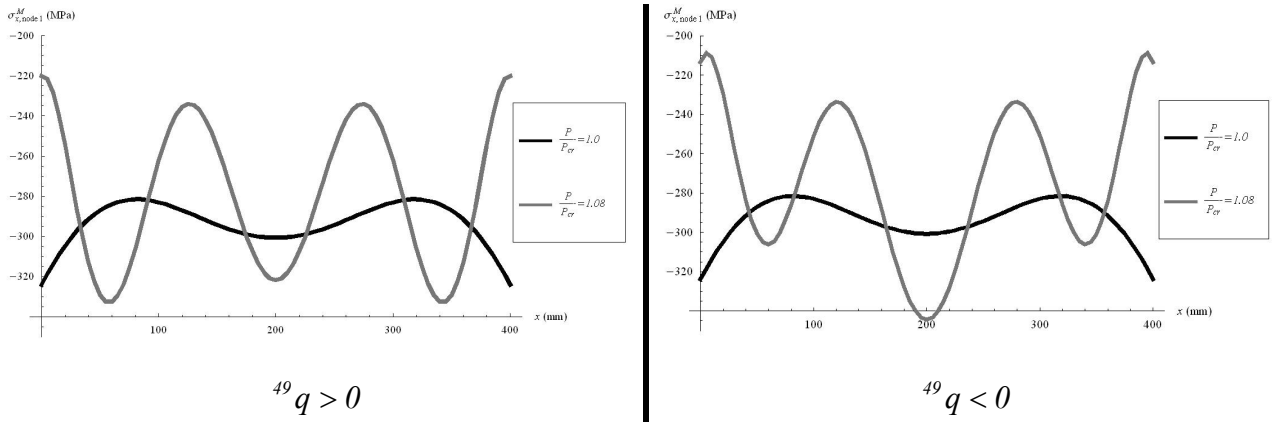

$^{49}q > 0$ $^{49}q < 0$

Fig. 6.20 – Longitudinal membrane stresses at node 1 along the longitudinal axis

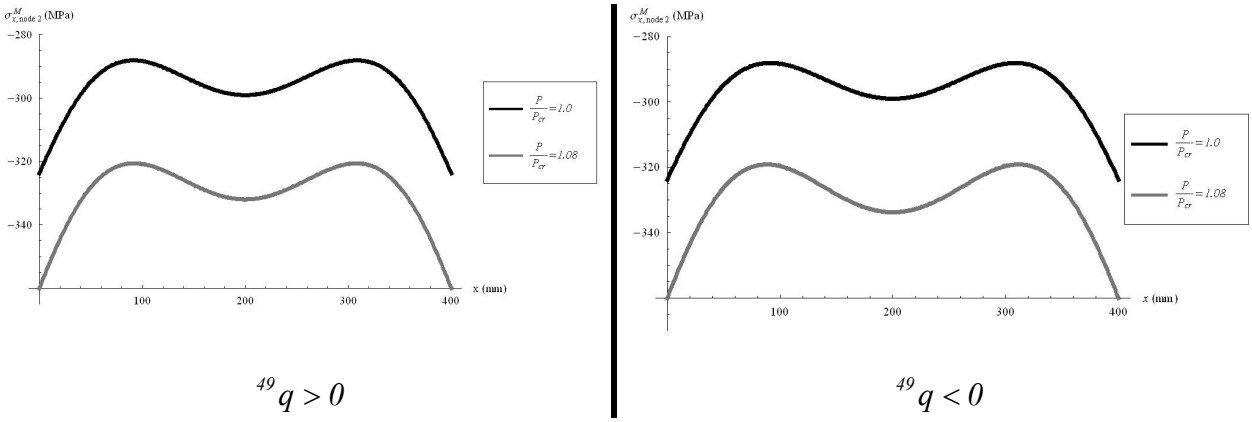

$^{49}q > 0$ $^{49}q < 0$

Fig. 6.21 – Longitudinal membrane stresses at node 2 along the longitudinal

axis

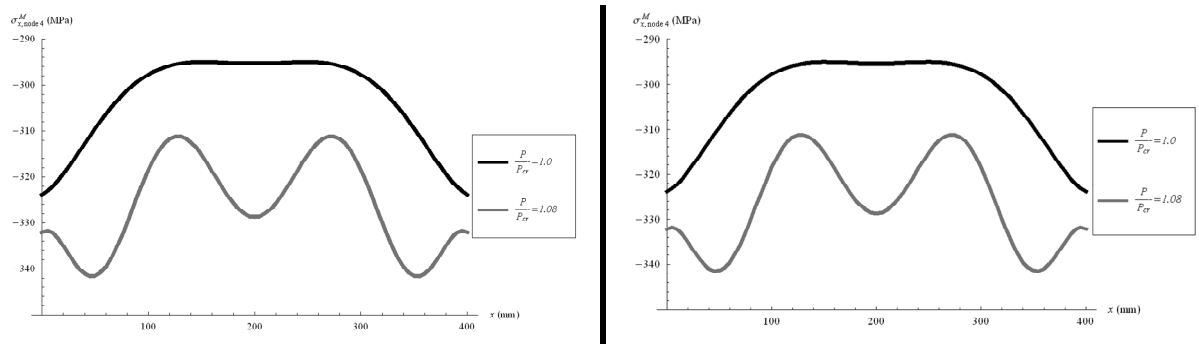

$^{49}q > 0$ $^{49}q < 0$

Fig. 6.22 – Longitudinal membrane stresses at node 4 along the longitudinal axis

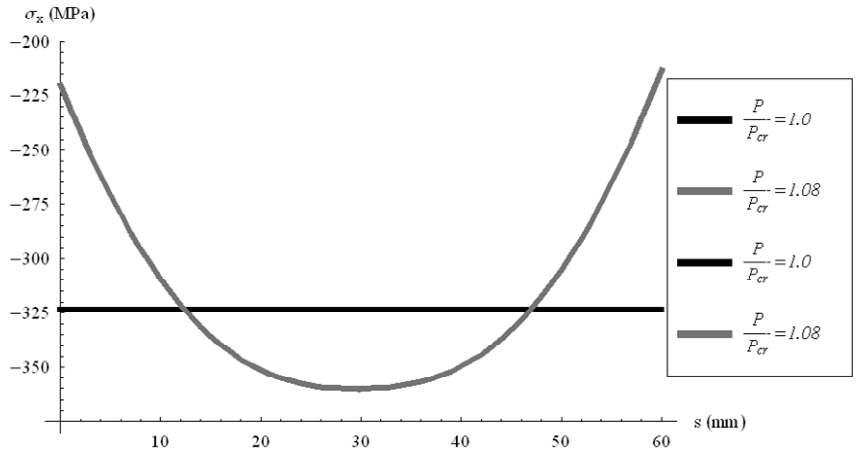

Fig. 6.23 – Longitudinal membrane stresses for plates 1 and 2 (upper flange) at $x = 0$, for $^{49}q > 0$

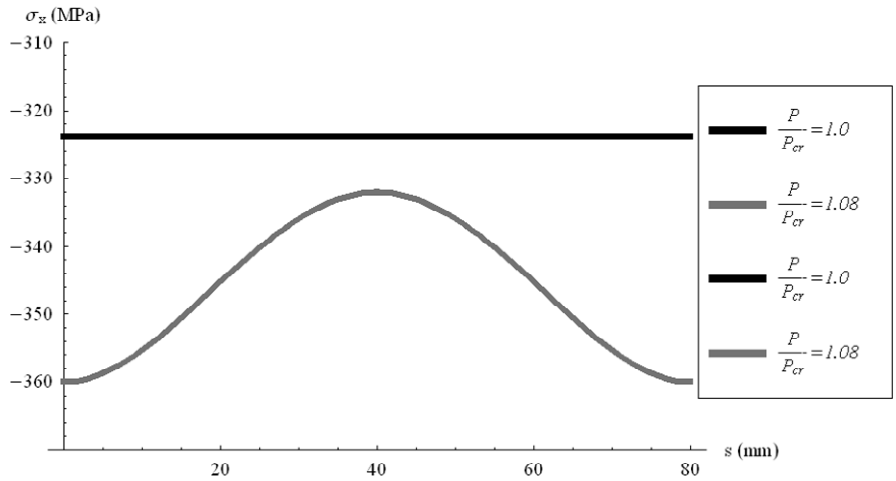

Fig. 6.27 – Longitudinal membrane stresses for plates 3 and 4 (web) at $x = 0$, for ${}^{49}q > 0$

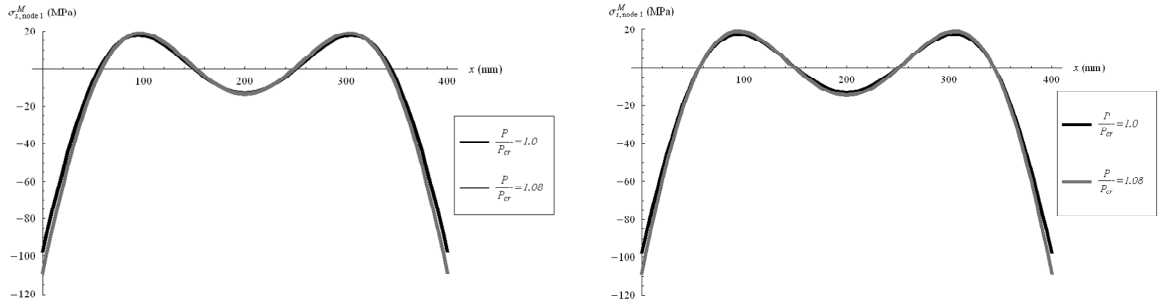

${}^{49}q > 0$ ${}^{49}q < 0$

Fig. 6.25 – Transversal membrane stresses at node 1 along the longitudinal axis

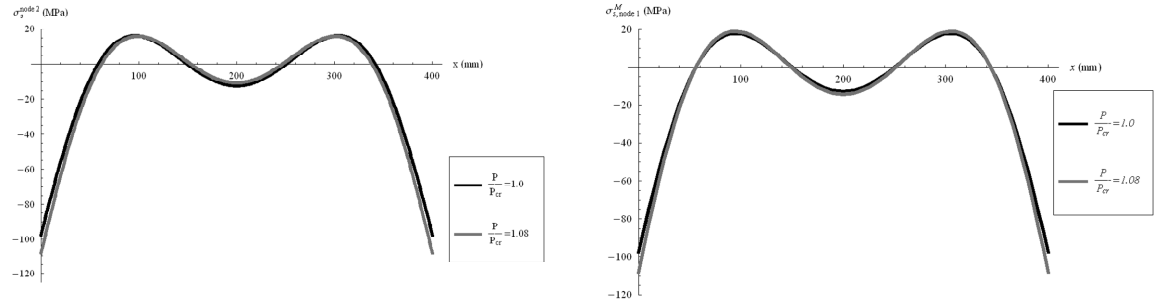

${}^{49}q > 0$ ${}^{49}q < 0$

Fig. 6.26– Transverse membrane stresses at node 2 along the longitudinal axis

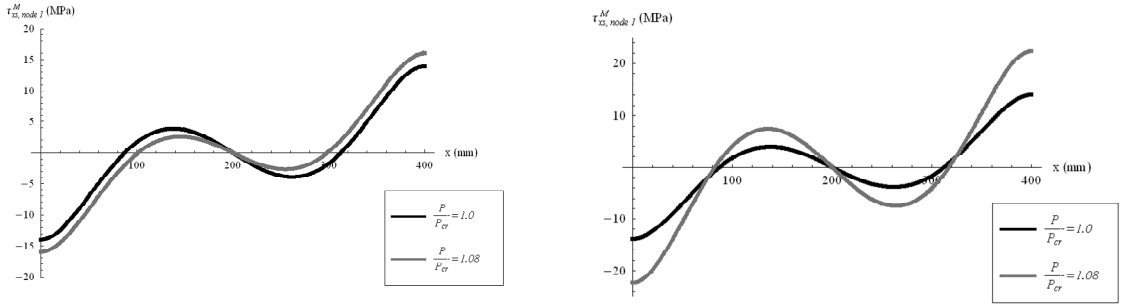

${}^{49}q > 0$ ${}^{49}q < 0$

Fig. 6.27 – Membrane shear stresses at node 1 along the longitudinal axis

6.3.3. The simply supported beam under uniform major axis bending moment

6.3.3.1 Introduction

For the I-section beam under uniform major axis bending moment, presented in Fig. 6.28, a more refined discretization was adopted in the web to allow the transverse bending of a portion of the web, which may occur in the post-buckling behaviour of the beam if the web and/or the flanges buckle. So, three web nodes were considered, as shown in Fig. 6.29, and 24 modes of deformation were obtained, being presented in Figures 6.30 and 6.31. It was obtained twelve modes of cross section's rigid body motion and twelve of cross section distortion, the last five involving transversal extension of the plates.

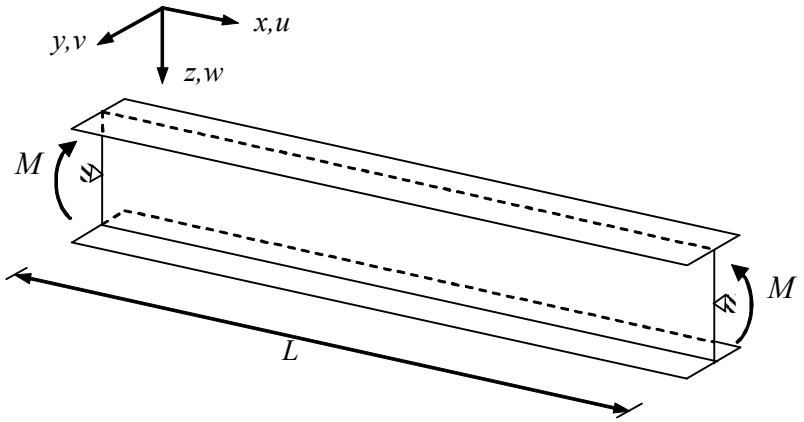

Fig. 6.28 – The I-section beam under major axis uniform bending moment

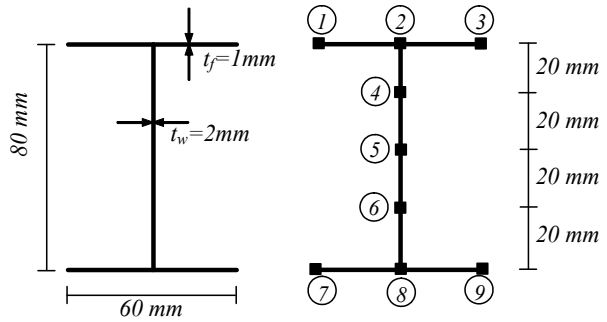

Fig. 6.29 – The cross section and the adopted nodes for beam analysis

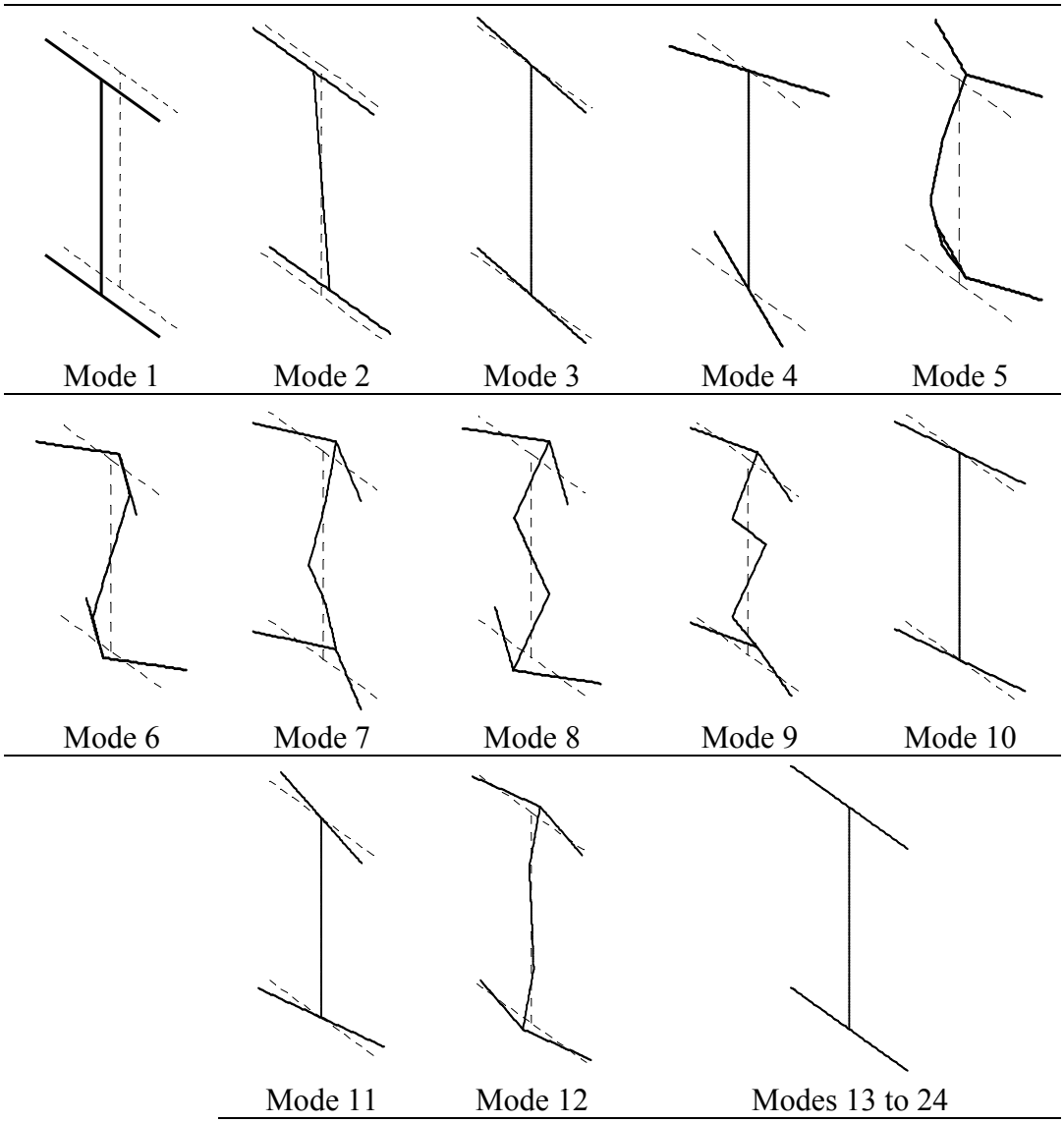

Fig. 6.30 - The unitary longitudinal warping displacements shapes for the orthogonal modes of deformation

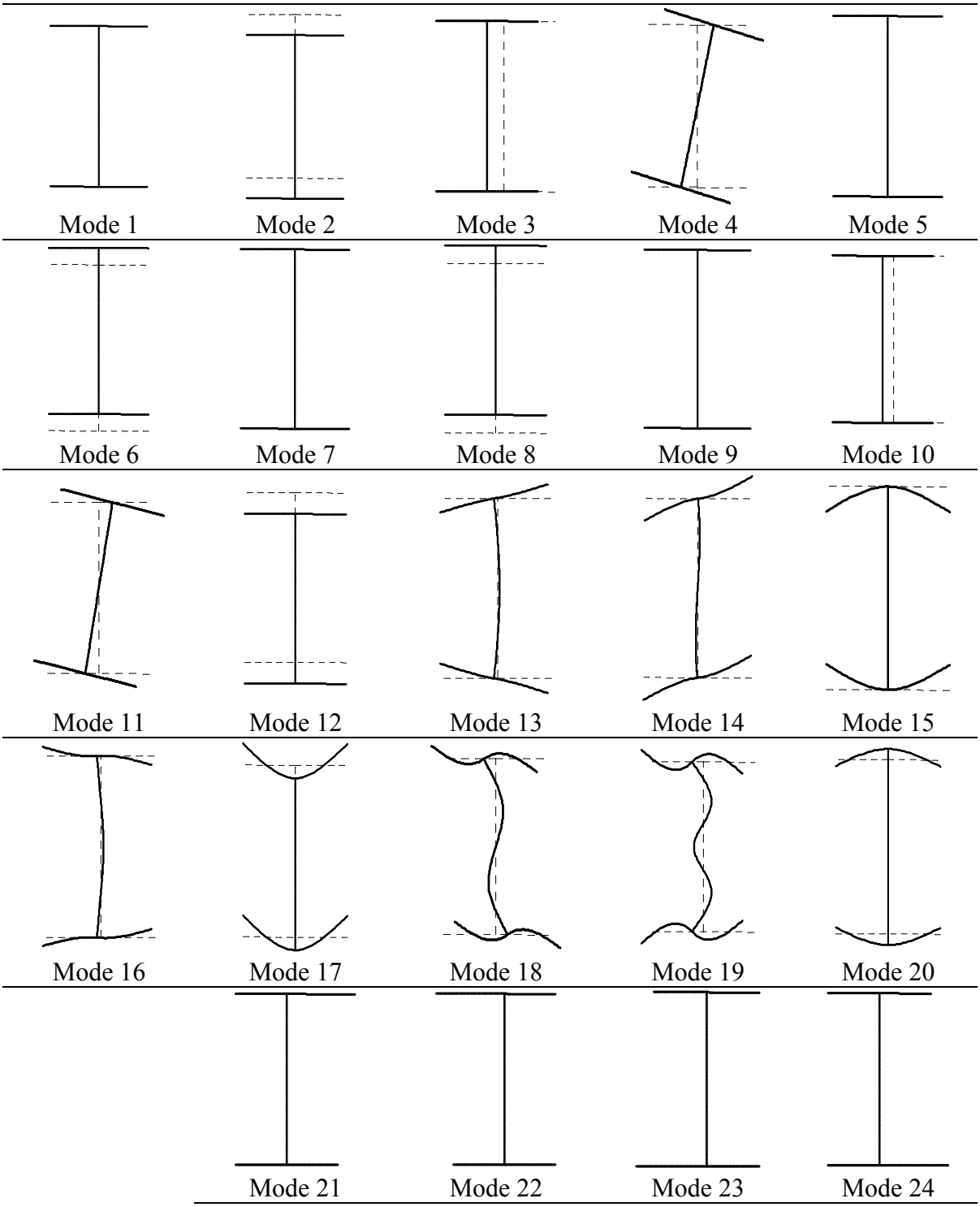

Fig. 6.31 - The unitary cross section displacements shapes for the orthogonal modes of deformation

The load was introduced as a longitudinal stress pattern $\sigma(s)$ illustrated in Fig. 6.32, whose stress distribution is equivalent to a binary with resultant 1 kNm, and these

stress distributions were applied with opposite sense, in relation to the other, in each edge cross section, so that the potential of the external loading is computed through the traditional way, i.e., using the expression:

$$\Pi = \sum_{k=1}^{n_{MD}} \left[\int_s t\, \sigma(s)_{x=L}\ {}^k u\, ds \times {}^k A' \Big|_{x=L} \right] + \sum_{k=1}^{n_{MD}} \left[\int_s t\, \sigma(s)_{x=0}\ {}^k u\, ds \times {}^k A' \Big|_{x=0} \right], \qquad (6.1)$$

and becomes a polynomial related to the generalized coordinates related to modes 2, 6, 8, and 12, since for these modes only the following integral

$$\int_s t\, \sigma(s)_{x=L}\ {}^k u\, ds\,, \qquad (6.2)$$

is non null. Therefore, only these modes are present in the potential of the external work and the corresponding coordinate functions were computed from the cinematic boundary conditions only, i.e., they are given by expressions (3.38), while for the remaining modes the corresponding coordinate functions were computed from the cinematic and the static boundary conditions, corresponding to expressions (3.37). It is noted here that, in the forthcoming examples of beams, the potential of the external loading is modelled this way, and so only the modes involved in potential of the external loading will be referred.

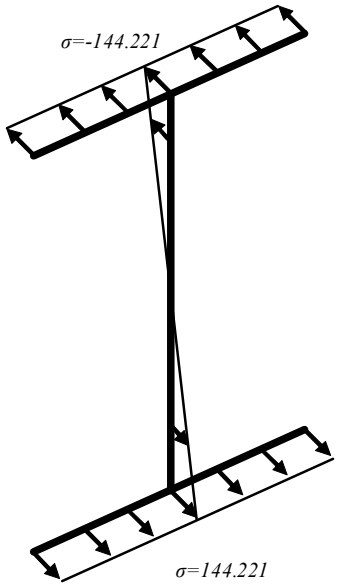

Fig. 6.32 - Longitudinal stress pattern $\sigma(s)$ for the introduction of the major axis bending moment – the units are computed to originate a resulting moment of 1 kNm

6.3.3.2 The critical behaviour

The critical behaviour is investigated here, and Fig. 6.33 validates the critical bending moments obtained using GBT by comparing them against the FSM solutions using CUFSM (Schaefer 2004). The agreement is perfect, despite the differences between both methods of analysis. The effect of the number of adopted coordinate functions per mode of deformation is illustrated in Fig. 6.34, showing that the critical bending moments are constant for the smaller lengths range, about 1.75 kNm, and the number of adopted polynomials is very important for this lengths range. For higher lengths, the global modes govern the buckling behaviour and the number of adopted polynomials has negligible influence in the critical behaviour of the beam. Fig. 6.35 shows the participation factors of the modes at the critical state and highlights the existence of the two referred buckling regions. For members with length smaller than *1000* mm modes 11, 12 and 14 rule the critical state, hence denoted by local plate buckling of the compressed web. For bigger lengths mode 3 rules the critical behaviour and buckling becomes global.

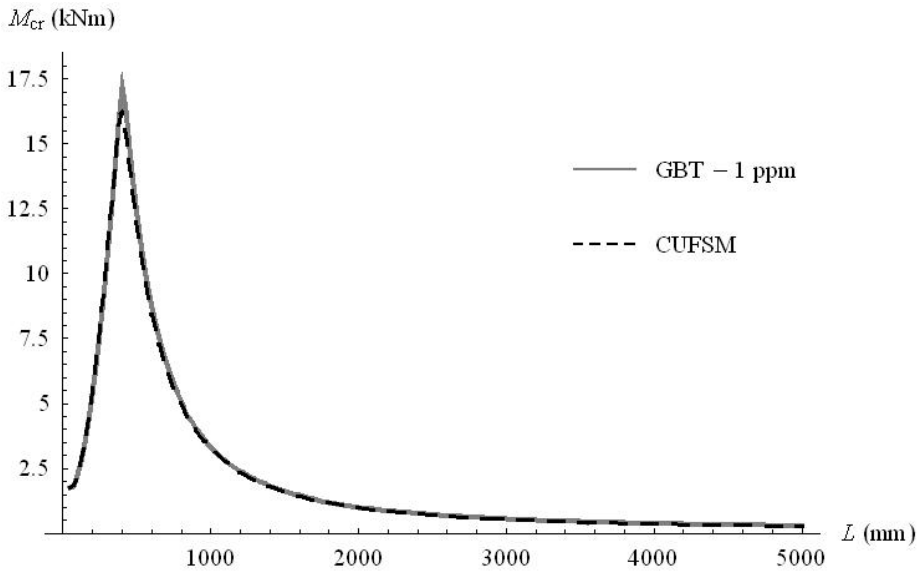

Fig. 6.33 – Buckling moments for the simply supported I-section beam under a constant major axis bending moment: benchmark comparison between GBT (with only one polynomial – with one half-wave – as coordinate function for each mode of deformation) and CUFSM analysis

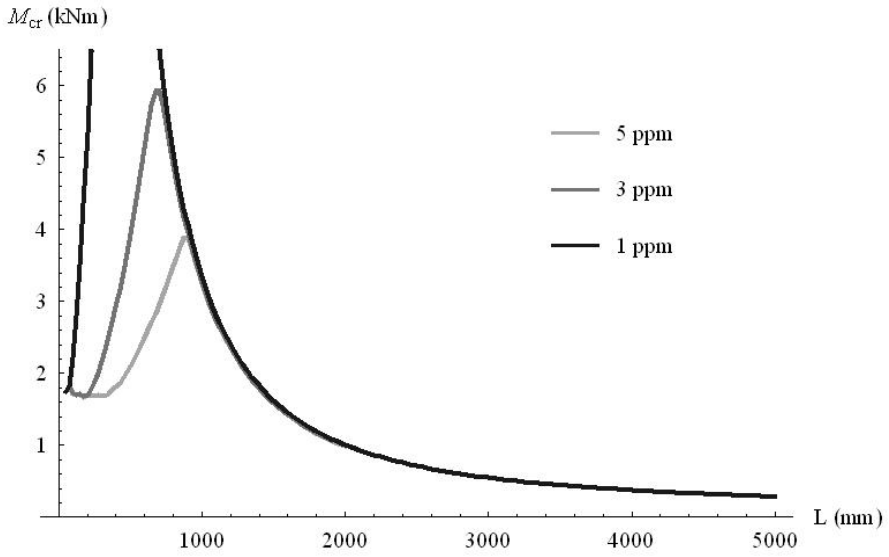

Fig. 6.34 – Buckling moments for the simply supported I-section beam under a constant major axis bending moment: the decrease of the critical moments with the increase of the number of adopted polynomials per mode of deformation

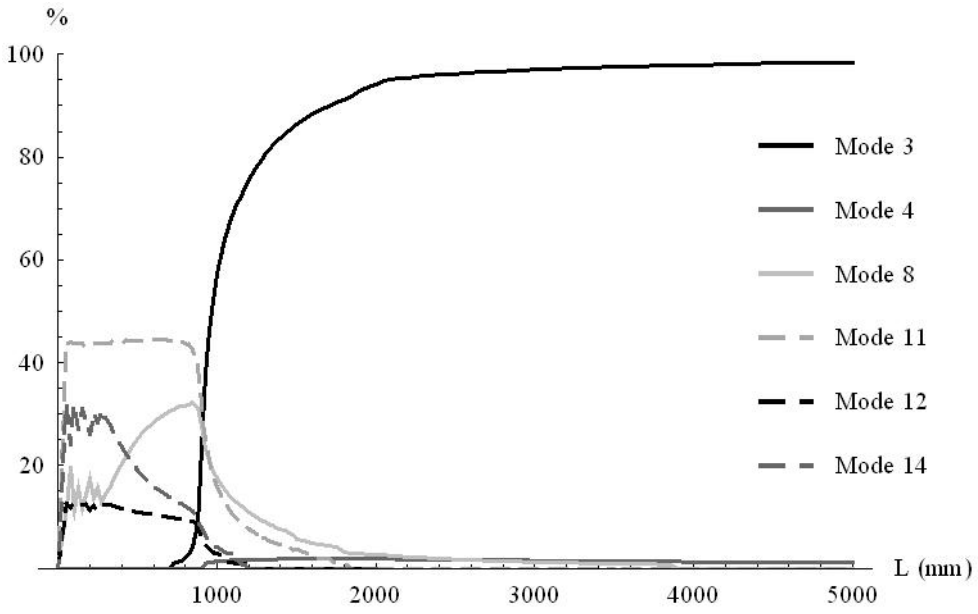

Fig. 6.35 – The simply supported I-section beam under a constant major axis bending moment: the participation of the modes of deformation at the critical state, considering 5 polynomials per mode

6.3.3.3 Post-buckling behaviour in the local plate buckling range

The post-buckling behaviour is analysed here for the length *L=400* mm, once more

through the procedures presented in Chapter 3. For this length modes 8, 11, 12 and 14 are the most active ones. Due to the limitations of the available computer resources, the post-buckling analysis was performed using only the first three polynomials from expressions (3.37) and (3.38) for the coordinate functions per mode of deformation, thus the resulting critical bending moment becomes equal to *2.98149* kNm.

Fig. 6.36 shows the vertical displacements observed at the compressed flange edge nodes, highlighting a stable symmetric post-buckling behaviour, while Fig. 6.37 presents the member's deformed shape for an applied moment of *5.75* kNm.

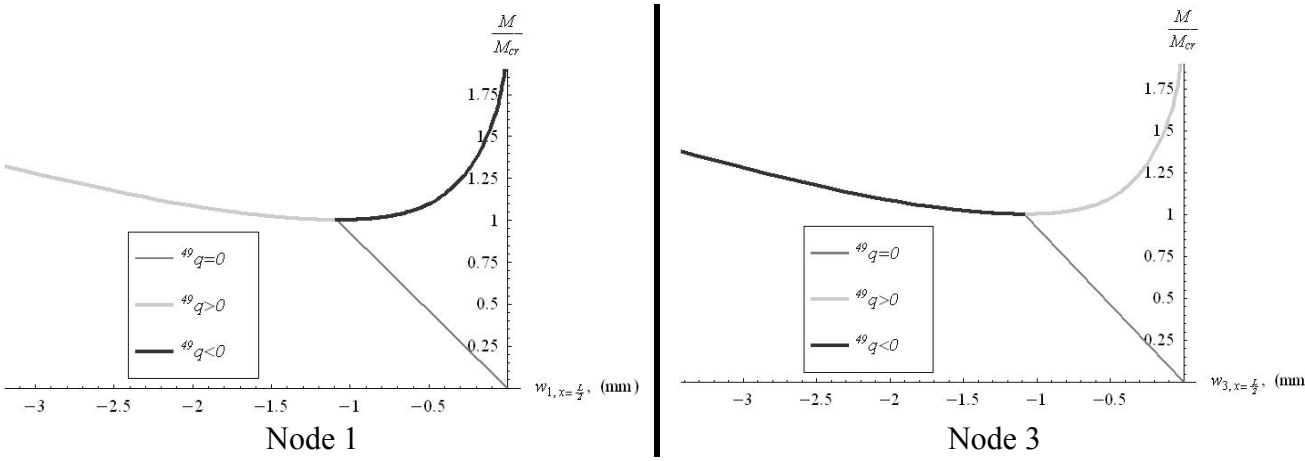

Fig. 6.36 – Vertical displacement of the compressed flange edge nodes 1 and 3 at the mid-span cross section

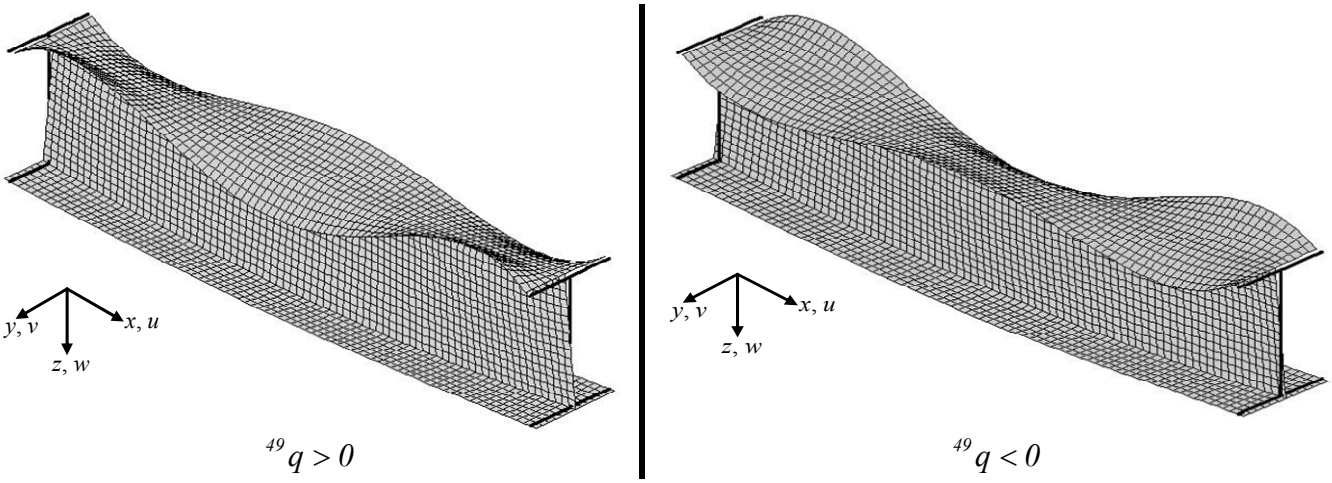

Fig. 6.37 – Member's deformed configuration for $M = 1.93 \times M_{CR}$ (all displacements are amplified by factor 5)

Figures 6.38 to 6.40 present the evolution of the longitudinal normal membrane stresses at the initial edge cross section, and it can be clearly observed, in Fig. 6.39, the shift of the neutral axis to the compressed part of the member, due to the decrease of the compressed stress in some points of the compressed part – actually, in certain points, the longitudinal stresses reach tensile values, implying a decrease of the member's stiffness.

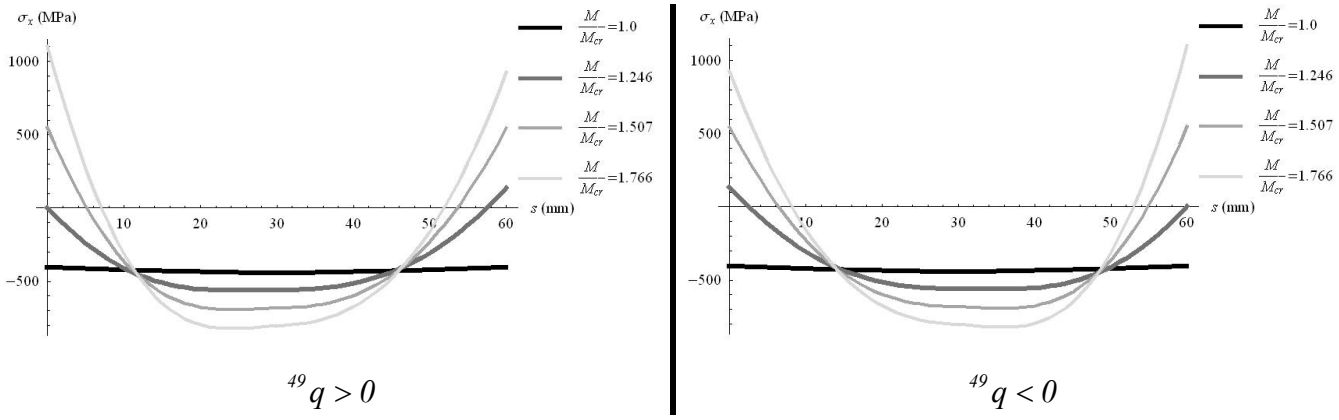

$^{49}q > 0$ $^{49}q < 0$

Fig. 6.38 - Longitudinal normal stresses σ_x along the compressed flange for $x=0$

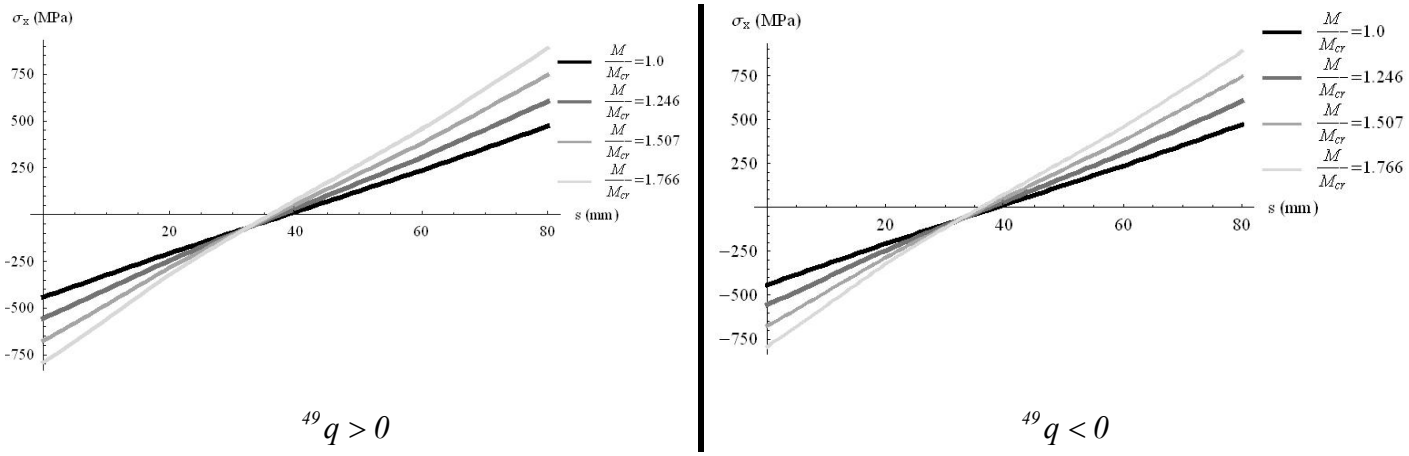

$^{49}q > 0$ $^{49}q < 0$

Fig. 6.39 - Longitudinal normal stresses σ_x along the web for $x=0$

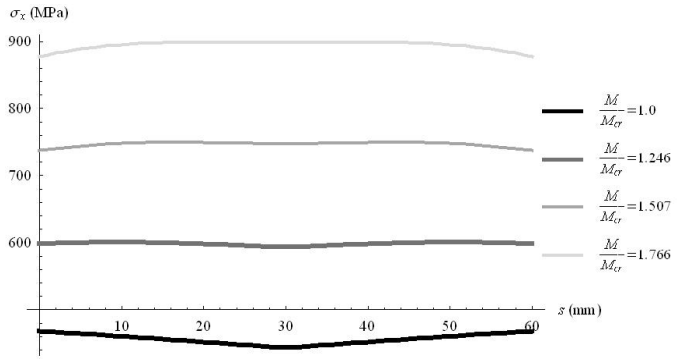

Fig. 6.40 - Longitudinal normal stresses σ_x along the traction flange for $x=0$
(similar for the positive and the negative branches of the post-buckling path)

6.4 – The bi-cellular closed cross section

6.4.1 Introduction

The extension of the GBT methodology to the analysis of multi-cellular closed cross sections with perpendicular plates is realized here and, for the quest of simplicity, is illustrated by a two cells section, described in Figure 6.41 – the generalization to a n-cells section becomes trivial. Just like in the I-section case, the inner nodes warping, plate bending and plate transversal extension modes pass over unchanged from Chapter 5 to the analysis of multi-cellular cross sections, and only the warping and plate distortional modes are transformed in order to accommodate the new cross section type geometric properties. For these later mode types, the scheme follows closely the one developed for I-sections and is explained here for the warping-plate distortional modes associated with main nodes 1 and 2 – once again, the generalization for the warping-plate distortional modes associated with the remaining nodes is trivial.

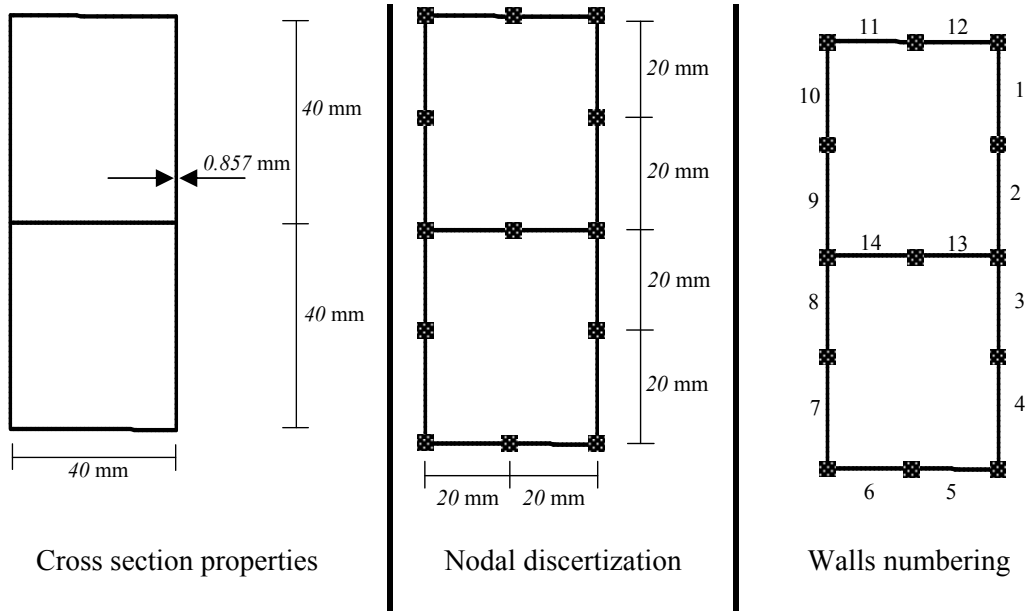

Fig. 41 - The two cells cross section

6.4.2 The basic modes involving warping of the main nodes and distortion of the main plates

Taking into account the wall and node numbering presented in Fig. 6.41and starting by establishing the warping mode associated with main node 1, first a unitary warping displacement at node 1 is introduced in a two-cells member with longitudinal length *dx* (along which it is considered that the modal amplitude function ${}^{k}A$ for any mode of deformation *k* is constant, together with its any order derivative, just like the previous cases), neglecting cross section continuity and in such a way that no plate distortion occurs at plates 1 and 6, as shown in Fig. 6.42-a). Then, continuity between consecutive plates is restored in terms of nodes translations, and so plate 2 is forced to twist an angle of

$$\gamma_2 = \frac{1}{b_1\, dx} \tag{6.3}$$

to accommodate the translation of node 2 in the perimeter's direction. After, plates 6, 1, 2, 3, 5, 6 and 7 bend transversally to render compatible the translational displacements between them. Finally, the resulting translational displacements are introduced in a displacements method problem related to the cross section, as shown in Chapter 5, to

derive the nodal rotations, again similarly to the I-section, and the cross section shows the shape presented in Figure 6.42-b).

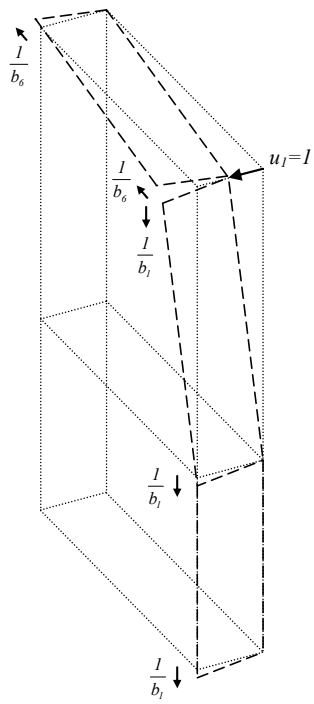

a) imposing a warping displacement to node 1, neglecting the continuity of the cross section at $x+dx$

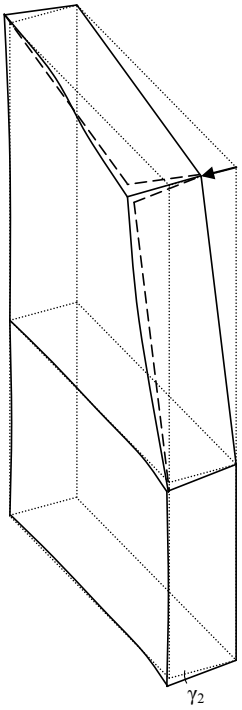

b) compatible rendering of the cross section

Fig. 6.42 - Setting up the warping mode associated with node 1

For the warping modes associated with node 2, one starts by imposing a unitary longitudinal displacement this node, neglecting cross section continuity, as shown in Fig. 6.43-a). For the compatible rendering of translational displacements in cross section plane at node 2, two ways are possible: i) plates 1 and 7 suffer transverse bending with no distortion, and plate 2 has to suffer distortion – Figure 6.43-b), or ii) plates 2 and 7 bend in the transversal direction while plate 1 suffers also distortion – Fig. 6.43-c. Since these two distinct configurations are possible, both shall be considered in the analysis and, similarly to the open I-section previously analysed, two distinct modes of deformation correspond to the warping of one main node.

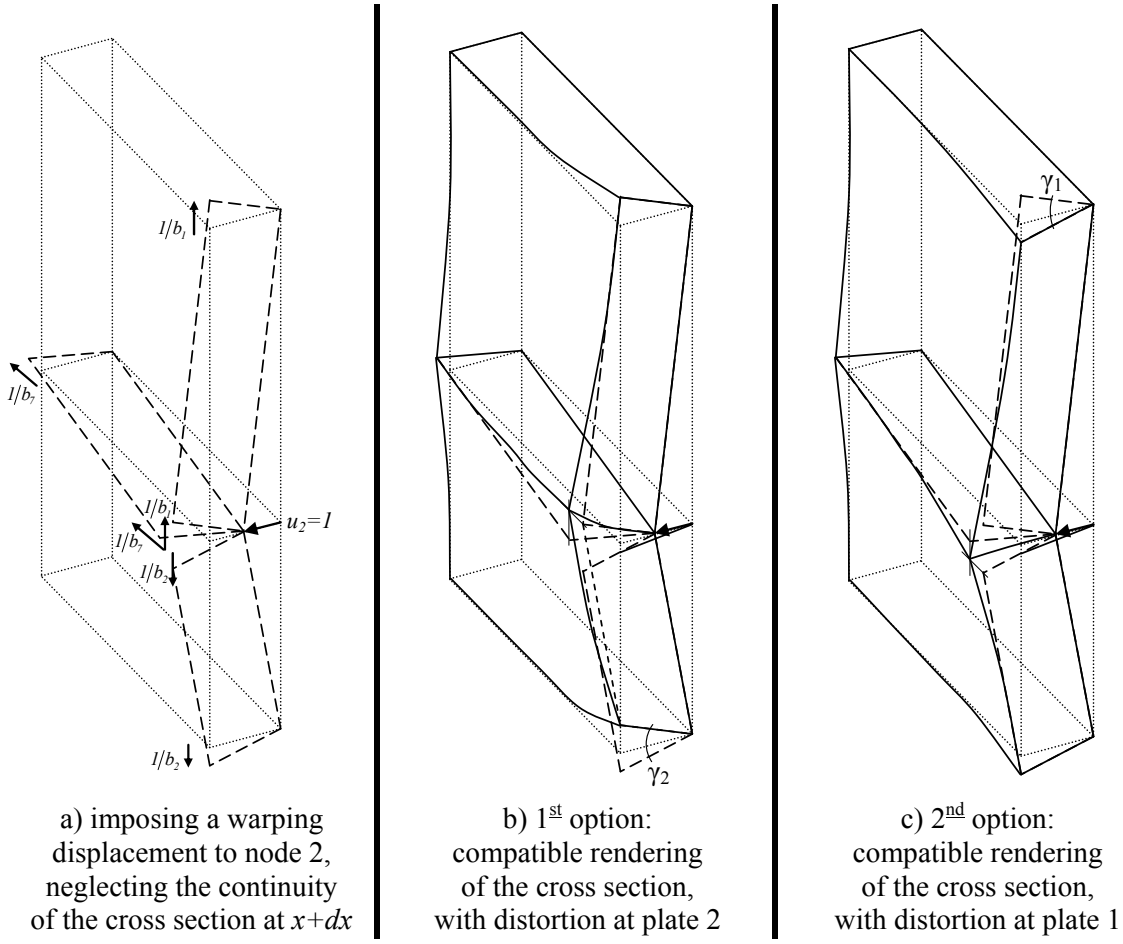

a) imposing a warping displacement to node 2, neglecting the continuity of the cross section at $x+dx$

b) 1st option: compatible rendering of the cross section, with distortion at plate 2

c) 2nd option: compatible rendering of the cross section, with distortion at plate 1

Fig. 6.43 - Setting up the warping modes associated with node 2

The establishment of the warping modes for nodes 3, 4 and 6 follows the procedure of mode 1, and the two warping modes related to node 5 follow the scheme of the modes associated with warping of node 2. Finally, 8 modes are obtained, involving distortion of plates 1, 2, 4 and 5. So, for the establishment of the plate distortional modes, only those associated with twist of plates 3, 6 and 7 are retained, since the plate distortional modes related to the remaining plates can be obtained as linear combination of the first 8 modes. In the end, 11 warping-plate distortional modes are obtained and, in the following example, these modes are illustrated for a real bi-cellular cross section.

6.5 – Illustrative example for the bi-cellular closed cross section

6.5.1 Presentation and derivation of the modes of deformation

To illustrate the extension of the GBT scheme to multi-cellular rectangular cross sections explained in the paragraph just above, the buckling and post-buckling behaviours of a two-cells member, whose cross section is defined in Figure 6.41, are analysed. The GBT analysis of this cross section starts by generating 11 warping-plate distortional modes shown in Figures 6.44 and 6.45, which, together with the remaining plate bending, inner nodes warping and plate transversal extension modes, generate the 32 orthogonal modes of deformation shown in Figures 6.46 and 6.47, 16 of them being classified as rigid-body modes since they show no transverse bending nor transverse extension.

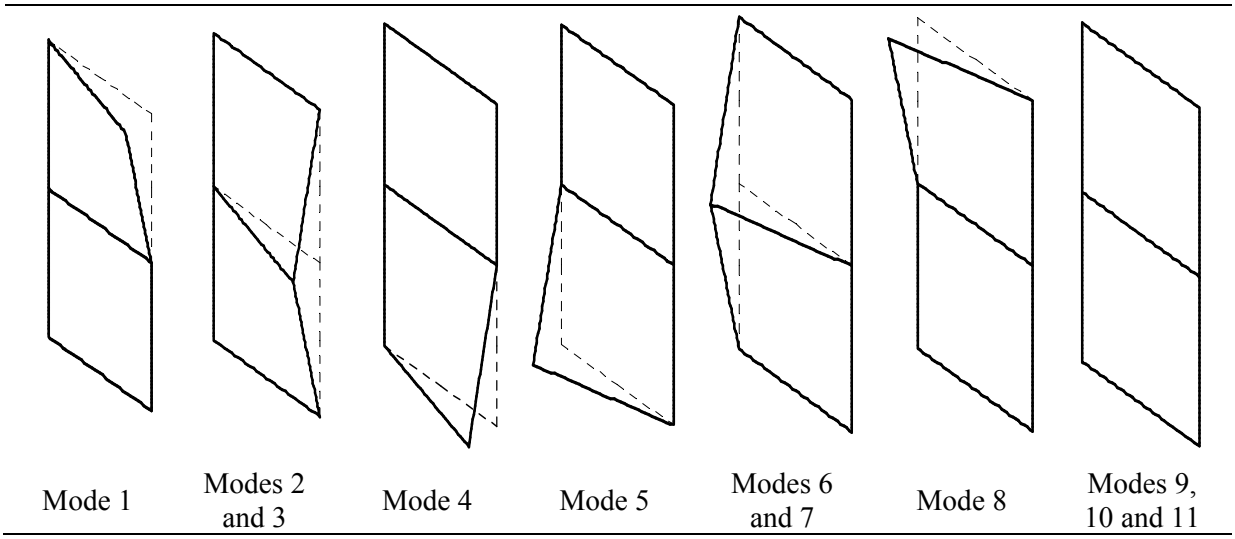

Fig. 6.44 - Longitudinal displacements for the initial warping-plate distortion mode of deformation

Like the closed RHS cross section analysed in Chapter 5 but in opposition to the open section case previously analysed – the open I-section –, for present cross section the torsion mode does not appear explicitly but can be obtained through a linear combination of modes 5, 9 and 16. Observing the rigid-body modes, mode 1 corresponds to axial elongation, modes 2 and 3 are the major and minor axis bendings, respectively, modes 5, 9

and 16 are torsion modes, affected by "shear-lag", and the remaining modes are involved with "shear-lag" deformations, exclusively or combined with bending. For the distortional modes, modes 17 to 25 are associated with transverse bending of the plates only, and modes 26 to 32 correspond mainly to the transverse extension of the cross section's plates.

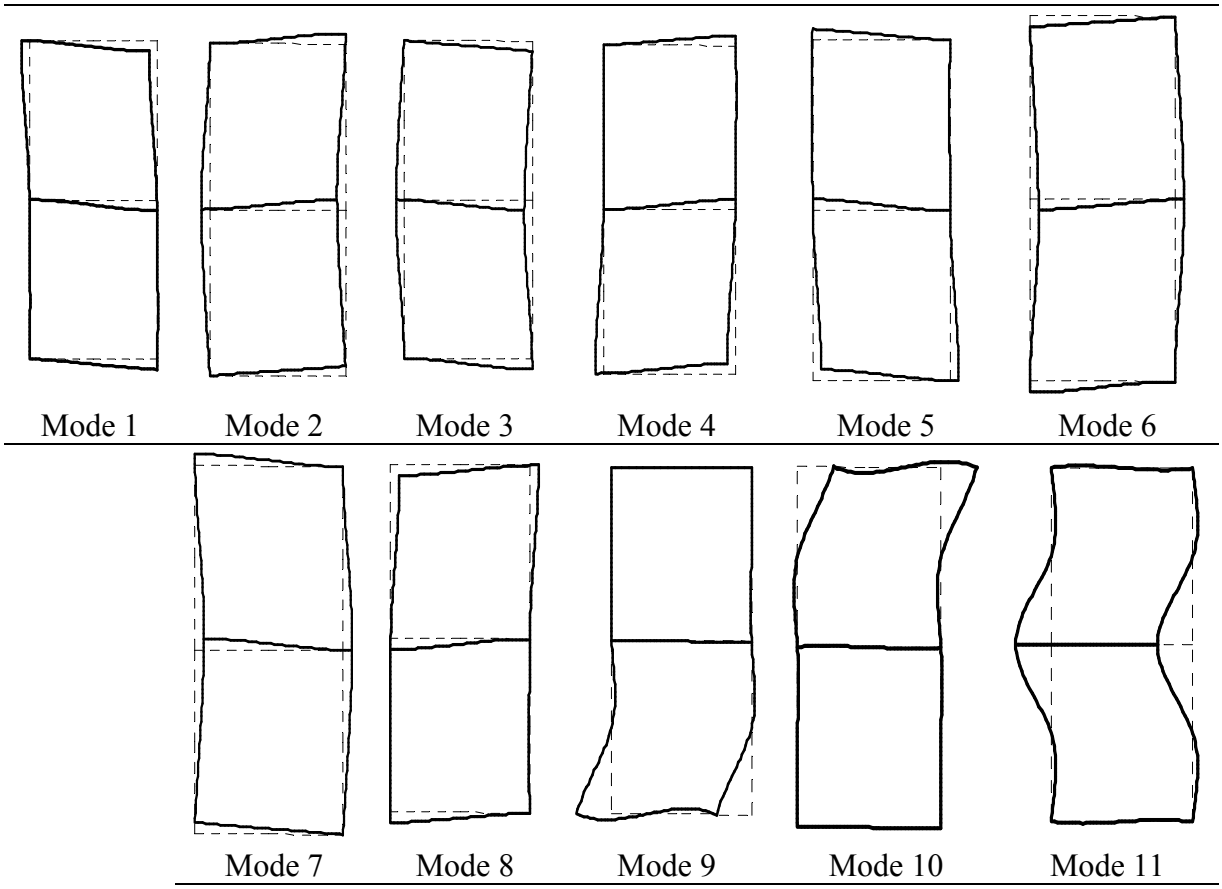

Fig. 6.45 - Cross section plane displacements for the initial warping-plate distortion mode of deformation

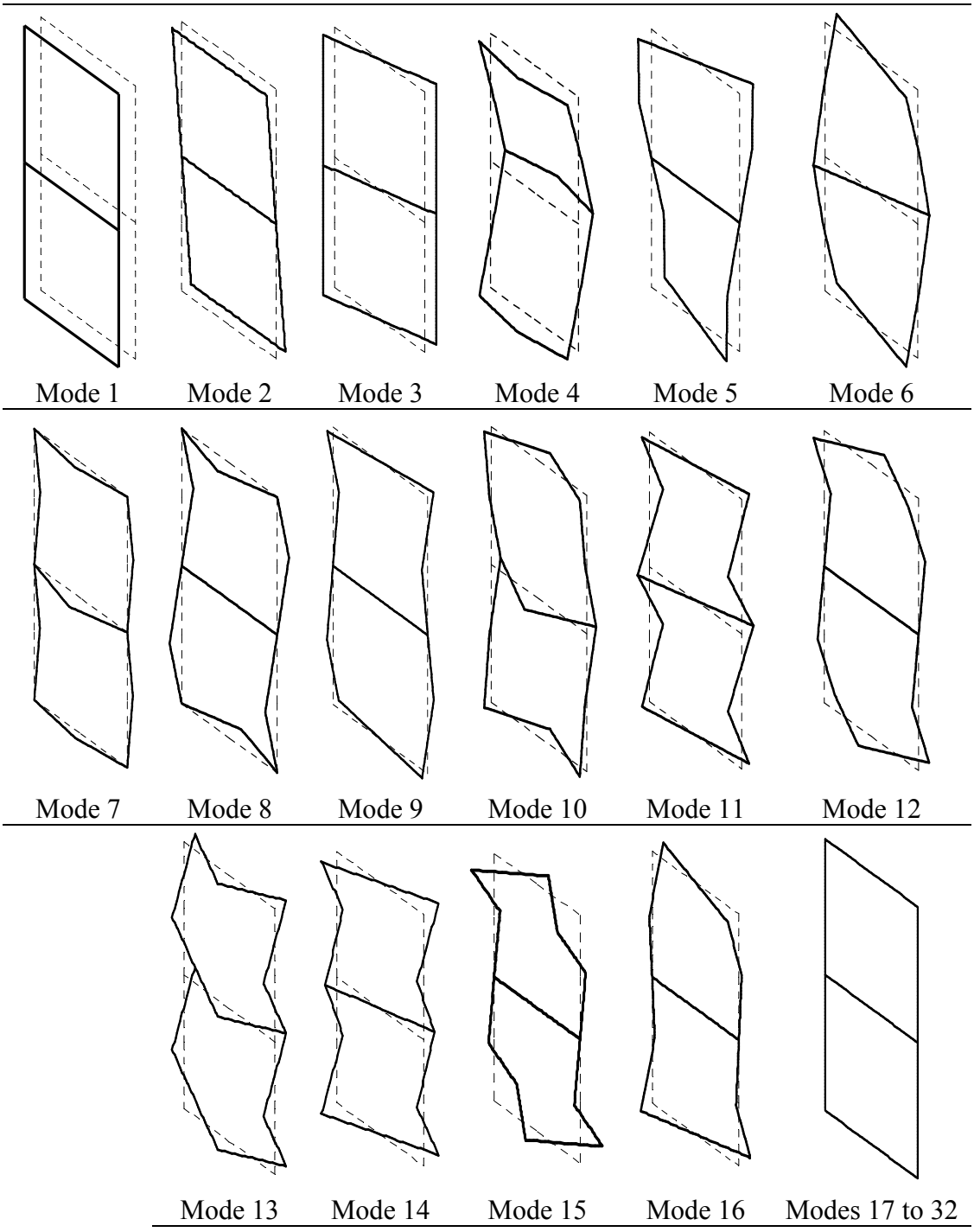

Fig. 6.46 - The unitary longitudinal warping displacements shapes for the orthogonal modes of deformation

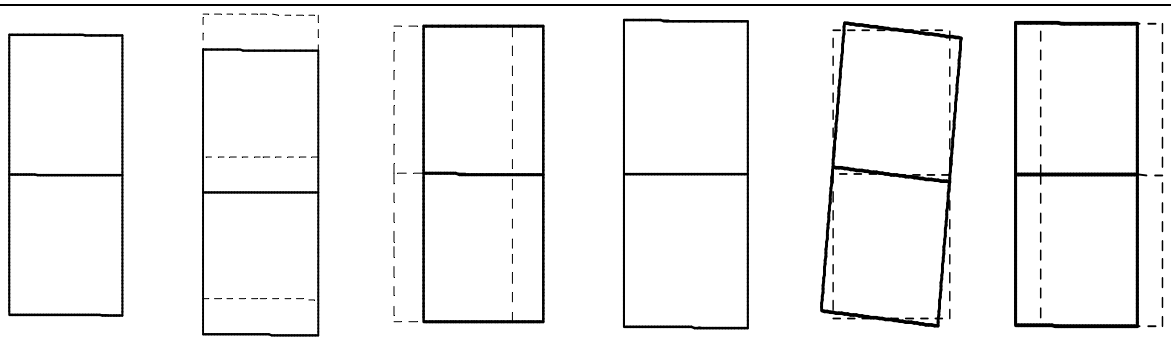

Mode 1 Mode 2 Mode 3 Mode 4 Mode 5 Mode 6

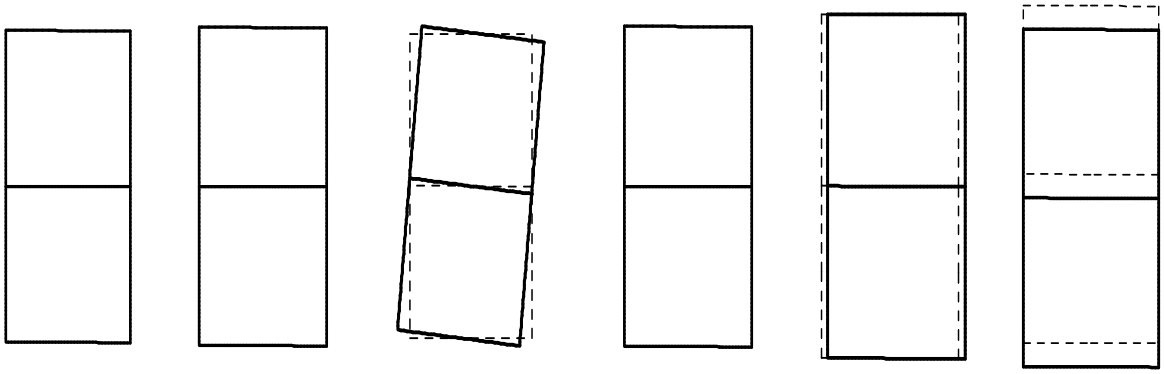

Mode 7 Mode 8 Mode 9 Mode 10 Mode 11 Mode 12

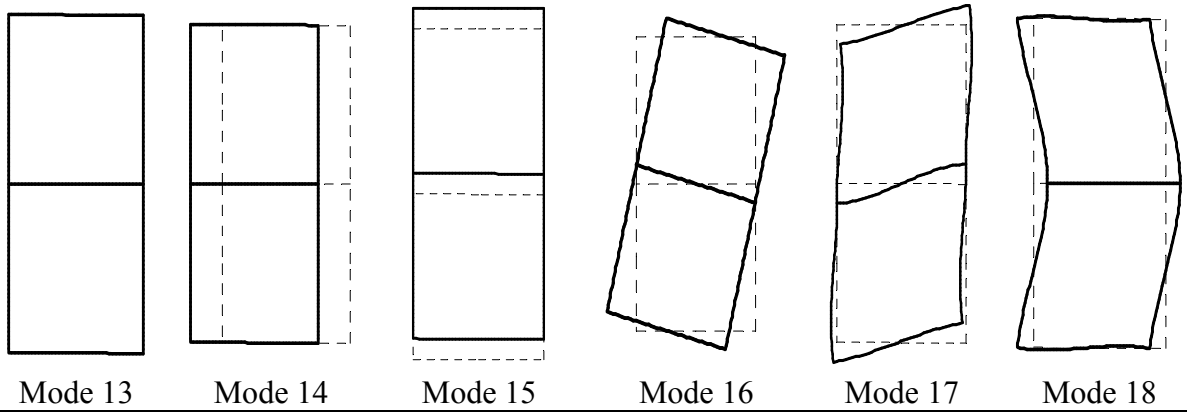

Mode 13 Mode 14 Mode 15 Mode 16 Mode 17 Mode 18

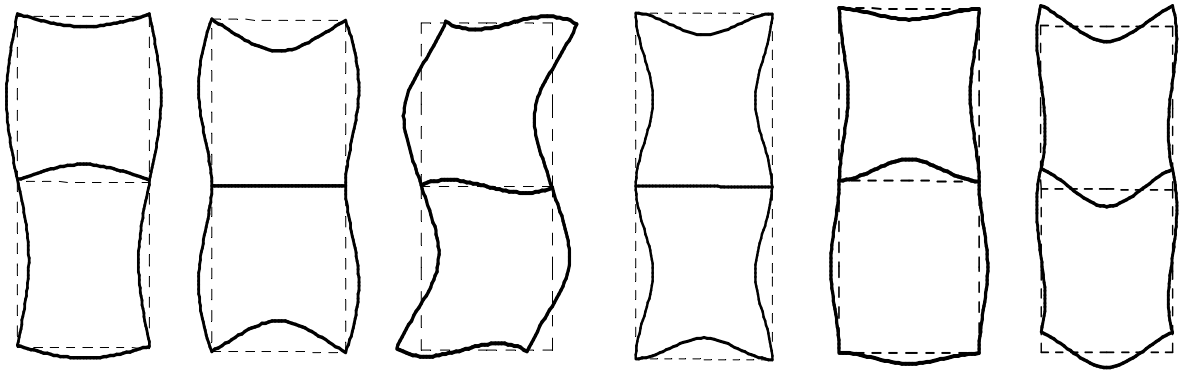

Mode 19 Mode 20 Mode 21 Mode 22 Mode 23 Mode 24

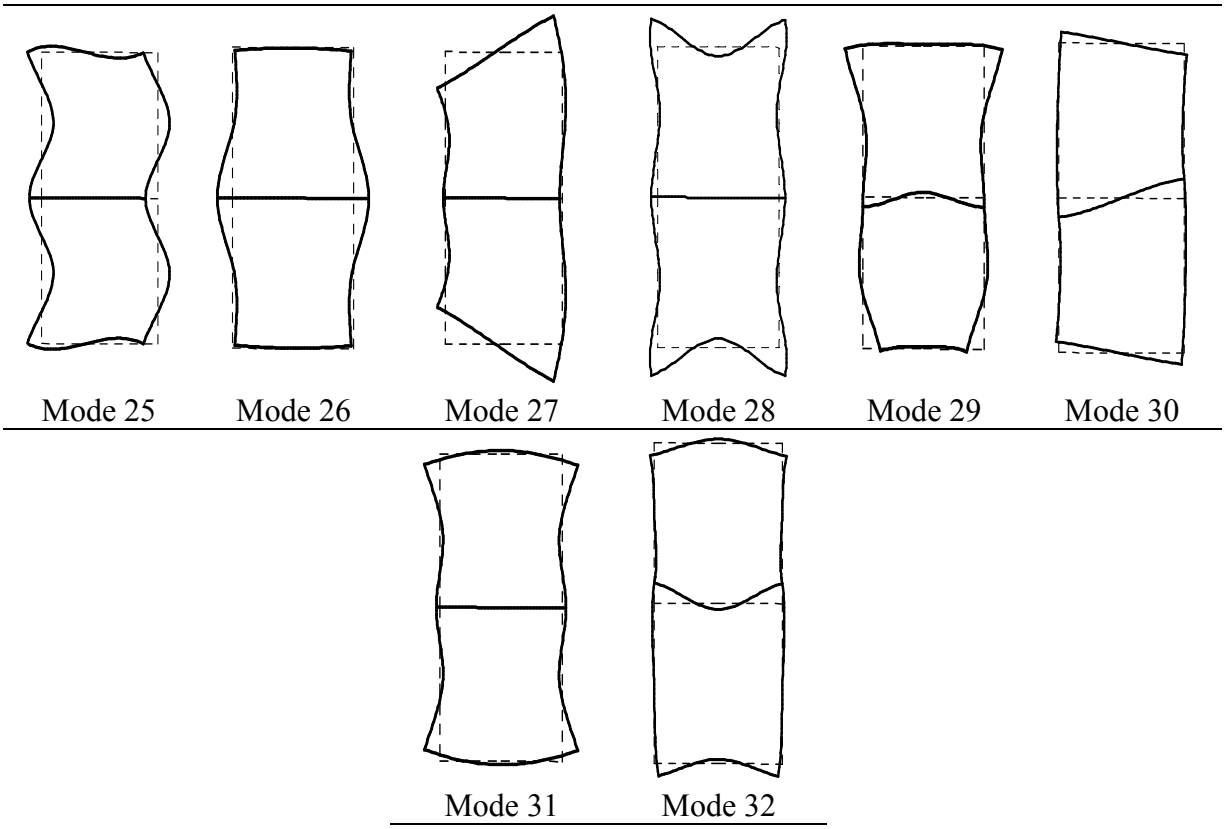

Fig. 6.47 - The unitary displacements shapes along the cross section plane for the orthogonal modes of deformation

6.5.2 The critical behaviour for the simply supported column

Using the coordinate function (3.24) for mode 1 and the coordinate function (3.37-a) for the remaining modes – considering only one half-wave – the buckling behaviour of the simply supported column of Figure 6.48 is analysed, and the graphic of Figure 6.49 is obtained, where the critical loads from the GBT analysis are compared to those arising from the FSM program CUFSM (Schafer 2003), a perfect agreement between both analyses being observed. Then, the precision of the analysis is increased by augmenting the number of coordinate functions for modes 2 to 32, as far as the available computer resources allow, and the graphics of Figures 6.50 and 6.51 for the buckling loads and modal participation at the critical state are obtained and show two distinct buckling zones: for smaller lengths the compressed column buckles through a local plate pattern, for which

modes 15, 19 and 24 are the most relevant, while for higher lengths buckling is global, ruled almost exclusively by mode 3 – minor axis bending. As expected, the number of half-waves is very relevant in the local plate buckling range and in Figure 6.50 it is observed how the critical load decreases when the number of coordinate functions is augmented in the local plate buckling domain, where the critical load becomes nearly constant against the member's length, with a value of P_{cr} around *78* kN.

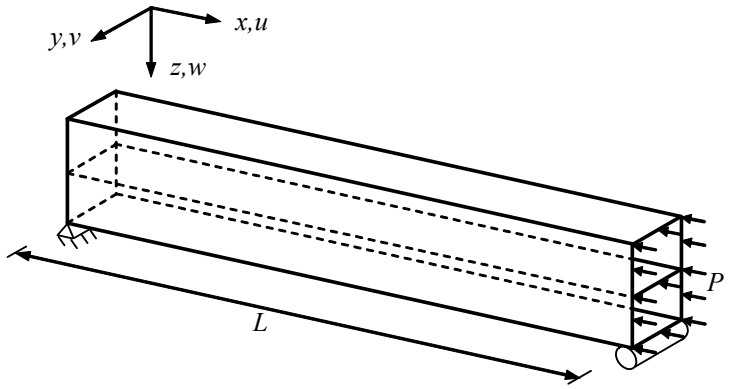

Fig. 6.48 - The compressed bi-cellular column

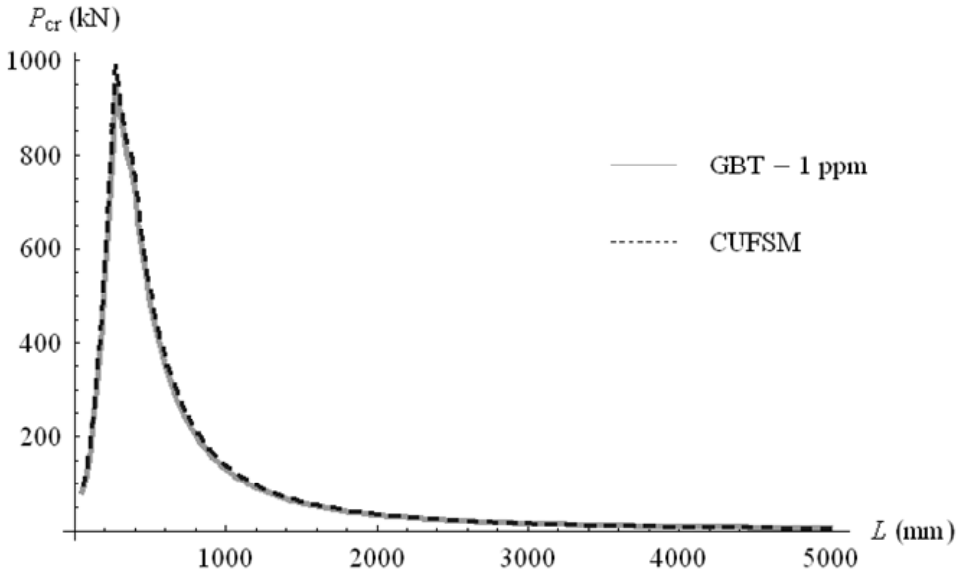

Fig. 6.6.49– Buckling loads for the simply supported bi-cellular section column under uniform compression: benchmark comparison between GBT (with only the first polynomial – with one half-wave – as coordinate function for each mode of deformation 2 and higher) and CUFSM analysis

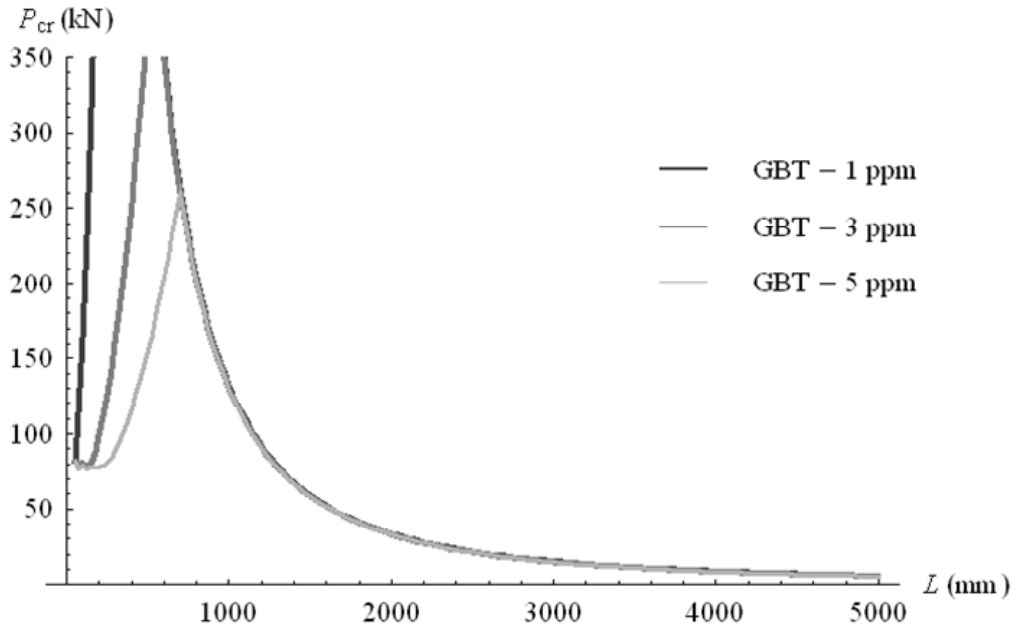

Fig. 6.50 – Buckling loads for the simply supported bi-cellular section column under uniform compression: decrease of the critical load with the number of adopted polynomials per mode of deformation

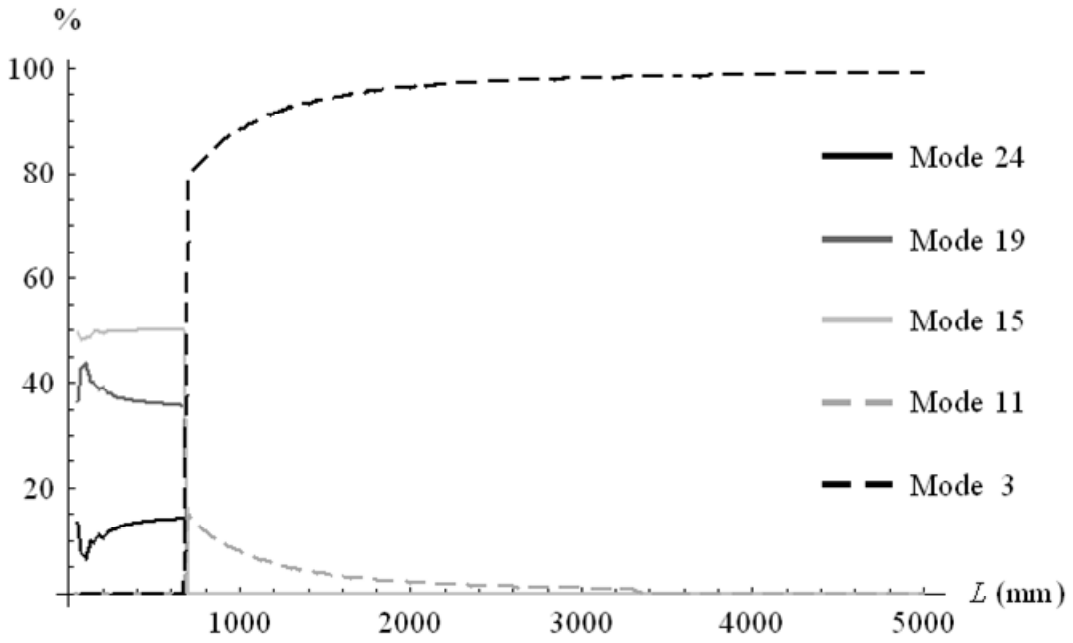

Fig. 6.51 – Modal participations at the critical state for the compressed bi-cellular section column, considering 5 polynomials per mode of deformation

6.5.3 Post-buckling behaviour in the cross section distortional range

The post-buckling behaviour is inspected here for a member's length of *250* mm, standing in the plate buckling lengths range, corresponding to a critical load of *80.905* kN. As coordinate functions, for modes 2 and higher only polynomials (3.37 a), (3.37 c) and (3.37 e) are adopted due to computer limitations. For the search of the post-buckling equilibrium path, the coordinate associated with mode 19 and with coordinate function (3.37-e) was chosen to control the calculations. Fig. 6.52 describes the displacement of the mid-point of the lateral wall, showing a stable post-buckling behaviour, and Figures 6.53 and 6.54 present the overall shape of the member for a load of *107.852* kN, for both branches of the post-buckling path. The post-buckling path was shown to be very stiff, so no significant changes were observed in the longitudinal stresses due to buckling. Observing Figures 6.52 and 6.53 it can be viewed that the longitudinal displacement for the edge cross section has higher magnitude than the transversal ones, implying great stiffness of the member – actually, it showed no significant reduction during the transition between the fundamental path to the post-buckling one.

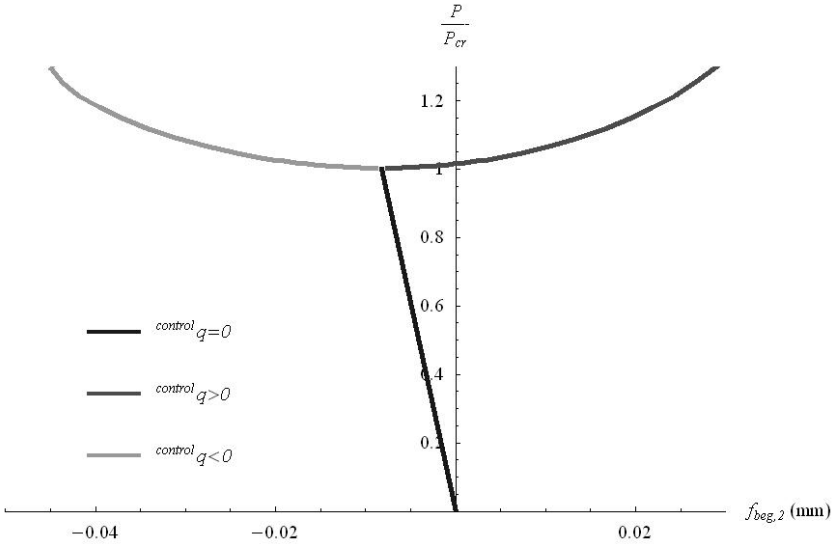

Fig. 6.52 – Horizontal displacement of the initial node of secondary wall N. 2, at $x = \frac{3}{10}L$

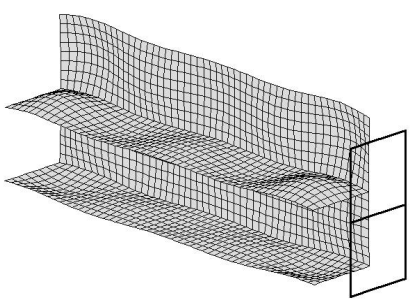

a) View without walls 7, 8, 9, 10, 11 and 12

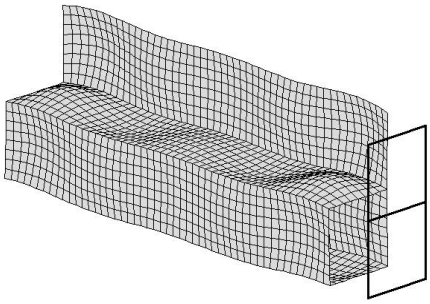

b) View without walls 9, 10, 11 and 12

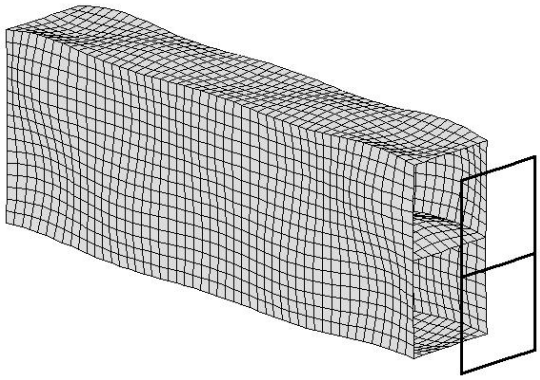

c) General view

Fig. 6.53 – Member's deformed configuration for $P = 1.33 \times P_{CR}$, for ${}^{control}q > 0$ (all displacements are amplified by a factor 50)

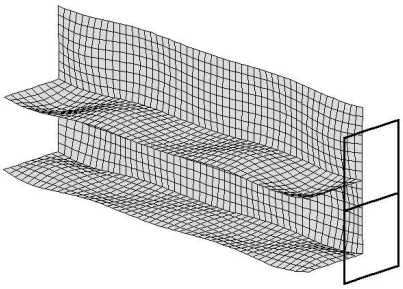

a) View without walls 7, 8, 9, 10, 11 and 12

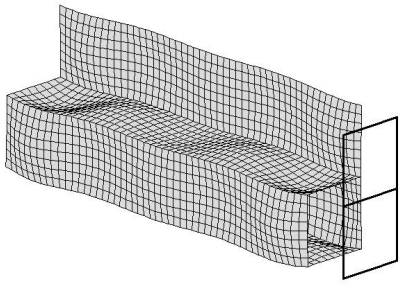

b) View without walls 9, 10, 11 and 12

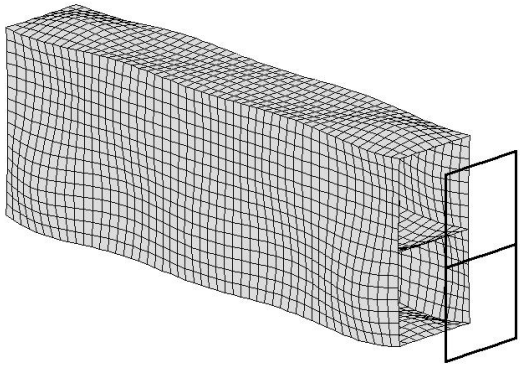

c) General view

Fig. 6.54 – Member's deformed configuration for $P = 1.33 \times P_{CR}$, for ${}^{control}q < 0$ (all displacements are amplified by a factor 50)

6.6 – GBT analysis of a any-type cross section member

6.6.1 Introduction

From the enhancements contained in the two previous particular cases – the I- and the bi-cellular sections – the following conclusions may be drawn with respect to the enlargement of GBT skills to the analysis of a general cross section:

i) The procedure developed for closed mono-cellular and open non-branched sections for the inner nodes warping, plate bending and plate transverse extension modes performed perfectly in the analysis of the I- and bi-cellular cross sections, so this strategy is kept in the analysis of a general cross section.

ii) The basic modes of deformation associated with warping of the main nodes and plates distortion were built together in the analysis of I- and bi-cellular sections, and both deformation patterns were combined to perform the compatible rendering of cross section's plane displacements at branching points, often generating more that one mode of deformation for one longitudinal displacements pattern (the warping displacements are established through the traditional GBT scheme with no need of special treatment); this constitutes the withdraw of one traditional GBT property and did not carry any problem in the member's analysis, since in the end all resulting modes of deformation were linearly independent.

iii) The fact that several modes of deformation may have similar longitudinal displacements patterns is related to the existence of more than one compatible rendering possibilities for the cross sectional translation displacements, provoked by the f_s displacements, along the perimeter's direction, that occur after having imposed the warping displacement to the main node with null distortion at the plates; since it was not possible to render compatible all plates

connected to a branching node at the same time, the rendering process for a node that connects three or more plates was performed through the traditional GBT way by pairs of plates, the remaining plates being forced to twist – in the end, all possible combinations were retained.

iv) This fact leads to several admissible configurations for the cross section's displacements, associated with only one warping displacements configuration, and their number is increased with the increasing number of branching points at the cross section – note that, after having analysed one branching node, if any plate connected to this node is connected, in the other side, to other branching node, more possibilities to the in plane's displacements shape will exist.

v) Despite of the existence of several modes with similar warping displacements patterns, the resulting n_{WD} basic warping-plate distortion modes of deformation were linearly independent and the corresponding equilibrium matrix $\boldsymbol{C}$ was always invertible, which is strictly necessary to solve the generalized eigenproblems involved in the orthogonalization procedure; since the calculus of matrix $\boldsymbol{C}$ involves all displacements of a plate, u, f_s (indirectly) and f, it shall be investigated if its rank is a good measure of the number of linearly independent warping-plate distortional modes of deformation for a general cross section.

All in all, based on the aspects described above, the procedure used in the above paragraphs for the I- and the bi-cellular sections for the establishment of the warping-plate distortional modes of deformation, will be extended below for a general cross section having several branching nodes connecting several plates each one, and whose plates can form a generic angle between them. Moreover, if the resulting modes of deformation are linearly dependant, a selection process to extract the independent modes of deformation, those that constitute the vector space basis for the modes of deformation and that will be

used after in the member's global analysis, will be released, based on the rank of matrix ***C*** related only with the basic warping-plate distortional modes. Finally, in order to illustrate the general scheme, the stability behaviour of two hollow flange sections is analysed.

6.6.2 – A general rule for compatible rendering of the cross-section's plane displacements

In the above examples of I- and bi-cellular cross sections, first the warping modes were established and only after the pure plate distortional modes were built, these later by imposing the distortional displacements patterns to those plates that did not twist during the establishment of the warping modes. So, the problem of enhancing GBT to a general analysis consists in creating a compatible rendering procedure for a general cross section that generates all relevant information to the member's equilibrium system, i.e., that is capable of generating all possible linearly independent warping-plate distortional modes of deformation. The strategy considered here is to generate all possible modes of deformation, considering all feasible compatible rendering options for the cross sectional plane displacements, and after to extract the linearly independent modes.

Starting by the compatible rendering procedure for the cross sectional's plane displacements, let's admit, with no loss of generality, that Figure 6.55 represents the plates configuration for a part of a general cross section just after having imposed the warping displacements pattern related to a unitary longitudinal displacement at node *j* (the patterned arrows represent the adopted plates direction) – at this step, only the main plates connected to node *j* move along their perimeter and outwards the node, with no distortion, each plate *k* experiencing a displacement along the perimeter's direction given by:

$$f_{s,k} = \frac{1}{b_k},\ k=i+1,\ i+2,\ i+4 \qquad (6.4)$$

as shown in the figure.

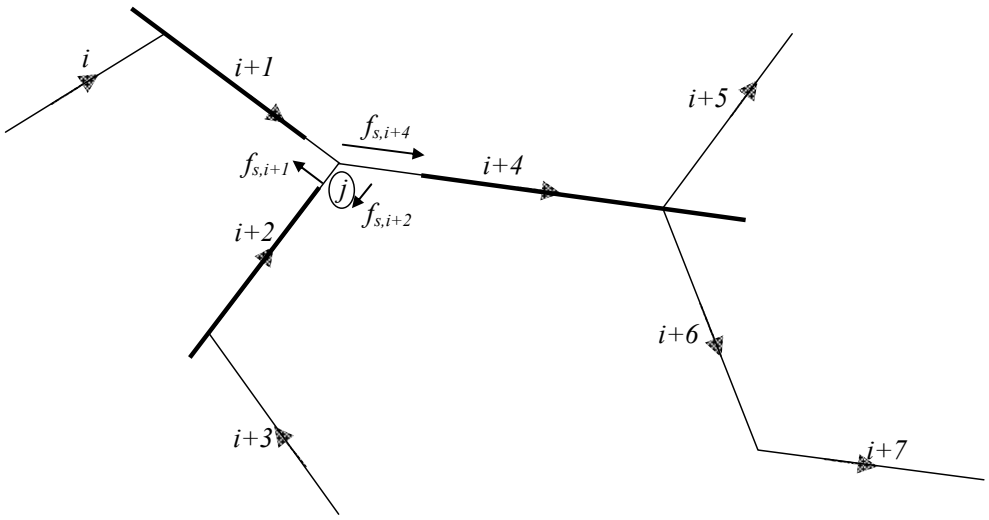

Fig. 6.55 – Cross section's displacements just after having imposed $u_j=1$

Now, the task is merely to derive the cross section's plane translational displacements at the main nodes, which will be used as prescribed displacements in the displacements method problem that computes the rotations of all nodes (thus defining completely all movements of the plates along the entire cross section), and that restore continuity along the cross section, by using only feasible deformation patterns for the plates. Therefore, concern will be taken upon the chord's movements for all plates only. Starting at main node *j* (the one that has been longitudinally displaced), plates *i+1*, *i+2* and *i+4* must be reconnected, but it is not possible to do it for the three plates at once, only for two at a time. Consequently, the three existing options must be carried out, as shown in Figure 6.56-a), where plate *i+4* is dragged to connect to point $P_{i+1,i+2}$, obtained as the concordance point between plates *i+1* and *i+2* through the traditional GBT scheme, Figure 6.56-b) , where plate *i+2* is dragged to connect to point $P_{i+1,i+4}$, and Figure 6.56-c), where plate *i+1* is dragged to connect to point $P_{i+2,i+4}$. In Figure 6.56 a), b) and c), the displacements obtained by dragging are signalled as f_s^* or f^*.

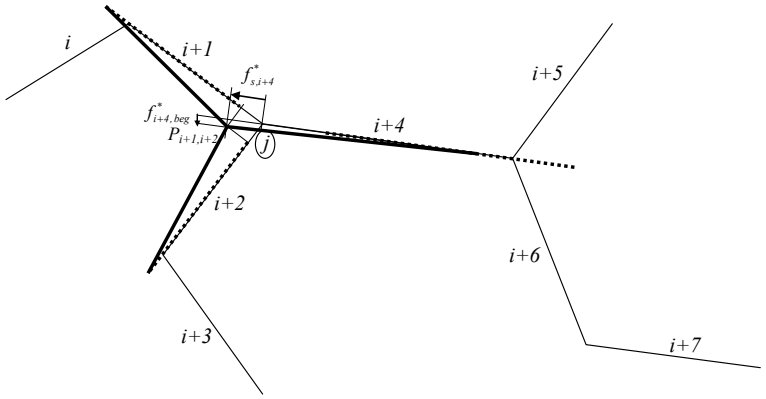

a) Option 1: starting by rendering compatible the displacements between plates *i+1* and *i+2* (plate *i+4* twists).

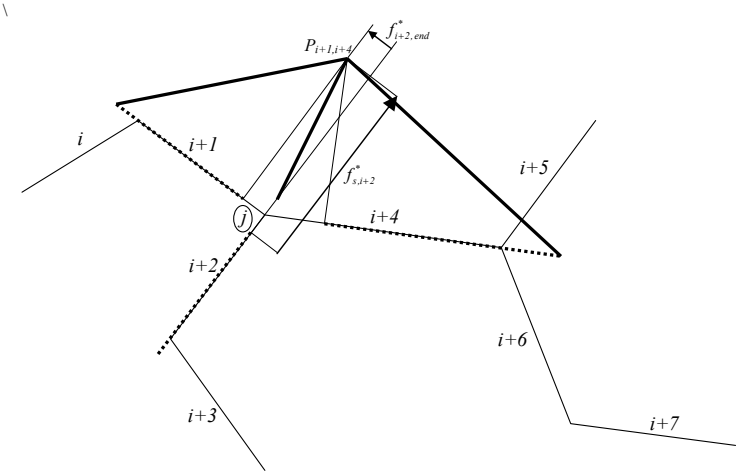

b) Option 2: starting by rendering compatible the displacements between plates *i+1* and *i+4* (plate *i+2* twists).

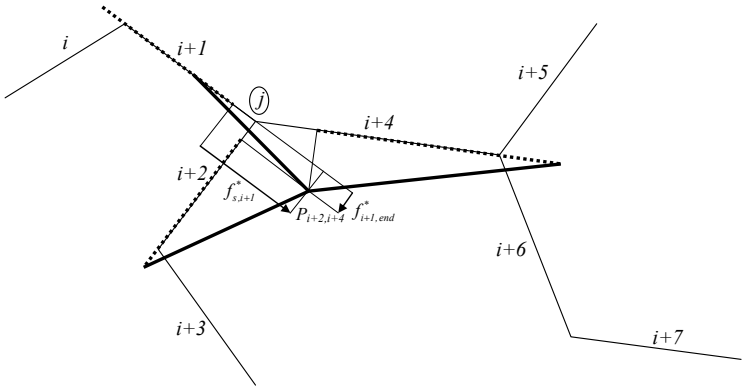

c) Option 3: starting by rendering compatible the displacements between plates *i+2* and *i+4* (plate *i+1* twists).

Fig. 6.56 – Compatible rendering configurations associated with node *j* – step 1

Subsequently, the compatible rendering procedure proceeds for each option of Fig. 6.56, independently from the others, and is illustrated here just for option 1, the remaining ones being treated similarly. From now on plate *i+4* can only suffer displacements provoked by transverse bending and then, as for node *j*, for the compatible rendering of the end node of plate *i+4* two possibilities exist, shown in Fig. 6.57: it can be done between plates *i+4* and *i+5* through the traditional GBT scheme based on transverse bending only with distortion at plate *i+6*, shown in Fig. 6.57-a) (option 1.1), or between plates *i+4* and *i+6*, with distortion at plate *i+5*, shown in Fig. 6.57-b) (option 1.2). Both ways are considered, thus generating two distinct configurations from option 1, each one generating (at least) one distinct mode of deformation. Note that each remaining option represented above, options 2 and 3, will give rise to more than one mode of deformation through the present scheme, for example options 2.1, 2.2, 3.1 and 3.2, thus the total number of resulting modes of deformation may have a great increment.

Finally, the pure plate distortional modes of deformation are computed similarly to the I- and bi-cellular sections considering, and using the present scheme, all possibilities of compatible rendering between plates shall be accounted for. They are computed only for those plates that did not experience twist before – if the plate distortional modes are computed for all plates, including those that have experienced distortion during the establishment of the warping modes, no problem will occur since in the end only the linearly independent modes are retained for the member's global analysis, as it will be seen in the following paragraph, but it was observed that it was sufficient to create the plate distortional modes for the plates that did not twist in any previous warping-plate distortional mode, the pure plate distortional modes being redundant.

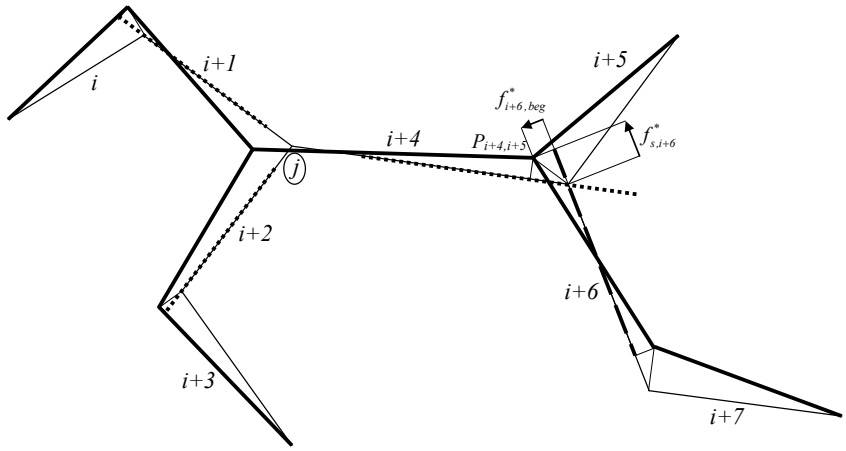

a) Option 1.1: compatible rendering for the displacements between plates *i+4* and *i+5* (plate *i+6* twists).

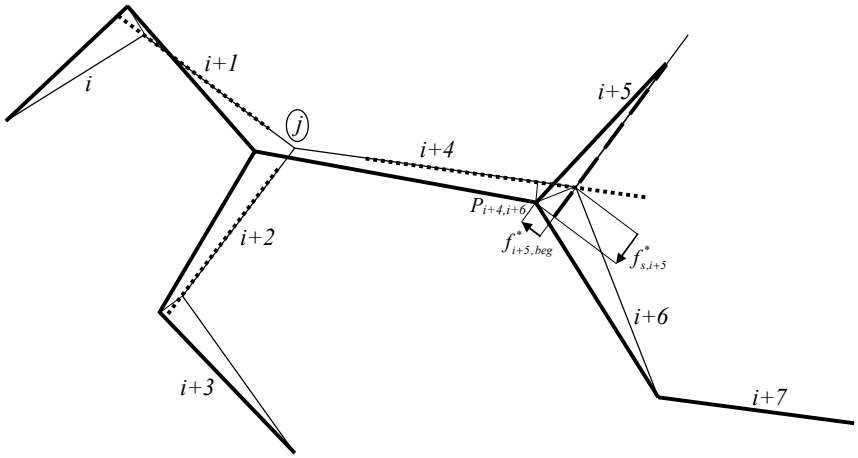

b) Option 1.2: compatible rendering for the displacements between plates *i+4* and *i+6* (plate *i+5* twists).

Fig. 6.57 – Option 1: compatible rendering configurations associated with the end node of plate *i+4*

6.6.3 The extraction of the warping-plate distortional basic linearly independent modes of deformation

Having established all admissible warping-plate distortional modes of deformation through the tree-type scheme presented above, let's suppose in total number n_{WPD}, it is seen that, in general, some of the resulting modes of deformation can be obtained from the remaining ones, which is equivalent to say that the basis dimension for the vector space related to the warping-plate distortional modes of deformation is smaller than n_{WPD}.

Furthermore, it can be seen that the $n_{WPD} \times n_{WPD}$ equilibrium system matrix $\boldsymbol{C}$ corresponding to all the warping-plate distortional modes is not invertible, whereas in the traditional or extended GBT formulations matrix $\boldsymbol{C}$ was always invertible, in order that the generalized eigenproblems solution techniques, such as the Jacobi method (Wilkinson 1965), employed in the orthogonalization of the modes of deformation could be applied. Therefore, for the classical and for the extended GBT formulations, the columns (or rows) of matrix $\boldsymbol{C}$ form a n_{WPD}-dimensional vector space base, and the rank of matrix $\boldsymbol{C}$ is always equal to n_{WPD}. Since for the branched sections analysed through the present tree-type scheme the rank of matrix $\boldsymbol{C}$ is no longer equal to n_{WPD}, and since it can be observed that some modes of deformation can be computed as linear combinations of the remaining, an extraction procedure that gives the linearly independent modes of deformation from the initial ones, which will form the n_{LI}-dimensional vector-space basis, $n_{LI} \leq n_{WPD}$, is needed.

Since it is necessary that the resulting matrix $\boldsymbol{C}$, related to the warping-plate distortional modes only, is invertible, its diagonalization shall render an invertible n_{LI}-dimensional diagonal matrix. Therefore, based on the eigenproblem properties (Noble and Daniel 1998), the extraction procedure runs in the following way:

i) From the scheme presented just above, n_{WPD} warping-plate distortional modes of deformation are established, being defined by the $n_{walls} \times n_{WPD}$ matrices $\boldsymbol{\Delta_{initial}}$ that store the unitary modal displacements or transverse bending moments in columns; they generate a non-invertible $n_{WPD} \times n_{WPD}$ dimensional matrix $\boldsymbol{C}$.

ii) The following eigenproblem is solved:

$$\left[\boldsymbol{C} - \lambda\, \boldsymbol{I}\right]\{x\} = \boldsymbol{0}\,, \tag{6.5}$$

yielding n_{LI} non-zero eigenvalues and $n_{WPD} - n_{LI}$ zero eigenvalues, and their corresponding eigenvectors.

iii) Using the n_{WPD} eigenvectors determined in expression (6.5), stored as columns of the $n_{WPD}\times\ n_{WPD}$ matrix $\boldsymbol{T_{tot}}$, the $n_{WPD}\times\ n_{WPD}$ matrix $\boldsymbol{C}$ is diagonalized to the form

$$\boldsymbol{T}_{tot}^{T}.\boldsymbol{C}.\boldsymbol{T}_{tot}=\begin{bmatrix}\lambda_1 & & & & & \\ & \ddots & & & 0 & \\ & & \lambda_{n_{LI}} & & & \\ & & & 0 & & \\ & 0 & & & \ddots & \\ & & & & & 0\end{bmatrix}, \tag{6.6}$$

where $\lambda_1,\ldots,\lambda_{n_{LI}}$ are the non-zero eigenvalues of $\boldsymbol{C}$ – from expression (6.6) it is seen that rank of matrix $\boldsymbol{C}$ is n_{LI}, thus there are n_{LI} linearly independent warping-plate distortional modes of deformation.

iv) Only the n_{LI} eigenvectors related to the n_{LI} non-zero eigenvalues $\lambda_1,\ldots,\lambda_{n_{LI}}$ are retained, generating a $n_{WPD}\times n_{LI}$ transformation matrix $\boldsymbol{T_{LI}}$ that stores them in columns, and the unitary modal displacements for the final linearly independent modes of deformation are defined by the $n_{walls}\times n_{LI}$ matrices $\boldsymbol{\Delta_{final}}$, that contains the unitary displacements or transverse bending moments and are given by:

$$\boldsymbol{\Delta}_{final}=\boldsymbol{\Delta}_{initial}\ \boldsymbol{T_{LI}}. \tag{6.7}$$

In the end, the final n_{LI} linearly independent warping-plate distortional modes of deformation are established and contain all the information of the initial modes, in the sense that any initial mode of deformation may be always given as a unique linear combination of the later modes, i.e., if a linear algebraic system of following type is established for the unknowns c_k:

$$\delta_{initial}=\sum_{k=1}^{n_{LI}} c_k\ {}^{k}\delta_{LI}\ , \tag{6.8}$$

where $\delta_{initial}$ represents any initial mode and ${}^{k}\delta_{LI}$ represents the linearly independent modes determined through the extraction procedure, this system is always possible and renders a unique solution in c_k for any $\delta_{initial}$. The linearly independent modes will then participate, together with the remaining modes, in the orthogonalization procedure explained in Chapters 2 and 5 that builds the transformation matrix, required to compute the orthogonal modes of deformation. In the following, the above scheme is deeply illustrated and validated with the GBT analysis of two hollow flange beam sections.

6.7 – Illustrative example for a general cross section: the compact hollow flange beam section

6.7.1 Cross sectional properties and the corresponding modes of deformation

The enhancement of the GBT scheme just presented is illustrated here, without loss of generality, by the GBT analysis of a compact hollow flange cross section (HFB). This cross section was invented recently in Australia by Palmer Tube Mills Pty Ltd (nowadays known as Smorgon Steel Tube Mills) and is devoted mainly to beam elements due to its double symmetry, high major axis moment of inertia and high torsion stiffness, provided by the closed triangular flanges at the top and bottom of the cross section, that enables a high critical major axis bending moment, despite a low minor axis moment of inertia. The geometric properties of the analysed cross section are presented in Figure 6.58, and Figures 6.59 to 6.64 illustrate how the scheme presented above performs to generate the set of orthogonal modes of deformation that will later be used in the member's analysis. The GBT analysis of the HFB section begins by setting up the warping-plate distortional modes of deformation, initially 26 for the considered cross section and illustrated in Figures 6.59 and 6.60. These modes are not linearly independent one from each other, so that the

extraction procedure at the beginning of the orthogonalization scheme excludes 15 modes, since they are dependent from the remaining, and retains only the 11 linearly independent modes presented in Figures 6.61 and 6.62. These later 11 modes constitute the admissible basis of the vector space related to all the first 26 warping-plate distortional modes of deformation, contain the same information than the initial modes and will take part, together with the inner nodes warping, plate bending and plate transverse extension modes, in the orthogonalization procedure that will render the final modes used in the member's analysis, presented in Figures 6.63 and 6.64.

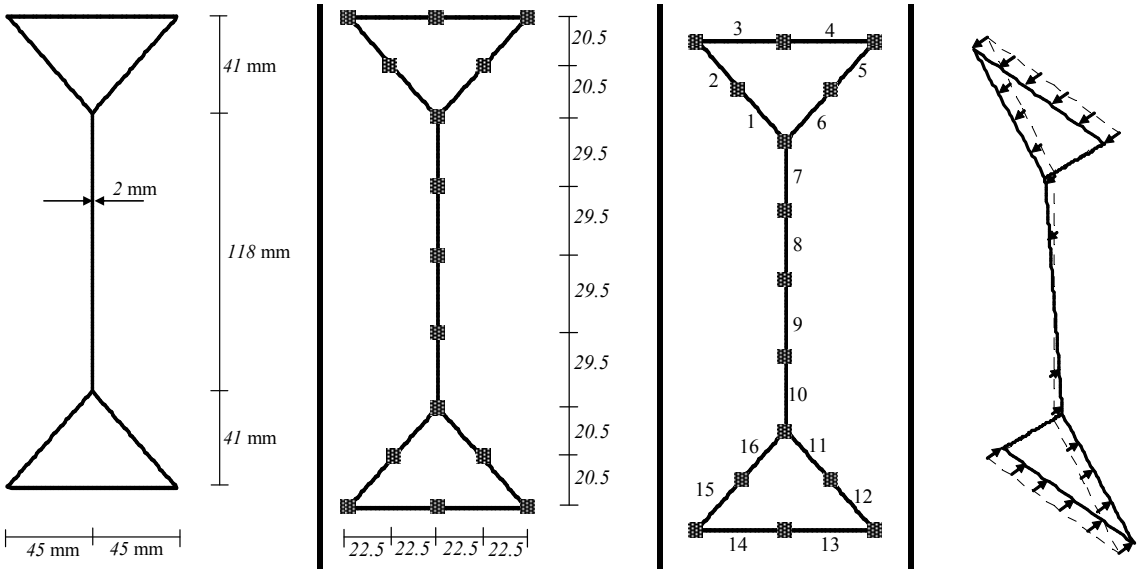

a) Cross section properties | b) Nodal discretization | c) Plate numbering | d) Applied stress distribution

Fig. 6.58 - The analysed compact HFB section

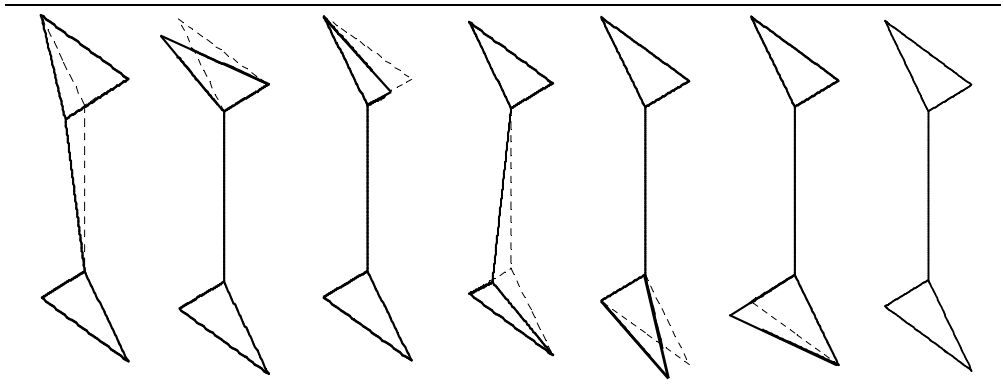

Modes 1 to 6 | Modes 7 to 9 | Modes 10 to 12 | Modes 13 to 18 | Modes 19 to 21 | Modes 22 to 24 | Mode 25 and 26

Fig. 6.59 - The unitary longitudinal warping displacements for the initial modes of deformation, for the compact HFB section

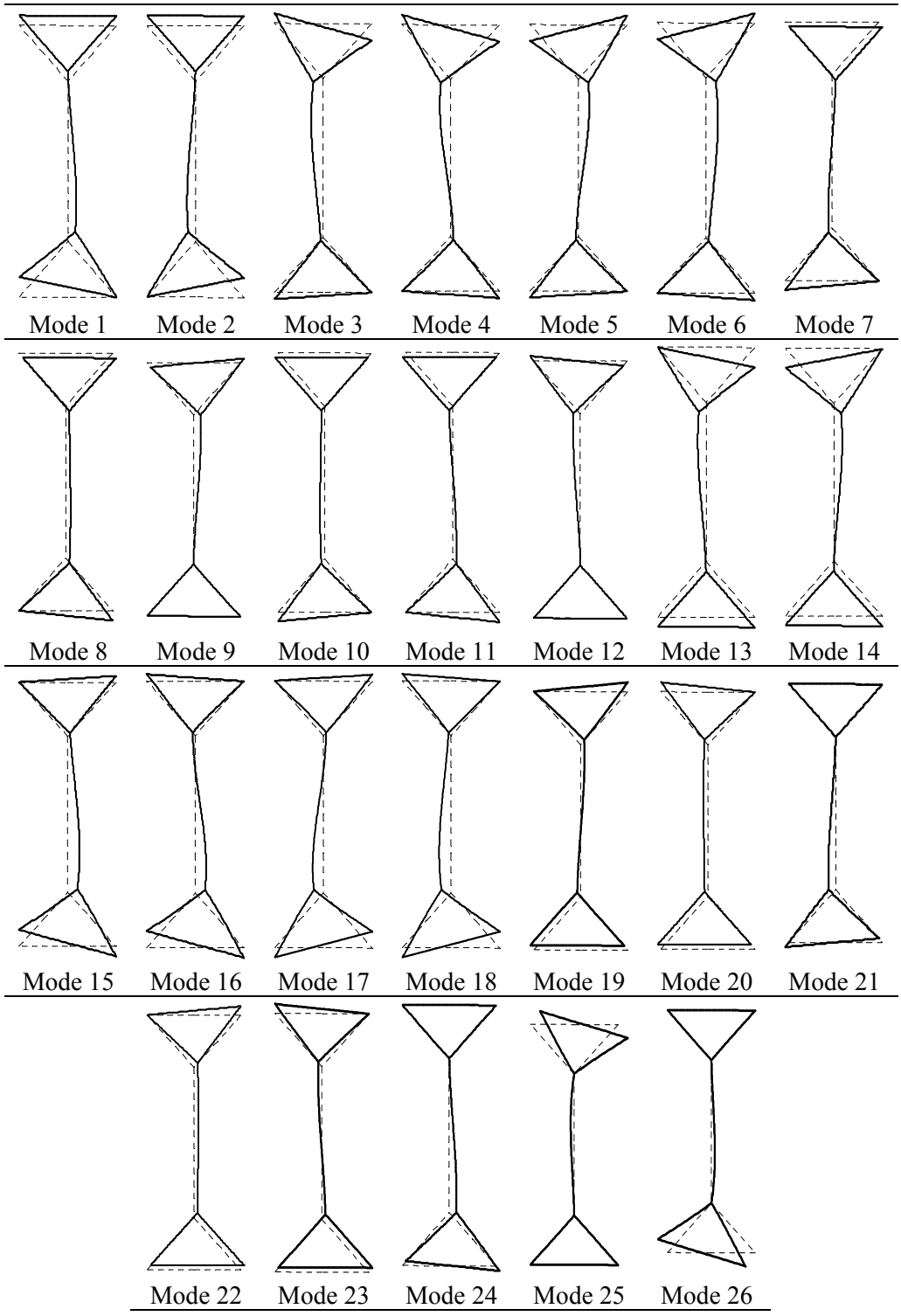

Fig. 6.60 - The unitary displacements along the cross section plane for the initial modes of deformation, for the compact HFB section

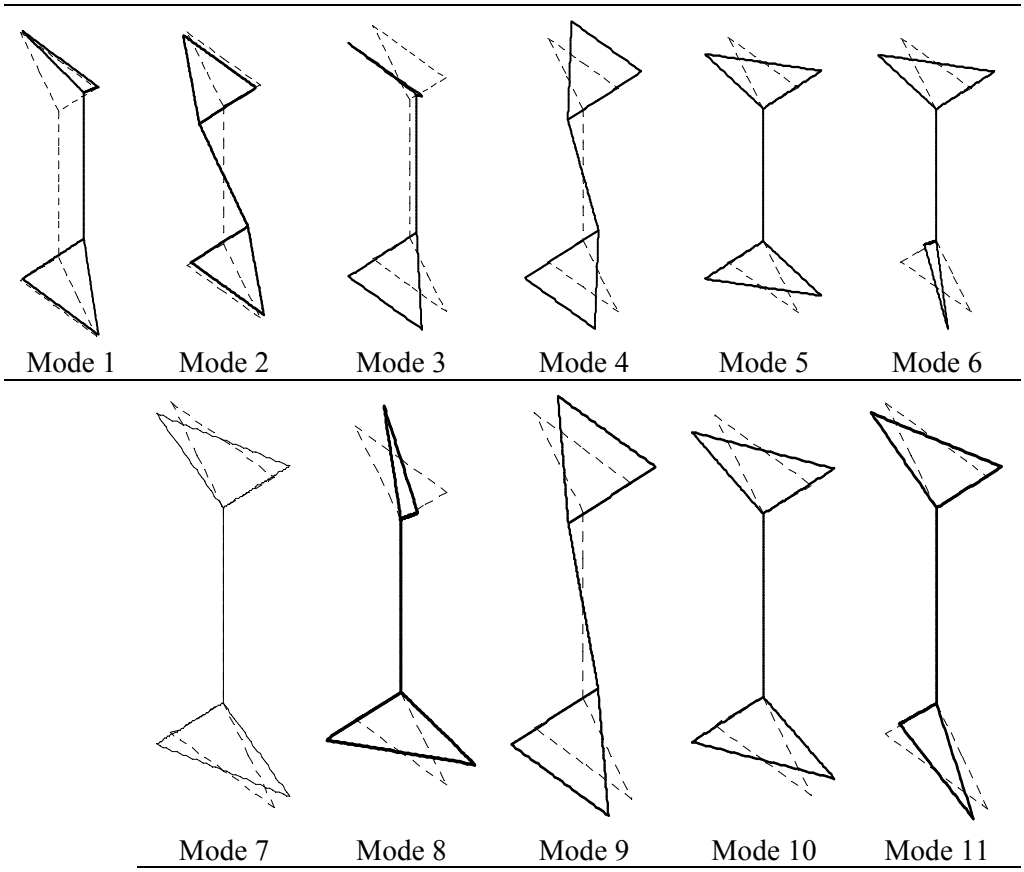

Fig. 6.61- The unitary longitudinal warping displacements for the linearly independent warping-plate distortional modes of deformation, for the compact HFB section

6.7.2 Critical behaviour of the simply supported beam

The critical behaviour of the simply supported beam is represented in Fig. 6.65, where the critical major axis bending moments from GBT analysis are validated against the FSM solutions arising from CUFSM (Schaefer 2003), being evident the perfect agreement between both methods. The GBT analysis considers function (3.37) for all modes with the exception of mode 1, which is removed from the analysis because the beam edges are considered longitudinally fixed, thus modelling the simply supported boundary conditions. To model modes 2, 6, 8, 12, 14 and 16 functions (3.38) are considered, obtained by withdrawing the static boundary conditions, since for these modes the following integral is non null:

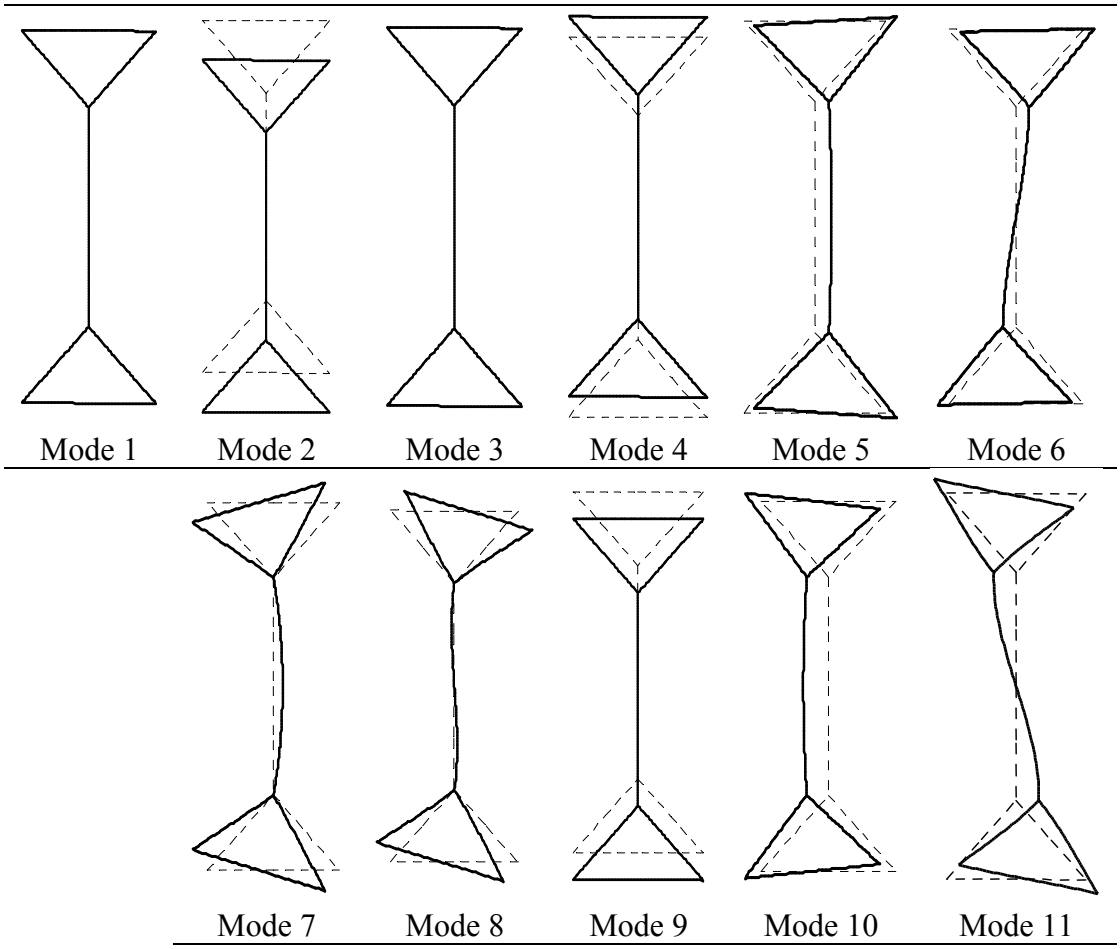

Fig. 6.62 - The unitary displacements along the cross section plane for the linearly independent warping-plate distortional modes of deformation, for the compact HFB section

$$\int_s t\,\sigma_b(s)\,{}^k u(s)\,ds\,, \tag{6.9}$$

where $\sigma_b(s)$ refers to the applied stress distribution presented in Fig. 6.58-d), being equivalent to a *1* kNm major axis bending moment. Expression (6.9) is related to the general expression (6.1) for the potential of the external loading, for the beam under uniform bending moment case, and the referred modes provoke a non-zero potential of the external work, so that functions (3.38) were chosen for these modes to enable a constant generalized modal force along the member's length, the corresponding coordinates appearing in Π in a linear form.

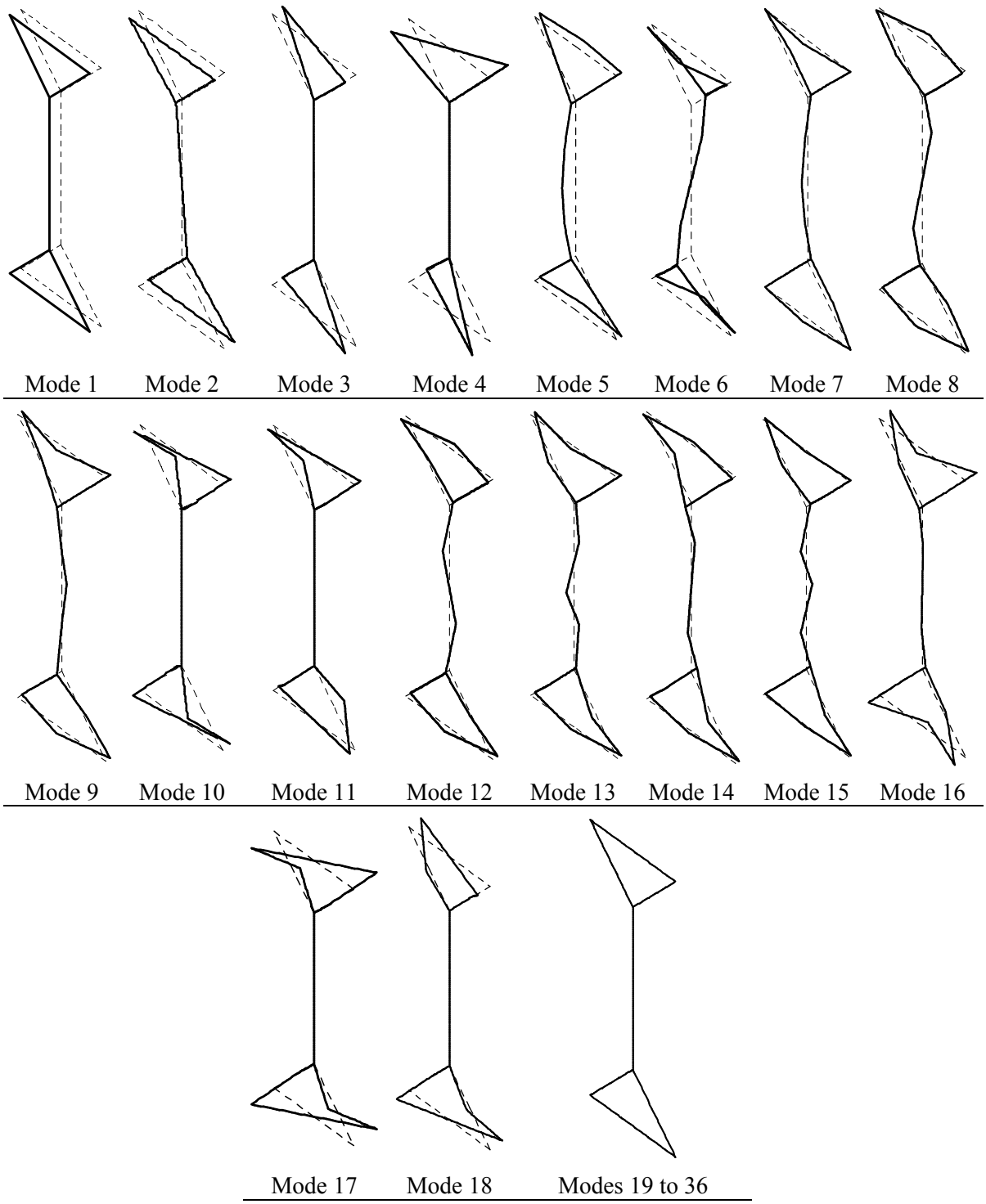

Fig. 6.63 - The unitary longitudinal warping displacements for the orthogonal modes of deformation, for the compact HFB section

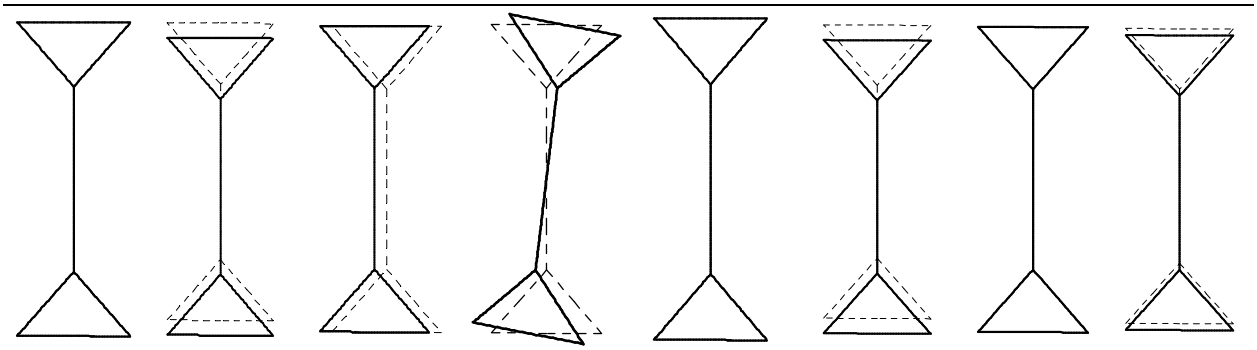
Mode 1
Mode 2
Mode 3
Mode 4
Mode 5
Mode 6
Mode 7
Mode 8

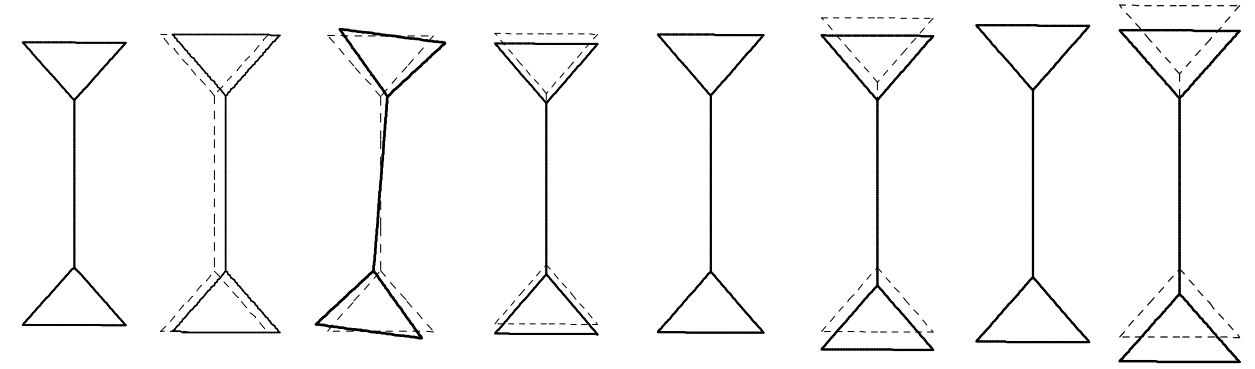
Mode 9
Mode 10
Mode 11
Mode 12
Mode 13
Mode 14
Mode 15
Mode 16

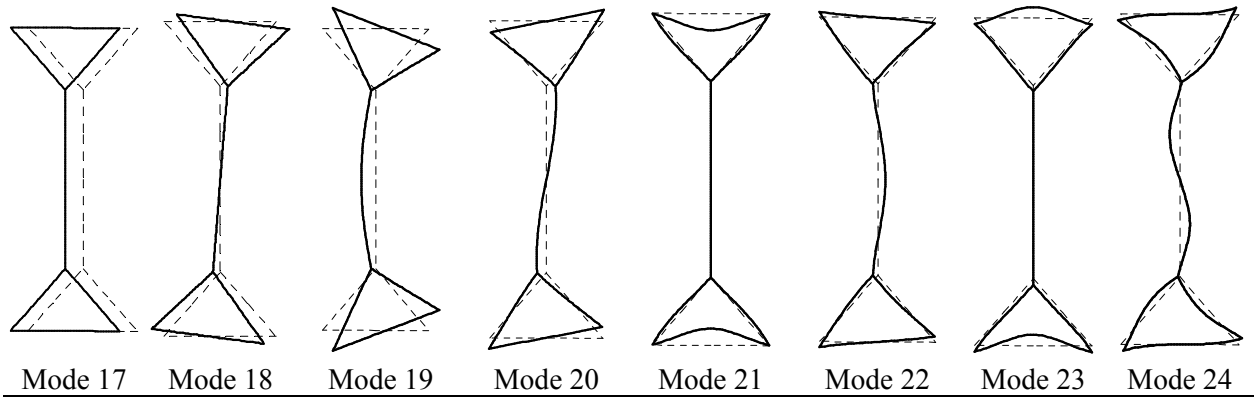
Mode 17
Mode 18
Mode 19
Mode 20
Mode 21
Mode 22
Mode 23
Mode 24

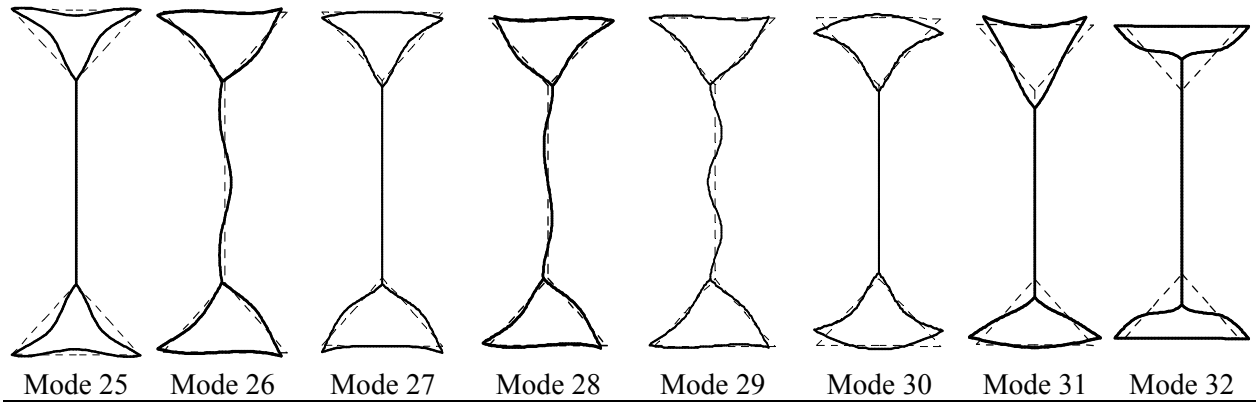
Mode 25
Mode 26
Mode 27
Mode 28
Mode 29
Mode 30
Mode 31
Mode 32

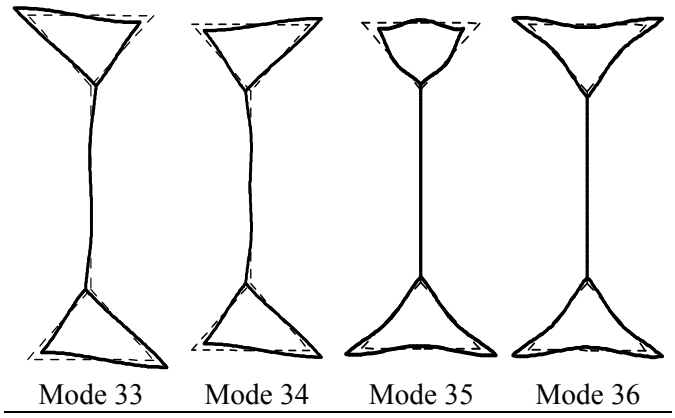

Fig. 6.64 - The unitary displacements along the cross section plane for the orthogonal modes of deformation, for the compact HFB section

The influence of the number of coordinate polynomials per mode of deformation adopted in the analysis is illustrated in Fig. 6.66, highlighting that for the smaller lengths range the critical moments remain constant as the lengths increase. Fig. 6.67 informs that for these lengths buckling is governed mainly by modes 21, 23 and 27, corresponding to the plate buckling of the compressed flange. For higher lengths the buckling moments are no longer constant against the member's length and the critical states are dependent of modes 3 and 20, i.e., a combination of minor axis bending and transverse bending of the flange, provoking a decrease of the critical resistance from the rigid cross section analysis, as observed in Avery, Mahendran and Nasir (2000). As the member's length increases, mode 20 smoothly becomes less significant, denoting that for larger members the transverse bending phenomenon becomes less important.

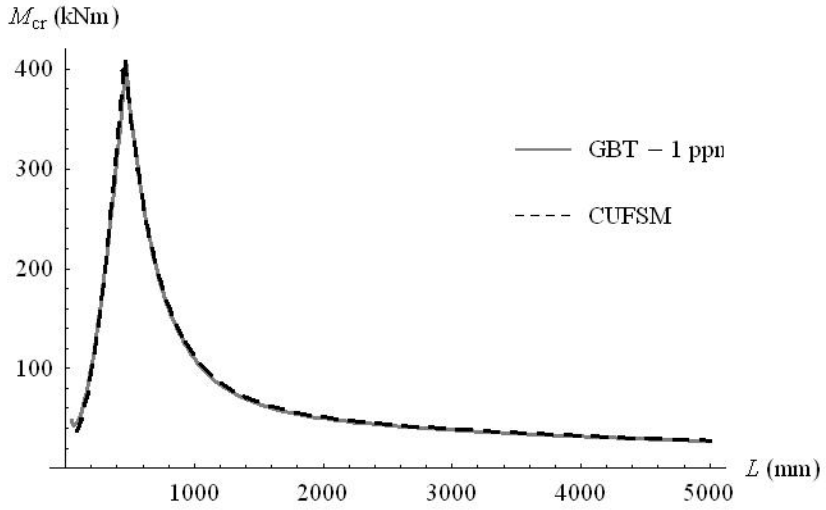

Fig. 6.65 – Critical major axis bending moments for the simply supported compact HFB section member: benchmark comparison between GBT and CUFSM analysis

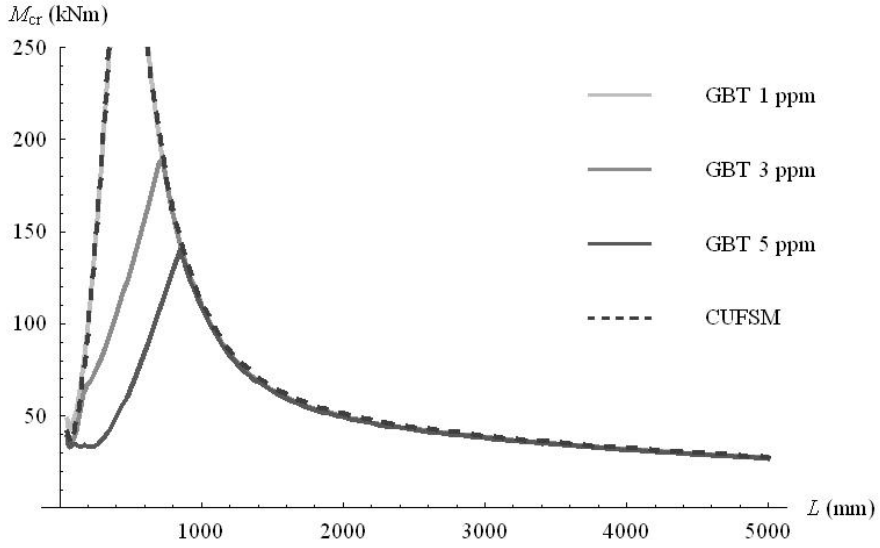

Fig. 6.66 – Critical major axis bending moments for the simply supported compact HFB section member: the decrease of the critical moments with the increase of the number of adopted polynomials per mode of deformation

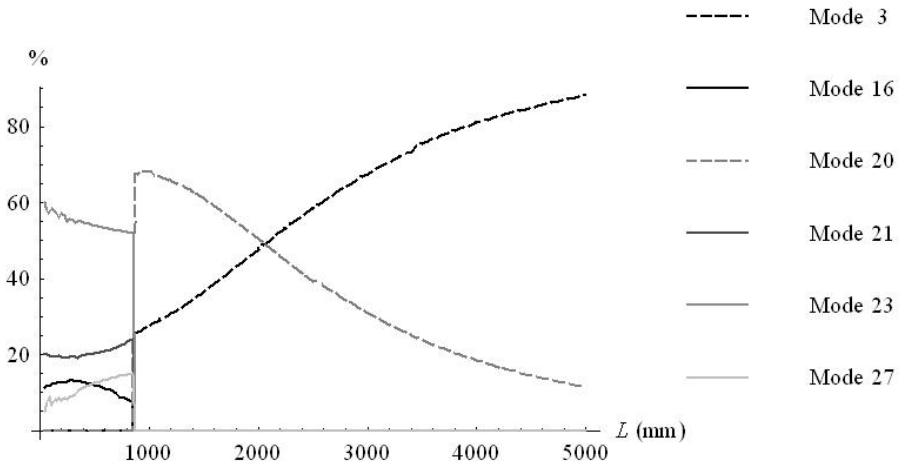

Fig. 6.67 – Modal participations at the critical state for the simply supported compact HFB section member under uniform major axis bending moment, considering 5 polynomials per mode of deformation

6.7.3 Post-buckling behaviour of a beam in the flange-buckling mode range

The post-buckling behaviour of the compact HFB section member is investigated here for a length of *300* mm, for which buckling is local. Due to computer limitations, only the first 5 polynomials of expression (3.37) are considered for modes 2 and higher, with the exception of modes 2, 6, 8, 12, 14 and 16, for which, as referred above, the static boundary conditions are neglected in the calculus of the corresponding coordinate functions, since the integral of the corresponding unitary warping displacements times the stress pattern presented in Fig. 6.58 is not null, so that for these modes the first 5 polynomials of expression (3.38) are considered in the analysis. The computed critical moment was *36.9826* kNm, and, for the search of the post-buckling path, as control it was chosen the coordinate corresponding to mode 23 and to coordinate function (3.37-c). The member's configurations presented in Fig. 6.68 are obtained for both branches for a moment of *71.298* kNm and Fig. 6.69 shows the vertical displacement for the mid-point of the compressed flange – end node of secondary wall 3 or initial node of wall 4, considering

the numbering given in Fig. 6.58-c) – at $x = \frac{L}{2}$, illustrating a stable post-buckling behaviour. Figures 6.70 to 6.72 present the longitudinal normal stresses along the laid-out cross section, and it is clearly perceptible the decrease of the longitudinal stresses as the applied load increases above M_{cr} in walls 3 and 4, for perimeter coordinate s between *60.877* mm and *150.877* mm, due to their buckling. To help the reading of these figures, Table 6.1 presents the correspondence between the perimeter coordinate and the secondary walls, whose numbering is given in Fig. 6.58-c).

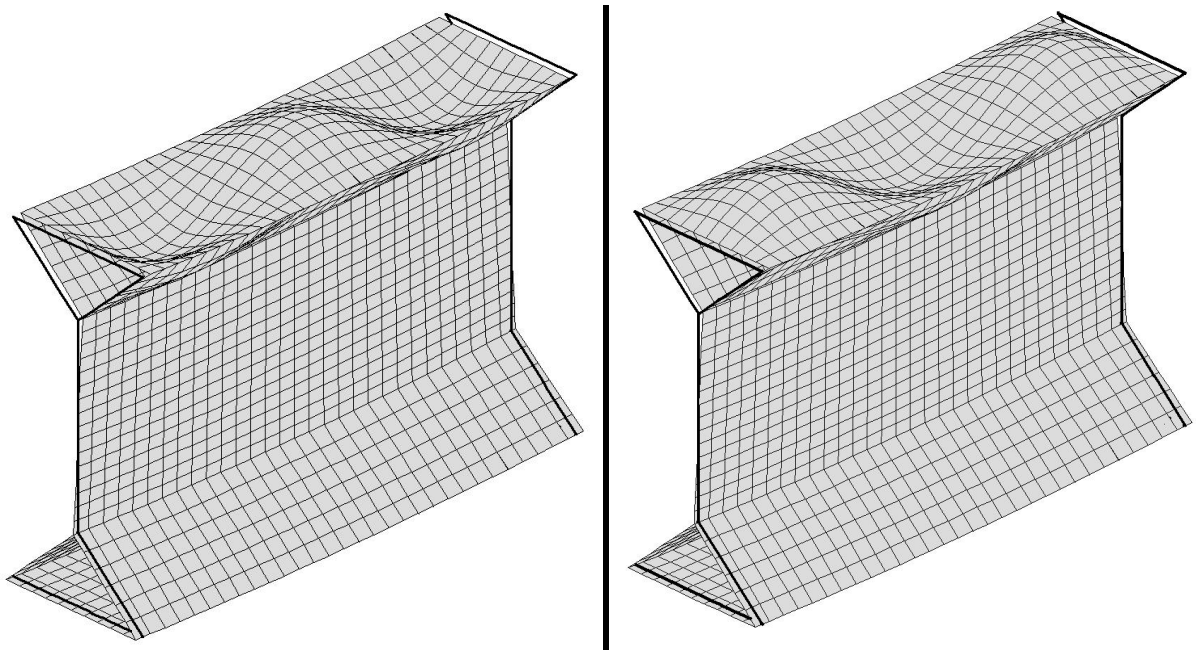

$^{control}q > 0$ $^{control}q < 0$

Fig. 6.68 – Member's deformed configuration for $M = 1.928 \times M_{CR}$ (all displacements are amplified by a factor 10)

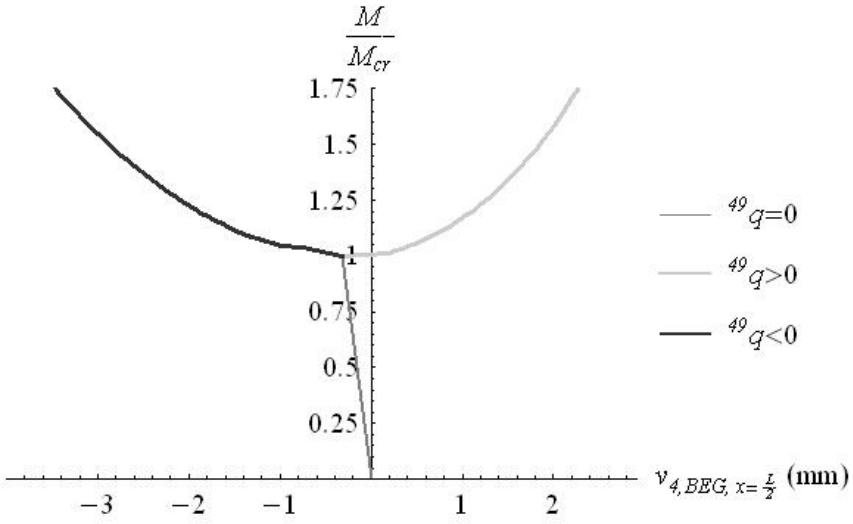

Fig. 6.69 – Vertical displacement of compressed flange mid-point at $x = \frac{L}{2}$

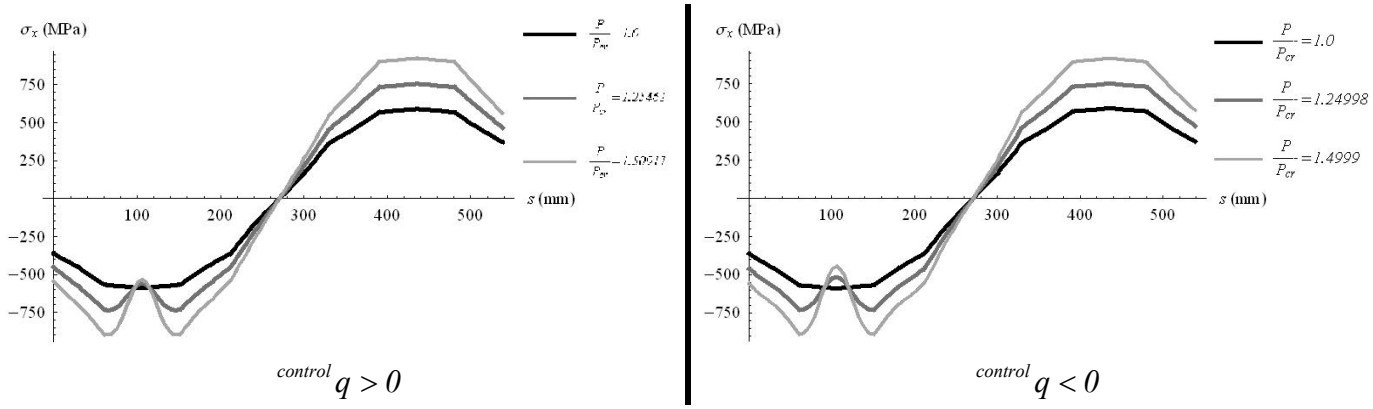

$^{control}q > 0$ $^{control}q < 0$

Fig. 6.70 – Longitudinal normal stresses σ_x^M along the (laid out) cross section at $x = L/4$

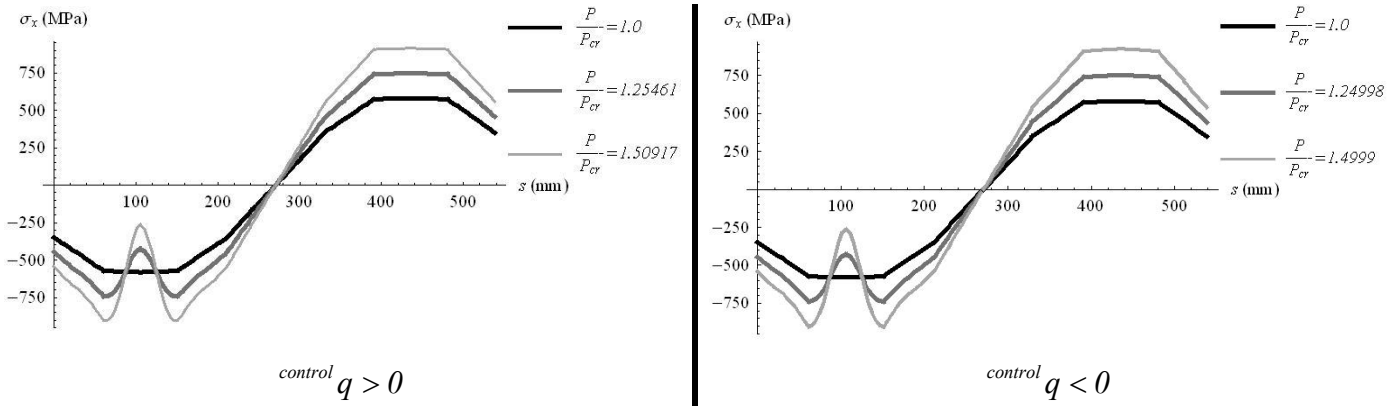

$^{control}q > 0$ $^{control}q < 0$

Fig. 6.71 – Longitudinal normal stresses σ_x^M along the (laid out) cross section at $x = L/3$

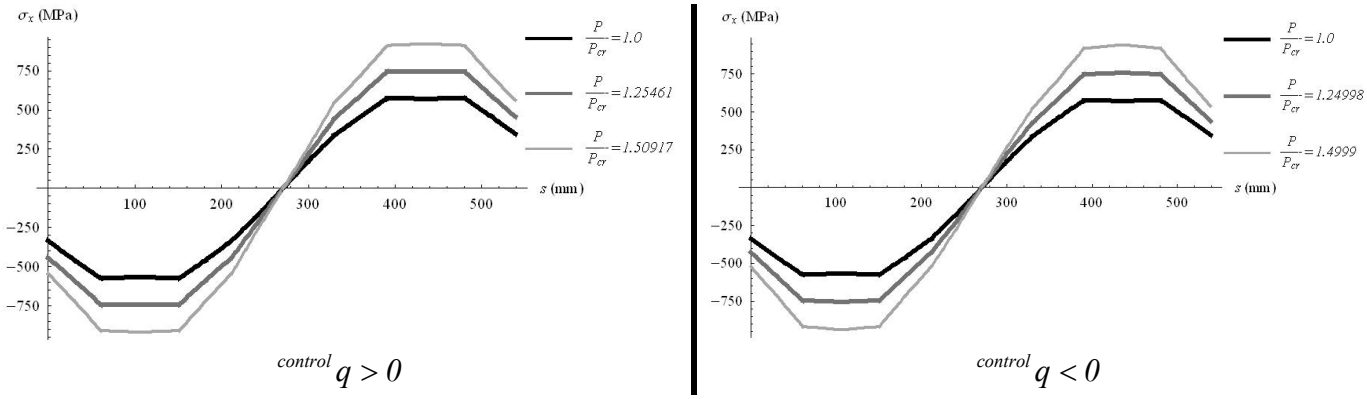

Fig. 6.72 – Longitudinal normal stresses σ_x^M along the (laid out) cross section at $x = L/2$

Wall	s_{ini} (mm)	s_{end} (mm)	Wall	s_{ini} (mm)	s_{end} (mm)
1	0	30.439	**9**	270.754	300.254
2	30.439	60.877	**10**	300.254	329.754
3	60.877	105.877	**11**	329.754	360.192
4	105.877	150.877	**12**	360.192	390.631
5	150.877	181.315	**13**	390.631	435.631
6	181.315	211.754	**14**	435.631	480.631
7	211.754	241.254	**15**	480.631	511.069
8	241.254	270.754	**16**	511.069	541.508

Table 6.1 - The analysed slender HFB section: perimeter coordinates corresponding to the secondary walls for the laid out cross section

6.8 – Illustrative example for a general cross section: the slender hollow flange beam section

6.8.1 Introduction, cross sectional properties and modes of deformation

According to Avery, Mahendran and Nasir (2000), there are three main buckling modes for HFB members under uniform bending. The plate buckling mode of the compressed flange was investigated in the previous section, just above, so that here the

remaining two types are analysed. To do so, a new cross section is adopted, being described in Fig. 6.73. It is noted that this cross section contains a slender web, whereas in the previous example the cross section's web was much shorter, therefore it was unlike to buckle. The GBT analysis considering one intermediate node for all plates, with the exception of the web, for which three intermediate nodes are considered, gives rise to 36 orthogonal modes of deformation, presented in Fig. 6.74 for the unitary warping displacements and in Fig. 6.75 for the cross section displacements. Like in the previous example, modes 30 to 36 deal mainly with transverse extension of the main plates and modes 19 to 29 are associated with transverse bending along the cross section. Modes 5 to 18 are the so-called shear-lag modes and are associated with non-zero terms in the main diagonal of matrix $\boldsymbol{D}$, mode 4 corresponds to the traditional torsion mode, here appearing explicitly despite of the two closed cells, modes 2 and 3 are the traditional bendings and mode 1 is the axial elongation. Finally, Table 6.2 establishes the correspondence between the perimeter coordinate s and the numbering of the secondary plates given in Fig. 6.73-d), in order to help the reading of the stress graphics for the laid-out cross section that will be presented below.

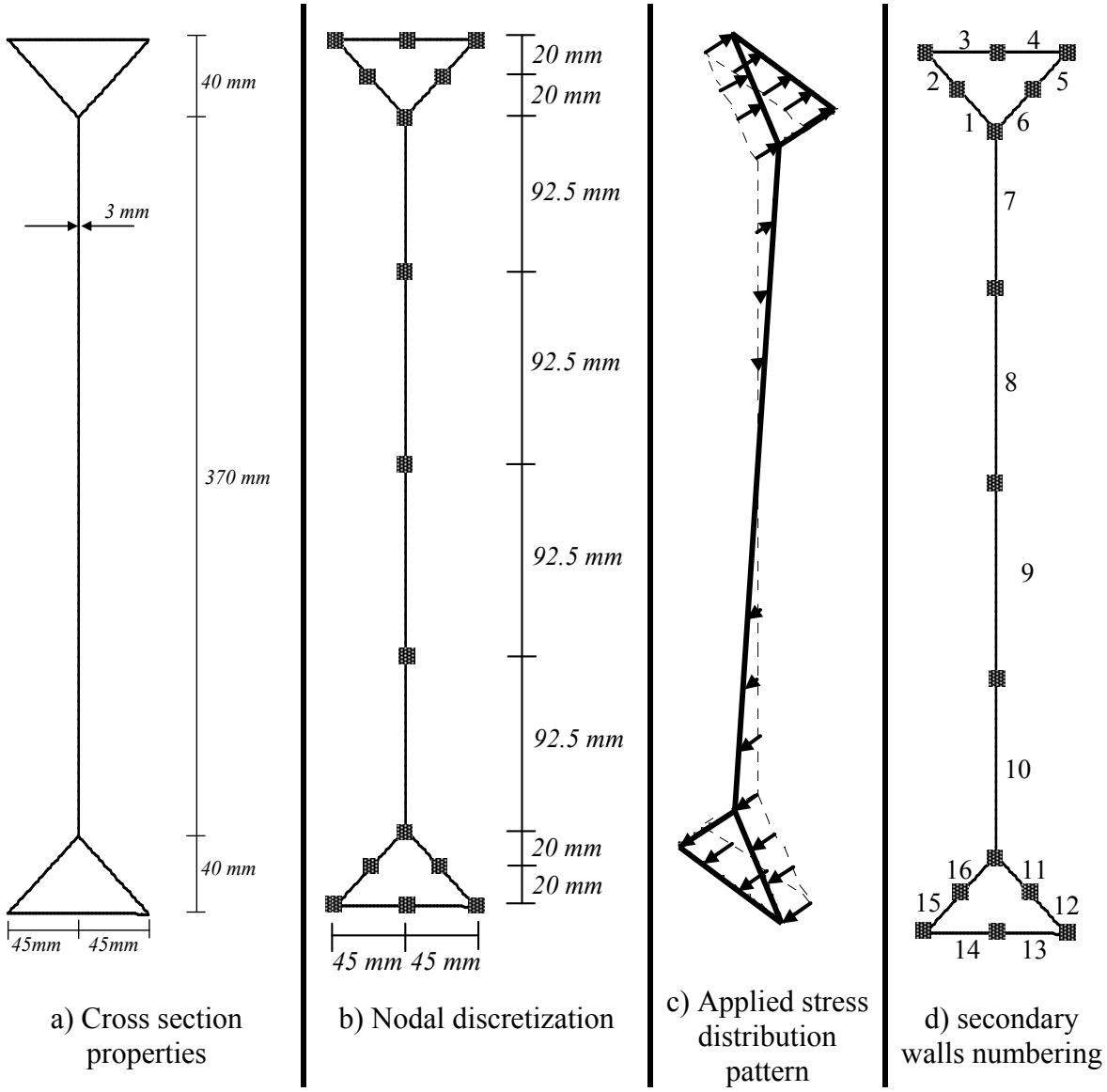

Fig. 6.73 - The analysed slender HFB section

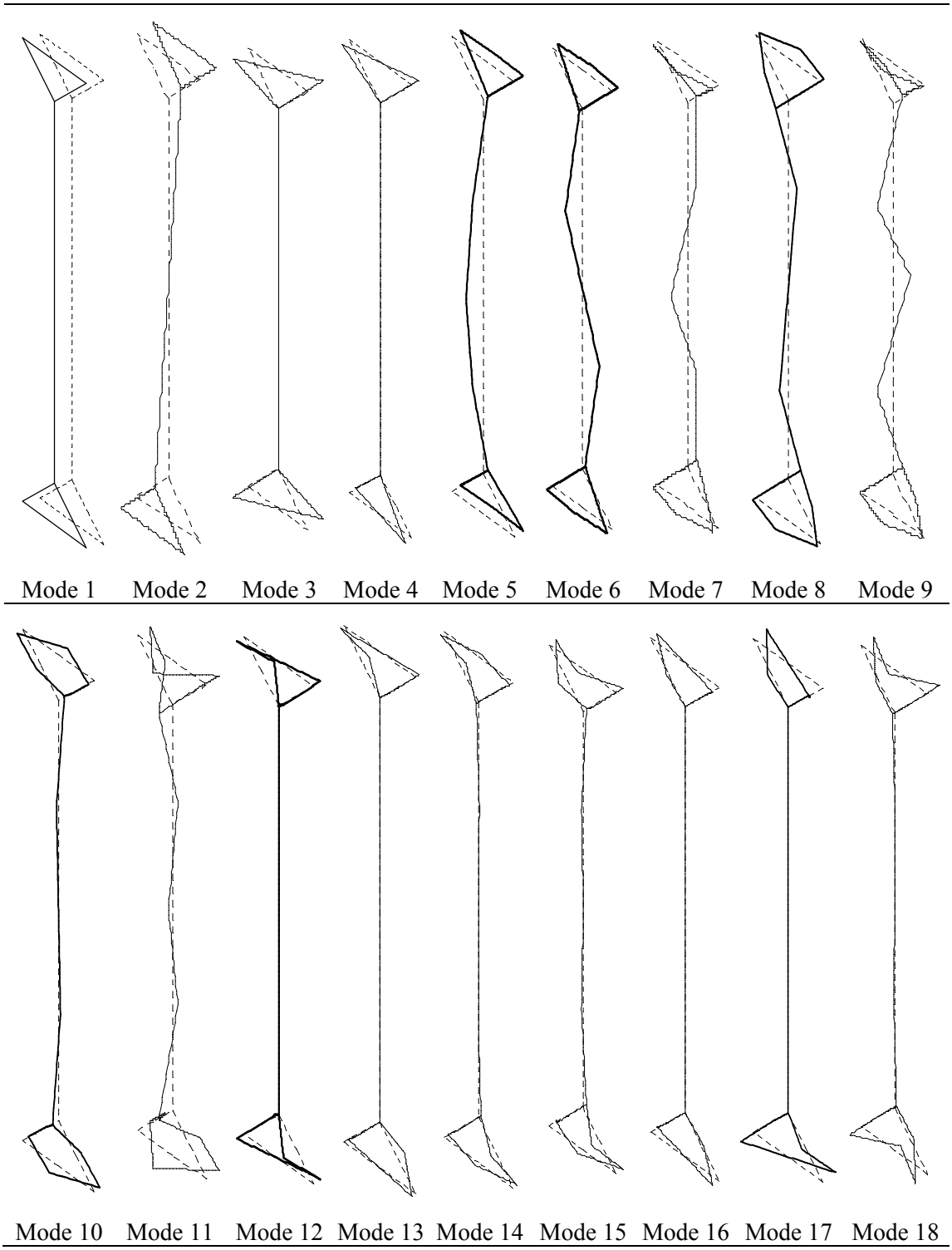

Fig. 6.74 - The unitary longitudinal warping displacements for the orthogonal modes of deformation (for modes 19 to 36 the longitudinal displacements are null all over the cross section), for the slender HFB section

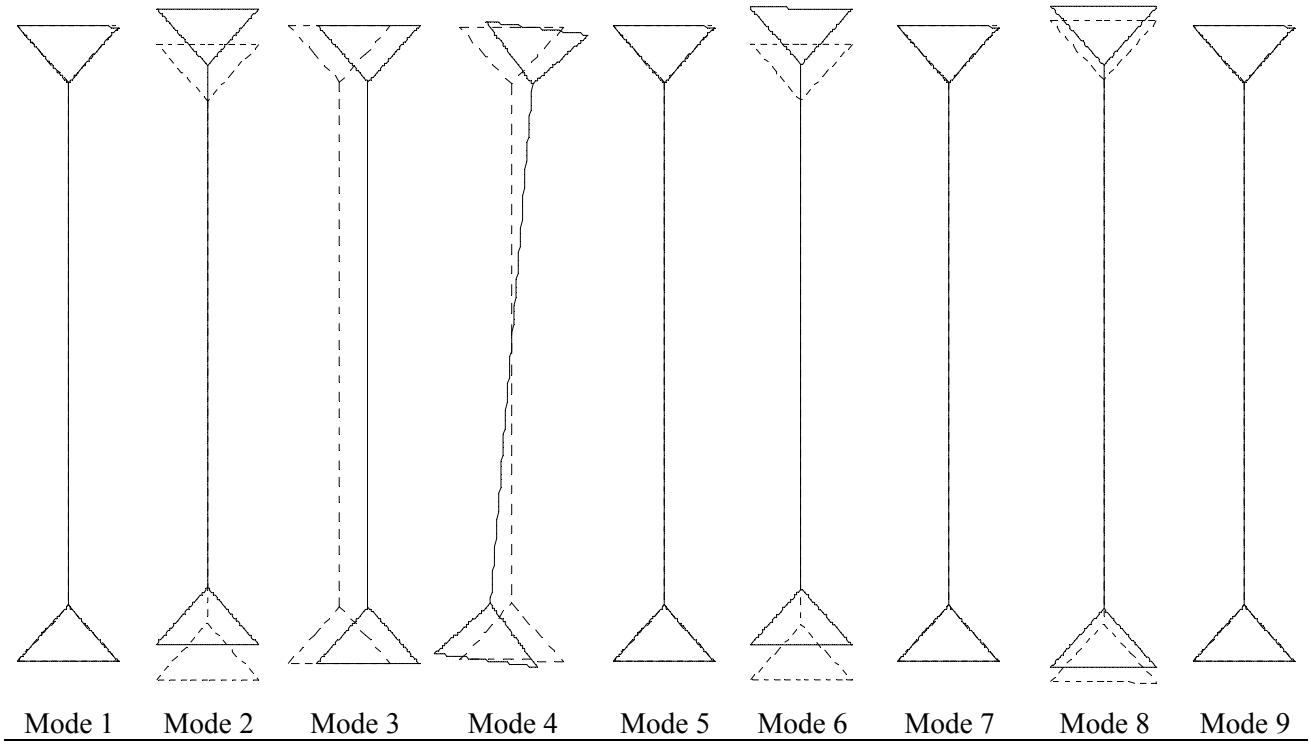
Mode 1
Mode 2
Mode 3
Mode 4
Mode 5
Mode 6
Mode 7
Mode 8
Mode 9

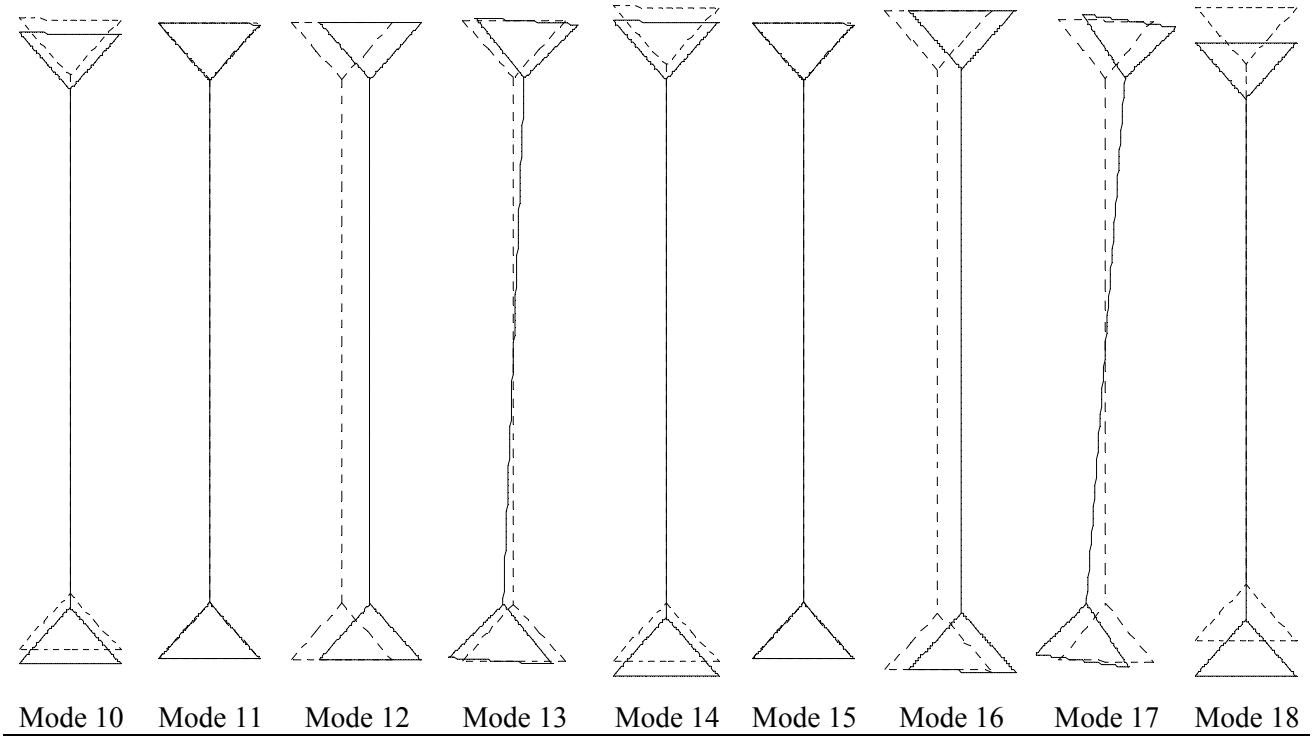
Mode 10
Mode 11
Mode 12
Mode 13
Mode 14
Mode 15
Mode 16
Mode 17
Mode 18

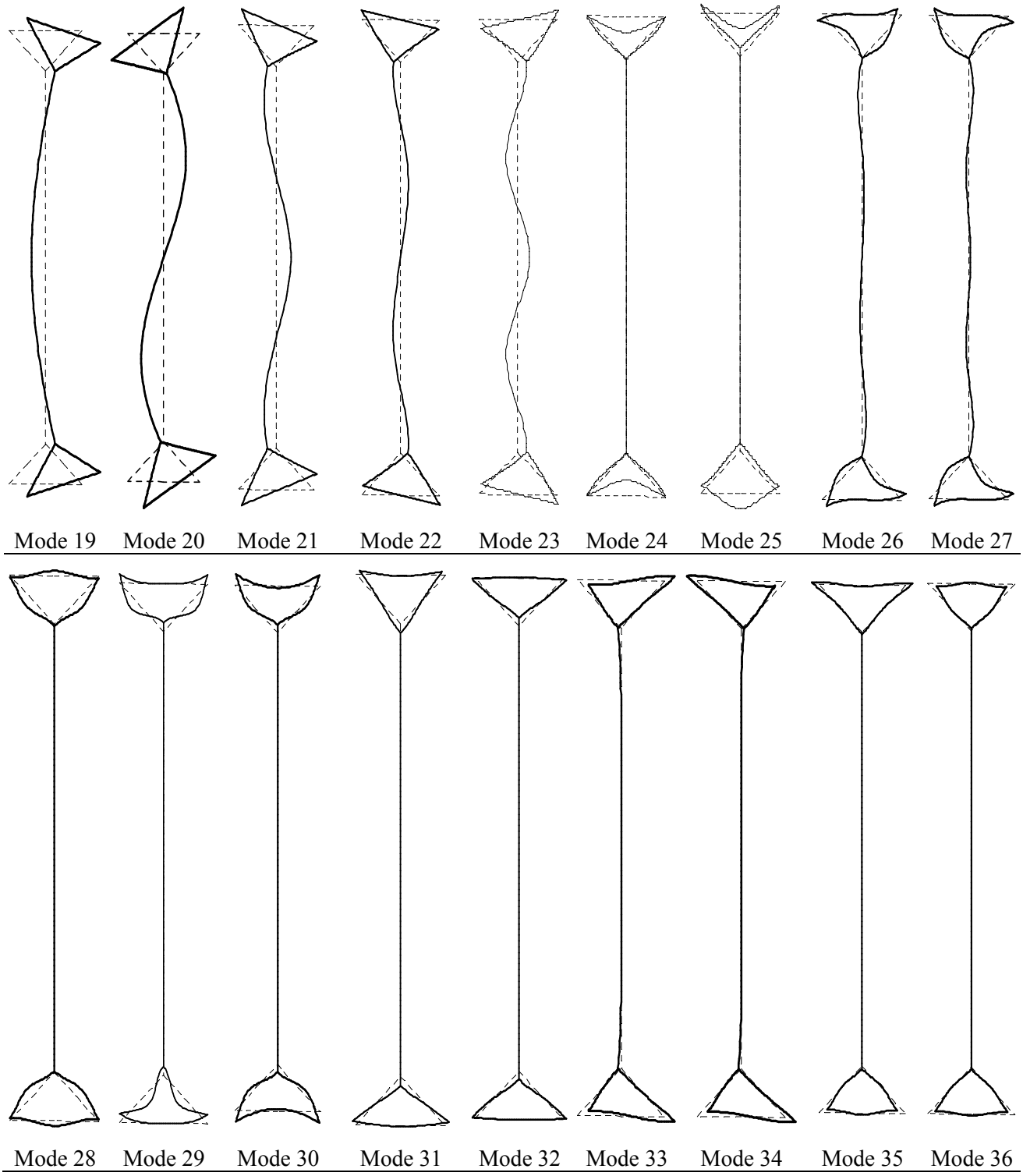

Fig. 6.75 - The unitary displacements along the cross section's plane for the orthogonal modes of deformation, for the slender HFB section

Wall	s_{ini} (mm)	s_{end} (mm)	Wall	s_{ini} (mm)	s_{end} (mm)
1	0	30.104	9	395.416	487.916
2	30.104	60.208	10	487.916	580.416
3	60.208	105.208	11	580.416	610.520
4	105.208	150.208	12	610.520	640.624
5	150.208	180.312	13	640.624	685.624
6	180.312	210.416	14	685.624	730.624
7	210.416	302.916	15	730.624	760.728
8	302.916	395.416	16	760.728	790.832

Table 6.2 - The analysed slender HFB section: perimeter coordinates corresponding to the secondary walls for the laid-out cross section

6.8.2 Critical behaviour of the simply supported beam

The critical behaviour of the simply supported HFB section beam is described in Fig. 6.76, where the critical major axis bending moments are validated against the solutions derived from CUFSM (Schaefer 2003), and in Figures 6.77 to 6.79. In Fig. 6.77, the influence of the number of adopted polynomials in the buckling load is addressed, showing the decrease of the buckling moments with the increasing number of adopted polynomials per mode of deformation. Figures 6.78 and 6.79 contain the variation of the modal participations at the critical state against the member's length, and highlight the existence of three buckling regions. For very short lengths, buckling is associated mainly with modes 25 and 24, related to the plate buckling of the compressed flange, like in the previous example. For lengths between 80 and 1200 mm buckling is associated with modes 22 and 23 and is provoked by the buckling of the compressed part of the web – hence the designation of "slender HFB section" for the present case and "compact HFB section" for the previous case, where buckling of the web never occurred, whichever was the member's length. For lengths higher than 1200 mm, buckling is ruled mainly by modes 2, 21 and 22 and becomes global, mode 2 playing and increasingly significant role as the member's length increases, and modes 21 and 22 disclose the influence of the web's transversal bending that provokes a decrease on the critical load capacity of the beam, as referred in

Avery and Mahendran (1997) and Avery, Mahendran and Nasir (2000).

Here and in the post-buckling analysis presented below, modes 2, 6, 8, 10, 14 and 18 are present in the potential of the external loading, applied, as in the previous cases, as a normal longitudinal stress pattern given in Fig. 6.73-c) at the beam's edge sections, so that the correspondent coordinate polynomials are derived from boundary conditions only, being given by expressions (3.38). The remaining modes are rendered discrete by adopting polynomials (3.37) and mode 1 is removed from the analysis since it is supposed that the edge cross sections are not allowed to move along the longitudinal direction – this assumption implies that the web's midpoint at the edge cross sections does not move longitudinally, as seen below. In the following the post-buckling behaviour is investigated for lengths lying in the two later buckling regions.

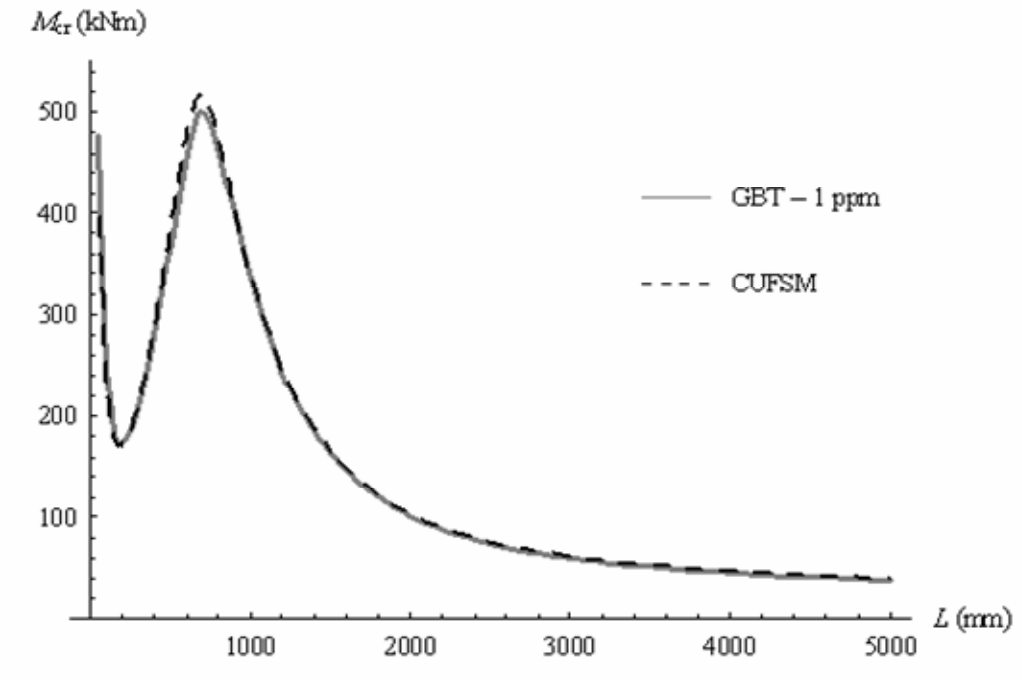

Fig. 6.76– Critical major axis bending moments for the simply supported slender HFB section member: benchmark comparison between GBT and CUFSM analysis

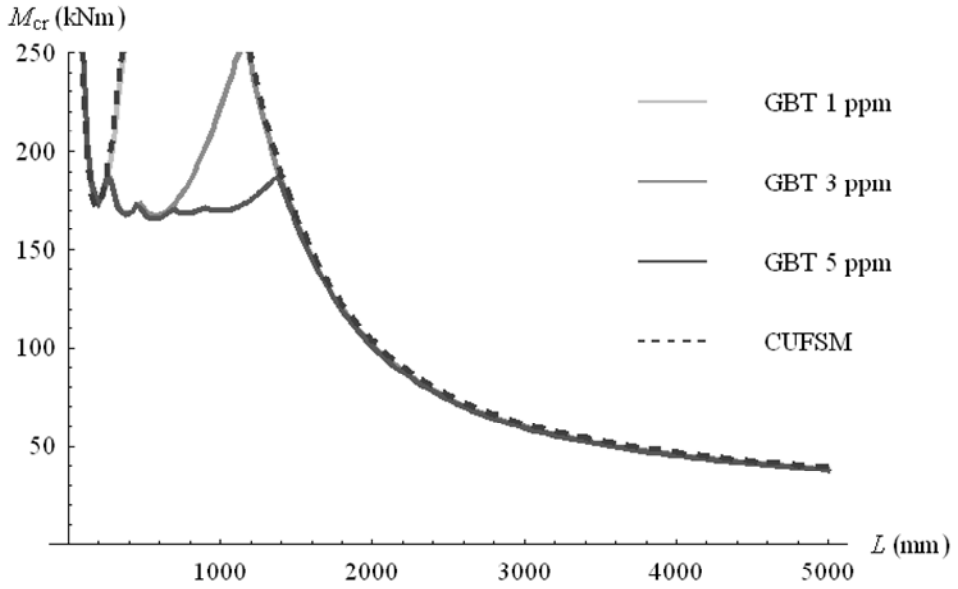

Fig. 6.77 – Critical major axis bending moments for the simply supported slender HFB section member: the decrease of the critical moments with the increase of the number of adopted polynomials per mode of deformation

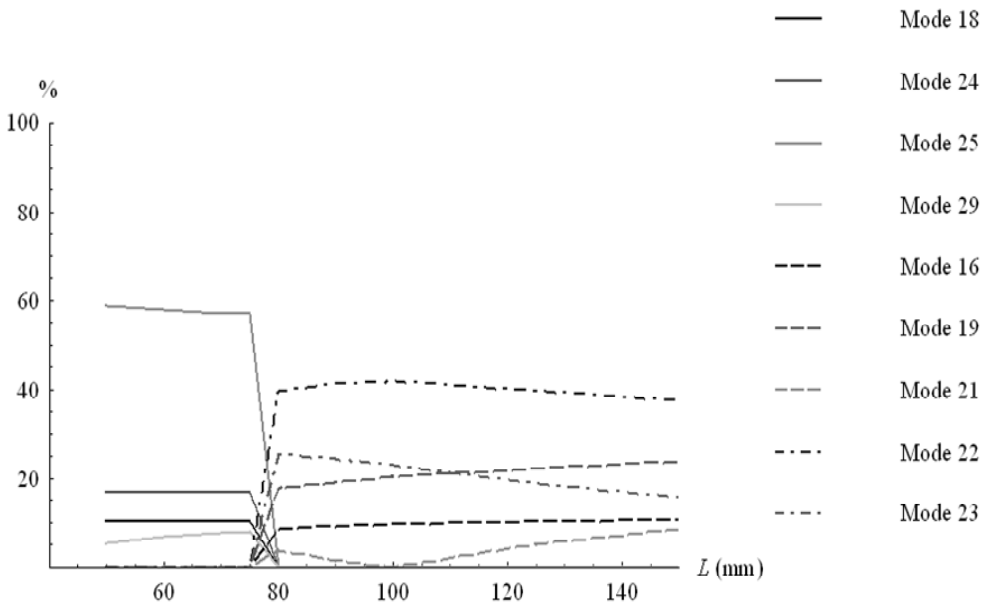

Fig. 6.78– Modal participations at the critical state for the simply supported HFB section member under uniform major axis bending moment, considering 5 polynomials per mode of deformation: lengths between 50 and 150 mm

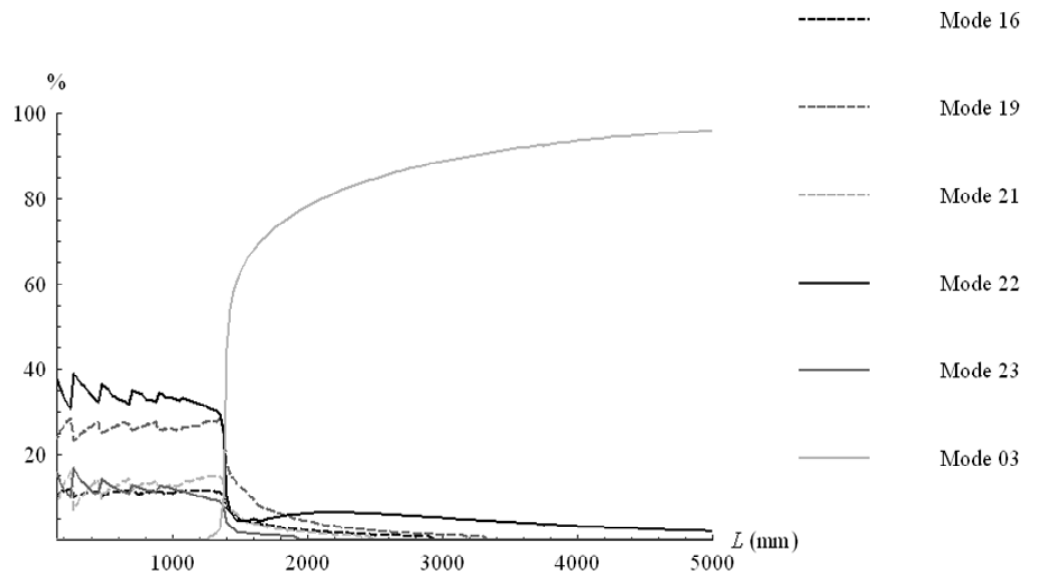

Fig. 6.79 – Modal participations at the critical state for the simply supported HFB section member under uniform major axis bending moment, considering 5 polynomials per mode of deformation: lengths between 150 and 5000 mm

6.8.3 Post-buckling behaviour of a simply supported beam under uniform major axis bending moment in the web-buckling mode range

The post-buckling in the web's distortional buckling zone is investigated for a member's length of *L=600* mm. For the discretization referred above, here limited to the first 3 polynomials for each mode of deformation due to computer limitations, the obtained critical moment is M_{cr}*=204.812* kNm and the obtained post-buckling behaviour is stable and symmetric, as displayed in Fig. 6.80, where a plot of the horizontal displacement of the initial node of wall 8 versus the applied load is presented. The member's global configuration is illustrated at Fig. 6.81 for both branches of the post-buckling path and for an applied moment of *257.485* kNm. Figures 6.82 and 6.83 present the longitudinal normal membrane stresses at $x = 0$ and $x = L/2$ along the laid-out cross section, and they clearly identify the reduction of the stress levels along the compressed part of the web – plates 7 and 8 – at *x=0* due to buckling.

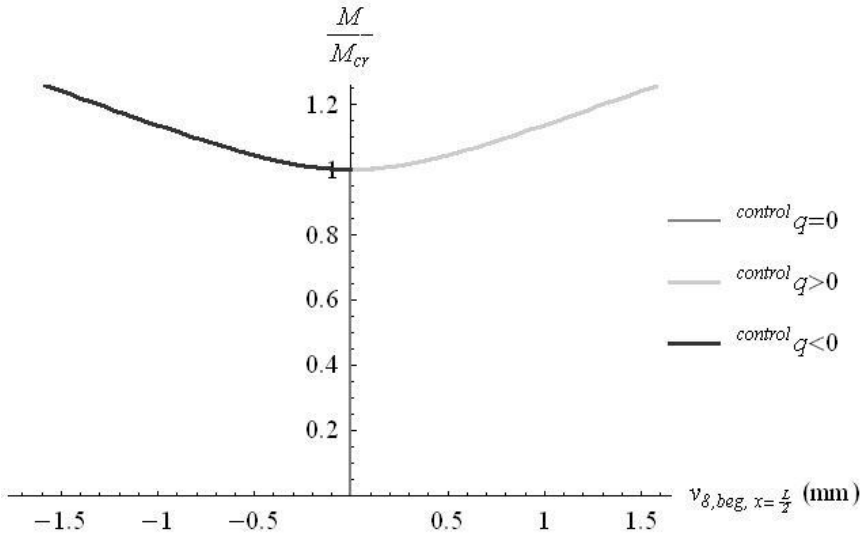

Fig. 6.80 – Horizontal displacements at the initial node of secondary wall n. 8, at $x = L/2$

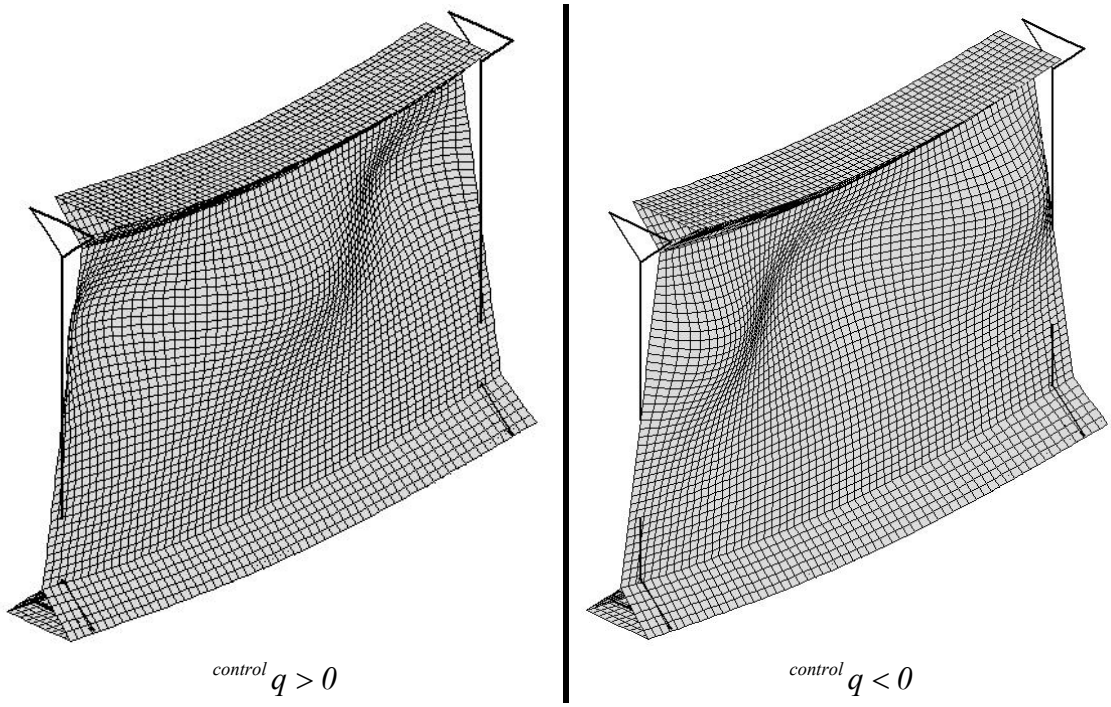

$^{control}q > 0$ $^{control}q < 0$

Fig. 6.81 – Member's deformed configuration for $M = 1.257 \times M_{CR}$ (all displacements are amplified by a factor 30)

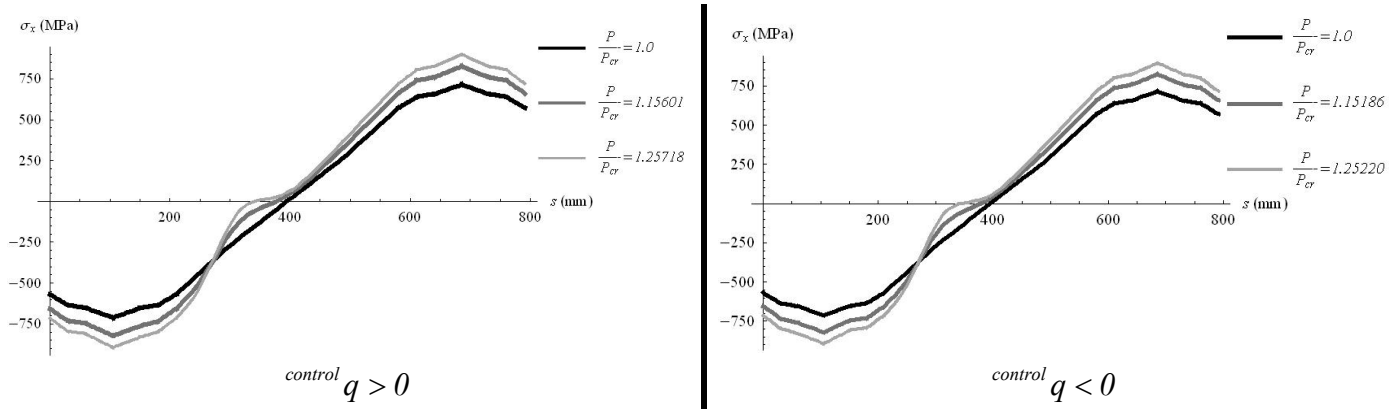

$^{control}q > 0$ $^{control}q < 0$

Fig. 6.82 – Longitudinal normal stresses σ_x^M along the (laid out) cross section at $x = 0$

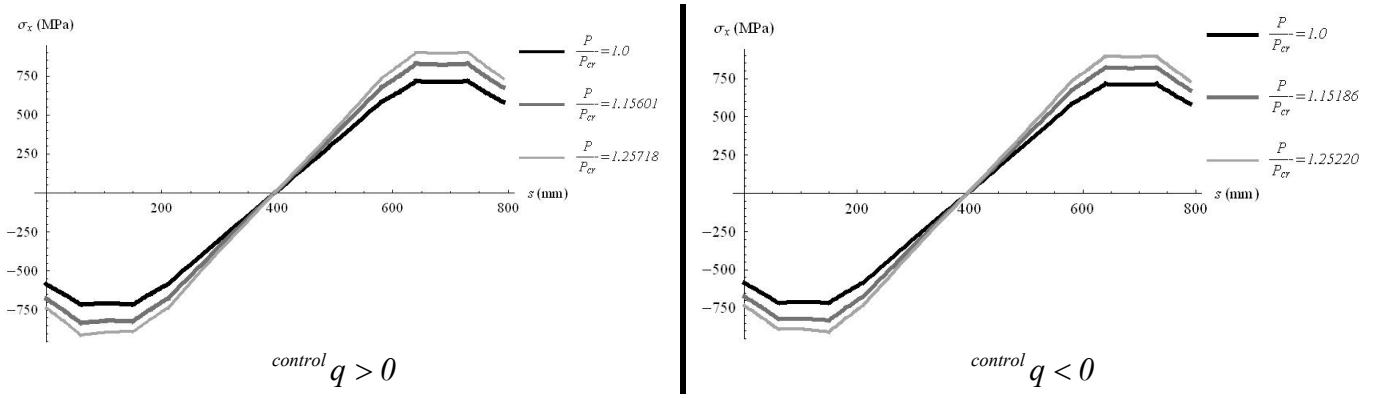

$^{control}q > 0$ $^{control}q < 0$

Fig. 6.83 – Longitudinal normal stresses σ_x^M along the (laid out) cross section at $x = L/2$

6.8.4 – Post-buckling behaviour of a simply supported beam under uniform major axis bending moment in the global flexural-distortional mode range

For higher lengths buckling is global-distortional and the correspondent post-buckling behaviour is investigated here for *L=1600* mm. For the discretization referred above and considering only the first 3 coordinate polynomials for each mode of deformation, due to computer limitations, the resulting critical moment is *M=147.812* kNm, and the most active coordinate is the one related to mode 3 and to the first coordinate polynomial. The post-buckling behaviour is shown to be stable, as seen in Fig. 6.84, where the horizontal displacement of the initial node of wall 7 is plotted against the applied load. This figure illustrates another very important fact, related to the adopted stability

procedures. As referred in chapter 3.3.4, far from the critical point the search of equilibrium states two ways are admissible to search post-buckling equilibrium states. One way is the solving of the transformed equilibrium system W_i given by expression (3.61) or (3.62), whereas the other option is the solving of the initial equilibrium system V_i given in expression (3.54), being both ways equivalent. In the problem under observation, profit is taken from this fact and the post-buckling path is initially calculated using the *W*-formulation, illustrated by the continuous line, but for $M > 1.05\, M_{cr}$ the equilibrium states are found by solving the *V*-system, illustrated by the dotted line. So, Fig. 6.84 illustrates that the post-buckling equilibrium trajectories are the same, regardless of the equilibrium systems used to find them, due to the prefect agreement between continuous sections of the same post-buckling equilibrium path.

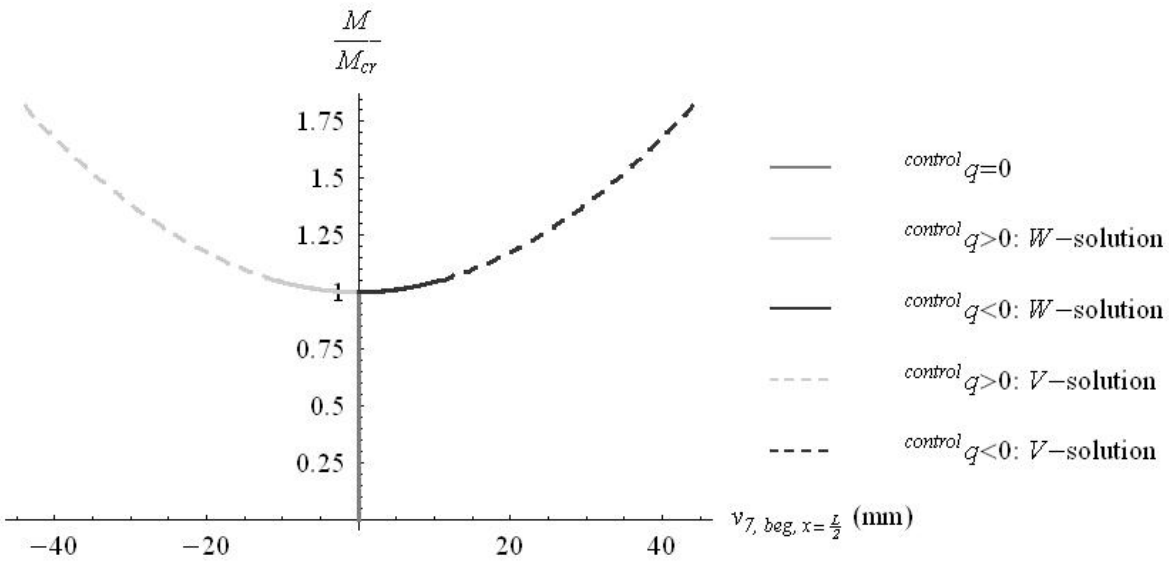

Fig. 6.84 – Horizontal displacements at the initial node of secondary wall n. 7, at $x = L/2$

The member's general configuration is presented in Fig. 6.85 for *M=263.969* kNm and in Figures 6.86 and 6.87 the longitudinal normal membrane stresses are presented along the laid-out cross section for $x = 0$ and $x = L/2$. The variation of the stresses along

the compressed flanges due to buckling is highlighted, and it is clearly perceptible that a stress pattern associated with minor axis bending is present along the cross section, mainly along the compressed hollow flange, which can show tension stresses due to the secondary minor axis bending moment. Once again, it is referred that high stress levels are rached, since the performed analysis assumes the material to be elastic, regardless of the applied stress levels.

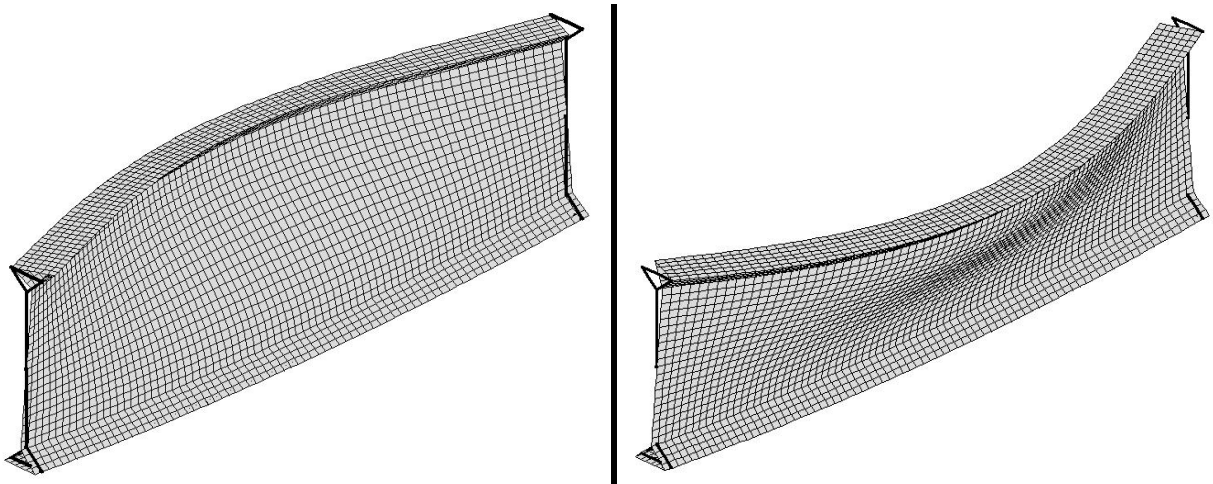

$^{control}q > 0$ $^{control}q < 0$

Fig. 6.85 – Member's deformed configuration for $M = 1.78594 \times M_{CR}$, for (all displacements are amplified by factor 5)

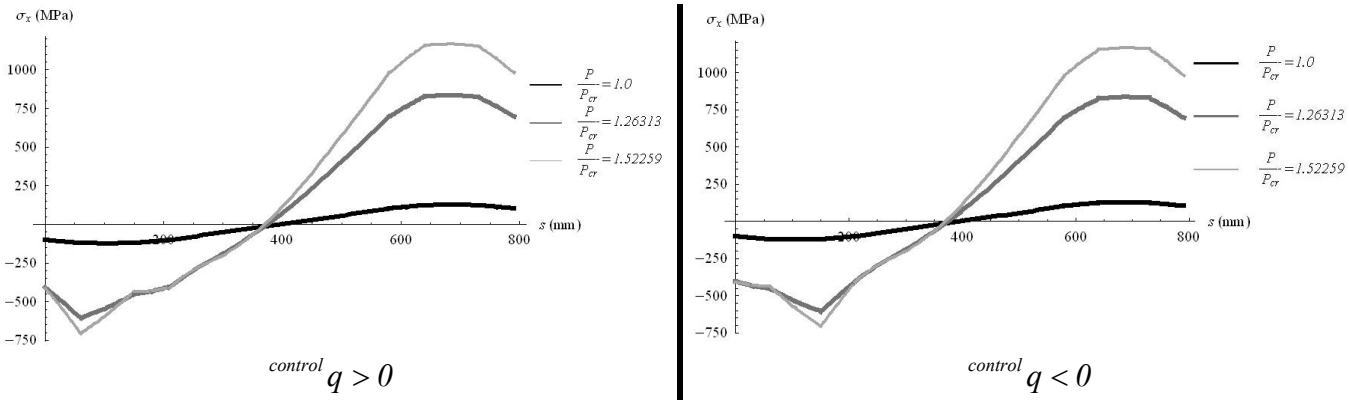

$^{control}q > 0$ $^{control}q < 0$

Fig. 6.86 – Longitudinal normal stresses σ_x^M along the (laid out) cross section at $x = 0$

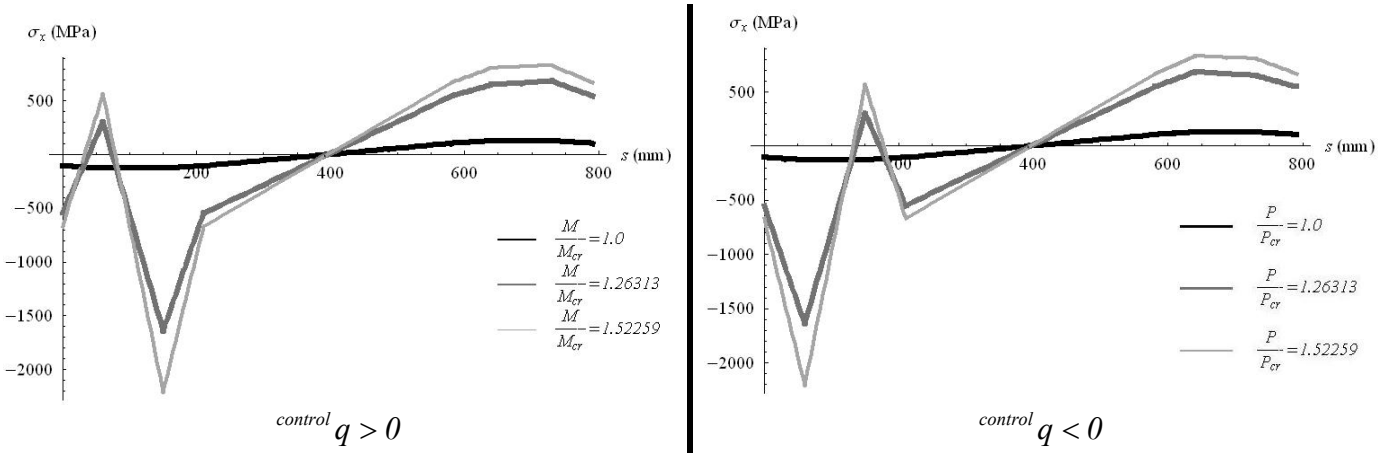

Fig. 6.87 – Longitudinal normal stresses σ_x^M along the (laid out) cross section at $x = L/2$

6.9 – Chapter synopsis

The present chapter enhanced the extended GBT scheme to the analysis of a member with general cross section geometry, made from plane folded plates. The general cross section may have branching nodes and closed cells, and the correspondent basic warping and plate distortional modes of deformation are established at the same time and are combined to assure cross section continuity, while the remaining initial mode types are established similarly to the closed or open non-branched sections given in Chapter 5. The presentation traduces chronologically the way the procedure was developed: first, it was developed for I- and bi-cellular cross sections, then for a general section: at the present stage, any cross section made from the rigid union of plane plates, forming a prismatic member, can be analysed through the GBT scheme. Finally, for each case, illustrative examples of thin-walled members having I-, bi-cellular or hollow flange beam section, under uniform compression or uniform major axis bending moment, were presented and the correspondent critical behaviour was compared to a FSM analysis, showing perfect agreement. Some developments contained in this chapter are already presented in two articles presented in two scientific conferences (Simão and Simões da Silva 2005a, Simão

& Simões da Silva 2005b).

7 – GENERAL CONCLUSIONS AND FURTHER WORK

7.1 – Final remarks

Emphasis in this thesis has been towards providing a consistent basis for the buckling and post-buckling analysis of elastic thin-walled prismatic members in the context of GBT, and, by implication, to the related numerical techniques involved.

After an introductory review of the state of the art, presented in Chapter 1, Chapter 2 contains a deep presentation of the Schardt's GBT theory and establishes a unified energy formulation for it, applicable to open non-branched and closed mono-cellular cross sections only since it follows the basic Schardt's assumptions. This energy formulation enables the consistent post-buckling analysis of thin-walled members by deriving the stress-strain relations consistently from the correspondent elasticity relations because the involved strains and the correspondent stresses are conjugate. The developments presented in this chapter are subsequently illustrated in Chapter 4 for the comparative buckling analysis of an open channel and rectangular hollow section column, the analysis of a RHS under uniform bending and the post-buckling analysis of a channel column. Clear benefits from GBT are noted for the identification of the relevant mode interaction, which is inexistent in the traditional FSM or FEM: it is there highlighted that channel columns, undergoing buckling in the distortional range with one half-wave, have non-symmetric post-buckling behaviour, the inwards movement corresponding to the unstable branch and the outwards movement corresponding to the stable branch. However, as the equilibrium state moves away from the critical one, in the inwards deformation the system regains stability and the trajectory's slope passes from negative to positive. This phenomenon can not be detected if imperfections are introduced to the system since by doing it there is no chance to analyse the member's behaviour in the neighbourhood of the critical state.

Chapter 3 may be divided in two parts. The first part contains a consistent

methodology to derive appropriate coordinate functions to the Rayleigh-Ritz method, i.e., to render discrete the member's energy functional. The coordinate functions are assumed to be polynomials that are computed from the boundary conditions of the problem, together with a normalization and orthogonality rules, through a sequential scheme that generates a complete set of appropriate coordinate functions. Therefore, the coordinate functions are no longer chosen by chance and the ability of the resulting polynomials to model several boundary conditions and to perform easy integrations is addressed and illustrated by calculating some sets of functions for usual boundary conditions, together with a brief discussion on the influence of the normalization factor to the numerical stability of the solving methods. It is noted here that the range of application of the presented methodology goes beyond the problem under observation and that the scheme can constitute a general method to the determination of appropriate coordinate functions for the Rayleigh-Ritz method in general: all in all, for a general problem being solved using the Rayleigh-Ritz method, an appropriate set for coordinate functions can be extracted from the boundary conditions of the problem itself.

The second part of Chapter 3 is devoted to the adaptation of the traditional stability procedures of Thompson and Hunt to the post-buckling analysis of structural members modelled by large equilibrium systems, for which algebraic manipulation and power expansions are no longer feasible due to the large size of the problem. Therefore, a matrix scheme is developed from the Thompson and Hunt procedures for the search of critical points and the path switching from the trivial path to the unknown post-buckling branches. The scheme forces the yet unknown post-buckling equilibrium states to lie outside the trivial path and determines them explicitly by solving the member's equilibrium system in each equilibrium state, instead of determining them as power expansions around the critical state. By doing this, the introduction of imperfections is avoided, so that no further complexities are introduced in the member's equilibrium system and, therefore, better insights can be obtained on the post-buckling behaviour of the structural members, as

observed in several examples along this thesis. The developed methodology proved to be able to deal with stability points, since it uses coordinate control, although load control is also possible, and explores, as far as the computer resources allow, the large skills enabled by the modern symbolic programming language MATHEMATICA.

Chapter 5 presents a GBT formulation alternative to the traditional Schardt's one. It starts by replacing the Force Method, for the analysis of the cross section's plane displacements, by the Displacement method, providing more consistency to the GBT analysis of cross sections and the computations of the transverse bending moments, and enabling the direct formulation of the plate's transverse extension modes, as referred below. The traditional Schardt's modes of deformation pass over unchanged to the present formulation, with the exception of the Bredt's torsional mode around closed cells that is removed from the analysis, while three additional modes of deformation are introduced, some of them already present in the bibliography, using a structured procedure. The inner nodes modes pretend to model the shear lag phenomenon, withdraw the Schardt's assumption of linear warping displacements between main nodes and consist merely in the longitudinal displacement of each inner node at the time, while the remaining nodes rest unmoved. The plate distortional modes pretend to substitute the Bredt's torsional mode and are defined as shear deformation patterns applied to each main plate at the time, the remaining ones experiencing only transverse bending deformations required to assure cross section continuity, and are used either in open or closed sections, thus unifying the GBT analysis of open and closed cross sections, similarly to the traditional FSM and FEM. The traditional Bredt's torsional mode for closed cells becomes then a particular case of the plate distortional modes. Finally, the modes of transversal extension of the plates are formulated directly by applying, for each mode, a pair of appropriate fixation forces at the edges of the correspondent main plate in the cross section's Displacement Method problem, forcing a constant transverse enlargement of each main plate at the time along the longitudinal slice *dx*. The procedure is then validated by solving two illustrative examples,

the channel column and the rectangular hollow section, and by comparing the solutions against independent results derived from the FSM and FEM. A third example is also solved and shows the ability of the GBT theory, together with the numerical analysis scheme for perfect systems, to detect phenomena that otherwise would not be observed, such as the post-buckling behaviour of the channel cross section in the flexural-distortional (asymmetric) range.

Chapter 6 enlarges the extended GBT theory to the analysis of general cross sections. The extension makes resource to exactly the same modes of deformation previously defined in Chapter 5, thus keeps the generality of the GBT theory and the plate bending, plate transverse extension and inner nodes warping modes pass over unchanged to the analysis of general cross sections. For general cross sections the method just combines the warping and the plate distortional modes at the initial step to assure cross section continuity, thus keeping the generality of GBT analysis for any type cross section, like in the FSM and FEM. The scheme is first developed to branched I-type and two-cells sections having perpendicular main plates, and is illustrated by the analysis of a I-section under compression or pure bending, and of a two cells section having equal area as the RHS analysed in Chapter 5. In each of these examples, the critical behaviour was compared to CUFSM and showed perfect agreement. After, a general procedure was implemented, requiring an additional step, previous to the orthogonalization process, to extract the linearly independent modes of deformation, given by the eigenvectors corresponding to non-null eigenvalues of matrix $\boldsymbol{C}$. The scheme is exemplified by the analysis of two hollow flange beam sections, covering all buckling modes these sections may present when submitted to a constant major axis bending moment. It is stressed that the modes of deformation for general sections are the same used in the extended GBT theory for open and mono-cellular sections, thus the generality of the GBT formulation is kept. At last, it is worth referring that the scheme presented in this chapter takes huge profit from the adoption of the Displacement Method for the determination of the transverse

bending moments, since care must be taken upon the translation displacements only, which are then introduced as prescribed displacements in the Displacement Method problem that easily computes the transverse bending moments, branching bringing no special difficulty.

All in all, the present thesis took profit from the ability of GBT to model the modal interaction in the buckling and post-buckling of thin-walled members, bringing much better physical explanation of the involved phenomena than the FSM or the FEM, extending these abilities to general cross sections, and from the ability of the adopted numerical strategies to model a wide range of boundary conditions and to deal with the perfect system, thus keeping the bifurcational behaviour these elements present and analysing the behaviour in the neighbourhood of the critical states, which is an impossible task if imperfections are introduced into the member's equilibrium system.

7.2 – Future research

Evidently, much remains to be done in the research area of the stability of thin-walled prismatic members. Several of the tasks presented below can be completed in the future, bringing deeper insights to GBT theory and to the behaviour of thin-walled members in general. Apart the evident application of the developed GBT scheme to other cross section shapes and to other load cases and supporting conditions, which constitutes an endless research range, other topics deserve special attention.

The modes related to the transversal extension of the plates can be refined by associating them with the secondary plates. The adaptation requires at first an adjustment of the plate's displacements, introducing perimeter displacements for the inner nodes also, as shown in Fig. 7.1, with the corresponding (trivial) changes in the plate's stiffness matrix and transformation matrix. Then, for each secondary plate the corresponding mode is established by applying two opposite forces at the edges of the secondary plate, as illustrated in Fig. 7.2 a) and b). From this point forward the procedure is similar to the one

exposed in Chapter 5, but an adjustment to the orthogonalization procedure is necessary. The Schardt's orthogonalization procedure is based on the fact that for a problem with n_{MD} modes of deformation matrix $\boldsymbol{C}$ is invertible, so that has rank n_{MD}. However, looking at the general expression of the terms of matrix $\boldsymbol{C}$ given in Chapter 5, it is expectable that the submatrix of $\boldsymbol{C}$ related to the plates transversal extension modes becomes singular, and therefore the traditional Schardt's is no longer applicable, although the modes of deformation are linearly independent one from each other. A case like this is not new: in Chapter 5 the transverse extension modes related to edge plates are removed from the global orthogonalization procedure since the correspondent lines and columns of $\boldsymbol{C}$ are null. In the present case it is suggested that at first an specific eigenproblem involving the present modes only is established between matrices $\boldsymbol{C}$ and $\boldsymbol{B}$, and only those related to non-null eigenvalues are included in the global orthogonalization procedure, although all modes are accounted in the global member analysis. It shall be investigated if there is any eigenproblem involving only the withdrawn modes and established between matrices $\boldsymbol{D}$ and $\boldsymbol{B}$ that has special significance and introduces any significant simplifications in the member's equilibrium matrices.

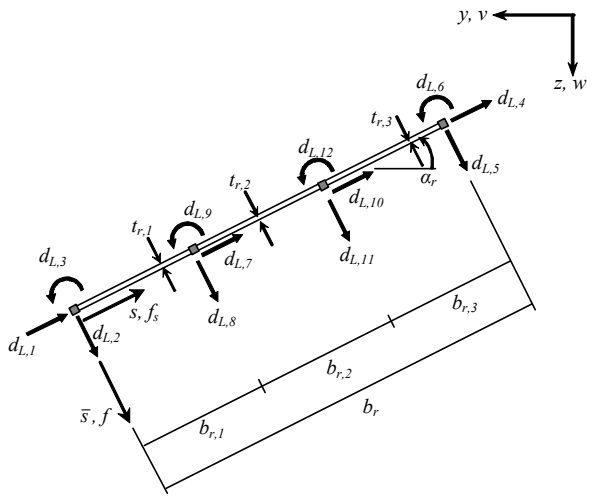

Fig. 7.1 – Plate displacements for a main plate *r*

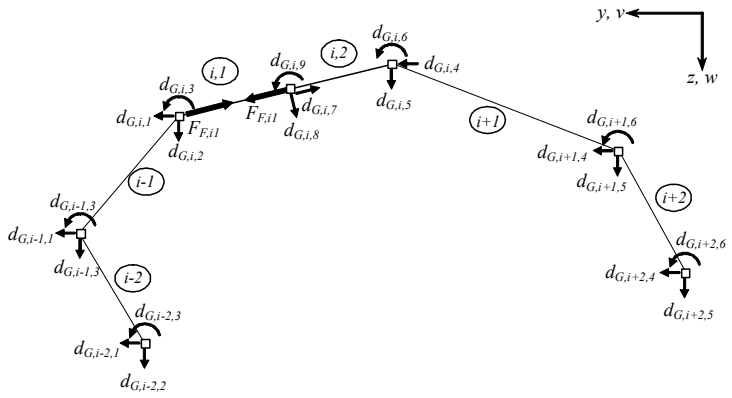

a) The transversal extension of the first secondary plate of major plate *i* - (*i, 1*)

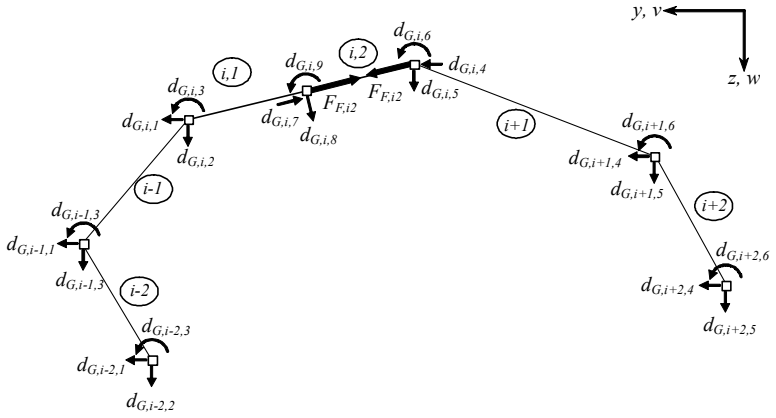

b) The transversal extension of the second secondary plate of major plate *i* - (*i, 2*)

Fig. 7.1 - The establishment of the two transversal extension plate modes for major plate *i*

The extension of the scheme developed in Chapter 3 to generate a complete set of orthogonal coordinate functions, in the context of the Rayleigh-Ritz method, to *n*-dimensional problems and to problems other than structural analysis may enable deeper understanding on the analysed phenomena and improves clearly the numerical RRM skills. Obvious applications are the study on the influence of the supporting conditions to the stability of plates under compressive loading, uniform or not, and the influence of the supporting conditions on the buckling and post-buckling behaviour of thin-walled prismatic members under a wide range of loading conditions. Also, with the development of the computer capacities commonly available and with the recent release of 64-bit personal computers that calculate numbers with an accuracy of 31 decimal places instead

of 15 for the 32-bit PC used in this thesis, numerical accuracy of the methods presented above, together with more refined discrete renderings, can enable better understanding of the post-buckling phenomena.

In the near future it is desirable to release a consistent GBT based program, for the automatic computation of the unitary modal displacements of general cross sections, similarly to the FSM based CUFSM software developed by Schaefer (2003) that computes the critical loading factor for prismatic simply supported members with general cross sections. It is suggested to base the automatic process in the general Theory of Graphs (Berge 2001, Deo 1974, Even 1979), in order to render systematic the modelling of the cross section with general geometry and the establishment of the correspondent modes of deformation. A useful and simple strategy is to compute the modal unitary displacements only, thus defining completely the modes of deformation for the posterior use of the research community and general audience.

The improved GBT formulation may be used in the near future to bring better insights on the complex shear-lag phenomenon and can be extended to materials other than isotropic. Actually, some extension of the GBT theory to materials other than isotropic is already done, as referred in Chapter 1, but profit can be taken from the adoption of the Displacement Method and the coupling between transverse extension and transverse bending can be thus easily modelled, simply by adapting adequately the terms in the stiffness matrix of the plates.

However, in the author's point of view, the most challenging research topic in the near future is the thorough study of the localized buckling in thin-walled prismatic members, principally the passage from a multi-wave shape to a localized shape, related to the appearing of secondary critical states (Coman 2004) in the post-buckling range. A wide research on the localized buckling in sandwich panels (Hunt & Ahmer Wadee 1998, Wadee 1998), in thin elastic plates (Everall & Hunt 1999) and cylindrical shells (Lord, Champneys and Hunt 1997) has already come to light but no references appear for

localization in thin-walled prismatic members such as RHS columns, although this phenomenon has already been experimentally observed (Graves-Smith & Sridharan 1980), as referred above. Moreover, due to the random shape of the geometric imperfections in real members, localization is strongly influenced by the shape of the imperfection, as observed by Abdelmoula, Damil & Potier-Ferry (1992) for cylindrical shells. Therefore, the study shall consider perfect members to decrease the number of intervenient parameters in the analysis. It is the belief of the author that the GBT theory developed in Chapter 5, together with the numerical strategies presented in Chapter 3, by adopting an increasingly larger number of orthogonal polynomials per mode, forms a powerful tool to the analysis of localized buckling in thin-walled members, namely in RHS. Note that, because the similarity between the member on elastic foundation and the thin-walled member (Schardt 1989), for the equilibrium differential equations system, has already been observed, it is expectable that localization phenomena occur also in thin walled members, since it was already observed in columns on elastic foundation (Sandstede 1997). The analysis shall consider that the primary and secondary critical states are independent one from the other, so the *W*-transformation must be established independently for the primary and for the secondary paths, relating it in both cases to the original TPE, due to the conservative character of the involved phenomena. An introductory research topic is evidently the analysis of simple models, like the beam on elastic foundation, using the orthogonal polynomials to render the system discrete and to extend the numerical procedures to the search of secondary critical states and switch to terciary paths. Despite of having been attempted, this strategy requires modern and powerful computer resources, like grid-computing software and clusters, which are not yet available to the author. Note that, due to computer limitations, the post-buckling analyses presented along the thesis were limited to the adoption of a small number of polynomials per mode of deformation, thus limiting their accuracy in spite of the orthogonality between the polynomials. As these resources become available, the scheme presented here will be applied to the study of localized

buckling in thin-walled members.

The last words of the thesis go, in a different speech, to express the author's greatest admiration for two researchers, perhaps the two most cited ones in this thesis, whom the author has still not met. Evidently, the author is referring to Richard Schardt, the creator of a whole new subject in solid mechanics – the GBT theory –, and to Giles W. Hunt, for his priceless contribution to the knowledge on the stability of elastic structures.

REFERENCES

Abdelmoula, R., Damil, N., Potier-Ferry, M. (1992), *Influence of distributed and localized imperfections on the buckling of cylindrical shells under external pressure*, International Journal of Solids and Structures, V. 29, N. 1, pp. 1-25.

AISI (1997), *Cold-formed steel design manual*, 1996 Edition, Washington: AISI - American Iron and Steel Institute .

Alfano, G., Marotti de Sciarra, F., Rosati, L. (1996), *Automatic analysis of multicell thin-walled sections*, Computers & Structures, V. 59, N. 4, pp. 641-655.

Ali, M. A., Sridharan, S. (1989), *A special beam element for the analysis of thin-walled structural components*, International Journal of Numerical Methods in Engineering, V. 28, pp. 1733-1747.

Allgower, E. L., Georg, K. (1990), *Numerical continuation methods – An introduction*, Berlin-Heidelberg: Springer-Verlag.

Allman, D. J. (1988), *Calculation of the stable equilibrium paths of discrete conservative systems with singular points*, Computers & Structures, V. 32, N. 5, pp. 1045-1054.

Amabili, M., Graziera, R. (1999), *A technique for the systematic choice of admissible functions in the Rayleigh-Ritz Method*, Journal of Sound and Vibration, V. 224 (3), pp. 519-539.

Arantes e Oliveira, E. R. (1999), *Elementos da teoria da elasticidade*, Lisboa: IST Press.

Avery, P., Mahendran, M. (1997), *Finite-element analysis of hollow flange beams with web stiffeners,* Journal of Structural Engineering, ASCE, V. 123, N. 9 (September), pp. 1123-1129.

Avery, P., Mahendran, M., Nasir, A. (2000), *Flexural capacity of hollow flange beams*, Journal of Constructional Steel Research, V. 53, pp. 201-223.

Baláž, I. (1999), *Dünnwandige Stäbe mit offenem oder geschlossenem deformierbarem Querschnitt*, Stahlbau, B. 68, H. 1, S. 70-77.

Batista, E., Camotim, D., Prola, L. C., Vasquez, E. (1998), On the stability and strength of steel columns affected by distortional buckling, Journal of Constructional Steel Research, V. 46, N. 1-3, paper N. 86.

Benito, R., Sridharan, S. (1984-85), *Mode interaction in thin walled structural members*, Journal of Structural Mechanics, V. 12, N. 4, pp. 517-542.

Benito, R., Sridharan, S. (1985), *Interactive buckling analysis with finite strips*, International Journal for Numerical Methods in Engineering, V. 21, pp. 145-161.

Berge, C. (2001), *Theory of graphs*, Mineola, NY: Dover.

Bleich, F. (1952), *Buckling strength of metal structures*, NY: McGraw Hill.

Bogensperger, T. (2000), *Erweiterte Stabtheorie und der Gevoutete Träger im Brückenbau*, Doktorat-Ingenieurs Dissertation, Graz: Technische Universität Graz.

Born, J. (1954), *Faltwerke – Ihre Theorie und Berechnung*, Stuttgart: Verlag Konrad Wittwer.

Boutyour, E. H., Zahrouni, H., Potier-Ferry, M., Boudi, M. (2004), *Bifurcation points and bifurcation branches by an asymptotic numerical method and Padé approximants*, International Journal for Numerical Methods in Engineering, V. 60, pp. 1987-2012.

Brown, R. E., Stone, M. A. (1997), *On the use of polynomial series with the Rayleigh-Ritz method*, Composite Structures, V. 39, N. 3-4, pp. 191-196.

Bulson, P. S. (1967), *Local stability and strength of structural members*, in: Chilver, A. H. (Ed.), *Thin-walled structures*, NY: John Wiley & Sons, pp. 153-207.

Camotim, D., Silveste, N. (2003), *GBT-based computational approach to analyse the geometrically non-linear behaviour of steel and composite thin-walled members*, in: Iu, V. P., Lamas, L. N., Pi, Y.-P., Mok, K. M. (Eds.), *Computational Methods in Engineering and Science* – Proceedings of the 9th International Conference on Enhancement and Promotion of Computational Methods in Engineering and Science – EPMESC IX, 25-28 November, Macao, Lisse: A. A. Balkema Publishers, p. 3-15.

Camotim, D., Silvestre, N., Gonçalves, R. and Borges Dinis, P. (2004), *GBT analysis of thin-walled members: new formulations and applications*, in: Loughlan, J. (Ed.), *Thin-walled structures* - International workshop in recent advances and future trends in thin-walled structures and technology, Loughborough University, 25 June, Bath: Canopus Publishing Ltd.

Caraça, B. J. (1954), *Lições de álgebra e análise*, Vol II, Fasc. 1º, Lisboa: Livraria Sá da Costa.

CEN - European Committee for Standardization (2004), *Eurocode 3: Design of Steel Structures, Part 1.3 – General Rules – Supplementary rules for cold-formed members and sheeting*. Brussels: European Committee for Standardization.

Chajes, A. (1974), *Principles of structural stability theory*, Englewood Cliffs, N. J.: Prentice Hall.

Champneys, A. R., Hunt, G. W., Thompson, J. M. T. (Eds.) (1999), *Localization and solitary waves in solid mechanics*, Singapore: World Scientific Publishing.

Chen, G., Baker, G. (2003), *Rayleigh-Ritz analysis for localized buckling of a strut on a softening foundation by Hermite functions*, International Journal of Solids and Structures, V. 40, pp. 7463-7474.

Chen, W. F., Lui, E. M. (1987), *Structural stability – Theory and implementation*, Upper Saddle River, N.J.: Prentice-Hall.

Cheung, M. S., Li, W., Chidiac, S. E. (1996), *Finite strip analysis of bridges*, London: E&FN Spon.

Cheung, Y. K. (1976), *Finite strip method in structural analysis*, Oxford: Pergamon Press.

Cheung, Y. K. Tham, L. G. (2000), *A review on the finite strip method*, Progress in Structural Engineering and Materials, V. 2, pp. 369-375.

Cheung, Y. K., Tham, L. G. (1998), *Finite strip method*, Boca Raton: CRC Press.

Coman, C. D. (2004), *Secondary bifurcations and localisation in a three-dimensional buckling model*, Zeitschrift für angewandte Mathematik und Physik ZAMP, V. 55, pp. 1050-1064.

Conchon, R. (2001), *Berechnung von Platten mit der Verallgemeinerten Technischen Biegetheorie (VTB)*, Institut Für Statik, Darmstadt: Technische Universität Darmstadt.

Cook, R. D., Malkus, D. S., Plesha, M. E. (1989), *Concepts and applications of Finite Element Analysis*, 3rd Ed., NY: John Wiley & Sons.

Courant, R., Hilbert, D. (1953), *Methods of mathematical physics*, Vol. I, NY: Interscience Publishers.

Crisfield, M. A. (1980), *Numerical analysis of structures*, in: Rhodes, J., Walker, A. C. (Eds.), *Developments in thin-walled structures – 1*, London: Applied Science Publishers, p. 235-284.

Croll, J. G. A., Walker, A. C. (1972), *Elements of Structural Stability*, NY: John Wiley & Sons.

Davies, J. M. (1998), *Generalized Beam Theory (GBT) for Coupled Instability Problems*, in: Rondal, J. (Ed.), *Coupled Instabilities in Metal Structures, Theoretical and Design Aspects*, CISM Courses and Lectures N. 379, p. 151-223, Wien – NY: Springer – Verlag.

Davies, J. M. (2000), *Recent research advances in cold-formed steel structures*, Journal of Constructional Steel Research, V. 55, p. 267-288.

Davies, J. M., Brian, E. R. (1982), *Manual on stressed skin diaphragm design*, London: Granada.

Davies, J. M., Jiang, C. (1996a), *Design of thin-walled columns for distorsional buckling*, in: Rondal, J., Dubina, D., Gioncu, V. (Eds.), *Coupled Instabilities in Metal Structures – CIMS 96*, London: Imperial College Press, pp. 165-172.

Davies, J. M., Jiang, C. (1996b), *Design of thin-walled beams for distortional buckling*, in: Proceedings of the 13th International Specialty Conference on Cold Formed Steel Structures, St. Louis, Missouri, U.S.A., October 17-18, pp. 141-153.

Davies, J. M., Jiang, C. (1998), *Design for distorsional buckling*, Journal of Constructional Steel Research, 46, 1-3, Paper N. 104.

Davies, J. M., Jiang, C., Ungureanu, V. (1998), *Buckling mode interaction in cold formed steel columns and beams*, in: Proceedings of the 14th International Specialty Conference on Cold Formed Steel Structures, St. Louis, Missouri, U.S.A., October 15-16, pp. 53-67.

Davies, J. M., Jiang, C., Voutay, P. (2000), *Intermediately-stiffened compression flanges*, in Camotim, D., Dubina, D., Rondal, J. (Eds.), *Coupled Instabilities in Metal Structures – CIMS 2000*, London: Imperial College Press, pp. 197-204.

Davies, J. M., Leach, P. (1992), *Some applications of Generalized Beam Theory*, in: Proceedings of the 11th International Specialty Conference on Cold Formed Steel Structures, St. Louis, Missouri, U.S.A., October 20-21, pp. 479-501.

Davies, J. M., Leach, P. (1994), *First-order Generalized Beam Theory*, J. Constuct. Steel Research, V. 31, N. 2-3, pp. 187-220.

Davies, J. M., Leach, P., Heinz, D. (1994), *Second-order Generalised Beam Theory*, J. Constuct. Steel Research, V. 31, N. 2-3, pp. 221-241.

Deo, N. (1974), *Graph theory with applications to engineering and computer science*, Englewood Clifs, NJ, Prentice-Hall.

Dinis, P. B., Camotim, D., Silvestre, N. (2006), *GBT formulation to analyse the buckling behaviour of thin-walled members with arbitrarily 'branched' open cross-sections*, Thin-Walled Structures, V. 44, pp. 20-38.

Dubina, D., Davies, J. M., Jiang, C., Ungureanu (1996), V., *Recent interactive buckling approaches for cold-formed thin-walled members*, In: Rondal, J., Dubina, D., Gioncu, V. (Eds.), *Coupled Instabilities in Metal Structures – CIMS 96*, London: Imperial College Press, pp. 173-180.

Dubina, D., Goina, D., Georgescu, M., Ungureanu, V., Zaharia, R. (1998), *Recent research on stability analysis of thin-walled cold-formed steel members*, Journal of Constructional Steel Research, V. 46, N. 1-3, Paper n. 103.

ECCS (1987), *European recommendations for the design of light gauge steel members*, 1st Ed., European Convention for Constructional Steelwork, Technical Committee 7 – Working Group 7.1, Publ. n. 49, Brussels: ECCS.

Eriksson, A. (1988), *On some path-related measures for non-linear structural F.E. problems*, International Journal for Numerical Methods in Engineering, V. 26, pp. 1791-1803.

Eriksson, A. (1989), *On linear constraints for Newton-Raphson corrections and critical point searches in structural F.E. problems*, International Journal for Numerical Methods in Engineering, V. 28, pp. 1317-1334.

Eriksson, A., Pacoste, C. (1999), *Symbolic software tools in the development of finite elements*, Computers & Structures, V. 72, pp. 579-593.

Even, S. (1979), *Graph algorithms*, London: Pitman.

Everall, P. R., Hunt, G. W. (1999), *Arnold tongue predictions of secondary buckling in thin elastic plates*, Journal of the Mechanics and Physics of Solids, V. 47, pp. 2187-2206.

FEA Ltd (2002), *LUSAS Manual (Version 15.3)*.

Felippa, C. (2001), *Nonlinear finite element methods*, Boulder, Colorado: University of Colorado.

Fujikake, M. (1985), *A simple approach to bifurcation and limit point calculations*, International Journal for Numerical Methods in Engineering, V. 21, pp. 183-191.

Fung, Y. C. (1965), *Foundations of solid mechanics*, Englewood Cliffs, N.J.: Prentice Hall.

Garcea. G. (2001), *Mixed formulation in Koiter analysis of thin-walled beams*, Computer Methods in Applied Mechanics and Engineering, V. 190, pp. 3369-3399.

Gautschi, W., Golub, G. H., Opfer, G. (Eds.) (1999), *Applications and computation of orthogonal polynomials* (Proceedings of the Conference at the Mathematical Research Institute Oberwolfach, Gemany, March 22-28, 1998), Basel: Birkäuser Verlag.

Geannakakes, G. N. (1995), *Natural frequencies of arbitrarily shaped plates using the Rayleigh-Ritz method together with natural co-ordinate regions and normalized characteristic orthogonal polynomials*, Journal of Sound and Vibration, V. 182, N. 3, pp. 441-478.

Gervásio. H., Simões da Silva, L., Simão, P. (2004), *Avaliação numérica do comportamento pós-encurvadura de pilares em secção de parede fina*, in: Congresso de Métodos Computacionais em Engenharia, Lisboa, 31 Maio a 2 Junho.

Ghali, A., Neville, A. M. (1997), *Structural analysis – a unified classical and matrix approach*, 4th Ed., London: E&FN Spon.

Girkmann, K. (1959), *Flächentragwerke*, 5th Ed., Berlin-Heidelberg: Springer-Verlag.

Godoy, K. A., Mook, D. T. (1996), *Higher-order sensitivity to imperfections in bifurcation buckling analysis*, International Journal of Solids and Structures, V. 33, N. 4, pp. 511-520.

Godoy, L. A. (2000), *Theory of elastic stability – analysis and sensitivity*, Philadelphia: Taylor & Francis.

Golub, G. H., Van Loan, C. F. (1996), *Matrix computations*, Baltimore: The John Hopkins University Press.

Gonçalves, R., Camotim, D. (2003), *Aplicação da Teoria Generalizada de Vigas (GBT) ao estudo da estabilidade de colunas de alumínio e aço inoxidável (Application of the Generalized Beam Theory (GBT) to the study of the stability of aluminium and stainless steel columns)*, in: Barbosa, J. I. (Ed.), VII Congresso de Mecânica Aplicada e Computacional, Évora, 14-16 Abril,, pp. 199-210.

Gonçalves, R., Camotim, D. (2004), *Thin-walled member plastic bifurcation analysis using Generalized Beam Theory*, In: Topping, B. H. V., Mota Soares, C. A. (Eds.), Proceedings of the 7th International Conference on Computational Structures Technology, Paper 122.

Graves-Smith, T. R. (1987), *The finite strip analysis of thin-walled structures*, in: Rhodes, J., Walker, A. C. (eds.), *Developments in thin-walled structures – 3*, London: Elsevier Applied Science Publ., pp. 205-235.

Graves-Smith, T. R., Sridharan, S. (1980), *Elastic collapse of thin-walled columns*, In: Rhodes, J., Walker, A. C. (Eds.), *Thin-walled structures – Recent technical advances and trends in design, research and construction*, Proceedings on the International Conference at the University of Strathclyde, Glasgow, 3-6 April 1979, pp. 718-730, London: Granada.

Haakh, A. U. (2004), *Die Erweiterung der VTB für allgemeine dünnwandige Querschnitte sowie die Lösung des Differentialgleichungssystems mit Potenzreihen*, Fachbereich für Bauingenieurwesen und Geodäsie, Dissertation D17, Darmstadt: Technische Universität Darmstadt.

Hancock, G. J. (1978), *Local, distortional, and lateral buckling of I-beams*, Journal of the Structural Division – Proceedings of the American Society of Civil Engineers, V. 104, n. ST11, November, pp. 1787-1798.

Hancock, G. J. (1981), *Interaction buckling in I-section columns*, Journal of the Structural Division – Proceedings of the American Society of Civil Engineers, V. 107, n. ST1, January, pp. 165-179.

Hancock, G. J. (2003), *Cold-formed steel structures*, Journal of Constructional Steel Research, V. 59, pp. 473-487.

Hancock, G. J., Kwon, Y. B., Bernard, E. S. (1994), *Strength design curves for thin-walled sections undergoing distortional buckling*, Journal of Constructional Steel Research, V. 31, pp. 169-186.

Hancock, G. J., Rogers, C. A., Schuster, R. M. (1996), *Comparison of the distortional buckling method for flexural members with tests*, in: Proceedings of the 13th International Specialty Conference on Cold Formed Steel Structures, St. Louis, Missouri, U.S.A., October 17-18, pp. 125-139.

Hanf, M. (1989), *Die geschlossene Lösung der linearen Differentialgleichungssysteme der Verallgemeinerten Technischen Biegetheorie mit einer Anwendung auf die Ermittlung plastischer Grenzlasten*, Bericht N. 9 des Institut für Statik, Darmstadt: TH Darmstadt.

Hangai, H., Kawamata, S. (1972), *Perturbation method in the analysis of geometrically nonlinear and stability problems*, in Oden, J. T., Clough, R. W., Yamamoto, Y. (Eds.), Advances in Computational Methods in Structural Mechanics and Design, pp. 473-489, Huntsville: University of Alabama in Huntsville Press.

Heinz, D. (1994), *Application of Generalized Beam Theory to the design of thin-walled purlins*, Thin-Walled Structures , V. 19, pp. 311-335.

Heinz, D. (1994), *Ein Verfahren zur Berechnung von Plattentragenwerken Durch Unterteilung in Makro-Plattenelemente*, Institut für Statik, Darmstadt: Technische Hochschule Darmstadt.

Heinz, D., Mark, H.-J. (1990), *Statisch nichtlineare Berechnungen mit der Verallgemeinerten Technischen Biegetheorie*, in Festschrift Richard Schardt, Darmstadt: T. H. Darmstadt, pp. 221-257.

Heldt, T. J., Mahendran, M. (1992), *The buckling behaviour of hollow flange beams*, Proceedings of the 11th International Specialty Conference on Cold Formed Steel Structures, Orlando, FL., U.S.A., October 20-21, pp. 131-144.

Heténi, M. (1952), *Beams on elastic foundation*, Ann Arbor: University of Michigan Press.

Huang, B.-Z., Atluri, S. N. (1995), *A simple method to follow post-buckling paths in Finite Element Analysis*, Computers & Structures, V. 57, N. 3, pp. 477-489.

Hunt, G. W. (1981), *An algorithm for the nonlinear analysis of compound bifurcation*, Philosophical Transactions – The Royal Society of London, V. 300 – A1455, pp. 443-481.

Hunt, G. W., Lucena Neto, E. (1991), *Localized buckling in long axially loaded cylindrical shells*, Journal of the Mechanics and Physics of Solids, V. 39, N. 7, pp. 881-894.

Hunt, G. W., Peletier, M. A., Champneys, A. R., Woods, P. D., Ahmer Wadee, M., Budd, C. J., Lord, G. J. (2000), *Cellular buckling in long structures*, Nonlinear Dynamics, V. 21, pp. 3-29.

Hunt, G. W., Williams, K. A. J. (1984), *On truncation of the structural potential function*, Mathematical Proceedings of the Cambridge Philosophical Society, V. 95, pp. 495-510.

Ignatiev, V. A., Sokolov, O. L. (1999), *Thin-walled cellular structures*, Roterdam: A. A. Balkema.

Jennings, A., McKeown, J. J. (1992), *Matrix computation*, 2nd Ed., Chichester: John Wiley & Sons.

Jiang, C. (1994), *Stability analysis of light gauge steel members using the finite element method and the Generalized Beam Theory*, PhD. Thesis, Salford: University of Salford.

Jiang, C. (1996), *Program to compute section properties using GBT* (Public Domain), Manchester: Manchester School of Engineering.

Jönsson, J. (1999), *Distortional warping functions and shear distributions in thin-walled beams*, Thin-Walled Structures, V. 33, pp. 245-268.

Kármán, Th. von, Christensen, N. B. (1944), *Methods of analysis for torsion with variable twist*, Journal of the Aeronautical Sciences (II), April, pp. 110-124.

Keller, H. B. (1987), *Lectures on numerical methods in bifurcation problems*, Bombay: Tata Institute of Fundamental Research.

Kesti, J. (2000), *Local and distortional buckling of perforated steel wall studs*, PhD. Thesis, Helsinki: Helsinki University of Technology.

Koiter, W. T. (1945), *On the stability of elastic equilibrium*, Dissertation, Delft, The Netherlands (English translation: Tech. Report AFFDL-TR-70-25, Air Force Flight Dyn. Lab., 1970)

Kolbrunner, C. F., Hajdin, N. (1975), *Dünnwandige Stäbe – Band 2: Stäbe mit deformierbaren Querschnitten, Nicht-elastisches Verhalten dünnwandige Stäbe*, Berlin – Heidelberg: Springer-Verlag.

Kollbrünner, C. F., Basler (1966), *Torsion*, Berlin-Heidelberg: Springer-Verlag.

Kouhia, R., Mikkola, M. (1989), *Tracing the equilibrium path beyond simple critical points*, International Journal for Numerical Methods in Engineering, V. 28, pp. 2923-2941.

Kouhia, R., Mikkola, M. (1999), *Tracing the equilibrium path beyond compound critical points*, International Journal for Numerical Methods in Engineering, V. 46, pp. 1049-1074.

Krätzig, W. B. (1995), *Time-invariant instability problems*, in: Kounadis, A. N., Krätzig, W. B. (Eds.), *Nonlinear stability of structures – Theory and computational techniques*, CISM Courses and Lectures N. 342, pp. 313-336, Wien – NY: Springer-Verlag.

Kreyszig, E. (1999), *Advanced Engineering Mathematics*, 8th Ed., NY: John Wiley & Sons.

Lanzo, A. D., Garcea. G., Casciaro, R. (1995), *Asymptotic post-buckling analysis of rectangular plates by HC finite elements*, International Journal of Numerical Methods in Engineering, V. 38, pp. 2325-2345.

Lau, S. C. W., Hancock, G. J. (1987), *Distortional buckling formulas for channel columns*, Journal of Structural Engineering – American Society of Civil Engineering, V. 113, N. 5, pp. 1063-1078.

Leach, P. (1989), *The Generalized Beam Theory with finite difference application*s, PhD. Thesis, Salford: University of Salford.

Lord, G. J., Champneys, A. R., Hunt, G. W. (1997), *Computation of localized post buckling in long axially compressed cylindrical shells*, Philosophical Transactions – The Royal Society of London, V. 355 , pp. 2137-2150.

Lucena Neto, E. (1992), *Localized post-buckling solutions in long axially-compressed cylindrical shells*, PhD Thesis, London: Imperial College of Science, Technology and Medicine.

Mahendran, M., Avery, P. (1997), *Buckling experiments of hollow flange beams with web stiffeners,* Journal of Structural Engineering, ASCE, V. 123, N. 9 (September), pp. 1130-1134.

Mahendran, M., Doan, V. (1999), *Lateral distortional buckling tests of hollow flange beams*, research monograph 99-3, Physical Infrastructure Centre, Queensland University of Technology, Brisbane, Australia.

Mandić, R., Hajdin, N. (1988), *A contribution to the analysis of box beams with deformable cross section*, Journal of Constructional Steel Research, V. 9, pp. 137-146.

Miosga, G. (1976), *Vorwiegend längsbeanspruchte dünnwandige prismatische Stäbe und Platten mit endlichen elastischen Verformungen*, Dissertation D 17, Institut für Statik, Darmstadt: T. H. Darmstadt.

Mirasso, A. E., Godoy, L. A. (1992), *Iterative Techniques for Non-Linear Eigenvalue Buckling Problems*, Communications in Applied Numerical Methods, Vol. 8, pp. 311-317.

Möller, R. (1982), *Zur Berechnung prismatischer Strukturen mit beliebigem nicht formtreuem Querschnitt*, Bericht N. 2 des Institut für Statik, Darmstadt: Technische Hochschule Darmstadt.

Mörschardt, S. (1990), *Die Verallgemeinerte Technische Biegetheorie für Faltwerke mit Kragteilen*, in Festschrift Richard Schardt, Darmstadt: T. H. Darmstadt, S. 259-275.

Murdock, J. A. (1999), *Perturbations – Theory and methods*, Philadelphia: SIAM – Society for Industrial and Applied Mathematics.

Murray, N. W. (1986), *Introduction to the theory of thin-walled structures*, NY: Oxford University Press.

Nakai, H., Yoo, C. H. (1988), *Analysis and Design of Curved Steel Bridges*, NY: McGraw Hill.

Narayanan, S., Mahendran, M. (2003), *Ultimate capacity of innovative cold-formed steel columns*, Journal of Constructional Steel Research, V. 59, pp. 489-508.

Natanson, I. P. (1964), *Constructive function theory*, Vol. 1, NY: Ungar.

Noble, B. Daniel, J. W. (1998), *Applied linear algebra*, Upper Saddle River, NJ: Prentice Hall.

Ovesy, H. R., Loughlan, J., Assaee, H. (2004), *The compressive post-local buckling behaviour of thin plates using a semi-energy finite strip approach*, Thin-Walled Structures, V. 42, pp. 449-474.

Pavazza, R., Blagojević, B. (2005), *On the cross-section distortion of thin-walled beams with multi-cell cross-sections subjected to bending*, International Journal of Solids and Structures, V. 42, pp. 901-925.

Pi, Y.-L., Trahair, N. S. (1997), *Lateral-distortional buckling of hollow flange beams*, Journal of Structural Engineering, ASCE, V. 123, N. 6 (June), pp. 695-702.

Poston, T., Stewart, I. (1978), *Catastrophe theory and its applications*, London: Pitman Publishing Ltd.

Prola, L. C. (2001), *Estabilidade local e global de elementos estruturais de aço enformados a frio* (*Local and global stability of cold-formed steel structural members*), PhD thesis, Lisboa: Instituto Superior Técnico (in Portuguese).

Przemieniecki, J. S. (1985), *Theory of Matrix Structural Analysis*, NY: Dover.

Rasmussen, K. J. R. (2000), *General Report – Experimental techniques in the testing of thin-walled structural members*, in Camotim, D., Dubina, D., Rondal, J. (Eds.), *Coupled Instabilities in Metal Structures – CIMS 2000*, London: Imperial College Press, pp. 225-239.

Rasmussen, K. J. R., Hancock, G. J. (2000), *Buckling analysis of thin-walled structures: numerical developments and applications*, Progress in Structural Engineering and Materials, V. 2, pp. 359-368.

Razaqpur, A. G., Li, H. G. (1991), *A finite element with exact shape functions for shear lag analysis in multi-cell box girders*, Computers & Structures, V. 39, N. 1-2, pp. 155-163.

Rhodes, J. (Ed.) (1991), *Design of Cold Formed Steel Members*, Elsevier.

Richards, T. H. (1977), *Energy Methods in Stress Analysis*, Chichester: Ellis Horwood.

Riks, E. (1984), *Some computational aspects of the stability analysis of nonlinear structures*, Computer Methods in Applied Mechanics and Engineering, V. 47, N. 3, pp. 219-259.

Rockey, K. C., Hill, H. V. (Eds.) (1969), *Thin Walled Steel Structures – Their design and use in buildings*, NY: Gordon & Breach Science Publishers.

Rondal, J. (2000), *Cold-formed steel members and structures – general report*, Journal of Constructional Steel Research, V. 55, N. 1-3, pp. 155-158.

Saal, G. (1974), *Ein Beitrag zur Schwingungsberechnung von dünnwandigen, prismatischen Schalentragwerken mit unverzweigtem Querschnitt*, Dissertation, D17, Darmstadt: Technische Hochschule Darmstadt.

Sandstede, B. (1997), *Instability of localized buckling modes in a one-dimensional strut model*, Philosophical Transactions – The Royal Society of London, V. 355, pp. 2083-2097.

Sarawit, A. T., Kim, Y., Bakker, M. C. M., Peköz, T. (2003), *The finite element method for thin-walled members – applications*, Thin-Walled Structures, V. 41, pp. 191-206.

Sarawit, A. T., Peköz, T. (2003), *Cold-formed steel frame and column design*, Report 03-03, NY: Cornell University.

Schafer, B. W. (1997), *Cold-formed steel behaviour and design: analytical and numerical modeling of elements and members with longitudinal stiffeners*, PhD. Thesis, NY: Cornell University.

Schafer, B. W. (2002), *Progress on the Direct Strength Method*, Proceedings of the 16th International Specialty Conference on Cold Formed Steel Structures, Orlando, FL., U.S.A., October 17-18, pp. 647-662.

Schafer, B. W. (2003), *CUFSM Manual* (downloadable at www.ce.jhu.edu/bschafer).

Schafer, B. W., Peköz, T. (1998a), Computational modeling of cold-formed steel: characterizing geometric imperfections and residual stresses, Journal of Constructional Steel Research, V. 47, pp. 193-210.

Schafer, B. W., Peköz, T. (1998b), *Direct strength prediction of cold-formed steel members using numerical elastic buckling solutions*, in Shanmugam, N. E., Richard Liew, J. Y., Thevendran, V. (Eds.), *Thin-walled structures – Research and development*, Oxford: Elsevier, pp. 137-144.

Schafer, B. W., Peköz, T. (1999), *Laterally braced cold-formed steel flexural members with edge stiffened flanges*, Journal of Structural Engineering, ASCE – American Society of Civil Engineers, V. 125, N. 2, February, pp. 118-127.

Schardt, R. (1966), *Eine Erweiterung der Technischen Biegetheorie zur Berechnung prismatischer Faltwerke*, Der Stahlbau, 35, S. 161–171.

Schardt, R. (1970), *Anwendung der Erweiterten Technischen Biegetheorie auf die Berechnung prismatischer Faltwerke und Zylinderschalen nach Theorie I. und II. Ordnung*, Proceedings of the IASS-Symposium on Folded Plates and Prismatic Structures, Vol. I, Wien.

Schardt, R. (1983), *The Generalized Beam Theory*, em Morris, L. J. (Ed.), *Instability and plastic collapse of Steel Structures*, Proceedings of M. R. Horne Conference, University of Manchester, London: Granada, pp. 469-475.

Schardt, R. (1989), *Verallgemeinerte Technische Biegetheorie*, Berlin-Heidelberg: Springer-Verlag.

Schardt, R. (1994a), *Generalized Beam Theory — An adequate method for coupled stability problems*, Thin-Walled Structures, V. 19, pp. 161-180.

Schardt, R. (1994b), *Lateral torsional and distorsional buckling of channel- and hat-sections*, J. Constuct. Steel Research, V. 31, N. 2-3, pp. 243-265.

Schardt, R., Hanf, M., Schardt, C. (1987), *Massnahmen zur besseren Ausnutzung und zur Steigerung der Trafähigkeit von Kaltprofilen*, Bericht N. 7 des Institut für Statik, Darmstadt: T. H. Darmstadt.

Schardt, R., Heppner, K.-U., Neujahr, M.(1995), *Über die Ermittlung eines Schwingbeiwertes für prismatische Brücken mit der VTB*, Bauingenieur, B. 70., S. 531–539.

Schardt, R., Issmer, H., Mörschardt, S. (1986), *Gesamstabilität Dünnwandiger Stäbe*, Bericht N. 5 des Institut für Statik, Darmstadt: T. H. Darmstadt.

Schardt, R., Schrade, W. (1982), *Kaltprofil-Pfetten*, Bericht N. 1 des Institut für Statik, Darmstadt: TH Darmstadt.

Schardt, R., Strehl, C. (1976), *Theoretische Grundlagen für die Bestimmung der Schubsteifigkeit von Trapezblechscheiben – Vergleich mit anderen Berechnungsansätzen und Versuchsergebnissen*, Der Stahlbau, 45. Jahrgang, S. 97–108.

Schardt, R., Zhang, X. (1989), *Die Anwendungen der Verallgemeinerten Technischen Biegetheorie im Nichtlineare Beulbereich*, em Stein, E. (Ed.), *Nicht Lineare Berechnungen in Konstruktiven Ingenieurbau*, , S. 482-500, Berlin-Heidelberg: Springer-Verlag.

Schrade, W. (1984), *Ein Beitrag zum Stabilitätsnachweis dünnwandiger, durch Bindebleche versteifter Stäbe mit offenem Querschnitt*, Bericht N.4 des Institut für Statik, Darmstadt: TU Darmstadt.

Sedlacek, G. (1971), *Die Anwendung der erweiterten Biege– und Verdrehtheorie auf die Berechnung von Kastenträgern mit verformbarem Querschnitt*, Straße Brücke Tunnel, B. 23., S. 241–244, 329–335.

Seidel, R. (1988), *From equilibrium to chaos – Practical bifurcation and stability analysis*, NY: Elsevier.

Shanmungam, N. E., Balendra, T. (1991), *An experimental and theoretical study of multi-cell structures curved in plan*, Thin-Walled Structures, V. 12, pp. 373-387.

Silva, V. D. (2004), *Mecânica e resistência dos materiais* (*Mechanics and strength of materials*), 3rd Ed., Coimbra: Zuari (in Portuguese).

Silvestre, N. (2005), *Teoria generalizada de vigas: formulações, implementação numérica e aplicações*, PhD Thesis, Lisboa: Instituto Superior Técnico (in Portuguese).

Silvestre, N., Camotim, D. (2002a), *First-order Generalized Beam Theory for arbitrary orthotropic materials*, Thin-Walled Structures, V. 40, N. 6, pp. 749-783.

Silvestre, N., Camotim, D. (2002b), *Second-order Generalized Beam Theory for arbitrary orthotropic materials*, Thin-Walled Structures, V. 40, N. 6, pp. 791-820.

Silvestre, N., Camotim, D. (2003), *GBT buckling analysis of pultruded FRP lipped channel members*, Computers & Structures, V. 81, pp. 1889-1904.

Silvestre, N., Camotim, D. (2004a), *Distortional buckling formulae for cold-formed steel C and Z-section members: Part I - derivation*, Thin-Walled Structures, V. 42, N. 11, pp. 1567-1597.

Silvestre, N., Camotim, D. (2004b), *Distortional buckling formulae for cold-formed steel C and Z-section members: Part II – validation and application*, Thin-Walled Structures, V. 42, N. 11, pp. 1599-1629.

Silvestre, N., Simão, P., Camotim, D. e Simões da Silva, L. (2001), *Aplicação da teoria generalizada de vigas (GBT) à análise de estabilidade de perfis de aço enformados a frio*, in: A. Lamas, P. Vila Real e L. Simões da Silva (Eds), Construção Metálica e Mista III, pp 617-626.

Simão, P., Simões da Silva, L. (2002), *Comparative analysis of the stability of open and closed thin-walled section members in the framework of Generalised Beam Theory*, in: Lamas, A., Simões da Silva, L. (Eds.), Proceedings of the 3rd European Conference on Steel Structures – EUROSTEEL 2002, Coimbra, Portugal, 19-20 September, Coimbra: CMM, pp. 711-721.

Simão, P., Simões da Silva, L. (2003a), *Stability behavior of closed cross-section thin-walled prismatic members in the framework of the Generalised Beam Theory*, in: Hancock, G.J., Bradford, M.A., Wilkinson, T.J., Uy, B. and Rasmussen, K.J.R. (Eds.), Proceedings of the International Conference on Advances in Structures – Steel, Concrete, Composite and Aluminium – ASSCCA'03, Sydney, Australia, Lisse: A. A. Balkema, pp. 503-510.

Simão, P., Simões da Silva, L. (2003b), *Post-buckling behaviour of open cross-section thin-walled columns in the context of the Generalized Beam Theory*, in: Iu, V. P., Lamas, L. N., Pi, Y.-P., Mok, K. M. (Eds.), *Computational Methods in Engineering and Science* – Proceedings of the 9th International Conference on Enhancement and Promotion of Computational Methods in Engineering and Science – EPMESC IX, 25-28 November, Macao, Lisse: A. A. Balkema Publishers, pp. 891-898.

Simão, P., Simões da Silva, L. (2003c), Comportamento pós-bifurcacional de colunas metálicas enformadas a frio de secção de parede fina no contexto da GBT, in Infante Barbosa, J. (Ed.), VII Congresso Nacional de Mecânica Aplicada e Computacional, Évora, pp 269-278.

Simão, P., Simões da Silva, L. (2004a), *A unified energy formulation for the stability analysis of open and closed thin-walled members in the framework of the Generalized Beam Theory*, Thin-Walled Structures, V. 42, N. 10, pp. 1495-1517.

Simão, P., Simões da Silva, L. (2004b), *A numerical scheme for post-buckling analysis of thin-walled members in the context of GBT*, in: Proceedings of the International Conference on Computational and Experimental Engineering and Sciences, Funchal, Madeira, pp. 2079-2086.

Simão, P., Simões da Silva, L. (2005a), *Post-Buckling Analysis of Thin-Walled I-Section Columns in the Framework of Generalized Beam Theory*, Proceedings of the 5th International Conference on Computation of Shell and Spatial Structures, June 1-4, Salzburg, Austria, CD-Rom extended abstract N. 265.

Simão, P., Simões da Silva, L. (2005b), *Análise pós-encurvadura de secções I de paredes finas no contexto da GBT*, in: Proceedings da Conferência Métodos Numéricos en Ingeniería 2005, Granada, Espanha, pp. 141 (abstract) and CD-Rom (full paper).

P. Simão, P, Simões da Silva,, L. (2005c), *Post-Buckling Analysis of Thin-Walled Channel Columns in the Framework of the Generalized Beam Theory*, in Proceedings of the Tenth International Conference on Civil, Structural and Environmental Engineering Computing, B.H.V. Topping, (Editor), Civil-Comp Press, Stirling, United Kingdom, paper n. 38.

Simões da Silva, L., Simão, P. (2002), *GBT – Teoria generalizada de peças lineares: aplicação a perfis metálicos enformados a frio com secção aberta* (GBT – Generalized Beam Theory: application to the study of cold-formed steel elements with open section), Revista Portuguesa de Engenharia de Estruturas, n. 50 (Fevereiro 2002), pp. 49-67 (in Portuguese).

Singh, B., Chakraverty, S. (1992), *On the use of orthogonal polynomials in the Rayleigh-Ritz method for the study of transverse vibration of elliptic plates*, Computers & Structures, V. 43, N. 3, pp. 439-443.

Singhvi, S., Kapania, K. (1994), *Comparison of simple and Chebychev polynomials in Rayleigh-Ritz analysis*, ASCE – Journal of Engineering Mechanics, V. 120, N. 10 (October), pp. 2126-2135.

Smith, S. T., Bradford, M. A., Oehlers, D. J. (1999a), *Numerical convergence of simple and orthogonal polynomials for the unilateral plate buckling problem using the Rayleigh-Ritz Method*, International Journal for Numerical Methods in Engineering, V. 44, pp. 1685-1707.

Smith, S. T., Bradford, M. A., Oehlers, D. J. (1999b), *Elastic buckling of unilaterally constrained rectangular plates in pure shear*, Engineering Structures, V. 21, pp. 443-453.

Sridharan, S., Graves-Smith, T. R. (1981), *Postbuckling analyses with finite strips*, Journal of the Engineering Mechanics Division, Proceedings of the ASCE – American Society of Civil Engineers, V. 107, N. EM5, October, pp. 869-888.

Steindl, A., Troger, H. (2001), *Methods for dimension reduction and their application in nonlinear dynamics*, International Journal of Solids and Structures, V. 38, pp. 2131-2147.

Stoer, J., Bulirsch, R. (1993), *Introduction to numerical analysis*, 2nd Ed., NY: Springer-Verlag.

Storch, J., Strang, G. (1988), *Paradox lost: natural boundary conditions in the Ritz-Galerkin Method*, International Journal for Numerical Methods in Engineering, Vol. 26, pp. 2255-2266.

Takanashi, K., Ishihara, N., Nakamura, H. (2000), *Analytical and numerical solutions for distortional instabilities of thin-walled beams under bending moments*, in Camotim, D., Dubina, D., Rondal, J., *Coupled instabilities in metal structures – CIMS 2000*, London: Imperial College Press, pp. 73-80.

Thompson, J. M. T., Hunt, G. (1973), *A general theory of elastic stability*, London: John Wiley & Sons.

Thompson, J. M. T., Hunt, G. (1984), *Elastic instability phenomena*, Chichester: John Wiley & Sons.

Thompson, J. M. T., Stewart, H. B. (2002), *Nonlinear dynamics and chaos*, 2nd Ed., Chichester: John Wiley & Sons.

Trahair, N. S. (1993), *Flexural-torsional buckling of structures*, London: E&FN Spon.

Troger, H., Steindl, A. (1991), *Nonlinear stability and bifurcation theory*, Wien: Springer-Verlag.

Uhlmann, W. (1970), *Die Berechnung von im Grundriß gekrümmten biegesteifen Faltwerken mit offenem in Längsrichtung unveränderlichem Querschnitt*, Der Stahlbau, 39. Jahrgang, S. 193–199, 240–247, 279–286.

van Erp, G. M., Menken, C. M. (2004), *Initial post-buckling analysis with the spline Finite-Strip method*, Computers & Structures, V. 40, N. 5, p. 1193-1201.

Vannucci, P., Cochelin, B., Damil, N., Potier-Ferry, M. (1998), *An asymptotic-numerical method to compute bifurcation branches*, International Journal for Numerical Methods in Engineering, V. 41, pp. 1365-1389.

Vlasov, V. Z. (1961), *Thin walled elastic beams*, 2nd Ed., Washington: The National Science Foundation and the Department of Commerce.

Wadee, M. A. (1998), *Localized buckling in sandwich structure*s, PhD Thesis, Bath: University of Bath.

Wadee, M. K., Hunt, G. W. and Withing, I. M. (1997), *Asymptotic and Rayleigh-Ritz routes to localized buckling solutions in an elastic instability problem*, Proceedings of The Royal Society of London, V. 453 – A, pp. 2085-2107.

Waldron, P. (1986), *Sectorial properties of straight thin-walled beams*, Computers & Structures, V. 24, N. 1, pp. 147-156.

Wilkinson, J. H. (1965), *The algebraic eigenvalue problem*, Oxford: Clarendon Press.

Winter, G. (1962), *Commentary on the 1962 Edition – Light gage cold-formed steel design manual*, NY: American Institute and Steel Institute.

Wolfram, S. (2003), *The Mathematica book*, 5th Ed., Champaign: Wolfram Media.

Wriggers, P. (1995), *Solution strategies for nonlinear equations and computation of singular points*, in: Kounadis, A. N., Krätzig, W. B. (Eds.), *Nonlinear stability of structures – Theory and computational techniques*, CISM Courses and Lectures N. 342, pp. 271-311, Wien – NY: Springer-Verlag.

Wriggers, P., Simo, J. C. (1990), *A general procedure for the direct computation of turning and bifurcation points*, International Journal for Numerical Methods in Engineering, V. 30, pp. 155-176.

Yamada, S., Croll, J. G. A. (1999), *Contributions to understanding the behaviour of axially compressed cylinders*, Journal of Applied Mechanics – ASME (American Society of Mechanical Engineers), V. 66, June, pp. 299-309.

Yan, J., Young, B. (2001), *Compression tests of thin-walled lipped channels with return lips*, in: Zaraś, J., Kowal-Michalska, K., Rhodes, J. (Eds.), *Thin-Walled Structures – Advances and Developments*, Oxford: Elsevier, pp. 249-256.

Yang, D., Wilkinson, T. (2005), *LiteSteel beams (LSB) under interior and end bearing forces*, Research Report N. 849, School of Civil Engineering, Sydney: the University of Sydney (downloadable at www.civil.usyd.edu.au).

Yap, D. C. Y., Hancock, G. J. (2006), *Interaction buckling and postbuckling in the distortional mode of thin-walled sections*, Research Report N. R870, School of Civil Engineering, Sydney: The University of Sydney (downloadable at www.civil.usyd.edu.au).

Young, B., Hancock, G. J. (2000), *Experimental investigation of cold-formed channels subjected to combined bending and web crippling*, Proceedings of the 15th International Specialty Conference on Cold Formed Steel Structures, St. Louis, Missouri, U.S.A., October 19-20, pp. 71-90.

Young, B., Rasmussen, K. J. R. (1998), *Tests on cold-formed channel columns*, , in: Proceedings of the 14th International Specialty Conference on Cold Formed Steel Structures, St. Louis, Missouri, U.S.A., October 15-16, pp. 239-264.

Yu, C., Schafer, B. J. (2002), *Local buckling tests on cold-formed steel beams*, in: Proceedings of the 16th International Specialty Conference on Cold Formed Steel Structures, Orlando, FL, U.S.A., October 17-18, pp. 127-144.

Yu, W. W. (2000), *Cold-formed steel design*, 3rd Ed., NY: John Wiley & Sons.

Zhang, X. (1988), *Ein Beitrag zur Bestimmung der Traglast dünnwandiger, durch Knicken und Beulen gefährdeter U–Profile unter Längsdruckbelastung in der Symmetrieebene*, Bericht N. 8 des Institut für Statik, Darmstadt: TH Darmstadt.

Zhao, X. L., Mahendran, M. (1998), *Recent innovations in cold-formed tubular sections*, Journal of Constructional Steel Research, V. 46, N. 1-3, CD-Rom Paper N. 228.